The Institute for Solid State Physics
The University of Tokyo

Activity Report 2021

ISSP

Activity Report 2021

Contents

Preface

We would like to offer the readers the scientific activity report of the Institute for Solid State Physics (ISSP) for the Japanese FY 2021.

ISSP was established in 1957 as a joint usage/research institute attached to the University of Tokyo. In every era, we aim to lead the frontier of “condensed matter physics and materials science” and contribute to science and technology from the view of basic research. We have promoted activities focused on research, education, and joint usage/research.

The first and second parts of the report, Research Highlights/Joint Research Highlights, exhibit experimental and theoretical achievements in condensed matter physics and materials science. In 2021, the number of adapted joint usage/research is 1,803 and the total number of researchers is 6,489, whose number was recovered even in the COVID-19 pandemic.

The third part includes the reports on progress of facilities in 2021 as follows. (1) In International MegaGauss Science Laboratory, the pulse magnets can generate up to 86 Tesla (T) by non-destructive manner, and from 100 T up to 1200 T, the world strongest as an in-door record, by destructive methods to promote materials science under high magnetic field. (2) In the Supercomputer Center (SCC), the System C is scheduled to be settled in June 2022. In Center of Computational Materials Science, the website "MateriApps" for information on application software in computational science has been constructed to support community members. (3) In Neutron Science Laboratory, it is really good news that JRR-3 has restarted in February 2021 after long shutdown and the normal General User Program came back from July 2021. The technical progress of High Resolution Chopper (HRC) spectrometer has been proceeded under high pressure and low temperature environment in cooperation with KEK. (4) The Laser and Synchrotron Research (LASOR) center has 10 groups in 2021 where ISSP has integrated the two streams, namely the extreme lasers and synchrotron radiations, into the common platform. In Synchrotron Radiation Laboratory, operand spectroscopy is available by using lasers at Harima branch. (5) The Laboratory of Quantum Material Nanostructures (Q-NanoLab) has opened on March 10, 2022 as a joint facility. The Q-NanoLab provides a common infrastructure for investigating nanostructures, non-equilibrium phenomena, or device operations of newly synthesized materials and novel quantum structures.

In the following parts, seven reports of international and domestic online and hybrid conferences and workshops owing to COVID-19 pandemic, subjects of joint research, and list of publications have been presented.

For the development of material science studying the various physical properties of matters, it is essential to further expand the research area and promote the diversity of the researchers. The ISSP Workshop entitled "ISSP WOMEN'S WEEK 2021" was held to further promote the activities of female researchers who still remain a minority in the field of science and engineering research. We invited female researchers who are active on the cutting edge in a wide range of fields of material science, ranging from leading professors representing each research field, who serve as a role model for female students, to up-and-coming young female researchers. Moreover, special lectures on the efforts of the institutions to promote diversity and a panel discussion with invited speakers were given.

All these facts confirm that ISSP continues to develop successfully and dynamically as the global center of excellence of condensed matter physics and materials science. We appreciate continuous support and cooperation of communities for our activities.

July, 2022
MORI Hatsumi
Director of the Institute for Solid State Physics
The University of Tokyo

Simplest Model for Doped Conducting Polymer: Single-Crystalline Dimer Radical Cation Salts

Mori and Ozaki Groups

Conjugated polymers are essential materials in organic electronic device technologies owing to their mechanical flexibility, lightness, and solution processability. Among them, poly(3,4-ethylenedioxythiophene):poly(styrenesulfonate) (PEDOT:PSS, Fig. 1a), a polyion complex in which the positively charged PEDOT is stabilized by PSS anions, is one of the most widely used conducting polymers. The high conductivity (up to > 4000 S cm^{-1}), transparency, and solution processability have increasingly led them to a wide range of applications, for example, as a hole injection layer in organic photovoltaic (OPV) devices. Nevertheless, in-depth structural information of PEDOT:PSS is sorely lacking, which has severely limited the understanding of the structure-based conducting mechanism requisite for performance improvement; this also hampers molecular design strategies of next-generation electric conductors. One promising approach to elucidate the structure-property relationships of doped PEDOT is to utilize discrete oligo-EDOT·A models (A: counter anion, Fig. 1b). Recently, we developed oligo-EDOT·A models with less bulky methylthio (MeS) groups (i.e., 2MeS-2EDOT·A; A = BF_4^-, ClO_4^-, PF_6^-) that facilitate the growth of X-ray quality single crystals with adequately tight π-stacking. Combination of the atomic-level structural analyses and physical property measurements of the discrete oligomer systems revealed strong π–π interactions along the stacking direction as the origin of the excellent conductivity of doped PEDOT.

Single crystals of charge-transfer salts 2MeS-2EDOT·A were then synthesized by the electrochemical oxidation of 2MeS-2EDOT in the presence of n-Bu_4N·A electrolyte. The X-ray structural analyses at 293 K revealed a 1:1 composition of oxidized 2MeS-2EDOT (i.e., monovalent radical cation 2MeS-2EDOT$^+$) and counter anion A located in the voids of 2MeS-2EDOT$^+$ donors (Figs. 2a, b). In each structure of 2MeS-2EDOT·A, the donors were tightly stacked in a one-dimensional (1D) configuration with a head-to-tail pattern and with the donors rotated 1–3° at the centroid along the π-stacking axis. Interestingly, the donors were uniformly π-stacked in the range 3.46–3.48 Å, consistent with those predicted for PEDOT:PSS (3.43–3.51 Å).

We investigated the band structures based on the crystal structures using first-principles density functional theory (DFT) calculations (OpenMX software). Concerning the 1+ electronic charge of the molecule and its crystallographycally uniform π-stacking structure, the HOCO band exhibited a half-filled state with no energy gaps at the Fermi level (Fig. 2c), suggesting a metallic electronic state. The band width W of the HOCO band was determined to be as high as 0.998 eV (Fig. 2c). This result indicates the exclusively strong molecular interaction (W ≈ 1 eV) found in 2MeS-2EDOT·A. The geometric and electronic structures of π-stacking are the most critical factors for the high conductivity of doped PEDOT.

We then measured the electrical resistivity (ρ) of 2MeS-2EDOT·A. The ρ along the long axis direction of the crystal shape (the donor stacking *a*-axis) of 2MeS-2EDOT·BF_4 was determined as 2.8 × 10^2 Ω cm (Fig. 2d) at room temperature. From an Arrhenius plot, the activation energy was determined as 177.2 ± 0.9 meV, exhibiting almost no *T*-dependence. Considering the metallic

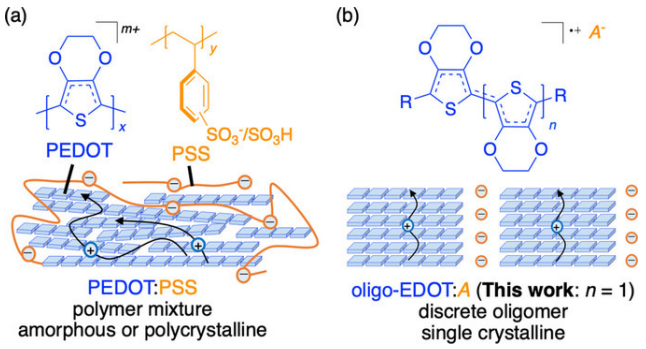

Fig. 1. Oligomer approach for doped PEDOT demonstrated in this study. (a) Structure of poly(3,4-ethylenedioxythiophene):poly(styrenesulfonate) (PEDOT:PSS). (b) Structure of discrete oligomer models: oligo-3,4-ethylenedioxythiophene (oligo-EDOT)·A (A = BF_4, ClO_4, PF_6).

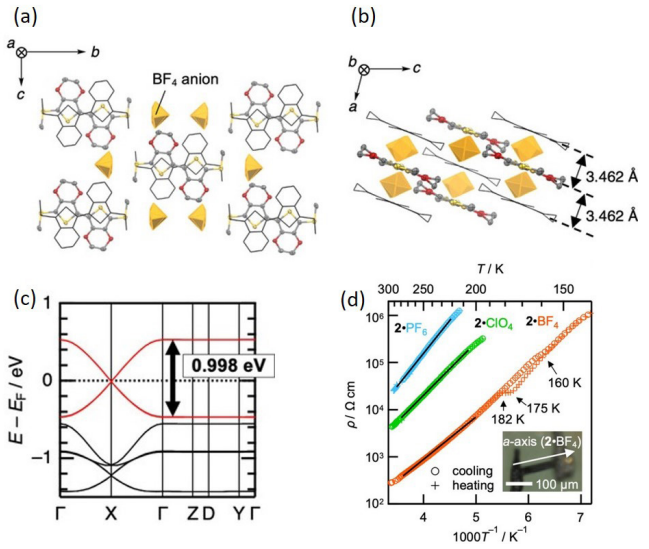

Fig. 2 Structures of 2MeS-2EDOT·BF_4 along (a) the a-axis and (b) the b-axis. The orange polyhedra represent the disordered BF_4 anions. (c) Calculated band structure of 2MeS-2EDOT·BF_4 and (d) ρ (resistivity) – Temperture−1 plots of 2MeS-2EDOT·A (A = BF_4, ClO_4, PF_6) Inset: a picture for the single crystal of 2MeS-2EDOT·BF_4 used in the measurement. Solid lines show fittings of the Arrhenius law.

half-filled electronic state indicated by the band calculations (Fig. 2c), the semiconducting behavior suggests that 2MeS-2EDOT·BF_4 is in a "genuine (half-filled) Mott state" with localized and poorly conducting electrons because of on-site Coulomb repulsion (U). The semiconducting behavior despite large W indicates that U is dominant over W in this system. Such a genuine Mott state (expressed as $U > W$) with large W is quite rare in organic conductor series. The semiconducting behaviors were likewise observed in 2MeS-2EDOT·ClO_4 and 2MeS-2EDOT·PF_6, and the room temperature ρ was determined as $4.3 \times 10^3\ \Omega$cm for 2MeS-2EDOT·ClO_4 and $4.3 \times 10^4\ \Omega$ cm for 2MeS-2EDOT·PF_6, respectively. The increase of ρ by one order of magnitude each was observed as the anion size increased and the π-stacking distances elongated (BF_4^-<ClO_4^-<PF_6^-, Fig. 2d). Activation energies were also determined as 223.6 ± 0.5 meV for 2MeS-2EDOT·ClO_4 and 277.9 ± 1.4 meV for 2MeS-2EDOT·PF_6, reflecting the chemical pressure effect from the anion sizes. It is to be noted that in the ρ–T^{-1} plot for 2MeS-2EDOT·BF_4, we observed a slight transition at 160 and 175 K for the cooling and heating processes, respectively, with a hysteresis of T (Fig. 2d), suggesting that a first-order phase transition is involved.

In conclusion, we developed tightly π-stacked models for discrete EDOT dimers 2MeS-2EDOT·A. These models exhibited unique 1D half-filled electronic structures with exclusively large band width ($W \approx 1$ eV) along the intracolumnar direction, implying the origin of the high electrical conductivity of doped PEDOT. The room temperature conductivities ($\sigma = \rho^{-1}$; < 3.6 μS cm^{-1}) were lower than that of doped PEDOT (> 4000 S cm^{-1}), which may originate in the genuine Mott state of our models caused by large U relative to W. The control of the competition between U and W in these systems (e.g., by elongating conjugation lengths to reduce U) may realize a variety of electronic states, including the metallic and even superconducting states. This unique approach of controlling U is accessible exclusively using our oligomer strategy. The construction of an oligomer library will further elucidate relationships between the structures and electronic properties.

References

[1] R. Kameyama, T. Fujino, S. Dekura, M. Kawamura, T. Ozaki, and H. Mori, A European Journal, **27**, 6696 (2021).
[2] R. Kameyama, T. Fujino, S. Dekura, and H. Mori, Phys. Chem. Chem. Phys. **24**, 9130 (2022).
[3] R. Kameyama, T. Fujino, S. Dekura, S. Imajo, T. Miyamoto, H. Okamoto, and H. Mori, J. Mater. Chem. C. **10**, 7543 (2022).

Authors

R. Kameyama, T. Fujino, S. Dekura, M. Kawamura, T. Ozaki and H. Mori

Topological Thermoelectric Effects in Organic Dirac Fermion System

Osada Group

Two topological thermoelectric effects, the nonlinear anomalous Ettingshausen effect and the quantized thermoelectric Hall effect, were investigated in the two-dimensional (2D) organic Dirac fermion (DF) system α-(BEDT-TTF)$_2$I$_3$.

(1) Nonlinear anomalous Ettingshausen effect (AEE)

So far, we have experimentally confirmed that the weak charge ordering (CO) state of α-(BEDT-TTF)$_2$I$_3$, which is the region close to the 2D massless DF phase in the CO phase, is a 2D massive DF state with a small CO gap. Because the finite Berry curvature dipole was expected in the massive DF state with tilted Dirac cones, we experimentally searched for the nonlinear anomalous Hall effect (AHE) in the current-carrying state in the weak CO state at zero magnetic field, and successfully observed it.

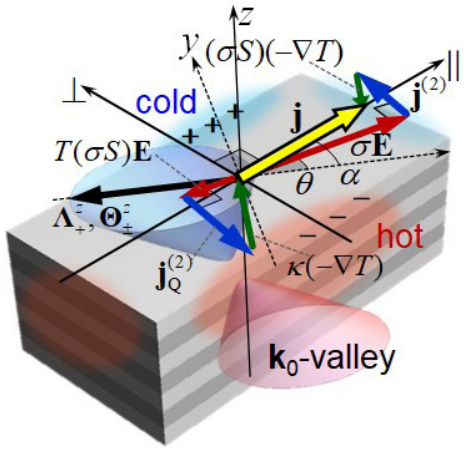

Fig. 1. Schematic of the current-induced topological transport phenomena, nonlinear anomalous Hall and Ettingshausen effects, in the current-carrying state in the thermally isolated 2D massive Dirac fermion system. $\mathbf{\Lambda}$ ($\mathbf{\Theta}$) indicates the (thermoelectric) Berry curvature dipole.

Here, we newly proposed a novel current-induced thermoelectric phenomenon, the nonlinear AEE, which is a thermoelectric analogue of the nonlinear AHE [1]. The thermoelectric Berry curvature dipole was introduced to explain this thermoelectric effect instead of the Berry curvature dipole. The nonlinear AEE is a phenomenon in which a temperature gradient proportional to the square current is induced in the direction perpendicular to the current. It exhibits rectifying characteristics (nonreciprocity). The generated transverse heat current flows unidirectionally even under an AC current. The nonlinear AEE occurs simultaneously with the nonlinear AHE as shown in Fig. 1. We estimated that the nonlinear AEE is sufficiently observable in the current-carrying state in the weak CO state of α-(BEDT-TTF)$_2$I$_3$.

(2) Quantized thermoelectric Hall effect (QTHE)

The high-performance thermoelectricity, that is boundless increase of the Seebeck coefficient S_{xx}, has been theoretically and experimentally investigated in 3D topological semimetals with nodal points (Dirac/Weyl semimetals) at the high-magnetic-field quantum limit. Recently, more advantageous thermoelectric effect called QTHE was proposed in the 2D massless DF system at the clean limit. The thermoelectric conductivity α_{xy} takes a quantized constant value of $(4\log 2)k_B e/h$, which is independent of temperature, magnetic field, and carrier density. It causes the boundless increase of S_{xx} even at low temperatures. α-(BEDT-TTF)$_2$I$_3$ was considered as one of candidate materials.

We investigated the thermoelectricity of the 2D massless DF system in real α-(BEDT-TTF)$_2$I$_3$ under high magnetic fields [2]. Because of its small electron group velocity, the Zeeman splitting becomes relatively important and cannot be ignored in α-(BEDT-TTF)$_2$I$_3$. We showed that the Zeeman splitting of the $n = 0$ Landau level suppresses the QTHE: α_{xy} decreases from the quantized value at low temperatures leaving a shoulder-like structure, and S_{xx} decreases after linear increase at high magnetic fields leaving a hump-

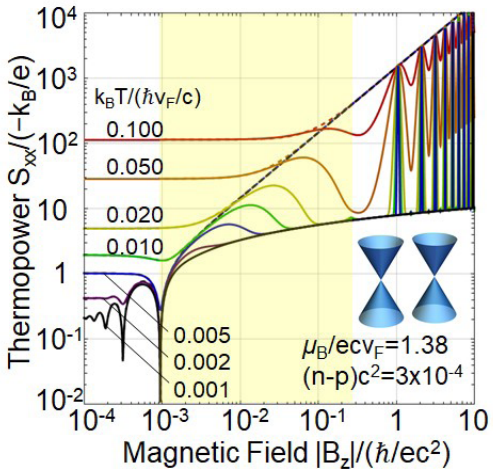

Fig. 2. The magnetic field dependence of the Seebeck coefficient of the 2D massless Dirac fermion system at a fixed carrier density around the charge neutrality point. The solid and dashed curves are for cases with and without the Zeeman effect.

like structure (Fig. 2). These features were observed in our previous experiment. In contrast to 3D nodal-point semimetals with robust gapless features, it is difficult to realize the QTHE in real 2D Dirac fermion systems due to the Zeeman gap in the $n = 0$ Landau level under high magnetic fields.

References
[1] T. Osada and A. Kiswandhi, J. Phys. Soc. Jpn. **90**, 053704 (2021).
[2] T. Osada, J. Phys. Soc. Jpn. **90**, 113703 (2021).

Authors
T. Osada, A. Kiswandhi, M. Sato, K. Uchida, and T. Taen

Discrete Time Crystals in Solids

Tsunetsugu Group

A discrete time crystal (DTC) is an exotic nonequilibrium phase of matter that is realized in periodically driven quantum systems and characterized by the breakdown of the discrete time translation symmetry [1]. The DTC phase has been well studied and experimentally demonstrated

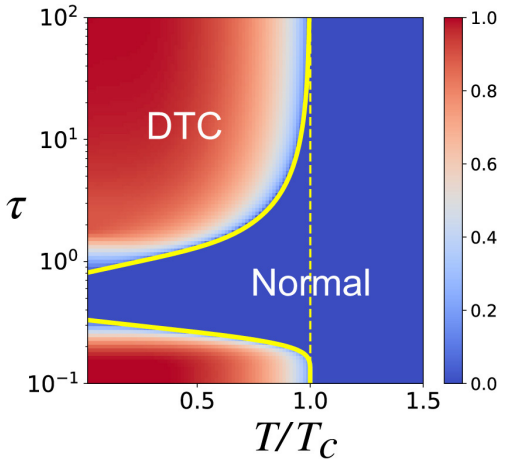

Fig. 1. Phase diagram of the discrete time crystal in solids, and the amplitude of the DTC order parameter is shown by color. The temperature T of the bath is normalized by the equilibrium ferromagnetic transition temperature T_c. τ is the interval between the consecutive pulses in units of $J = \hbar = 1$ (J is the exchange energy).

in artificial quantum systems without dissipation, such as trapped ions, NV centers in diamonds, and digital quantum computers. However, it had not been explored in solid-state materials, in which unavoidable dissipation is hard to control. Therefore, if one realizes the DTC phase in those materials, it could offer a new possibility of controlling their properties and functionalities.

In this study [2], we have studied the DTC phase in solid-state materials and uncovered its mechanism and properties. We have analyzed a ferromagnetic quantum Ising model periodically driven by a train of magnetic field pulses each corresponding to (nearly) π-pulse (period τ). Using the Floquet-Redfield equation, we have incorporated dissipations due to the couplings of the quantum spins to their surrounding phonon bath. This is much harder to solve than the usual Schrödinger equation because it requires treating a $D \times D$ density matrix rather than a D-dimensional wave function (D denotes the Hilbert space dimension, which increases exponentially with the number of spins). To circumvent this problem, we have employed the mean-field theory and numerically obtained the DTC order parameter in a self-consistent manner.

Performing massive numerical calculations on the supercomputer at ISSP, we have determined the DTC phase diagram in solids as shown in Fig. 1. In the normal phase, the system relaxes to a nonequilibrium steady state which oscillates periodically with the same period τ as the drive's. On the other hand, in the DTC phase, the system turns into a time crystal which oscillates with the doubled period 2τ. These results show that DTCs can be realized in real magnetic materials subject to dissipation at low temperatures if the pulse interval is either long or short enough. Interestingly, this phase diagram highlights a reentrant behavior of the DTC phase as the pulse interval is varied.

We have further proposed how to realize and detect the DTC in experiments. We have analyzed the robustness of the DTC against imperfections in pulse shapes unavoidable in experiments such as their height and duration; We have shown that those imperfections do not break the DTC phase. We have also shown that critical phenomena accompany the DTC phase transition. In particular, when temperature is varied to cross the DTC/normal phase boundary, the decay of the DTC order parameter exhibits a power-law in time rather than an exponential. This characteristic behavior can be used as an indicator for the DTC in finite-time experiments. We have finally estimated the parameters for realizing DTC phase and proposed that the electron spin resonance on some magnetic materials may be a promising experimental platform. We believe that these results pave the way for a new research field of time crystals in material science.

References
[1] K. Sacha and J. Zakrzewski, Rep. Prog. Phys. **81**, 016401 (2018).
[2] K. Chinzei and T. N. Ikeda, Phys. Rev. Research **4**, 023025 (2022).

Authors
K. Chinzei and T. N. Ikeda

High-Harmonic Generation in GaAs beyond the Perturbative Regime

Itatani and Kato Groups

Recently, high-harmonic generation (HHG) has been experimentally observed in solids. In contrast to gaseous media, solids have the vastly diverse nature such as in their band structures, energy gaps, crystalline anisotropy, and magnetism. It has thus far been experimentally and theoretically investigated in various solids, but comprehensive understanding of the crossover behavior from the perturbative to the nonperturbative regime has not been gained yet. Such an understanding requires a unified viewpoint connecting the perturbative to nonperturbative regimes.

In the perturbative regime, it is well known that the intensity of the nth-order harmonics obeys an E^{2n} scaling law with respect to the field amplitude E. In the conventional formulation of nonlinear optics using the Bloch basis, this scaling law is successfully explained by the multiphoton interband transition of Bloch electrons. The E^{2n} scaling, however, breaks down at sufficiently high fields (typically at several MV/cm). In recent theoretical studies, this nonperturbative nature of HHG is explained by the alternative formulation, in which intraband electron acceleration motion is taken into account with a new basis called the Houston basis. In spite of these theoretical developments, it has not been clarified yet how the properties of HHG in the nonperturbative regime are seamlessly connected to those in the perturbative regime where the E^{2n} scaling holds. For a clear understanding on this crossover behavior, accurate measurement of the field-intensity dependences of HHG is crucial and indispensable.

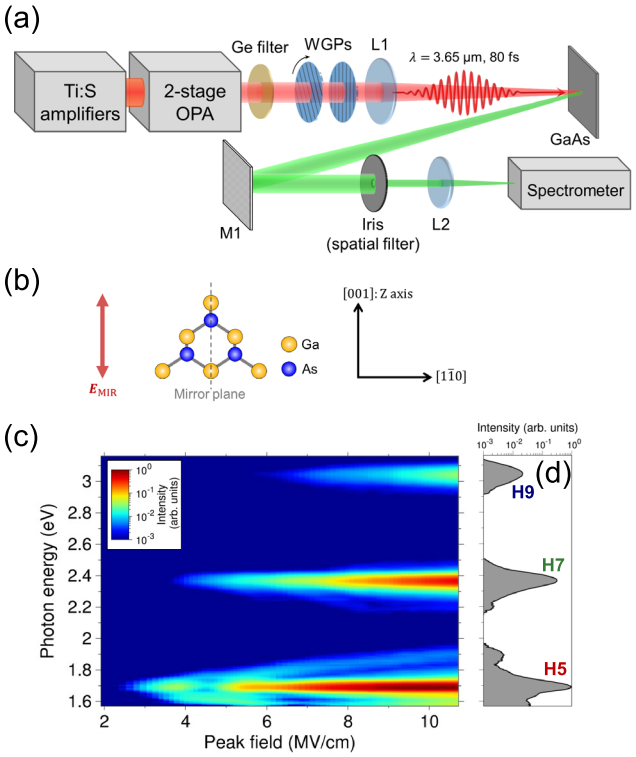

Fig. 1. (a) Experimental setup for HHG in reflection geometry using bulk GaAs and MIR laser source. Ti:Sapphire regenerative and multi-pass amplifiers (450Hz, 5 mJ, 70 fs) were used to pump the optical parametric amplifier (OPA). WGPs, a pair of wire-grid polarizers; L1 (f = 300 mm) and L2 (f = 50 mm), CaF_2 lenses; M1 (R = 100 mm), Al-coated concave mirror. (b) Structure of the (110) surface of GaAs and direction of the laser polarization. (c) Field-intensity dependences of the 5th, 7th, and 9th harmonic spectra. (d) HHG spectrum at the peak field of 10 MV/cm.

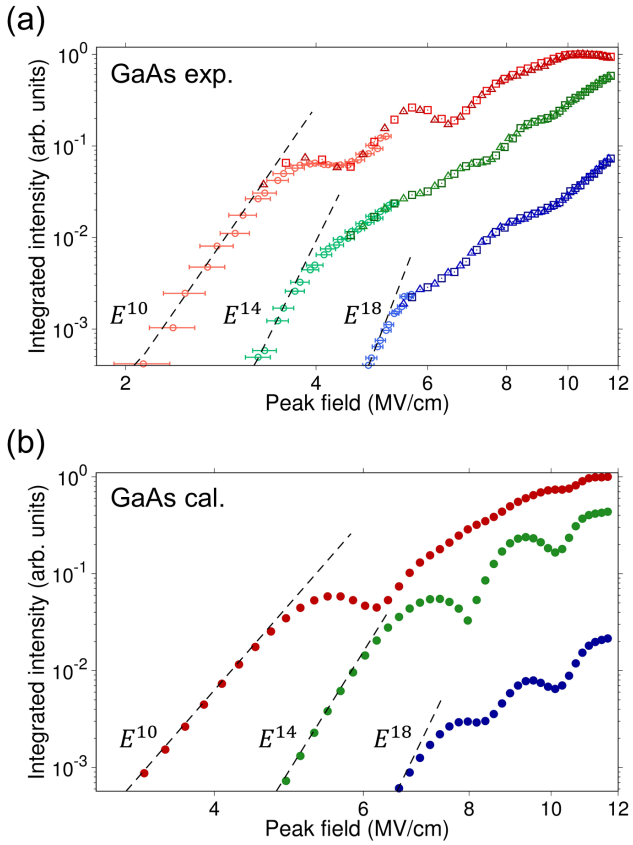

Fig. 2. (a) Field-intensity dependences of the 5th (red), 7th (green), and 9th (blue) HHG intensities. Two datasets (squares and triangles) were measured in a single sweep starting from 2 to 12 MV/cm and then from 12 to 2 MV/cm, respectively. Small HHG signals (circles) were measured with a longer acquisition time. (b) Calculated results of the Luttinger-Kohn model. In the weak-field regime, the harmonic intensities almost obey an E^{2n} perturbative scaling law for both the measured and calculated results (dashed black lines).

Based on this motivation, we experimentally and theoretically investigated the field-intensity dependence of HHG in GaAs [1]. The experiments were carried out by using an intense mid-infrared laser irradiating a GaAs sample, as shown in Fig. 1(a) , in the reflection geometry to minimize nonlinear propagation effects and phase mismatch [2]. We set the pulse duration and the wavelength of the incident light to be 80 fs and 3.65 μm. The peak field was estimated to be up to 12 MV/cm inside the sample. We measured the HHG intensities as a function of the peak field of the incident pulses from 2 to 12 MV/cm. We show in Figs. 1(c) and 1(d) the obtained HHG spectra which indicate only odd-order harmonics due to the inversion symmetry of GaAs (Fig. 1(b)). Fig. 2(a) shows the intensities of the 5th, 7th, and 9th harmonics as a function of laser intensity. This figure indicates that harmonic intensities did not saturate monotonically with increasing laser intensity, but rather exhibited oscillations. As the field intensity was increased, the oscillatory behaviors appeared above 4, 5, and 6 MV/cm for the 5th, 7th, and 9th harmonics, respectively, where they started to deviate from the perturbative scaling law. An explanation of these experimental results will require clarification of the crossover of HHG from the perturbative to the nonperturbative regime as well as the physical origin of the oscillatory behavior.

To analyze these experimental results, we employed an eight-band Luttinger-Kohn model, which includes conduction, heavy-hole, light-hole, and split-off bands for both spin-up and spin-down components. We introduce our

theoretical framework by applying our previous works [3,4] to the Luttinger-Kohn model and calculate the intensities of the 5th, 7th, and 9th harmonics originating from GaAs. Consequently, we succeed in reproducing E^{2n} scaling laws in the perturbative regime as well as the oscillatory behaviors in the non-perturbative regime (Fig.2(b)). By performing further analyzation, we concluded that the diagonal elements of the Hamiltonian representing field-induced dynamic band modification is crucial in the nonperturbative regime. Since this field-induced dynamic band modification can naturally be ignored in the perturbative regime, we can easily obtain the HHG intensities showing the crossover behavior from the perturbative to the nonperturbative regime. The findings of our work give important foundation for understanding a variation of nonlinear optics from the perturbative to nonperturbative regime and open up the possibility of novel optical technologies, such as strong-field coherent control of solid HHG and Floquet engineering of dressed states in solids.

References

[1] T. Tamaya, P. Xia, C. Kim, F. Lu, T. Kanai, N. Ishii, J. Itatani, H. Akiyama, and T. Kato, Phys. Rev. B **104**, L121202 (2021).
[2] P. Xia, C. Kim, F. Lu, T. Kanai, H. Akiyama, J. Itatani, and N. Ishii, Opt. Express **26**, 29393 (2018).
[3] T. Tamaya, A. Ishikawa, T. Ogawa, and K. Tanaka, Phys. Rev. Lett. **116**, 016601 (2016).
[4] T. Tamaya and T. Kato, Phys. Rev. B **100**, 081203(R) (2019).

Authors

T. Tamaya*, P. Xia*, C. Kim, F. Lu, T. Kanai, N.Ishii, J. Itatani, H. Akiyama, and T. Kato

*T. T. and P. X contributed equally to this work

Einstein-de Haas Nanorotor

Kato Group

The angular-momentum conversion phenomena between spin and mechanical rotation are recognized as the gyromagnetic effects discovered in the early 20th century by S. J. Barnett, A. Einstein, and W. J. de Haas. They observed magnetization induced by mechanical rotation [1] and mechanical rotation induced by magnetization [2] known as the Einstein-de Haas (EdH) effect, revealing the origin of magnetism is the angular momentum. The gyromagnetic effects are universal phenomena that appeared even in nonmagnetic materials ranging from macroscopic to microscopic scales in various branches of physics, including ultracold atoms, spintronics, nuclear spin physics, and quark-hadron physics.

In our study [3], we developed a quantum theory to describe the microscopic mechanism of a nanorotor driven by electron spin injection via the EdH effect. As a feasible setup, we considered the double-wall carbon nanotube rotor as shown in Fig. 1 (a). For the double-walled carbon nanotube, mechanical rotational motion of the inner carbon nanotube was already studied both experimentally [4] and theoretically [5]. However, efficient driving forces for the rotational motion are still lacking.

In this system, the rotor (the inner carbon nanotube) is driven by four transitions as shown in Fig. 1 (b). By applying a bias voltage between two half-metallic ferromagnetic electrodes, an electron with a spin $s_z = \hbar/2$ tunnels from the left electrode into the nanorotor (from (b-1) to (b-2)). This electron cannot tunnel to the drain electrode as long as its spin state remains $s_z = \hbar/2$ because there is no electronic

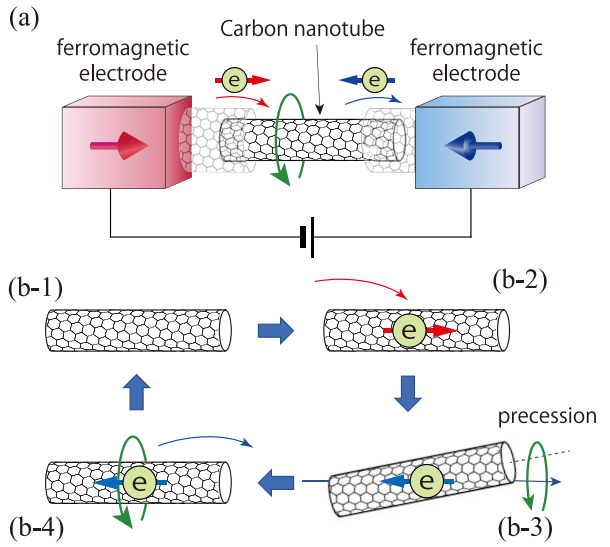

Fig. 1 Schematic diagram of the nanorotor rotationally driven by spin injection. (a) The system consisting of a double-wall carbon nanotube and two ferromagnetic electrodes. (b) The four processes for driving of rotational motion of the nanoroter.

state for the spin $s_z = \hbar/2$ in the half-metallic ferromagnetic drain. Electron accumulation by additional electron tunneling is also forbidden because of the Coulomb blockade in the nanorotor that acts like a quantum dot. Therefore, only spin flipping of the injected electron enables continuous current flow through the rotor (from (b-2) to (b-3)). Simultaneously with this spin flipping, angular momentum $\hbar$ is eventually transferred from the injected electron to the mechanical rotational motion. After this angular momentum transfer, the electron with the spin $s_z = -\hbar/2$ can leave the nanotube into the right electrode. Therefore, the current through the nanorotor is expected to be a driving force of the rotational motion of the nanorotor in this system. In our study, we clarified that the precession of the nanorotor as shown in Fig. 1 (b-3) always occurs in the angular momentum transfer from the electron spin to the nanorotor. Therefore, in order to drive the nanorotor efficiently, the state of the nanoroter is needed to be relaxed from a precession state into a sleeping top state (from (b-3) to (b-4)).

The transition into the precession state is explained as follows. When the nanoroter is assumed to be a rigid body, its quantum states are specified by three quantum numbers, L, M, and k, where L is the quantum number corresponding

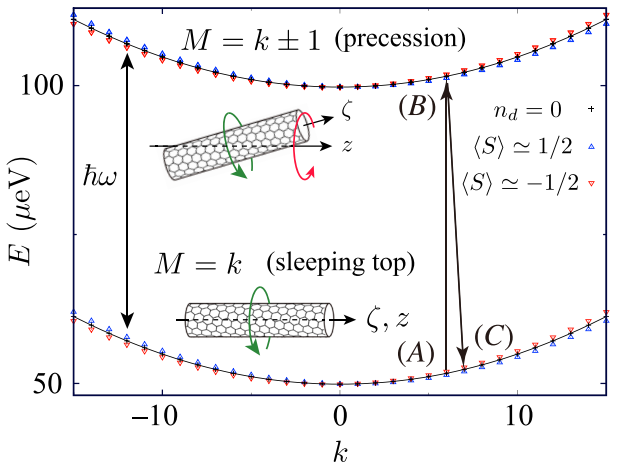

Fig. 2. Eigenenergies of rotational motion as a function of k. The upper and lower branches correspond to the precession state ($M = k \pm 1$) and the sleeping top state ($M = k$), respectively.

to the magnitude of the angular momentum, M is the z component of the angular momentum, and k is the angular momentum around the axis of the rotor. In Fig. 2, we show the eigenenergies of the roter for the sleeping top state ($M = k$, the lower inset of Fig. 2) and the precession state ($M = k \pm 1$, the upper inset of Fig. 2). We showed that the spin-rotation coupling between electron spins and the nanoroter induces only the transition from (A) to (B) in Fig. 2 because the spin-rotation coupling only changes M without changing k. Therefore, we need to introduce a phonon heat bath which causes relaxation from the precession state (B) to the sleeping top state (C). In our work [3], we discussed a detailed condition for efficient and stable driving of the rotational motion of the nanoroter.

The present driving mechanism is not restricted to carbon nanotubes; it applies to other materials as well. The process discussed here would be a minimal model for the momentum transfer from an electron to rotor that effectively includes the other possible processes.

This study has been performed as a joint study with Mamoru Matsuo, who was a visiting professor of ISSP in the academic year 2016.

References

[1] S. J. Barnett, Phys. Rev. **56**, 239 (1915).
[2] A. Einstein and W. J. de Haas, KNAW proc. **18 I**, 696 (1915).
[3] W. Izumida, R. Okuyama, K. Sato, T. Kato, and M. Matsuo, Phys. Rev. Lett. **128**, 017701 (2022).
[4] A. M. Fennimore, T. D. Yuzvinsky, W.-Q. Han, M. S. Fuhrer, J. Cumings, and A. Zettl, Nature **424**, 408 (2003).
[5] S. W. D. Bailey, I. Amanatidis, and C. J. Lambert, Phys. Rev. Lett. **100**, 256802 (2008).

Authors

W. Izumida[a], R. Okuyama[b], K. Sato[c], T. Kato, and M. Matsuo[d]
[a]Tohoku University
[b]Meiji University
[c]National Institute of Technology, Sendai College
[d]Kavli Institute for Theoretical Sciences, University of Chinese Academy of Sciences

Orbital Torque in Ferromagnetic-Metal/ Ru/Al_2O_3 Trilayers

Otani Group

For the development of spintronic memory and logic devices, the efficient current-induced spin-torque effect is critical. Spin-orbit torque, which uses spin-orbit coupling (SOC) in heavy metals (and/or Rashba interfaces) to create spin current and resulting torque to switch the magnetization of a neighboring ferromagnetic layer, has received a lot of attention in the last decade. The torque effect based on orbital angular momentum injection and SOC in the ferromagnet, known as orbital torque (OT), has recently attracted much attention. While each electronic state in a spin current may only carry $\hbar/2$ angular momentum, the angular momentum carried by a state in an orbital current has no limit, implying that OT has higher efficiency. Indeed, in most metal elements, orbital-current production efficiency is substantially higher than its spin equivalent. Furthermore, because SOC is not required, the materials choices for the orbital source are pretty broad, rather than being confined to a few types of heavy metals like spin-current generation. As a result, OT is a strong contender for the operating principle of practical spintronic devices.

The development of OT devices based on polycrystalline stacks is beneficial for industrial on-silicon manufacture. OT was previously discovered primarily due to the interfacial orbital Rashba effect (ORE) in polycrystalline layered structures grown by room-temperature evaporation or sputtering, which can modulate OT through layer design. These studies use an interface or a bulk containing Cu or Pt as a source of orbital angular momentum. The full d-shell of Cu and the high SOC of Pt obstruct orbital transport and make OT analysis in polycrystalline stacks more difficult. Oxidation helps orbital transport in Cu, adding complexity to the structure. Meanwhile, theoretical works have focused on the orbital generation and transport in single-crystalline systems because of the complexity of orbital transport in polycrystalline heterostructures. It is highly warranted to bridge the gap between experiment and theory by obtaining efficient, long-range orbital transport in a uniform polycrystalline layer and developing a corresponding theoretical approach to orbital transport that remains elusive.

We experimentally study the current induced torque effect in polycrystalline ferromagnetic metal (FM)/Ru/Al_2O_3 stacks shown in Fig. 1(a). FM is either $Co_{40}Fe_{40}B_{20}$ or $Ni_{80}Fe_{20}$. Using a device structure, we demonstrate a high torque efficiency due to the ORE at the Ru/Al_2O_3 interface (Fig. 1(b)). Ru is chosen because of its electronic configuration of $4d^75s^1$ and a small bulk-originating spin-orbit torque so that orbital-current generation is allowed by orbital hybridization; the absence of d-electrons does not limit orbital-current propagation at the Fermi level or SOC-related relaxation, and OT is not disturbed by the conventional spin Hall torque. We performed spin-torque ferromagnetic resonance (ST-FMR) measurements

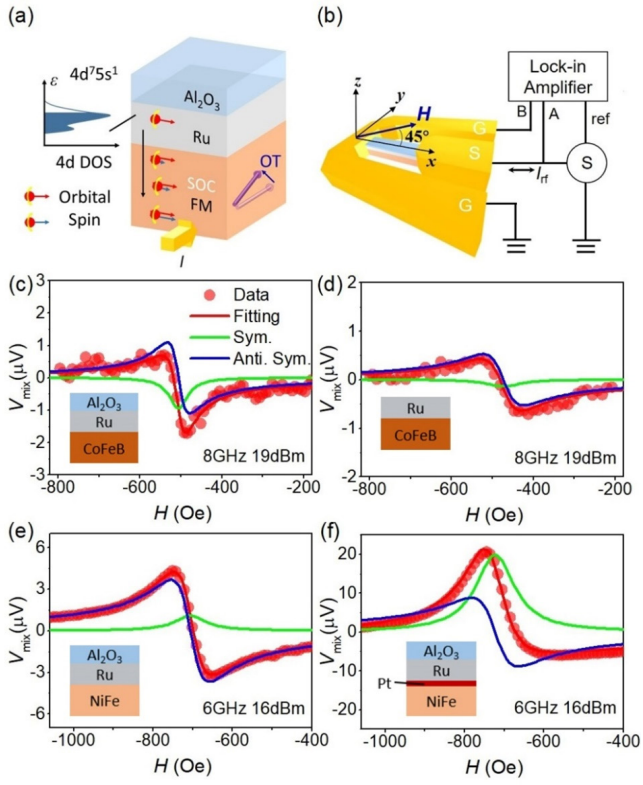

Fig. 1. (a) Schematic of the orbital torque in FM/Ru/Al_2O_3. (b) Experimental setup of the ST-FMR measurement. (c)–(f) ST-FMR spectra and fitting for the CoFeB(7)/Ru(6)/Al_2O_3(2) (c) and CoFeB(7)/Ru(6) (d) devices at 8 GHz, and NiFe(7)/Ru(6)/Al_2O_3(2) (e) and NiFe(7)/Pt(1)/Ru(6)/Al_2O_3(2) (f) devices at 6 GHz. The red circles are experimental data; the red lines are fitting curves. The symmetric and antisymmetric components plots are in the right panel with green and blue lines. Schematics of the sample layout are shown in the inset.

(Fig. 1(b)) on the polycrystalline FM/Ru/Al_2O_3 stacks. Figure 1(c) shows the V_{mix} signal obtained from the ST-FMR measurement of a $Co_{40}Fe_{40}B_{20}$(7)/Ru(6)/Al_2O_3(2) (units in nanometers) trilayer. The signal V_{mix} is decomposed into symmetric (S) and asymmetric (A) Lorentzian components, revealing sizable negative S components that indicates the current-induced damping-like torque. From systematic studies in this work, we find characteristic behaviors of OT: (i) the sign and magnitude of the torque efficiency are strongly dependent on the FM materials and insertion layers according to the sign and magnitude of their SOC (Fig. 1(c) and (e)); and (ii) torque efficiency is enhanced with increasing CoFeB layer thickness t_F, with a large saturation torque efficiency of 0.3 for t_F = 12 nm, consistent with the long propagation length of the orbital current in the ferromagnet. Our quantum evolution simulation shows the unique random processing feature of orbital transport in polycrystalline materials, enabling long-range orbital transport in polycrystalline samples, even in a crystal field.

This study concludes that transition metal-based materials with a small SOC, simple structure, and itinerant d-electrons can provide a suitable platform for studying orbital transport in polycrystalline structures and developing torque devices.

Reference
[1] L. Liao, F. Xue, L. Han, J. Kim, R. Zhang, L. Li, J. Liu, X. Kou, C. Song, F. Pan, and Y. Otani, Phs. Rev. B **105**, 104434 (2022).

Authors
L. Liao, F. Xue[a], L. Han[b], J. Kim[c], R. Zhang[b], L. Li[a], J. Liu[a], X. Kou[a], C. Song[b], F. Pan[b], and Y. Otani
[a]ShanghaiTech University
[b]Tsinghua University

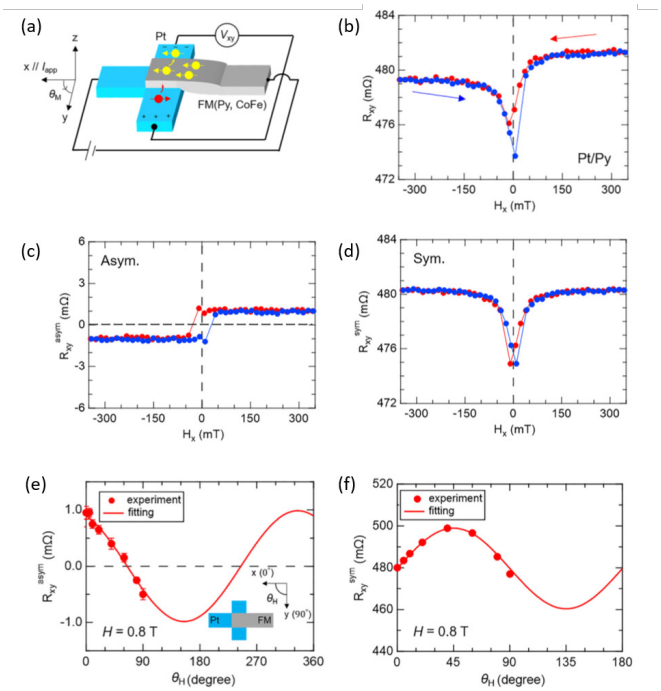

Fig. 1. (a) Schematic of ISHE measurement in the T-shaped spin conversion device. (b) Magnetic field dependence of the transverse resistance *Rxy* in the Pt/FeNi device with $\theta = 0°$. Red and blue arrows show the magnetic field sweeping direction. (c), (d) asymmetric and symmetric components of *Rxy*. (e), (f) Magnetic field angle dependences of the asymmetrical and symmetrical components $H = 0.8$ T.

Planar Hall Effect on the Output Signal in T-Shaped Spin Conversion Device

Otani Group

The T-shaped spin conversion device consisting of ferromagnetic and spin Hall (or spin conversion) materials is an indispensable component in a new type of logic circuit: magnetoelectric spin-orbit logic circuit. In this device, a spin polarized current is directly injected into the spin Hall material from the ferromagnet, and the inverse spin Hall effect (ISHE) is detected as the transverse voltage as shown in Fig. 1 (a). The output signal can be an order of magnitude greater than that of the nonlocal methods. Pham et al. have demonstrated an increase in the ISHE signal by scaling down the T-shaped device structure, that is favorable for the high-density device [1]. They also discussed the adverse effects of the adjacent ferromagnet on the total signal via a transverse anisotropic magnetoresistance, the planar Hall effect (PHE), concluding that it only causes the offset of the output signal. However, our recent experiments showed the superposition of the signal induced by PHE which change its sign upon magnetization reversal.

In this work, we investigated the influence of PHE on the ISHE induced voltage on the T-shaped device. The T-shaped Pt wires were first formed on the Si/SiO_2 substrate using e-beam lithography, e-beam deposition, and liftoff. The thickness of Pt is 20 nm. We then deposited a ferromagnetic wire on the Pt. Figure 2(b) shows the magnetic field dependence of R_{xy} in the Pt/FeNi device. One can extract the asymmetric contribution in R_{xy} by calculating the difference between the signals measured at trace and retrace scan. Figures 1(c) and (d) show asymmetric and symmetric components as a function of the applied field, respectively. Figure 1 (e) and (f) show the magnetic field angle dependences of the symmetric and symmetric components, respectively. The ISHE causes an asymmetric component of the transverse resistance in the T-shaped device structure. On the other hand, we found that the PHE contributes to the transverse voltage as a symmetric component because the magnetic moment continuously rotates clockwise (or counterclockwise). From the experimental results, the spin Hall angle of Pt and the anisotropic magnetoresistance ratio of FeNi were estimated to be ~ 3.0% and ~ 1.0%, respectively, that are in the same order as the reported value. We did same measurement on a Pt/CoFe device. The overall change in the asymmetric component is almost the same as that in the Pt/FeNi, while the change in the symmetric component is about half of that in the Pt/FeNi device. This reduction of the symmetric signal is attributed to the lower anisotropic magnetoresistance ratio of CoFe than that of FeNi. Therefore, it is essential to use the ferromagnet that has small anisotropic magnetoresistance ratio to reduce the adverse effect in the T-shaped device.

In conclusion, our systematic studies reveal that the PHE causes a symmetric component in the output signal because of the continuous clockwise (or counterclockwise) magnetic rotation. We find that we can suppress the undesired signal by choosing a low AMR ferromagnet such as the CoFe alloy. These results help us to design the T-shaped device structure for studying spin conversion in spin Hall materials, topological insulators, and Rashba interface for developing the spintronic logic devices.

References
[1] V. T. Pham, I. Groen, S. Manipatruni, W. Y. Choi, D. E. Nikonov, E. Sagasta, C.-C. Lin, T. A. Gosavi, A. Marty, L. E. Hueso, I. A. Young, and F. Casanova, Nat. Electron. **3**, 309 (2020)
[2] H. Mizuno, H. Isshiki, K. Kondou, Y. Zhu, and Y. Otani, Appl. Phys. Lett. **119**, 092401 (2021)

Authors
Y. Otani and H. Isshiki

Squeezed Abrikosov-Josephson Vortex

Hasegawa Group

Two-dimensional (2D) superconductors are sensitive to the presence of disorder, which induces electron localization, phase fluctuation, and eventually the superconducting-insulator transition at zero temperature. Here we present a new way of introducing disorder into high-quality monolayer superconductors by forming them on vicinal substrates. We fabricated the striped incommensurate (SIC) structure, one of the Pb monolayer superconducting phases, on vicinal Si(111) substrates tilted by 1.1° or 0.5°. Since each step works as a disorder and behaves like a Josephson junction, by just adjusting the miscut angle, the step separation, or disorder density, can be controlled precisely.

The role of a single step on atomic-layer superconductors has been investigated by scanning tunneling microscopy (STM) [1]. The shape of vortex cores trapped at steps depends on how the step decouples the superconducting terraces. When the decoupling is weak, round Abrikosov vortex is pinned at the step. With the intermediate decoupling, trapped vortices are elongated along the step, which is called a Abrikosov-Josephson vortex (AJV) and their local density of states (DOS) within the gap is not fully recovered at the core. In the case of the strongly decoupling step, a further elongated vortex with local DOS almost same as that of superconducting states, that is, Josephson vortex, is formed along the step.

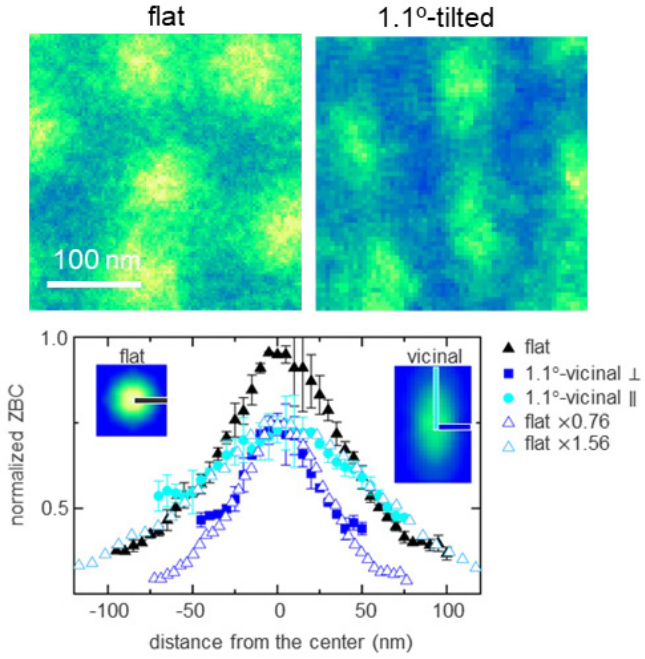

Fig. 1. (upper panels) ZBC maps taken on flat and 1.1°-tilted vicinal SIC samples showing vortices under out-of-plane magnetic field of 120 mT. (lower panel) ZBC profiles across the vortex center taken on the flat (black triangles) and the vicinal (blue squares and light blue circles) samples, respectively. Blue squares (light blue circles) indicate the profiles taken in the direction perpendicular (parallel) to the steps. Empty blue (light blue) triangles are the profile taken on the vortices of the flat sample multiplied by 0.78 in height and by 1.56 (0.76) along the horizontal axis, demonstrating similarity in the three profiles. Insets show the averaged vortices taken on the flat and vicinal samples.

Through the electron transport measurement under out-of-plane magnetic fields B, we found that the critical magnetic field (B_{c2}) of the superconducting phase formed on vicinal substrates is higher than that formed on the flat substrate. Using STM at 0.36 K, we estimated B_{c2} from the magnetic field that saturates the conductance at the bottom of the superconducting gap, that is, zero bias conductance (ZBC), and found consistent with those of the transport measurements.

In order to understand the enhanced B_{c2} microscopically, we investigated vortices by STM. The upper panels of Fig. 1 are ZBC maps showing the vortices taken on the flat and 1.1°-tilted SIC sample under B = 120 mT. Compared with the round vortices observed on the flat sample, the vortices on the tilted sample are elongated along the step direction. In addition, ZBC at the center is suppressed. Since both are characteristic features of AJV we attribute them to an AJV.

According to the Ginzburg-Landau (GL) equation, the critical field is inversely proportional to ξ^2. Since the size of vortex is closely related to ξ, we investigated the size and shape of the vortices. The lower panel of Figure 1 shows the ZBC cross-sectional profiles taken on vortices on the flat sample (black triangles), on the vicinal sample in the directions parallel (//, light blue circles) and perpendicular ($\perp$, blue squares) to the steps. From the plot we found that these three profiles have a similar shape. First, on the vortices of the vicinal sample, ZBC at the center is suppressed by a factor of 0.78. Then, the suppressed profile was laterally expanded by a factor of 1.56 (shrunk by 0.76) to find good agreements with the parallel (perpendicular) profiles of the vicinal sample's vortices.

Curiously, the squeezing ratio in the perpendicular direction, 0.76, corresponds well to the inverse of the B_{c2} enhancement ratio ($B_{c2,flat}/B_{c2,vicinal}$). According to the anisotropic 2D GL model, $B_{c2,vicinal}$ is given by $\Phi_0/2\pi\xi_\perp\xi_{//}$, where $\xi_\perp$ and $\xi_{//}$ are the coherence length in the directions perpendicular and parallel to the steps. Thereby the correspondence suggests us that the B_{c2} enhancement is due to the reduced coherence length $\xi_\perp$ by the presence of the steps.

The reduction in ξ by the high-density steps is explained by the suppression of mean free path l by disorder according to the equation $\xi = \sqrt{\xi_0 l}$, where ξ_0 is the coherence length without disorder. Since l is written as $h/e^2k_F\rho$ for a 2D system, where ρ is the resistivity, in a 2D metallic layer with an array of linear resistors at equal interval w as shown in the inset of Fig. 2(a), we found $B_{c2.vicinal}/B_{c2.flat}$ is written as $(1 + \alpha/w)^{-1/2}$, where $\alpha \equiv \rho_{step}/\rho_{terrace}$ is a ratio of step and terrace resistivity. Figure 2(a) shows B_{c2} dependence on the terrace width w obtained from our experimental results including those of 0.5°-tilted vicinal sample. A solid curve is a fitted one with α = 15.4 nm, showing good agreement. Since $l_{flat} \sim 3.3$ nm we estimates $l_\perp$ for 1.1° (0.5°) -tilted vicinal SIC phases is 1.6 (2.3) nm, respectively.

One of the characteristic features of AJV is the suppression of DOS within the gap at the vortex core. According to the calculations of AJV [1], the DOS suppression is described as t^2, where t is the ratio of hopping strength across the step to that within the terrace. Since the width of the elongated vortex core is given by $2\xi_\perp$, vortices on the

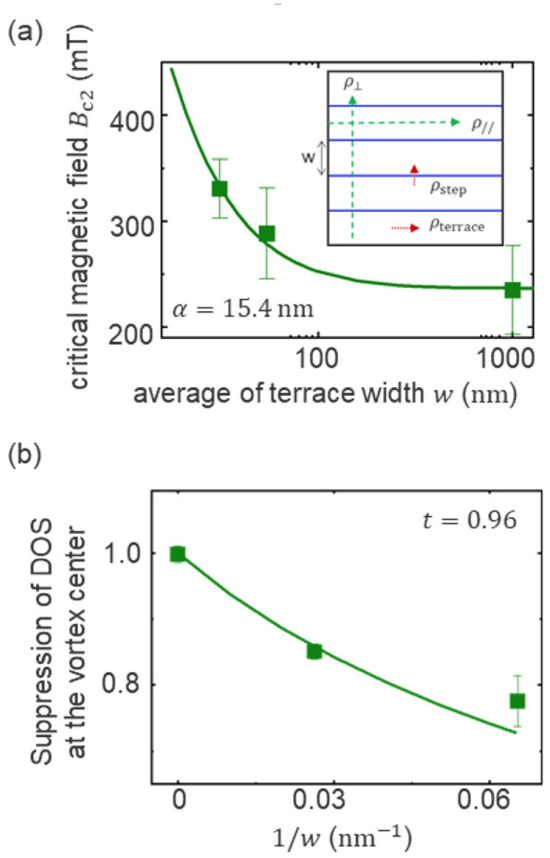

Fig. 2. (a) Terrace width dependence of the critical magnetic field. The solid curve is a fitting described in the text. The inset shows a schematic of the arrayed resistors to model the vicinal SIC phases. (b) terrace width dependence of the suppressed DOS at the vortex center. The solid curve is a fitting written in the text.

vicinal substrates cross the steps $2\xi_\perp/w$ times. The effective hopping strength ratio across the steps is thus given as $t^{2\xi_\perp/w}$. Figure 2(b) shows the terrace width dependence of the suppression factor $t^{4\xi_\perp/w}$. A solid green curve is a fitting one with $\xi_\perp = \xi_{flat}\,(1 + \alpha/w)^{-1/2}$, showing a good agreement when $t = 0.96$. Considering an almost round shape of vortices trapped at a single step of the same SIC phase [1], the estimated value close to 1 is reasonable. We thus conclude that the elongated vortices observed on the vicinal samples are due to the formation of AJV. They are, however, different from ones formed on a single step that have the width of the coherence length. In the vicinal SIC phases, AJV are squeezed in the direction perpendicular to the steps because of the limited mean free path in the direction.

Reference
[1] S. Yoshizawa *et al.*, Phys. Rev. Lett. **113**, 247004 (2014).

Authors
Y. Sato, M. Haze, S. Yoshizawa[a], T. Uchihashi[a], and Y. Hasegawa
[a]National Institute for Materials Science

Thin Film Growth by Energy-Moderated Laser Ablation

Lippmaa Group

Pulsed laser deposition (PLD) is one the most successful thin film growth methods for oxides and other materials with very high melting points. The main merit of PLD is the ability to grow thin films of almost any material for which stoichiometric bulk evaporation sources are available. This universal nature of PLD stems from the near-stoichiometric transfer of material from the source to the film in the laser ablation process. However, despite this universal nature of PLD, it is also generally understood that the highest crystalline quality in thin films can be achieved by molecular beam epitaxy (MBE), rather than PLD. The inferior quality of PLD-grown films often manifests itself in the form of higher defect density, lower carrier mobility in semiconductors, inferior dielectric permittivity compared to bulk crystals, and in systematic shifts of film lattice parameters compared to known bulk reference values. These functional property differences in PLD films can be traced back to stoichiometry shifts in the deposition process and mechanical damage to the film due to the high-energy plasma in the laser ablation plume.

The stoichiometry shift may be related to nonstoichiometric evaporation of different elements from an ablation target, to a difference in the scattering spread of atoms with different weight in the gas phase as the ablation plume expands and interacts with the ambient background gas, or to selective re-evaporation of some atomic species from a film surface at the growth temperature. Depending on which mechanism is responsible, the target composition, ablation laser pulse power density, or the growth temperature and growth rate can be adjusted to correct for the stoichiometry errors.

A more difficult question is how to handle the formation of point defects in the film due to the high kinetic energy of atoms that impinge on the film surface. Time-of-flight measurements have shown that the kinetic energy of atomic species in a laser ablation plume can reach 100 eV, depending on the energy transfer from laser light to the expanding plasma. This energy is sufficient to cause sputtering damage on the film surface and thus leads to the formation of point defects that are not related to any stoichiometry errors. For oxide thin films, such point defect damage can be detected as an expansion of the film lattice compared to known bulk reference value. An effective way to reduce such sputter damage is to reduce the kinetic energy of the plume by introducing a dense background gas. As illustrated in Fig. 1, the position of a $SrTiO_3$ film x-ray diffraction (XRD) peak changes as a function of the ambient oxygen pressure. An overlap of the homoepitaxial film peak with the

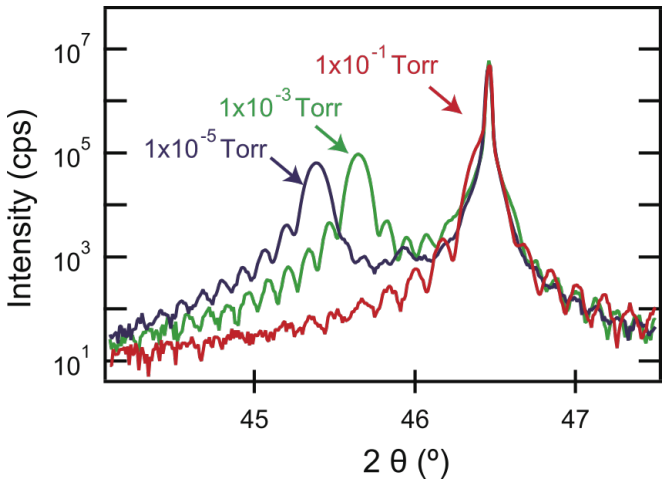

Fig. 1. X-ray diffraction patterns of homoepitaxial $SrTiO_3$ films grown by PLD at several oxygen pressures. The film peaks separate from the substrate position 46.4° due to lattice expansion caused by point defects. An overlap with the substrate is achieved only at very high oxygen pressure (100 mTorr).

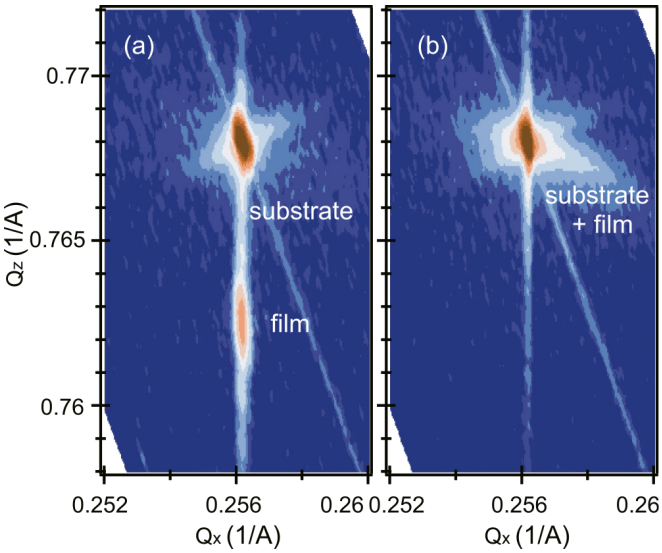

Fig. 2. Reciprocal space maps of homoepitaxial $SrTiO_3$ films grown in (a) 10^{-5} Torr of O_2 and (b) mixture of 10^{-5} Torr O_2 / 600 mTorr He. The film peak exactly overlaps with the substrate peak when the kinetic energy of the plasma plume is moderated by the presence of He in the film growth chamber.

$SrTiO_3$ substrate peak was obtained at 100 mTorr oxygen pressure. Using very high oxygen pressure during film growth is not a good solution because it reduces the deposition rate, may cause gas-phase stoichiometry errors, and degrades the surface flatness of oxide films.

In this work, plasma kinetic energy moderation was therefore done by introducing He gas into the process chamber to a pressure of 600 mTorr [1]. Despite the high pressure, the presence of He does not reduce the deposition rate significantly and allows for independent adjustment of the reactive oxygen pressure while the kinetic energy of the plume can be reduced by an order of magnitude. As the maximum energy of plasma species drops below about 20 eV, sputter damage of the thin film is nearly eliminated. A dramatic change in the film structure can be seen in the reciprocal space maps in Fig. 2. The map shown in panel (a) is for a homoepitaxial $SrTiO_3$ film grown at an oxygen pressure of 10^{-5} Torr. The film diffraction peak is clearly shifted away from the substrate, indicating that the film lattice is strongly expanded. Separate composition analysis showed that the film was very close to stoichiometric and a Sr/Ti ratio error cannot be the cause of the lattice expansion. In contrast, panel (b) shows a map for a film grown in a mixture of 10^{-5} Torr of oxygen and 600 mTorr of He. No separate film peak is visible in this case since the homoepitaxial film peak overlaps exactly with the substrate peak.

High-pressure He in the PLD chamber thus effectively moderates the kinetic energy of the ablation plume and eliminates the sputtering damage of the oxide film. The kinetic energy is a function of the laser peak power and thus depends not only on the pulse energy but also on the pulse length. The kinetic energy moderation is thus an especially important technique for improving thin film quality when a Nd:YAG lasers with a pulse length of close to 4 ns are used for PLD growth of thin films.

Reference

[1] R. Takahashi, T. Yamamoto, and M. Lippmaa, Cryst. Growth. Des. **21**, 5017 (2021).

Authors
R. Takahashi[a], T. Yamamoto[b], and M. Lippmaa
[a]Nihon University
[b]Nagoya University

Functionalization of the MoS_2 Basal Plane for Activation of Molecular Hydrogen by Pd Deposition Studied by Ambient-Pressure X-ray Photoelectron Spectroscopy

Yoshinobu and I. Matsuda Groups

Molybdenum disulfide (MoS_2) is one of the transition-metal dichalcogenides (TMDs) and has a layered structure. The monolayer or multilayer MoS_2 is expected to have various applications such as field-effect transistors, optoelectronic devices, and gas sensors due to the unique optical properties, sufficiently high carrier mobility, and excellent chemical and thermal stability. In addition, MoS_2 has been used as industrial catalysts for many years. For example, the Co-MoS_2/Al_2O_3 catalyst has been industrially used as a hydrodesulfurization catalyst that hydrogenates sulfur contained in crude oil to improve the purity. Thus, the MoS_2 surface is a reaction field for various catalytic reactions involving hydrogen atoms. The dissociative adsorption of hydrogen molecules on MoS_2 surfaces is considered to be a thermally activated process. At room temperature, the basal plane of MoS_2 is inert for the dissociation of molecular hydrogen. Therefore, creating active sites for the hydrogen dissociation on the MoS_2 basal surface is expected to lead to higher efficiency of hydrogenation reactions and hydrogen gas sensors using the MoS_2 crystal.

We investigated the effects of gaseous hydrogen exposure on the bare MoS_2 and Pd-deposited MoS_2 basal surfaces using ambient-pressure X-ray photoelectron spectroscopy [1]. In the Mo 3d core-level, S 2p core-level, and valence-band photoelectron spectra of a bare MoS_2 surface, little change was observed in the energy shift before and after exposure to hydrogen gas. Upon hydrogen gas exposure on the Pd-deposited MoS_2 surface, the Pd 3d XPS spectra changed (Figs. 1(a) and (b)), which can be interpreted as the adsorption of dissociated hydrogen atoms on the Pd sites; each peak in the photoelectron spectra (Mo 3d, S 2p, and valence-band) shifted to a lower binding energy with

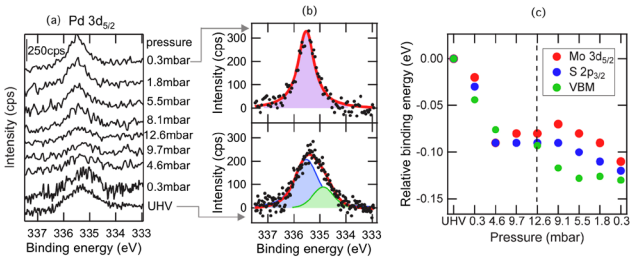

Fig. 1. (a) Pd $3d_{5/2}$ spectra of the Pd/MoS_2 as a function of H_2 gas pressure at 300 K. The amount of deposited Pd was estimated to be 2.0 % for the amount of Mo atoms on the outermost MoS_2 layer. (b) The upper and lower figure are the fitting results for the Pd $3d_{5/2}$ AP-XPS spectra before and after the hydrogen exposure, respectively. The green component and blue component in the lower figure are assigned to be surface and bulk components of the Pd islands, while the pink component would consist of both the bulk component and hydrogen atoms-adsorbed surface component. (c) The relative binding energies for the Mo $3d_{5/2}$ core-level, S $2p_{3/2}$ core-level, and valence band maximum (VBM) as a function of H_2 gas pressure.

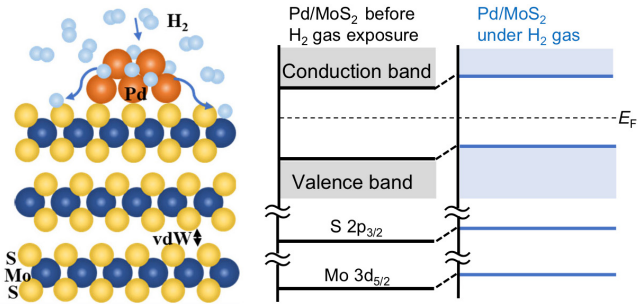

Fig. 2. (Left) The schematic of the dissociation of molecular hydrogen, the adsorption of atomic hydrogen on the Pd-deposited sites on the MoS_2 surface and the spillover of hydrogen atoms onto the MoS_2 surface. (Right) The energy diagram of the Pd-deposited MoS_2 surface before and after hydrogen exposure.

0.1 eV (Fig. 1(c)). When hydrogen gas was evacuated, the peak energy remained lower compared with that before hydrogen gas exposure (Fig. 1(a)). These results indicate that the dissociation of molecular hydrogen and the adsorption of atomic hydrogen occur on the Pd-deposited sites on the MoS_2 surface, and thereafter hydrogen atoms spillover onto the MoS_2 surface. This study shows that the active site for the dissociation of molecular hydrogen is created on an inert MoS_2 basal surface by Pd deposition. In addition, the electronic states of the MoS_2 substrate have been modulated by hydrogen atoms spilled over onto the MoS_2 surface. These processes and the energy diagram are schematically shown in Fig. 2.

Reference
[1] F. Ozaki, S. Tanaka, W. Osada, K. Mukai, M.Horio, T. Koitaya, S. Yamamoto, I. Matsuda, and J. Yoshinobu, Applied Surface Science **593**, 153313 (2022).

Authors
F. Ozaki, S. Tanaka, W. Osada, K. Mukai, M. Horio, T. Koitaya[a], S. Yamamoto[b], I. Matsuda, and J. Yoshinobu
[a]Institute for Molecular Science
[b]Tohoku University

Development of Accurate Density Functional Theory

Sugino Group

Significance of the density functional theory (DFT) is in the ability to obtain the particle density ρ and the energy E without knowing the many-body wave function or the Green's function. Establishing the ρ-to-E mapping (or the functional $E[\rho]$), or equivalently the mapping to the external potential ($V_{\text{ext}}[\rho]$), is a grand challenge of computational materials science. This can be done, in principle, by inverting the V_{ext}-to-ρ relations that are provided by performing extremely-high-precision simulations; but there was no such trial until very recently. Such machine-learning (ML) based approach may be enabled by overcoming problems associated with handling very large dataset. With this in mind, we have previously done accurate quantum chemical simulations of a few molecules and the resulting density-to-energy relation was modeled with the neural network technique. The functional thus developed was found to improve the accuracy of molecular calculations showing a promise of achieving the chemical accuracy with DFT; however, application to solids was hampered by the fact that the molecular ρ is qualitatively different from the solid-state ρ and the non-availability of accurate ρ for solid states. In this context, we have shown that the insufficient information contained the molecular ρ can be augmented by adding the theoretically established ρ-to-E relations that hold for general ρ. To demonstrate this, we have reconstructed the functional using the theoretical relations as constraints of ML. The functional was developed using a semilocal functional format, called meta-generalized-gradient-approximation (meta-GGA), where the density, gradient of the density, and the kinetic energy density are used as the descriptor. By applying thus-established functional ($V_{\text{ext}}[\rho]$) to various crystalline solids, we have shown improved predictability of the lattice parameters. The functional was made public for the benefit of supercomputer uses [1].

Further improvement in the accuracy is most likely to be brought by using more sophisticated descriptors, such as the weighted densities. To get insights into it, classical systems provide a suitable benchmark because of the simple structure as compared to quantum systems. In this context, we investigated the structure of classical fluids of Lennard-Jones particles. In the classical systems, the density to the free-energy mapping can be rigorously described through the Bogoliubov-Born-Green-Kirkwood-Yvon (BBGKY) hierarchical equations and establishing the mapping corresponds to finding a universal closure relation, or simply a closure, that can appropriately truncate the hierarchy. To investigate it, we used the method of adiabatic continuation of the interaction and the scheme of functional renormalization group (FRG). We have obtained this way the flow equation that is suitable for deriving a working equation for numerical work. We focused herein on the Kirkwood super-

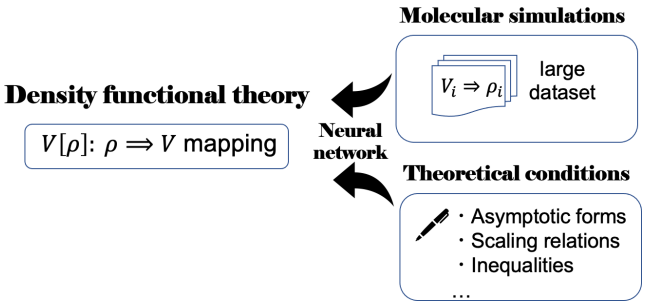

Fig. 1. Machine learning of the density functional $V[\rho]$ made possible using combined molecular data and theoretical conditions. The functional thus constructed can be applied to extended systems like solids not included in the learning set.

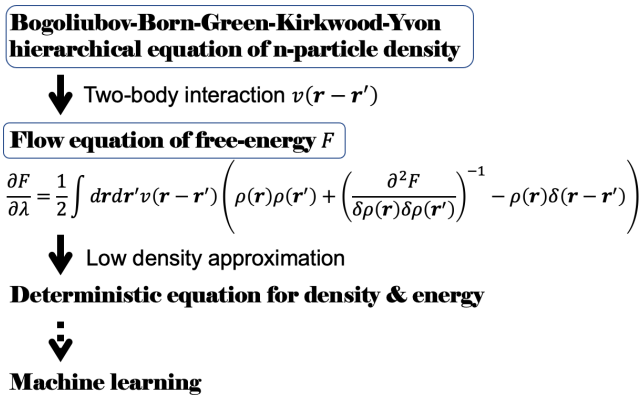

Fig. 2. Density functional theory for classical systems. Flow equation suitable for numerical work was developed to be used for the machine learning of the density-to-free energy mapping.

position with which to decompose the n-particle density into two-particle densities, which is strikingly accurate in the low-density region. By applying the resulting equation to a one-component one-dimensional fluid, we found it possible to obtain accurate density and energy when compared with other liquid theories. This result is already a demonstration of the power of the Kirkwood approximation combined with FRG in describing classical liquids, but more importantly, the resulting method has a form suitable for ML and thus encourages future work on the construction of the functional [2].

References

[1] R. Nagai, R. Akashi, and O. Sugino, npj Compt. Mater. **6**, 1 (2020); *ibid*, Phys. Rev. Res. **4**, 013106 (2022).
[2] T. Yokota, J. Haruyama, and O. Sugino, Phys. Rev. E **104**, 014124 (2021).

Authors

R. Nagai, [a]R. Akashi, [b]T. Yokota, and O. Sugino
[a]National Institute for Quantum Science and Technology
[b]Interdisciplinary Theoretical and Mathematical Science Program, RIKEN.

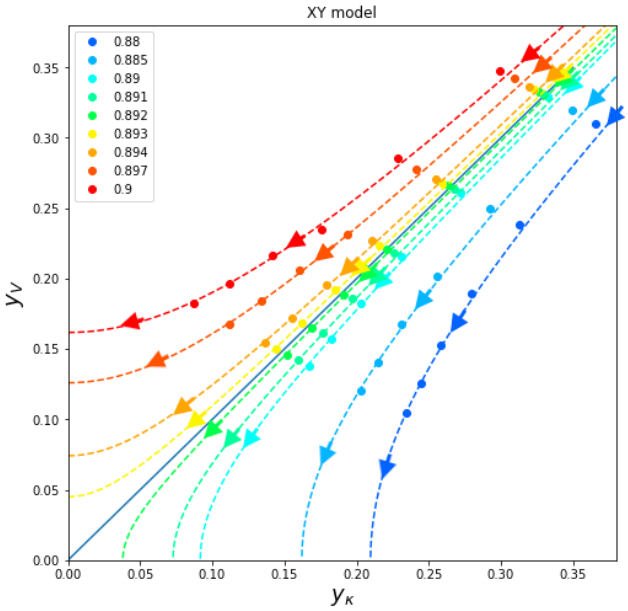

Fig. 2. The Renormalization-Group flow for the BKT transition in the classical two-dimensional XY model, constructed numerically from the transfer matrix spectrum based on the combination of tensor-network renormalization and conformal field theory.

Resolving the Berezinskii-Kosterlitz-Thouless Transition in the Two-Dimensional XY Model with Tensor-Network-Based Level Spectroscopy

Oshikawa Group

The Berezinskii-Kosterlitz-Thouless (BKT) transition was historically the first example of topological phase transitions, which is now an essential concept in physics as signified by the Nobel Prize in Physics in 2016. The canonical model exhibiting the BKT transition is the classical XY model in two dimensions. The BKT transition is conceptually well understood in terms of the Kosterlitz Renormalization Group (RG) equation. However, the famous "Kosterlitz RG flow" has remained a rather abstract concept, which cannot be seen directly. Moreover, because of the notorious logarithmic corrections, significant finite-size effects persist even in a large system, making conventional finite-size scaling of Monte Carlo methods such as Binder plot powerless. Even with considerable efforts over decades, an accurate determination of the critical temperature remains difficult, even with a huge computational power, for the system as simple as the classical XY model in two dimensions.

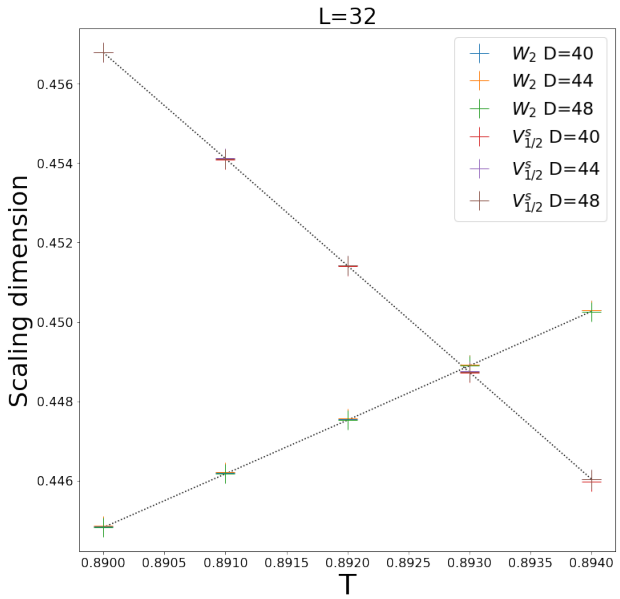

Fig. 1. The "level spectroscopy" applied to the classical two-dimensional XY model with the tensor-network renormalization. The crossing of the two "energy levels" (eigenvalues of the transfer matrix) in a finite-size system gives a precise estimate of the BKT transition temperature, as the logarithmic correction is cancelled out.

On the other hand, many one-dimensional quantum systems can be also described by the same effective theory and thus also exhibit the BKT transition. Interestingly, a powerful numerical finite-size scaling method called "level spectroscopy" was developed specifically for those 1D quantum systems by Okamoto and Nomura. Based on the conformal field theory results on the finite-size energy spectrum thanks to Cardy, they found that the BKT transition can be identified with a level crossing between a certain pair of the energy levels, canceling the logarithmic corrections. This allows a surprisingly accurate determination of the BKT transition point with exact numerical diagonalization of rather small systems. However, the applications of level spectroscopy have been limited to one-dimensional quantum BKT system such as quantum spin chains so far. While it should be applicable to the spectrum of the transfer matrix for the classical two-dimensional XY model, the level spectroscopy has not been applied there, because of the difficulty in calculating the spectrum for the system with continuous variables such as the angle of the XY spin.

In this work, we demonstrated a successful implementation of level spectroscopy on the classical two-dimensional XY model, based on the tensor network renormalization (TNR) scheme. The TNR enables us to obtain a precise spectrum of the transfer matrix, to which the level spectroscopy can be applied. As in the case of the one-dimensional quantum system, it allows a very accurate determination of the critical point by removing the logarithmic corrections from systems of moderate sizes, which can be described by a tensor network with a finite bond dimension. As a result, we have improved the accuracy of the BKT transition tempera-

ture in the classical two-dimensional XY model, by an order of magnitude over the best numerical estimate in the literature.

Furthermore, our TNR study covers larger system sizes than those in the existing level spectroscopy studies on one-dimensional quantum systems. We found a new feature of the finite-size scaling, that leads to a further improvement of level spectroscopy. Finally, we also applied our methodology to visualize the celebrated Kosterlitz RG flow of the BKT transition based on the numerical data, for the first time to our knowledge.

Reference
[1] A. Ueda and M. Oshikawa, Phys. Rev. B **104,** 165132 (2021). [Editor's Suggestion]

Authors
A. Ueda and M. Oshikawa

Large Anomalous Nernst Effect and Nodal Plane in an Iron-Based Kagome Ferromagnet

Nakatsuji Group

Anomalous Nernst effect (ANE), a thermoelectric effect in magnetic material, has recently attracted attention as unique energy-harvesting technology. It holds promise in developing high-efficiency energy-harvesting devices with a simple lateral structure, high flexibility, and low production cost. The design of magnetic materials that exhibits a large ANE will help develop a novel energy harvesting technology. Here, we observed a high ANE exceeding 3 μV/K above room temperature in the kagome ferromagnet Fe_3Sn with a high Curie temperature of 760 K [1].

Figure 1a shows the temperature dependence of anomalous Nernst coefficient S_{ij} and transverse thermoelectric conductivity α_{ji}. With increasing temperature up to 400 K, the magnitude of the ANE coefficient increases monotonically and reaches 3 μV/K above room temperature. The temperature dependence of α_{ij}/T exhibits logarithmic behavior over almost a decade of temperature from 400 K down to 40 K, and remains roughly constant at ˜0.02 $Am^{-1}K^{-2}$ below ˜40 K (Fig. 1b). The logarithmic behavior of α_{ij}/T signals a nontrivial electronic structure close to the Fermi energy.

To investigate the origin of ANE, we carried out first-principles calculations to analyze α_{ij}, and the calculated result agrees well with the experimental data (Fig. 1b). We then conclude that the origin of the ANE is a pair of partially flat

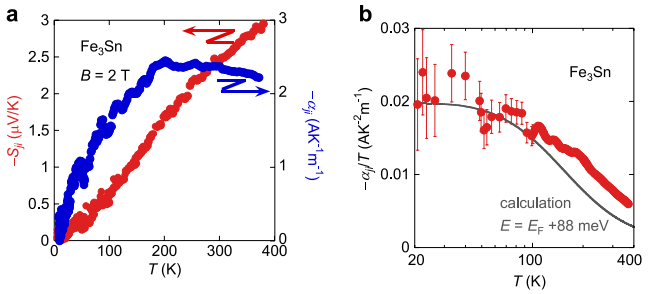

Fig. 1. (a) Temperature dependence of the Nernst signal (S_{ji}) and the transverse thermoelectric conductivity (α_{ij}) measured under an external magnetic field of 2 T. (b) Temperature dependence of the transverse thermoelectric conductivity (α_{ji}/T). The dark line represents α_{ji}/T obtained by DFT calculation at E_F = +88 meV.

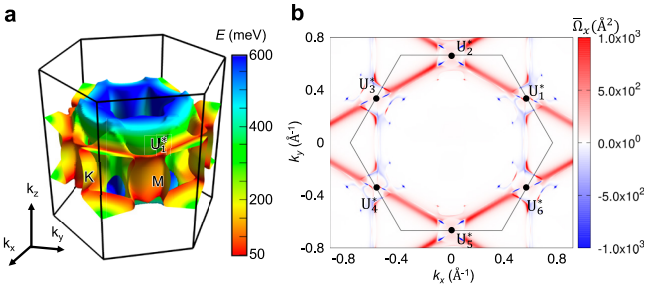

Fig. 2. (a) Nodal plane in the hexagonal Brillouin zone obtained as follows: $\Delta\varepsilon(\boldsymbol{k}) \equiv \varepsilon^{\alpha}(\boldsymbol{k}) - \varepsilon^{\beta}(\boldsymbol{k}) = 0$, where $\Delta\varepsilon(\boldsymbol{k})$, $\varepsilon^{\alpha(\beta)}(\boldsymbol{k})$, and $\boldsymbol{k}$ are the energy difference between two bands, eigenvalue for up- and down-spin bands, and wave vector, respectively. The color bar shows the energy of the nodal plane calculated without SOC. (b) Contour plot of the sum of the Berry curvature over the occupied states ($E = E_F + 50$ meV) on $k_z = 0.13$ plane.

bands of up- and down-spins, known as the "nodal plane" (Fig. 2a). Indeed, strong intensity of the Berry curvature arising from the flat nodal plane appears at specific chemical potentials (Fig. 2b). Similar to the nodal lines, nodal planes are ubiquitous in electronic band structures without SOC. Nodal planes often turn into nodal lines at constant energy cuts, and these constant energy lines lead to partially flat bands with a small energy gap after introducing SOC. Such characteristic band structure is not unique to Fe_3Sn and could be realized in other kagome lattice materials. It is well known that M points in kagome lattice may result in van Hove singularities (namely, the derivative of energy dispersion is zero). Therefore, energy dispersion on lines connecting M points could be flat compared with other k paths. Our theoretical analysis based on the first-principles calculation clarifies that a "nodal plane" induces strongly enhanced Berry curvature, resulting in the large ANE. The flat degenerate electronic bands provide a valuable guide to designing magnetic materials with a large ANE.

Reference
[1] T. Chen, S. Minami, A. Sakai, Y. Wang, Z. Feng, T. Nomoto, M. Hirayama, R. Ishii, T. Koretsune, R. Arita, and S. Nakatsuji, Sci. Adv. **8**, eabk1480 (2022).

Authors
T. Chen, S. Minami[a], A. Sakai, Y. Wang[a], Z. Feng, T. Nomoto[a], M. Hirayama[b], R. Ishii, T. Koretsune[c], R. Arita[a,b], and S. Nakatsuji
[a]The University of Tokyo
[b]RIKEN Center of Emergent Matter Science (CEMS)
[c]Tohoku University

Anomalous Scaling Behavior of Transverse Thermoelectric Conductivity in Ferromagnet CoMnSb

Nakatsuji Group

Transverse transport effects such as anomalous Hall and Nernst effects are effective probes to topological texture in electronic band structures. In particular, large Berry curvature originating from Weyl nodes or nodal line structures is known to enhance these effects significantly. In contrast to the Hall conductivity σ_{yx}, which measures the summation of the Berry curvature below Fermi energy, the transverse thermoelectric conductivity α_{yx} sensitively captures the Berry curvature in the vicinity of the Fermi energy [1]. Therefore, the Nernst effect provides complementary information about the characteristics of the topological band structure. Moreover, scaling behavior $\alpha_{yx} \sim -T \log T$ is recently reported

in ferromagnet Co_2MnGa [2]. This anomaly is attributed to the Weyl semimetal state tuned close to the quantum Lifshitz critical point. However, the universality of this critical behavior is still yet to be confirmed experimentally.

Here, we report magnetic, transport, and thermoelectric properties of single crystals of ferromagnetic CoMnSb with a high Curie temperature of 470 K [3]. The actual experimental crystal structure of CoMnSb is a $2\times2\times2$ superstructure of the previously predicted half-Heusler structure. Since theoretical understanding of the transverse transport phenomena in the superstructure CoMnSb is lacking, we performed first-principles calculation of superstructure CoMnSb to compare with experimental results.

We find a sizable anomalous Hall conductivity σ_{yx} and transverse thermoelectric conductivity α_{yx} experimentally. We observe substantial anomalous Hall conductivity σ_{yx} and transverse thermoelectric conductivity α_{yx}. The experimental σ_{yx} (T) is well described by DFT calculation for the chemical potential E - $E_F \approx$ -130 meV (Fig. 1(a)), which is consistent with the valence electron count estimated from the sample composition measured by Inductively Coupled Plasma (ICP) method. Moreover, α_{yx} exhibits $-T\log T$ cr itical behavior instead of the conventional Fermi liquid behavior $\alpha_{yx} \sim T$ over a decade of temperature between 10 and 400 K (Fig. 1(b)). This behavior is similar to ferromagnetic Weyl semimetal Co_2MnGa and nodal-line semimetals Fe_3X (X = Al, Ga) [2, 5]. Our theoretical calculation shows that in the vicinity of the chemical potential E - $E_F \approx$ -130 meV, the scaling behavior $\alpha_{yx} \sim -T\log T$ arises from Weyl nodes in the band structure (Fig. 2).

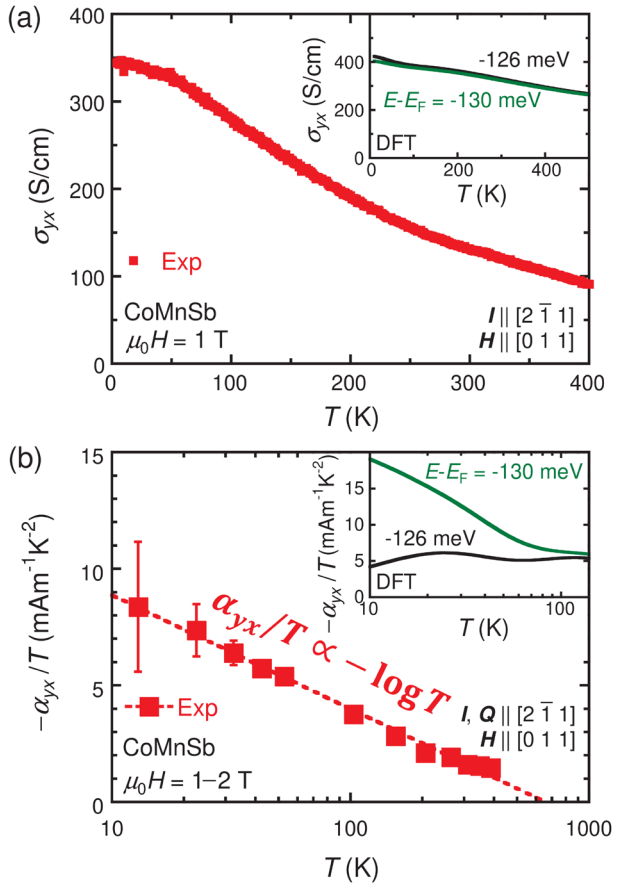

Fig. 1. Temperature T dependence of (a) the Hall conductivity σ_{yx}, and (b) the transverse thermoelectric conductivity divided by T, α_{yx} / T in comparison with theoretical calculations (insets) for CoMnSb. Two different chemical potentials, E - E_F = -126 meV (black) and E - E_F = -130 meV (green), are selected for calculating σ_{yx} (T) and α_{yx} (T) / T.

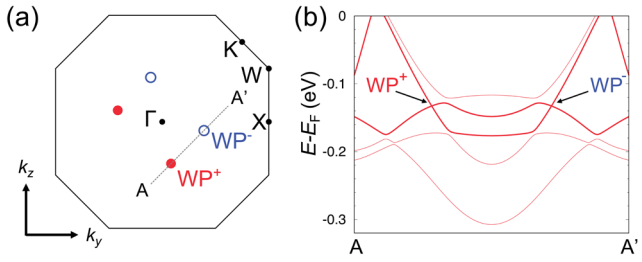

Fig. 2. (a) Momentum-space distribution of Weyl nodes in CoMnSb on the k_x = 0 plane, which shows the Weyl node pair WP$^-$ (open blue circle) and WP$^+$ (closed red circle). The coordinate of WP$^-$ and WP$^+$ (k_y, k_z) are (0.21, -0.04) and (0.04, -0.21) in the unit of angstrom inverse, respectively. Black solid lines correspond to the boundary of the fcc Brillouin zone. (b) Band structure along A--A' (the black-dotted line) shown in (a).

In summary, we have successfully synthesized single-crystal samples of superstructure CoMnSb and explored their transverse transport properties. The observed critical scaling behavior in the transverse thermoelectric conductivity $\alpha_{yx} \sim -T\log T$ clearly deviates from the conventional Fermi liquid behavior, providing a hallmark of topological texture in the band structure. The comparison of experimental results with DFT calculations shows that this critical behavior results from Weyl nodes. This result indicates that the logarithmic criticality in the transverse thermoelectric conductivity provides a highly sensitive signature to reveal the topological band texture.

References

[1] G. Sharma, P. Goswami, and S. Tewari, Phys. Rev. B **93**, 035116 (2016).
[2] A. Sakai *et al.*, Nat. Phys. **14**, 1119 (2018).
[3] H. Nakamura *et al.*, Phys. Rev. B **104**, L161114 (2021).
[4] S. Minami *et al.*, Appl. Phys. Lett. **113**, 032403 (2018).
[5] A. Sakai *et al.*, Nature **581**, 53 (2020).

Authors

H. Nakamura, S. Minami[a], T. Tomita, A. A. Nugroho[b], and S. Nakatsuji
[a]The University of Tokyo
[b]Institut Teknologi Bandung

Phonon Spectrum of Quantum Pyrochlores $Pr_2Zr_2O_7$ and $Pr_2Ir_2O_7$

Nakatsuji Group

Experimental realization of a quantum spin liquid (QSL) state is among the central topics of condensed matter physics. In a QSL state, spins do not form long-range order even down to absolute zero, characterized by strong long-range entanglement[1]. Geometric frustrations and competing interactions are central ingredients to realizing QSL states. However, almost all candidate materials discovered possess chemical or structural disorders. Thus, it is crucial to understand the role of structural disorders. Can structural disorder be a factor that stabilizes a QSL state, as proposed in some theoretical studies [2]? How to experimentally distinguish the effects of structural disorders from that induced by the intrinsic lattice dynamics?

To answer these questions, we performed Raman scattering spectroscopy to separate dynamic lattice effects from the structural disorders on the Pr-based pyrochlore oxides $Pr_2Zr_2O_7$ and $Pr_2Ir_2O_7$[3,4]. Both materials host exotic ground states without long-range orders. Their CEF

ground state is an E_g non-Kramers doublet, which is unprotected by the time-reversal symmetry and thus can be split by a slight deviation from the D_{3d} local symmetry. As a result, structural disorders may play an essential role in shaping the ground-state properties of both systems.

Our Raman studies reveal that splitting of the ground state E_g doublet and the E_g doublet at 55 meV results from different physical origins [3]. Figures 1(a) and (b) show the Raman spectra of CEF excitation and the CEF level scheme of $Pr_2Zr_2O_7$ at 14 K, respectively. The E_g level at 55 meV is split by the T_{2g} phonons instead of structural disorder. The observed splitting characterized by a well-defined symmetry can only occur in the presence of mixing with another excitation of E symmetry, leading to a vibronic state (Fig. 1(c)). Based on DFT calculations, the vibronic state in $Pr_2Zr_2O_7$ is most likely driven by T_{2g} phonon lying at 64.6 meV at the Γ point (Fig. 1(d)). The associated eigenvectors involve motion of O1 oxygens that modulates the Pr^{3+} oxygen environment (Fig. 1(e)).

Our second study [4] reveals that $Pr_2Zr_2O_7$ exhibits phonon softening, which modulates the Pr-O-Pr angle and changes the magnetic super-exchange interaction. Compared to $Pr_2Zr_2O_7$, $Pr_2Ir_2O_7$ shows a similar but much broader phonon spectrum (Fig. 2). Given that the metallic $Pr_2Ir_2O_7$ features phonon-electron scattering mechanisms, which are absent in the insulating $Pr_2Zr_2O_7$, the difference in their phonon spectrum is likely a result of phonon-electron scattering rather than disorders.

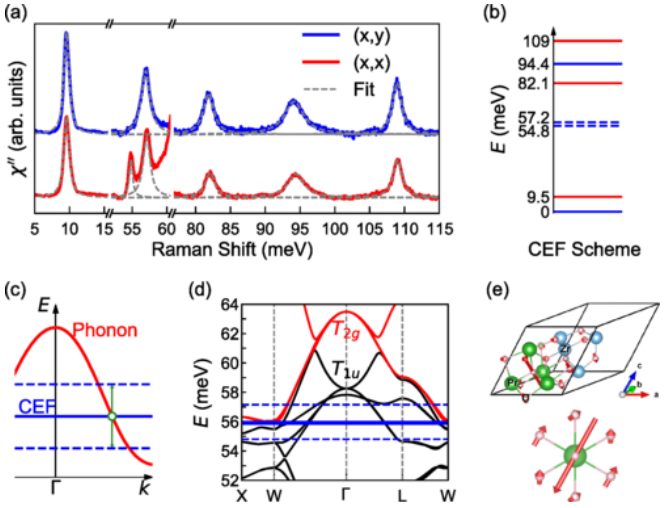

Fig. 1. (a) Raman spectra of $Pr_2Zr_2O_7$ at 14 K. (b) A schematic diagram of the Pr^{3+} CEF levels in $Pr_2Zr_2O_7$. (c) A schematic diagram of the vibronic coupling between the phonons and CEF states. (d) The $Pr_2Zr_2O_7$ phonon dispersion obtained by DFT calculations. The energy range close to the vibronic features is shown. Dashed blue lines represent the experimentally observed CEF vibronic excitations. The vibronic coupling is expected to occur at the intersection point of the nonsplit CEF doublet (solid blue line) and the T_{2g} phonon branch (red curve). (e) Atomic displacements of the T_{2g} phonon mode. Upper panel: View of the unit cell. Lower panel: PrO_8 octahedron site viewed from the [111] direction.

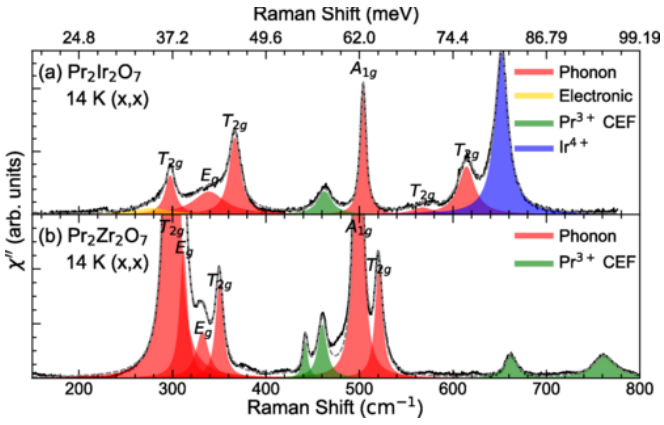

Fig. 2. Raman scattering spectra of (a) $Pr_2Ir_2O_7$ and (b) $Pr_2Zr_2O_7$ at 14 K in parallel polarization configuration.

References

[1] P.W. Anderson, Mat. Res. Bull. **8**, 153 (1973).
[2] L. Savary and L. Balents, Phys. Rev. Lett. **118**, 087203 (2017).
[3] Y. Xu, H. Man, N. Tang, T. Ohtsuki, S. Baidya, S. Nakatsuji, D. Vanderbilt, and N. Drichko, Phys. Rev. B **89**, 075137 (2022).
[4] Y. Xu, H. Man, N. Tang, S. Baidya, H. Zhang, S. Nakatsuji, D. Vanderbilt, and N. Drichko, Phys. Rev. B **104**, 075125 (2021).

Authors

Y. Xu[a], H. Man[a], N. Tang, T. Ohtsuki, S. Baidya[b], S. Nakatsuji, D. Vanderbilt[b], and N. Drichko[a], and H. Zhang[b]
[a]John Hopkins University
[b]Rutgers University

Ferrimagnetic Compensation and its Thickness Dependence of TbFeCo Alloy Thin Films

Nakatsuji Group

Rare earth (RE)-transition metal (TM) ferrimagnetic materials have compositions in which the antiferromagnetically coupled magnetization of RE and TM atoms compensates, resulting in a zero net magnetization. Tuning magnetization to zero is particularly advantageous in creating efficient memory devices based on magnetic materials. Moreover, such materials exhibit bulk perpendicular magnetic anisotropy (PMA), whose origin is different from the interfacial PMA. This property offers another advantage for applications. This study reports a systematic investigation into the magnetic properties of ferrimagnetic TbFeCo thin films deposited on a Pt underlayer. Our results show that the Tb concentration, at which magnetic moments of Tb and Fe or Co sublattices are compensated, increases with the thickness of TbFeCo thin films because the Tb atoms are magnetically inert as they are mixed with the Pt underlayer (Fig. 1). Furthermore, we clarify the relationship between the loss of magnetism of Tb atoms and bulk PMA. This study provides a prospect for designing ferrimagnetic ultrathin films with large PMA, which is essential for fabricating magnetic memory devices.

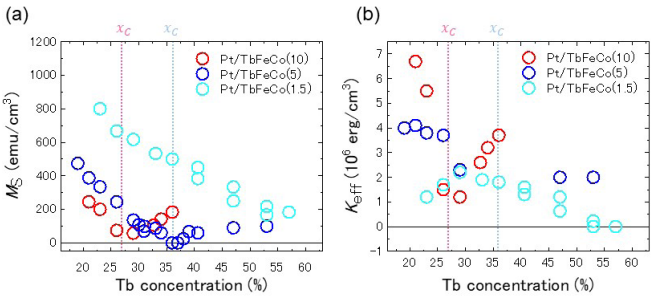

Fig. 1. (a) and (b) Tb concentration dependence of the saturation magnetization M_S (a) and the effective magnetic anisotropy energy density K_{eff} (b) for TbFeCo thin films with different thicknesses. The underlayer is Pt. Red circles: Pt/TbFeCo(10 nm), blue circles: Pt/TbFeCo(5 nm), and light blue circles: Pt/TbFeCo(1.5 nm). Red and blue broken vertical lines denote the compensation composition x_c for Pt/TbFeCo(10 nm) and Pt/TbFeCo(5 nm), respectively.

Reference
[1] M. Ishibashi, K. Yakushiji, M. Kawaguchi, A. Tsukamoto, S. Nakatsuji, and M. Hayashi, Appl. Phys. Lett. **120**, 022405 (2022).

Authors
M. Ishibashi[a], K. Yakushiji[b], M. Kawaguchi[a], A. Tsukamoto[c], S. Nakatsuji[a, d, e, f], and M. Hayashi[a, e]
[a]The University of Tokyo
[b]National Institute of Advanced Industrial Science and Technology
[c]Nihon University
[d]CREST, Japan Science and Technology Agency
[e]Trans-scale Quantum Science Institute, University of Tokyo
[f]Johns Hopkins University

Enhanced Anomalous Hall Signal by Electrical Manipulation in Antiferromagnetic Weyl Metal Mn_3Sn

Nakatsuji, Otani, and Miwa Groups

Topological properties may play a significant role in developing next-generation electronic devices. Weyl semimetals characterized by linearly dispersive band touching points may exhibit surprisingly large topological transport responses, such as anomalous Hall effect (AHE), anomalous Nernst effect (ANE), and chiral anomaly. Manipulation of such topological responses electrically may lead to a new type of nonvolatile memory device.

Recently, electrical manipulation of topological responses for a magnetic Weyl semimetal has been demonstrated. Magnetic switching using spin-orbit torque (SOT) is established in the antiferromagnet Mn_3Sn (Fig. 1(a)) [1]. Figure. 1b shows the schematic of the electrical switching in Mn_3Sn/W memory devices. The polarization of the flowing current determines the orientation of the magnetization of Mn_3Sn. The different states of Mn_3Sn can be read by measuring the Hall voltage, namely "0" and "1" states. For application purposes, it is essential to develop means to enhance the readout signal of the magnetic switching in Mn_3Sn. Several ingredients determine the signal's magnitude, such as geometrical factors of a memory cell, shunting current, and volume fraction of the switching domain. While the former two are extrinsic and tunable by changing the magnetic cell and layer structure, the latter is intrinsic to the cell that consists of a multilayer stack.

This work optimizes the multilayer structure and deposition process and realizes a three-time enhancement of the readout signal (Hall resistance). The Ru buffer layer is removed from the reported Ru/Mn_3Sn/W layer to decrease the current shunting effect, and the Mn_3Sn/W bilayer is directly deposited on the Si/SiO_2 substrate. Moreover, additional annealing progress at the Mn_3Sn/W interface is applied to suppress the roughness at the Mn_3Sn /W interface; as a result, the roughness is decreased to 0.5 nm, one order of magnitude smaller than that of the reported Ru/Mn_3Sn/W thin film.

The obtained AHE signal of the Mn_3Sn/W thin film is twice larger than the previous value reported for Ru/ Mn_3Sn /W thin film. Based on the X-ray diffraction analysis, both the decreased current shunting effect and the different orientation of Mn_3Sn domains contribute to the enhancement of the AHE signal. In the current switching measurement, the switching volume fraction calculated by the ratio between electrical and field switching signals is 50%, around 1.5 times larger than the reported value. The enhancement of the switching fraction is likely related to the higher spin injection efficiency at the interface due to the smooth interface. The enhancement of AHE and the switching fraction result in a three-time enhancement of the switching Hall resistance (Fig. 1(c)). This finding may bring memory devices based on topological antiferromagnet closer to real-world applications [2].

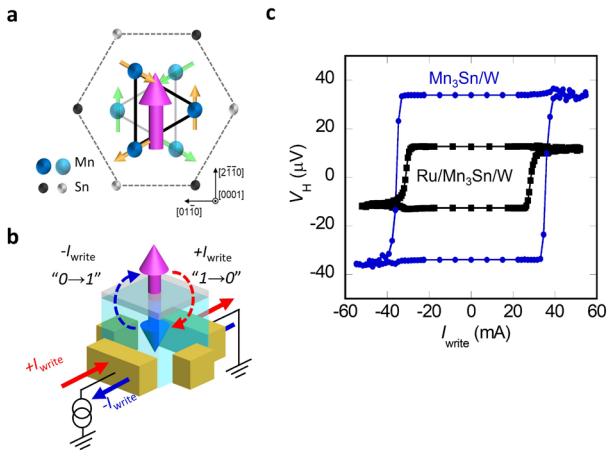

Fig. 1. (a) Crystal and spin structures of Mn_3Sn. The non-collinear spin structure consisting of six Mn magnetic moments (yellow and green arrows) can be viewed as the ferroic ordering of a magnetic octupole (purple arrow). (b) The schematic of the electrical switching in Mn_3Sn/W memory devices. Two different states of Mn_3Sn, "0" and "1" states, can be determined by the polarity of applying current. (c) Enhancement of the switching Hall voltage in the Mn_3Sn/W bilayer is three times larger than the value observed in the previous Ru/Mn_3Sn/W multilayer.

References
[1] H. Tsai, T. Higo, K. Kondou, T. Nomoto, A. Sakai, A. Kobayashi, T. Nakano, K. Yakushiji, R. Arita, S. Miwa, Y. Otani, snd S. Nakatsuji, Nature **580**, 608 (2020).
[2] H. Tsai, T. Higo, K. Kondou, S. Sakamoto, A. Kobayashi, T. Matsuo, S. Miwa, Y. Otani, and S. Nakatsuji, Small Sci. **1**, 2000025 (2021).

Authors
H. Tsai, T. Higo, K. Kondou[a], S. Sakamoto, A. Kobayashi, T. Matsuo, S. Miwa, Y. Otani, and S. Nakatsuji
[a]RIKEN CEMS

Observation of Spontaneous X-ray Magnetic Circular Dichroism in the Chiral Antiferromagnet Mn_3Sn Thin Film

Miwa and Nakatsuji Groups

Antiferromagnets without a net magnetic moment are invisible to many magnetic probes, including X-ray magnetic circular dichroism (XMCD). Recently, it was proposed that the inverse triangular spin (ITS) structure of a noncollinear antiferromagnet can give rise to finite XMCD signals through the non-vanishing magnetic dipole term T, which is probed by XMCD, even without net magnetization [1,2], as schematically shown in Fig. 1(a).

A chiral antiferromagnet Mn_3Sn with the $D0_{19}$ structure [3] is an ideal material for observing the XMCD signals originating from the ITS structure (also referred to as the ferroic order of cluster magnetic octupoles) because the direction of the ITS structure or the octupole polarization can be controlled by external magnetic fields through finite spin canting.

In the present study, to test if finite XMCD signals are observable in the ITS structure, we grew a Mn_3Sn epitaxial

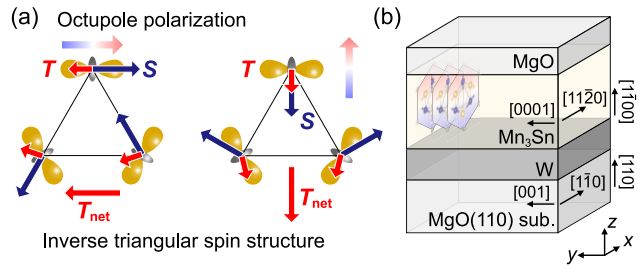

Fig. 1. (a) Inverse triangular spin (*S*) structure with magnetic dipole term (*T*). (b) Thin film structure.

thin film and performed XMCD measurements on it. The sample structure was MgO(110) substrate/W (15 nm)/ Mn_3Sn (40 nm)/MgO (3 nm), as schematically shown in Fig. 1(b). X-ray absorption spectroscopy (XAS) and XMCD measurements were performed on the BL-16A2 beamline at the Photon Factory. Measurement temperature was room temperature. The incident x-ray and magnetic field directions were perpendicular to the sample surface so that the octupole polarization becomes parallel to the incident x-rays.

Figure 2(a) shows a typical XAS spectrum of the Mn_3Sn thin film. The XAS spectral line shape did not depend on the magnetic field strength or direction. The XMCD spectra obtained with magnetic fields of 0.1 T and 5 T are shown by the red and blue curves in Fig. 2(b), respectively. The spectral line shapes significantly differ from each other: The spectrum obtained with 0.1 T shows a strong positive pre-edge peak, denoted by α in Fig. 2(b), while the spectrum obtained with 5 T shows an intense negative peak at the XAS peak position, denoted by β in Fig. 2(b).

The XMCD spectra are expected to consist of the spin-canting component, which develops with increasing magnetic fields, and the field independent octupole component. Because the peak β develops with increasing magnetic fields, it most likely originates from spin canting. Indeed, if the spectrum taken with 0.1 T is subtracted from the spectrum taken with 5 T, a broad featureless XMCD spectrum without peak α is obtained, as shown by the green curve in Fig. 2(b). This broad spectrum resembles the XMCD spectra of metallic systems, suggesting that it reflects the spin component. This argument also indicates that the spectrum taken with 0.1 T, which shows multiple sharp peaks, predominantly reflects the octupole component because it is independent of magnetic fields.

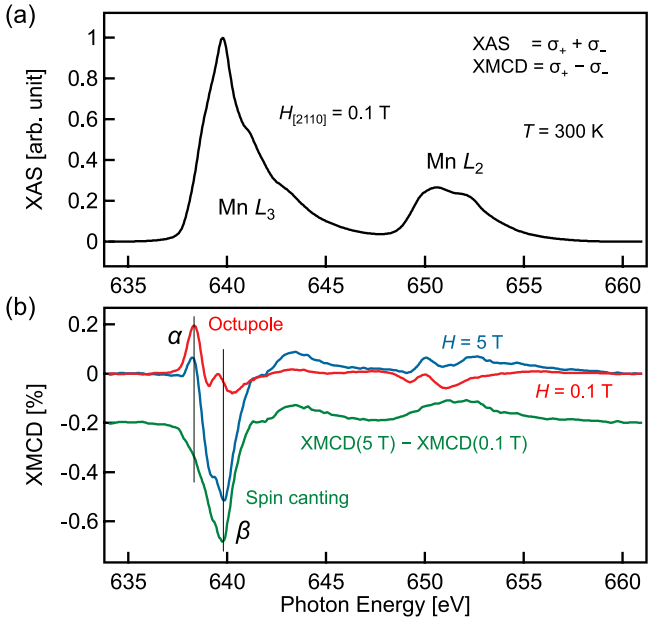

Fig. 2. (a) Typical XAS spectrum of the Mn_3Sn thin film. (b) XMCD spectra taken with magnetic fields (*H*) of 0.1 T (red curve) and 5 T (blue curve). The spin canting component (green curve) is extracted by subtracting the 0.1 T spectrum from the 5 T spectrum.

In summary, we demonstrated that the ITS structure can give rise to finite XMCD signals by performing XMCD measurements on a Mn_3Sn epitaxial thin film [4]. This finding should allow one to quantitatively evaluate the magnitude of the octupole polarization and spin canting, which would be difficult otherwise. The present results should also lead to the resolution of antiferromagnetic domains and antiferromagnetic domain walls using the scanning XMCD technique.

References
[1] Y. Yamasaki, H. Nakao, and T.-h. Arima, J. Phys. Soc. Jpn **89**, 083703 (2020).
[2] N. Sasabe, M. Kimata, and T. Nakamura, Phys. Rev. Lett. **126**, 157402 (2021).
[3] S. Nakatsuji, N. Kiyohara, and T. Higo, Nature **527**, 212 (2015).
[4] S. Sakamoto, T. Higo, M. Shiga, K. Amemiya, S. Nakatsuji, and S. Miwa, Phys. Rev. B **104**, 134431 (2021).

Authors
S. Sakamoto, T. Higo, M. Shiga, K. Amemiya[a], S. Nakatsuji, and S. Miwa
[a]KEK

Electron-Correlation-Driven Enhancement of Orbital Polarization at the Fe/MgO Interface

Miwa Group

Utilizing electron spins in electronic devices is a central theme in the field of spintronics. The giant tunneling magnetoresistance (TMR) effect and interfacial perpendicular magnetic anisotropy (PMA) in Fe/MgO-based multilayer systems are the foundation of such spintronics applications. For both effects, the atoms located at the interface play crucial roles. That is, the interfacial spin and orbital polarization determines TMR and PMA, respectively. Therefore, it is essential to understand how Fe atoms behave at the interface with MgO by characterizing their spin and orbital magnetic moments to further improve TMR and PMA.

For such a purpose, we performed depth-resolved x-ray magnetic circular dichroism (XMCD) measurements on the V/Fe/MgO trilayer grown on an MgO(001) substrate (Fig. 1(a)) The trilayer showed PMA, as confirmed by magneto-optical Kerr effect measurements with out-of-plane magnetic fields (Fig. 1(b)). The principle of the depth-resolved XMCD [1] is shown in Fig. 1(c). Here, photoelectrons emitted at different angles were detected separately. Because electrons have a finite inelastic mean free path λ_e in solids, the probability of inelastic electrons at depth z escaping into the vacuum depends on the electron emission angle θ_d. Therefore, detecting electrons as a function of θ_d yields probing depth (λ_{eff}) dependent XMCD spectra and hence the depth profiles of the spin and orbital magnetic moments. The depth-resolved XMCD measurements were conducted at the beamline BL-7A at the Photon Factory.

The obtained spin and orbital magnetic moments were plotted against the detection angles in Figs. 2(a) and 2(b),

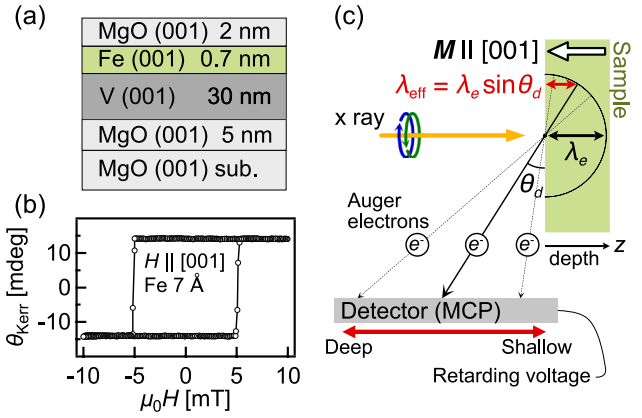

Fig. 1. (a) Sample structure. (b) Out-of-plane magnetization curve measured based on the magneto-optical Kerr effect. (c) Schematic illustration of experimental setup and principle of depth-resolved XMCD technique, where probing depth (λ_{eff}) depends on the electron emission angle (θ_d).

respectively. Both the spin and orbital magnetic moments increased as the detection angles decreased, suggesting that they enhanced near the Fe/MgO interface. By performing curve fitting, we estimated the magnetic moment of each layer, as shown by the solid staircase-like lines in Figs. 2(c) and 2(d). The obtained depth profiles show interfacial enhancement of the Fe orbital and spin magnetic moments at the Fe/MgO interface. By contrast, the spin magnetic moment diminished at the Fe/V interface.

To interpret the experimental observations, we performed first-principles calculations. Figure 2(e) shows the used supercell. The calculated magnetic moments are shown by the gray shaded bars in Figs. 2(c) and 2(d). Although the calculations reproduced interfacial enhancement of the spin magnetic moments, it significantly underestimated the orbital counterpart. To resolve this discrepancy, we performed the calculations with orbital polarization (OP) correction. This correction accounts for the electron–electron correlation

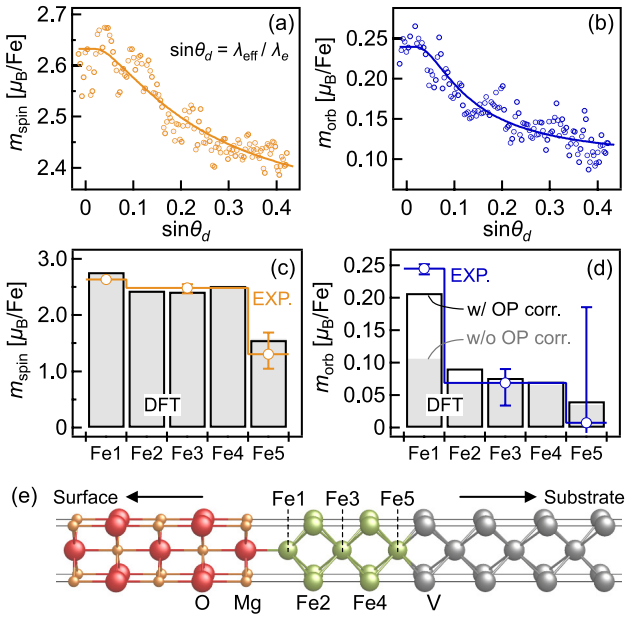

Fig. 2. Detection-angle-dependent (a) spin magnetic moment m_{spin}, (b) orbital magnetic moment m_{orb}. Solid curves represent the fit. Depth profiles of (c) spin magnetic moment and (d) orbital magnetic moment. Staircase-like lines with open markers represent experimental data; black bars and gray shaded bars represent results of first-principles calculations with and without orbital polarization (OP) correction, respectively. (e) Supercell used for calculations.

by satisfying Hund's second rule and provide an accurate description of orbital magnetic moments and PMA. The OP correction calculations considerably increased the orbital magnetic moment at the Fe/MgO interface close to the experimental value, as shown by the black bars in Figs. 2(c) and 2(d). This agreement suggests that the electron–electron correlation, probably strengthened by interfacial electron localization, enhance the orbital magnetic moment at the Fe/MgO interface and the PMA.

The present findings [2] should also apply to other ferromagnetic metal/oxide interfaces, including CoFeB/MgO systems, as enhanced electron−electron correlation is generic to such interfaces with the abrupt termination of metallic bonds. Furthermore, this study provides insights into the importance of considering electron−electron correlation, which have often been disregarded in spintronics, to understand various phenomena that emerge at interfaces.

References
[1] K. Amemiya, Phys. Chem. Chem. Phys. **14**, 10477 (2012).
[2] S. Sakamoto, M. Tsujikawa, M. Shirai, K. Amemiya, and S. Miwa, ACS Appl. Electron. Mater. **4**, 1794 (2022).

Authors
S. Sakamoto, M. Tsujikawa[a], M. Shirai[a], K. Amemiya[b], and S. Miwa
[a]Tohoku University
[b]KEK

Mott-Insulator-Like Bose-Einstein Condensation in a Tight-Binding System of Interacting Bosons with a Flat Band

Kawashima Group

We considered a Bose-Hubbard model on a two-dimensional lattice. We showed that the model parameters (the lattice structure, the hopping constants, and the chemical potential) can be tuned in such a way that the ground state is generated by applying, to the vacuum, N creation operators of locally-defined quasi-particles, where N is proportional to the total number of lattice points. The resulting model has a free parameter β that controls the degree of quantum fluctuation; β = 0 for no fluctuation and β = 1/2 for the maximum fluctuation. We carried out Monte Carlo simulation of this model at zero temperature, and discovered that the model undergoes a quantum phase transition when we change this parameter. While the system is 2+1 dimensional, the new phase transition exhibits the characteristics of 2 dimensions, i.e., the Kosterlitz-Thouless phase transition analogous to the classical XY model in 2 dimensions. Accordingly, the large β phase is the quasi Bose-Einstein condensation phase.

The above-mentioned ground state is expressed exactly as a tensor network with the bond dimension 2. Tracing out this tensor network is equivalent to calculating the partition function of some classical loop gas model. This is why the quantum criticality exhibits the purely 2-dimensional characteristics. It also allows us to construct a Monte Carlo algorithm for efficient sampling from the space of classical occupation-number configurations. In other words, we can stochastically trace out the tensor network to obtain various physical quantities of interest, such as the static structure factors and the helicity modulus.

The lattice is generated from the square lattice by duplicating each bond into p copies and introducing an additional site in the middle of each copy. (Fig. 1) The direct hopping

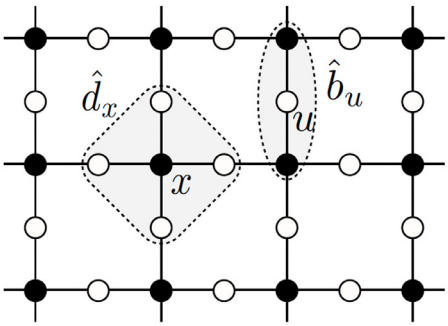

Fig. 1. The lattice considered (p=1). Within each cluster specified by x or u, a tuned hopping between the black and the white sites is defined.

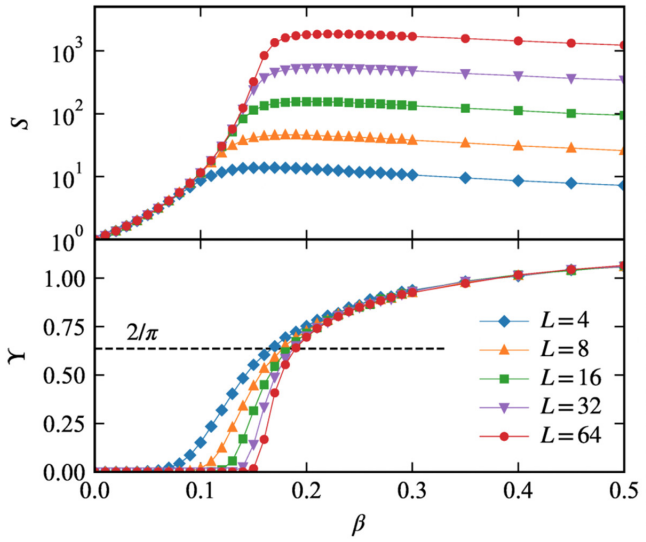

Fig. 2. The static structure factor S (top) and the helicity modulus (bottom) as functions of β for p=2. The horizontal line in the bottom panel indicates the universal jump 2/π, the thermodynamic value characteristic to the KT transition point.

is allowed only within local clusters labelled by either x or u. While bosons interact with each other, the model is constructed in such a way that the dispersion of a single particle has a flat band if influence of the other paricles could be neglected. The result of the Monte Carlo simulation are shown in Fig. 2. The static structure factor diverges around β = 0.2 and, at the same time, the helicity modulus jumps from 0 to 2/π, the universal value characteristic to the KT transition.

Reference

[1] H. Katsura, N. Kawashima, S. Morita, A. Tanaka, and H. Tasaki, Phys. Rev. Research, **3** 033190 (2021).

Authors
H. Katsura[a], N. Kawashima, S. Morita, A. Tanaka[b], and H. Tasaki[c]
[a]The University of Tokyo
[b]National Institute of Technology
[c]Gakushuin University

Double Superconducting Dome and Triple Enhancement of T_c in the Kagome Superconductor CsV_3Sb_5 under High Pressure

Uwatoko Group

The newly discovered kagome metals AV_3Sb_5 (A = K, Rb, Cs) have aroused tremendous research interest as a novel platform to study the interplay between nontrivial band topology, superconductivity (SC) and charge-density-wave (CDW) order [1-4]. At ambient conditions, these materials crystallize into a layered structure with hexagonal symmetry (space group *P6/mmm*), inset of Fig. 1(a), consisting of A layer and V-Sb slab stacked alternatively along the c-axis. The most prominent feature of this structure is the presence of quasi-2D ideal kagome layers of V ions coordinated by Sb. These compounds are metallic and enter a superconducting ground state below T_c = 0.93, 0.92, and 2.5 K for A= K, Rb, and Cs [2-4], respectively. In the normal state, their transport and magnetic properties exhibit a clear anomaly at T^* = 78, 104, and 94 K, respectively, due to the formation of CDW-like order as revealed by the x-ray diffraction and scanning tunning microscopy measurements [2-4]. The charge order in KV_3Sb_5 has been found to display a chiral anisotropy [5], which can lead to giant anomalous Hall effect in the absence of magnetic order or local moments [6,7]. It was also argued as a strong precursor of unconventional SC. Moreover, angle-resolved photoemission spectroscopy measurements and density-functional-theory calculations have characterized their normal state as a Z_2 topological metal with multiple Dirac nodal points near the Fermi level [1,4], consistent with the observations of Shubnikov-de Haas quantum oscillations and small Fermi surfaces (FSs) with low effective mass in RbV_3Sb_5 [3].

At present, the topologically related phenomena and SC have been actively studied in these AV_3Sb_5 compounds, but

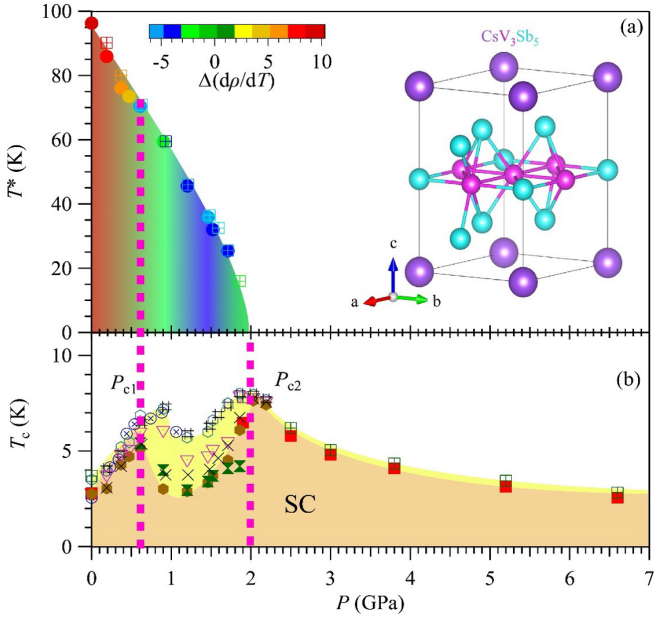

Fig. 1. Temperature-pressure phase diagram of CsV_3Sb_5. Pressure dependence of the transition temperatures for (a) the CDW-like order and (b) superconductivity. The color scale in (a) represents the sign of $\Delta(d\rho/dT)$ around T^*, which changes sign near P_{c1} due to the modification of CDW order. Inset of (a) shows the crystal structure of CsV_3Sb_5. The yellow region between P_{c1} and P_{c2} in (b) corresponds to a relatively broad superconducting transition.

the rich physics related to the electron correlation, especially the relationship between the intertwined electronic orders, has been barely revealed. In this regard, it is interesting to unveil the correlation between the CDW-like order and SC commonly observed in these AV_3Sb_5 materials. Thus, we have chosen to study CsV_3Sb_5 with the highest T_c among this series of compounds by applying a high-pressure approach, which has been widely used in disentangling the competing electronic orders of strongly correlated metals. The interplay between CDW and SC in CsV_3Sb_5 was studied via measurements of resistivity, DC and AC magnetic susceptibility under various pressures up to 6.6 GPa [8]. We find that the CDW transition decreases with pressure and experience a subtle modification at $P_{c1} \approx 0.6$-0.9 GPa before it vanishes completely at $P_{c2} \approx 2$ GPa. Correspondingly, $T_c(P)$ displays an unusual M-shaped double dome with two maxima around P_{c1} and P_{c2}, respectively, leading to a tripled enhancement of T_c to about 8 K at 2 GPa. The obtained temperature-pressure phase diagram, Fig. 1, resembles those of many unconventional superconductors, illustrating an intimated competition between CDW-like order and SC. The competition is found to be particularly strong for the intermediate pressure range $P_{c1} \leq P \leq P_{c2}$ as evidenced by the broad superconducting transition and reduced superconducting volume fraction. The modification of CDW order around P_{c1} has been discussed based on the band structure calculations. Our work not only demonstrates the potential to raise T_c of the V-based kagome superconductors, but also offers more insights into the rich physics related to the electron correlations in this novel family of topological kagome metals.

References

[1] B. R. Ortiz, L. C. Gomes, J. R. Morey *et al.*, Phys. Rev. Mater. **3**, 094407 (2019).
[2] B. R. Ortiz, E. Kenney, P.M. Sarte *et al.*, Phys. Rev. Mater. **5**, 034801 (2021).
[3] Q.W. Yin, Z. J. Tu, C. S. Gong *et al.*, Chin. Phys. Lett. **38**, 037403 (2021).
[4] B. R. Ortiz, S. M. L. Teicher, Y. Hu *et al.*, Phys. Rev. Lett. **125**, 247002 (2020).
[5] Y. X. Jiang, J. X. Yin, M. M. Denner *et al.*, Nature Mater. **20**, 1353 (2021).
[6] S. Y. Yang, Y. J. Wang, B. R. Ortiz *et al.*, Sci. Adv. **6**, eabb6003 (2020).
[7] E. M. Kenney, B. R. Ortiz, C. N. Wang *et al.*, J. Phys. Condens. Matter. **33**, 235801 (2021).
[8] K. Y. Chen, N. N. Wang, Q. W. Yin *et al.*, Phys. Rev. Lett. **126**, 247001 (2021).

Authors

K. Y. Chen[a], N. N. Wang[a], Q. W. Yin[b], Y. H. Gu[a], K. Jiang[a], Z. J. Tu[b], C. S. Gong[b], Y. Uwatoko, J. P. Sun[a], H. C. Lei[b], J. P. Hu[a], and J.-G. Cheng[a]

[a]Institute of Physics, Chinese Academy of Science
[b]Renmin University of China

Nearly Room Temperature Ferromagnetism in a Pressure-Induced Correlated Metallic State of van der Waals Insulator $CrGeTe_3$

Uwatoko Group

Discovery of two-dimensional (2D) magnetism in van der Waals (vdW) materials have unfurled diverse range of possibilities for development of novel spintronics, multiferroic and quantum computing devices using atomically

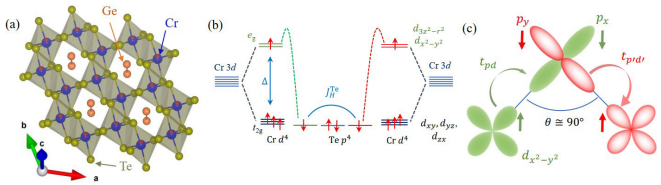

Fig. 1. (a) Single layer of $CrGeTe_3$ illustrating the honeycomb network of edge sharing $CrTe_6$ octahedra. In case of CrX_3, the place of Ge-Ge dimers remains vacant. (b) Crystalline electric field splitting of Cr 3*d* orbitals into t_{2g} - and e_g -manifolds. Δ is the energy difference between t_{2g}- and e_g levels. J_H^{Te} is the Hund's coupling energy at Te site. (c) Schematic picture of indirect superexchange FM interaction between Cr e_g-orbitals via two Te *p*-orbitals. $t_{pd}(t_{p'd'})$is the virtual hopping between e_g (e'_g) and *p* (*p*') orbitals. θ is the geometrical Cr-Te-Cr bond angle.

thin materials [1]. Among the vast pool of vdW materials, $CrGeTe_3$ and CrX_3 (X = Cl, Br, I) are Mott insulators with a charge gap, thus facilitating suitable platforms to exploit both charge and spin degrees of freedom. At low temperature, these insulators share a common layered rhombohedral $R\bar{3}$ -crystal structure held together by weak vdW forces along the *c*-axis. Each single layer consists of a honeycomb network of edge sharing octahedra formed by a central Cr atom bonded to six ligand atoms (Te or X), as illustrated in Fig. 1(a) for $CrGeTe_3$.

The crystalline field effect ensuing from this octahedra splits the Cr-3d orbitals into t_{2g} - and e_g-manifolds [Fig.1(b)]. The onsite Coulomb repulsion localizes the t_{2g}-electrons driving the system into an insulating state significantly well above T_C. Although, a direct antiferromagnetic exchange interaction exists between t_{2g}-electrons, thermal fluctuation inherent to 2D suppress the long-range magnetic order. The spin orbit coupling (SOC) emanating through the covalent bond between ligand *p* and Cr-e_g orbital generates the magnetocrystalline anisotropy energy to counteract the thermal fluctuation. Below T_C, the superexchange interaction between Cr-e_g electrons via two different ligand p-orbitals, as schematically portrayed in Fig.1(c), benefits from the distortion of $CrTe_6$ octahedra and the Hund's energy gain at the ligand Te (or X) site to stabilize the FM order. The correlation between t_{2g}-electrons also move up the ligand *p* bands close to Fermi level, thus opening a band gap between the Cr *d* conduction band and the ligand *p* valence band indicating a charge transfer type Mott behaviour.

However, one drawback for the practical technological application is the low Curie temperature, T_C, mostly below liquid nitrogen temperature. For exploitation of these attributes, it is essential to realize this novel FM state at or close to room temperature. Recently, T_C of $CrGeTe_3$ has been raised around 200 K either by intercalating large organic ions into single crystals [2] or using sophisticated process like electrochemical doping to field effect transistor devices [3]. Although, these results are promising, such filling control methods lead to strong charge inhomogeneity as well as structural and chemical defects, including creation of magnetic impurity, unfavourable for device application.

On the other hand, application of pressure is advantageous, which not only controls the bandwidth but also the spin exchange pathways via subtle modification of bond length and angle between atoms avoiding the complication of disorder. Here, for the first-time we show the evidence of nearly room temperature FM in $CrGeTe_3$ bulk single crystals with application of pressure [4]. Using highly sensitive dc magnetic susceptibility and resistivity measurement under high quality hydrostatic pressure, we found that T_C of $CrGeTe_3$ exceeds 250 K above 9.1 GPa. In Fig. 2, we present

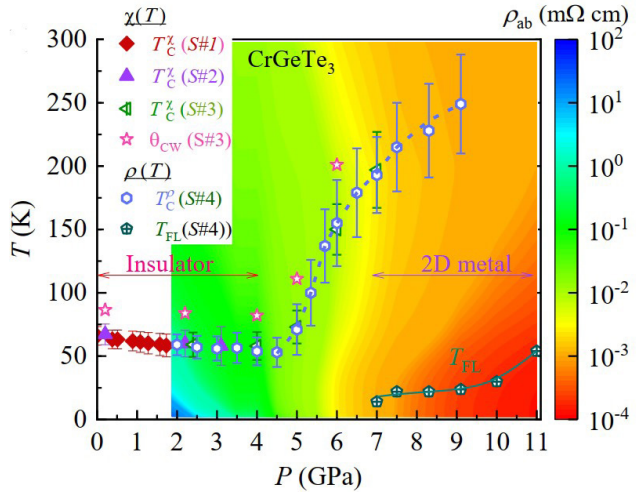

Fig. 2. Pressure temperature phase diagram of $CrGeTe_3$. Color scale represents the magnitude of ρ_{ab}. θ_{CW} and T_C^{χ} respectively are the Curie-Weiss temperature and Curie temperature, estimated from magnetic susceptibility. T_C^{ρ} and T_{FL} are Curie temperature and Fermi liquid temperature determined from ρ_{ab}.

the pressure-temperature phase diagram of $CrGeTe_3$ which uncovers a rare example of bandwidth-controlled insulator-metal transition (IMT) in a vdW materials. Moreover, the remarkable absence of accompanied structural transition and spin crossover involving magnetic to non-magnetic states across IMT, clearly indicates the pressure driven changes of electronic property are purely electronic in origin. Furthermore, these findings show that electronic property of $CrGeTe_3$ can be switched much more responsively using external perturbation, such as strain, doping compared to other vdW insulators.

References

[1] C. Gong *et al.,* Nature, **546**, 265 (2017).
[2] N. Wang *et al.,* J. Am. Chem. Soc, **141**, 17166 (2019).
[3] I. A. Verzhbitskiy *et al.,* Nat. Electron., **3**, 460 (2020).
[4] Dilip Bhoi, J. Gouchi, N. Hiraoka, Y. Zhang, N. Ogita, T. Hasegawa, K. Kitagawa, H. Takagi, K. H. Kim, and Y. Uwatoko, Phys. Rev. Lett. **127**, 217203 (2021)

Authors

D. Bhoi, J. Gouchi, N. Hiraoka[a], Y. Zhang[b], N. Ogita[c], T. Hasegawa[c], K. Kitagawa[a], H. Takagi[a,d,e], K. H. Kim[f,g], and Y. Uwatoko

[a]The University of Tokyo
[b]Southeast University
[c]Hiroshima University
[d]Institute for Functional Matter and Quantum Technologies, University of Stuttgart
[e]Max Planck Institute for Solid State Research
[f]CeNSCMR, Seoul National University
[g]Institute of Applied Physics, Seoul National University

Pressure-Induced Superconductivity in the Excitonic Insulator Candidate Ta_2NiSe_5

Uwatoko Group

Superconductor hosts a condensate of electron pairs (Cooper pairs), which can conduct electricity without any loss of energy. In conventional superconductivity, an attractive interaction mediated by lattice vibrations can lead electrons to form pairs. The bound states through attractive Coulomb attraction between electrons and holes, similar to Cooper pairs in superconductivity, are called excitons. A spontaneous condensation of excitons with lowering temperature is expected to occur due to weakly screened Coulomb interactions in narrow gap semiconductors and semimetals. In that case, the system becomes an insulator known as an excitonic insulator. The excitonic insulator was theoretically proposed more than 50 years ago, however, experimental facts for excitonic state are far from conclusive.

A layered chalcogenide Ta_2NiSe_5 located near the semiconductor-semimetal boundary has in recent years attracted attention as a promising candidate for the excitonic insulator. At ambient pressure, semiconductor-to-insulator transition occurs at $T_c \sim 328$ K, accompanied with a structural phase transition from high-temperature orthorhombic to low-temperature monoclinic. The transition at T_c has been discussed to be the excitonic transition as manifested by the characteristic flattening of the valence band [1]. Furthermore, the control of energy gap using a solid-solution $Ta_2Ni(Se_{1-x}S_x)_5$ and an application of moderate pressure reproduce the canonical phase diagram for the excitonic insulator [2]. Here we show a high-pressure phase diagram of Ta_2NiSe_5 covering the whole range from semiconducting to semimetallic region for the first time, and discovered pressure-induced superconductivity in the semimetallic phase [3].

Figure 1 depicts a pressure-temperature phase diagram of Ta_2NiSe_5 based on bulk measurements under pressure. Ta_2NiSe_5 exhibits a first-order structural transition under pressure at $P_s \sim 3$ GPa, which is accompanied by the change from an almost zero-gap semiconductor to a semimetal. In the pressure-induced semimetallic phase, there appears a transition to another semimetal with a partial-gap at T^*, accompanied with a lattice distortion analogous to that occurs at the excitonic transition at low-pressure semiconducting phase. With increasing pressure, T^* is suppressed and reaches to zero temperature around $P_c \sim 8$ GPa. A dome-like superconducting phase with a maximum $T_{sc} \sim 1.2$ K emerges around P_c. Since the Coulomb interactions between electrons and holes should be screened out substantially due to the increased carrier density, applying pressure changes the character of the gap from excitonic dominant to hybridization gap dominant on increasing the band overlap. Our results evidence the presence of the electron-lattice coupling may be one of the key ingredients for the occurrence of superconductivity and the excitonic transition in the low-pressure phase.

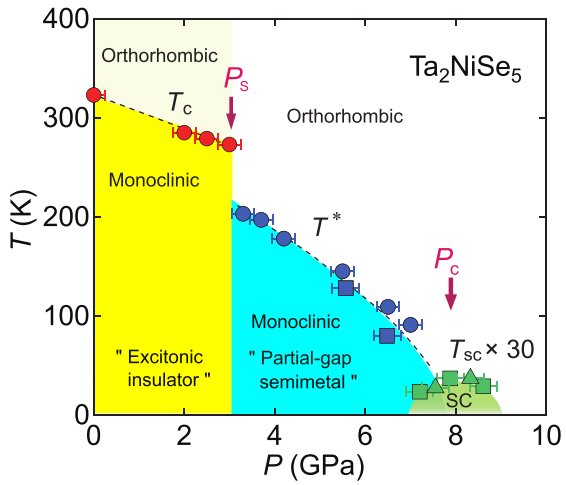

Fig. 1. Temperature-pressure phase diagram of Ta_2NiSe_5 obtained from bulk measurements under pressure. The lines are guides for the eye.

References
[1]Y. Wakisaka, T. Sudayama, K. Takubo, T. Mizokawa, M. Arita, H. Namatame, M. Taniguchi, N. Katayama, M. Nohara, and H. Takagi, Phys. Rev. Lett. **103**, 026402 (2009).
[2]Y. F. Lu, H. Kono, T. I. Larkin, A. W. Rost, T. Takayama, A. V. Boris, B. Keimer, and H. Takagi, Nat. Commun. **8**, 14408 (2017).
[3]K. Matsubayashi, H. Okamura, T. Mizokawa, N. Katayama, A. Nakano, H. Sawa, T. Kaneko, T. Toriyama, T. Konishi, Y. Ohta, H. Arima, R. Yamanaka, A. Hisada, T. Okada, Y. Ikemoto, T. Moriwaki, K. Munakata, A. Nakao, M. Nohara, Y. Lu, H. Takagi, and Y. Uwatoko, J. Phys. Soc. Jpn. **90**, 074706 (2021).

Authors
K. Matsubayashi[a], H. Okamura[b], T. Mizokawa[c], N. Katayama[d], A. Nakano[d], H. Sawa[d], T. Kaneko[e], T. Toriyama[e], T. Konishi[e], Y. Ohta[e], H. Arima[a], R. Yamanaka, A. Hisada[b], T. Okada, Y. Ikemoto[f], T. Moriwaki[f], K. Munakata[g], A. Nakao[g], M. Nohara[h], Y. Lu [i], H. Takagi[i], and Y. Uwatoko
[a]The University of Electro-Communications
[b]Tokushima University
[c]Waseda University
[d]Nagoya University
[e]Chiba University
[f]JASRI
[g]CROSS
[h]Hiroshima University
[i]The University of Tokyo

Difference in Curvature Sensing of Isotropic and Anisotropic Curvature-Inducing Proteins

Noguchi Group

In living cells, biomembrane shapes are controlled by various curvature-inducing proteins. We have studied the binding of these proteins using mean-field theories. Clathrin and coat protein complexes bend membranes in a laterally isotropic manner and generate spherical buds. In contrast, Bin/Amphiphysin/Rvs (BAR) superfamily proteins bend the membrane along their BAR domain axes and generate cylindrical membrane tubes. The former and latter proteins can be modeled as laterally isotropic objects and anisotropic objects of a crescent elliptic shape, respectively.

For isotropic proteins, we derived the free energy, including the Gaussian curvature and area expansion by the protein insertion [1]. Then, we investigated the formation of spherical buds [1] and binding onto a tethered vesicle [2]. Experimentally, a narrow membrane tube (tether) is elongated from a spherical vesicle by an external force imposed by a micropipette and optical tweezers. A first-order transition occurs between a small number of large buds and a large number of small buds with increasing chemical potential of protein binding [2]. For the tethered vesicle, interestingly, a first-order transition occurs twice between low and high protein densities in the tube. The force-dependence curves of the protein density in the membrane tube and the tube curvature are reflection symmetric and point symmetric, respectively, from the force point, in which the tube curvature matches the protein (sensing) curvature (see Figs. 1(a) and (b)) [2]. This theory reproduces the meshless membrane simulation results of the homogeneous phases very well. In addition, beaded-necklace-like tubes with microphase separation were found in the simulation.

For anisotropic proteins, an orientational-dependent excluded volume interaction is included in the free energy. We studied binding onto membrane tubes [3]. The proteins exhibit a second-order or first-order nematic transition with increasing protein density for intermediate and small radii of

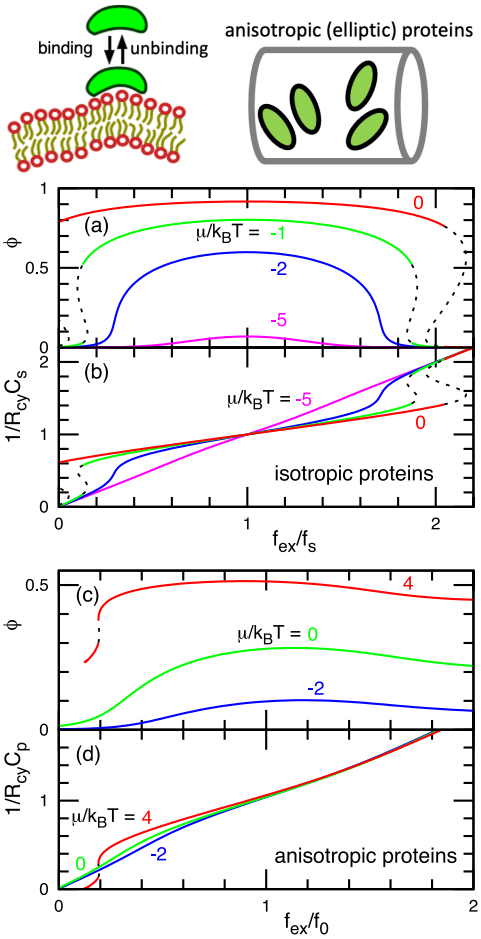

Fig. 1. Binding of proteins onto tubular membranes. External force f_{ex} dependence of protein density φ and tube radius R_{cy}. (a),(b) Isotropic proteins with sensing curvature C_s. (c),(d) Anisotropic proteins with a spontaneous curvature C_p along proteins axis. With increasing binding chemical potential m, more proteins are bound.

the membrane tube, respectively. The tube curvatures for the maximum protein binding (sensing) and orientational order are differently varied by the protein density and rigidity. As the external force along the tube axis increases, a first-order transition from a large tube radius with low protein density to a small radius with high density occurs only once, and subsequently, the protein orientation tilts to the tube-axis direction (see Figs. 1 (c) and (d)). The density-dependent sensing curvature and the number of transitions are characteristics due to the anisotropic bending energy. In contrast, each isotropic protein has a constant sensing curvature. This density-dependent sensing curvature has been measured in the experiment of BAR proteins. This theory quantitatively reproduces the results of meshless membrane simulation for short proteins. For long proteins, the formation of protein clusters generates a quantitative deviation from the theory, although qualitative agreements still hold.

The present theories can be used to estimate the bending rigidity and curvature of bound proteins in experiments and atomistic simulations. These mechanical parameters are keys to quantitatively understand the curvature sensing and generation of proteins.

References
[1] H. Noguchi, Phys. Rev. E **104**, 014410 (2021).
[2] H. Noguchi, Soft Matter **17**, 10469 (2021).
[3] H. Noguchi, C. Tozzi, and M. Arroyo, Soft Matter **18**, 3384 (2022).

Author
H. Noguchi

Structure of Glass-Forming Molecular Liquids under High Pressure

Yamamuro Group

Glass transition is one of the most important unsolved problems in condensed matter physics. The history of the glass transition study might start when Giauque found a heat capacity jump of glycerol in 1923 [1]. After that many people have studied the mechanism of the glass transition both through experimental and theoretical approaches. High pressure studies have played important roles in the glass transition research since they provide direct information for the validity of the two important concepts of the mechanism of the glass transition; i.e., the entropy theory and free-volume theory. At present, the entropy theory, particularly Adam-Gibbs (AG) theory [2], is dominant to explain thermodynamic properties of the glass transition [3] and the pressure dependence of the glass transition temperature (T_g) [4]. An extended version of the AG theory, random first-order transition (RFOT) theory [5], can also explain the non-linear dynamics of the glass transition. Molecular liquids are important materials in the glass transition research since they are similar to the systems treated in theoretical and computer simulation studies. We are interested in van der Waals molecules which are condensed only by the van der Waals interaction, and hydrogen-bonding molecules which have network structures formed by intermolecular hydrogen bonds.

Recently, we have measured X-ray diffraction (XRD) data of toluene ($C_6H_5CH_3$, T_g = 117 K) and glycerol [$(CH_2(OH)CH(OH)CH_2(OH)$, T_g = 187 K] under high pressures (toluene: < 0.9 GPa, glycerol: < 3.6 GPa) at RT. This work is a collaboration with Prof. Yoshio Kono (Ehime Univ.). We used a Paris-Edinburg cell and BL37XU, SPring-8, on which very precise horizontal focusing and collimation are available.

Figure 1 shows the structure factors of toluene at 0.9 GPa. The result of the MD simulation (AMBER force field, 0.2 ns, 500 molecules) is also shown. The MD simulation well reproduces the experimental data. Good agreement was obtained also for the data at 0 and 0.4 GPa. Figure 2 shows the pair distribution functions $g(r)$ of aromatic (benzene-ring) carbons obtained by the MD simulations. As the density (pressure) increases, three peaks between 3 and 6 Å become more prominent. These peaks are known to be due to the T-type pair correlation as shown in the inset. It is noteworthy that this trend is the same as the cooling effect at ambient pressure. Hence, we concluded that the AG concept is valid also for the glass transition by pressurization.

On the other hand, the structure factor of glycerol cannot be reproduced by the MD simulation using the potential parameters at ambient pressure. Therefore, we performed ab initio (Car-Parrinello) MD simulations using a smaller system (50 molecules) and shorter simulation time (0.15 ps) to determine the short-range structure, and then adjusted the Lenard-Jones parameters as a function of pressure so as to reproduce the $g(r)$ obtained by the ab initio MD. Figure 3 shows the structure factors using the adjusted potential parameters. Good agreement is obtained between the experimental and MD data. Form the obtained structure, we found that the molecular structure is deformed to be more compact keeping hydrogen bonds. The C-O intermolecular correlation is also important under high pressure. The present conclusion is quite different from the common sense that

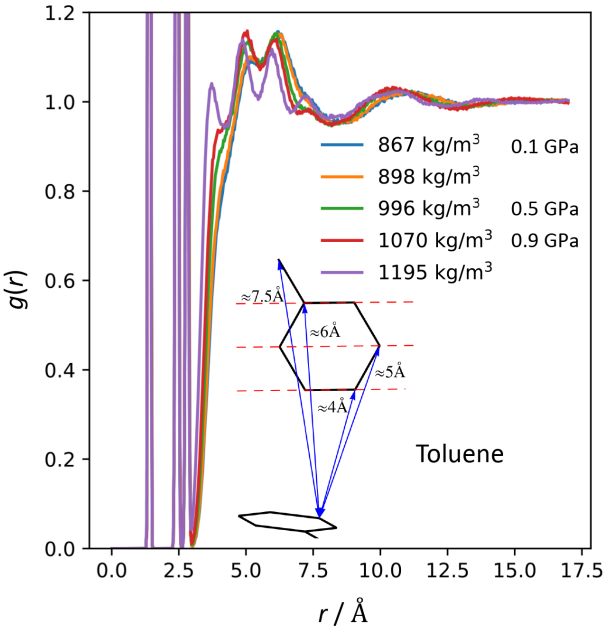

Fig. 2. Pair distribution function for aromatic carbon atoms of toluene. Preferred pair correlation is shown by inset.

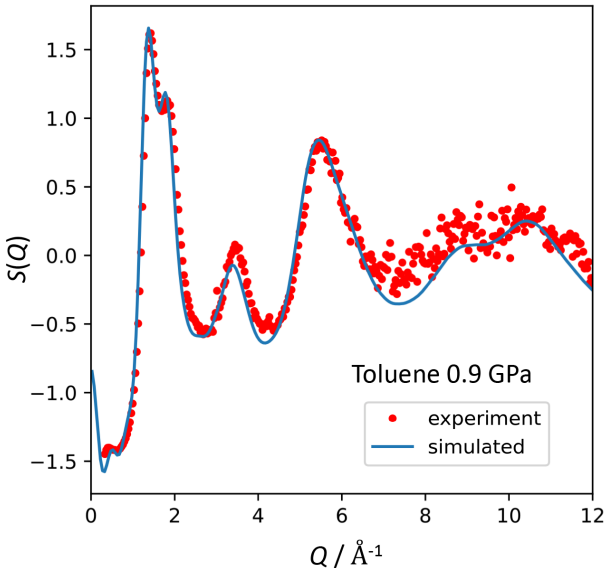

Fig. 1. Structure factor of toluene at 0.9 GPa.

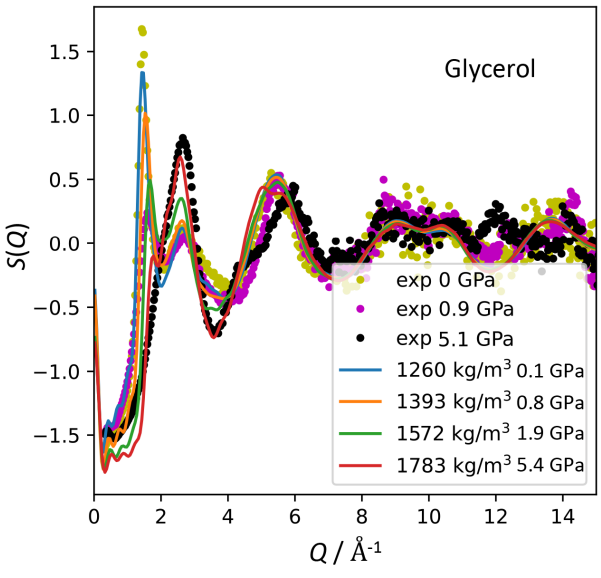

Fig. 3. Structure factor of glycerol under high pressure.

hydrogen bonds are just broken by pressurization. A neutron diffraction experiment is under planning to determine the position of the hydrogen atoms and make clearer discussion on the competing hydrogen-bond and van der Waals interactions under high pressure.

References

[1] G. E. Gibson and W. F. Giauque, J. Am. Chem. Soc. **40**, 93 (1923).
[2] G. Adam and J. H. Gibbs, J. Chem. Phys. **43**, 139 (1965).
[3] S. Tatsumi *et al*., Phys. Rev. Lett. **109**, 045701 (2012).
[4] O. Yamamuro *et al*., J. Non-Cryst. Solids, **183**, 144 (1995).
[5] T. R. Kirkpatrick *et al*., Phys. Rev. A **40**, 1045 (1989).

Authors

Y. Zhao, H. Akiba, N. Kondo[a], Y. Kono[a], and O. Yamamuro
[a]Ehime University

Nontrivial Temperature Dependence of Magnetic Anisotropy in Multiferroics $Ba_2MnGe_2O_7$

Masuda group

Spin-driven multiferroics have been extensively studied since the discovery of an enhanced magnetoelectric effect in $TbMnO_3$. Through spin-orbit coupling (SOC), a spin order induces a change of charge distribution, leading to emergence of electric polarization. The microscopic mechanisms of the multiferroics are categorized into three types: the spin current, the exchange striction, and the spin dependent *d-p* hybridization. A notable feature of the third one is that hybridized *d* and *p* orbitals of magnetic ion and ligand are modulated by spin states via SOC, and this induces an electric polarization. The relation between the electric polarization $\boldsymbol{P}$ and the spin moment $\boldsymbol{S}$ is locally described. The mechanism has been identified in several compounds including åkermanite compounds $Ba_2CoGe_2O_7$. Since the direction of the local spin moment determines the direction of the electric polarization, magnetic anisotropy plays a key role in forming multiferroic structure, *i.e.*, the simultaneous structures of the spin and polarization. The magnitude of the anisotropy gives the energy scale for the control of the magnetism by the electric field as well as magnetic field. Although the temperature (T) dependence of the anisotropy gap in magnon spectrum in a conventional magnet scales as a power of the sublattice magnetic moment, it may not be the case for the multiferroics. The change of the polarization with T affects the spin-interaction parameters through the *d-p* hybridization, which can lead to a nontrivial behavior in T dependence of the anisotropy and a low-energy spin dynamics. Here we study spin dynamics on a square-lattice antiferromagnet $Ba_2MnGe_2O_7$ known as multiferroic compound by using a state-of-art spectrometer with ultra-high resolution.

Figure 1(a) shows the INS spectrum measured at 0.05 K. Two dispersive modes with the boundary energy of 0.55 meV and with gaps ~ 0.05 meV and ~ 0.1 meV are clearly observed. The gap of the low-energy (T_1) mode is ascribed to easy-axis anisotropy in the square lattice by spin nematic interaction/electric polarization interaction; $\mathcal{H}_N = \sum_{i,j} J_N O_i^{XY} O_j^{XY} = \sum_{i,j} J_P P_i^Z P_j^Z$, where J_N is nematic interaction, O^{XY} is Stevens operator, and J_P is an effective interaction between the electric polarizations. Anisotropy gap of the high-energy (T_2) mode is ascribed to easy-plane anisotropy by a single-ion anisotropy. We find that the former gap is

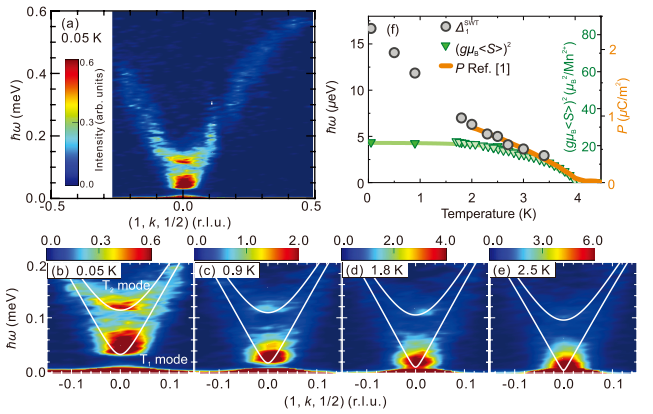

Fig. 1. Inelastic neutron scattering (INS) spectra. (a) False color plot of the INS spectrum measured at 0.05 K projected onto the $\hbar\omega$ - (1, k, 1/2) plane. The spectrum is integrated in the range of $0.9 \le h \le 1.1$ and $0.45 \le l \le 0.55$. White solid curves are calculated magnon-dispersions. (b)-(e) The INS spectra focused on the low-energy range measured at (b) 0.05 K, (c) 0.9 K, (d) 1.8 K and (e) 2.5 K. White solid curves are calculated dispersions. (f) T dependences of Δ_1^{SWT} (black circles), electric polarization P (orange curve from Ref. [1]) and the second power of the sublattice moment (light green triangles).

drastically suppressed with the increase of T, while the latter gap is moderately suppressed as shown in Figs. 1(b)-1(e). We also find that J_N is strongly dependent on T.

T dependences of the easy-axis anisotropy Δ_1^{SWT}, a scaled electric polarization P, and the second power of the scaled sublattice moment $(g\mu_B S)^2$ are shown in Fig. 1(f). We find that Δ_1^{SWT} does not scale as $(g\mu_B S)^2$, but is rather consistent with the temperature dependence of P. Indeed, our spin-wave calculation including the spin nematic term $\mathcal{H}_N$ exhibits that the formula of the anisotropy gap is proportional to P. Furthermore, the calculation shows that the drastic T dependence of J_N results from the change of orbital with T; the modification of the hybridized orbitals of Mn^{2+} and O^{2-} ions with T leads to a small change of the energy, which is negligible in highly anisotropic system but is enhanced in the nearly isotropic system such as the symmetric half-filled shell of Mn^{2+} ion, and it is probed as the change of J_N thorough SOC. We, thus, find a characteristic quasiparticle of the multiferroics originating from the hybridization of spin and orbital momenta.

References

[1] H. Murakawa, Y. Onose, S. Miyahara, N. Furukawa, and Y. Tokura, Phys. Rev. B **85**, 174106 (2012).
[2] S. Hasegawa, S. Hayashida, S. Asai, M. Matsuura, I. Zaliznyak, and T. Masuda, Phys. Rev. Research **3**, L032023 (2021).

Authors

S. Hasegawa, S. Hayashida, S. Asai, M. Matsuura[a], I. Zaliznyak[b], and T. Masuda
[a]CROSS
[b]Brookhaven National Laboratory

Polarized Neutron Scattering Study on a Centrosymmetric Skyrmion Host Gd_2PdSi_3

Nakajima Group

Gadolinium based intermetallic compounds have been intensively investigated since the discovery of magnetic skyrmion lattice, which is topologically-nontrivial vortex-like spin texture, with the large topological Hall effect in a

triangular lattice itinerant magnet Gd_2PdSi_3 [1]. Although magnetic skyrmions were discovered in chiral ferromagnets such as MnSi [2], the recent study on Gd_2PdSi_3 has demonstrated that centrosymmetric magnets can also host magnetic skyrmions owing to coupling between local magnetic moments and conduction electrons. Subsequent studies on a breathing kagome system $Gd_3Ru_4Al_{12}$ [3] and a tetragonal magnet $GdRu_2Si_2$ [4] also reported emergence of skyrmion lattice states. In these studies, resonant X-ray magnetic scattering techniques were used because the L_2 absorption edge of Gd is located at 7.935 keV, which is suited for conventional scattering measurements. By analyzing light polarizations of scattered X-rays, magnetic structures in these compounds were investigated. However, resonant X-ray scattering is quite sensitive not only to the magnetic moments but also charge density waves. A recent STM study on $GdRu_2Si_2$ reported possible coexistence of magnetic and charge modulations [5]. To verify the magnetic structures in Gd-based skyrmion systems, we employ polarized neutron scattering technique, which can unambiguously distinguish magnetic modulations from charge/nuclear modulations.

In the present study, we focus on Gd_2PdSi_3, in which the triangular skyrmion lattice state was discovered in the first field-induced phase. In zero field, this system exhibits two magnetic phase transitions, which were identified by previous specific heat measurements, below 21 K. According to the previous resonant X-ray study, the ground state has screw-type magnetic modulations, while the thermally-induced phase was not investigated in detail. We thus studied the temperature evolution of the magnetic order near zero magnetic field by means of polarized neutron scattering.

Gd is one of the strongest neutron absorbers, and thus we used an isotope-enriched $^{160}Gd_2PdSi_3$ crystal, which has relatively weak absorption, for the present study. The experiment was performed at the polarized neutron triple-axis neutron spectrometer PONTA in JRR-3. The sample was mounted in a closed-cycle refrigerator with the $(H,K,0)$ scattering plane. The spectrometer was operated in the P_{zz} and P_{xx} longitudinal polarization analysis modes. In the former mode, the direction of the neutron polarization is perpendicular to the horizontal scattering plane. In the latter, neutron polarization is set to be parallel or antiparallel to the scattering vector Q $(= k_i - k_f)$.

Figure 1(a) shows a polarized neutron scattering profile of a magnetic Bragg reflection at $(0,q,0)$ measured at 2.5 K. Red and blue symbols correspond to spin-flip (SF) and non-spin-flip (NSF) scattering intensities, which are proportional to Fourier-transformed magnetic moments parallel to the c axis and those perpendicular to both the c axis and q-vector, respectively. Note that NSF signals may also be attributed to a charge or lattice modulation with the same q-vector. We thus measured the same reflection with the P_{xx} configuration, in which all the magnetic signals are observed only in the SF channel. As shown in Fig. 1(b), we found that the reflection does not contain NSF intensity, demonstrating that the reflection at $(0,q,0)$ is purely magnetic. We thus conclude that the magnetic structure in the ground state is an elliptic screw-type structure. We also measured temperature dependence of the SF and NSF intensities with varying temperature, and found that the c-axis component of the magnetic moments disappears upon the phase transition to the intermediate phase. More detailed analyses are ongoing and will be published elsewhere.

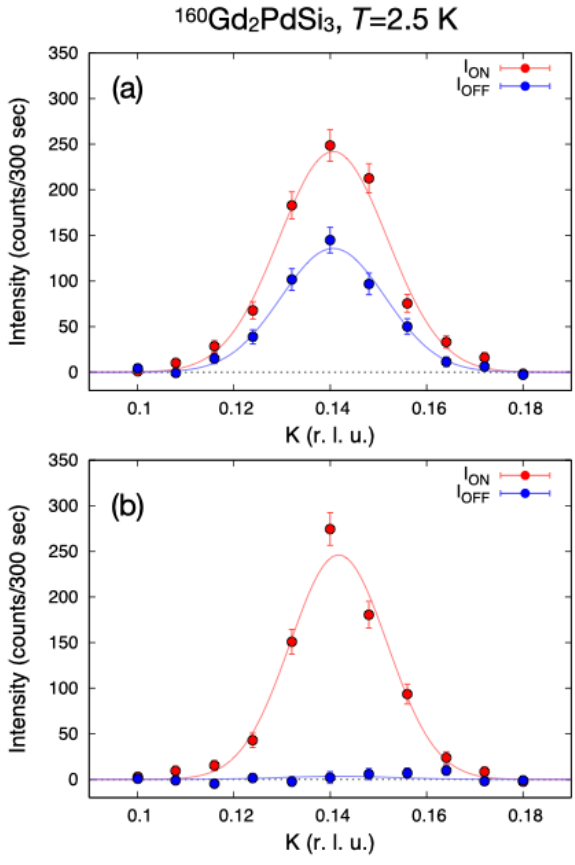

Fig. 1. Polarized neutron scattering profile of a magnetic Bragg reflection at (0,q,0) measured at 2.5 K in (a) P_{zz} and (b) P_{xx} configurations.

References

[1] T. Kurumaji *et al*., Science. **365**, 914 (2019).
[2] S. Muhlbauer *et al*., Science **323**, 915 (2009).
[3] M. Hirschberger *et al*., Nat. Commun. **10**, 5831 (2019).
[4] N. D. Khanh *et al*., Nat. Nanotech. **15**, 444 (2020).
[5] Y. Yasui *et al*., Nat. Commun. **11**, 5925 (2020).

Authors
J. Ju, H. Saito, and T. Nakajima

Tough and Highly Recoverable Hydrogel Reinforced by Strain-Induced Crystallization

Mayumi Group

Hydrogels, cross-linked polymer networks containing water, are expected to be applied for biomaterials such as artificial cartilage, ligaments, and prosthetic joints due to their high water content and biocompatibility. For the applications as the biomaterials, the mechanical toughness and instant recoverability are needed because artificial ligaments and prosthetic joints should survive under repeated high stress at a high frequency (ex. 1 Hz). Most tough hydrogels are reinforced by introducing sacrificial structures that can dissipate input energy [1]. However, since the sacrificial damages cannot recover instantly, the toughness of these gels drops substantially during consecutive cyclic loadings. In this work, we have developed for the first time a tough and instantly recoverable hydrogels utilizing strain-induced crystallization (SIC) [2].

We used slide-ring (SR) gel containing movable figure-of-eight cross-links that work as pulleys to eliminate stress heterogeneities during deformation. SR hydrogel was

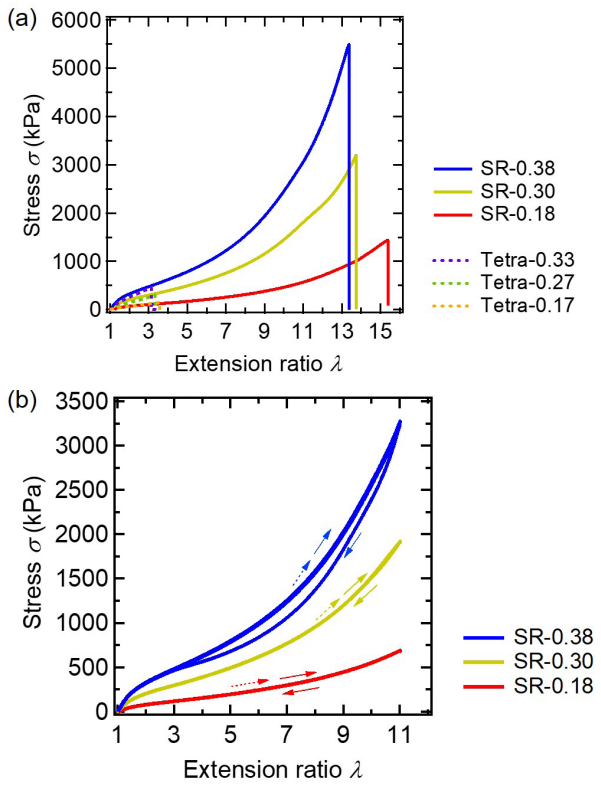

Fig. 1. Stress-extension ratio curves of SR and Tetra gels, (b) loading-unloading curves of SR gels under repeated cyclic stretching.

prepared from polyrotaxane in which only 2 % of its polyethylene glycol (PEG) axis was threaded with a-cyclodextrin (CD) rings. The CDs are covalently cross-linked by adding cross-linkers. The slidable cross-linking points in SR gels can slide on the PEG chains to homogenize stress in the polymer network. For comparison, fixed cross-link PEG gels were prepared via end-crosslinking of Tetra-armed PEG prepolymers. The PEG concentrations and molecular weights of polymer strands between cross-linking points in the Tetra gels were almost the same as those in the SR gels.

Fig. 1 (a) shows the tensile stress–extension ratio curves until rupture for the SR and Tetra gels. The SR gels can survive at higher stress (> 5 MPa) and higher strain (> 1000%) compared with the Tetra-PEG gels. The toughness of the SR gels is comparable to that of the most tough polymer gel with the breakable sacrificial structure. Also, as shown in Fig.1 (b), the mechanical hysteresis of the SR gels under repeated cycle is quite small, and the instant recovery of extension energy between two consecutive cycles is 95 %, which is much higher than the low recoverability of the tough polymer gels having breakable structure (< 50%).

The high toughness of the SR gels originates from strain-induced crystallization (SIC). As shown in Fig. 2, at large strains, we observed diffraction spots in the wide-angle X-ray scattering (WAXS) patterns, indicating the occurrence of SIC of the stretched PEG chains. On the other hand, no diffraction spots were observed for the Tetra gels. The slidability of the cross-liinking points homogenizes the orientation and deformation of PEG chains, which results in the remarkable high toughness of the SR gels. During the unloading process, the strain-induced crystalline structure disappeared immediately. The reversible formation/destruction of the PEG crystals under repeated cycles leads to the high mechanical reversibility of the SR gels.

Although SIC has been reported in rubbers without any

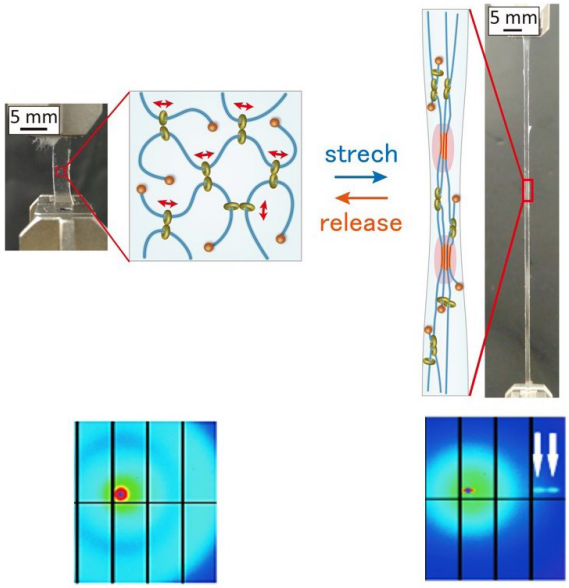

Fig. 2. Schematic illustration and WAXS patterns of SR gels.

solvent, it is the first time to discover the reversible SIC in polymer gels with much lower polymer concentrations. This self-reinforcement strategy by SIC is a novel concept for realizing simultaneously high mechanical toughness and rapid recoverability under cyclic deformation, which are required for the biomedical materials for artificial joints and ligaments.

References
[1] J. P. Gong, Soft Matter **6**, 2583 (2010).
[2] C. Liu, N. Morimoto, L. Jiang, S. Kawahara, T. Noritomi, H. Yokoyama, K. Mayumi, K. Ito, Science **372**, 1078 (2021).

Author
K. Mayumi

Phase Transition in $5d^1$ Double Perovskite Ba_2CaReO_6 Induced by High Magnetic Field

Kindo, Y. Matsuda, and Hiroi Groups

Physical properties emerging from the combination effect of electron correlation and spin-orbit coupling have attracted considerable attention in the last decade. In 5*d* transition metal ions with partially filled t_{2g} orbital, large spin-orbit coupling of 0.4 eV may entangle the effective orbital angular momentum and the spin angular momentum. The electronic state is described by the effective total angular momentum J_{eff}. For example, an unpaired electron in the d^1 ion in the cubic octahedral crystal field occupies the J_{eff} = 3/2 quartet. In solids, interactions among spin-orbital entangled electrons may give rise to exotic ground states such as a spin liquid and multipolar orders. When the d^1 ions with the J_{eff} = 3/2 state interact on the face-centered-cubic (FCC) lattice, unconventional ground states such as multipolar orders, spin-orbit dimer phase, and spin-orbital liquid may emerge. In the multipolar ordered states, magnetic dipolar, electric quadrupolar, and magnetic octupolar moments can be the order parameter. Magnetic properties of double perovskite-type oxides, chlorides, bromides, and lacunar spinel selenides have been investigated as Mott insula-

tors with the J_{eff} = 3/2 state on the FCC lattice [1-4]. These examples demonstrate that various multipolar and dimer orders can be realized by applying a certain perturbation via non-magnetic cations and ligand anions.

Another way for exploring a novel electronic phase is applying strong magnetic field comparable to the magnitude of interactions among electrons. In the spin-1/2 Heisenberg model on the tetragonally distorted FCC lattice as seen in the rhenium double perovskite oxides at low-temperature, successive field induced magnetic phases including the 1/2-magnetization plateau may appear in the magnetization process. While the electric quadrupoles do not couple with magnetic field directly, a possibility of magnetic field induced quadrupolar transition has been discussed in CeB_6, where the Ce atom with $4f^1$ electron configuration has Γ_8 quartet ground state of which symmetry is identical to the J_{eff} = 3/2 quartet.

We focused on a rhenium double perovskite oxide Ba_2CaReO_6, which is a candidate of the J_{eff} = 3/2 Mott insulator with Re^{6+} ($5d^1$) ions. The magnetization of Ba_2CaReO_6 was measured in the pulsed high magnetic field by changing the maximum magnetic field values up to 66 T as shown in Fig. 1 [5]. The magnetization curve at 4.2 K deviates from the linear behavior around 35 T and exhibits a steep increase at around 45 T, indicating the presence of a magnetic field induced phase transition. The full magnetic moment of Ba_2CaReO_6 estimated from the effective magnetic moment is 0.38 μ_B and thus the magnetization of 0.2 μ_B at the high field region is clearly smaller than the full moment. The magnetic field induced phase transition in Ba_2CaReO_6 was also clearly detected in the magnetostriction $\Delta L/L_{0T}$ measured at 4.2 K as shown in Fig. 2. The longitudinal magnetostriction is positive and amounts to 2-3 $\times 10^{-4}$ at around 60 T, while the transverse magnetostriction is negative and amounts to ~1 $\times 10^{-4}$ at around 60 T. The longitudinal magnetostriction is plotted against magnetization in the inset of Figure 2. The magnetostriction changes quadratically to magnetization up to around 40 T. The deviation from the quadratic behavior is observed as increasing the field, suggesting a change in the way of spin-lattice coupling via orbital degrees of freedom. The magnetic field induced phase transition is attributed to the transition from the collinear to the canted antiferromagnetic orders with possible changes in the orbital states. Ba_2CaReO_6 would reside in the parameter regime close to the boundary between the two magnetic orders, representing a suitable material for investigating the interplay between the spin-orbital entangled electrons and magnetic field.

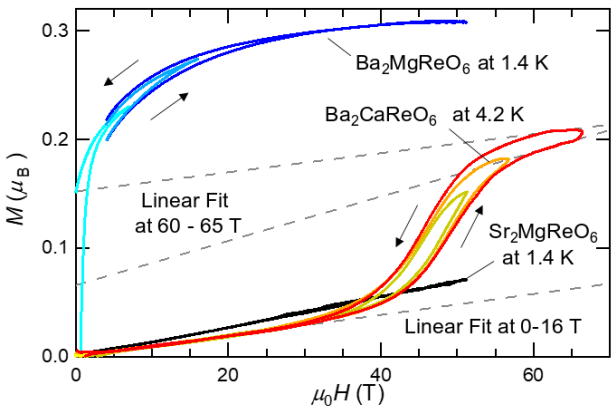

Fig. 1. Magnetization curves of Ba_2CaReO_6 measured up to 66 T (red) and those of relative compounds Ba_2MgReO_6 (blue) and Sr_2MgReO_6 (black).

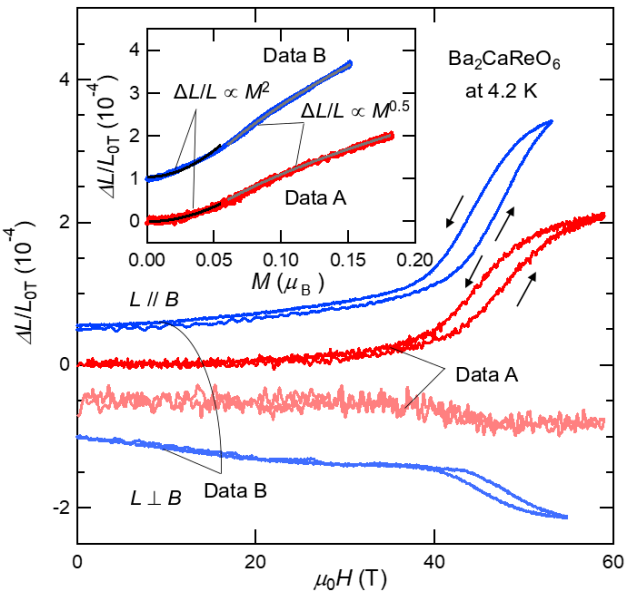

Fig. 2. Magnetostriction $\Delta L/L_{0T}$ of Ba_2CaReO_6 measured at 4.2 K. The magnetostriction with positive and negative values correspond to the longitudinal and transverse magnetostriction, respectively. The longitudinal magnetostriction is plotted against the magnetization in the inset.

References

[1] H. Ishikawa, T. Takayama, R. K. Kremer, J. Nuss, R. Dinnebier, K. Kitagawa, K. Ishii, and H. Takagi, Phys. Rev. B, **100**, 045142 (2019).
[2] H. Ishikawa, T. Yajima, A. Matsuo, Y. Ihara, and K. Kindo, Phys. Rev. Lett. **124**, 227202 (2020).
[3] H. Ishikawa, T. Yajima, A. Matsuo, and K. Kindo, J. Phys.: Condens. Matter **33**, 125802 (2021).
[4] D. Hirai, H. Sagayama, S. Gao, H. Ohsumi, G. Chen, T. Arima, and Z. Hiroi, Phys. Rev. Research **2**, 022063 (2020).
[5] H. Ishikawa, D. Hirai, A. Ikeda, M. Gen, T. Yajima, A. Matsuo, Y. H. Matsuda, Z. Hiroi, and K. Kindo Phys. Rev. B **104**, 174422 (2021).

Authors

H. Ishikawa, D. Hirai, A. Ikeda, M. Gen, T. Yajima, A. Matsuo, Y. H. Matsuda, Z. Hiroi, and K. Kindo

New Material Exhibiting the Interplay between Non-magnetic 3*d*-electron Kagome Bands and 4*f*-electron Magnetism

Kindo, Ozaki, and Tokunaga Groups

Kagome lattice, a two-dimensional network made of corner shared triangles, has attracted condensed matter physicists as a platform for realizing novel electronic states. A localized spin system on the kagome lattice is a typical example that exhibits a quantum spin liquid ground state due to the geometrical frustration. Itinerant electrons on the kagome lattice produces a band structure with uncommon features such as a Dirac point, van Hove singularity, and a flat band and may host unconventional density wave orders or superconductivity. Experimentally, 3*d* transition metal compounds with kagome lattice have been investigated in search for novel correlated electronic phases. Kagome cuprates are candidates for the Mott insulator with a quantum spin liquid ground state. Intermetallic compounds with the kagome layers of Cr, Mn, Fe, and Co have been investigated in recent years as a metal with large anomalous Hall effect and novel band structures. Recently, a series of vanadium

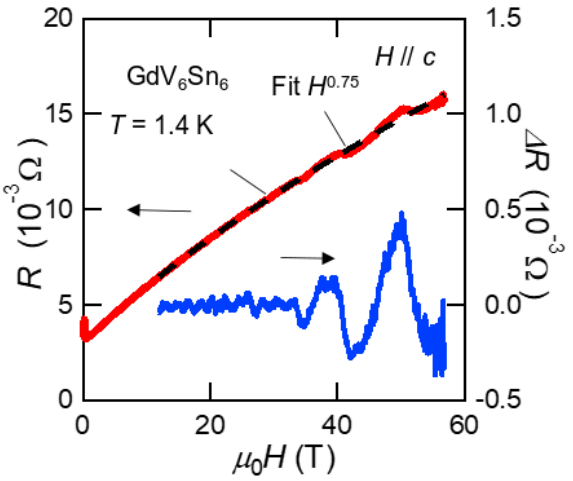

Fig. 1. Magnetoresistance of GdV_6Sn_6 at 1.4 K measured up to 56 T in pulsed magnetic field. A fit to $H^{0.75}$ magnetic field dependence, which is used to estimate the oscillating component ΔR, is shown by the dashed line.

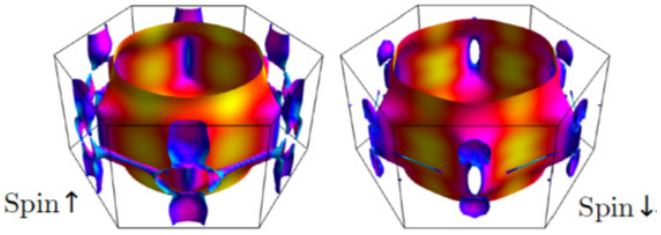

Fig. 2. Fermi surface plot of GdV_6Sn_6 including the effect of spin splitting.

antimonide AV_3Sb_5 (A = K, Rb, Cs) have attracted considerable attention as a new member of the kagome metal. AV_3Sb_5 compounds exhibit various phenomena such as the co-existence of charge density wave (CDW) order and superconductivity and the anomalous Hall effect without a magnetic order, suggesting that vanadium kagome metal is a promising platform for investigating unconventional electronic properties. Kagome layers made of vanadium are found in a series of stannide RV_6Sn_6 (R = Rare Earth), which are discovered in 2011 in the polycrystalline form [1]. Their physical properties are not investigated in the first report. The short V-V distances of approximately 2.7 Å may produce metallic conductivity within the kagome layer as seen in AV_3Sb_5. The variety of the rare earth ions, which separate the kagome layers instead of alkaline metals in AV_3Sb_5, may allow us to tune the physical properties.

We synthesized the high-quality single crystals of GdV_6Sn_6 and YV_6Sn_6 and investigate their electronic properties for the first time [2]. We revealed that GdV_6Sn_6 exhibits unique magnetotransport properties at low-temperature such as non-linear Hall resistivity and increase of resistance R in magnetic field H as $R \sim H^{0.75}$ up to 56 T with Shubnikov–De Haas oscillations as shown in the Fig. 1. The first principles band structure calculations revealed the presence of multiple Fermi surfaces with Dirac-like band crossings near the Fermi-energy as shown in the Fig. 2. The presence of multiple carriers is consistent with the non-linear Hall resistivity. The observed Shubnikov–De Haas oscillations can be attributed to the small Fermi pockets. The non-magnetic analogue YV_6Sn_6 turned out to exhibit similarly non-linear Hall resistivity, suggesting the two compounds host common electronic structure arising from the V-kagome layer. Moreover, a magnetic transition was observed at 5 K in GdV_6Sn_6. The magnetic order causes the negative magnetoresistance at weak magnetic field region below 1 T, which is absent in the non-magnetic YV_6Sn_6, pointing to a coupling between Gd-spins on the triangular lattice and carriers in the V-kagome layer. Our results demonstrate that RV_6Sn_6 family including GdV_6Sn_6 provide a new class of material to investigate the interplay between itinerant non-magnetic 3d-electron with bands inherent to the kagome lattice and magnetism of the 4f-electron on the triangular lattice.

References
[1] L. Romaka, Y. Stadnyk, V. V. Romaka, P. Demchenko, M. Stadnyshyn, and M. Konyk, J. alloys compd. **509**, 8862 (2011).
[2] H. Ishikawa, T. Yajima, M. Kawamura, H. Mitamura, and K. Kindo, J. Phys. Soc. Jpn. **90**, 124704 (2021).

Authors
H. Ishikawa, T. Yajima, M. Kawamura, H. Mitamura, and K. Kindo

Extraordinary π-electron Superconductivity in a Doped Quantum Spin Liquid

Kindo and Kohama Group

The realization of high-T_c superconductivity is one of the holy grails of condensed matter physics. As one idea to achieve this, P. W. Anderson proposed a possible pathway to the glory in 1987 just after the discovery of the high-T_c cuprates [1]. Strong geometric frustration of magnetically interacting spins suppresses magnetic orders, resulting in a quantum spin liquid (QSL) state. Sufficient carrier doping into a QSL yields mobility of the electrons keeping the correlated spin correlations, which perhaps lead to high-T_c charged superconducting pairs using the spin fluctuations. Nevertheless, it has been challenging to make superconductivity in a doped QSL stable in actual materials, and thus, the experimental understanding of the frustration effect on superconductivity has been less well developed.

Recently, several papers [2,3] reported that the organic superconductor, κ-(BEDT-TTF)$_4$Hg$_{2.89}$Br$_8$ (κ-HgBr), is one of the most plausible candidates for doped QSLs hosting superconductivity. This salt is classified into the strongly correlated dimer-Mott system and has the almost regular

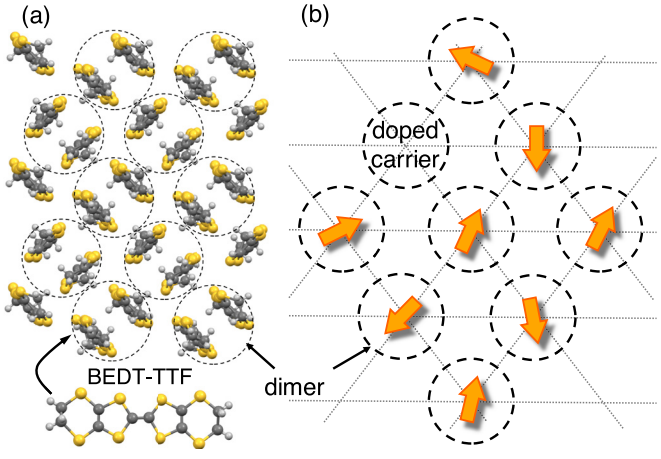

Fig. 1. (a) Molecular arrangement of the organic molecules in the two-dimensional organic layers in κ-HgBr. The dotted circles denote the molecular dimers forming the triangular lattice. (b) Schematic of the dimer lattice. The arrows represent spins of π-electrons.

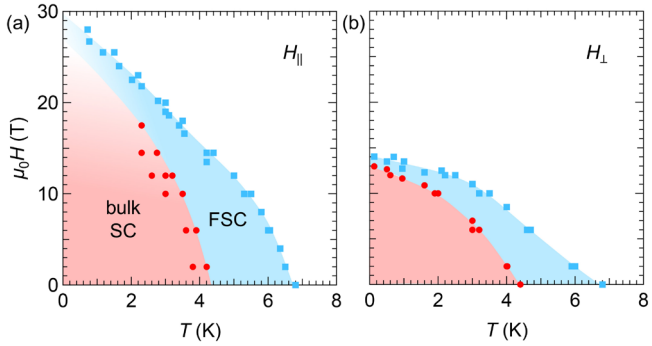

Fig. 2. Field-temperature superconducting phase diagrams in parallel (a) and perpendicular (b) fields. The blue and red shaded areas highlight the regions of the fluctuating superconductivity (FSC) and bulk superconductivity, respectively. The circles denote T_c whereas the boxes signify temperatures where FSC appears.

triangular lattice of the dimers, as shown in Fig. 1. Indeed, its magnetism can be described by antiferromagnetically interacting spins on a triangular lattice and does not exhibit any magnetic orders even at low temperatures. Thanks to the carrier doping by the nonstoichiometric ratio of the HgBr counter anions, the electronic state is an 11% hole-doped state from the half-filled Mott insulator, leading to metallic conductivity as well the superconductivity.

In this work [4], using various high-field measurements, we revealed that the superconductivity that emerged from the doped QSL exhibits unique field-temperature superconducting phase diagrams, as shown in Fig. 2. The red area represents the region of bulk superconductivity (SC) while the blue area indicates the region of fluctuating superconductivity (FSC). In a magnetic field, superconductivity is suppressed by the paramagnetic pair breaking effect and the orbital pair breaking effect, which yields limits of the upper critical field H_{c2} known as the Pauli limit H_P and orbital limit H_{orb}. When applying magnetic fields parallel to the superconducting plane for two-dimensional superconductivity, the orbital pair breaking effect is quenched and H_P governs H_{c2}. As H_P is proportional to the amplitude of the superconducting energy gap, the coupling strength of the superconductivity can be roughly estimated by the ratio H_{c2}/T_c. As shown in Fig. 2(a), amazingly, H_{c2}/T_c for κ-HgBr exceeds 6 TK^{-1}, which is much larger than not only 1.84 TK^{-1} expected in the conventional BCS framework, but also ~3 TK^{-1} observed in other strong-coupling organic superconductors. Besides, H_{c2}/T_c in perpendicular fields (Fig. 2(b)) reaches about 3 TK^{-1}, which is also much larger than those of other superconductors. Considering the results including the orbital limit in perpendicular fields, the superconductivity in κ-HgBr is realized by the extremely strong pairing of the anomalously heavy π-electrons. We discuss the origin of these anomalous features of the superconductivity and elucidate that these originate from quantum critical behavior developed near a quantum critical point of the QSL insulating phase.

In addition, we find that FSC appears even much above T_c (see the blue area in Fig. 2) compared to other organic superconductors. It is not clear at present why the fluctuation region appears in the wide temperature range above T_c, however, given the characteristic of the geometrical frustration to hinder long-range orders of spin-singlet pairing, this nature may be attributed to a characteristic of the superconductivity appearing in doped QSLs.

References
[1] P. W. Anderson, Science **235**, 1196 (1987).
[2] H. Oike, K. Miyagawa, H. Taniguchi, and K. Kanoda, Phys. Rev. Lett. **114**, 067002 (2015).
[3] H. Oike, Y. Suzuki, H. Taniguchi, Y. Seki, K. Miyagawa, and K. Kanoda, Nature Commun. **8**, 756 (2017).
[4] S. Imajo, S. Sugiura, H. Akutsu, Y. Kohama, T. Isono, T. Terashima, K. Kindo, S. Uji, and Y. Nakazawa, Phys. Rev. Research **3**, 033026 (2021).

Authors
S. Imajo, S. Sugiura[a], H. Akutsu[b], Y. Kohama, T. Isonoc, T. Terashima[c], K. Kindo, S. Uji[c], and Y. Nakazawa[b]
[a]Tohoku University
[b]Osaka University
[c]National Institute for Materials Science

Approaching the Best Wire for Non-Destructive Pulsed Magnet

Kindo Group

Non-destructive pulsed magnet is the most important tool for a precise measurement under very high magnetic field. Generating high magnetic field, however, has been hard task because the magnet is destroyed due to considerable Maxwell stress. The stress reaches about 2 GPa in the field of 70 Tesla(T). The simplest solution for generating high field non-destructively is making the coil-wire strong. Cu-Ag wire has been the best candidate for the coil-wire because the wire has the tensile strength of about 1.1 GPa and the conductivity of about 80% of copper. By using the wire, we succeeded in generating a field of 85.8 T in 2011. The best wire, unfortunately, was an accidental success. The wire was not reproduced though we continued to produce wires with similar physical properties. There were many wires having the same strength and conductivity but nothing could generate the field exceeding 80 T. This would be a mystery because the maximum field depends on the tensile strength of the wire mainly. Our efforts to reproduce the best wire were in vain. 10 years have passed since it became mystery.

To solve the mystery, we firstly classified the wire into good ones and bad ones. This classification indicated clearly that the quality of the wire depends on the manufacturing process, especially drawing one. In November 2021, we tested a wire regarded as an ideal combination of manufacturing process. Figure 1 shows the waveform of the magnetic

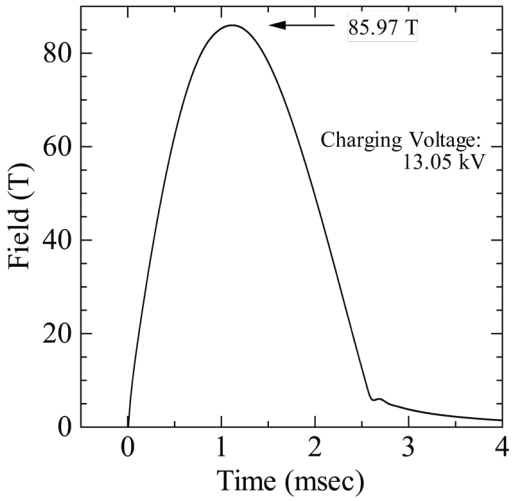

Fig. 1. The shape of completely non-destructive magnetic field of 85.97 Tesla.

field generated using this wire. There was no distortion of the waveform from the start to the end of the magnetic field generation, and we succeeded in generating a magnetic field of 85.97 T completely non-destructively, breaking the previous record.

The mystery of Cu-Ag wire was solved. The mystery lay in the manufacturing process, especially drawing one. Based on these results, we will develop wires that have undergone the ideal manufacturing process to generate even higher magnetic fields, and will provide a 100 T fields non-destructively contributing the joint research program.

Authors
K. Matsui, A, Matsuo, and K. Kindo

Particle-Hole Symmetry Breaking in a Spin-Dimer System $TlCuCl_3$ Observed at 100 T

Y. H. Matsuda and Kindo Group

In a pure dimer system, the transition between singlet state and the S_z = 1-triplet state under an external magnetic field drives a phase transition at the critical magnetic field $H_g \equiv \Delta/g\mu_B$ with Δ the spin gap. The H_g separates into two distinct critical points H_{c1} and H_{c2} in real spin-gap materials due to interdimer interactions; these two critical magnetic fields correspond to the beginning and saturation of the magnetization, respectively. It has been proposed that the field-induced ordering phase at H_{c1} in the dimer system with finite interdimer interactions (a three-dimensional S = 1/2 spin-gap dimer system) can be interpreted as a Bose-Einstein condensation (BEC) phase of magnons [1]. For a long time, this field-induced ordering phase at H_{c2} was thought to be the BEC phase of holes of magnons [2], e.g., the magnetic-field dependence of the order parameters in phase diagrams has a symmetry with respect to the particle-hole invariant point $H = (H_{c1} + H_{c2})/2$. However, the universality of this symmetry has been questioned in strong interdimer interaction system.

In present work, we study the magnetization (M) process of $TlCuCl_3$ (a strong interdimer interaction spin system) up to 100 T and discuss the particle-hole symmetry breaking of the BEC phase [3]. Figure 1 shows the magnetization process and the magnetic field dependence of the dM/dH at 2 K; the magnetization data simulated by the quantum Monte Carlo (QMC) calculation is also presented for the comparison of the M-H curves. The magnetization curve (M-H curve) has a monotonous convex downward shape, which manifests the difference between the critical behaviors around H_{c1} and H_{c2} and implies the absence of the particle-hole symmetry in $TlCuCl_3$.

The breaking of symmetry can be simply understood in the bond operator theoretical formalism. The magnetism around H_{c1} is contributed to by the outset of lowest triplet $|\uparrow\uparrow>$, namely, S_z = 1 condensations driven by the vanishing spin gap. In the pure-dimer limit $J_{intra} >> J_{inter}$, the other two higher-energy local excitations ($|\uparrow\downarrow> + |\downarrow\uparrow>$) and $|\downarrow\downarrow>$ can be neglected since they hardly affect the low-temperature physics. However, a finite J_{inter} interaction can mediate a four-particle interaction that accumulates highest-triplet $|\downarrow\downarrow>$ excitations in the presence of a partial lowest-triplet condensation and singlet condensation [4]. Therefore, $|\downarrow\downarrow>$

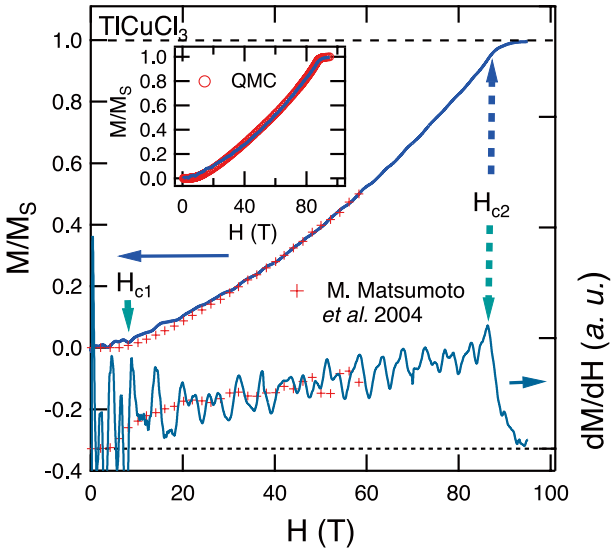

Fig. 1. The magnetization curve measured up to 95 T, as well as the dM/dH data. Red marks represent the results of Ref. [4]. The inset shows Comparison between the experimental magnetization curve and the QMC simulation results.

excitations suppress the magnetization from the $|\uparrow\uparrow>$ condensations when $H \gtrsim H_{c1}$. When the magnetic field increases beyond H_{c1}, such a suppression eventually becomes inefficient due to a large Zeeman gap to excite a $|\downarrow\downarrow>$ quasiparticle and is negligible near H_{c2}. Therefore, it can be concluded that the particle-hole symmetry in the weak interdimer spin system is broken in $TlCuCl_3$ due to the strong higher-order terms through the interdimer interactions.

References
[1] T. Nikuni, M. Oshikawa, A. Oosawa, and H. Tanaka, Phys. Rev. Lett. **84**, 5868 (2000).
[2] M. Jaime, V. F. Correa, N. Harrison, C. D. Batista, N. Kawashima, Y. Kazuma, G. A. Jorge, R. Stein, I. Heinmaa, S. A. Zvyagin, Y. Sasago, and K. Uchinokura, Phys. Rev. Lett. **93**, 087203 (2004).
[3] X.-G. Zhou, Y. Yao, Y. H. Matsuda, A. Ikeda, A. Matsuo, K. Kindo, and H. Tanaka, Phys. Rev. Lett. **125**, 267207 (2020).
[4] M. Matsumoto, B. Normand, T. M. Rice, and M. Sigrist, Phys. Rev. B **69**, 054423 (2004).

Authors
X.-G. Zhou, Yuan Yao, Y. H. Matsuda, A. Ikeda, A. Matsuo, K. Kindo, and H. Tanaka[a]
[a]Tokyo Institute of Technology

Two Spin-State Crystallizations in $LaCoO_3$ up to 200 T

Y. H. Matsuda Group

The puzzling properties of $LaCoO_3$ have been drawing the attention of researchers for more than 60 years, regarding the uncovered origin of the magnetic and insulating state at intermediate temperature range of 100 - 500 K. $LaCoO_3$ is characterized by the spin-state degrees of freedom that governs the temperature evolution of the electronic and magnetic properties. The origin of the magnetic and insulating state between 100 - 500 K is quite controversial, although it has been widely accepted that the ground state is the low spin (LS) non-magnetic insulator. As the origin of the magnetic states, some argue that the intermediate spin state (IS) is involved, while others claim that the mixture of the LS and high spin (HS) states is important. Many experimental results support each claim, being unable to put an end

to the long-standing discussion. We believe that this controversy is rooted in the itineracy-localization duality of correlated electrons in $LaCoO_3$.

We tackled this long-standing problem by using pulsed ultrahigh magnetic field beyond 100 T because beyond 100 T are supposed to be useful in controlling the excited spin-states. In the previous study of ours, we discovered two kinds of spin-state orderings, α and β phases that are extended beyond 100 T on the *B*-*T* phase diagram [1], by means of magnetization measurements using the induction method. However, the magnetization study shows only little information on the difference between the uncovered α and β phases, especially regarding the spin-state configurations.

We came up with an idea that magnetostriction measurement will supplement the magnetization study because the spin-state degree of freedom is coupled with the lattice volume even more directly than magnetization is. For this purpose, we have developed an ultrahigh speed magnetostriction measurement instrument utilizing the fiber Bragg grating (FBG) and optical filter method [2], for the measurement above 100 T. By means of the FBG based method, we have successfully revealed the magneto-lattice properties of $LaCoO_3$ up to 200 T [3]. The result shows very clearly that α and β phases are quite different in volume and that both have constant volume above 100 T, indicating both phases are super-lattice formations (crystallizations) of the spin-states. We have claimed several possible crystallizations in the paper [3]. The result clearly shows that the spin-state interactions lead to kinds of long-range ordering in $LaCoO_3$. At this moment, we still do not know why the ordering is present only in high magnetic fields. We further push the study to even higher magnetic field of 600 T using electromagnetic flux compression method and FBG based magnetostriction measurements, which have clarified even exotic phase diagram up to 600 T [4].

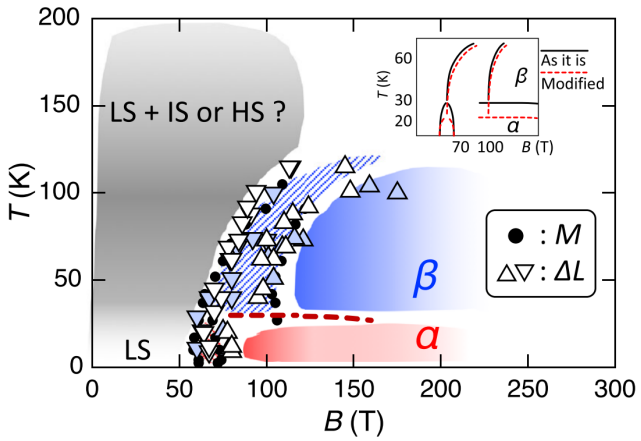

Fig. 1. Phase diagram of $LaCoO_3$ uncovered by the FBG based magnetostriction measurement up to 200 T.

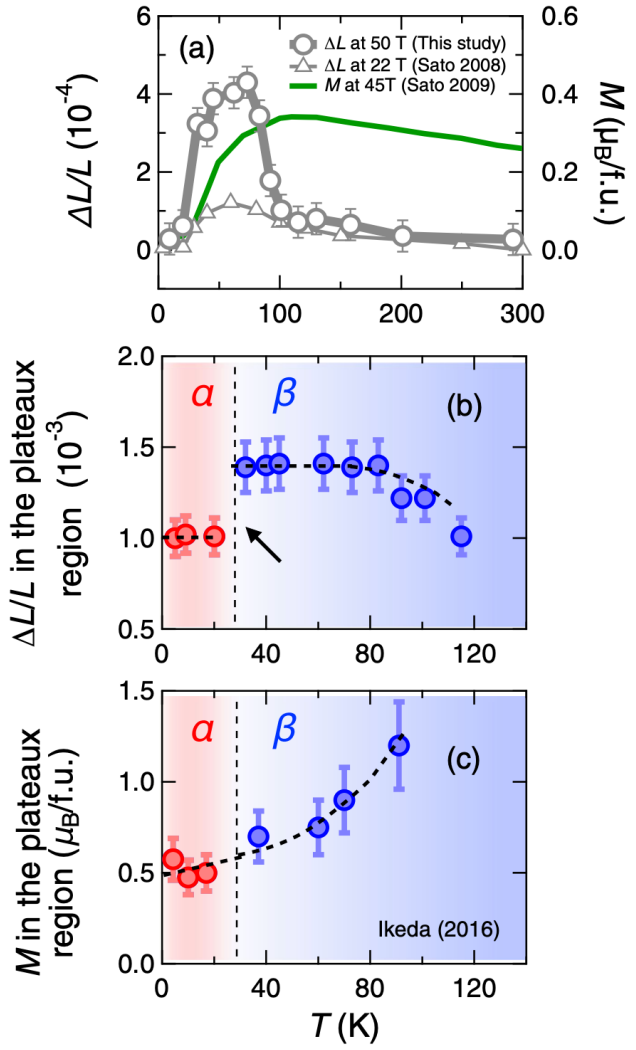

Fig. 2. Comparison of the temperature dependence between magnetization and magnetostriction at $B \sim 50$ T and 100 T and the sample temperatures from 4.2 to 300 K.

References

[1] A. Ikeda, T. Nomura, Y. H. Matsuda, A. Matsuo, K. Kindo, and K. Sato, Phys. Rev. B **93**, 220401(R) (2016).
[2] A. Ikeda, T. Nomura, Y. H. Matsuda, S. Tani, Y. Kobayashi, H. Watanabe, K. Sato, Rev. Sci. Instrum. **88**, 083906 (2017).
[3] A. Ikeda, Y. H. Matsuda, and K. Sato, Phys. Rev. Lett. **125**, 177202 (2020).
[4] A. Ikeda, Y. H. Matsuda, K. Sato, Y. Ishii, H. Sawabe, D. Nakamura, S. Takeyama, and J. Nasu, arXiv:2201.02704.

Authors
A. Ikeda[a], Y. H. Matsuda and K. Sato[b]
[a]University of Electro-Communications
[b]National Institute of Technology

Magnetic Field-Induced Phenomena in the Unconventional Superconductor UTe_2

Tokunaga Group

Unconventional superconductivity in UTe_2 is one of the hot topics in strongly correlated electron systems. The spin-triplet superconductivity is very likely because of its extremely high superconducting (SC) critical fields. Since its discovery three years ago, many experimental and theoretical works with intense competition revealed novel phenomena realized in UTe_2 [1]. External parameters, such as pressure and magnetic field (*H*), strongly affect superconductivity and magnetism in UTe_2. One of the intriguing phenomena induced by applied *H* is the reinforcement and reemergence of SC phases, which are sensitive to the *H* directions [2]. When the *H* applied along a hard magnetization *b* axis, the *H* reinforces the SC transition above 15 T. With increasing *H*, the superconducting transition temperature T_{sc} increases and is suppressed above $\mu_0 H_m \sim 35$ T, where a first-order metamagnetic transition takes place (see Fig. 1(b)) [3]. More surprisingly, the *H* along near the [011] direction induces another SC phase above H_m [2]. Thus, the metamagnetic

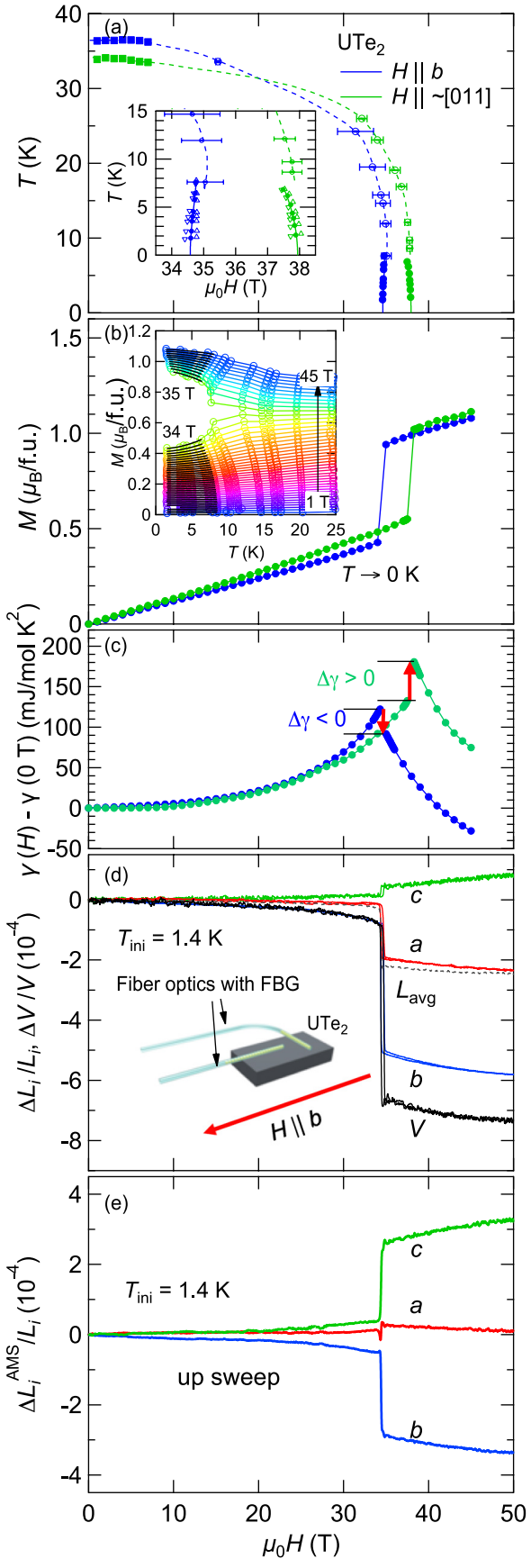

Fig. 1. (a)Phase diagrams of UTe_2 for $H \parallel b$ and ~[011]. The inset zooms near H_m. The filled (open) circles and squares indicate H_m (crossover) and T_χ^{max}, respectively. Magnetic field dependences of (b) magnetization extrapolated to 0 K, (c)electronic specific heat coefficient derived by thermodynamic relations, (d)linear and volume magnetostriction at T_{ini} = 1.4 K and (e)anisotropic magnetostriction at T_{ini} = 1.4 K.

transition strongly affects the SC transition. However, their relationship and the origin of metamagnetism leave many mysteries. Using state-of-the-art pulsed-high-field experiments developed in the International MegaGauss Science Laboratory at the ISSP, we have studied H-induced phenomena in UTe_2.

In order to address the relationship between metamagnetic and SC transition, we revealed the mass enhancement as a function of the magnetic field and its direction [4]. In general, the larger the density of state, the higher T_{sc} is. Field dependence of the electronic specific heat coefficient, γ (H), is derived thermodynamically by analyzing the T dependence of magnetization (M) at constant fields and phase diagram. Since the magnetocaloric effect (MCE) is significant [5], the sample temperature varies during the H sweep. To account for the MCE, we measure the sample T and M simultaneously using field-insensitive capacitance thermometers developed by Miyake et al. [6]. This method is also potent in determining the magnetic phase diagram more precisely.

The inset of Fig. 1 (b) shows the M (T) curves at constant H. On approaching H_m, T decreases significantly. This M (T, H) evaluation is the first attempt and a considerable breakthrough in the pulsed-field experiments. The sign change in dM/dT across H_m indicates the existence of a peak of γ (H) at H_m from Maxwell's relation. The γ (H) should change discontinuously across H_m because of the first-order transition. We solved this issue by employing Clausius-Clapeyron's equation. As shown in Fig. 1(a), dH_m/dT changes in its sign from positive for $H \parallel b$ to negative for $H \parallel$ ~[011]. This change means that the negative $\Delta\gamma$ (H) crossing H_m for $H \parallel b$ changes to positive for $H \parallel$ ~[011] [see Fig. 1(c)]. The negative (positive) $\Delta\gamma$ (H) for $H \parallel b$ (~[011]) is consistent with the suppression (reemergence) of SC at H_m. These findings hint at understanding the origin of the SC phases varying with the field directions.

Since the metamagnetic transition is of the first order, the volume at least should change across H_m. Thus, we tried to reveal volume/structural change, namely lattice instability, at H_m through the magnetostriction [7]. We performed magnetostriction measurements using the optical fiber with fiber-Bragg-grating and the optical filter method developed in Ikeda *et al.* [8]. The inset of Fig. 1 (d) is a schematic drawing of the setup for the magnetostriction measurements. The bare fiber optics were glued directly on the sample parallel and perpendicular to the field direction along the b axis, as in Ref. [9]. This method enables us to obtain the longitudinal and transverse magnetostriction simultaneously, the first example in pulsed fields.

$\Delta L_i/L_i$'s (i = a, b, c) show anisotropic H dependencies and change discontinuously at H_m, as expected for the first-order transition (Fig. 1 (d)). The volume magnetostriction $\Delta V/V$, i.e., a summation of $\Delta L_i/L_i$, shows a discontinuous change of -5.9×10^{-4} at H_m. Knowing ΔV and ΔM at H_m, we can estimate pressure (p) dependence of H_m from Clausius-Clapeyron's equation. The $H_m(p)$ obtained by the thermodynamic quantities are in good agreement with the $H_m(p)$ determined experimentally, confirming the reliability of our experiments. An important finding here is the anisotropic magnetostriction (AMS) defined as $\Delta L_i^{AMS}/L_i = \Delta L_i/L_i - \Delta L_{avg}/L_{avg}$ (the averaged linear magnetostrcition $\Delta L_{avg}/L_{avg} = \Delta V/3V$). For the isotropic case, the AMS is small. Interestingly, the strong anisotropy appears in the bc plane, while $\Delta L_a^{AMS}/L_a$ is very small. Thus, the metamagnetic transition in UTe_2 involves the lattice instability, which plays a crucial role in the SC phases near H_m. We also suggest the possible

valence instability in terms of the itinerant-localized duality picture of the uranium magnetism [7].

Without experimental developments, the fascinated *H*-induced phenomena in UTe_2 are not entirely solved. In other words, UTe_2 is our good trainer experimentally and physically. Our struggles for a complete understanding continue.

References

[1] D. Aoki, J.-P. Brison, J. Flouquet, K. Ishida, G. Knebel, Y. Tokunaga, and Y. Yanase, J. Phys.: Condens. Matter **34**, 243002 (2022).
[2] S. Ran, I.-L. Liu, Y. S. Eo, D. J. Campbell, P. Neves, W. T. Fuhrman, S. R. Saha, C. Eckberg, H. Kim, J. Paglione, D. Graf, J. Singleton, and N. P. Butch, Nat. Phys. **15**, 1250 (2019).
[3] A. Miyake, Y. Shimizu, Y. J. Sato, D. Li, A. Nakamura, Y. Homma, F. Honda, J. Flouquet, M. Tokunaga, and D. Aoki, J. Phys. Soc. Jpn. **88**, 063706 (2019).
[4] A. Miyake, Y. Shimizu, Y. J. Sato, D. Li, A. Nakamura, Y. Homma, F. Honda, J. Flouquet, M. Tokunaga, and D. Aoki, J. Phys. Soc. Jpn. **90**, 103702 (2021).
[5] S. Imajo, Y. Kohama, A. Miyake, C. Dong, J. Flouquet, K. Kindo, and D. Aoki, J. Phys. Soc. Jpn. **88**, 083705 (2019).
[6] A. Miyake, H. Mitamura, S. Kawachi, K. Kimura, T. Kimura, T. Kihara, M. Tachibana, and M. Tokunaga, Rev. Sci. Instrum. **91**, 105103 (2020).
[7] A. Miyake, M. Gen, A. Ikeda, K. Miyake, Y. Shimizu, Y. J. Sato, D. Li, A. Nakamura, Y. Homma, F. Honda, J. Flouquet, M. Tokunaga, and D. Aoki, J. Phys. Soc. Jpn. **91**, 063703 (2022).
[8] A. Ikeda, Y. H. Matsuda, and H. Tsuda, Rev. Sci. Instrum. **89**, 096103 (2018).
[9] M. Gen, A. Miyake, H. Yagiuchi, Y. Watanabe, A. Ikeda, Y. H. Matsuda, M. Tokunaga, T. Arima, and Y. Tokunaga, Phys. Rev. B **105**, 214412 (2022).

Authors

A. Miyake, M. Gen[a], A. Ikeda[b], K. Miyake[c], Y. Shimizu[d], Y. J. Sato[d], D. Li[d], A. Nakamura[d], Y. Homma[d], F. Honda[d, e], J. Flouquet[f], M. Tokunaga, and D. Aoki[d, f]

[a]The University of Tokyo
[b]University of Electro-Communications
[c]Osaka University
[d]Tohoku University
[e]Kyushu University
[f]CEA-Grenoble

Ultrasound Measurement under Ultrahigh Magnetic Fields

Kohama and Y. H. Matsuda Groups

Ultrasound is a powerful means to study numerous phenomena of condensed-matter physics as acoustic waves coupling strongly to structural, magnetic, orbital, and charge degrees of freedom. In this work, we have developed a new ultrasound measurement technique combined with the single-turn coil (STC) system, generating magnetic fields beyond 100 T [1].

Figure 1 summarizes the concepts of the ultrasound pulse-echo (PE) and continuous-wave excitation (CW) techniques. Usually, ultrasound measurements under pulsed magnetic fields are performed with the PE technique, where the pulsed ultrasound is excited and the transmitted echo signals are analyzed by a phase-sensitive technique. In this case, cross-talk noise and higher echoes that arrive after multiple reflections are separated in time. However, magnetic fields above 100 T are accessible only by destructive techniques, which generate fields only for several microseconds. This field duration is too short to perform PE ultrasound measurements. Instead, we have employed the CW technique, which excites and detects ultrasound waves continuously. In this case, the detected signal contains all echo signals. Only if the 0th echo signal is dominant, the

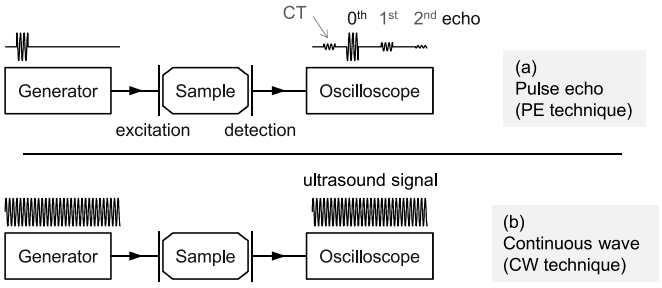

Fig. 1. Schematics of the (a) pulse-echo and (b) continuous-wave ultrasound techniques. Here, CT means crosstalk.

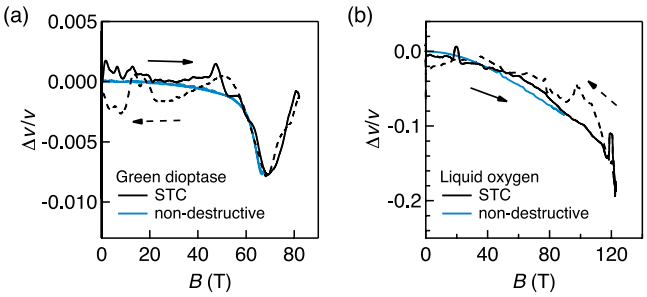

Fig. 2. Relative change in the sound velocity of (a) green dioptase at 4 K and (b) liquid oxygen at 77 K.

detected signal reflects the change of sound velocity. This condition is reasonably satisfied in various magnetic phase transitions, where acoustic attenuation increases and higher-echo signals do not affect the measurements. Therefore, the CW technique can be applied for detecting phase transitions under ultrahigh magnetic fields.

Figure 2 shows representative results on green dioptase and liquid oxygen. Results obtained by the STC (black) are compared with the ones by non-destructive magnets (cyan). These results reasonably coincide despite the significant difference in the field durations by the factor of 1000 (10 ms/10 μs). For the case of green dioptase [Fig. 2(a)], an anomaly corresponding to the magnetic phase transition is observed at 65 T. Here, the measurement resolution is of the order of $\Delta v/v \sim 10^{-3}$, which is sufficient for detecting various field-induced phase transitions. For the case of liquid oxygen [Fig. 2(b)], a continuous decrease of sound velocity is observed up to 120 T with the significant softening of $\Delta v/v \sim -0.2$. The observed change in sound velocity is extremely large, and cannot be explained by a magneto-volume effect. We point out that this sound-velocity change could be a precursor of a field-induced liquid-liquid transition of oxygen [2]. Now, the developed technique is open to users.

References

[1] T. Nomura, A. Hauspurg, D. I. Gorbunov, A. Miyata, E. Schulze, S. A. Zvyagin, V. Tsurkan, Y. H. Matsuda, Y. Kohama, and S. Zherlitsyn, Rev. Sci. Instrum. **92**, 063902 (2021).
[2] T. Nomura, A. Ikeda, M. Gen, A. Matsuo, K. Kindo, Y. Kohama, Y. H. Matsuda, S. Zherlitsyn, J. Wosnitza, H. Tsuda, and T. C. Kobayashi, Phys. Rev. B **104**, 224423 (2021).

Authors

T. Nomura, A. Hauspurg[a], D. I. Gorbunov[a], A. Miyata[a], E. Schulze[a], S. A. Zvyagin[a], V. Tsurkan[b], Y. H. Matsuda, Y. Kohama, and S. Zherlitsyn[a]

[a]Hochfeld-Magnetlabor Dresden (HLD-EMFL)
[b]University of Augsburg

Developing Novel Spectroscopy Techniques Using a Segmented Cross Undulator

I. Matsuda Group

Cross undulators, composed of a single set of insertion devices for linear horizontal and vertical polarization with a phase shifter in between, have become available at worldwide synchrotron and x-ray free electron laser facilities. To achieve higher degree of the light polarization, a segmented type of the cross undulator, was designed and successfully installed at SPring-8 BL07LSU [1]. At the beamline, the continuous variation of the phase shifts has realized smooth polarization controls of soft X-ray beam between linear and circular ones with fast switching (13 Hz) [1]. The oscillatory regulation has allowed us to determine the element-specific complex permittivity in soft X-ray [1]. In the present research, we demonstrated a new control of linear polarization at any angle with a segmented undulator.

The segmented cross undulator at SPring-8 BL07LSU is composed of eight segments of insertion device (ID) and seven phase shifters (PSs), as shown in Fig. 1 (a). The ID segment is a horizontal figure-8 undulator or a vertical figure-8 undulator. The horizontal (H) and vertical (V) ID segments are placed alternatively and sandwich a PS. A PS is used to adjust the relative phase of radiation emitted from each segment by changing the path length of the electron orbit in magnetic field. To realize linearly polarized light with arbitrary angle, θ, we combine two waves of the left- and right-handed circularly polarized light, generated by sets of the ID segments, Set A and Set B, as shown in Fig.1(a). Set A or B is composed of the two H and two V segments. When Set A produces right-handed (left-handed) circular polarized light, we make Set B generate lefthanded (right-handed) circular polarized light. Then, the rotation angle (θ) of linearly polarized light is controlled by changing the phase shift between the left and right circularly polarized light at the center PS. In other words, we can generate soft X-ray beam with linear polarization that continuously rotates its angle over 2π.

For demonstration, we made measurements of near-edge X-ray absorption fine structure (NEXAFS) on a 2D film of h-BN (Fig. 1(b)) [2]. Focusing on the π* and σ* NEXAFS peaks, we traced their intensity variations with angle of the linear polarization, θ. Since this NEXAFS methodology is different from the conventional one, we hereafter call it the rotational NEXAFS measurement. When the incident angle is 80°, as illustrated in Fig. 1(c), intensity of hν = 401.5 eV (π*) becomes the maximum at θ = 0, π, 2π (horizontal) and the minimum at θ = π/2, 3π/2 (vertical), while that of hν=408.0 eV (σ*) shows the opposite, as shown in Fig. 1(d). The rotational NEXAFS experiment enhances the clear electronic contrast between the π* (out-of-plane) and σ* (in-plane) orbitals of h-BN. The experimental plot is expected to be useful in making assignments of the electronic states and in determining the precise configuration of molecules.

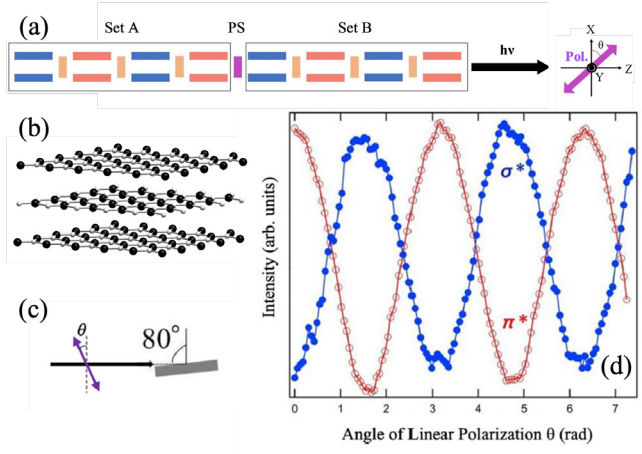

Fig. 1. (a) A schematic drawing of the segmented undulator with H (blue) and V (red) ID segments and PS's (orange). (b) An illustration of a h-BN film. (c) The measurement configuration. (d) The rotational NEXAFS spectra at the π* peak (hν = 401.5 eV) and the σ* peak (hν = 408.0 eV) [2].

Figure 2 shows another demonstration of the rotational X-ray spectroscopy experiment of the X-ray magnetic linear dichroism (XMLD) [3]. Figure 2 (a) shows an Ni L-edge XAS spectra of a NiO crystal taken with horizontal and vertical linearly polarized light at the incident angle of 80° from the surface normal. XMLD spectra of the NiO crystal is obtained by taking difference between the XAS spectra taken with the horizontal and vertical linear polarizations (Fig. 2 (b)), showing clear linear dichroisms. Focusing on the L2a and L2b peaks, the former has a large horizontal intensity, while the latter has a large vertical intensity. The spectral feature appears opposite in the XMLD signals. Figures 2(c,d) show results of the rotational XMLD, taken at the incident angle of 80°. The intensity changes with a period of π, showing a clear XMLD contrast. The reversed features between the ID section orders confirm the genuine XMLD signals (red and blue lines in the figure). The technique can

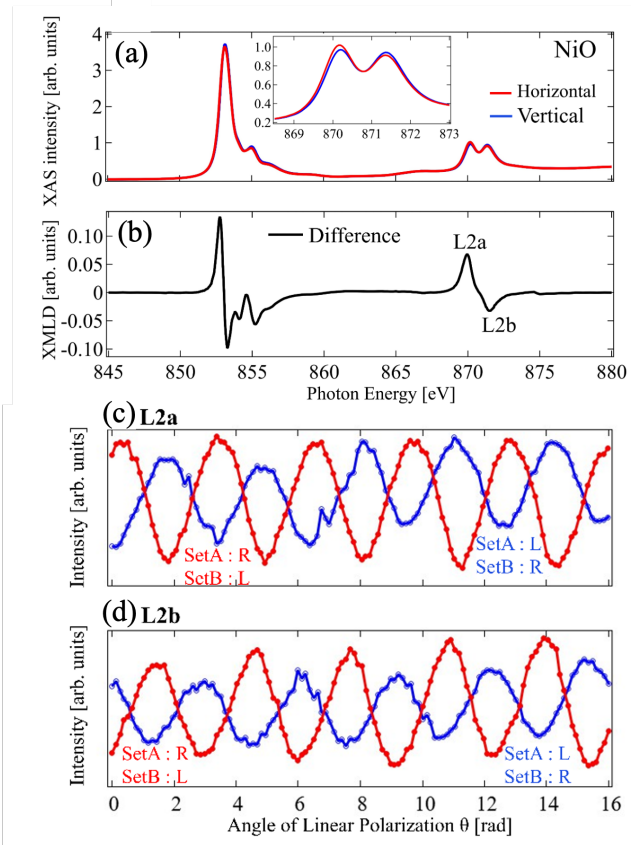

Fig. 2. (a) XAS and (b) XMLD spectra of a NiO crystal at the Ni L-edge and at an incident angle of 80°. In (a), the red (blue) curve indicates a spectrum, taken by the horizontal (verticals) linear polarization. (c)(d) Plots of the Rotational XMLD, shown as intensity at the L2a (hν = 869.95 eV) and L2b (hν = 871.55 eV) peaks at various angles of linear polarization. The red plot shows the results for Set A with right-handed polarization and Set B with left-handed polarization, while the blue plot shows the results with the opposite polarization configuration [3].

be combined with a lock-in-amplification and it is expected to detect fine magnetic signals of various materials.

References

[1] J. Miyawaki, S. Yamamoto, Y. Hirata, M. Horio, Y. Harada, and I. Matsuda, AAPPS Bulletin **31**, 25 (2021).
[2] Y. Kudo, Y. Hirata, M. Horio, M. Niibe, and I. Matsuda, Nucl. Instrum. Meth. Phys. Res. A **1018**, 165804 (2021).
[3] Y. Kudo, M. Horio, Y. Hirata, T. Ohkochi, T. Kinoshita, and I. Matsuda, e-J. Surf. Sci, Nanotechnol. **20**, 124 (2022).

Author

I. Matsuda

Visualization of the Strain-Induced Topological Phase Transition in a Quasi-One-Dimensional Superconductor $TaSe_3$

Kondo Group

The control of the phase transition from topological to normal insulators can allow for an on/off switching of the spin current. Topological phase transitions realized by elemental substitution [1] require the preparation of materials with various compositions and are thus far from a feasible device application, which demands a reversible operation.

In this study, we use angle-resolved photoemission spectroscopy (ARPES) and spin-resolved ARPES (SARPES) to visualize the strain-driven band-structure evolution of the quasi-one-dimension (quasi-1D) superconductor $TaSe_3$. Our results demonstrate that it undergoes reversible strain-induced topological phase transitions from a strong topological insulator phase with spin-polarized, quasi-one-dimensional topological surface states to topologically trivial semimetal and band insulating phases. The quasi-one-dimensional superconductor $TaSe_3$ provides a suitable platform for engineering the topological spintronics with the functionality to on/off switch a spin current that is robust against impurity scattering.

In the transition-metal trichalcogenides MX_3 (M = Nb, Ta; X = S, Se), physical properties vary and electronic orders evolve differently in accordance with the distinctive stacking sequences of the 1D chain variants [2]. Among them, $TaSe_3$ is especially appealing in that superconductivity emerges at low temperatures (~2 K) [3], in contrast with the other members, which typically undergo charge density wave transitions [2]. More intriguingly, recent ab initio calculations predict that semimetallic $TaSe_3$ belongs to a three-dimensional (3D) strong TI phase [4]. Therefore, it has been further suggested as a candidate for a topological superconductor with the topological surface states (TSSs) formed near E_F. Thanks to the van der Waals stacking of 1D chains [2] and the electronic proximity to other topological phases [4], $TaSe_3$ potentially brings an attractive functionality of controlling topological properties by fine-tuning of a single physical parameter, i.e., the lattice variation via strain.

In Fig. 1 [5], we demonstrate the first unambiguous confirmation of the strong TI phase in $TaSe_3$. Figures 1c,d shows the calculated and correspondingly experimental band dispersions around the Brillouin zone edge, where the TSSs are expected (the sharp features in Figs. 1c,d). To elucidate more details, we magnify the dispersions in Figs. 1e,f, where one can see clearly two branches of TSSs. Utilizing ultra-high resolution SARPES, we map the spin-resolved states in

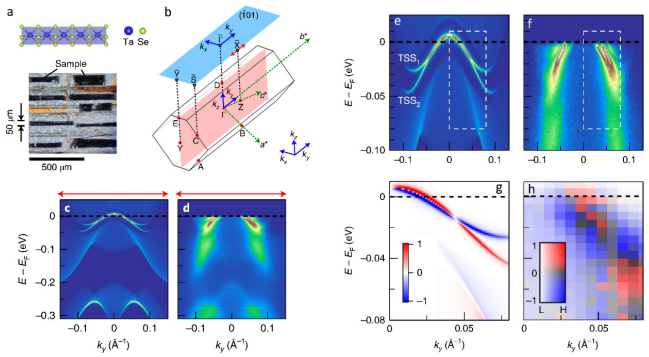

Fig. 1. Strong topological insulator phase in $TaSe_3$ revealed by ARPES [5]. (a) Crystal structure of the quasi-1D monoclinic $TaSe_3$ and a picture of single crystals mounted on a sample holder for ARPES measurements. (b) 3D bulk Brillouin zone and its 2D projection. (c, d) Calculated and experimental band dispersions along the red arrow in (b) near the zone edge where topological surface states (TSSs) are expected to emerge. (e, f) Magnified dispersions of (c, d) near E_F. Two branches of TSSs are observed. (g, h) Calculated and experimental spin-polarization maps in the energy-momentum window marked by the dashed box in (e, f). Measurement temperature was 10 K and a 7 eV laser was used as a light source.

Fig. 1h within the energy-momentum window specified by the dashed box in Fig. 1f. Correspondingly, the calculations are also shown in Fig. 1g. One can see that our results nicely reproduce the theoretical predictions of spin-polarized states with a spin-degenerated node point.

We have designed a device to apply strain to the quasi-1D crystals, based on a bending mechanism, as shown in Fig. 2a [5]. After tightening four screws, one can apply uniaxial tensile strain to the crystals mounted on the platform. This can be seen in Fig. 2b representing with color scale the distribution of longitudinal strain produced by the finite-element analysis. We also used commercial strain gauges to measure the strain values and confirmed a good agreement of those with the simulations [5]. Figures 2d-f show the band dispersions around the zone edge obtained under different strains tuned *in-situ*, revealing two-step phase transitions. At zero strain (Fig. 2d), one can see sharp and high-intense TSSs that are consistent with those shown in Figs. 1d,f. With increasing strain up to around 1%, the TSSs vanished (Fig. 2e) as a result of the topological phase transition, i.e., the band inversion is lifted and the bulk gap collapsed, turning the bulk state to the trivial semimetallic phase. As the strain reached 2.4%,

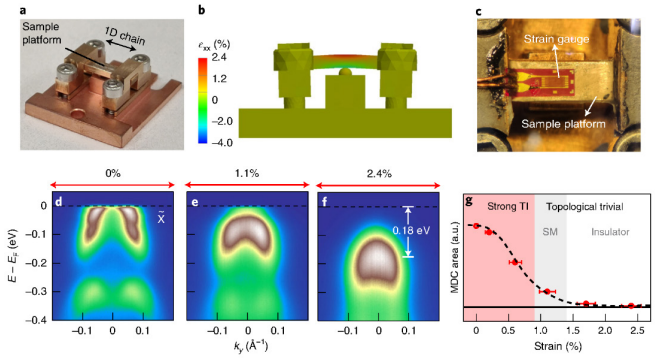

Fig. 2. Strain-induced topological and metal-insulator phase transitions revealed by ARPES for $TaSe_3$ [5]. (a) A picture of the strain device we designed and used for ARPES measurements. (b) Finite-element tensile strain simulation of the device (side view). (c) Top view of the device with a strain gauge attached. (d-f) ARPES band dispersions around the zone edge under strain controlled *in-situ*. The strain values applied are described on the top of each panel. (g) ARPES intensity at E_F as a function of the strain value, crossing three distinct phases, i.e., strong TI phase, trivial semimetal phase, and trivial insulator phase.

the band gap was reopened (Fig. 2f), and a metal-insulator transition occurred. These phase variations are reflected on the ARPES intensity at E_F , which is plotted in Fig. 2g as a function of strain values controlled in-situ. Comparing with our calculations, we conclude that we have realized two-step phase transitions, from a strong topological insulator phase, across a topologically trivial semimetallic phase, to a normal band insulator phase.

In summary, we have demonstrated that $TaSe_3$ hosts a strong TI phase in its ground state. By means of *in-situ* strain engineering of the band structure, we have observed two-step phase transitions in $TaSe_3$, including a topological phase transition from a strong TI phase to a trivial semimetal phase, and a subsequent metal-insulator transition. We note that $TaSe_3$ provides an excellent functionality of easily controlling the band topology by mechanical strain. Such a strain method is much simpler, reversible, and thus promising than element substitution method for future application utilizing topological phase transition. Furthermore, our results give prediction that the Majorana fermions emerge in the $TaSe_3$ superconductor and they are controllable by the strain method, so encouraging follow-up research toward the future realization of the quantum computation.

References

[1] S.-Y. Xu *et al.*, Science **332**, 560 (2011).
[2] P. Monceau, Adv. Phys. **61**, 325 (2012).
[3] T. Sambongi *et al.*, J. Phys. Soc. Jpn. **42**, 1421 (1977).
[4] S. Nie *et al.*, Phys. Rev. *B* **98**, 125143 (2018).
[5] C. Lin *et al.*, Nat. Mater. **20**, 1093 (2021).

Authors
C. Lin, M. Ochi[a], R. Noguchi, K. Kuroda, M. Sakoda[b], A. Nomura[c], M. Tsubota[d], P. Zhang, C. Bareille, K. Kurokawa, Y. Arai, K. Kawaguchi, H. Tanaka, K. Yaji[e], A. Harasawa, M. Hashimoto[f], D. Lu[f], S. Shin[g], R. Arita[g,h], S. Tanda[b], and T. Kondo
[a]Osaka University
[b]Hokkaido University
[c]Tokyo University of Science
[d]Gakushuin University
[e]National Institute for Materials Science
[f]SLAC National Accelerator Laboratory
[g]The University of Tokyo
[h]RIKEN

Multipole Polaron in the Devil's Staircase of CeSb

Kondo Group

An electron-boson coupling, that leads to a quasiparticle (QP) of an electron combined with a local bosonic field, can cause interesting properties of condensed matter. For examples, dynamical behavior of a QP often plays roles in electronic instabilities leading to strongly correlated phenomena such as high-temperature superconductivity and colossal magnetoresistance. Thus, the investigation of such a QP is important in materials science. One of the most famous QPs is the polaron by electron-phonon coupling but such a QP state can be realized by coupling to other bosonic modes. However, only three types of electron–boson coupling have been experimentally identified: electron–phonon (or polaron), electron–magnon (or magnetic polaron) and electron–plasmon (or plasmaron) couplings, despite a number of investigations.

In this study, we found a new type of electron–boson coupling which leads to a unique QP state, 'multipole polaron', by investigating a rare-earth intermetallic compound CeSb [1].This new coupling mediates between the itinerant electrons and the bosonic field constituted by the crystal-electric-field (CEF) excitations of the localized 4f states. As evidence for it, we present laser angle-resolved photoemission spectroscopy (ARPES) [2] revealing band renormalization via the coupling of the mobile electron with the CEF excitation. This low-energy feature corresponds to a quadrupole CEF excitation (Jz = ±2) in the J multiplets of the 4f orbitals, possessing the 'multipole' freedom.

We present ARPES maps at the anti-ferromagnetic (AF) phase taken by high-resolution laser-ARPES in Fig. 1a, b. A clear signature for the band renormalization of the Sb 5p band is revealed: the Fermi velocity is largely reduced with a prominent kink at energy $E-E_F = -7 \pm 1$ meV, which directly manifests the presence of an electron–boson coupling (Fig. 1b). In fact, this low energy scale of the kink structure is consistent with the CEF excitation of the Ce 4f orbitals. The CEF splitting in the ordered 4f states of CeSb shows the ground state with Jz ≈ 5/2 (hereafter $f\Gamma_{80}$) and the higher $f\Gamma_8$ states with Jz ≈ 1/2 (hereafter $f\Gamma^*_8$) (Fig. 1c) [3]. The energy scale of the $f\Gamma_{80}$ to $f\Gamma^*_8$ excitation is ~5–6 meV and shows good agreement with the kink energy (7 ± 1 meV). Since the quadrupole CEF excitation ($|\Delta J_z| = 2$) for $f\Gamma_{80}$ to $f\Gamma^*_8$ has multipole character, our observations of the prominent kink reflect a coupling of the electron with the multipole CEF excitation. Such a QP with a large mass enhancement can be described as a multipole polaron that propagates in a sea of lamellar $f\Gamma_{80}$ orbits but largely dressed with the self-induced quadrupole polarization of the longitudinal $f\Gamma^*_8$ orbits, as illustrated by Fig. 1d.

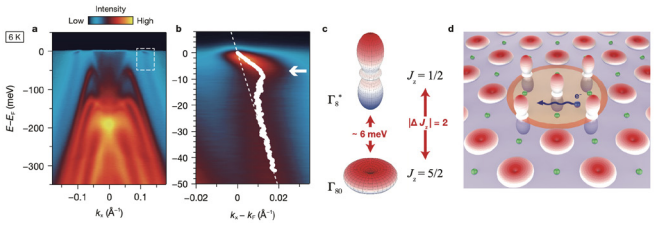

Fig. 1. (a) ARPES band map at T = 6 K (AF phase). (b) Magnified image for the prominent kink in the band dispersion within the dashed rectangles shown in (a). (c) CEF scheme of the localized 4f states in the ordered phase. (d) Schematic of the multipole polaron.

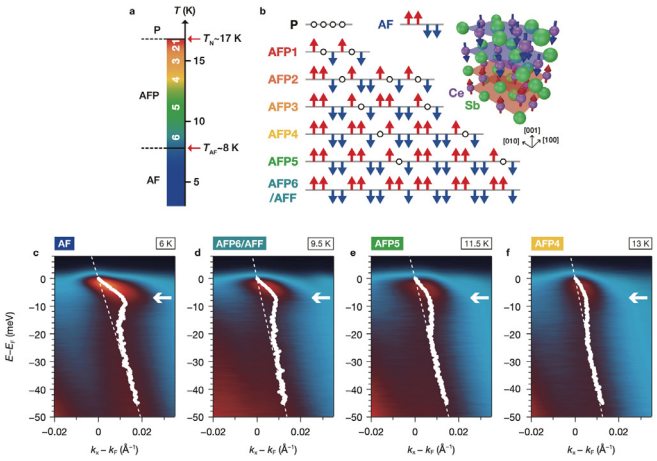

Fig. 2. (a) Temperature scale of the devil's staircase transition at zero field. (b) Schematics of magnetostructures that comprise stackings of ferromagnetic (arrows) and paramagnetic (circles) planes along the crystallography axis [001]. The inset shows the magnetic texture for the magnetic ground state (AF phase). (c-f) Magnified images for the prominent kink in the band dispersion for several distinct phases.

References
[1] Y. Arai *et al*., Nat. Mater. **21**, 410 (2022).
[2] K. Kuroda *et al*., Nat. Commun. **11**, 2888 (2021).
[3] J. Rossat-Mignod *et al*., J. Magn. Magn. Mater. **52**, 111 (1985).
[4] P. Bak, Phys. Today **39**, 38 (1986).

Authors
Y. Arai, K. Kuroda[a], T. Nomoto[b], Z. H. Tin[c], S. Sakuragi, C. Bareille, S. Akebi, K. Kurokawa, Y. Kinoshita, W.-L. Zhang[d], S. Shin[b], M. Tokunaga, H. Kitazawa[e], Y. Haga[f], H. S. Suzuki, S. Miyasaka[c], S. Tajima[c], K. Iwasa[g], R. Arita[b,h], and T. Kondo
[a]Present address: Hiroshima University
[b]The University of Tokyo
[c]Osaka University
[d]Sophia University
[e]National Institute for Materials Science
[f]Japan Atomic Energy Agency
[g]Ibaraki University
[h]RIKEN

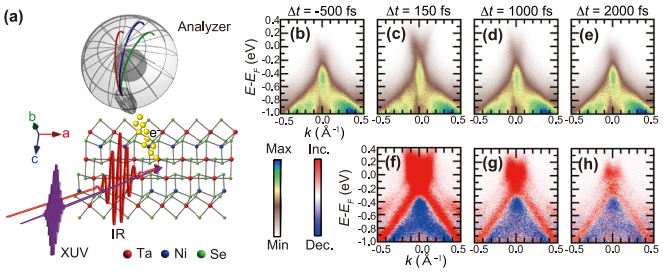

Fig. 1. (a) Schematic illustration of time- and angle-resolved photoemission spectroscopy (TARPES), as applied to Ta_2NiSe_5. The pump pulse is infrared light, whereas the probe pulse is extreme ultraviolet light produced by high harmonic generation. Photoelectrons are detected by a hemispherical electron analyzer. (b)–(e) TARPES spectra of Ta_2NiSe_5. The delay time between the pump and probe is indicated in each panel. (f)–(h) Differential images of TARPES. Red and blue points represent increasing and decreasing photoemission intensity, respectively.

Detecting Electron-Phonon Coupling During Photoinduced Phase Transition

Okazaki and Itatani Groups

Photoinduced phase transitions have been intensively studied owing to their potential capabilities to control a material of interest in an ultrafast manner, which can induce exotic phases unable to be attained at equilibrium. As materials of interest, strongly correlated electron systems provide very fruitful playgrounds because they exhibit very rich phases owing to intertwined couplings between multiple degrees of freedom including charge, orbital, spin, and lattice, where photoexcitation is a very promising way to control their physical properties. Recently, we revealed the photoinduced insulator-to-metal transitions (IMTs) in Ta_2NiSe_5 by using time- and angle-resolved photoemission spectroscopy (TARPES) as schematically shown in Fig. 1(a). Figures 1(b)-1(e) are TARPES spectra of Ta_2NiSe_5 in each delay time, and Figs. 1(f)-1(h) show differential images of TARPES, where red and blue regions correspond to increasing and decreasing intensity, respectively. One can notice that the photo-induced semimetallic bands shown as red regions in Figs. 1(f)-1(h) cross the Fermi level (E_F). However, the key mechanisms are still under debate, and it is currently a central issue as to how the couplings between the electron, lattice, and spin degrees of freedom are evolving during the photoinduced phase transition.

In order to reveal the underlying mechanism in terms of the electron-phonon couplings, we mapped out the frequency-dependent intensity of the Fourier components in the energy and momentum space, which we call frequency-domain angle-resolved photoemission spectroscopy (FDARPES). Figures 2(a)–2(e) show the FDARPES spectra corresponding to the frequencies of 1, 2, 3, 3.75, and 4 THz, respectively. To see each phonon mode associated with the FDARPES spectra, we performed the *ab initio* calculations. First, we calculated the band structure of Ta_2NiSe_5 based on the density functional theory within a generalized gradient approximation (GGA), and confirmed that the results can overall reproduce the photoemission results as shown in Fig. 2(f). Then, we employed the calculations to obtain the phonon modes based on the density functional perturbation theory. The calculated phonon modes corresponding to the 2- and 3-THz modes are shown in Figs. 2(g) and 2(h). Noticeably, the FDARPES spectra exhibit distinctively different behaviors depending on the frequency, which demonstrates that each phonon mode is selectively coupled to the specific electronic bands. Particularly, the 2-THz phonon mode has the strongest signal around E_F, where it consists of a mixture of Ta 5*d* and Se 4*p* orbitals, and this signature is responsible for the collapse of the excitonic insulating phase. In other words, the 2-THz phonon mode is revealed to be the most strongly coupled to the emergent photoinduced electronic bands crossing E_F. Furthermore, we proceeded to compare each FDARPES spectra with the band dispersions before and after photoexcitation. We found that the FDARPES spectrum at 1 THz matches the band dispersions after photoexcitation better than that before photoexcitation as shown in Fig. 2(a), while the FDARPES spectrum at 3 THz is closer to the band dispersions before photoexcitation as shown in Fig. 2(c). This means that both the semimetallic and semiconducting bands are coexistent in the transient state, and suggests the strong electron-phonon couplings for 1-THz and 3-THz phonon modes are associated with the semimetallic and semiconducting bands, respectively. Moreover, this finding demonstrates that, whereas the semimetallic and semiconducting states coexist after photoexciation, the FDARPES method can selectively reveal the coupling of each phonon mode to semimetallic and semiconducting states by the frequency-domain analysis.

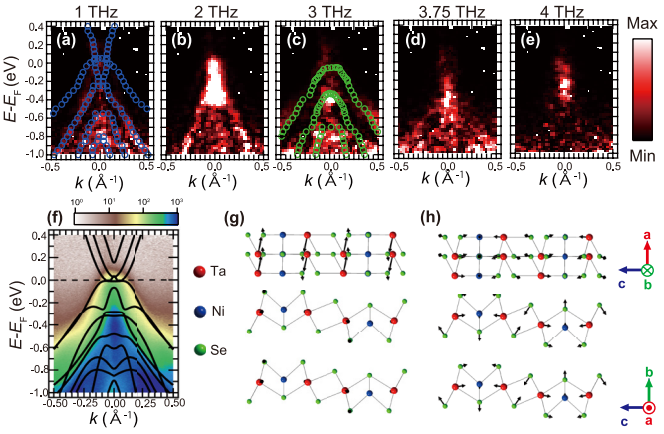

Fig. 2. (a)–(e) Frequency-domain angle-resolved photoemission spectroscopy (FDARPES) spectra shown as frequency-dependent intensities of the oscillation components as a function of energy and momentum. The peak positions in the TARPES spectra after and before photoexcitation are plotted as blue and green circles in (a) and (c), respectively. (f) Calculated band structure of Ta_2NiSe_5 based on the density functional theory within a generalized gradient approximation (GGA) superimposed onto the photoemission spectrum before pump excitation. (g), (h) Calculated phonon modes corresponding to (b) and (c), respectively.

Reference
[1] T. Suzuki, Y. Shinohara, Y. Lu, M. Watanabe, J. Xu, K. L. Ishikawa, H. Takagi, M. Nohara, N. Katayama, H. Sawa, M. Fujisawa, T. Kanai, J. Itatani, T. Mizokawa, S. Shin, and K. Okazaki, Phys. Rev. B **103**, L121105 (2021).

Authors
T. Suzuki, Y. Shinohara[a], Y. Lu[a], M. Watanabe, J. Xu, K. L. Ishikawa[a], H. Takagi[a,b], M. Nohara[c], N. Katayama[d], H. Sawa[d], M. Fujisawa, T. Kanai, J. Itatani, T. Mizokawa[e], S. Shin[a], and K. Okazaki
[a]The University of Tokyo
[b]Max Planck Institute
[c]Okayama University
[d]Nagoya University
[e]Waseda University

Multiband Superconductivity in Strongly Hybridized 1*T*'-WTe_2/$NbSe_2$ Heterostructure

Inducing superconductivity by proximity in materials with nontrivial band topology has become a method in the search for unconventional forms of superconducting pairing. At the one-dimensional (1D) edges of two-dimensional (2D) topological insulators the presence of non-Abelian parafermions has been predicted, which could have important applications in topological quantum computation. Here, we investigate heterostructures of the quantum spin Hall candidate 1*T*'-WTe_2, grown by *in situ* van der Waals epitaxy on a superconductor 2H-$NbSe_2$ by scanning tunneling spectroscopy down to 500 mK, which enables us to resolve the superconducting local density of states (LDOS) across the interface between the two materials.

Figure 1 shows scanning tunneling microscopy (STM) data of 1*T*'-WTe_2/2H-$NbSe_2$ heterostructures. In agreement with previous studies of WTe_2 on bilayer graphene, we observe islands with disordered boundaries and sizes up to a few tens of nanometer in diameter that are polycrystalline on $NbSe_2$ substrates. Lattice parameters estimated from FFT patterns of the STM images are $a \sim a_1 = 3.5 \pm 0.2$ Å, and $b \sim 2a_2\cos(30°) = 6.2 \pm 0.3$ Å, in good agreement with the lattice parameters of WTe_2 ($a = 3.48$ Å and $b = 6.28$ Å) and $NbSe_2$ ($a_1 = a_2 = 3.45$ Å). Local lattice matching implies a 5% compressive lattice strain along b, which has previously been shown to further stabilize the WTe_2 bulk gap.

In Fig. 2, tunneling spectra taken on the monolayer WTe_2 and the $NbSe_2$ substrate at 500 mK are presented, demonstrating the clear signature of a superconducting energy gap in the 2D monolayer WTe_2. The measured superconducting LDOS within a self-consistent multiband framework that considers a superconducting gap of each band and an interband Cooper-pair tunneling rate. It has been already known

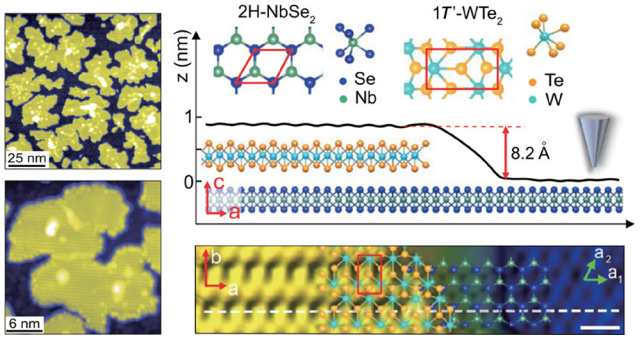

Fig. 1. (left panels) STM topography of monolayer 1*T*'-WTe_2 islands grown on a single crystal of 2H-$NbSe_2$ by van der Waals epitaxy. Upper right panel shows height profile corresponding to the dashed white line in the lower right panel, showing a monolayer height of 8.2 Å. The inset shows the respective 1*T*'-WTe_2 and 2H-$NbSe_2$ crystal structures. Atomic-resolution close-up of the 1*T*'-WTe_2 edge, showing detail of the atomic alignment.

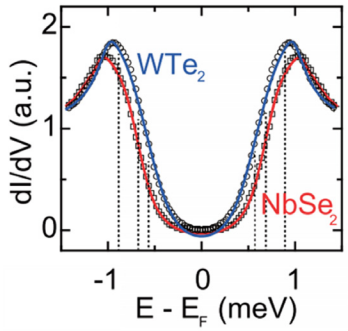

Fig. 2. tunneling spectra comparing the WTe_2/$NbSe_2$ spectrum with that measured on the bare $NbSe_2$ substrate. Solid red and blue lines are fits to our two-band ($NbSe_2$) and three-band (WTe_2) models, respectively.

that the gap of $NbSe_2$ is well described with a scheme of intrinsic two-band superconductor, and here we consider a third order parameter Δ_{WTe2}, coupled to the two $NbSe_2$ bands, assuming intrinsic $\Delta_{WTe2} = 0$. Fits to both a two-band ($NbSe_2$, red line) and a three-band (WTe_2/$NbSe_2$, blue line) model explain the data well (Fig. 2) and reproduce the known $NbSe_2$ order parameters. Self-consistently obtained $\Delta_{WTe2} = (0.57 \pm 0.02)$ meV, reflecting induced pairing, which suggests strong hybridization between the overlayer and substrate.

Our tight-binding calculations revealed that the strong hybridization in WTe_2/$NbSe_2$ heterostructure substantially weakens the topological edge state signature compared with WTe_2/HOPG, which is only weakly hybridized. In spite of

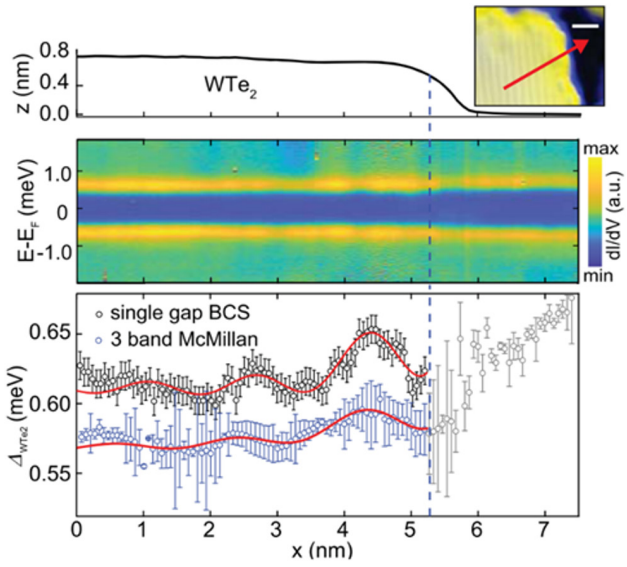

Fig. 3. (upper panel) STM-height profile measured across a clean edge of a WTe_2 monolayer crystal. The inset shows the corresponding STM topograph indicating position and direction of the line profile (red arrow). (middle) A series of tunneling spectra measured T = 500 mK for points across the edge. (lower) Extracted spatial profile of the induced order parameter $\Delta_{WTe2}(x)$ (blue), compared with a single-band BCS-Dynes model (black).

the suppressed edge states, however, we observed enhanced order parameter at the edge as shown in Fig. 3, where a spatial profile of the extracted order parameter $\Delta_{WTe2}(x)$ based on the three-band superconductivity analysis is shown. The plot also shows spatial oscillations with a period of ~2 nm. Oscillations of comparable period are also observed in the order parameter extracted from a simple single-band BCS model. This suggests that these arise from Friedel-like oscillations in the local density of states due to scattering of 2D bulk states at the WTe_2 edge. The exponential decaying 1D edge state, with decay length (1.1 ± 0.2) nm is comparable to the normal-state LDOS of the edge.

Reference
[1] W. Tao *et al.*, Phys. Rev. B **105**, 094512 (2022).

Authors
W. Tao[a], Z. J. Tong[a], A. Das[b], D.-Q. Ho[a], Y. Sato, M. Haze, J. Jia[a], Y. Que[a], F. Bussolotti[c], K. E. J. Goh[a,c], B. Wang[d], H. Lin[e], A. Bansil[d], S. Mukherjee[b], Y. Hasegawa, and B. Weber[a,f]
[a]Nanyang Technological University, Singapore
[b]Indian Institute of Technology Madras
[c]Agency for Science Technology and Research (A*STAR)
[d]Northeastern University
[e]Institute of Physics, Academia Sinica
[f]Monash University

PI of Joint-use project: B. Weber
Host lab: Hasegawa Group

Bayesian Optimization of Thin Film Growth Parameters

The use of thin films for developing new crystalline materials is an attractive approach because the crystal growth process is fast, the volume of required material is small, and a relatively large number of samples with varying composition or structure can be rapidly synthesized. However, the physical properties of thin films are very sensitive to small changes in the various process parameters that control the film growth. Besides the usual thermodynamic parameters, such as pressures or temperatures, thin film growth is also affected by kinetic effects, such the growth rate. For this reason, the process space, in addition to the composition space, can be very multi-dimensional. Exhaustive mapping of materials properties over the whole available temperature, pressure, growth rate, etc. ranges is therefore very time consuming and in practice, a human operator would struggle in determining the optimum combination of parameter combinations to test to complete a materials exploration or optimization task with the smallest number of experiments. In this regard, help may be available from the various machine learning methods that have been developed in recent years. In particular, the dimensionality problem of the process parameter space can be handled by Bayesian optimization, as illustrated in Fig. 1.

The thin film synthesis system illustrated in Fig. 1 was recently developed by Dr. Ohkubo at NIMS [1]. Nitride thin films are grown by metal-organic molecular beam epitaxy (MO-MBE) from an organic precursor in the presence of activated nitrogen plasma. In this work, the growth of TiN was attempted as a demonstration of the MO-MBE process using tetrakis(dimethylamido)titanium (TDMAT) as a Ti source. The TiN films were characterized by x-ray diffraction (XRD) and transport analysis. In particular, the superconducting transition temperature of TiN was used as a more sensitive measure of the crystalline quality of the films than

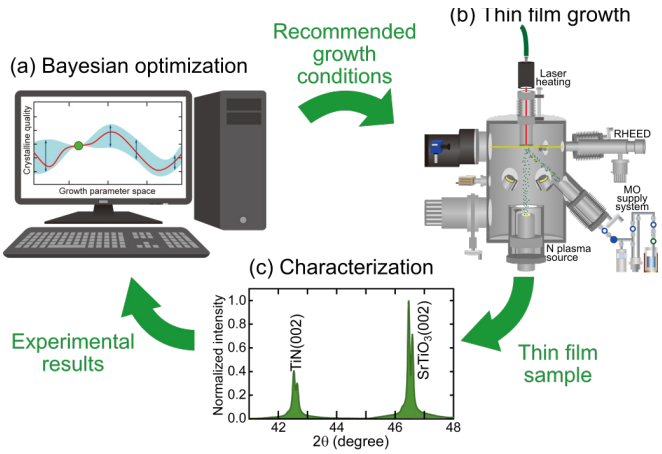

Fig. 1. Closed-loop optimization of epitaxial thin film growth conditions using a Bayesian approach. Nitride thin films were grown by metal-organic molecular beam epitaxy (b) and characterized by x-ray diffraction (c). The film peak intensity was used as the feedback for the Bayesian optimizer (a).

is possible by XRD analysis. A small set of initial samples was synthesized by manually selecting the primary process parameters: the film growth temperature, the TDMAT source foreline pressure, the nitrogen flow rate, and the excitation power of the nitrogen plasma source. These four parameters effectively determine the growth mode (temperature), rate (TDMAT flow rate), and the nitrogen activity.

After the initial set of samples were synthesized and characterized by XRD, further combinations of the four main parameters were selected by a Bayesian optimization process using the normalized TiN peak intensity in the XRD pattern as the objective function. The growth temperature range was limited to 550 to 900 °C, the TDMAT pressure was between 0.5 and 10.5 Torr, the N_2 flow rate was limited to 0.5 to 5 sccm, and the plasma source power limits were 270 to 500 W, forming a search grid of 7 × 100 × 45 × 23 points. After every film growth experiment, the XRD pattern was analyzed and a new process point was determined by the Bayesian process. The cycle was repeated for 20 times. No further improvement of the XRD peak intensity was obtained after 10 cycles.

The low-temperature superconducting transition temperature measurements were done at ISSP. The gradual improvement of the critical temperature in the Bayesian optimization process is shown in Fig. 2. It can be seen that the maximum T_c of 5.2 K was obtained on the tenth cycle, after which no further increase was obtained.

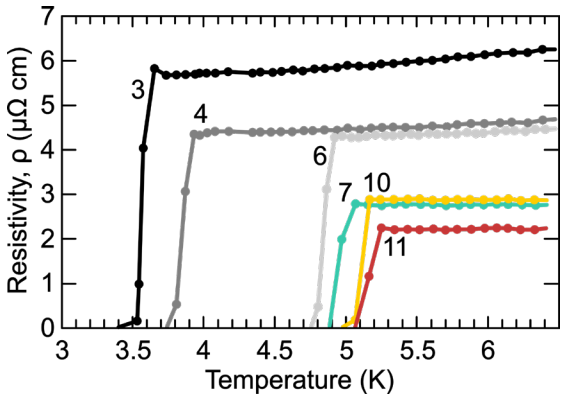

Fig. 2. Gradual improvement of the superconducting transition temperature of TiN thin films as a function of the synthesis-characterization-selection cycle index. No further improvement was obtained after just 10 synthesis experiments.

This experiment was the first demonstration of closed-loop thin film synthesis controlled by a machine learning algorithm for reducing the number of film growth experiments required to reach the optimal physical properties. In this work, XRD was used as the source of the feedback signal for the Bayesian process. This means that the cycle time (Fig. 1) was limited by the diffraction analysis, not by synthesis. In addition to the XRD and transport data, in situ electron diffraction data was also collected. In the future, it may be possible to greatly increase the rate of materials development by using real-time in situ characterization tools for providing the feedback signal for a Bayesian process optimizer.

Reference
[1] I. Ohkubo, Z. Hou, J. N. Lee, T. Aizawa, M. Lippmaa, T. Chikyow, K. Tsuda, and T. Mori, Mater. Today Phys. **16**, 100296 (2021).

Authors
I. Ohkubo[a], Z. Hou[a], J. N. Lee, T. Aizawa[a], M. Lippmaa, T. Chikyow[a], K. Tsuda[a], and T. Mori[a]
[a]NIMS

PI of Joint-use project: I. Ohkubo
Host lab: Lippmaa Group

Adsorption and Reaction of Formic Acid on Cu(111)

Hydrogen is one of the promising energy sources toward the carbon neutral and sustainable society. Formic acid (HCOOH) has attracted attention as a candidate for the hydrogen storage material because it is nontoxic and exists as a stable molecule at standard temperature and pressure conditions. In general, HCOOH can be catalytically converted into CO_2 and H_2 via dehydrogenation or into CO and H_2O via dehydration. Among others, a Cu surface is one of the attractive catalysts, because HCOOH is selectively decomposed into CO_2 and H_2 via the formate (HCOO) intermediate without generating CO. However, the mechanism of HCOOH dehydrogenation is not yet fully understand. One of the reasons may be that the state of HCOOH on a Cu surface, in which HCOOH is adsorbed in a polymeric form, is not yet determined. Furthermore, there is a discrepancy between the computational and experimental adsorption energies [1]. Toward the full understanding of the HCOOH dehydrogenation on Cu catalyst, we conducted density functional theory studies on monomeric as well as polymeric adsorption of HCOOH on Cu(111), as well as their dehydrogenation reactions.

We used the rev-vdW-DF2 [2], a variant of the van der Waals density functional (vdW-DF). Use of vdW-DF is essential, as the interaction between HCOOH and Cu surface is very weak and is of dispersion type. The surfaces were represented using slab models, and the electrostatic interaction in the surface normal direction was treated rigorously by using the effective screening medium method.

We first investigated the monomeric adsorption of HCOOH on Cu(111) and found that the adsorption energy is much smaller than the experimental value, when the generalized gradient approximation is used, while it is in better agreement with the experiment, when the dispersion forces are properly described via vdW-DF [3].

We then investigated the molecular structures for the polymeric HCOOH adsorption. In the literature, there have been proposals of the so-called α- and β-polymeric structures on the surfaces (Fig. 1), according to the crystalline HCOOH, but the stable form on Cu(111) has yet to be resolved. We explored the stable structure of polymeric HCOOH by considering various structures and in-plane periodicities. HCOOH interacts weakly with the surface, while it interacts with the neighboring molecules via the H-bonding-like interaction. We found that the β-polymeric form is energetically more stable than the α one, although they are energetically competing. However, by simulating the vibrational spectra, scanning tunneling microscopy/atomic force microscopy (AFM) images (Fig. 2), and by comparing with the experiments, we concluded that α-polymeric HCOOH is more plausible and has been formed and observed in the experiments [4, 5]. We then studied the dehydrogenation reaction by taking the edge effect into account. We found that the dehydrogenation reaction is facilitated at the edge of the polymeric HCOOH chain, and it barely occurs within the polymeric HCOOH chain. Our results are consistent with the previous experiments.

The polymeric HCOOH is decomposed (in part) into HCOO and form complex nanostructures, depending on the annealing temperature. We performed extensive structure search of HCOOH-HCOO and HCOO with different compositions and successfully determined the structures of chain-like monodentate HCOO + HCOOH and monodentate HCOO + bidentate HCOO aggregates as well as bidentate HCOO clusters by evaluating the adsorption energies and simulating the AFM images [4].

In summary, we have clarified the adsorption states of HCOOH as well as the aggregates composed of HCOOH and HCOO and the mechanism of the dehydrogenation of HCOOH into HCOO on Cu(111), and succeeded in tracking the fate of HCOOH on Cu(111) upon annealing.

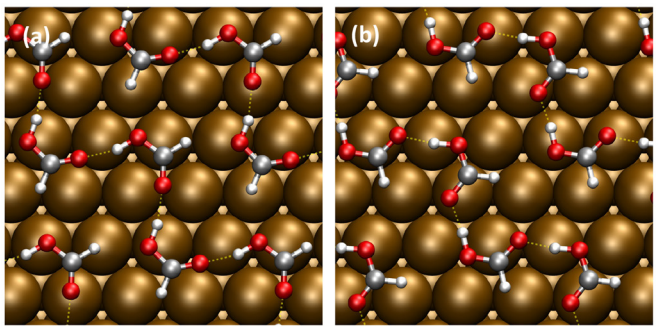

Fig. 1. Structures of (a) α-polymeric and (b) β-polymeric HCOOH's on Cu(111).

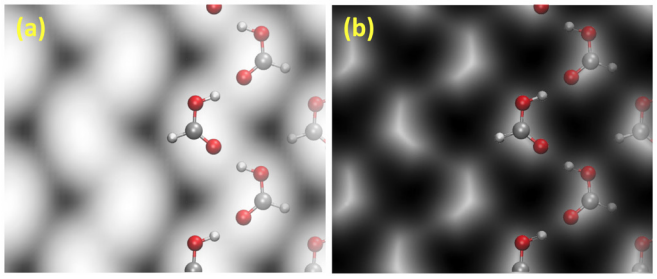

Fig. 2. (a) Simulated scanning tunneling microscopy image and (b) simulated atomic force microscopy image of polymeric HCOOH in the α-form on Cu(111). Tersoff-Hamann and probe particle methods were used to generate the former and the latter, respectively.

References
[1] Y. Shiozawa, T. Koitaya, K. Mukai, S. Yoshimoto, and J. Yoshinobu, J. Chem. Phys. **143**, 234707 (2015).
[2] I. Hamada, Phys. Rev. B **89**, 121103(R) (2014).
[3] S. E. M. Putra, F. Muttaqien, Y. Hamamoto, K. Inagaki, I. Hamada, and Y. Morikawa, J. Chem. Phys. **150**, 154707 (2019).
[4] A. Shiotari*, S. E. M. Putra*, Y. Shiozawa, Y. Hamamoto, K. Inagaki, Y. Morikawa, Y. Sugimoto, J. Yoshinobu, and I. Hamada, Small **17**, 2008010 (2021). (*: equal contribution)
[5] S. E. M. Putra, F. Muttaqien, Y. Hamamoto, K. Inagaki, A. Shiotari, J. Yoshinobu, Y. Morikawa, and I. Hamada, Phys. Rev. Materials **5**, 075801 (2021).

Authors
I. Hamada[a], S. E. M. Putra[a], F. Muttaqien[b], Y. Hamamoto[a], K. Inagaki[a], A. Shiotari[c], Y. Sugimoto[c], J. Yoshinobu, and Y. Morikawa[a]
[a]Osaka University
[b]Institut Teknologi Bandung
[c]The University of Tokyo

PI of Joint-use project: I. Hamada
Host lab: Yoshinobu Group

Photon Echo from Lensing of Fractional Excitations in Tomonaga-Luttinger Spin Liquid

Physicists routinely diagnose the properties of a material by its linear responses to external stimuli. The recently developed nonlinear spectroscopy measures nonlinear optical responses to obtain more information on the material. Yet, it is often unclear if there is a straightforward connection between such nonlinear responses and the material's properties, especially when its constituent particles strongly interact with one another. We addressed this question by studying theoretically a prototypical strongly interacting system, the Tomonaga-Luttinger spin liquid. Tomonaga was the first to point out that the low-energy excitations of fermions in one dimensions can be described in terms of quantized sound waves (phonons). Subsequent studies have established that the quantum theory of sound waves, which is now called Tomonaga-Luttinger liquid, can describe the universal low-energy physics of a wide variety of one-dimensional critical quantum many-body systems. This includes critical one-dimensional quantum spin systems, which are regarded as Tomonaga-Luttinger spin liquids.

A remarkable feature of the Tomonaga-Luttinger spin liquids is "fractionalization" of the spin excitations. In ordered magnets, the elementary excitation corresponds to a single spin flip and called "magnon". A single magnon is created by an absorption of photon (or a scattering of neutron), resulting in a sharp peak in the spectrum of linear response. In contrast, in the Tomonaga-Luttinger spin liquid, the single spin flip caused by an absorption of photon fractionalizes into two "spinon" excitations. This leads to a continuum in the linear response spectrum. While this "two-spinon continuum" is a characteristic signature of the fractionalization, the absence of the sharp peak makes the analysis difficult.

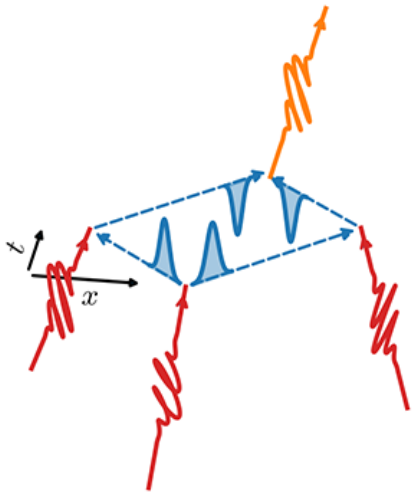

Fig. 1. Schematic diagram of the photon echo. The first photon creates a pair of fractionalized spinon excitations, the second and third photons reflect them back, refocusing them to give rise a sharp echo.

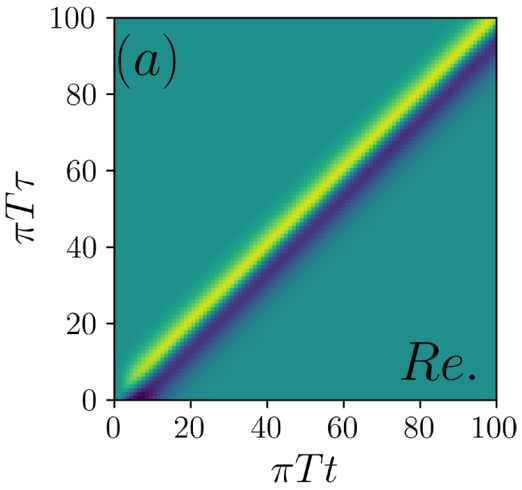

Fig. 2. The photon echo signal in real time. Despite the fractionalization, the sharp signal remains over a long period of time thanks to the spinon lensing effect.

We analyzed nonlinear optical responses of the Tomonaga-Luttinger spin liquids in the context of terahertz (THz) two-dimensional coherent spectroscopy (2DCS), which is developing rapidly in recent years. We find a direct link between a specific nonlinear response, known as photon echo, and the dynamical properties of the excitations in this system.

The central finding in our work was that we can recover the sharp peak even in the Tomonaga-Luttinger spin liquid with the fractionalized spinon excitations, if we look at the nonlinear responses in a particular manner. The photon echo is measured by three successive optical pulses. The sharp response appears as a surge in the response after the last pulse. In the Tomonaga-Luttinger spin liquid, we trace the origin of the photon echo to a unique "lensing" phenomenon: The first pulse creates a pair of spinons moving in opposite directions. The second and third pulses change their directions of motion. These two excitations thus come back toward each other and reunite, thereby giving rise to the echo. Dissipation and dispersion effects, which suppress the lensing phenomenon, are sensitively picked up by the echo signal. This will make the 2DCS a very useful experimental probe to study these effects, which would be quite difficult with conventional experimental measurements.

Our work thus uncovers one aspect of the many uses of the nonlinear spectroscopy and related dynamical phenomena. We believe that more interesting physics is yet to be explored in the nonlinear responses of strongly correlated systems, and hope that our work will stimulate further theoretical and experimental studies.

Reference
[1] Z.-L. Li, M. Oshikawa, and Y. Wan, Phys. Rev. X **11**, 031035 (2021).

Authors
Z.-L. Li[a], M. Oshikawa, and Y. Wan[a]
[a]Institute of Physics, Chinese Academy of Sciences

PI of Joint-use project: Y. Wan
Host lab: Oshikawa Group

Pressure-Induced Multicriticality and Electronic Instability in the Quasi-Kagome Ferromagnet URhSn

URhSn crystallizes in the hexagonal ZrNiAl-type structure without inversion symmetry. The U atom forms the quasi-kagome structure, in which the magnetic frustration is potentially expected. The rare-earth based family, such as CePdAl and YbAgGe, indeed shows the novel magnetic phase diagram due to this magnetic frustration. In U based system, the ferromagnetic quantum critical behavior is well established, for example in UCoAl and URhAl, where the wing-shaped temperature-pressure-field phase diagram associated with the first order metamagnetic transition is demonstrated.

In URhSn, two successive transitions had been reported in the previous literature. The one is the ferromagnetic Curie temperature at T_C = 16 K with the relatively large ordered moment of 2.1 μ_B directed along c-axis, the other transition occurs at T_O = 54 K with the large specific heat jump. The origin for the latter transition is still unclear from the neutron scattering experiments and Mossbauer spectroscopy, meaning that the order parameter remains "hidden". Thus a quadrupole or multipole order is inferred [1].

In this study, we performed the electrical resistivity measurements under pressure up to 11 GPa [2]. The two transitions are abruptly switched to the two different transitions at the critical pressure, P_C ~ 6.3 GPa, indicating two bicritical points associated with the Fermi surface reconstructions.

High quality single crystals were grown using the Czochralski method in a tetra-arc furnace. The obtained single crystals were then annealed at 800 °C under vacuum for one month. The residual resistivity ratio (RRR) is about 40, and the de Haas-van Alphen oscillations are successfully detected, revealing the mean free path of ~1000 Å, indicating the high quality of our sample. A bar shaped single crystal was set into a cubic anvil cell for the resistivity measurements at high pressure up to 11 GPa and at low temperatures down to 2.5 K. The electrical current was applied along the [11-20] direction.

Figure 1 shows the temperature-pressure phase diagram determined from the resistivity measurements. Two transitions at T_C and T_O were clearly detected with two kinks in the resistivity measurements. Interestingly, T_O decreases with pressure, while T_C slightly increases up to the critical pressure, P_C ~ 6.3 GPa. Further increasing pressure, T_O increases, displaying a sharp minimum at Pc as a function of pressure, while T_C drops suddenly, and increases again. These abrupt changes of T_C and T_O indicate that the first order phase boundary exists at P_C, shown at the ABC line in the phase diagram of Fig. 1. The residual resistivity also abruptly increases at P_c and remains the large value, suggesting the drastic change of the electronic state. The resistivity A coefficient, assuming the T^2 dependence of the resistivity, also shows a sudden increase above P_C, which also supports the drastic change of the electronic state, possibly associated with the Fermi surface reconstruction.

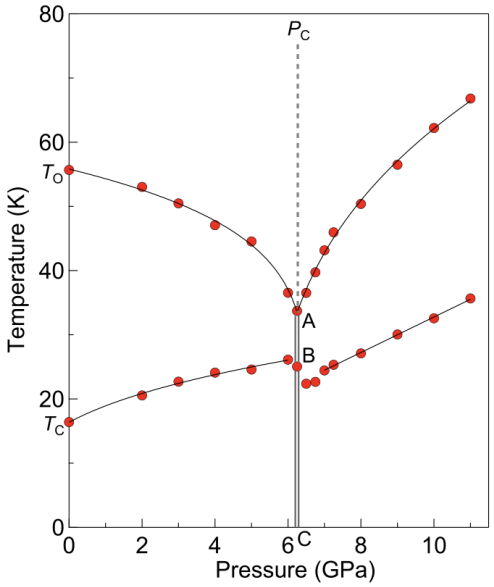

Fig. 1. Temperature-pressure phase diagram of URhSn.

Of course, we don't know yet what are the order parameters for the different two phases above P_C. The present results, however, reveals the novel pressure-induced quantum phase transitions. Interestingly, this multicriticality is possibly related to the higher order multiple order and the associated multiple phases, which occurs in the 5*f*-electron systems without inversion symmetry in the crystal structure. Further experiments with microscopic probes are required.

References
[1] Y. Shimizu, A. Miyake, A. Maurya, F. Honda, A. Nakamura, Y. J. Sato, D. Li, Y. Homma, M. Yokoyama, Y. Tokunaga, M. Tokunaga, and D. Aoki, Phys. Rev. B. **102**, 134411 (2020).
[2] A. Maurya, D. Bhoi, F. Honda, Y. Shimizu, A. Nakamura, Y. J. Sato, D. Li, Y. Homma, M. Sathiskumar, J. Gouchi, Y. Uwatoko, and D. Aoki, Phys. Rev. B **104**, 195119 (2021).

Authors
D. Aoki[a] and A. Maurya[a]
[a]IMR, Tohoku University

PI of Joint-use project: A. Maurya
Host lab: Uwatoko Group

Pressure-Induced Lifshitz Transition Observed from Nuclear Magnetic Resonance in S-Substituted FeSe

We performed ^{77}Se-nuclear magnetic resonance (NMR) measurements under pressures of up to 3.9 GPa on 12 % S-substituted FeSe and observed a pressure-induced Lifshitz transition at around 1.0 GPa from the Knight shift (K) and relaxation rate ($1/T_1$) [1].

FeSe is unique among iron-based superconductors in the point that small unconnected Fermi surfaces induce superconductivity without magnetism. The left panel of Fig. 1(a) shows the Fermi surfaces in the tetragonal phase. The Fermi surfaces consist of the small hole pockets at point Γ, $\boldsymbol{k}$ = (0, 0), and anisotropic electron pockets at point X, $\boldsymbol{k}$ = (π, 0) or (0, π) [2-4]. The superconductivity appears in the nematic phase where four-fold rotational

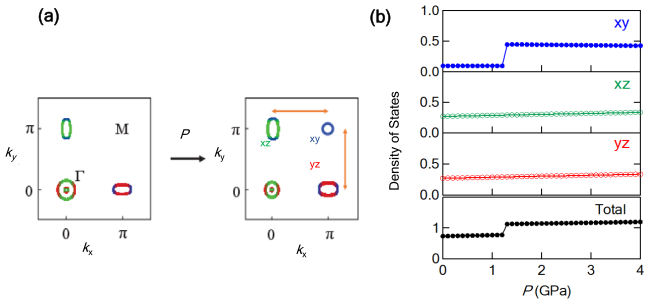

Fig. 1. (a) Schematic Fermi surfaces of pure FeSe in a tetragonal phase theoretically derived at ambient pressure and high pressure. The Fermi surfaces colored in green, red, and blue represent d_{xz}, d_{yz}, and d_{xy} orbitals, respectively. Arrows indicate the nesting of d_{xy} orbitals between points M and X. (b) The density of states (DOS) originating from each orbital and the total DOS calculated theoretically for 10% S-substituted FeSe.

symmetry is broken. Unlike iron-based pnictides, this orbital configuration reduces the likelihood of nesting between electron and hole pockets with the same orbital, leading to the absence of magnetism.

Upon pressure application, FeSe undergoes an antiferromagnetic (AF) order instead of the nematic order [5]. Although the nematic and AF phases are complicatedly entangled in the pressure versus temperature (P-T) phase diagram, S substitution makes possible to resolve the complex overlap between them [6].

Figure 2(a) shows the P-T phase diagram for 12% S-substituted FeSe determined from ac susceptibility and ^{77}Se-NMR measurements [1]. A single crystal with dimensions of approximately 1.0mm × 1.0mm × 0.5mm was used for these experiments. Figure 2(b) shows $1/T_1T$ for the field parallel to the FeSe plane. The color plot in Fig. 2(a) obtained from $1/T_1T$ provides a measure of low-energy spin fluctuations. As seen from the color plot, AF fluctuations below and above 1 GPa are of different origins. Strong AF fluctuations develop without magnetism in the nematic phase below 1 GPa, whereas AF fluctuations seem to be weak above 1 GPa despite of the AF-phase boundary.

The anomaly at 1 GPa is also observed in the shift K. The NMR spectra at 60 K and K at 60 and 70 K are shown in Fig. 3(a) and 3(b), respectively. The shift is decomposed as $K = K_{orb} + K_{spin}$ where K_{spin} and K_{orb} represent the spin and orbital parts, respectively. The former and latter are T-dependent and T-independent, respectively. The orbital part K_{orb} is

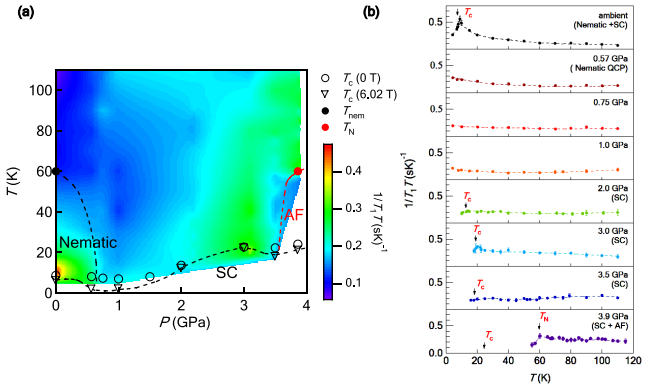

Fig. 2. (a) Color plot of relaxation rate divided by temperature ($1/T_1T$). The superconducting (SC) phase shows a double-dome structure at 6.02 T. T_Cs shown by circles and inverted triangles are determined from AC susceptibility measurements at 0 T and 6.02 T, respectively. Both nematic and SC orders are absent at 1.0 GPa at 6.02 T. (b) T dependence of $1/T_1T$ measured at 6.02 T for the field parallel to the FeSe plane. T_Cs shown by arrows are the same with those in Fig. 2(a).

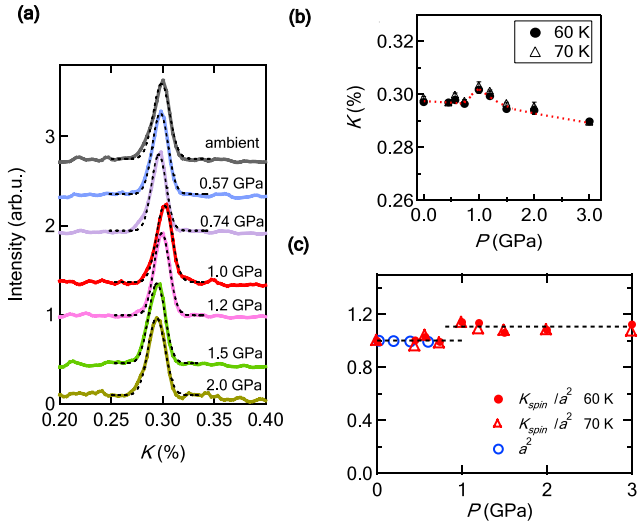

Fig. 3. (a) Pressure dependence of the NMR spectra at 60 K. Each spectrum is fitted with a Gaussian function, as indicated by dotted curves. (b) Pressure dependence of the Knight shift (K) measured at 60 and 70 K. The dotted curves are guides to the eye. (c) Pressure dependence of the spin part of K divided by a^2 (K_{spin}/a^2) where a represents the square of the a-axis lattice constant. In the figure, K_{spin}/a^2 and a^2 are normalized by those at ambient pressure. The dashed lines represent the average of K_{spin}/a^2 at pressure regions below and above 1 GPa. The results in Fig. 3(c) are comparable to theoretical calculations in Fig. 1(b).

~0.26% at low pressures below 1 GPa and decreases 0.005 and 0.01 % at 2 and 3 GPa, respectively. The decrease at high pressures is estimated from the decrease in K_{spin} due to superconductivity [1]. The spin part K_{spin} and the uniform susceptibility $\chi(0)$ are related to $K_{spin} = A\chi(0)$ where A is the hyperfine coupling. Since $\chi(0)$ can be described using the density of states (DOS) of a 2D free electron system, K_{spin} is expressed as $K_{spin} \propto (Na)^2m/\hbar$ where N^2, a, and m are the total number of lattices, lattice constant, and electron mass, respectively. Two quantities, K_{spin}/a^2 and a^2, normalized by those at ambient pressure are shown in Fig. 3(c).

The step-like enhancement of K_{spin}/a^2 at 1 GPa implies the appearance of other Fermi surfaces, as expected theoretically at high pressures [4] (See the right panel of Fig. 1(a)). The results of K_{spin}/a^2 are comparable to the theoretically calculated total DOS shown in Fig. 1(b). The Fermi surface at point M, $\boldsymbol{k} = (\pi, \pi)$, is of d_{xy}-orbital origin, leading to the nesting with unconnected Fermi surfaces with the same d_{xy} orbital (See yellow arrows in Fig. 1(a)). In fact, the enhancement of K_{spin}/a^2 seems to be smaller than that shown in Fig. 1(b), implying that the size of the hole pocket at the point M is fairly small. This unbalanced nesting would induce very weak AF fluctuations observed at high pressures above 1 GPa.

In conclusion, we performed ^{77}Se-NMR measurements on 12% S-substituted FeSe under pressures of up to 3.9 GPa. We observed the anomalies of K and $1/T_1T$ corresponding to the theoretically predicted Lifshitz transition. Our results suggest that the emergence of the d_{xy} orbital and its orbital-selective coupling play a key role to understand the electronic properties of FeSe at high pressures.

References

[1] T. Kuwayama, *et al.*, Scientific Reports **11**, 17265 (2021).
[2] M. D. Watoson, *et al.*, Phys. Rev. B **91**, 155106 (2015).
[3] L. Fanfarillo, *et al.*, Phys. Rev. B **97**, 121109 (2018).
[4] Y. Yamakawa, *et al.*, Phys. Rev. B **96**, 144509 (2017).
[5] J. P. Sun, *et al.*, Nat. Commun. **7**, 12146 (2016).
[6] K. Matsuura, *et al.*, Nat. Commun. **8**, 1143 (2017).

Authors
T. Kuwayama[a], K. Matsuura[b], J. Gouchi, Y. Yamakawa[c], Y. Mizukami[b], S. Kasahara[a], Y. Matsuda[a], T. Shibauchi[b], H. Kontani[c], Y. Uwatoko, and N. Fujiwara[a]
[a]Kyoto University
[b]University of Tokyo
[c]Nagoya University

PI of Joint-use project: N. Fujiwara
Host lab: Uwatoko Group

High-Pressure Phase Diagrams of $FeSe_{1-x}Te_x$: Correlation Between Suppressed Nematicity and Enhanced Superconductivity

The interplay among magnetism, electronic nematicity, and superconductivity is the key issue in strongly correlated materials including iron-based, cuprate, and heavy-fermion superconductors. Magnetic fluctuations have been widely discussed as a pairing mechanism of unconventional superconductivity, but recent theory predicts that quantum fluctuations of nematic order may also promote high-temperature superconductivity. This mechanism of unconventional superconductivity is distinctly different from the one based on spin fluctuations, and its experimental verification remains elusive. This is partly due to the closeness between nematic and antiferromagnetic orders in iron-pnictide superconductors, and the enhanced superconductivity can be found near both ends of these two ordered phases, where both magnetic and nematic fluctuations are enhanced. FeSe with a superconducting transition temperature $T_c \approx 9$ K serves as an ideal platform to study the relationship between the nematicity and superconductivity, because unlike other iron-based superconductors its nematic order below the structural transition at $T_s \approx 90$ K is accompanied by no magnetic order [1].

In this study, we have succeeded in growing high-quality single crystals of $FeSe_{1-x}Te_x$ superconductors, another family of FeSe-based materials, which we use to study the electronic phase diagram in a wide range of Te composition under pressure [2]. The single crystals of $FeSe_{1-x}Te_x$were grown by the chemical vapor transport technique, which overcomes the phase separation issue reported in the previous crystal growth for a low Te composition range. The resistivity and synchrotron X-ray diffraction measurements show that the electronic nematic transition

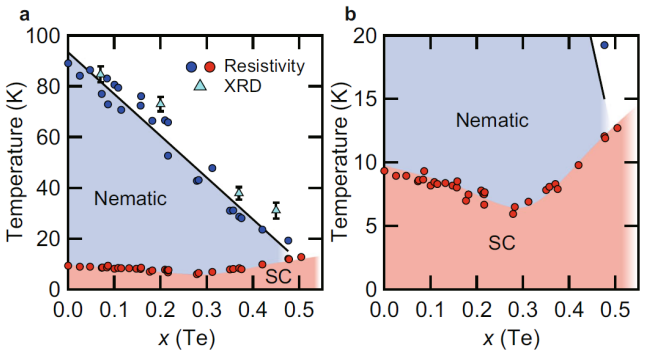

Fig. 1. a, Nematic and superconducting transition temperatures as a function of Te composition x(Te). The blue and red circles represent the nematic (T_s) and superconducting (T_c) transition temperatures, respectively, determined by the resistivity measurements. The light blue triangles represent T_s, determined by the splitting of the Bragg peaks in the XRD measurements. b, The same as in a, but the temperature range is 0–20 K.

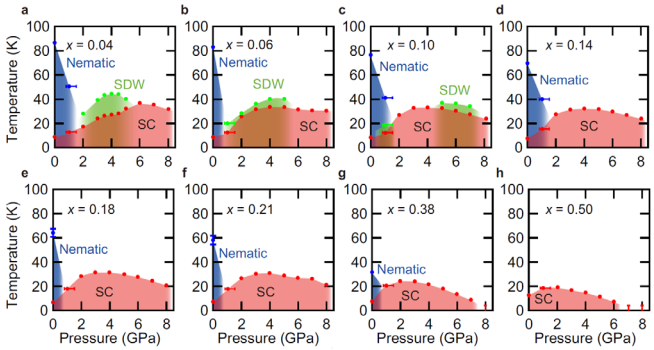

Fig. 2. Pressure dependence of T_c, T_s, and T_m indicated by red, blue, and green circles, respectively, for x(Te) ≈ 0.04 (a), 0.06 (b), 0.10 (c), 0.14 (d), 0.18 (e), 0.21 (f), 0.38 (g), and 0.50 (h).

temperature T_s is monotonically suppressed with increasing Te composition. As shown in Fig. 1, the nematic transition can be completely suppressed by ~50% substitution, while the superconducting transition temperature T_c shows a nonmonotonic composition dependence. We find that this nonmonotonic dependence of $T_c(x)$ does not correlate with the x(Te) dependence of residual resistivity ratio, implying that the T_c increase found for x(Te) > 0.3 has an intrinsic origin.

Figure 2 shows the high-pressure phase diagrams of $FeSe_{1-x}Te_x$ up to 8 GPa determined by the resistivity measurements performed by using the constant-load cubic anvil cell in Uwatoko group, ISSP, University of Tokyo. When Te composition x(Te) becomes larger than 0.1, the high-pressure magnetic order disappears, whereas the pressure-induced superconducting dome near the nematic end point is continuously found up to x(Te) ≈ 0.5. In contrast to $FeSe_{1-x}S_x$, enhanced superconductivity in $FeSe_{1-x}Te_x$ does not correlate with magnetism but with the suppression of nematicity. It is generally expected that the quantum fluctuations of electronic order are intensified near the end point of the associated order, so in the present case, nematic fluctuations are expected to be enlarged when the nematic order is suppressed wither by the Te substitution or pressure. Our results show that the superconducting dome exists near the end point of nematic order in $FeSe_{1-x}Te_x$, near which we have no magnetic order. These results highlight the paramount role of nonmagnetic nematic fluctuations for high-temperature superconductivity in this system.

References
[1] See, for a review, T. Shibauchi, T. Hanaguri, and Y. Matsuda, J. Phys. Soc. Jpn. **89**, 102002 (2020).
[2] K. Mukasa, K. Matsuura, M. Qiu, M. Saito, Y. Sugimura, K. Ishida, M. Otani, Y. Onishi, Y. Mizukami, K. Hashimoto, J. Gouchi, R. Kumai, Y. Uwatoko, and T. Shibauchi, Nat. Commun. **12**, 381 (2021).

Authors
K. Mukasa[a], K. Matsuura[a], M. Qiu[a], M. Saito[a], Y. Sugimura[a], K. Ishida[a], M. Otani[a], Y. Onishi[a], Y. Mizukami[a], K. Hashimoto[a], J. Gouchi, R. Kumai[b], Y. Uwatoko, and T. Shibauchi[a]
[a]The University of Tokyo
[b]KEK

PI of Joint-use project: T. Shibauchi
Host lab: Uwatoko Group

Topological Spin Orders in a Centrosymmetic Tetragonal Magnet $EuAl_4$ Investigated by Polarized Neutron Scattering

Topologically nontrivial magnetic orders have been intensively investigated since the pioneering work on magnetic skyrmion lattice in MnSi, in which Dzyaloshinski-Moriya (DM) interactions arising from the chiral crystal structure and ferromagnetic interactions lead to long-period modulated magnetic orders including the skyrmion lattice state. Therefore, the early studies on magnetic skyrmions were focusing mainly on ferromagnetic systems with broken spatial inversion symmetry. However, a recent study on an itinerant triangular lattice magnet Gd_2PdSi_3 [1] has revealed that centrosymmetric system can host magnetic skyrmion lattice owing to frustration in magnetic interactions or coupling between local magnetic moments and conduction electrons. In fact, subsequent studies have found the emergence of skyrmion lattice states in centrosymmetric magnets.

In the present study, we have found that $EuAl_4$, which is also a centrosymmetric magnet, exhibits two distinct skyrmion lattice states in magnetic field [2]. This system has a tetragonal crystal structure belonging to the space group of $I4/mmm$. By applying magnetic field along the c axis below 15 K, the system shows successive field-induced phase transitions, which is accompanied by anomalies in Hall resistivity. This is indicative of the topological Hall effect arising from a non-coplanar magnetic structure like skyrmion lattice state. To determine the magnetic structures in the field-induced phases, we performed polarized neutron scattering in a magnetic field at TAIKAN instrument (BL15) in the materials and life science experimental facility in J-PARC. By utilizing supermirror neutron spin polarizer and analyzer, we measured spin-flip and non-spin-flip scattering intensities of magnetic Bragg reflections appearing in the small-angle region in a magnetic field of 1 T with varying temperature. As a result, we found that this system exhibits rhombic and square lattices of Bloch-type magnetic skyrmion lattices in a magnetic field. We have further investigated magnetic phase transitions in zero magnetic field using the polarized triple-axis neutron spectrometer PONTA in JRR-3. The spectrometer was operated in the P_{zz} longitudinal polarization analysis mode, in which the polarization direction of the neutron spins was set to be perpendicular to the horizontal scattering plane. Figure 1 shows the summary of the measurements at PONTA. We have identified four magnetic phases below 15 K in zero field. Phase I and V have the magnetic modulation wave vectors (q-vectors) of (q,0,0), while phase IV does (q,q,0). By analyzing the neutron spin polarization of the scattered neutrons, the low temperature phases (I and V) and the highest temperature phase (IV) are found to have screw-type and fan-type magnetic modulations, respectively. Interestingly, the intermediate phase, phase VI, has both (q,0,0) and (q,q,0) wave vectors. By assuming a multi-q magnetic order in this phase, a superposition of these wave vectors (and their counterparts (0,q,0) and (q,–q,0)) results in another topologically-nontrivial magnetic order, which is distinct from the well-known magnetic skyrmion lattice state. We would also like to emphasize that the modulation periods of these incommensurate magnetic orders are relatively short, specifically, 2-3 nm, which cannot be resolved by Lorentz transmission electron microscope. The present study also demonstrates that polarized neutron scattering is quite useful to study short-period topological magnetic orders.

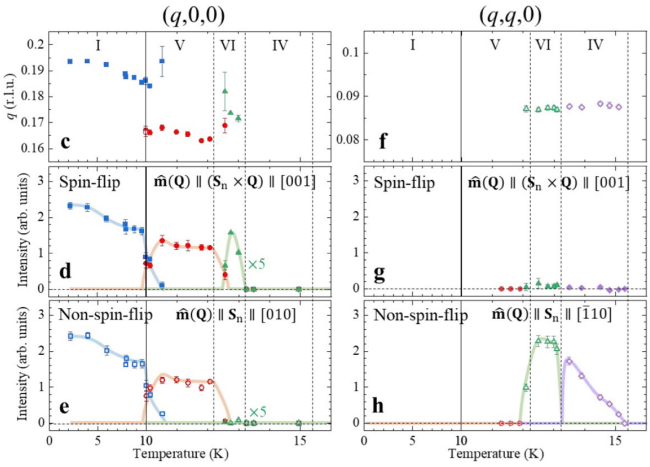

Fig. 1. Temperature dependence of spin-flip and non-spin-flip intensities of magnetic Bragg reflections in $EuAl_4$ measured by PONTA spectrometer in JRR-3.

References

[1] T. Kurumaji *et al*., Science. **365**, 914 (2019).
[2] R. Takagi *et al*., Nat. Commun. **13**, 1472 (2022).

Authors

R. Takagi[a], N. Matsuyama[a], V. Ukleev[b], L. Yu[b], J. S. White[b], S. Francoual[c], J. R. L. Mardegan[c], S. Hayami[a], H. Saito, K. Kaneko[d], K. Ohishi[e], Y. Ōnuki[f], T. Arima[a], Y. Tokura[a,f], T. Nakajima, and S. Seki[a]

[a]The University of Tokyo
[b]Paul Scherrer Institute
[c]Deutsches Elektronen Synchrotron (DESY)
[d]Japan Atomic Energy Agency (JAEA)
[e]Comprehensive Research Organization for Science and Society (CROSS)
[f]RIKEN-CEMS

PI of Joint-use project: R. Takagi
Host lab: Neutron Science Laboratory

High Field Quantum Phase in the Chromium Spinel Oxide $HgCr_2O_4$

The spin nematic state, which has long been discussed for magnets with frustrated interactions, is a spin analog of the nematic state in a liquid crystal. In this unconventional magnetic state, the fluctuations of spins, behaving like rod- or disk-shaped molecules, spontaneously select a preferred direction without conventional magnetic order. In this study, we have confirmed a possible spin nematic order in the chromium spinel oxide $HgCr_2O_4$ This compound is known as a highly frustrated pylochlore antiferromagnet with significant spin-lattice coupling. In fact, the wide half-magnetization plateau, which was stabilized by the lattice distortion, was reported in $HgCr_2O_4$ [1]. The magnetization process in the chromium spinel oxides has been accounted for the classical model with the bilinear and biquadratic interactions, derived by integrating out the lattice degrees of freedom [2]. However, the result of previous high field magnetization measurements indicated the existence of a phase, which cannot be explained by the classical model, just below the saturation field H_{c4} [3]. From the subsequent theory, this unknown phase was suggested to be the spin nematic phase, which is stabilized by the interplay of the spin-lattice coupling, geometrical spin frustration and quantum fluctuation [4]. To gain thermodynamic evidence for the existence

of the magnetic ordering in the phase just below H_{c4}, we have performed the specific heat and the magnetocaloric effect measurements under pulsed high magnetic fields up to 42 T [5]. Figure 1 shows the results of the magnetocaloric effect measurements. The sharp dips at $H_{c3} \sim 37$ T and $H_{c4} \sim 40$ T in the magnetocaloric effect under the quasi-isothermal condition unambiguously exhibit the magnetic phase for $H_{c3} < H < H_{c4}$, whereas the fact that only a small kink is observed at H_{c3} under the quasiadiabatic condition indicates that the phase between H_{c3} and H_{c4} is gapless. From a peak of the specific heat at 38.5 K, we have also confirmed the ordering for $H_{c3} < H < H_{c4}$. From these thermodynamic measurements, we have obtained the magnetic field and temperature phase diagram, shown in Fig. 4. In the Heisenberg-type pyrochlore lattice magnet, the lowest-energy magnon states in a fully spin-polarized region above the saturation field are localized with flat dispersions owing to the geometrical configuration of the lattice. Therefore, the hopping of the single lowest-energy magnon is prohibited, thereby preventing kinetic energy gain. Meanwhile the spin-lattice coupling in $HgCr_2O_4$ brings the effective biquadratic interaction in Eq. (1). This biquadratic interaction contains a term $(S_i^-)^2(S_j^+)^2$, which induces hopping of a two-spin flipped state on a Cr^{3+} site to the nearest neighbor sites. Because of this hopping term, the two-magnon bound state

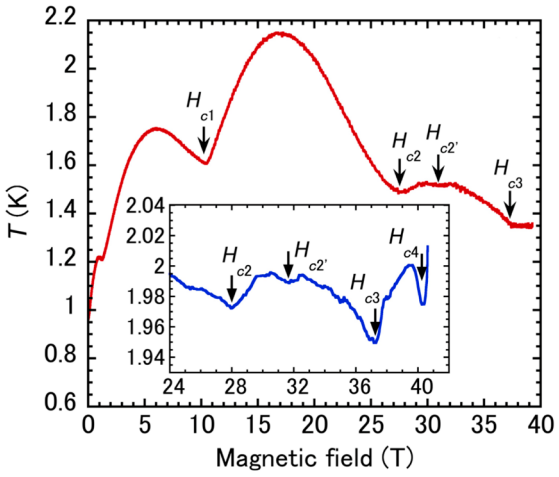

Fig. 1. Magnetocaloric effect of $HgCr_2O_4$, observed under quasi-adiabatic condition. The inset shows that obtained under a quasi-isothermal condition.

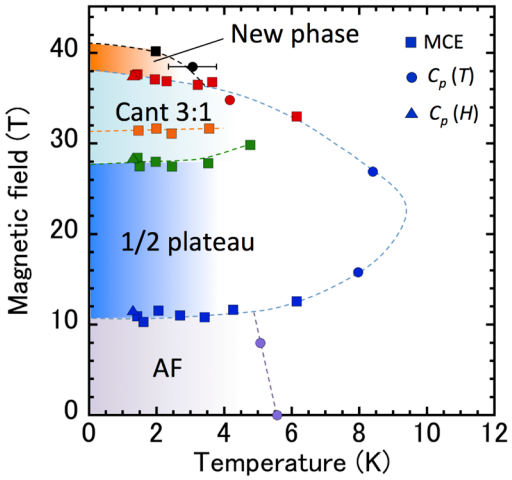

Fig. 2. Magnetic field and temperature phase diagram of $HgCr_2O_4$, obtained from thermodynamic experiments. Squares, circles, and triangles are the transition points obtained from the magnetocaloric effect, temperature, and field dependencies of the specific heat, respectively. Dashed curves are drawn as guides for the eyes.

becomes stable and has a lower energy than two independent localized magnons in the fully polarized spin state. Decreasing the magnetic field in the fully polarized spin state causes softening of the two-magnon bound state. Then, the bound state touches to the ground state at the saturation field, resulting in its condensation, which leads to the spin nematic state. According to the calculation, the spin-component distribution, of which the projection to the plane perpendicular to the magnetic field has an ellipsoid shape, is aligned owing to the spin nematic order, thereby breaking the rotational symmetry around field. From our experimental results that suggest the existence of the gapless magnetic ordered phase between H_{c3} and H_{c4}, we consider that such a spin nematic order most probably appears in $HgCr_2O_4$. The existence of an unknown magnetic phase just below the saturation was also reported for other chromium spinel oxides, $CdCr_2O_4$ and $ZnCr_2O_4$ from high-field experiments It is possible that the appearance of the spin nematic phase is of universal nature in chromium spinel oxides.

References

[1] H. Ueda, H. Mitamura, T. Goto, and Y. Ueda, Phys. Rev. B **73**, 094415 (2006).
[2] K. Penc, N. Shannon, and H. Shiba, Phys. Rev. Lett. **93**, 197203 (2004).
[3] S. Kimura, M. Hagiwara, T. Takeuchi, H. Yamaguchi, H. Ueda, Y. Ueda, and K. Kindo, Phys. Rev. B **83**, 214401 (2011).
[4] E. Takata, T. Momoi, and M. Oshikawa, arXiv:1510.02373.
[5] S. Kimura, S. Imajo, M. Gen, T. Momoi, M. Hagiwara, H. Ueda, and Y. Kohama, Phys. Rev. B **105**, L180405 (2022).

Authors

S. Kimura[a], S. Imajo, M. Gen, T. Momoi[b], M. Hagiwara[c], H. Ueda[d], and Y. Kohama
[a]Tohoku University
[b]RIKEN
[c]Osaka University
[d]Kyoto University

PI of Joint-use project: S. Kimura
Host lab: Kindo and Kohama Groups

A portable 77 Tesla Generator "PINK" for Novel Quantum Beam Experiments

The high magnetic field beyond 100 T is a promising tool to induce and uncover hidden or magnetic properties of materials thanks to its large Zeeman energy, that amounts to 134 K at 100 T for an electron spin of 1/2. However, experimentally, its usage is greatly regulated. First, the generation of B well above 100 T is principally difficult, being restricted to the destructive pulse magnets, where high magnetic fields last only a few μ-seconds, and a large explosion and electromagnetic noises accompany. Second, the experimental probe of material properties is limited. To overcome this situations, young researchers have made great effort for making possible to conduct electric resistivity, magnetization, ultrasound and magnetostriction measurements. Ikeda *et al.*, realized the magnetostriction measurement by using fiber Bragg grating technique and optical filter method, which is useful up to 1000 T range generated using electromagnetic flux compression method.

All these techniques are restricted to macroscopic measurements. In condensed matter physics, microscopic measurements and macroscopic ones complement with each other. Thus, microscopic measurements are in great demand. Recent single shot quantum beams like x-ray free electron laser (XFEL) [1] and femto-second Terahertz pulse

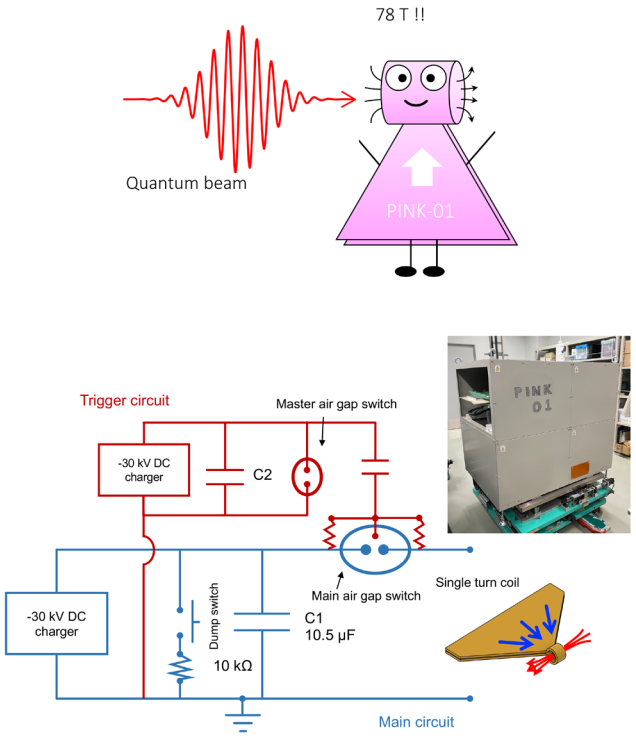

Fig. 1. Schematic image of PINK-01 and the electric circuit.

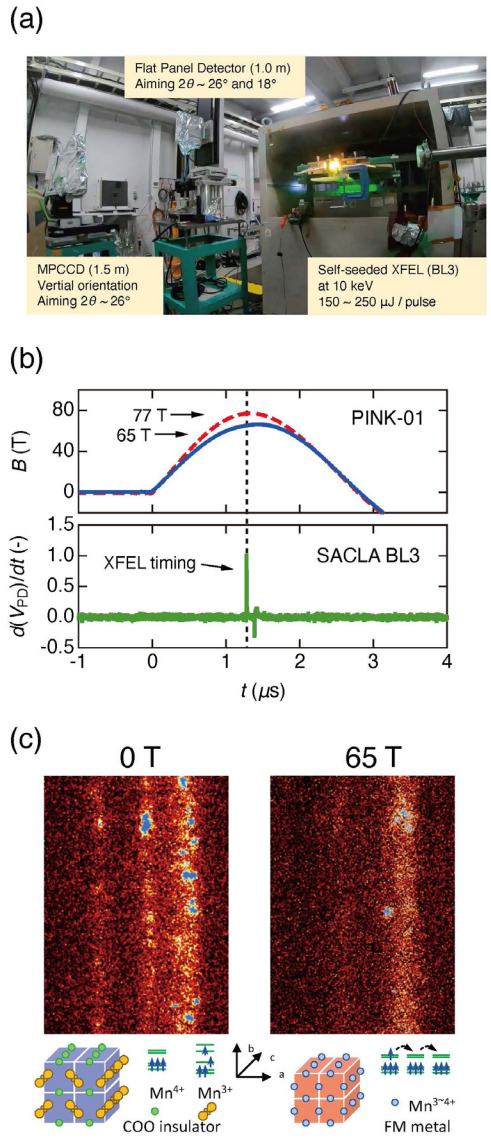

Fig. 2. (a) A photo, (b) synchronization between B pulse and XFEL pulse, and (c) a part of Debye-Scherrer ring of $Bi_{0.5}Ca_{0.5}MnO_3$ with and without magnetic field of 65 T.

techniques are in principle applicable for such purposes. However, the 100 T and 1000 T generators are built in a few large facilities. Besides, they are regularly occupied by daily experiments. For this reason, it is unable to move it to the x-ray facilities, or it is possible one to occupy the experimental site for developing new measurement only when the developing set-up is easily removable from the site.

This problem is solved if the ultrahigh magnetic field generator becomes portable. In the present study we have developed an ultrahigh magnetic field generator called PINK-01 (Portable INtense Kyokugenjiba with numbering 01). PINK-01 is shown to generate 77 T with a single turn coil with a 2.5 mm bore. We have carried PINK-01 to the XFEL facility SACLA in Japan. We have succeeded in obtaining XRD of powdered $Bi_{0.5}Ca_{0.5}MnO_3$ under 77 T where the charge ordered insulator phase is melted by the magnetic field inducing the forced ferromagnetic metallic phase. We clearly observe the lattice state change by the phase transition. We are now building new set up PINK-02 for 100 T generation and low temperature experiment with XFEL. Microscopic change of lattice will be uncovered in many kinds of materials at 100 T soon [2].

References
[1] A. Ikeda, Y. H. Matsuda, X. Zhou, T. Yajima, Y. Kubota, K. Tono, and M. Yabashi, Phys. Rev. Research **2**, 043175 (2020).
[2] A. Ikeda, Y. H. Matsuda, X. Zhou, S. Peng, Y. Ishii, T. Yajima, Y. Kubota, I. Inoue, Y. Inubishi, K. Tono, and M. Yabashi, Appl. Phys. Lett., **120**, 142403 (2022).

Authors
A. Ikeda[a], Y. H. Matsuda, X. Zhou, S. Peng, Y. Ishii, T. Yajima, Y. Kubota[b], I. Inoue[b], Y. Inubishi[b,c], K. Tono[b,c], and, M. Yabashi[b,c]
[a]University of Electro-Communications
[b]RIKEN SPring-8 Center
[c]Japan Synchrotron Radiation Research Institute

PI of Joint-use project :A. Ikeda
Host lab: Y. H. Matsuda Group and X-ray Laboratory

Field-Induced Multiple Metal-Insulator Crossovers of Correlated Dirac Electrons of Perovskite $CaIrO_3$

The quantum phenomena of high-mobility relativistic electrons are issues of great interest in the modern condensed matter physics. So far, the quantum phenomena of relativistic electrons have been extensively studied in Dirac semimetals in which the electron correlation effect is small, but there is a growing interest in the quantum phenomena due to the strong electron correlations. One of fertile grounds to study this issue is the magnetically induced quantum limit (QL) in which the electrons are quasi-one-dimensionally

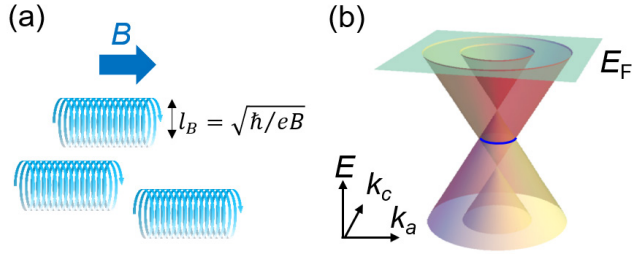

Fig. 1. (a) Quasi-one-dimensional confinement under high magnetic field in the quantum limit. (b) Schematic illustration of Dirac like dispersion near the line node.

(1D) confined under a sufficiently strong magnetic field B. In the QL, electrons in the lowest Landau level with the index $n = 0$ are confined in a scale of magnetic length $l_B = \sqrt{\hbar/eB}$ within a plane perpendicular to the magnetic field, while the momentum along the magnetic field is preserved (Fig. 1(a)). Previous theoretical studies proposed that nontrivial phases such as the axion charge density wave (CDW) and excitonic insulator can be induced, if the QL of the Dirac/Weyl electron can be realized in materials with the strong electron correlation [1]. However, the experimental realization of quantum limit in the strongly correlated electron material is a challenge and hence it has rarely been explored so far.

In this context, the correlated Dirac semimetal of perovskite $CaIrO_3$ provides an ideal arena to study the collective phenomena of high-mobility relativistic electrons in the QL. It has been proposed that the electron pocket emerging around U-point in the Brillouin zone of $CaIrO_3$ is caused by the Dirac band dispersion with a closed line-node protected by the nonsymmorphic crystalline symmetry (*Pbnm*), as illustrated in Fig. 1(b). Recently, it has been shown that the line node is precisely tuned close to E_F (~10 meV below E_F) and yields the Dirac electrons with dilute carrier density (less than 2×10^{17} cm^{-3}) and high mobility exceeding 60,000 cm^{2}V^{-1}s^{-1} due to strong electron correlations in the proximity to the Mott criticality [2]. As a result, the correlated Dirac electrons reach the QL at a modest magnetic field less than 10 T. However, the transport property in the QL of this material has not been explored so far, and a possibly striking feature of collective phenomena of the Dirac electrons remains elusive.

In this study, we have investigated the quantum limit transport of correlated Dirac electrons in the perovskite $CaIrO_3$ by means of magneto-transport measurements up to 55 T and theoretical calculations [3]. In the QL, the magnetoresistivity steeply increases around 10 T and the insulating state with a finite energy gap emerges around 18 T (Fig. 2). By further increasing the magnetic field, both the gap and resistivity dramatically decrease, resulting in the quasi-1D metallic state in the deep QL regime. The non-monotonic field dependence of the gap suggests that the field-induced insulating state originates from the collective electronic ordering, likely the charge density wave or spin density wave driven by the Fermi surface instability inherent to the quasi-one-dimensional $n = 0$ Landau levels with the enhanced density of states under the magnetic field. The field-induced crossover between the metallic state and the gapped state appears in the fairly low magnetic field regime (10-30 T) among the conventional semimetals, highlighting the highly field-sensitive character of strongly correlated Dirac electrons relevant to the Mott criticality.

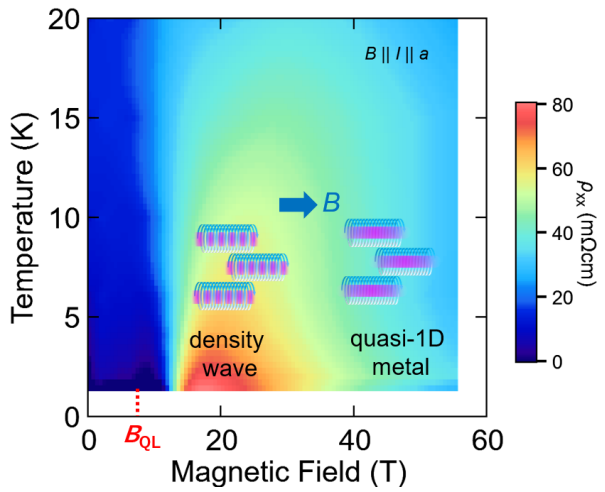

Fig. 2. The contour plot of resistivity as a function of temperature and magnetic field. The density wave and quasi-one-dimensional metallic phase may appear in the quantum limit of Dirac electrons around the line node.

References

[1] Z. Pan and R. Shindo, Phys. Rev. B **100**, 165124 (2019).
[2] J. Fujioka, R. Yamada, M. Kawamura, S. Sakai, M. Hirayama, R. Arita, T. Okawa, D. Hashizume, M. Hoshino, and Y. Tokura, Nat. Commun. **10**, 362 (2019).
[3] R. Yamada, J. Fujioka, M. Kawamura, S. Sakai, M. Hirayama, R. Arita, T. Okawa, D. Hashizume, T. Sato, F. Kagawa, R. Kurihara, M. Tokunaga, and Y. Tokura, npj Quantum Mater. **7**, 13 (2022).

Authors

R. Yamada[a], J. Fujioka[b], M. Kawamura[c], S. Sakai[c], M. Hirayama[a,c], R. Arita[a,c], T. Okawa[a], D. Hashizume[c], T. Sato[c], F. Kagawa[a,c], R. Kurihara, M. Tokunaga, and Y. Tokura[a,c]
[a]The University of Tokyo
[b]Tsukuba University
[c]CEMS RIKEN

PI of Joint-use project: J. Fujioka
Host lab: Tokunaga Group

NMR Relaxation Time Measurements in Pulsed Field

Interesting electronic states are frequently found in magnetic fields, where magnetic interactions inherent in material compete with magnetic energy provided by the external magnetic fields. To cause significant impact on the electronic state, extremely high magnetic fields generated by the pulsed-field technology should be applied to the material. The recent advances in pulsed-field technology allow us to access novel field-induced quantum states by its ability to generate extreme magnetic fields. However, various experiments in pulsed field have been a challenge because of the short duration of field generation time. In this work, we incorporate a versatile NMR spectrometer with the dynamically controlled pulsed field to perform NMR measurement in pulsed field and demonstrate the nuclear spin-lattice and spin-spin relaxation rate measurements.

NMR experiment in pulsed field was difficult because the resonant frequency determined by the external field strength continuously and rapidly changes following the pulsed-field profile. Previously the field-sweep NMR spectrum has been obtained by quickly recording the NMR intensity during the rapid variation of field strength [1,2]. To achieve a sufficiently long measurement time, which is determined by the total pulse width, a large-scale electromagnet with a long time duration of typically ~100 ms has been used for the NMR experiment. In contrast, we combined our NMR spectrometer with the "flat-top" pulsed field; a novel type of pulsed field realized by controlling the pulsed-field strength dynamically [3]. Since the field drift can be suppressed to less than 100 ppm during when the pulsed field is under the feedback control, we can perform any conventional NMR measurements developed for the steady fields even in a rather short time duration of ~30 ms. Since a smaller energy is required to generate a shorter pulsed field, this development facilitates the pulsed-field NMR experiment in any kinds of pulse magnets, such as a portable pulsed-field generator installed in a small laboratory.

The most important advantage of the flat-top pulse is that the relaxation of physical quantities can be traced during the quasi-steady field state. With this feature, we can perform the nuclear spin-lattice relaxation time T_1 measurement with conventional saturation-recovery method, which was believed to be impossible in pulsed field. In addition to the quasi-steady condition of the magnetic fields, we need high reproducibility of field strength to obtain the relaxation profile of the nuclear magnetization. As the spin-echo pulses to observe NMR signal disturb the nuclear spin states, we need to repeat several NMR measurements with various delays between the saturation and the spin-echo pulses at independent pulsed fields. We confirmed the reproducibility of field strength and the NMR intensity by repeating 10 independent field pulses and by measuring ^{65}Cu-NMR signal with the same condition at each pulse [4]. Encouraged by the high reproducibility of flat-top pulse we performed the T_1 measurement for a metallic antiferromagnet CrB_2, and the obtained relaxation profile is shown in Fig.1(a) as the filled symbols. The open symbols are the result obtained at the same field in a real-steady condition. The agreement between the results in pulse and steady fields manifests the feasibility of relaxation time measurement in pulsed fields. However, as the total pulse duration was ~30 ms for the pulse magnet used in the current study, the accessible time scale of T_1 is limited up to ~4 ms which is usually too short to achieve the thermal equilibrium state. To solve this issue, we are now working to implement the NMR spectrometer to a larger pulse magnet with longer pulse duration, which will allow us to extend the accessible time scale of T_1. We also successfully performed the nuclear spin-spin relaxation time T_2 measurement with the same setup [5]. As the typical timescale for T_2 is shorter than 1 ms, T_2 measurement is more suitable for pulsed fields. Figure 1 (b) shows the T_2 decay profiles obtained in the pulsed field (filled) and steady field (open). The consistent results again confirm the feasibility of T_2 measurement in pulsed fields.

Besides the T_1 and T_2 measurements, combination of versatile NMR spectrometer and flat-top pulse enables the frequency-sweep NMR spectrum measurement and the constant-rate field-sweep NMR spectrum measurement. [4,5] With these developments, microscopic magnetism in materials can be unveiled up to very high magnetic fields. So far, microscopic experiment that can be performed at such high magnetic field is still limited. Our pulsed-field NMR technique developed here will provide crucial information to understand the field-induced quantum states.

References

[1] J. Kohlrautz, J. Haase, E. L. Green, Z. T. Zhang, J. Wosnitza, T. Herrmannsdörfer, H. A. Dabkowska, B. D. Gaulin, R. Stern, and H. Kühne, J. Magn. Reson. **271**, 52 (2016).
[2] A. Orlova, E. L. Green, J. M. Law, D. I. Gorbunov, G. Chanda, S. Krämer, M. Horvatić, R. K. Kremer, J. Wosnitza, and G. L. J. A. Rikken, Phys. Rev. Lett. **118**, 247201 (2017).
[3] Y. Kohama and K. Kindo, Rev. Sci. Instrum. **86**, 104701 (2015).
[4] Y. Ihara, K. Hayashi, T. Kanda, K. Matsui, K. Kindo, and Y. Kohama, Rev. Sci. Instrum. **92**, 114709 (2021).
[5] Y. Kohama, T. Nomura, S. Zherlitsyn, and Y. Ihara, submitted to J. Appl. Phys.

Authors

Y. Ihara[a], K. Hayashi[a], T. Kanda, K. Matsui, K. Kindo, and Y. Kohama
[a]Hokkaido University

PI of Joint-use project: Y. Ihara
Host lab: Kindo and Kohama Groups

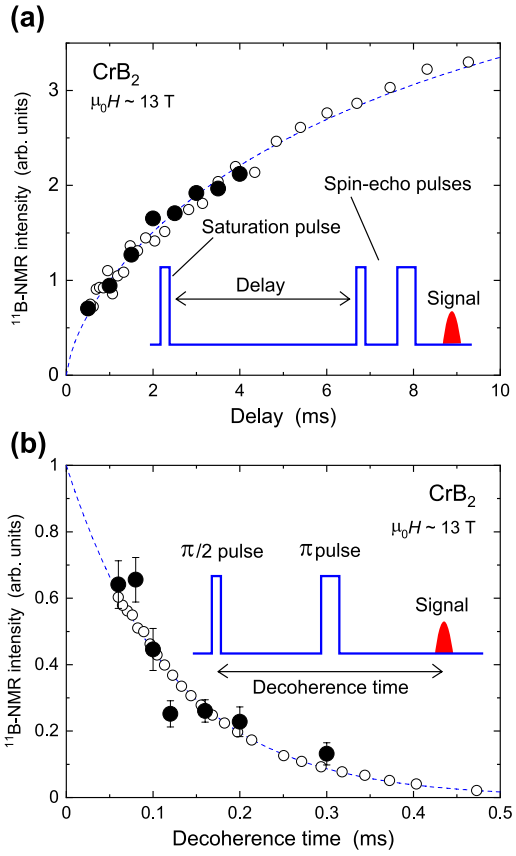

Fig. 1. Recovery (a) and decay (b) profiles of nuclear magnetization measured for a metallic antiferromagnet CrB_2. The filled (open) symbols are the data obtained in pulsed (steady) fields. Consistent results in both cases confirm the feasibility of relaxation measurement in flat-top pulse. Insets are the sketches of the NMR pulse sequences used for corresponding measurements.

Time-Resolved X-Ray Photoelectron Diffraction Using an Angle-Resolved Time-of-Flight Electron Analyzer

Photoelectron spectroscopy (PES) is a powerful experimental approach for investigating chemical composition, electronic states, and atomic structure of a material. Recently, the PES measurement method is conducted with temporal resolutions and the experiment becomes a successful method to track these quantities during the dynamical events of a sample. At SPring-8 BL07LSU, such a time-resolved PES technique is developed and the beamline endstation has been opened for users. In the present research, we combined it with angular resolution and demonstrated a time-resolved experiment of X-ray photoelectron diffraction (XPD) [1].

The time-resolved measurements were performed by a pump-probe method that combined synchrotron radiation (SPring-8 BL07LSU) and laser (BL07LASER) pulses [2,3]. Photon energy of synchrotron radiation was set at hv = 300eV, while that of laser at hv = 1.55 eV. Angle-resolved spectra were obtained with a two-dimensionally angle-resolved time-of-flight (2DARTOF) analyzer [3]. The photoelectrons, detected by the 2D delay line detector, were recorded at the arrival time (t) and position (x, y), subsequently converted into energy (E) and 2D emission angle (θx, θy). A demonstration experiment was made on a silicene layer, a honeycomb lattice of Si atoms, on a ZrB_2 substrate. Figures 1 (a) and 1 (b) show the Si 2p XPD patterns of two atomic sites, α and β, in the silicene. The two sites appear at different binding energies of PES, as shown in Fig. 1 (c). One can find in Fig.1 (a,b) that the experimental XPD pattern

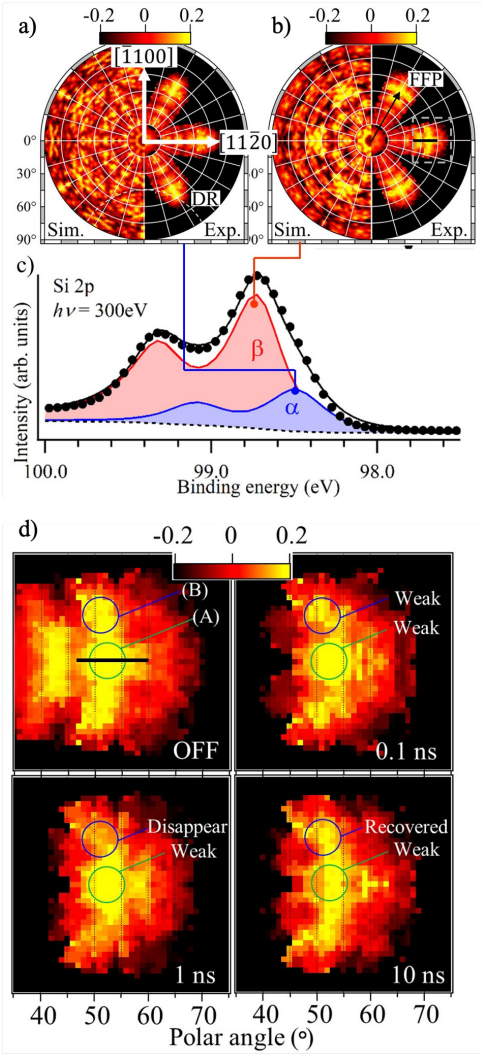

Fig. 1. (a,b) XPD patterns of the Si 2p core levels at the α and β sites in (c) XPS spectrum. (d) Time-resolved XPS pattern of the β site taken at various delay times [1].

is reproduced by the simulation. Focusing on the pattern at the β site, the temporal variation can be detected after the delay time. As presented in Fig. 1(d), the features, labeled A and B, shows temporal changes, weakening, disappearance, and recovery, during sub-nanoseconds (ns) to 10 ns. These results indicate that the time-resolved XPD experiment can be effectively made with a 2DARTOF analyzer. The novel approach is useful to examine the structural changes during dynamical events, such as photocatalysis and photo-induced phase transition.

References

[1] A. K. Ang, Y. Fukatsu, K. Kimura, Y. Yamamoto, T. Yonezawa, H. Nitta, A. Fleurence, S. Yamamoto, I. Matsuda, Y. Yamada-Takamura, and K. Hayashi, Jpn. J. Appl. Phys. **59**, 100902 (2020).
[2] J. Miyawaki, S. Yamamoto, Y. Hirata, M. Horio, Y. Harada, and I. Matsuda, AAPPS Bulletin **31**, 25 (2021).
[3] M. Ogawa *et al.,* Rev. Sci. Instrum. **83**, 023109 (2012).

Authors
K. Hayashi[a] and I. Matsuda
[a]Nagoya Institute of Technology

PI of Joint-use project: K. Hayashi
Host lab: I. Matsuda Group

Progress of Facilities

Supercomputer Center

The Supercomputer Center (SCC) is a part of the Materials Design and Characterization Laboratory (MDCL) of ISSP. Its mission is to serve the whole community of computational condensed-matter physics of Japan, providing it with high performance computing environment. In particular, the SCC selectively promotes and supports large-scale computations. For this purpose, the SCC invites proposals for supercomputer-aided research projects and hosts the Steering Committee, as mentioned below, that evaluates the proposals.

The ISSP supercomputer system consists of two subsystems: System B, which was last replaced in Oct. 2020, is intended for larger total computational power and has more nodes with relatively loose connections whereas System C is intended for higher communication speed among nodes. System B (ohtaka) consists of 1680 CPU nodes of AMD EPYC 7702 (64 cores) and 8 FAT nodes of Intel Xeon Platinum 8280 (28 cores) with total theoretical performance of 6.881 PFlops. System C (enaga) consists of 252 nodes of HPE SGI 8600 with 0.77 PFLOPS, which stopped operation in Dec. 2021 for replacement. The new machine (kugui), which consists of 128 nodes of AMD EPYC 7763 (128 cores) and 8 nodes of AMD EPYC 7763 (64 cores) with total theoretical performance of 0.973 PFLOPS, will start operation in June 2022.

In addition to the hardware administration, the SCC puts increasing effort on the software support. Since 2015, the SCC has been conducting “Project for advancement of software usability in materials science (PASUMS).”In this project, for enhancing the usability of the ISSP supercomputer system, we conduct several software-advancement activities: developing new application software that runs efficiently on the ISSP supercomputer system, adding new functions to existing codes, help releasing private codes for public use, creating/improving manuals for public codes, etc. Three target programs were selected in fiscal year 2021 and developed or enhanced the ustablity of software were released as (1) ESM-RISM (proposal made by M. Otani (AIST)), and (2) 2DMAT (proposal made by T. Hoshi (Tottori Univ.)). In 2021, we also started the data repository service for storing results of numerical calculation and enhancing their reusability.

All staff members of university faculties or public research institutes in Japan are invited to propose research projects (called User Program). The proposals are evaluated by the Steering Committee of SCC. Pre-reviewing is done by the Supercomputer Project Advisory Committee. In fiscal year 2021, totally 321 projects were approved including the ones under the framework of Supercomputing Consortium for Computational Materials Science (SCCMS), which specially supports FUGAKU and other major projects in computational materials science. The total points applied and approved are listed on Table. 1 below.

The research projects are roughly classified into the following three (the number of projects approved, not including SCCMS):

First-Principles Calculation of Materials Properties (142)
Strongly Correlated Quantum Systems (29)
Cooperative Phenomena in Complex, Macroscopic Systems (128)

In all the three categories, most proposals involve both methodology and applications. The results of the projects are reported in 'Activity Report 2020' of the SCC. Every year 3-4 projects are selected for “invited papers” and published at the beginning of the Activity Report. In the Activity Report

Class	Max Points		Application	Number of Projects	Total Points			
					Applied		Approved	
	System B	System C			System B	System C	System B	System C
A	100	50	any time	17	1.7k	0.7k	1.7k	0.7k
B	1k	100	twice a year	96	68.0k	5.3k	37.9k	4.1k
C	10k	1k	twice a year	169	1053.3k	79.6k	532.4k	57.4k
D	10k	1k	any time	3	16.0k	0k	13.5k	0k
E	30k	3k	twice a year	14	323.0k	31.2k	193.0k	22.7k
S			twice a year	0	0k	0k	0k	0k
SCCMS				22	54.1k	7.4k	54.1k	7.4k
Total				321	1516.1k	124.2k	832.6k	92.3k

Table 1: Research projects approved in Academic Year 2021.
The maximum points allotted to the project of each class are the sum of the points for the two systems; Computation of one node for 24 hours corresponds to one point for the CPU nodes of System B and System C. The FAT nodes require four points for a 1-node 24-hours use.

2020, the following three invited papers are included:

1. "Theory, practice, and application of the van der Waals density functional", Ikutaro HAMADA (Osaka U.)
2. "Development of permanent magnet materials--from the view point of first-principles calculation", Hisazumi AKAI (ISSP) and Shinji TSUNEYUKI (Univ. Tokyo)
3. "Development of Bayesian optimization tool and its applications in materials science", Ryo TAMURA (NIMS), Yuichi MOTOYAMA (ISSP), and Kazuyoshi YOSHIMI (ISSP)

Neutron Science Laboratory

The Neutron Science Laboratory (NSL) has been playing a central role in neutron scattering activities in Japan since 1961 by performing its own research programs as well as providing a strong General User Program (GUP) for the university-owned various neutron scattering spectrometers installed at the JRR-3 (20 MW) operated by Japan Atomic Energy Agency (JAEA) in Tokai, Ibaraki (Fig. 1). In 2003, the Neutron Scattering Laboratory was reorganized as the Neutron Science Laboratory to further promote the neutron science with use of the instruments in JRR-3. Under GUP supported by NSL, 12 university-group-owned spectrometers in the JRR-3 reactor are available for a wide scope of researches on material science. The submitted proposals were about 300 and the visiting users reached over 6000 person-day in FY2010. In 2009, NSL and Neutron Science Division (KENS), High Energy Accelerator Research Organization (KEK) built a chopper spectrometer, High Resolution Chopper Spectrometer, HRC, at the beam line BL12 of MLF/J-PARC (Materials and Life Science Experimental Facility, J-PARC) (Fig. 2). HRC covers wide energy transfer (100 μeV < $\hbar\omega$ < 0.5 eV) and momentum transfer (0.03 Å^{-1} < Q < 30 Å^{-1}) ranges, and therefore becomes complementary to the existing inelastic spectrometers at JRR-3. HRC has accepted general users through the J-PARC proposal system since FY2011.

Triple axis spectrometers, HRC, a four-circle diffractometer, and a high resolution powder diffractometer are utilized for a conventional solid state physics and a variety of research fields on hard-condensed matter, while in the field of soft-condensed matter science, researches are mostly carried out by using a small angle neutron scattering

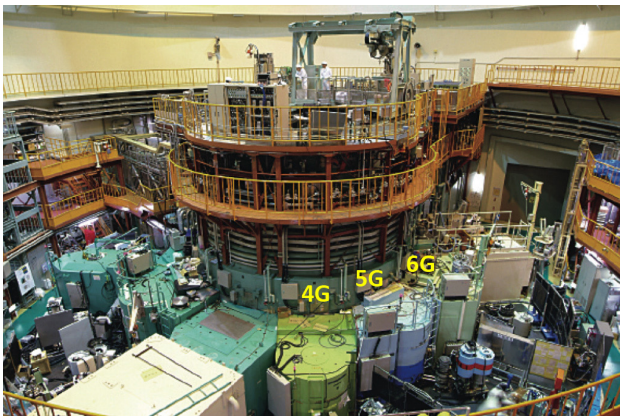

Fig. 1. Reactor hall of JRR-3. Three triple axis spectrometers are shown in the photo.

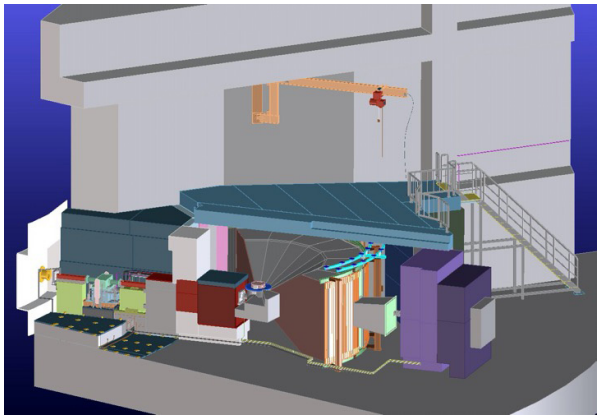

Fig. 2. Schematic view of HRC.

(SANS-U) and/or neutron spin echo (iNSE) instruments. The upgraded time-of-flight (TOF) inelastic scattering spectrometer, AGNES, is available both for hard- and soft-matter science. Our GUP has produced 2076 publications and 285 dissertations until February 28, 2022. Their lists for the last 10 years is given in Activity Report on Neutron Scattering Research which is available in ISSP and NSL web pages.

Since the Great East Japan Earthquake on March 11, 2011, JRR-3 has been closed mainly from safety issues. Hence, our domestic activity is only on HRC. From FY2012 to FY2020, NSL have managed User-Program Supports for Overseas Experiments. 398 people (for 297 proposals) have performed their experiments in various foreign facilities and published 118 papers (as for February 28, 2022). The lists for this program are also available in Activity Report on Neutron Scattering Research mentioned above.

As for international cooperative programs, NSL operates the U.S.-Japan Cooperative Program on neutron scattering, providing further research opportunities to material scientists who utilize the neutron scattering technique for their research interests. In 2010, relocation of the U.S.-Japan triple-axis spectrometer, CTAX, was completed, and it is now open to users. NSL has another agreement with Australian Centre for Neutron Scattering (ANSTO), which was the main foreign facility for the User-Program Supports for Overseas Experiments.

It was really good news that JRR-3 restarted in February 2021 after long shutdown and the normal GUP came back from July 2021. During the shutdown period, we made a lot of efforts on upgrading the instruments and neutron beam circumstances. Specific actions taken include: the installation of focusing collimation systems, such as focusing monochromator and focusing analyzer, and material lens; and the introduction of polarization optics together with the installation of non-magnetization neutron shield. The neutron guides in the Guide Hall have also been upgraded by replacing the existing ones with super-mirror guides. These upgrades should result in increase in neutron beam flux several times. For example, the neutron intensity of AGNES (high resolution cold neutron spectrometer) increased seven times. The sample environments such as cryostat and pressure cells have also been upgraded. We had 4 operation cycles and 91 days of beam time in 2021. 107 experiments, selected from 176 proposals by NSPAC, were performed and many significant results were obtained.

International MegaGauss Science Laboratory

The objective of this laboratory (Fig. 1) is to study the physical properties of solid-state materials (such as metals, semiconductors, insulators, superconductors, and magnetic materials) in a high magnetic field of 100 T or even higher. Such a high magnetic field can control material phases and functions. Our pulsed magnets, at moment, can generate up to 87 Tesla (T) by non-destructive manner, and up to 1200 T by destructive manner. The world record indoor magnetic field 1200 T was achieved in 2018. The laboratory is opened for scientists in domestic as well as from overseas. Lots of fruitful results have come out not only from the collaborative researches but also from our in-house activities.

Fig. 1. The building C of the IMGSL.

Our interests cover the study on quantum phase transitions (QPT) induced by high magnetic fields. Field-induced QPT has been explored in various materials such as quantum spin systems, strongly correlated electron systems and other magnetic materials. One of our ultimate goals is to provide the joint-research users with a 100 T millisecond-long pulse using a non-destructive magnet, and to offer versatile high-precision physical measurements. Measurable physical quantities or properties are magneto-optical spectra, magnetization, magnetostriction, electrical transport, specific heat, nuclear magnetic resonance, and ultrasound propagation. They can be carried out with sufficiently high accuracy. Another ultimate goal is to extend the magnetic field region and discover novel phenomena happening only in extremely strong magnetic fields exceeding 100 T. Recent technical developments allow us to even measure magnetostriction and ultrasound propagation in the destructive magnetic fields over 100 T, that can directly reach potential structural changes in the ultrahigh magnetic fields. Recent discovery of magnetic field induced insulator-metal transitions of strongly correlated materials in 500 T would open new direction of the megagauss field research, namely exploration of field-induced novel phases in materials with strong interactions comparable to thermal energy of a room temperature.

A 210 MJ flywheel generator (Fig. 2), which is the world largest DC power supply (recorded in the Guinness Book of World Records) was installed in the DC flywheel generator station at our laboratory, and used as an energy source of super-long pulse magnets. The magnet technologies are intensively devoted to the quasi-steady long pulse magnet

	Alias	Type	B_{max}	Pulse width Bore	Power source	Applications	Others
Building C Room 101-113	ElectroMagnetic Flux Compression	Destructive	1200 T	3μs (100-1200T) 10 mm	5 MJ, 50 kV 2 MJ, 50 kV	Magneto-Optical Magnetization	5 K – room temperature
	Horizontal Single-turn Coil	Destructive	300 T 200 T	6μs 5 mm 10 mm	0.2 MJ, 50 kV	Magneto-Optical measurements Magnetization	5 K – room temperature
	Vertical Single-turn Coil	Destructive	300 T 200 T	8μs 5 mm 10 mm	0.2 MJ, 40 kV	Magneto-Optical Magnetization	2 K – room temperature
Building C Room 114-120	Mid-pulse Magnet	Non-destructive	60 T 70 T	40 ms 18 mm 40 ms 10 mm	0.9 MJ, 10 kV	Magneto-Optical measurements Magnetization Magneto-Transport Hall resistance Polarization Magneto-Striction Magneto-Imaging Torque Magneto- Calorimetry Heat Capacity	Independent Experiment in 5 site Lowest temperature 0.1 K
Building C Room 121	PPMS	Steady	14 T			Resistance Heat Capacity	Down to 0.3 K
	MPMS	Steady	7 T			Magnetization	
Building K	Short-Pulse Magnet	Non-destructive	87 T (2-stage pulse) 86 T	5 ms 10 mm 5 ms 18 mm	0.5 MJ, 20 kV	Magnetization Magneto-Transport	2 K – room temperature
	Long-Pulse Magnet	Non-destructive	43.5 T	1 s 30 mm	210 MJ, 2.7 kV	Resistance Magneto-Calorimetry	2 K – room temperature

Table 1. Available Pulse Magnets, Specifications

Fig. 2. Upper: The K-building for the flywheel generator (left-hand side) and a long pulse magnet station (right-hand side). Lower: The flywheel giant DC generator which is 350 tons in weight and 5 m high (bottom). The generator, capable of a 51 MW output power with the 210 MJ energy storage, is planned to energize the long pulse magnet generating 100 T without destruction.

(an order of 1-10 sec) energized by the giant DC power supply. The giant DC power source will also be used for the giant outer-magnet coil to realize a 100 T nondestructive magnet by inserting a conventional pulse magnet coil in its center bore. Recently, the super-long pulsed magnet has been intensively used to investigate thermal properties such as specific heat and magnetocaloric effects.

Magnetic fields exceeding 100 T can only be obtained with destruction of a magnet coil. The ultrahigh magnetic fields are obtained in a microsecond time scale. The project, financed by the ministry of education, culture, sports, science and technology aiming to generate 1000 T with the electromagnetic flux compression (EMFC) system (Fig. 3), has been completed. Our experimental techniques using the destructive magnetic fields have intensively been developed. The system which is unique to ISSP in the world scale is comprised of a power source of 5 MJ main condenser bank and 2 MJ condenser bank. Two magnet stations are constructed and both are energized from each power source. Both systems are fed with another 2 MJ condenser bank used for a seed-field coil of which magnetic flux is to be compressed. The 2 MJ EMFC system can generate 450 T. The 5 MJ system is used for generation of 1000 T-class

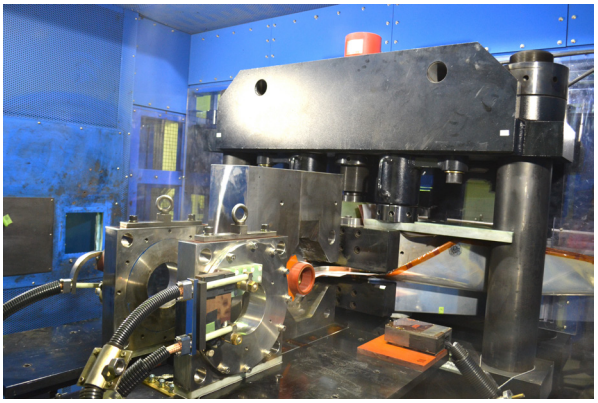

Fig. 3. A view of the coil setup of the electromagnetic flux compression inside of an anti-explosive house. The world's strongest indoor magnetic field 1200 T was achieved in 2018.

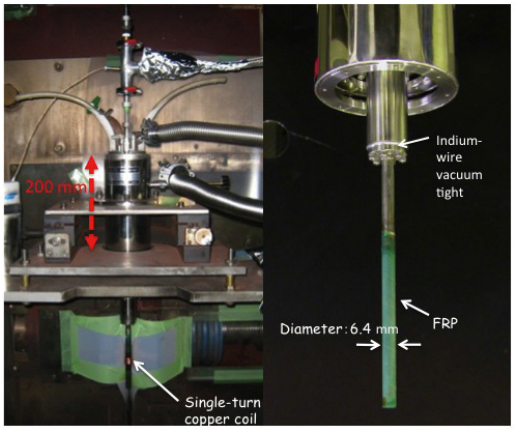

Fig. 4. Schematic picture of the V-type single-turn coil equipped with a 40 kV, 200 kJ fast capacitor bank system. The liquid-helium-bath cryostat with a plastic tail is also shown.

magnetic field. For the research in magnetic field range of 100 - 300 T, we have two single-turn coil (STC) systems that have a fast-capacitor bank system of 200 kJ for each. One is the horizontal type (H-type) and the other is a vertical type (V-type, Fig. 4). Various kinds of laser spectroscopy experiments such as the cyclotron resonance and the Faraday rotation are possible using the H-type STC, while a stable low temperature condition of 2 K is available for the V-type STC.

Center of Computational Materials Science

With the advancement of hardware and software technologies, large-scale numerical calculations have been making important contributions to materials science and will have even greater impact on the field in the near future. CCMS is a specialized research center established in 2011 for promoting computer-aided materials science with massively parallel computers, such as the Fugaku supercomputer, which has been recently developed in Kobe as the core of a billion-dollar national project. Activities of CCMS are divided into the following three categories: (1) highly efficient and large-scale use of the Fugaku supercomputer and its application to grand-challenge problems in computational materials science, (2) activities as the center for the community of computational condensed matter physics and materials science, and (3) computational physics research aiming to solve rare-element problems.

For the first category, each group in CCMS is carrying out various individual research projects in its own expertise to efficiently utilize large-scale parallel computers. For example, the Ozaki group has been developing efficient and accurate methods and software packages to extend the applicability of DFT to more realistic systems, and investigated the structural and electronic properties of various 2D materials in successful collaboration with experimental groups and industrial companies. There are other activities such as development of Tensor Network (TN) based numerical methods and Markov-chain Monte Carlo methods by the Kawashima group and the Todo group.

As for the activities in the second category, apart from major annual conferences and formal international meetings, the CCMS provided a series of lectures and training sessions at Kashiwa. For example, training sessions "Kashiwa Hands-

Fig. 1. Software in the CCMS community

Fig. 2. MateriApps Website

On" for getting accustomed to various application programs, such as OpenMX, Hphi, mVMC, AkaiKKR, and MateriApps LIVE!, as shown in Fig. 1, have been held monthly. Each session is designed for more than 10 trainees and takes 4-5 hours. We also coordinate the use of the computational resources available to our community, and support community members through various activities such as administrating the website "MateriApps" for information on application software in computational science as shown in Fig. 2.

For the third category, the Akai team and the Fukushima group were working on the development of new permanent magnet materials. In order to meet the ever-increasing demands for new permanent magnet materials that are used for high performance permanent magnets, CCMS is theoretically investigating the various magnetic properties, such as saturation magnetization, Curie temperature, and magnetic anisotropy, of iron-based magnetic materials, including rare-earth magnet materials, $R_2(Fe,Co)_{14}B$, $R_2(Fe,Co)_{17}$, and $RFe_{11.5}Ti_{0.5}$ (R = La, Ce, … , Lu, Y) on the basis of first-principles calculations.

These activities are supported by funds for various governmental projects including Element Strategy Initiative and the Program for Promoting Researches on the Supercomputer Fugaku.

The following is the selected list of meetings organized by CCMS in recent years:

- 2021/2/22,24 Workshop for data science in materials science.
- 2021/4/8-2021/7/29 On-line lecture series for advanced computational science and technology A (2021).
- 2021/5/10,11 AiiDA-tutorial-Japan-2021-Spring.
- 2021/9/3,10,17,24 MP-CoMS on-line lecture series for fundamentals and applications of first-principles electronic structure calculations.
- 2021/8/5 Workshop for the Fugaku permanent magnet project.
- 2021/6/2,3 Matching Workshop for industries & graduate students/ postdocs, Online.
- 2022/2/3,4 4th Element Strategy Symposium: Building a Carbon-Neutral Society with Innovative Materials, on-line.

In addition to the events listed above, we organize regular hands-on program for various application, such as Open MX and PHYSBO.

Laser and Synchrotron Research Center (LASOR Center)

Laser and synchrotron research center (LASOR Center) was established in October 2012 to push the frontiers of the photon and materials science. LASOR has 10 groups in 2021, which is the biggest division in ISSP. Most of the research activities on the development of new lasers with an extreme performance and the application to materials science are studied in specially designed buildings D and E with large clean rooms and the isolated floor from the vibrations in Kashiwa Campus. On the other hand, the experiments utilizing the synchrotron radiation are performed at beamline BL07LSU in SPring-8 (Hyogo). We also have a clean room for a laser processing platform in Kashiwa II Campus.

The development of novel laser-based light sources in the vacuum-ultraviolet to soft-X-ray regions innovated materials investigations as represented by the highest-energy-resolution photoemission, ultrafast time-domain, and ultrafast non-linear spectroscopies. Materials science research powered by lasers thus has entered a new era. The ultra-short and high-power lasers are more and more attractive light source for both basic science and industry. The state-of-the-art laser source and spectroscopy are intensively explored.

Another stream pursued at ISSP is the synchrotron-based research. The drastic advance in brilliance of the synchrotron radiation has also opened a new field of its own in photon science. The soft-X-ray beam-line in SPring-8 (BL07LSU) was implemented with a longest undulator in the world: The end stations illuminated by the brilliant soft-X-rays are used to output innovative achievements based on high-resolution spectroscopy data. In 2018, Japanese government has made a statement to construct a new synchrotron facility in Tohoku.

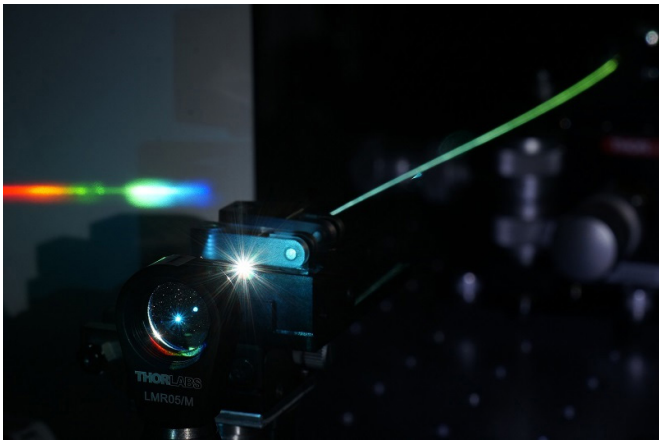

Fig. 1. Optical frequency comb

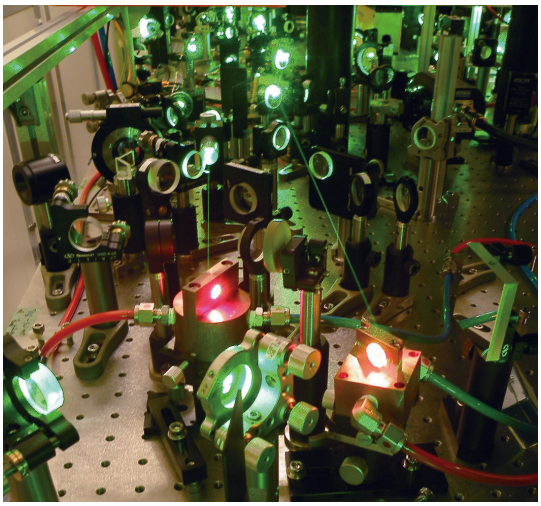

Fig. 2. Close look of a high-peak-power ultrashort-pulse laser

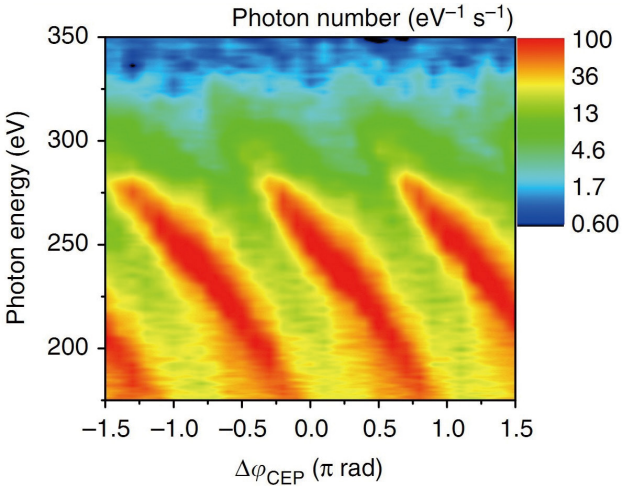

Fig. 4. Phase-dependence of high harmonic spectra in soft X rays.

LASOR has decided to subjectively contribute to this facility from the design to the operation.

Lasers and synchrotrons have developed independently; now both light sources cover a wide photon-energy range with an overlap in the vacuum-ultraviolet to soft-X-ray regions. Foreseeing their common interests in research fields and technologies, ISSP integrated the two streams, namely the extreme lasers and synchrotron radiations, into the common platform. Through the mutual interactions between the forefronts of lasers and synchrotrons, LASOR will be the center of innovations in light and materials science, with the aid of world-wide joint research and close collaborations with other divisions in ISSP such as New Materials Science, Nanoscale Science, and Condensed Matter Theory.

The mission of LASOR is to cultivate and propel the following three scientific fields:

1. Laser Science,
2. Synchrotron radiation Science,
3. Extreme Spectroscopy,

• Laser science group

We were committed to continuing to develop various state-of-the-art laser systems such as high-power solid-state or gas lasers, high-intensity lasers, ultra-short pulse lasers down to attosecond time scale (Peta-Hz linewidth), ultrastable lasers with 1-Hz linewidth, optical frequency combs, mid-infrared lasers, THz light source, and semiconductor lasers.

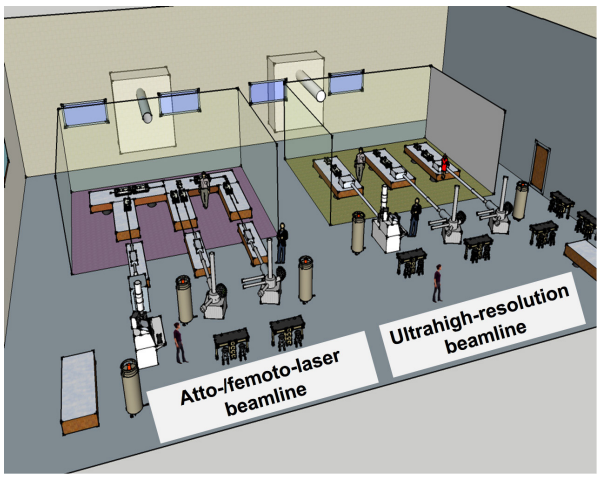

Fig. 3. Design of E building for extreme VUV- and SX-lasers and new spectroscopy.

High-power and ultrashort pulse laser technology has progressed for this 10 years. It opened two directions of research. One is a coherent extreme ultraviolet light source realized by a high-harmonic generation (HHG) scheme. The average power of HHG became high enough to use it for a photoemission spectroscopy. The photon energies of 7 eV to 60 eV are now available. They can be either very narrow band width or ultrashort pulse. The other is an industrial science such as a laser processing. Pulse duration variable, 100-W average power, femtosecond laser is now available in LASOR for any collaborative research including companies. We have a laser processing platform for both industrial and scientific applications.

We also aim to develop novel laser spectroscopy and coherent non-linear optical physics, enabled via emerging lasers and optical science/technology, and extensively study basic light-matter physics, optical materials science, and applied photonics. Such researches include ultrafast spectroscopy for excited state dynamics, terahertz magnetic-field spectroscopy for spin dynamics, quantitative micro-spectroscopy on semiconductor lasers and nano-structure photonics devices, such as quantum wire lasers, gain-switch semiconductor laser, multi-junction solar cells, and bio-luminescent systems.

• Synchrotron radiation science group

By inheriting and developing the synchrotron techniques cultivated for more than 20 years, we continuously develop world cutting-edge spectroscopies such as time-resolved

Fig. 5. 10-MHz high harmonic generation in an enhancement cavity.

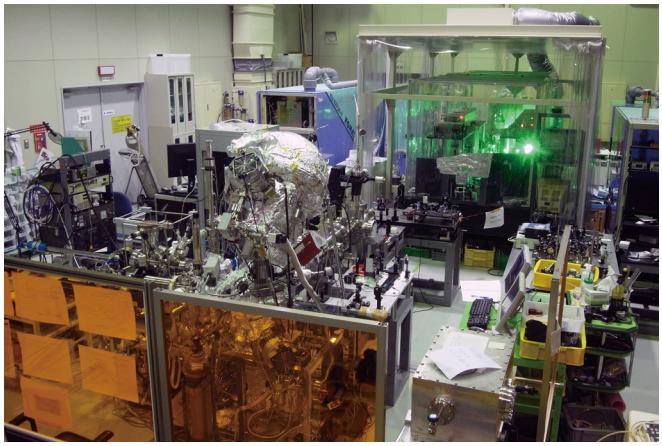

Fig. 6. Pump-probed photoemission system using 60-eV laser

photoemission /diffraction, ultrahigh resolution soft X-ray emission, 3D (depth + 2D microscopy) nano ESCA and X-ray magneto-optical effect and provide these techniques both for basic material science and for applied science, which contributes to the device applications in collaboration with outside researchers. In order to pioneer new spectroscopies for the next-generation light sources, we upgrade fast polarization switching of the undulator light source in cooperation with SPring-8. In addition, we promote frontier works on the use of X-ray free electron lasers, SACLA with high spatial and temporal coherence comparable to optical lasers in collaboration with scientists of laser light sources and spectroscopies.

• Extreme spectroscopy group

The advent of laser-based light sources in the soft-X-ray region is opening a new stage in the field that has been cultivated by the synchrotron radiations. One of the milestones is to develop a laser-based light source of ~7 eV for the sub-meV-resolution photoemission spectroscopy. In this five years, available photon energy became 11 eV with help of Yb-fiber laser technology. It has high photon flux (1014 photons/sec) with sub picosecond time resolution. Laser-based spin-resolved ARPES is realizing in LASOR. This technology would open brand-new spectroscopy. High-harmonic generation based photoemission spectroscopy in the 20-60 eV region is another direction to be pursued. Time-domain spectroscopy in the femtosecond region was achieved. Combined with the picosecond time-domain spectroscopy utilizing the pulsed light delivered from synchrotrons, we investigate the electronic structures and dynamics of matter in bulk, on surface, and into the nano-scale. The ultimate objective is to expand the soft-X-ray operando methodologies by lasers. Diffractions, magneto-optical effects, and inelastic scatterings now done at synchrotrons will be performed by lasers, to access the real-time dynamics of chemical reactions and phase transitions down to the femtoseconds.

State-of-the-art laser based organism spectroscopy is new direction in LASOR. ISSP research area is shifting from simple material and science to complex one including living body and functional material with excited state physics.

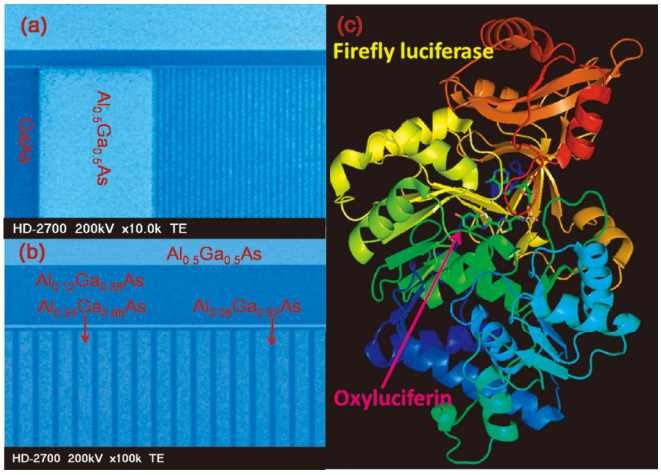

Fig. 7. Photonics devices under study: (left panel) semiconductor quantum wires and (right panel) firefly-bioluminescence system consisting of light emitter (oxyluciferin) and enzyme (luciferase)

Synchrotron Radiation Laboratory

The Synchrotron Radiation Laboratory (SRL) was established in 1975 as a research division dedicated to solid state physics using synchrotron radiation (SR). Currently, SRL is composed of two research sites, the Harima branch and the E-building of the Institute for Solid State Physics.

• Brilliant soft X-ray beamline at Harima branch

In 2006, the SRL staffs have joined the Materials Research Division of the Synchrotron Radiation Research Organization (SRRO) of the University of Tokyo and they have played an essential role in constructing a new high brilliant soft X-ray beamline, BL07LSU, in SPring-8. The light source is the polarization-controlled 25-m long soft X-ray undulator with electromagnetic phase shifters that allow fast switching of the circularly (left, right) and linearly (vertical, horizontal) polarized photons. The monochromator is equipped with a varied line-spacing plain grating, which covers the photon energy range from 250 eV to 2 keV. At the downstream of the beamline, a lot of experimental stations have been developed for frontier spectroscopy researches: three endstations, i.e. ambient pressure X-ray photoemission (Fig. 1), three-dimensional (3D) nano-ESCA (Fig. 2), high resolution soft X-ray emission spectroscopy (XES) (Fig. 3) stations are regularly maintained by the SRL staffs and open for public use, and at free-port station many novel spectroscopic tools have been developed and installed such as soft X-ray imaging (ptychography) station using an originally developed Wolter-type focusing miller system. The beamline

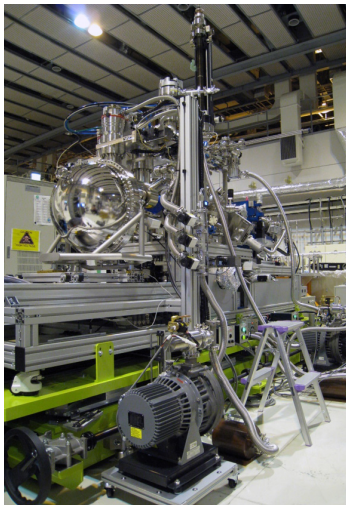

Fig. 1. Ambient pressure photoemission station

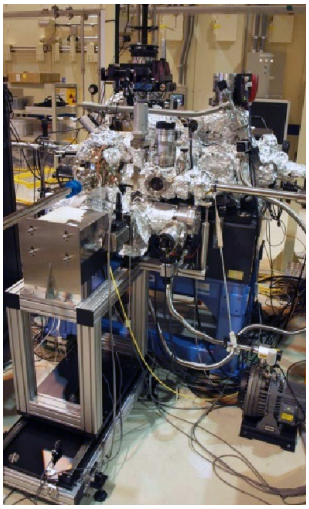

Fig. 2. 3D nano-ESCA station

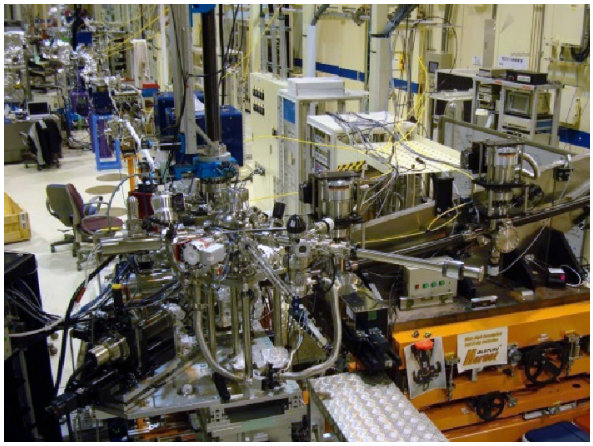

Fig. 3. Soft X-ray emission station

construction was completed in 2009 and SRL established the Harima branch laboratory in SPring-8. At SPring-8 BL07LSU, each end-station has achieved high performance: the ambient pressure X-ray photoemission (APXPS) system has achieved the 100 Torr XPS measurement and is used for various catalytic reactions including CO2 reduction; the 3Dnano-ESCA station reaches the spatial resolution of 70 nm and is equipped with a sample holder with a 5-terminal electrode, which is dedicated for the analysis of secondary battery materials, high electron mobility transistors etc.; the XES station provides spectra with the energy resolution around 70 meV at 400 eV and enables real ambient pressure experiments on various targets including solution and its interface with solids and gases. In 2021, 34 user groups made their experiments during the SPring-8 operation time, which was the largest number in the past 15 years. Scientific themes related to new materials and phenomena were also conducted for social implementation as a trial use of industry-academia collaboration which will be facilitated in the next-generation synchrotron radiation facility which is now under construction and will be operational since 2024 at Sendai.

• High-resolution Laser SARPES at E-building

High-resolution Laser Spin- and Angle-Resolved Photoemission Spectroscopy (SARPES) is a powerful technique to investigate the spin-dependent electronic states in solids. In FY 2014, LASOR and SRL staffs constructed a new SARPES apparatus (Fig. 4), which was designed to provide high-energy and -angular resolutions and high efficiency of spin detection using a laser light at E-building. The achieved energy resolution of 1.7 meV in SARPES spectra is the highest in the world at present. From FY 2015, the new SARPES system has been opened to outside users. The Laser-SARPES system consists of an analysis chamber, a carousel chamber connected to a load-lock chamber, and a molecular beam epitaxy chamber, which are kept ultra-high vacuum (UHV) environment and are connected to UHV gate valves. The electrons are excited with 6.994 eV photons, yielded by 6th harmonic of a Nd:YVO4 quasi-continuous wave laser with a repetition rate of 120 MHz, and 10.7 eV photons, driven by the third harmonic radiation at 347 nm of an Yb:fiber chirped pulse amplifier laser, which was developed by Kobayashi's lab in LASOR. The hemispherical electron analyzer is a custom-made Scienta Omicron DA30-L, modified for installing the spin detectors. The spectrometer is equipped with two high-efficient spin detectors orthogonally placed each other, associating very low energy electron diffraction, which allows us to analyze the three-dimensional spin polarization of electrons. At the exit of the hemispherical analyzer, a multi-channel plate and a CCD camera are also installed, which enables us to perform the angle-resolved photoelectron spectroscopy with two-dimensional (energy-momentum) detection. The laser-SARPES with 7 eV laser can provide both high-resolution spin-integrated and spin-resolved photo-emission spectra in various types of solids, such as spin-orbit coupled materials and ferromagnetic materials. In addition, using the 10.7 eV makes it possible to follow their ultrafast spin dynamics in the time domain by pump-probe scheme.

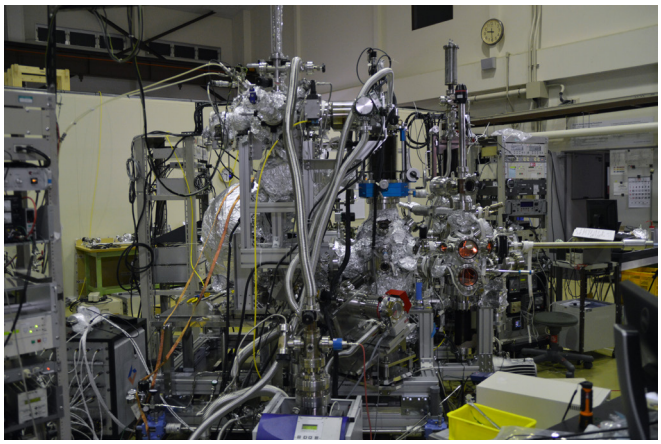

Fig. 4. Laser-SARPES system at E-building

The time-resolved soft X-ray spectroscopy (TR-SX) station was moved from SPring-8 BL07LSU to the E-building in 2020. The measurement chamber is equipped with a unique electron spectrometer, the two-dimensional (2D) angle-resolved time-of-flight (ARTOF) analyzer. The system is currently operational for measurements of 2D angle-resolved photoemission spectroscopy with pulsed laser of 6 eV photon energy, produced by high harmonic generations from a 1.2 eV laser. Time-resolved measurements can also be conducted with temporal resolution of 600 fs.

Conferences and Workshops

Frontier Research on Glasses and Related Complex Systems

May 10-12, 2021

O. Yamamuro, H. Tanaka, K. Miyazaki, T. Kanaya, T. Hayakawa, K. Fukao,
R. Nozaki, N. Shinyashiki, O. Urakawa, H. Shirota, and N. Yamamuro

This workshop was organized for discussing the present frontiers and future directions of the experimental, theoretical and computational studies on glasses and related systems including granular materials, spin/electronic glasses, proteins, foods, medicines, etc. ISSP has held workshops related to the glass every 3-4 years since 2002 and played a leading role of this field. Though a face-to-face meeting was planned at the time of application, it was unfortunately changed to an online meeting due to prolonged COVID-19 effects. The workshop contained 2 plenary lectures, 20 invited talks, and 21 contributed talks. The poster session, which was held in previous workshops, was cancelled. There were 208 participants including some special guests from China. This number was the largest ever, which is the biggest advantage of the online meeting. The discussion was quite active and many questions were asked from the audience though the online meetings are usually quiet. This reflects the activity of the present field. Actually, a related international meeting, International Discussion Meeting on Relaxations in Complex Systems (https://9idmrcs.jp/), will be held in Makuhari, Chiba in 2023, based on the domestic members of this workshop.

2nd Workshop on the Frontline and Future Trends in Nanoscale Science

June 22, 2021

S. Katsumoto, Y. Otani, T. Osada, Y. Yamashita, S. Miwa, and Y. Hasegawa

Recent rapid progress in nanoscale science, such as elucidation and precise control of novel quantum phenomena by nanofabricated devices, and emerging topological properties at surfaces, interfaces, and atomic-layer two-dimensional materials, attracts tremendous attentions in the community of condensed matter physics. In order to overview relevant cutting edge researches and explore future directions of the interdisciplinary research field, we organized this workshop following the first one held in July 2020. Looking ahead of the foundation of Laboratory of Nanoscale Quantum Materials (Q-Nano Lab, later founded in March 2022), the present workshop focused on the subjects of low-dimensional and topological materials, spintronics, quantum transport, q-bits, quantum computing etc., and invited 8 young researchers working in universities and research institutes in Japan.

Since the workshop was held online through the network, more than 200 participants, some of which are from abroad, joined the workshop, and actively participated in the discussion after the presentations. Although a half-day short event, the workshop was so exciting because all the presentations provides us new amazing and stimulating results on the frontline nano science. The organizing members are also delighted to find many young promising researchers performing high-quality sciences based on their new ideas and concepts. We expect that the workshop will further encourage the activity of nano science in Japan and promote joint researches with our institute through the newly founded Q-Nano Lab.

New Trends in Quantum Condensed Matter Theory 2021

July 26-30, 2021

T. Oka, M. Oshikawa, G. Chen, R. Moessner, and A. Vishwanath

Quantum material is a stage where various exotic quantum phenomena such as phase transitions and non-trivial dynamics are manifested, and active research is being done worldwide. We held an online workshop with a focus on recent developments in the theory of quantum materials, where both Japanese and international young active theorists were invited.

Talks on twisted bilayer graphene, quantum computation, nonequilibrium many-body quantum states, photoinduced superconductivity, quantum chaos, topological states, etc. were given by 11 Japanese, 5 from Asia, 3 from Europe, and 6 from the US, including 3 women.

The invited speakers were young researchers only, and the presentations were full of energy and enthusiasm. Despite the late-night (Japan time), there were always more than 70 participants, and a lively Q&A session was held. One aim of the workshop was to support young researchers in building their career paths by providing a stage for them to stimulate each other actively and by shining a spotlight on their achievements. We think that this workshop was successful in this aim and feel that it should be continued, for example, bi-annually.

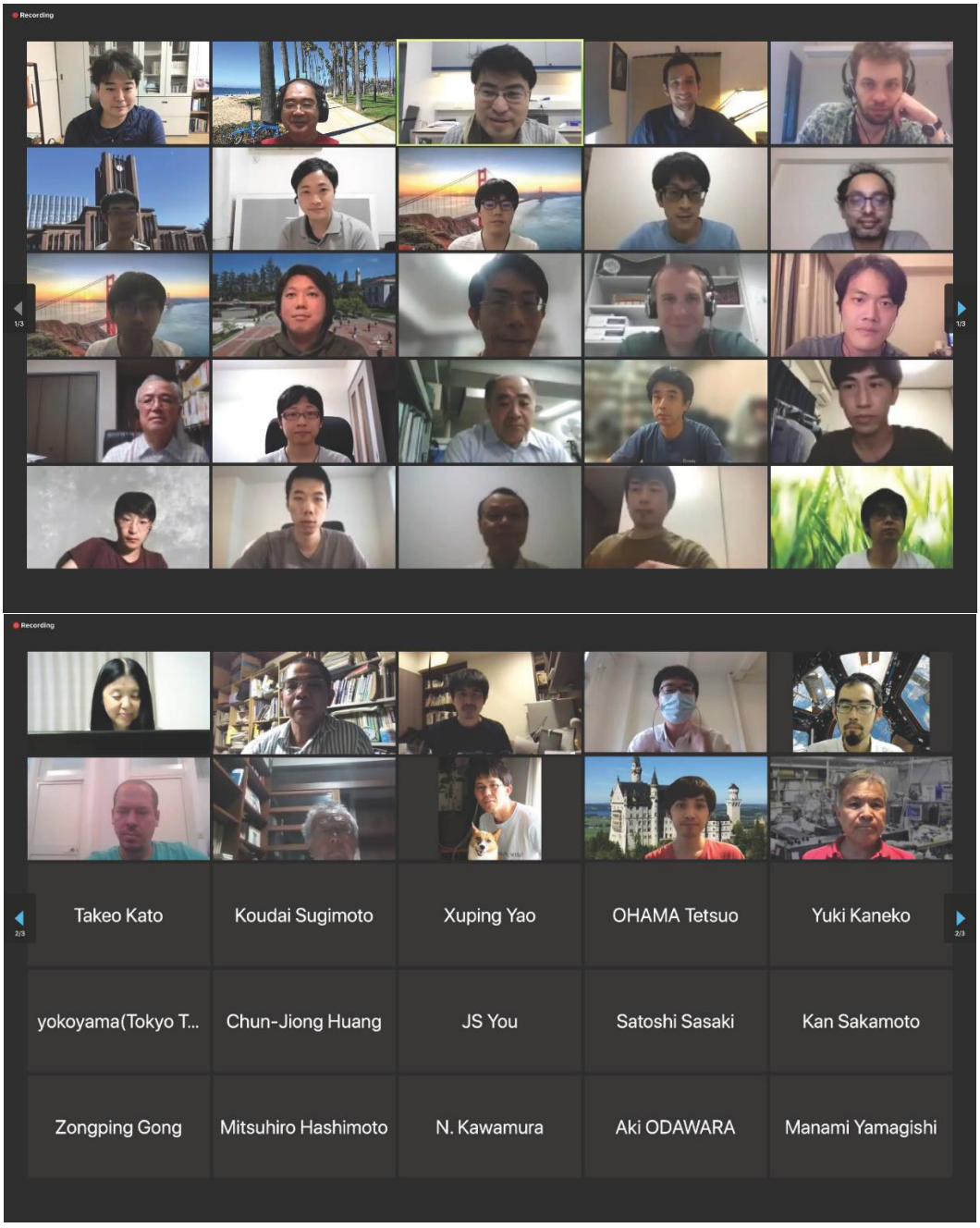

ISSP WOMEN'S WEEK 2021

August 3-5, 2021
H. Akiyama, T. Ozaki, M. Oshikawa, M. Tokunaga, I. Matsuda,
S. Miwa, H. Mori, M. Yamashita, and J. Yoshinobu

For the development of material science studying the various physical properties of matters, it is essential to further expand the research area and promote the diversity of the researchers. The ISSP Workshop entitled "ISSP WOMEN'S WEEK 2021" was held to further promote the activities of female researchers who still remain a minority in the field of science and engineering research. We invited female researchers who are active on the cutting edge in a wide range of fields of material science, ranging from leading professors representing each research field, who serve as a role model for female students, to up-and-coming young female researchers. In contrast to an ordinary workshop with a focused topic, this workshop covers a wide range of topics – including biophysics, chemistry, surface physical sciences, and strong-correlated electrons – for creating new networks of female researchers. All speakers are thus asked to briefly introduce themselves in addition to the introduction for broad audiences. All speakers are also asked to give comments with respect to current issues to promote diversity. On the second day, Dr. Kaori Hayashi (Vice President of the University of Tokyo) and Dr. Kaoru Tamada (Vice President of Kyushu University) gave special lectures on the efforts of their institutions to promote diversity, which is followed by a panel discussion with invited speakers. There were about 166 pre-registered participants for this workshop, with 60-90 participants / day over the three days.

10th International Workshop on Advanced Spectroscopy of Organic Materials for Electronic Applications: ASOMEA-X

October 25-28, 2021
J. Yoshinobu, R. Arafune, K. Akaike, K. Ozawa, Y. Yamada, H. Yoshida,
Y. Nakayama, Y. Harada, T. Kondo, K. Okazaki, K. Kuroda

ASOMEA has been held every two to three years since 2001 as an international workshop to discuss structures, electronic states, and properties of electronically functionalized organic materials and the related phenomena at surface/interface from the viewpoint of spectroscopy. This ASOMEA-X has expanded its scope to include not only electronically functionalized organic materials, but also low-dimensional and topological materials that have recently been attracting much attention. In order to obtain deeper understanding of the microscopic and dynamic properties of these materials as well as the behavior of electrons, atoms and molecules during device operation and reactions, we have focused not only on studies using conventional spectroscopies but also those by the state-of-the-art spectroscopies including operando spectroscopy, time-resolved spectroscopy and local probe microscopy/spectroscopy. The presentations at ASOMEA-X consisted of 3 invited tutorial talks, 20 invited talks, 22 general oral presentations and 18 poster presentations. For oral presentations, the web conference tool (Zoom) was used together with the breakout rooms for the intimate discussion with speakers after their presentations. For poster presentations, a virtual poster room was prepared using SpatialChat, allowing participants to approach the presenter for discussion, similar to a face-to-face poster presentation. The number of participants is as follows: 103 from Japan and 60 from eight foreign countries (Sweden, Germany, U.S.A., China, Korea, Singapore, India, and New Zealand). The program and abstracts are available from the web site (https://yoshinobu.issp.u-tokyo.ac.jp/ASOMEAX_web/index.html).

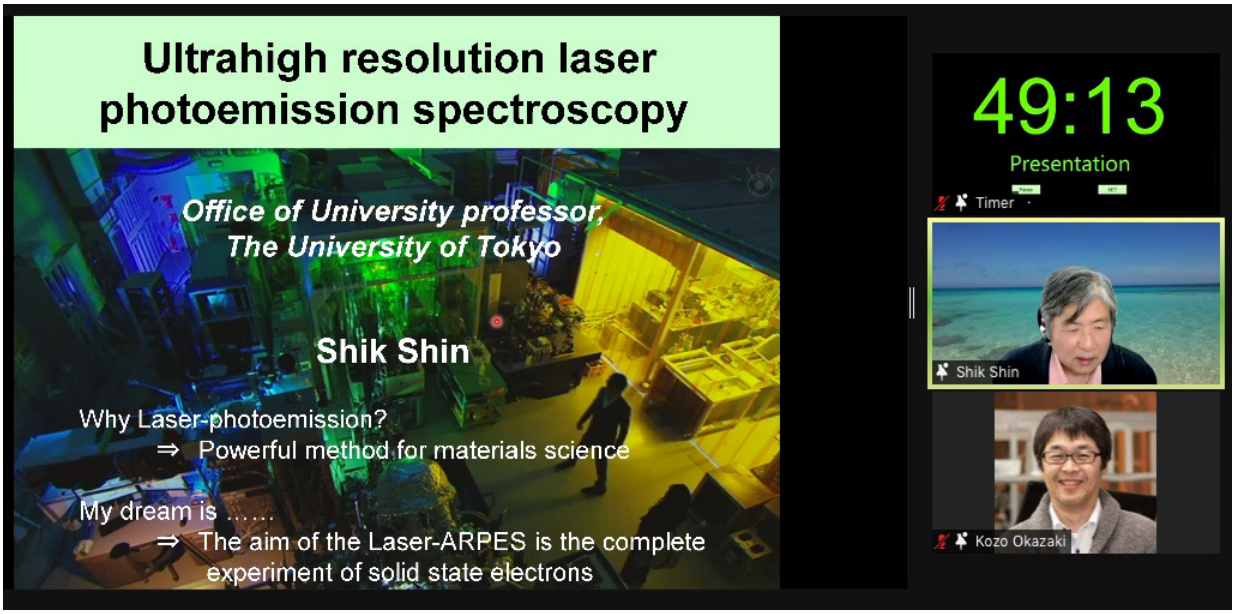

A screen shot of one of the online tutorial lectures, in which Prof. Shin gave his last invited talk among many international conferences. Prof. Shin passed away on June 7, 2022.

Frontiers in Molecular Crystals Research: New Materials and Novel Phenomena

December 1-2, 2021
H. Ito, T. Kusamoto, M. Naka, T. Osada, H. Seo (chair), M. Suda, N. Tajima, A. Ueda, M. Yamashita, and K. Yoshimi

This workshop was organized to gather researchers working on a rich variety of molecular solids to exchange discussions about recent progresses in different fields. The presentations included a broad range of topics: e.g., development of new metal complexes showing novel cross-correlated functionalities among magnetic, optical, and electric responses, elucidation of novel phenomena by first-principles calculations and strongly-correlated theories, design of pi-electron system in newly synthesized molecular materials, photo-induced nonlinear phenomena explored by state-of-the-art optical sources, and measurements and analyses of nontrivial electronic states in molecular topological materials. We had 12 invited talks, 18 contributed talks, and 41 poster presentations. The workshop was held as a hybrid-type organization with oral talks onsite at ISSP and online otherwise, and successfully had extensive discussions between researchers with different backgrounds.

High-Pressure Workshop “Recent topics”

March 5, 2022
Y. Uwatoko, Z. Hiroi, H. Takahashi, and M. Hasegawa

Pressure is an important thermodynamic parameter frequently used for understanding and tuning the fundamental physical properties of materials in a controlled manner and also synthesize new materials not existing in ambient pressure and temperature. Apart from these, in recent years, the growing importance of high pressure has been realized in many other research fields. To review and update the status of recent research in various fields using high pressure as a keyword as well as to discuss the future research prospects, the ISSP workshop was held on March 5th, 2022. Considering the ongoing COVID-19 situation, the workshop was held online via ZOOM with 183 participants from universities, companies and including research institutes working in various fields. In this workshop, 14 researchers were invited to deliver talk about the latest trends in science and discuss the new direction that is expected to emerge from their current research activity. Each speaker presented various research results ranging from synthesis of new materials, measurement techniques under high pressure, essential pressure technologies to various applied measurements. In addition, each presentation was followed by an active question and answer session. Finally, Prof. Mori, Director of ISSP, gave a presentation on the prospects and direction of ISSP.

Frontier of Scanning Probe Microscopy and Related Nano Science

March 30-31, 2022,
M. Haze, T. An, Y. Okada, Y. Kim, Y. Sugimoto, Y. Hasegawa, T. Hanaguri, and Y. Yoshida

Scanning tunneling microscopy (STM) provides us atomically resolved images of materials' surfaces. It has been known that electronic states, magnetic properties, and vibrational spectra can be obtained by tunneling spectroscopy, spin-polarized STM, and inelastic tunneling spectroscopy, respectively. Recently, combined with pico-second pulsed light or THz light, new atomistic information of time-resolved phenomena were revealed. Recent progress of photo STM has made meV-resolution of single-molecule photo luminescence possible. Spin-polarized STM with GHz waves successfully detects spin resonance of single atoms. Dilution refrigerator STM achieves meV energy resolution to reveal fine structures in a superconducting gap. Improvement of atomic force microscopy (AFM) is also amazing; atomic framework of molecules is now imaged by using CO-terminated tip. The orientation of water molecules are successfully visualized.

In order to overview above-mentioned recent advancements of probe microscopy, we organized this workshop. In addition to young domestic invited speakers and poster presenters, we also invited several prominent researchers from abroad, making the most of the online workshop.

Since the schedule was arranged loosely and each speaker has a plenty of time for the presentation (40 min), speakers gave us a very clear and informative talk, which may not be possible in usual tight-scheduled conferences. The discussion after the presentation was also quite active, which obviously helped scientific and technical understandings of the audience. More than 150 researchers joined the workshop including some from abroad. It would be our pleasure if the workshop revise the perspective about the probe microscopes and promote joint researches among the participants.

Open Topological System in Biology, Quantum Systems, and Statistical Mechanics

March 28-30, 2022
T. Oka and K. Inoue

Transport processes of particles, energy, and information have been widely studied in both condensed matter physics and life sciences. In this workshop, we invited researchers from 3 fields, namely condensed matter physics, life sciences, and statistical mechanics, to discuss the topics of open topological systems.

Talks on non-Hermite quantum systems, correlated electrons, Liouville systems, Floquet systems, and biological systems (experiments) were given. Naomichi Hatano, who pioneered the field, gave the first talk with an excellent overview. Many of the speakers were young, including two Ph.D. students. The format of the workshop was hybrid, with about 50 on-site audiences and 20 online audiences. Extremely lively Q&A sessions were held, and although we had a relaxed schedule (60 mins for each speaker), the discussions continued for a long time. The workshop aimed to bring young researchers from different fields and help them communicate their ideas. We think that this workshop was successful in this aim and feel that it should be continued, for example, bi-annually.

Publications (2021.1 - 2022.4)

Division of Condensed Matter Science

Mori group

We have successfully developed and unveiled unprecedented functional properties for the molecular materials and systems. The major achievements in 2021 are (1) to develop the simplest model for doped PEDOT (Poly(3,4-ethylenedioxythiophene)), single-crystalline EDOT dimer radical cation salts, (2) to investigate effects of mechanical grinding on the phase behavior and anhydrous proton conductivity of imidazolium hydrogen succinate, and (3) to investigate modulation of the electronic states and magnetic properties of Nickel catecholdithiolene complex by oxidation-coupled deprotonation.

1. †Effects of mechanical grinding on the phase behavior and anhydrous proton conductivity of imidazolium hydrogen succinate: S. Dekura, Y. Sunairi, K. Okamoto, F. Takeiri, G. Kobayashi, Y. Hori, Y. Shigeta and H. Mori, Solid State Ionics **372**, 115775 (2021).
2. †Proton Conduction Mechanism for Anhydrous Imidazolium Hydrogen Succinate Based on Local Structures and Molecular Dynamics: Y. Hori, S. Dekura, Y. Sunairi, T. Ida, M. Mizuno, H. Mori and Y. Shigeta, J. Phys. Chem. Lett. **12**, 5390 (2021).
3. * 水素を活かすセラミクス　プロトン－電子カップル型分子性結晶および二分子膜における機能開拓： 森 初果 , 加藤 浩之 , 藤野 智子 , 上田 顕 , 吉信 淳 , セラミックス **56**, 88-91 (2021).
4. Effect of Alkyl Chain Length on Charge Transport Property of Anthracene-Based Organic Semiconductors: D. Zhang, S. Yokomori, R. Kameyama, C. Zhao, A. Ueda, L. Zhang, R. Kumai, Y. Murakami, H. Meng and H. Mori, ACS Appl. Mater. Interfaces **13**, 989 (2021).
5. Terahertz-field-induced polar charge order in electronic-type dielectrics: H. Yamakawa, T. Miyamoto, T. Morimoto, N. Takamura, S. Liang, H. Yoshimochi, T. Terashige, N. Kida, M. Suda, H. M. Yamamoto, H. Mori, K. Miyagawa, K. Kanoda and H. Okamoto, Nat Commun **12**, 953 (2021).
6. *Ferromagnetism out of charge fluctuation of strongly correlated electrons in κ-(BEDT-TTF)$_2$Hg(SCN)$_2$Br: M. Yamashita, S. Sugiura, A. Ueda, S. Dekura, T. Terashima, S. Uji, Y. Sunairi, H. Mori, E. I. Zhilyaeva, S. A. Torunova, R. N. Lyubovskaya, N. Drichko and C. Hotta, npj Quantum Mater. **6**, 87 (2021).
7. *The Simplest Model for Doped Poly(3,4-ethylenedioxythiophene) (PEDOT): Single-crystalline EDOT Dimer Radical Cation Salts: R. Kameyama, T. Fujino, S. Dekura, M. Kawamura, T. Ozaki and H. Mori, Chem. Eur. J. **27**, 6696 (2021).
8. Modulation of the electronic states and magnetic properties of nickel catecholdithiolene complex by oxidation-coupled deprotonation: S. Yokomori, S. Dekura, A. Ueda, R. Kumai, Y. Murakami and H. Mori, J. Mater. Chem. C **9**, 10718-10726 (2021).
9. †Magnetic and Structural Properties of Organic Radicals Based on Thienyl- and Furyl-Substituted Nitronyl Nitroxide: T. Sugano, S. J. Blundell, W. Hayes and H. Mori, Magnetochemistry **7**, 62 (2021).
10. Conjugation length effect on the conducting behavior of single-crystalline oligo(3,4-ethylenedioxythiophene) (*n* EDOT) radical cation salts: R. Kameyama, T. Fujino, S. Dekura and H. Mori, Phys. Chem. Chem. Phys. **24**, 9130 (2022).
11. Proton–electron-coupled functionalities of conductivity, magnetism, and optical properties in molecular crystals: H. Mori, S. Yokomori, S. Dekura and A. Ueda, Chem. Commun., 10.1039.D1CC06826A (2022), in print.
12. 水素を使いこなすためのサイエンス　ハイドロジェノミクス：森 初果 , (共立出版 , ISBN 978-4-320-04498-2, 2022).

Osada group

Two topological thermoelectric effects were investigated in the organic Dirac fermion system: (1) The nonlinear anomalous Ettingshausen effect (AEE) was predicted as a thermoelectric analogue of the nonlinear anomalous Hall effect (AHE) in the

* Joint research among groups within ISSP.

current-carrying state in two-dimensional (2D) massive Dirac fermion system. The thermoelectric Berry curvature dipole was introduced instead of the Berry curvature dipole. We estimated the possible nonlinear AEE in the weak charge ordering (CO) state in an organic conductor α-(BEDT-TTF)$_2$I$_3$, and found that it is in the observable range. (2) The quantized thermoelectric Hall effect (QTHE), which was theoretically proposed in the 2D massless Dirac fermion system at the high-magnetic-field quantum limit, was investigated in the real organic Dirac system α-(BEDT-TTF)$_2$I$_3$. The relatively large Zeeman splitting of the n=0 Landau level suppresses the QTHE causing the hump-like structure of Seebeck coefficient, which was observed in the experiment.

1. Experimental Confirmation of Massive Dirac Fermions in Weak Charge-Ordering State in α-(BEDT-TTF)$_2$I$_3$: K. Yoshimura, M. Sato and T. Osada, J. Phys. Soc. Jpn. **90**, 033701(1-5) (2021).
2. Possible Nonlinear Anomalous Thermoelectric Effect in Organic Massive Dirac Fermion System: T. Osada and A. Kiswandhi, J. Phys. Soc. Jpn. **90**, 053704(1-5) (2021).
3. Thermoelectric Effect at Quantum Limit in Two-Dimensional Organic Dirac Fermion System with Zeeman Splitting: T. Osada, J. Phys. Soc. Jpn. **90**, 113703(1-4) (2021).
4. Observation of possible nonlinear anomalous Hall effect in organic two-dimensional Dirac fermion system: A. Kiswandhi and T. Osada, J. Phys.: Condens. Matter **34**, 105602(1-7) (2022).
5. Thermoelectric Hall Effect at High-Magnetic-Field Quantum Limit in Graphite as a Nodal-Line Semimetal: T. Osada, T. Ochi and T. Taen, J. Phys. Soc. Jpn. **91**, 063701(1-4) (2022).
6. 有機ディラック電子系におけるトポロジカル輸送現象：長田 俊人，固体物理 **57**, 227-240 (2022).
7. 有機ディラック電子系における非線形トポロジカル輸送現象： 長田 俊人，キスワンディ アンディカ，日本物理学会誌 **77**, 233-238 (2022).

Yamashita group

We have been studying (1) quantum criticality in heavy-fermion materials by ultralow temperature cryostat, (2) thermal-Hall conductivity of exotic excitations in frustrated magnets and (3) a new technique for the study of strongly-correlated electron systems. In this year, we have performed (1) developments of ultralow-temperature resistivity measurements of $YbRh_2Si_2$, (2) thermal-Hall measurements of AFM skyrmions in $MnSc_2S_4$, (3) planar thermal Hall measurements of Kitaev candidate $Na_2Co_2TeO_6$, and (4) electric transports and NMR of $EuIn_2As_2$.

1. *Pressure-induced phase transition in the J_1-J_2 square lattice antiferromagnet $RbMoOPO_4Cl$: H. Takeda, T. Yamauchi, M. Takigawa, H. Ishikawa and Z. Hiroi, Phys. Rev. B **103**, 104406 (2021).
2. Tuning the Parity Mixing of Singlet-Septet Pairing in a Half-Heusler Superconductor: K. Ishihara, T. Takenaka, Y. Miao, Y. Mizukami, K. Hashimoto, M. Yamashita, M. Konczykowski, R. Masuki, M. Hirayama, T. Nomoto, R. Arita, O. Pavlosiuk, P. Wisniewski, D. Kaczorowski and T. Shibauchi, Phys. Rev. X **11**, 041048 (2021).
3. *Strongly correlated superconductivity in a copper-based metal-organic framework with a perfect kagome lattice: T. Takenaka, K. Ishihara, M. Roppongi, Y. Miao, Y. Mizukami, T. Makita, J. Tsurumi, S. Watanabe, J. Takeya, M. Yamashita, K. Torizuka, Y. Uwatoko, T. Sasaki, X. Huang, W. Xu, D. Zhu, N. Su, J. -G. Cheng, T. Shibauchi and K. Hashimoto, Sci. Adv. **7**, eabf3996(1-8) (2021).
4. *Ferromagnetism out of charge fluctuation of strongly correlated electrons in κ-(BEDT-TTF)$_2$Hg(SCN)$_2$Br: M. Yamashita, S. Sugiura, A. Ueda, S. Dekura, T. Terashima, S. Uji, Y. Sunairi, H. Mori, E. I. Zhilyaeva, S. A. Torunova, R. N. Lyubovskaya, N. Drichko and C. Hotta, npj Quantum Mater. **6**, 87 (2021).
5. * ヘリウムリサイクルへの取り組み―東京大学物性研究所の活動―: 勝本 信吾，鷺山 玲子，土屋 光，山下 穣，低温工学 **56**, 119 (2021).
6. Field-induced topological Hall effect in antiferromagnetic axion insulator candidate $EuIn_2As_2$: J. Yan, Z. Z. Jiang, R. C. Xiao, W. J. Lu, W. H. Song, X. B. Zhu, X. Luo, Y. P. Sun and M. Yamashita, Phys. Rev. Research **4**, 013163 (2022).

Division of Condensed Matter Theory

Tsunetsugu group

† Joint research with outside partners.

We have continued to study several topics of correlated electron systems and their nonequilibrium dynamics this year. One topic is the thermodynamics of a frustrated spin system, and we have studied the Kagome spin system with breathing lattice deformation. Mapping this system to an effective model of spin and chirality degrees of freedom, we have performed classical Monte Carlo simulations to investigate their thermodynamic properties. We have found a glassy behavior of chiralities, which may be understood as a nematic liquid. We have also continued a study of electric quadrupoles in the heavy fermion system. An analysis on the complex spatial structure of quadrupoles has been developed further to examine the effects of the cubic interactions characteristic to this system. As for the nonequilibrium issues, we have analyzed nonlinear optical responses of a Kitaev spin liquid and proposed their use for identifying such a liquid. We have also developed a WKB theory to study nonperturbative nonlinear optical effects. For statistical-mechanical aspects of periodically driven quantum systems, we have characterized the heating rate in isolated systems based on the Fermi golden rule. We have also developed a theory for determining nonequilibrium steady states in the systems subject to Markovian dissipation. In particular, a setup was proposed for realizing a time crystalline steady state accompanied by critical phenomena.

1. Dynamics of Composite Domain Walls in Multiferroics in Magnetic Field and Their Instability: K. Kawahara and H. Tsunetsugu, J. Phys. Soc. Jpn. **90**, 014703 (2021).
2. Nematicity Liquid in a Trimerized-Kagome Antiferromagnet: I. Tanaka and H. Tsunetsugu, J. Phys. Soc. Jpn. **90**, 063707 (2021).
3. Quadrupole Orders on the fcc Lattice: H. Tsunetsugu, T. Ishitobi and K. Hattori, J. Phys. Soc. Jpn. **90**, 043701 (2021).
4. Analytical WKB theory for high-harmonic generation and its application to massive Dirac electrons: H. Taya, M. Hongo and T. N. Ikeda, Phys. Rev. B **104**, L140305 (2021).
5. Fermi's golden rule for heating in strongly driven Floquet systems: T. N. Ikeda and A. Polkovnikov, Phys. Rev. B **104**, 134308 (2021).
6. Generalized hydrodynamics study of the one-dimensional Hubbard model: Stationary clogging and proportionality of spin, charge, and energy currents: Y. Nozawa and H. Tsunetsugu, Phys. Rev. B **103**, 035130 (2021).
7. Linear and nonlinear optical responses in Kitaev spin liquids: M. Kanega, T. N. Ikeda and M. Sato, Phys. Rev. Research **3**, L032024 (2021).
8. Nonequilibrium steady states in the Floquet-Lindblad systems: van Vleck's high-frequency expansion approach: T. N. Ikeda, K. Chinzei and M. Sato, SciPost Phys. Core **4**, 033 (2021).
9. Criticality and rigidity of dissipative discrete time crystals in solids: K. Chinzei and T. N. Ikeda, Phys. Rev. Research **4**, 023025 (2022).
10. 複数の秩序が生むドメイン壁の不安定性 -- 複合ドメイン壁の構造不安定性 --: 川原 光滋 , 常次 宏一 , 固体物理 **56**, 467-475 (2021).
11. ユニークな四極子秩序の安定化機構の発見 : 服部 一匡 , 石飛 尊之 , 常次 宏一 , 固体物理 **57**, 255-266 (2022).

Kato group

The main research subject of Kato Lab. is transport properties in mesoscopic and spintronic devices. We studied (1) heat transport via small quantum systems, (2) transmission properties of Josephson junction arrays, (3) spin pumping from ferromagnetic insulator to metallic systems, (4) many-body effect in multielectron quantum dot systems, (5) high-harmonic generation in semiconductors, (6) nonequilibrium transport through Kondo quantum dots, (7) nanorotors driven by the spin-rotation coupling, and (8) the fluctuation theorem in spin-Hall magnetoresistance.

1. Heat transport through a two-level system embedded between two harmonic resonators: T. Yamamoto and T. Kato, J. Phys.: Condens. Matter **33**, 395303(1-10) (2021).
2. *High-harmonic generation in GaAs beyond the perturbative regime: P. Xia, T. Tamaya, C. Kim, F. Lu, T. Kanai, N. Ishii, J. Itatani, H. Akiyama and T. Kato, Phys. Rev. B **104**, L121202(1-6) (2021).
3. Nonlinear Fermi liquid transport through a quantum dot in asymmetric tunnel junctions: K. Tsutsumi, Y. Teratani, R. Sakano and A. Oguri, Phys. Rev. B **104**, 235147(1-17) (2021).
4. Piezo-optic effect of high-harmonic generation in semiconductors: T. Tamaya and T. Kato, Phys. Rev. B **103**, 205202(1-10) (2021).
5. Spin current at a magnetic junction as a probe of the Kondo state: T. Yamamoto, T. Kato and M. Matsuo, Phys. Rev. B **104**, L121401(1-5) (2021).

* Joint research among groups within ISSP.

6. Spin pumping of two-dimensional electron gas with Rashba and Dresselhaus spin-orbit interactions: M. Yama, M. Tatsuno, T. Kato and M. Matsuo, Phys. Rev. B **104**, 054410(1-9) (2021).

7. Transmission of waves through a pinned elastic medium: T. Yamamoto, L. I. Glazman and M. Houzet, Phys. Rev. B **103**, 224211(1-17) (2021).

8. *Preparation and Readout of Multielectron High-Spin States in a Gate-Defined GaAs/AlGaAs Quantum Dot: H. Kiyama, K. Yoshimi, T. Kato, T. Nakajima, A. Oiwa and S. Tarucha, Phys. Rev. Lett. **127**, 086802(1-6) (2021).

9. Three-body correlations in nonlinear response of correlated quantum liquid: T. Hata, Y. Teratani, T. Arakawa, S. Lee, M. Ferrier, R. Deblock, R. Sakano, A. Oguri and K. Kobayashi, Nat. Commun. **12**, 3233(1-7) (2021).

10. †*DSQSS: Discrete Space Quantum Systems Solver: Y. Motoyama, K. Yoshimi, A. Masaki-Kato, T. Kato and N. Kawashima, Comput. Phys. Commun. **264**, 107944(1-9) (2021).

11. Kondo Effect and Phase Measurement in Double Quantum Dot in Parallel: Y. Zhang, R. Sakano and M. Eto, J. Phys. Soc. Jpn. **91**, 014703(1-10) (2022).

12. Current noise and Keldysh vertex function of an Anderson impurity in the Fermi-liquid regime: A. Oguri, Y. Teratani, K. Tsutsumi and R. Sakano, Phys. Rev. B **105**, 115409(1-37) (2022).

13. Einstein–de Haas Nanorotor: W. Izumida, R. Okuyama, K. Sato, T. Kato and M. Matsuo, Phys. Rev. Lett. **128**, 017701(1-6) (2022).

14. Fluctuation theorem for spin transport at insulating ferromagnetic junctions: T. Sato, M. Tatsuno, M. Matsuo and T. Kato, Journal of Magnetism and Magnetic Materials **546**, 168814(1-6) (2022).

15. 一歩進んだ理解を目指す物性物理学講義：加藤 岳生，(サイエンス社，東京 , 2022).

Division of Nanoscale Science

Katsumoto group

A shot noise measurement system using a handmade HEMT and a preamplifier has been completed. Numerical simulation on the spin precession and division of electrons propagating on spin-resolved quantum Hall edge was carried out with the recursive Green function method. The simulation successfully reproduced the experimentally observed probability partition. Shot noise measurement was carried out on the flying spin qubit interferometer. We have found an anomalous decrease in the shot noise at higher bias, which has been explained by the approach of spin-resolved edge states.

1. Commensurability oscillations in the Hall resistance of unidirectional lateral superlattices: A. Endo, S. Katsumoto and Y. Iye, Phys. Rev. B **103**, 235303 (2021).

2. Homemade-HEMT-based transimpedance amplifier for high-resolution shot-noise measurements: T. Shimizu, M. Hashisaka, H. Bohuslavskyi, T. Akiho, N. Kumada, S. Katsumoto and K. Muraki, Review of Scientific Instruments **92**, 124712 (2021).

3. * ヘリウムリサイクルへの取り組み―東京大学物性研究所の活動―: 勝本 信吾，鷺山 玲子，土屋 光，山下 穣，低温工学 **56**, 119 (2021).

Otani group

This year, we focused on the topic related to the antiferromagnetic spintronics, namely the manipulation of the cluster magnetic octupole state in Mn_3X (X=Mn or Sn) thin films. Last year, we succeeded in the magnetic octupole state manipulation in Mn_3Sn by using spin-orbit torque. We further improved the readout voltage beyond 1 mV, a milestone for future applications for memory technology. Besides, we also demonstrated that the absence of shape anisotropy enables omnidirectional control and lifts the shape constraint in designing magnetic devices. Our international collaboration with Pohang University of Science and Technology in Korea and Peter Grünberg Institut in Germany on the novel spin-charge conversion study showed that the flow of orbital angular momentum plays a vital role in exerting nontrivial torque in ferromagnetic metal/Cu/Aluminum oxide trilayers. Another international collaboration on magnon-phonon coupling study with Huazhong University of Science and Technology demonstrated numerically that antiferromagnetic domain walls could oscillate at a relatively low frequency of the order of MHz. This finding is beneficial for antiferromagnetic devices, which require a stable antiferromagnetic domain wall velocity.

† Joint research with outside partners.

1. Nontrivial torque generation by orbital angular momentum injection in ferromagnetic-metal/Cu/Al_2O_3 trilayers: J. Kim, D. Go, H. Tsai, D. Jo, K. Kondou, H.-W. Lee and Y. Otani, Phys. Rev. B **103**, L020407 (2021).

2. *Domain structure and domain wall dynamics in topological chiral antiferromagnets from the viewpoint of magnetic octupole: Y. Otani and T. Higo, Appl. Phys. Lett. **118**, 040501 (2021).

3. Influence of planar Hall effect on the output signal in a T-shaped spin conversion device: H. Mizuno, H. Isshiki, K. Kondou, Y. Zhu and Y. Otani, Appl. Phys. Lett. **119**, 092401 (2021).

4. *Omnidirectional Control of Large Electrical Output in a Topological Antiferromagnet: T. Higo, Y. Li, K. Kondou, D. Qu, M. Ikhlas, R. Uesugi, D. Nishio-Hamane, C. L. Chien, Y. Otani and S. Nakatsuji, Adv. Funct. Mater. **31**, 2008971 (2021).

5. *Spin-orbit torque switching of the antiferromagnetic state in polycrystalline Mn_3Sn/Cu/heavy metal heterostructures: H. Tsai, T. Higo, K. Kondou, A. Kobayashi, T. Nakano, K. Yakushiji, S. Miwa, Y. Otani and S. Nakatsuji, AIP Advances **11**, 045110 (1-6) (2021).

6. Strain-induced Megahertz Oscillation and Stable Velocity of an Antiferromagnetic Domain Wall: F. Chen, X. Ge, W. Luo, R. Xing, S. Liang, X. Yang, L. You, R. Xiong, Y. Otani and Y. Zhang, Phys. Rev. Applied **15**, 014030 (2021).

7. *Fabrication of polycrystalline Weyl antiferromagnetic Mn_3Sn thin films on various seed layers: T. Nakano, T. Higo, A. Kobayashi, S. Miwa, S. Nakatsuji and K. Yakushiji, Phys. Rev. Materials **5**, 054402 (1-9) (2021).

8. Nanochannels for spin-wave manipulation in $Ni_{80}Fe_{20}$ nanodot arrays: S. Sahoo, S. N. Panda, S. Barman, Y. Otani and A. Barman, Journal of Magnetism and Magnetic Materials **522**, 167550 (2021).

9. *Giant Effective Damping of Octupole Oscillation in an Antiferromagnetic Weyl Semimetal: S. Miwa, S. Iihama, T. Nomoto, T. Tomita, T. Higo, M. Ikhlas, S. Sakamoto, Y. Otani, S. Mizukami, R. Arita and S. Nakatsuji, Small Science **1**, 2000062 (1-8) (2021).

10. *Large Hall Signal due to Electrical Switching of an Antiferromagnetic Weyl Semimetal State: H. Tsai, T. Higo, K. Kondou, S. Sakamoto, A. Kobayashi, T. Matsuo, S. Miwa, Y. Otani and S. Nakatsuji, Small Science **1**, 2000025 (1-9) (2021).

11. Interaction between surface acoustic waves and spin waves in a ferromagnetic thin film: K. Yamamoto, M. Xu, J. Puebla, Y. Otani and S. Maekawa, Journal of Magnetism and Magnetic Materials **545**, 168672 (2022).

12. Efficient and controllable magnetization switching induced by intermixing-enhanced bulk spin–orbit torque in ferromagnetic multilayers: K. Zhang, L. Chen, Y. Zhang, B. Hong, Y. He, K. Lin, Z. Zhang, Z. Zheng, X. Feng, Y. Zhang, Y. Otani and W. Zhao, Applied Physics Reviews **9**, 011407 (2022).

Hasegawa group

We studied superconductivity of Pb atomic layers formed on vicinal substrates to investigate how surface steps with an interval shorter than the coherence length affect the two-dimensional superconductivity. Transport measurements revealed reduced critical temperature and enhanced critical magnetic field. Scanning tunneling microscopy (STM) exhibited elongated vortices along the steps. The oval-shaped vortices are Abrikosov-Josephson vortices squeezed in the direction perpendicular to the steps due to the reduced coherence length, which is also responsible for the enhanced critical fields. Our work demonstrates that vicinal substrates provide a unique platform to control macroscopic properties through the precise tuning of disorder. In collaboration with Prof. Bent Weber, Nanyang Univ., Singapore, we investigated heterostructures of a quantum spin Hall candidate *1T′*-WTe_2 grown by van der Waals epitaxy on superconductor $NbSe_2$ by STM. By analyzing the normal and superconducting density of states (DOS) by scanning probe spectroscopy across the interface, we found that strong hybridization of electronic states gives rise to a semimetallic DOS in the 2D bulk even in nominally band insulating crystals. Despite the strong hybridization, we found a measurable enhancement of the local DOS at the crystal edges in the normal state and a slight enhancement of the order parameter in the superconducting state.

1. Enhanced critical magnetic field for monoatomic-layer superconductor by Josephson junction steps: F. Oguro, Y. Sato, K. Asakawa, M. Haze and Y. Hasegawa, Phys. Rev. B **103**, 085416(1-7) (2021).

2. †Reduction in magnetic coercivity of Co nanomagnets by Fe alloying: H.-H. Yang, C.-C. Hsu, K. Asakawa, W.-C. Lin and Y. Hasegawa, Nanoscale **13**, 16719-16725 (2021).

3. †Multiband superconductivity in strongly hybridized 1T′−WTe_2/$NbSe_2$ heterostructures: W. Tao, Z. J. Tong, A. Das, D.-Q. Ho, Y. Sato, M. Haze, J. Jia, Y. Que, F. Bussolotti, K. E. Johnson Goh, B. Wang, H. Lin, A. Bansil, S. Mukherjee, Y. Hasegawa and B. Weber, Phys. Rev. B **105**, 094512(1-14) (2022).

---

* Joint research among groups within ISSP.

4. Superconductivity near the saddle point in the two-dimensional Rashba system Si(111)−√3×√3−(Tl,Pb): T. Machida, Y. Yoshimura, T. Nakamura, Y. Kohsaka, T. Hanaguri, C. -R. Hsing, C. -M. Wei, Y. Hasegawa, S. Hasegawa and A. Takayama, Phys. Rev. B **105**, 064507(1-9) (2022).

5. Numerical simulations for ferromagnetic resonance of nano-size island structures probed by radio-frequency scanning tunneling microscopy: Y. Sato, M. Haze, H.-H. Yang, K. Asakawa, S. Takahashi and Y. Hasegawa, Jpn. J. Appl. Phys. **61**, 025001(1-6) (2022).

6. スパースモデリングを活用した走査トンネル顕微鏡像解析：土師 将裕，吉田 靖雄，長谷川 幸雄，表面と真空 **65**, 78-83 (2022).

7. 走査トンネル分光法：長谷川 幸雄，「図説表面分析ハンドブック」，日本表面真空学会，(朝倉出版 , 2021), 428-433.

Lippmaa group

We have worked on developing the pulsed laser deposition process. In particular, we have studied the effect of the high-energy ions in the ablation plume have on the properties of ceramic thin films. Our recent work shows that the plume energy is sufficient to cause local damage in thin films, as shown by thin film lattice parameter shifts from known bulk values. We have shown that the kinetic damage to thin films can be effectively reduced by introducing a light inert buffer gas into the process chamber. Deposition of films in the presence of high-pressure He ambient gas does not significantly reduce the deposition rate, but reduces the kinetic energy of the plume and thus enables the growth of higher-quality thin films with fewer point defects.

1. Nanopillar composite electrodes for solar-driven water splitting: M. Lippmaa, S. Kawasaki, R. Takahashi and T. Yamamoto, MRS Bulletin **46**, 142-151 (2021).

2. †He Buffer Gas for Moderating the Kinetic Energy of Pulsed Laser Deposition Plumes: R. Takahashi, T. Yamamoto and M. Lippmaa, Cryst. Growth Des. **21**, 5017-5026 (2021).

3. 単結晶薄膜の自立化プロセスの開発：高橋 竜太，リップマー ミック，セラミックス **56**, 451-454 (2021).

4. *Observation and control of the weak topological insulator state in $ZrTe_5$: P. Zhang, R. Noguchi, K. Kuroda, C. Lin, K. Kawaguchi, K. Yaji, A. Harasawa, M. Lippmaa, S. Nie, H. Weng, V. Kandyba, A. Giampietri, A. Barinov, Q. Li, G. D. Gu, S. Shin and T. Kondo, Nat. Commun. **12**, 406 (2021).

5. †Realization of closed-loop optimization of epitaxial titanium nitride thin-film growth via machine learning: I. Ohkubo, Z. Hou, J. N. Lee, T. Aizawa, M. Lippmaa, T. Chikyow, K. Tsuda and T. Mori, Mater. Today Phys. **16**, 100296 (1-6) (2021).

Functional Materials Group

Yoshinobu group

We conducted several research projects in the fiscal year 2021: (1) The surface chemistry of hydrogen, formic acid and CO_2 on Cu(977), Pd-Cu(111) and Pd-Cu(997) surfaces was studied by SR-PES, IRAS, HREELS and TPD. (2) The adsorption/desorption of CH_4 on Pt(997) was studied by TPD, IRAS and SR-XPS. (3) The dry reforming of CH_4 with CO_2 on Pt(997) was studied by AP-XPS at SPring-8. (4) The reaction dynamics of CO + O -> CO_2 on Pt(111) was studied by van der Waals DFT calculations. (5) The micro-beam SR-XPS and AP-XPS were applied to study the MoS_2 edge in vacuum and under hydrogen pressure. (6) The narrow band and broad band THz pulse generation system has been newly constructed.

1. †Adsorption of CO_2 on Terrace, Step, and Defect Sites on Pt Surfaces: A Combined TPD, XPS, and DFT Study: Y. Wong, Y. H. Choi, S. Tanaka, H. Yoshioka, K. Mukai, H. H. Halim, A. R. Mohamed, K. Inagaki, Y. Hamamoto, I. Hamada, J. Yoshinobu and Y. Morikawa, J. Phys. Chem. C **125**, 23657 (2021).

2. †*Band Bending of n-GaN under Ambient H_2O Vapor Studied by X-ray Photoelectron Spectroscopy: Y. Imazeki, M. Sato, T. Takeda, M. Kobayashi, S. Yamamoto, I. Matsuda, J. Yoshinobu, M. Sugiyama and Y. Nakano, J. Phys. Chem. C **125**, 9011 (2021).

3. C–H Bond Activation of Methane through Electronic Interaction with Pd(110): T. Koitaya, A. Ishikawa, S. Yoshimoto and J. Yoshinobu, J. Phys. Chem. C **125**, 1368 (2021).

4. †*Comparative Study of H_2O and O_2 Adsorption on the GaN Surface: M. Sato, Y. Imazeki, T. Takeda, M. Kobayashi, S. Yamamoto, I. Matsuda, J. Yoshinobu, Y. Nakano and M. Sugiyama, J. Phys. Chem. C **125**, 25807 (2021).

† Joint research with outside partners.

5. * 水素を活かすセラミクス　プロトン－電子カップル型分子性結晶および二分子膜における機能開拓：森 初果，加藤 浩之，藤野 智子，上田 顕，吉信 淳，セラミックス **56**, 88-91 (2021).

6. Role of Intermolecular Interactions in the Catalytic Reaction of Formic Acid on Cu(111): A. Shiotari, S. E. M. Putra, Y. Shiozawa, Y. Hamamoto, K. Inagaki, Y. Morikawa, Y. Sugimoto, J. Yoshinobu and I. Hamada, Small **2021**, 2008010 (2021).

7. Theoretical study on adsorption and reaction of polymeric formic acid on the Cu(111) surface: S. E. M. Putra, F. Muttaqien, Y. Hamamoto, K. Inagaki, A. Shiotari, J. Yoshinobu, Y. Morikawa and I. Hamada, Phys. Rev. Materials **5**, 075801 (2021).

8. †*Structure and electronic structure of van der Waals interfaces at a Au(1 1 1) surface covered with a well-ordered molecular layer of n-alkanes: H. Mizushima, H. Koike, K. Kuroda, K. Yaji, A. Harasawa, Y. Ishida, M. Nakayama, K. Mase, K. Mukai, T. Kitazawa, T. Kondo, J. Yoshinobu, S. Shin and K. Kanai, Applied Surface Science **535**, 147673 (2021).

9. †*Functionalization of the MoS_2 basal plane for activation of molecular hydrogen by Pd deposition: F. Ozaki, S. Tanaka, W. Osada, K. Mukai, M. Horio, T. Koitaya, S. Yamamoto, I. Matsuda and J. Yoshinobu, Applied Surface Science **593**, 153313 (2022).

10. †*Hydrogen absorption and diffusion behaviors in cube-shaped palladium nanoparticles revealed by ambient-pressure X-ray photoelectron spectroscopy: J. Tang, O. Seo, D. S. R. Rocabado, T. Koitaya, S. Yamamoto, Y. Nanba, C. Song, J. Kim, A. Yoshigoe, M. Koyama, S. Dekura, H. Kobayashi, H. Kitagawa, O. Sakata, I. Matsuda and J. Yoshinobu, Applied Surface Science **587**, 152797 (2022).

11. *Tracking Ultrafast Change of Multiterahertz Broadband Response Functions in a Photoexcited Dirac Semimetal Cd_3As_2 Thin Film: N. Kanda, Y. Murotani, T. Matsuda, M. Goyal, S. Salmani-Rezaie, J. Yoshinobu, S. Stemmer and R. Matsunaga, Nano Letters **22**, 2358 (2022).

12. ZrB_2(0001) 薄膜表面上の二次元 Ge 二重三角格子：深谷 有喜，吉信 淳，アントワーヌ フロランス，高村 (山田) 由紀子，PF News **39-3**, 21-27 (2021).

13. 巻頭言　界面におけるエネルギー変換・輸送と現代の課題：吉信 淳，表面と真空 **64**, 539 (2021).

14. Hydrogenomics: Efficient and Selective Hydrogenation of Stable Molecules Utilizing Three Aspects of Hydrogen: K. Fukutani, J. Yoshinobu, M. Yamauchi, T. Shima and S. Orimo, Catal Lett **152**, 1583-1597 (2022).

15. 図説 表面分析ハンドブック：日本表面真空学会 (編集), (朝倉書店，東京都 , 2021).

16. “水素 " を使いこなすためのサイエンス　ハイドロジェノミクス：折茂 慎一，福谷 克之，藤田 健一（編），(共立出版，東京都文京区，2022).

Akiyama group

In 2021, we fabricated new series of gain-switched 1030-1060nm InGaAs laser diodes (LDs) changing various device parameters and investigated stable short seed-pulse generation conditions below 10 ps by current injection. We started study on heat-recovery (HERC) solar cells, and photo-voltaic and thermo-electric hybrid tandem cells, in collaboration with AIST team. Collaborations on four-junction solar cells with China team and on CIGC cells with Tsukuba team have been started. As for bio- and chemical-physics, we had significant progress in time-resolved Raman spectroscopy on channel rhodopsin with semiconductor-laser-based light sources (collaboration between a D3 student Shibata-kun and Inoue-group). Good progress has been made in quantitative spectroscopy on bioluminescence quantum yield of new luciferin analogs (Akalumine, Tokeoni, etc.) and on photo-cleavage/photo-bleaching quantum yields of D-luciferin and coumarin-caged-luciferins, in collaboration with Gunma-university team.

1. *High-harmonic generation in GaAs beyond the perturbative regime: P. Xia, T. Tamaya, C. Kim, F. Lu, T. Kanai, N. Ishii, J. Itatani, H. Akiyama and T. Kato, Phys. Rev. B **104**, L121202(1-6) (2021).

2. *Direct generation of sub-picosecond pulse via multi-section gain switching: T. Nakamura, T. Ito, H. Nakamae, C. Kim, Y. Hazama, Y. Kobayashi, R. Kuroda and H. Akiyama, Opt. Lett. **46**, 1277 (2021).

3. Unidirectional output from a quantum-dot single-photon source hybrid integrated on silicon: R. Katsumi, Y. Ota, T. Tajiri, M. Kakuda, S. Iwamoto, H. Akiyama and Y. Arakawa, Opt. Express **29**, 37117 (2021).

4. Fabricating over 7%-efficient $Sb_2(S,Se)_3$ thin-film solar cells by vapor transport deposition using Sb_2Se_3 and Sb_2S_3 mixed powders as the evaporation source: X. Hu, J. Tao, R. Wang, Y. Wang, Y. Pan, G. Weng, X. Luo, S. Chen, Z. Zhu, J. Chu and H. Akiyama, Journal of Power Sources **493**, 229737 (2021).

---

* Joint research among groups within ISSP.

5. Superior single-mode lasing in a self-assembly $CsPbX_3$ microcavity over an ultrawide pumping wavelength range: G. Weng, J. Yan, S. Chen, C. Zhao, H. Zhang, J. Tian, Y. Liu, X. Hu, J. Tao, S. Chen, Z. Zhu, H. Akiyama and J. Chu, Photon. Res. **9**, 54 (2021).

6. Reducing Shockley–Read–Hall recombination losses in the depletion region of a solar cell by using a wide-gap emitter layer: T. Nakamura, W. Yanwachirakul, M. Imaizumi, M. Sugiyama, H. Akiyama and Y. Okada, Journal of Applied Physics **130**, 153102 (2021).

7. Absorption Spectra for Firefly Bioluminescence Substrate Analog: TokeOni in Various pH Solutions: H. Ogawa, R. Ono, Y. Noguchi, N. Kitada, R. Saito-Moriya, S. A. Maki, H. Akiyama, H. Itabashi and M. Hiyama, Photochem Photobiol **97**, 1016 (2021).

8. High performance single-mode vertical cavity surface emitting lasers based on $CsPbBr_3$ nanocrystals with simplified processing: C. Zhao, J. Tao, J. Tian, G. Weng, H. Liu, Y. Liu, J. Yan, S. Chen, Y. Pan, X. Hu, S. Chen, H. Akiyama and J. Chu, Chemical Engineering Journal **420**, 127660 (2021).

9. Electron–Hole Plasma Lasing Dynamics in $CsPbCl_m Br_{3-m}$ Microplate Lasers: G. Weng, J. Tian, S. Chen, J. Yan, H. Zhang, Y. Liu, C. Zhao, X. Hu, X. Luo, J. Tao, S. Chen, Z. Zhu, J. Chu and H. Akiyama, ACS Photonics **8**, 787 (2021).

10. Adaptive automatic solar cell defect detection and classification based on absolute electroluminescence imaging: Y. Wang, L. Li, Y. Sun, J. Xu, Y. Jia, J. Hong, X. Hu, G. Weng, X. Luo, S. Chen, Z. Zhu, J. Chu and H. Akiyama, Energy **229**, 120606 (2021).

11. Enhanced Magneto-Optical Kerr Effect of GaAs-Based P-N Junctions in the Terahertz Range: K. Miyagawa, M. Nagai, M. Ashida, C. Kim and H. Akiyama, J Infrared Milli Terahz Waves **42**, 325 (2021).

12. Diagnosing breakdown mechanisms in monocrystalline silicon solar cells via electroluminescence imaging: Y. Jia, Y. Wang, X. Hu, J. Xu, G. Weng, X. Luo, S. Chen, Z. Zhu and H. Akiyama, Solar Energy **225**, 463 (2021).

13. Improving the performance of Sb_2S_3 thin-film solar cells by optimization of VTD source-substrate proximity: R. Wang, Y. Wang, Y. Pan, D. Qin, G. Weng, X. Hu, J. Tao, X. Luo, S. Chen, Z. Zhu, J. Chu and H. Akiyama, Solar Energy **220**, 942 (2021).

14. Electroluminescence imaging of laser induced defect formation in Cu(In, Ga)Se_2 solar cell: Y. Jia, Y. Wang, X. Hu, G. Weng, J. Tian, X. Luo, S. Chen, Z. Zhu and H. Akiyama, Solar Energy Materials and Solar Cells **230**, 111160 (2021).

15. レーザー加工用 LD シード光源の開発―ピコ秒利得スイッチ半導体レーザー：中村 考宏 , 中前 秀一 , 金昌 秀 , ソダーバンル ハッサネット , 杉山 正和 , 秋山 英文 , レーザ加工学会誌 **28**, 30-35 (2021).

16. Subcells Analysis of Thin-Film Four-Junction Solar Cells Using Optoelectronic Reciprocity Relation: J. Long, Q. Sun, X. Li, P. Dai, M. Song, L. Zhu, H. Akiyama, J. Lu and S. Lu, Sol. RRL **5**, 2000542 (2021).

17. Photo-bleaching of firefly luciferin with UV irradiation: R. Kumagai, R. Ono, H. Akiyama, H. Itabashi and M. Hiyama, Chemical Physics Letters **792**, 139414 (2022).

18. Carrier dynamics of AlGaAs/AlAs asymmetric double quantum wells with different barrier thickness: Y. Liu, G. Weng, F. Cao, Y. Wang, W. Wan, C. Wang, H. Nakamae, C. Kim, X. Hu, X. Luo, S. Luo, S. Chen, J. Chu and H. Akiyama, Opt. Mater. Express **12**, 1291 (2022).

Sugino group

Target of Sugino group is to advance computational materials science using modern density functional theory (DFT). This was proceeded by improving the density functional through machine-learning of the many-body wave function of materials. Our machine-learning method was found to provide reasonably accurate electronic structures not only for molecules but also bulk solids, showing a promise for further improvement toward the chemical accuracy. Electron-phonon coupling is another key to the improvement. Effect of nuclear motion on the band gap was investigated using perturbative or non-perturbative method gaining insight into the material dependence. Applying DFT to various materials was intensively done for the phase problems of graphite intercalations, solid oxygen, and cuprates in addition to our continued study on electrochemical interfaces.

1. Optical representation of thermal nuclear fluctuation effect on band-gap renormalization: K. Ishii, J. Haruyama and O. Sugino, Phys. Rev. B **104**, 245144 (2021).

2. Functional-renormalization-group approach to classical liquids with short-range repulsion: A scheme without repulsive reference system: T. Yokota, J. Haruyama and O. Sugino, Phys. Rev. E **104**, 014124 (2021).

3. †Thermodynamic Analysis of Li-Intercalated Graphite by First-Principles Calculations with Vibrational and Configura-

† Joint research with outside partners.

tional Contributions: J. Haruyama, S. Takagi, K. Shimoda, I. Watanabe, K. Sodeyama, T. Ikeshoji and M. Otani, J. Phys. Chem. C **125**, 27891 (2021).

4. †*Ab initio* construction of the energy density functional for electron systems with the functional-renormalization-group-aided density functional theory: T. Yokota and T. Naito, Phys. Rev. Research **3**, L012015 (2021).

5. †Advances and challenges for experiment and theory for multi-electron multi-proton transfer at electrified solid-liquid interfaces: K. Sakaushi, T. Komeda, S. Hammes-Schiffer, M. M. Melander and O. Sugino, PHYSICAL CHEMISTRY CHEMICAL PHYSICS **22**, 19401-19442 (2021).

6. †Machine-learning-based exchange correlation functional with physical asymptotic constraints: R. Nagai, R. Akashi and O. Sugino, Phys. Rev. Research **4**, 013106 (2022).

7. †Roadmap on Machine Learning in Electronic Structure: R. Nagai, R. Akashi and O. Sugino, Electron. Struct. **1**, 37-38 (2022).

Oka group

The Oka group has proposed a theory of geometric effects in non-adiabatic tunneling and applied it to strong field excitations in Dirac and Weyl semimetals.

1. Nonperturbative topological current in Weyl and Dirac semimetals in laser fields: R. M. A. Dantas, Z. Wang, P. Surówka and T. Oka, Phys. Rev. B **103**, L201105 (2021).

2. Scanning Tunneling Microscopy as a Single Majorana Detector of Kitaev's Chiral Spin Liquid: M. Udagawa, S. Takayoshi and T. Oka, Phys. Rev. Lett. **126**, 127201 (2021).

3. Nonadiabatic nonlinear optics and quantum geometry — Application to the twisted Schwinger effect: S. Takayoshi, J. Wu and T. Oka, SciPost Phys. **11**, 075 (2021).

Inoue group

In 2021, we reported a new machine learning method to predict rhodopsin genes having red-shifted absorption. By applying this method, ion pumping rhodopsin exhibiting absorption wavelength 40-nm longer than known proteins was discovered. The crystal structure of schizorhodopsin (SzR), which is a new type of inward proton pump first characterized in 2020, by X-ray crystallography. It revealed that transmembrane helices of SzR are shortened on the cytoplasmic side enabling rapid proton release to the cytoplasmic solvent. We found thermostable SzRs from thermophilic archaea. This finding suggests that in addition to general outward proton pumping rhodopsins, various types of microbial rhodopsins are used in high-temperature environments.

1. TAT Rhodopsin Is an Ultraviolet-Dependent Environmental pH Sensor: C. Kataoka, T. Sugimoto, S. Shigemura, K. Katayama, S. P. Tsunoda, K. Inoue, O. Béjà and H. Kandori, Biochemistry **60**, 899-907 (2021).

2. Crystal structure of schizorhodopsin reveals mechanism of inward proton pumping: A. Higuchi, W. Shihoya, M. Konno, T. Ikuta, H. Kandori, K. Inoue and O. Nureki, Proc. Natl. Acad. Sci. USA **118**, e2016328118 (2021).

3. Thermostable light-driven inward proton pump rhodopsins: Y. Kawasaki, M. Konno and K. Inoue, Chemical Physics Letters **779**, 138868 (2021).

4. Exploration of natural red-shifted rhodopsins using a machine learning-based Bayesian experimental design: K. Inoue, M. Karasuyama, R. Nakamura, M. Konno, D. Yamada, K. Mannen, T. Nagata, Y. Inatsu, H. Yawo, K. Yura, O. Béjà, H. Kandori and I. Takeuchi, Commun. Biol. **4**, 362 (2021).

5. Pro219 is an electrostatic color determinant in the light-driven sodium pump KR2: Y. Nakajima, L. Pedraza-González, L. Barneschi, K. Inoue, M. Olivucci and H. Kandori, Commun. Biol. **4**, 1185 (2021).

6. Ion Transport Activity Assay for Microbial Rhodopsin Expressed in Escherichia coli Cells: M. Konno, K. Inoue and H. Kandori, bio-protocol **11**, e4115 (2021).

7. Heliorhodopsin Evolution Is Driven by Photosensory Promiscuity in Monoderms: P.-A. Bulzu, V. S. Kavagutti, M.-C. Chiriac, C. D. Vavourakis, K. Inoue, H. Kandori, A.-S. Andrei, R. Ghai and S. J. Hallam, mSphere **6**, e00661-21 (2021).

8. Structural characterization of proton-pumping rhodopsin lacking a cytoplasmic proton donor residue by X-ray crystallography: K. Suzuki, M. D. C. Marín, M. Konno, R. Bagherzadeh, T. Murata and K. Inoue, J. Biol. Chem. **298**, 101722 (2022).

---

* Joint research among groups within ISSP.

9. Diverse heliorhodopsins detected via functional metagenomics in freshwater *Actinobacteria* , *Chloroflexi* and *Archaea*: A. Chazan, A. Rozenberg, K. Mannen, T. Nagata, R. Tahan, S. Yaish, S. Larom, K. Inoue, O. Béjà and A. Pushkarev, Environmental Microbiology **24**, 110-121 (2022).

10. Saccharibacteria harness light energy using type-1 rhodopsins that may rely on retinal sourced from microbial hosts: A. L. Jaffe, M. Konno, Y. Kawasaki, C. Kataoka, O. Béjà, H. Kandori, K. Inoue and J. F. Banfield, ISME J, published on the web (2022).

11. 第3のロドプシン：ヘリオロドプシン：井上 圭一 , 化学と工業 **74**, 307 (2021).

12. Expanding horizons of biosciences by light-control: M. Kataoka and T. Nagata, Biophysics and Physicobiology **18**, 13-15 (2021).

13. Microbial Rhodopsins: The Last Two Decades: A. Rozenberg, K. Inoue, H. Kandori and O. Béjà, Annu. Rev. Microbiol. **75**, published on the web (2021).

14. Rhodopsins at a glance: T. Nagata and K. Inoue, J. Cell Sci. **134**, jcs258989 (2021).

15. Application of Optogenetics for Muscle Cells and Stem Cells: T. Asano, D. B. L. Teh and H. Yawo, in: *Optogenetics*, edited by Hiromu Yawo, Hideki Kandori, Amane Koizumi, Ryoichiro Kageyama, (Springer Nature, 2021), 359-375.

16. Diversity, Mechanism, and Optogenetic Application of Light-Driven Ion Pump Rhodopsins: K. Inoue, in: *Optogenetics*, edited by Hiromu Yawo, Hideki Kandori, Amane Koizumi, Ryoichiro Kageyama, (Springer Nature, 2021), 89-126.

17. ロドプシンが拓くタンパク質科学の地平：井上 圭一 ,「未来探究２０５０　東大 30 人の知性が読み解く世界」, 東京大学未来ビジョン研究センター , (日本経済新聞出版 , 2021), 74-83.

Quantum Materials Group

Oshikawa group

We continued theoretical studies on a wide range of subjects in many-body physics. In particular, we successfully implemented the "Level Spectroscopy" based on tensor-network renormalization group on the 2-dimensional classical XY model. This model is a canonical model to exhibit the Berezinskii-Kosterlitz-Thouless (BKT) transition, which is a prototypical topological phase transition. Although it has been studied for more than half century, the logarithmic correction makes a precise determination of the transition point rather challenging. By utilizing the powerful finite-scaling of conformal field theory and the modern numerical algorithm, we have succeeded in an extremely accurate determination of the BKT transition point, as well as a visualization of the Renormalization-Group flow based on the actual numerical data.

1. Resolving the Berezinskii-Kosterlitz-Thouless transition in the two-dimensional XY model with tensor-network-based level spectroscopy: A. Ueda and M. Oshikawa, Phys. Rev. B **104**, 165132 (2021).

2. †SU(4)-symmetric quantum spin-orbital liquids on various lattices: M. G. Yamada, M. Oshikawa and G. Jackeli, Phys. Rev. B **104**, 224436 (2021).

3. †Two-wire junction of inequivalent Tomonaga-Luttinger liquids: Y.-T. Kang, C.-Y. Lo, M. Oshikawa, Y.-J. Kao and P. Chen, Phys. Rev. B **104**, 235142 (2021).

4. †Non-Fermi Liquids in Conducting Two-Dimensional Networks: J. M. Lee, M. Oshikawa and G. Y. Cho, Phys. Rev. Lett. **126**, 186601 (2021).

5. Twisted Boundary Condition and Lieb-Schultz-Mattis Ingappability for Discrete Symmetries: Y. Yao and M. Oshikawa, Phys. Rev. Lett. **126**, 217201 (2021).

6. †Photon Echo from Lensing of Fractional Excitations in Tomonaga-Luttinger Spin Liquid: Z.-L. Li, M. Oshikawa and Y. Wan, Phys. Rev. X **11**, 031035 (2021).

7. Chiral approximation to twisted bilayer graphene: Exact intravalley inversion symmetry, nodal structure, and implications for higher magic angles: J. Wang, Y. Zheng, A. J. Millis and J. Cano, Phys. Rev. Research **3,**, 023155 (2021).

8. Topological field theories and symmetry protected topological phases with fusion category symmetries: K. Inamura, Journal of High Energy Physics **2021**, 204 (2021).

9. †Parafermionization, bosonization, and critical parafermionic theories: Y. Yao and A. Furusaki, J. High Energ. Phys.

† Joint research with outside partners.

2021, 285 (2021).

10. Fermionization and boundary states in 1+1 dimensions: Y. Fukusumi, Y. Tachikawa and Y. Zheng, SciPost Phys. **11**, 082 (2021).

11. †Remarks on compatibility between conformal symmetry and continuous higher-form symmetries: Y. Lee and Y. Zheng, Physical Review D **104**, 085005 (1-7) (2021).

12. Kramers-Wannier-like Duality Defects in (3+1)D Gauge Theories: J. Kaidi, K. Ohmori and Y. Zheng, Phys. Rev. Lett. **128**, 111601 (2022).

13. On lattice models of gapped phases with fusion category symmetries: K. Inamura, J. High Energ. Phys. **2022**, 36 (2022).

Nakatsuji group

A new era in quantum materials research arises, featuring discoveries of novel topological phases of matter and emergent quasi-particle excitations behaving as elusive elementary particles. Our research activities focus on designing and synthesizing new materials with emergent quantum properties that have never been seen before, then exploring the physics behind such properties with our world-leading measurement facilities. We aim to lead the innovative quest for new quantum materials that bear a far-reaching impact not only on basic science but also on our everyday life in the future. Major research themes: 1. Solid-state analogs of relativistic particles and new quantum phenomena · Weyl fermion and chiral anomaly · Quantum spin ice, magnetic monopole, and emergent photon 2. Room-temperature quantum transport phenomena in topological magnetic materials · Weyl antiferromagnets and their application to spintronic devices · Giant thermal and optical responses driven by the Berry curvature 3. Quantum phase transition in strongly correlated systems · Non-Fermi-liquid behavior and exotic superconductivity in multipolar Kondo materials

1. 6-GHz lattice response in a quantum spin-orbital liquid probed by time-resolved resonant x-ray scattering: K. Takubo, T. Mizokawa, H. Man, K. Yamamoto, Y. Zhang, Y. Hirata, H. Wadati, D. I. Khomskii and S. Nakatsuji, Phys. Rev. B **104**, 205110 (2021).

2. Logarithmic criticality in transverse thermoelectric conductivity of the ferromagnetic topological semimetal CoMnSb: H. Nakamura, S. Minami, T. Tomita, A. A. Nugroho and S. Nakatsuji, Phys. Rev. B **104**, L161114 (2021).

3. *Low Gilbert damping in epitaxial thin films of the nodal-line semimetal $D0_3$-Fe_3Ga: S. Sakamoto, T. Higo, S. Tamaru, H. Kubota, K. Yakushiji, S. Nakatsuji and S. Miwa, Phys. Rev. B **103**, 165122 (1-5) (2021).

4. *Observation of spontaneous x-ray magnetic circular dichroism in a chiral antiferromagnet: S. Sakamoto, T. Higo, M. Shiga, K. Amemiya, S. Nakatsuji and S. Miwa, Phys. Rev. B **104**, 134431 (1-6) (2021).

5. *Domain structure and domain wall dynamics in topological chiral antiferromagnets from the viewpoint of magnetic octupole: Y. Otani and T. Higo, Appl. Phys. Lett. **118**, 040501 (2021).

6. Simultaneous enhancements of thermopower and electrical conductivity in quasi-one-dimensional α -$YbAlB_4$ single crystal: K. Kuga, M. Matsunami, S. Singh, S. Nakatsuji and T. Takeuchi, Appl. Phys. Lett. **119**, 223905 (2021).

7. トポロジカル磁性体が拓く新たな応用展開　量子制御による革新的機能の創製に向けて：中辻　知，応用物理 **90**, 221-229 (2021).

8. * ワイル反強磁性金属 Mn_3Sn 薄膜の室温テラヘルツ異常ホール効果：松田 拓也，肥後 友也，神田 夏輝，松永 隆佑，応用物理 **90**, 752 (2021).

9. *Omnidirectional Control of Large Electrical Output in a Topological Antiferromagnet: T. Higo, Y. Li, K. Kondou, D. Qu, M. Ikhlas, R. Uesugi, D. Nishio-Hamane, C. L. Chien, Y. Otani and S. Nakatsuji, Adv. Funct. Mater. **31**, 2008971 (2021).

10. *Spin-orbit torque switching of the antiferromagnetic state in polycrystalline Mn_3Sn/Cu/heavy metal heterostructures: H. Tsai, T. Higo, K. Kondou, A. Kobayashi, T. Nakano, K. Yakushiji, S. Miwa, Y. Otani and S. Nakatsuji, AIP Advances **11**, 045110 (1-6) (2021).

11. Anomalous transport due to Weyl fermions in the chiral antiferromagnets Mn_3X, X=Sn, Ge: T. Chen, T. Tomita, S. Minami, M. Fu, T. Koretsune, M. Kitatani, I. Muhammad, D. Nishio-Hamane, R. Ishii, F. Ishii, R. Arita and S. Nakatsuji, Nat. Commun. **12**, 572 (2021).

12. Monopolar and dipolar relaxation in spin ice $Ho_2Ti_2O_7$: Y. Wang, T. Reeder, Y. Karaki, J. Kindervater, T. Halloran, N. Maliszewskyi, Y. Qiu, J. A. Rodriguez, S. Gladchenko, S. M. Koohpayeh, S. Nakatsuji and C. Broholm, Science Advances **7**(1-10) (2021).

---

* Joint research among groups within ISSP.

13. Monopolar and dipolar relaxation in spin ice $Ho_2Ti_2O_7$: Y. Wang, T. Reeder, Y. Karaki, J. Kindervater, T. Halloran, N. Maliszewskyj, Y. Qiu, J. A. Rodriguez, S. Gladchenko, S. M. Koohpayeh, S. Nakatsuji and C. Broholm, Sci. Adv. **7**, eabg0908 (2021).

14. *Fabrication of polycrystalline Weyl antiferromagnetic Mn_3Sn thin films on various seed layers: T. Nakano, T. Higo, A. Kobayashi, S. Miwa, S. Nakatsuji and K. Yakushiji, Phys. Rev. Materials **5**, 054402 (1-9) (2021).

15. Spin-orbital liquid in $Ba_3CuSb_2O_9$ stabilized by oxygen holes: K. Takubo, H. Man, S. Nakatsuji, K. Yamamoto, Y. Zhang, Y. Hirata, H. Wadati, A. Yasui, T. Mizokawa and D. I. Khomskii, Phys. Rev. Materials **5**, 075002 (2021).

16. Giant field-like torque by the out-of-plane magnetic spin Hall effect in a topological antiferromagnet: K. Kondou, H. Chen, T. Tomita, M. Ikhlas, T. Higo, A. H. MacDonald, S. Nakatsuji and Y. Otani, Nat Commun **12**, 6491 (2021).

17. Inhomogeneous Kondo-lattice in geometrically frustrated $Pr_2Ir_2O_7$: M. Kavai, J. Friedman, K. Sherman, M. Gong, I. Giannakis, S. Hajinazar, H. Hu, S. E. Grefe, J. Leshen, Q. Yang, S. Nakatsuji, A. N. Kolmogorov, Q. Si, M. Lawler and P. Aynajian, Nat Commun **12**, 1377 (2021).

18. X-ray study of ferroic octupole order producing anomalous Hall effect: M. Kimata, N. Sasabe, K. Kurita, Y. Yamasaki, C. Tabata, Y. Yokoyama, Y. Kotani, M. Ikhlas, T. Tomita, K. Amemiya, H. Nojiri, S. Nakatsuji, T. Koretsune, H. Nakao, T.-H. Arima and T. Nakamura, Nat Commun **12**, 5582 (2021).

19. High-temperature antiferromagnetism in Yb based heavy fermion systems proximate to a Kondo insulator: S. Suzuki, K. Takubo, K. Kuga, W. Higemoto, T. U. Ito, T. Tomita, Y. Shimura, Y. Matsumoto, C. Bareille, H. Wadati, S. Shin and S. Nakatsuji, Phys. Rev. Research **3**, 023140 (2021).

20. *Giant Effective Damping of Octupole Oscillation in an Antiferromagnetic Weyl Semimetal: S. Miwa, S. Iihama, T. Nomoto, T. Tomita, T. Higo, M. Ikhlas, S. Sakamoto, Y. Otani, S. Mizukami, R. Arita and S. Nakatsuji, Small Science **1**, 2000062 (1-8) (2021).

21. *Large Hall Signal due to Electrical Switching of an Antiferromagnetic Weyl Semimetal State: H. Tsai, T. Higo, K. Kondou, S. Sakamoto, A. Kobayashi, T. Matsuo, S. Miwa, Y. Otani and S. Nakatsuji, Small Science **1**, 2000025 (1-9) (2021).

22. Logarithmic Criticality in Transverse Thermoelectric Conductivity of the Ferromagnetic Topological Semimetal CoMnSb: H. Nakamura, S. Minani, T. Tomita, A. A. Nugroho and S. Nakatsuji, Condensed Materials Materials Science arXiv:2105.12098, 1-6 (2021).

23. Phonon spectrum of $Pr_2Zr_2O_7$ and $Pr_2Ir_2O_7$ as evidence of coupling of the lattice with electronic and magnetic degrees of freedom: Y. Xu, H. Man, N. Tang, T. Ohtsuki, S. Baidya, S. Nakatsuji, D. Vanderbilt and N. Drichko, Phys. Rev. B **105**, 075137 (2022).

24. Ferrimagnetic compensation and its thickness dependence in TbFeCo alloy thin films: M. Ishibashi, K. Yakushiji, M. Kawaguchi, A. Tsukamoto, S. Nakatsuji and M. Hayashi, Applied Physics Letters **120**, 022405-1 and 4 (2022).

25. Topological Magnets: Functions Based on Berry Phase and Multipoles: S. Nakatsuji and R. Arita, Annu. Rev. Condens. Matter Phys. **13**, annurev-conmatphys-031620-103859 (2022).

Miwa group

We have studied the following topics this year: (1) Time-resolved spin dynamics and (2) x-ray magnetic circular dichroism on a chiral antiferromagnet Mn_3Sn, (3) microscopic understanding of perpendicular magnetic anisotropy at Fe/MgO. In topic (1), we find giant effective damping of the octupole polarization (ferroic order in the chiral antiferromagnet Mn_3Sn) due to exchange enhanced spin dynamics (Small Sci. **1**, 2000062). This is a work in collaboration with Nakatsuji and Otani groups. In topic (2), we have succeeded in preparing an epitaxial thin film of Mn_3Sn(1-100) and observing x-ray magnetic circular dichroism signals from the octupole polarization in Mn_3Sn. The signal comes from the magnetic dipole Tz term of Mn atoms (Phys. Rev. B **104**, 134431). This is a work in collaboration with Nakatsuji group. In topic (3), we find the perpendicular magnetic anisotropy in Fe/MgO system can be enhanced by reducing in-plane tensile strain in Fe ultrathin film (Phys. Rev. B **104**, L140406).

1. Influence of epitaxial strain on the perpendicular magnetic anisotropy of Fe/MgO systems: M. Shiga, S. Sakamoto, T. Tsujikawa, R. Ando, K. Amemiya and S. Miwa, Phys. Rev. B **104**, L140406 (1-6) (2021).

2. *Low Gilbert damping in epitaxial thin films of the nodal-line semimetal $D0_3$-Fe_3Ga: S. Sakamoto, T. Higo, S. Tamaru, H. Kubota, K. Yakushiji, S. Nakatsuji and S. Miwa, Phys. Rev. B **103**, 165122 (1-5) (2021).

3. *Observation of spontaneous x-ray magnetic circular dichroism in a chiral antiferromagnet: S. Sakamoto, T. Higo, M.

† Joint research with outside partners.

Shiga, K. Amemiya, S. Nakatsuji and S. Miwa, Phys. Rev. B **104**, 134431 (1-6) (2021).

4. Quasi-maser operation using magnetic tunnel junctions: Y. Yamada, M. Goto, T. Yamane, N. Degawa, T. Suzuki, A. Shimura, S. Aoki, T. Mizuno, J. Urabe, S. Hara, S. Miwa and Y. Suzuki, Appl. Phys. Lett. **118**, 192402 (1-5) (2021).

5. Physically Unclonable Functions With Voltage-Controlled Magnetic Tunnel Junctions: Y. Tanaka, M. Goto, A. K. Shukla, K. Yoshikawa, H. Nomura, S. Miwa, S. Tomishima and Y. Suzuki, IEEE Trans. Magn. **57**, 3400806 (1-6) (2021).

6. *Spin-orbit torque switching of the antiferromagnetic state in polycrystalline Mn_3Sn/Cu/heavy metal heterostructures: H. Tsai, T. Higo, K. Kondou, A. Kobayashi, T. Nakano, K. Yakushiji, S. Miwa, Y. Otani and S. Nakatsuji, AIP Advances **11**, 045110 (1-6) (2021).

7. *Fabrication of polycrystalline Weyl antiferromagnetic Mn_3Sn thin films on various seed layers: T. Nakano, T. Higo, A. Kobayashi, S. Miwa, S. Nakatsuji and K. Yakushiji, Phys. Rev. Materials **5**, 054402 (1-9) (2021).

8. Investigation of the thermal tolerance of silicon-based lateral spin valves: N. Yamashita, S. Lee, R. Ohshima, E. Shigematsu, H. Koike, Y. Suzuki, S. Miwa, M. Goto, Y. Ando and M. Shiraishi, Sci Rep **11**, 10583 (2021).

9. *Giant Effective Damping of Octupole Oscillation in an Antiferromagnetic Weyl Semimetal: S. Miwa, S. Iihama, T. Nomoto, T. Tomita, T. Higo, M. Ikhlas, S. Sakamoto, Y. Otani, S. Mizukami, R. Arita and S. Nakatsuji, Small Science **1**, 2000062 (1-8) (2021).

10. *Large Hall Signal due to Electrical Switching of an Antiferromagnetic Weyl Semimetal State: H. Tsai, T. Higo, K. Kondou, S. Sakamoto, A. Kobayashi, T. Matsuo, S. Miwa, Y. Otani and S. Nakatsuji, Small Science **1**, 2000025 (1-9) (2021).

11. Synthetic Rashba spin–orbit system using a silicon metal-oxide semiconductor: S. Lee, H. Koike, M. Goto, S. Miwa, Y. Suzuki, N. Yamashita, R. Ohshima, E. Shigematsu, Y. Ando and M. Shiraishi, Nat. Mater. **20**, 1228-1232 (2021).

12. Reservoir computing based on spintronics technology (p339-p360), Reservoir computing [Editor: K. Nakajima and I. Fischer]: T. Taniguchi, S. Tsunegi, S. Miwa, K. Fujii, H. Kubota and K. Nakajima, (Springer, Singapore, 2021).

13. Electron Correlation Enhances Orbital Polarization at a Ferromagnetic Metal/Insulator Interface: Depth-Resolved X-ray Magnetic Circular Dichroism and First-Principles Study: S. Sakamoto, M. Tsujikawa, M. Shirai, K. Amemiya and S. Miwa, ACS Appl. Electron. Mater. **4**, 1794-1799 (2022).

Division of Data-Integrated Materials Science

Fukushima group

This year, we have developed a fundamental simulation code for investigating the material properties of permanent magnets and spintronic materials. The automatic exhaustive calculations, which are based on the all-electron full-potential (Korringa-Kohn-Rostoker) KKR Green's function method (FPKKR), have been performed. Since the potential is anisotropic rather than spherically symmetric, it is possible to calculate not only the magnetization and Curie temperature but also the magneto-crystalline anisotropy energy constant with high accuracy. The KKR Green's function method can be conveniently combined with the coherent potential approximation (CPA). It is free from using supercells, resulting in reduced computational costs drastically. Therefore, our code can perform efficient calculations for a huge number of compositions of disordered alloys, compared to the other simulation code. We have applied this code to several magnetic materials, such as YCo_5 alloys, $SmCo_5$ alloys, and $Sm_2Fe_{17}N_3$ alloys. We have also systematically investigated the electronic structure, intrinsic defect formation, and transport properties of Cu_2S by first-principles calculations, using a theoretical model called an acanthite-like structure. The transport properties of Cu_2S system have been successfully reproduced using an electron-phonon scattering method, highlighting the important role of relaxation time prediction in conductivity estimation instead of regarding it as a constant.

1. First-principles calculation of electronic density of states and Seebeck coefficient in transition-metal-doped Si–Ge alloys: R. Yamada, A. Masago, T. Fukushima, H. Shinya, T. Q. Nguyen and K. Sato, Solid State Commun. **323**, 110227(1-8) (2021).

2. Effect of atomic configuration on magnetic properties and electronicstate of CoVMnAl quaternary heusler alloy: R. Y. Umetsu, K. Saito, K. Ono, T. Fukushima, F. Kuroda, T. Oguchi and T. Ishigaki, J. Alloys Compd. **855**, 157389(1-9) (2021).

3. Ferromagnetism and giant magnetoresistance in zinc-blende FeAs monolayers embedded in semiconductor structures:

* Joint research among groups within ISSP.

L. D. Anh, T. Hayakawa, Y. Nakagawa, H. Shinya, T. Fukushima, M. Kobayashi, H. Katayama-Yoshida, Y. Iwasa and M. Tanaka, Nat. Commun. **12**, 4201(1-10) (2021).

4. Theoretical prediction of large anisotropic magnetocaloric effect in MnP: H. B. Tran, T. Fukushima, H. Momida, K. Sato, Y. Makino and T. Oguchi, Comput. Mater. Sci. **188**, 110227(1-8) (2021).

5. Intrinsic defect formation and the effect of transition metal doping on transport properties in a ductile thermoelectric material α-Ag_2S: a first-principles study: H. N. Nam, R. Yamada, H. Okumura, T. Q. Nguyen, K. Suzuki, H. Shinya, A. Masago, T. Fukushima and K. Sato, Phys. Chem. Chem. Phys **23**, 9773-9784 (2021).

6. Low-temperature acanthite-like phase of Cu_2S: electronic and transport properties: H. N. Nam, K. Suzuki, T. Q. Nguyen, A. Masago, H. Shinya, T. Fukushima and K. Sato, Phys. Rev. B **105**, 075205(1-11) (2022).

7. A first-principles study on the electrical conductivity of $Ag_2S_{1-x}Se_x$ (x=0, 0.25, 0.5): Electron-phonon coupling: 71. H. N. Nam, K. Suzuki, A. Masago, T. Q. Nguyen, H. Shinya, T. Fukushima and K. Sato, Appl. Phys. Lett. **120**, 143903(1-6) (2022).

8. *Automatic exhaustive calculations of large material space by Korringa-Kohn-Rostoker coherent potential approximation method — Applied to equiatomic quaternary high entropy alloys: T. Fukushima, H. Akai, T. Chikyow and H. Kino, Pays. Rev. Mater. **6**, 023802(1-19) (2022).

9. Mn 基ホイスラー合金の磁気特性と電子状態：梅津 理恵 , 斉藤 耕太郎 , 小野 寛太 , 佐藤 和則 , 福島 鉄也 , 黒田 文彬 , 小口 多美夫 , まてりあ **60**, 205-211 (2021).

10. 半導体スピントロニクス材料のデザイン：佐藤 和則 , 真砂 啓 , 福島 鉄也 , 新屋ひ かり ,「スピントロニクスのための計算機ナノマテリアルデザイン」, 吉田博 , (内田老鶴圃 , 2022), 167-188.

Materials Design and Characterization Laboratory

Hiroi group

The high-pressure synthesis, crystal structure, and magnetic properties of four novel transition-metal oxyhydrides─$Ba_2NaVO_3H_3$, $Ba_2NaVO_{2.4}H_{3.6}$, $Ba_2NaCrO_{2.2}H_{3.8}$, and $Ba_2NaTiO_3H_3$─crystallizing in the double-perovskite structure were reported. We studied the pyrochlore oxide $Hg_2Os_2O_7$ through thermodynamic measurements, muon spin rotation (μSR) spectroscopy and neutron diffraction experiments. A magnetic transition, probably to an AIAO-type order, was observed at 88 K, while the resistivity showed a decrease at the transition and remained metallic down to 2 K. Thus, the ground state of $Hg_2Os_2O_7$ is most likely an AIAO semimetal, which is analogous to the intermediate-temperature state of $Cd_2Os_2O_7$. $Hg_2Os_2O_7$ exists on the verge of the metal–insulator boundary on the metal side and provides an excellent platform for studying the electronic instability of 5delectrons with moderate electron correlations and strong spin–orbit interactions. Substitution effects of Os for Ru in α-$RuCl_3$ are investigated in a wide composition range of $0 \le x \le 0.67$ in $Ru_{1-x}Os_xCl_3$ by X-ray and electron diffraction, magnetic susceptibility, heat capacity, and Raman spectroscopy measurements. Apart from the Kitaev physics with antiferromagnetic interactions increasing with x, a rich phase diagram is obtained, which includes an antiferromagnetic long-range order below 12 K for $x \le 0.15$, a dome-shaped spin-singlet dimer phase below 130 K for $0.15 \le x \le 0.40$, and a magnetic short-range order for $x > 0.40$. NaAlSi is an sp electron superconductor crystallizing in a layered structure of the anti-PbFCl type with a relatively high transition temperature Tc of ~7 K. We successfully prepared single crystals of NaAlSi by a Na–Ga flux method and characterized their superconducting and normal-state properties through electrical resistivity, magnetization, and heat capacity measurements. A sharp superconducting transition with a Tc of 6.8 K is clearly observed, and heat capacity data suggest an anisotropic superconducting gap. Surprisingly, despite the sp electron system, the normal state is governed by the electron correlations, which is indicated by a T^2 resistivity and a Wilson ratio of 2.0. The origin of the electron correlation may be related to the orthogonal saddle-shaped Fermi surfaces derived from the Si px and py states, which intersect with the light Al s bands to form the nodal lines near the Fermi level.

1. Extremely Large Magnetoresistance in the Hourglass Dirac Loop Chain Metal β-ReO2: D. Hirai, T. Anbai, S. Uji, T. Oguchi and Z. Hiroi, J. Phys. Soc. Jpn. **90**, 094708 (2021).

2. Superconductivity in the Topological Nodal-line Semimetal NaAlSi: T. Yamada, D. Hirai, H. Yamane and Z. Hiroi, J. Phys. Soc. Jpn. **90**, 034710 (2021).

3. *Universal Dynamics of Magnetic Monopoles in Two-Dimensional Kagomé Ice: H. Takatsu, K. Goto, T. J. Sato, J. W. Lynn, K. Matsubayashi, Y. Uwatoko, R. Higashinaka, K. Matsuhira, Z. Hiroi and H. Kadowaki, J. Phys. Soc. Jpn. **90**, 123705(1-4) (2021).

† Joint research with outside partners.

4. *Phase transition in the 5d(1) double perovskite Ba_2CaReO_6 induced by high magnetic field: H. Ishikawa, D. Hirai, A. Ikeda, M. Gen, T. Yajima, A. Matsuo, Y. H. Matsuda, Z. Hiroi and K. Kindo, Phys. Rev. B **104**, 174422(7) (2021).

5. *Pressure-induced phase transition in the J_1-J_2 square lattice antiferromagnet $RbMoOPO_4Cl$: H. Takeda, T. Yamauchi, M. Takigawa, H. Ishikawa and Z. Hiroi, Phys. Rev. B **103**, 104406 (2021).

6. †*Quantum antiferromagnet bluebellite comprising a maple-leaf lattice made of spin-1/2 Cu^{2+} ions: Y. Haraguchi, A. Matsuo, K. Kindo and Z. Hiroi, Phys. Rev. B **104**, 174439(6) (2021).

7. *Dimensional reduction by geometrical frustration in a cubic antiferromagnet composed of tetrahedral clusters: R. Okuma, M. Kofu, S. Asai, M. Avdeev, A. Koda, H. Okabe, M. Hiraishi, S. Takeshita, K. M. Kojima, R. Kadono, T. Masuda, K. Nakajima and Z. Hiroi, Nat. Commun. **12**, 4382(1-7) (2021).

8. Modern Alchemy: Making "Plastics" from Paper: Y. Iwamiya, M. Kawai, D. Nishio-Hamane, M. Shibayama and Z. Hiroi, Ind. Eng. Chem. Res. **60**, 355 (2021).

9. Pyrochlore oxide $Hg_2Os_2O_7$ on verge of metal–insulator boundary: K. Kataoka, D. Hirai, A. Koda, R. Kadono, T. Honda and Z. Hiroi, J. Phys.: Condens. Matter **34**, 135602 (2022).

10. Dimer Crystallization Induced by Elemental Substitution in the Honeycomb Lattice of $Ru_{1-x}Os_xCl_3$: K. Kataoka, D. Wulferding, T. Yajima, D. Nishio-Hamane, D. Hirai, S. Lee, K.-Y. Choi and Z. Hiroi, J. Phys. Soc. Jpn. **91**, 014801 (2022).

11. Unusual Resistive Transitions in the Nodal-Line Semimetallic Superconductor NaAlSi: D. Hirai, T. Ikenobe, T. Yamada, H. Yamane and Z. Hiroi, J. Phys. Soc. Jpn. **91**, 024702 (2022).

12. Electronic states of metallic electric toroidal quadrupole order in $Cd_2Re_2O_7$ determined by combining quantum oscillations and electronic structure calculations: H. T. Hirose, T. Terashima, D. Hirai, Y. Matsubayashi, N. Kikugawa, D. Graf, K. Sugii, S. Sugiura, Z. Hiroi and S. Uji, Phys. Rev. B **105**, 035116 (2022).

13. High-Pressure Synthesis of Transition-Metal Oxyhydrides with Double-Perovskite Structures: T. Yajima, K. Takahashi, H. Nakajima, T. Honda, K. Ikeda, T. Otomo and Z. Hiroi, Inorg. Chem. **61**, 2010 (2022).

14. Surface Functionalization of Non-Woven Fabrics Using a Novel Silica-Resin Coating Technology: Antiviral Treatment of Non-Woven Fabric Filters in Surgical Masks: C. Tsutsumi-Arai, Y. Iwamiya, R. Hoshino, C. Terada-Ito, S. Sejima, K. Akutsu-Suyama, M. Shibayama, Z. Hiroi, R. Tokuyama-Toda, R. Iwamiya, K. Ijichi, T. Chiba and K. Satomura, IJERPH **19**, 3639 (2022).

Kawashima group

We developed efficient methods, algorithms, parallelized programs, and sometimes new concepts, based on novel numerical techniques including the tensor network (TN) method and applied them to relevant physical problems. To list subjects of our research in 2021, (1) Development of new TN methods [Morita, PRB103][Tu, PRB103], (2) TN study of surface critical phenomena [Fukusumi, PRB104][Iino, JSP182], (3) Study of TN ground states such as Kitaev spin liquid [Lee, PRB104] [Katsura, PRR3], (4) Study of spin liquid in frustrated spin systems [Ogino, PRB103 & PRB104][Kohshiro, PRB104], (5) TN implementation of rael-space renormalization group [Lyu, PRR3], (6) Development of open-source applications [Motoyama, CPC264][Hoshi, CPC258], (7) Application of data-scientific techniques to materials science [Harashima, PRM5]

1. Effective Ruderman–Kittel–Kasuya–Yosida-like Interaction in Diluted Double-exchange Model: Self-learning Monte Carlo Approach: H. Kohshiro and Y. Nagai, J. Phys. Soc. Jpn. **90**, 034711 (2021).

2. Anisotropy as a diagnostic test for distinct tensor-network wave functions of integer- and half-integer-spin Kitaev quantum spin liquids: H.-Y. Lee, T. Suzuki, Y. B. Kim and N. Kawashima, Phys. Rev. B **104**, 024417(1-13) (2021).

3. Continuous phase transition between Neel and valence bond solid phases in a J-Q-like spin ladder system: T. Ogino, R. Kaneko, S. Morita, S. Furukawa and N. Kawashima, Phys. Rev. B **103**, 085117 (2021).

4. Generating function for tensor network diagrammatic summation: W.-L. Tu, H.-K. Wu, N. Schuch, N. Kawashima and J.-Y. Chen, Phys. Rev. B **103**, 205155 (2021).

5. Global optimization of tensor renormalization group using the corner transfer matrix: S. Morita and N. Kawashima, Phys. Rev. B **103**, 045131(1-6) (2021).

6. Multiple magnetization plateaus induced by farther neighbor interactions in an S=1 two-leg Heisenberg spin ladder: H. Kohshiro, R. Kaneko, S. Morita, H. Katsura and N. Kawashima, Phys. Rev. B **104**, 214409 (2021).

---

* Joint research among groups within ISSP.

7. Open spin chain realization of a topological defect in a one-dimensional Ising model: Boundary and bulk symmetry: Y. Fukusumi and S. Iino, Phys. Rev. B **104**, 125418 (2021).

8. Symmetry-protected topological phases and competing orders in a spin-1/2 XXZ ladder with a four-spin interaction: T. Ogino, S. Furukawa, R. Kaneko, S. Morita and N. Kawashima, Phys. Rev. B **104**, 075135 (2021).

9. †*DSQSS: Discrete Space Quantum Systems Solver: Y. Motoyama, K. Yoshimi, A. Masaki-Kato, T. Kato and N. Kawashima, Comput. Phys. Commun. **264**, 107944(1-9) (2021).

10. †*Kω— Open-source library for the shifted Krylov subspace method of the form (zI-H)x=b: T. Hoshi, M. Kawamura, K. Yoshimi, Y. Motoyama, T. Misawa, Y. Yamaji, S. Todo, N. Kawashima and T. Sogabe, Computer Physics Communications **258**, 107536 (2021).

11. "Data Assimilation Method for Experimental and First-Principles Data: Finite-Temperature Magnetization of $(Nd,Pr,La,Ce)_2(Fe,Co,Ni)_{14}B$": Y. Harashima, K. Tamai, S. Doi, M. Matsumoto, H. Akai, N. Kawashima, M. Ito, N. Sakuma, A. Kato, T. Shoji and T. Miyake, Phys. Rev. Materials **5**, 013806(1-10) (2021).

12. Mott-insulator-like Bose-Einstein condensation in a tight-binding system of interacting bosons with a flat band: H. Katsura, N. Kawashima, S. Morita, A. Tanaka and H. Tasaki, Phys. Rev. Research **3**, 033190 (2021).

13. Scaling dimensions from linearized tensor renormalization group transformations: X. Lyu, R. G. Xu and N. Kawashima, Phys. Rev. Research **3**, 023048 (2021).

14. Boundary CFT and Tensor Network Approach to Surface Critical Phenomena of the Tricritical 3-State Potts model: S. Iino, J Stat Phys **182**, 56 (2021).

15. Energy Scale Deformation on Regular Polyhedra: T. Eguchi, S. Oga, H. Katsura, A. Gendiar and T. Nishino, J. Phys. Soc. Jpn. **91**, 034001 (2022).

16. Universal and non-universal correction terms of Bose gases in dilute region: a quantum Monte Carlo study: A. Masaki-Kato, Y. Motoyama and N. Kawashima, J. Phys. Soc. Jpn. **90**, 034711(1-8) (2022).

17. *Unconventional dual 1D–2D quantum spin liquid revealed by ab initio studies on organic solids family: K. Ido, K. Yoshimi, T. Misawa and M. Imada, npj Quantum Mater. **7**, 48 (2022).

18. Cartesian Operator Factorization Method for Hydrogen: X. Lyu, C. Daniel and J. K. Freericks, Atoms **10**, 14 (2022).

Uwatoko group

The transport and optical properties of Ta_2NiSe_5 have been measured under high pressures up to ~ 9 GPa and present the complete phase diagram of the high-pressure semi-metallic phase above P_s ~ 3 GPa. Also, we discovered bulk superconductivity with transition temperature T_{sc} up to 1.2 K only around P_c, which further justifies the strong electron–lattice coupling. We study the interplay between CDW and SC in CsV_3Sb_5 via measurements of resistivity, dc and ac magnetic susceptibility under various pressures up to 6.6 GPa. The CDW transition decreases with pressure and experiences a subtle modification at $P_{c1} \approx 0.6$–0.9 GPa before it vanishes entirely at $P_{c2} \approx 2$ GPa. We study the electronic and magnetic properties of $CrGeTe_3$ single crystals by varying pressure up to 11.0 GPa using dc magnetic susceptibility and resistivity measurement. We demonstrate that pressure can be used as a suitable parameter to control both magnetic and electrical properties of $CrGeTe_3$ by tuning the charge transfer energy gap between the Te-p valence band and the Cr-e_g conduction band. Moreover, the lack of concurrent structural transition and spin crossover across the insulator-metal transition (IMT) makes $CrGeTe_3$ a unique vandal van der Waals material and provides a novel example of bandwidth-controlled IMT. We have systematically investigated superconductivity in Bi single crystal up to 6.2 GPa. These unusual regular state transport and superconducting properties suggest a possible unconventional superconductivity scenario for the Bi-III phase. We have investigated the external pressure effect on the resistance and the ARPES on $BiSbTe_3$. It is observed that with an increase of pressure, resistance decreases and at a value of 8 GPa a sharp drop in resistance is observed which indicates the occurrence of superconductivity. With further pressure increase, the superconducting transition temperature (T_c) increases and at 14 GPa it shows the maximum T_c (~ 3.3 K). This may indicate that the superconducting transition might be due to the change in the bulk band structure in $BiSbTe_3$. The theoretical study suggests that surface states remain topologically protected and bulk band structure changes under applied pressure.

1. Hybridization-Gap Formation and Superconductivity in the Pressure-Induced Semimetallic Phase of the Excitonic Insulator Ta_2NiSe_5: K. Matsubayashi, H. Okamura, T. Mizokawa, N. Katayama, A. Nakano, H. Sawa, T. Kaneko, T. Toriyama, T. Konishi, Y. Ohta, H. Arima, R. Yamanaka, A. Hisada, T. Okada, Y. Ikemoto, T. Moriwaki, K. Munakata, A. Nakao, M. Nohara, Y. Lu, H. Takagi and Y. Uwatoko, J. Phys. Soc. Jpn. **90**, 074706(1-6) (2021).

2. *Universal Dynamics of Magnetic Monopoles in Two-Dimensional Kagomé Ice: H. Takatsu, K. Goto, T. J. Sato, J. W.

† Joint research with outside partners.

Lynn, K. Matsubayashi, Y. Uwatoko, R. Higashinaka, K. Matsuhira, Z. Hiroi and H. Kadowaki, J. Phys. Soc. Jpn. **90**, 123705(1-4) (2021).

3. Crystallographic and superconducting properties of filled skutterudite $SrOs_4P_{12}$: Y. Kawamura, S. Deminami, K. Takeda, T. Kuzuya, L. Salamakha, H. Michor, E. Bauer, J. Gouchi, Y. Uwatoko, T. Kawae and C. Sekine, Phys. Rev. B **103**, 085139(1-9) (2021).

4. Effects of disorder and hydrostatic pressure on charge density wave and superconductivity in 2*H*-TaS_2: S. Xu, J. Gao, Z. Liu, K. Chen, P. Yang, S. Tian, C. Gong, J. Sun, M. Xue, J. Gouchi, X. Luo, Y. Sun, Y. Uwatoko, H. Lei, B. Wang and J. Cheng, Phys. Rev. B **103**, 224509(1-8) (2021).

5. High-pressure insulating phase of Mo_4O_{11} with collapsed volume: Z. Y. Liu, P. F. Shan, K. Y. Chen, M. Marshall, S. Zhang, T. Yong, H. S. Deng, X. Yin, Y. Ding, H. M. Weng, Y. Uwatoko, P. Dera, W. Xie, Y. Sui and J. -G. Cheng, Phys. Rev. B **104**, 024105(1-10) (2021).

6. †Pressure-induced multicriticality and electronic instability in the quasi-kagome ferromagnet URhSn: A. Maurya, D. Bhoi, F. Honda, Y. Shimizu, A. Nakamura, Y. J. Sato, D. Li, Y. Homma, M. Sathiskumar, J. Gouchi, Y. Uwatoko and D. Aoki, Phys. Rev. B **104**, 195119(1-5) (2021).

7. Superconducting phase diagram and the evolution of electronic structure across charge density wave in underdoped 1T-Cu_8TiSe_2 under hydrostatic pressure: S. Xu, P. Yang, K. Chen, Z. Liu, W. Cui, Q. Hu, J. Sun, R. Ang, Y. Uwatoko, B. Wang and J. Cheng, Phys. Rev. B **104**, 134503(1-9) (2021).

8. Double Superconducting Dome and Triple Enhancement of *Tc* in the Kagome Superconductor CsV_3Sb_5 under High Pressure: K. Chen, N. Wang, Q. Yin, Y. Gu, K. Jiang, Z. Tu, C. Gong, Y. Uwatoko, J. Sun, H. Lei, J. Hu and J. -G. Cheng, Phys. Rev. Lett. **126**, 247001(1-8) (2021).

9. Nearly Room-Temperature Ferromagnetism in a Pressure-Induced Correlated Metallic State of the van der Waals Insulator $CrGeTe_3$: D. Bhoi, J. Gouchi, N. Hiraoka, Y. Zhang, N. Ogita, T. Hasegawa, K. Kitagawa, H. Takagi, K. H. Kim and Y. Uwatoko, Phys. Rev. Lett. **127**, 217203(1-7) (2021).

10. Abnormal transport properties of Bi-III superconducting phase in pressurized bismuth single crystal: Y. Zhang, J. Gouchi, K. Ishigaki, S. Nagasaki, Z. Shi and Y. Uwatoko, Supercond. Sci. Technol. **34**, 075009(1-7) (2021).

11. Discovery of Superconductivity in the Quasi-One-Dimensional $SrBi_2Se_4$ Single Crystals: Y. Zhang, X. Xing, Y. Meng, X. Yi, J. Gouchi, D. Bhoi, J. Feng, Y. Fan, W. Zhou, N. Zhou, Y. Uwatoko and Z. Shi, Chem. Mater. **33**, 6752-6760 (2021).

12. Observation of antiferromagnetic ordering from muon spin resonance study and the Kondo effect in a Dy-doped Bi_2Se_3 topological insulator: V. K. Gangwar, S. Kumar, M. Singh, P. Singh, L. Ghosh, D. Pal, P. Shahi, Y. Uwatoko, E. F. Schwier, K. Shimada, D. K. Sharma, S. Kumar and S. Chatterjee, J. Phys. D: Appl. Phys. **54**, 455302(1-10) (2021).

13. *Strongly correlated superconductivity in a copper-based metal-organic framework with a perfect kagome lattice: T. Takenaka, K. Ishihara, M. Roppongi, Y. Miao, Y. Mizukami, T. Makita, J. Tsurumi, S. Watanabe, J. Takeya, M. Yamashita, K. Torizuka, Y. Uwatoko, T. Sasaki, X. Huang, W. Xu, D. Zhu, N. Su, J. -G. Cheng, T. Shibauchi and K. Hashimoto, Sci. Adv. **7**, eabf3996(1-8) (2021).

14. Pressure Dependence of Superconducting Properties, Pinning Mechanism, and Crystal Structure of the $Fe_{0.99}Mn_{0.01}Se_{0.5}Te_{0.5}$ Superconductor: K. Murugesan, G. Lingannan, K. Ishigaki, Y. Uwatoko, C. Sekine, Y. Kawamura, H. JunIchi, B. Joseph, P. Vajeeston, P. K. Maheswari, V. P. S. Awana and A. Sonachalam, ACS Omega **6**, 30419-30431 (2021).

15. †Author Correction: Experimental evidence for the existence of a second partially-ordered phase of ice VI: R. Yamane, K. Komatsu, J. Gouchi, Y. Uwatoko, S. Machida, T. Hattori, H. Ito and H. Kagi, Nat Commun **12**, 1800 (2021).

16. Continuous control of classical-quantum crossover by external high pressure in the coupled chain compound $CsCuCl_3$: D. Yamamoto, T. Sakurai, R. Okuto, S. Okubo, H. Ohta, H. Tanaka and Y. Uwatoko, Nat Commun **12**, 4263(1-9) (2021).

17. †Experimental evidence for the existence of a second partially-ordered phase of ice VI: R. Yamane, K. Komatsu, J. Gouchi, Y. Uwatoko, S. Machida, T. Hattori, H. Ito and H. Kagi, Nat Commun **12**, 1129(1-6) (2021).

18. †High-pressure phase diagrams of $FeSe_{1-x}Te_x$: correlation between suppressed nematicity and enhanced superconductivity: K. Mukasa, K. Matsuura, M. Qiu, M. Saito, Y. Sugimura, K. Ishida, M. Otani, Y. Onishi, Y. Mizukami, K. Hashimoto, J. Gouchi, R. Kumai, Y. Uwatoko and T. Shibauchi, Nat Commun **12**, 381(1-7) (2021).

19. Defect induced ferromagnetic ordering and room temperature negative magnetoresistance in MoTeP: D. Pal, S. Kumar,

---

* Joint research among groups within ISSP.

P. Shahi, S. Dan, A. Verma, V. K. Gangwar, M. Singh, S. Chakravarty, Y. Uwatoko, S. Saha, S. Patil and S. Chatterjee, Sci Rep **11**, 9104(1-9) (2021).

20. †Pressure-induced reconstitution of Fermi surfaces and spin fluctuations in S-substituted FeSe: T. Kuwayama, K. Matsuura, J. Gouchi, Y. Yamakawa, Y. Mizukami, S. Kasahara, Y. Matsuda, T. Shibauchi, H. Kontani, Y. Uwatoko and N. Fujiwara, Sci Rep **11**, 17265(1-7) (2021).

21. Quasi-one-dimensional superconductivity in the pressurized charge-density-wave conductor $HfTe_3$: Z. Y. Liu, J. Li, J. F. Zhang, J. Li, P. T. Yang, S. Zhang, G. F. Chen, Y. Uwatoko, H. X. Yang, Y. Sui, K. Liu and J. -G. Cheng, npj Quantum Mater. **6**, 90(1-12) (2021).

22. Competition between charge-density-wave and superconductivity in the kagome metal Rb_3Sb_5: N. N. Wang, K. Y. Chen, Q. W. Yin, Y. N. N. Ma, B. Y. Pan, X. Yang, X. Y. Ji, S. L. Wu, P. F. Shan, S. X. Xu, Z. J. Tu, C. S. Gong, G. T. Liu, G. Li, Y. Uwatoko, X. L. Dong, H. C. Lei, J. P. Sun and J. -G. Cheng, Phys. Rev. Research **3**, 043018(1-11) (2021).

23. Correlation of magnetocaloric effect through magnetic and electrical resistivity on Si doped Ni–Mn–In Heusler melt spun ribbon: P. Sivaprakash, S. Arumugam, S. Esakki Muthu, D. M. Raj Kumar, C. Saravanan, N. V. Rama Rao, Y. Uwatoko and R. Thiyagarajan, Intermetallics **137**, 107285(1-8) (2021).

24. Pressure induced superconducting state in ideal topological insulator $BiSbTe_3$: V. K. Gangwar, S. Kumar, M. Singh, L. Ghosh, Y. Zhang, P. Shahi, M. Muntwiler, S. Patil, K. Shimada, Y. Uwatoko, J. Sau, M. Kumar and S. Chatterjee, Phys. Scr. **96**, 055802(1-8) (2021).

25. Internal and External Pressure Effects on Superconductivity in $FeTe_xSe_{1-x}$(x = 0.46, 0.54) Single Crystals: G. Lingannan, K. Ganesan, S. Mariappan, R. Sankar, Y. Uwatoko and S. Arumugam, J Supercond Nov Magn **34**, 725-731 (2021).

26. Abrupt Change in Electronic States under Pressure in New Compound $EuPt_3Al_5$: T. Koizumi, F. Honda, Y. J. Sato, D. Li, D. Aoki, Y. Haga, J. Gouchi, S. Nagasaki, Y. Uwatoko, Y. Kaneko and Y. Ônuki, J. Phys. Soc. Jpn. **91**, 043704(1-5) (2022).

27. †Magnetization of Quaternary Heusler Alloy CoFeCrAl: S. Tsujikawa, I. Shigeta, J. Gouchi, T. Kanomata, R. Y. Umetsu, Y. Uwatoko and M. Hiroi, IEEE Trans. Magn. **58**, 1 (1-5) (2022).

28. †Sub-micrometer particle size effects on metastable phases for a photoswitchable Co–Fe Prussian blue analog: M. Itoi, I. Maurin, K. Boukheddaden, M. J. Andrus, D. R. Talham, E. Elkaim and Y. Uwatoko, Journal of Applied Physics **131**, 085110(1-11) (2022).

29. Pressure-driven superconducting dome in the vicinity of CDW in the pyrite-type superconductor CuS_2: L. F. Shi, Z. Y. Liu, J. Li, X. X. Zhang, N. N. Wang, Q. Cui, K. Y. Chen, Q. Y. Liu, P. T. Yang, J. P. Sun, B. S. Wang, Y. Uwatoko, Y. Sui, H. X. Yang and J. -G. Cheng, Phys. Rev. Materials **6**, 014802(1-8) (2022).

30. Temperature-Pressure Phase Diagram and Possible Pressure-Driven New Electronic Phase in the Polar Metal $LiOsO_3$: J. -G. Cheng, J. -S. Zhou and Y. Uwatoko, ECS J. Solid State Sci. Technol. **11**, 023008(1-4) (2022).

Ozaki group

To discover novel materials having unknown structures, we performed high-throughput calculations for structural exploration based on computational methods such as density functional theory (DFT) in two directions. One is to find densest binary and ternary sphere packing structures (DBSPs, DTSPs). The other is to find two dimensional compounds consisting of AB_2 composition. As the first issue, we addressed the DBSPs and DTSPs under periodic boundary conditions and present phase diagrams, including newly found 12 and 59 putative densest structures, respectively. To efficiently explore the DBSPs and DTSPs, we developed an unbiased random search approach based on both the piling-up method to generate initial structures in an unbiased way and the iterative balance method to optimize the volume of a unit cell while keeping the overlap of hard spheres minimized. It turned out that many of DBSPs and DTSPs correspond to real crystals, suggesting that the diverse structures of DBSPs and DTSPs can be effectively used as structural prototypes for searching ternary and quaternary crystal structures. As the second issue, we constructed a structure map for AB_2 type monolayers of 3844 compounds which are all the combinations of 62 elements selected from the periodic table. The structure map and its web version (http://www.openmx-square.org/2d-ab2/), which are obtained by symmetry-unconstrained geometry optimizations starting from ferromagnetic 1T, 1H and planar structures as the initial states, provide comprehensive structural trends of the 3844 compounds in two dimensional (2D) structures and correctly predict the structures of most of the existing 2D compounds such as transition metal dichalcogenides and MXenes having 1T or 1H type structures. Our structure map and database will promote efforts towards the synthesis of undiscovered 2D materials experimentally and investigating the properties of new structures theoretically.

† Joint research with outside partners.

1. Methods for constructing parameter-dependent flat-band lattices: T. Ogata, M. Kawamura and T. Ozaki, Phys. Rev. B **103**, 205119 (2021).

2. Scaling law for Rashba-type spin splitting in quantum-well films: R. Noguchi, K. Kuroda, M. Kawamura, K. Yaji, A. Harasawa, T. Iimori, S. Shin, F. Komori and T. Ozaki, Phys. Rev. B **104**, L180409 (2021).

3. The hidden competing phase revealed by first-principles calculations of phonon instability in the nearly optimally doped cuprate La1.875Sr0.125CuO4: C.-C. Lee, J.-Y. Chiu, Y. Yamada-Takamura and T. Ozaki, Phys. Rev. B **104**, 064114 (2021).

4. Densest ternary sphere packings: R. Koshoji and T. Ozaki, Phys. Rev. E **104**, 024101 (2021).

5. Diverse densest binary sphere packings and phase diagram: R. Koshoji, M. Kawamura, M. Fukuda and T. Ozaki, Phys. Rev. E **103**, 023307 (2021).

6. †*Kω— Open-source library for the shifted Krylov subspace method of the form (zI-H)x=b: T. Hoshi, M. Kawamura, K. Yoshimi, Y. Motoyama, T. Misawa, Y. Yamaji, S. Todo, N. Kawashima and T. Sogabe, Computer Physics Communications **258**, 107536 (2021).

7. †*RESPACK: An ab initio tool for derivation of effective low-energy model of material: K. Nakamura, Y. Yoshimoto, Y. Nomura, T. Tadano, M. Kawamura, T. Kosugi, K. Yoshimi, T. Misawa and Y. Motoyama, Computer Physics Communications **261**, 107781 (2021).

8. Structure of one-dimensional monolayer Si nanoribbons on Ag(111): L. Feng, A. Shiotari, K. Yabuoshi, M. Fukuda, T. Ozaki and Y. Sugimoto, Phys. Rev. Materials **5**, 034002 (2021).

9. Voltage-controlled magnetic anisotropy in antiferromagnetic MgO-capped MnPt films: P. -H. Chang, W. Fang, T. Ozaki and K. D. Belashchenko, Phys. Rev. Materials **5**, 054406 (2021).

10. *The Simplest Model for Doped Poly(3,4-ethylenedioxythiophene) (PEDOT): Single-crystalline EDOT Dimer Radical Cation Salts: R. Kameyama, T. Fujino, S. Dekura, M. Kawamura, T. Ozaki and H. Mori, Chem. Eur. J. **27**, 6696 (2021).

11. †*DCore: Integrated DMFT software for correlated electrons: H. Shinaoka, J. Otsuki, M. Kawamura, N. Takemori and K. Yoshimi, SciPost Phys. **10**, 117 (2021).

12. A structure map for AB2 type 2D materials using high-throughput DFT calculations: M. Fukuda, J. Zhang, Y. -T. Lee and T. Ozaki, Mater. Adv. **2**, 4392-4413 (2021).

Noguchi group

We have studied (1) reaction-diffusion waves on a deformable vesicle, (2) binding of isotropic curvature-inducing proteins onto membranes, (3) non-thermal fluctuations of membrane pushed by filament growth, (4) cavitation in Karman vortex of polymer solution, (5) fracture dynamics of polymer material, and (6) dynamics of water molecules on lipid membrane.

1. †Effects of polymers on the cavitating flow around a cylinder: A large-scale molecular dynamics analysis: Y. Asano, H. Watanabe and H. Noguchi, J. Chem. Phys. **155**, 014905 (2021).

2. Coarse-grained molecular dynamics simulations of void generation and growth processes in the fracture of the lamellar structure of polyethylene: Y. Higuchi, Phys. Rev. E **103**, 042502 (2021).

3. Vesicle budding induced by binding of curvature-inducing proteins: H. Noguchi, Phys. Rev. E **104**, 014410 (2021).

4. Rotational Dynamics of Water at the Phospholipid Bilayer Depending on the Head Groups Studied by Molecular Dynamics Simulations: Y. Higuchi, Y. Asano, T. Kuwahara and M. Hishida, Langmuir **37**, 5329 (2021).

5. Three-Phase Coexistence in Binary Charged Lipid Membranes in a Hypotonic Solution: J. Guo, H. Ito, Y. Higuchi, K. Bohinc, N. Shimokawa and M. Takagi, Langmuir **37**, 9683 (2021).

6. Binding of curvature-inducing proteins onto tethered vesicles: H. Noguchi, Soft Matter **17**, 10469-10478 (2021).

7. Binding of thermalized and active membrane curvature-inducing proteins: Q. Goutaland, F. van Wijland, J.-B. Fournier and H. Noguchi, Soft Matter **17**, 5560-5573 (2021).

8. Reaction-diffusion waves coupled with membrane curvature: N. Tamemoto and H. Noguchi, Soft Matter **17**, 6589-6596 (2021).

---

* Joint research among groups within ISSP.

9. Undulation of a moving fluid membrane pushed by filament growth: H. Noguchi and O. Pierre-Louis, Sci Rep **11**, 7985 (2021).

10. 荷電脂質膜の秩序形成：実験と粗視化分子動力学シミュレーションの融合：下川 直史 , 伊藤 弘明 , 樋口 祐次 , 分子シミュレーション学会誌「アンサンブル」**23**, 253-259 (2021).

11. Hydrophobic immiscibility controls self-sorting or co-assembly of peptide amphiphiles: R. Wakabayashi, R. Imatani, M. Katsuya, Y. Higuchi, H. Noguchi, N. Kamiya and M. Goto, Chem. Commun. **58**, 585 (2022).

12. Anisotropic, Degradable Polymer Assemblies Driven by a Rigid Hydrogen-Bonding Motif That Induce Shape-Specific Cell Responses: K. Fukushima, K. Matsuzaki, M. Oji, Y. Higuchi, G. Watanabe, Y. Suzuki, M. Kikuchi, N. Fujimura, N. Shimokawa, H. Ito, T. Kato, S. Kawaguchi and M. Tanaka, Macromolecules **55**, 15 (2022).

13. Nonequilibrium dynamics of a fluid vesicle: Turing patterns and traveling waves: H. Noguchi and N. Tamemoto, J. Phys.: Conf. Ser. **2207**, 012017 (2022).

14. †Binding of anisotropic curvature-inducing proteins onto membrane tubes: H. Noguchi, C. Tozzi and M. Arroyo, Soft Matter **18**, 3384--3394 (2022).

Yoshimi group

We have developed and enhanced the usability of programs adopted in the project for advancement of software usability in materials science (PASUMS). Our group's activity of 2021 include functional and usability enhancement of (1) 2DMAT and (2) RISM. We published four papers about the developed software packages (DCore, DSQSS, Kω, and RESPACK) in PASUMS. In addition, using these software packages, we have studied electronic properties of organic conductors β'-$[Pd(dmit)_2]_2$ and relaxation phenomena observed in quantum dot system. We also published the paper about the improvement of an analytic continuation method by combining sparse modeling with Pade approximation.

1. †Multiple-magnon excitations shape the spin spectrum of cuprate parent compounds: D. Betto, R. Fumagalli, L. Martinelli, M. Rossi, R. Piombo, K. Yoshimi, D. D. Castro, E. D. Gennaro, A. Sambri, D. Bonn, G. A. Sawatzky, L. Braicovich, N. B. Brookes, J. Lorenzana and G. Ghiringhelli, Phys. Rev. B **103**, L140409 (2021).

2. *Preparation and Readout of Multielectron High-Spin States in a Gate-Defined GaAs/AlGaAs Quantum Dot: H. Kiyama, K. Yoshimi, T. Kato, T. Nakajima, A. Oiwa and S. Tarucha, Phys. Rev. Lett. **127**, 086802(1-6) (2021).

3. †*DSQSS: Discrete Space Quantum Systems Solver: Y. Motoyama, K. Yoshimi, A. Masaki-Kato, T. Kato and N. Kawashima, Comput. Phys. Commun. **264**, 107944(1-9) (2021).

4. †*Kω— Open-source library for the shifted Krylov subspace method of the form (zI-H)x=b: T. Hoshi, M. Kawamura, K. Yoshimi, Y. Motoyama, T. Misawa, Y. Yamaji, S. Todo, N. Kawashima and T. Sogabe, Computer Physics Communications **258**, 107536 (2021).

5. †*RESPACK: An ab initio tool for derivation of effective low-energy model of material: K. Nakamura, Y. Yoshimoto, Y. Nomura, T. Tadano, M. Kawamura, T. Kosugi, K. Yoshimi, T. Misawa and Y. Motoyama, Computer Physics Communications **261**, 107781 (2021).

6. *Ab initio* derivation and exact diagonalization analysis of low-energy effective Hamiltonians for β′−[Pd(dmit)2]2: K. Yoshimi, T. Tsumuraya and T. Misawa, Phys. Rev. Research **3**, 043224 (2021).

7. †*DCore: Integrated DMFT software for correlated electrons: H. Shinaoka, J. Otsuki, M. Kawamura, N. Takemori and K. Yoshimi, SciPost Phys. **10**, 117 (2021).

8. Robust analytic continuation combining the advantages of the sparse modeling approach and the Padé approximation: Y. Motoyama, K. Yoshimi and J. Otsuki, Phys. Rev. B **105**, 035139 (2022).

9. *Unconventional dual 1D–2D quantum spin liquid revealed by ab initio studies on organic solids family: K. Ido, K. Yoshimi, T. Misawa and M. Imada, npj Quantum Mater. **7**, 48 (2022).

Neutron Science Laboratory

Yamamuro group

† Joint research with outside partners.

Our laboratory is studying chemical physics of complex condensed matters by using neutron scattering, X-ray diffraction, calorimetric, dielectric, and viscoelastic techniques. Our target materials are glasses, liquids, and various disordered systems. Following the vapor-deposited (VD) CS_2 and CCl_4 glasses, which were measured in 2018 and 2020, the inelastic neutron scattering (INS) experiment of VD H_2O glass (amorphous ice) was performed using AMATERAS in J-PARC MLF. By combining these three INS data , we have found a general relation between the low-energy excitations and local structures of glasses. The boson peak appears independently of the local structure, while the dispersive phonon excitations adjacent to the boson peak strongly depends on quasi-network structures of glasses (network formation degree: $H_2O > CCl_4 > CS_2$). The neutron diffraction (ND) of a novel hydrogen-cluster material Li_5MoD_{11} was measured on NOVA in J-PARC MLF. The Rietveld and pair distribution function (PDF) analyses revealed that the MoD_9 cluster is orientationally disordered down to 10 K, being consistent with the previous quasielastic neutron scattering (QENS) experiments. A ND work on amorphous D_2 deuterate was conducted on NOVA. The corresponding QENS work on amorphous H_2 hydrate was also performed using DNA and AGNES in JRR-3 which was restarted in 2021 after the long shutdown due to the Great East-Japan Earthquake in 2011. Other than these neutron works, the synchrotron-radiation X-ray diffraction works of toluene and glycerol liquids were carried out at high pressure up 4 GPa and room temperature using a Paris-Edinburgh cell and BL37XU at SPring-8. At higher pressures, we found drastic development in intermolecular correlation for toluene and more compact intramolecular structure keeping hydrogen bonds for glycerol.

1. Quasielastic Neutron Scattering Study on Polymorphism of Glycerol Deuterated Triacylglycerols: Comparison with Saturated, Trans-unsaturated and Cis-unsaturated Triacylglycerols: C. Takechi, T. Kawaguchi, F. Kaneko and O. Yamamuro, Chem. Lett. **50**, 435 (2021).
2. Spin glass behavior and magnetic boson peak in a structural glass of a magnetic ionic liquid: M. Kofu, R. Watanuki, T. Sakakibara, S. Ohira-Kawamura, K. Nakajima, M. Matsuura, T. Ueki, K. Akutsu and O. Yamamuro, Sci. Rep. **11**, 12098 (2021).
3. Quasielastic neutron scattering study on proton dynamics assisted by water and ammonia molecules confined in MIL-53: S. Miyatsu, M. Kofu, A. Shigematsu, T. Yamada, H. Kitagawa, W. Lohstroh, G. Simeoni, M. Tyagi and O. Yamamuro, Structural Dynamics **8**, 054501 (2021).
4. Intermolecular correlations of liquid and glassy CS_2 studied by synchrotron radiation x-ray diffraction: Y. Mizuno, Y. Zhao, H. Akiba, S. Kohara, K. Ohara, M. G. Tucker, M. T. McDonnell and O. Yamamuro, J. Chem. Phys. **156**, 034503 (2022).
5. Structure of water-in-salt and water-in-bisalt electrolytes: M. A. González, H. Akiba, O. Borodin, G. J. Cuello, L. Hennet, S. Kohara, E. J. Maginn, L. Mangin-Thro, O. Yamamuro, Y. Zhang, D. L. Price and M. -L. Saboungi, Phys. Chem. Chem. Phys. **24**, 10727-10736 (2022).
6. 熱測定・中性子散乱による液晶性イオン液体のナノ構造とダイナミクス研究：根本 文也 , 古府 麻衣子 , 山室 修 , 日本液晶学会誌 **25(4)**, 230-236 (2021).

Masuda group

The goal of our research is to discover a new quantum phenomenon and to reveal the mechanism of it. In this fiscal year we studied the following topics; Nontrivial temperature dependence of magnetic anisotropy in multiferroic $Ba_2MnGe_2O_7$,magnetic diffuse scattering of $YBaCo_4O_7$ and $LuBaCo_4O_7$ on Kagome and triangular lattices, crystalline electric field level scheme of non-centrosymmetric $CeRhSi_3$ and $CeIrSi_3$, etc.

1. Antiferromagnetic Kitaev interaction in Jeff = 1/2 cobalt honeycomb materials $Na_3Co_2SbO_6$ and $Na_2Co_2TeO_6$: C. Kim, J. Jeong, G. Lin, P. Park, T. Masuda, S. Asai, S. Itoh, H.-S. Kim, H. Zhou, J. Ma and J.-G. Park, J. Phys.: Condens. Matter **34**, 045802(1-11) (2021).
2. Complex Magnetic Phase Diagram in the Non-Centrosymmetric Compound $CePtSi_3$: D. Ueta, M. Yoshida, T. Kobuke, Y. Ikeda, T. Masuda and H. Yoshizawa, J. Phys. Soc. Jpn. **90**, 064712(1-4) (2021).
3. Crystalline Electric Field Level Scheme of Non-centrosymmetric $CeRhSi_3$ and $CeIrSi_3$: D. Ueta, T. Kobuke, H. Shibata, M. Yoshida, Y. Ikeda, S. Itoh, T. Yokoo, T. Masuda and H. Yoshizawa, J. Phys. Soc. Jpn. **90**, 104706(1-7) (2021).
4. Magnetic Diffuse Scattering of $YBaCo_4O_7$ and $LuBaCo_4O_7$ on Kagome and Triangular Lattices: M. Soda, K. Morita, G. Ehlers, F. Ye, T. Tohyama, H. Yoshizawa, T. Masuda and H. Kawano-Furukawa, J. Phys. Soc. Jpn. **90**, 074704(1-5) (2021).
5. Oval-cycloidal Magnetic Structure with Phase-shift in the Non-centrosymmetric Tetragonal Compound $CePdSi_3$: D. Ueta, M. Yoshida, T. Kobuke, Y. Ikeda, A. Nakao, T. Moyoshi, K. Munakata, Y. Liu, T. Masuda and H. Yoshizawa, J.

* Joint research among groups within ISSP.

Phys. Soc. Jpn. **90**, 114702(1-5) (2021).

6. †*Spin-gap formation due to spin-Peierls instability in π-orbital-ordered NaO_2: M. Miyajima, F. Astuti, T. Fukuda, M. Kodani, S. Iida, S. Asai, A. Matsuo, T. Masuda, K. Kindo, T. Hasegawa, T. C. Kobayashi, T. Nakano, I. Watanabe and T. Kambe, Phys. Rev. B **104**, L140402(5) (2021).

7. †*Coexistence of Magnetoelectric and Antiferroelectric-like Orders in $Mn_3Ta_2O_8$: K. Kimura, N. Yagi, S. Hasegawa, M. Hagihala, A. Miyake, M. Tokunaga, H. Cao, T. Masuda and T. Kimura, Inorg. Chem. **60**, 15078(1-7) (2021).

8. Topological Analysis of the Experimental Electron Density in Multiferroic Antiferromagnet $Ba_2MnGe_2O_7$: R. Dutta, H. Thoma, D. Chernyshov, B. Nafradi, T. Masuda, A. Kriele and V. Hutanu, IEEE Trans. Magn. **58**, 2500206(1-6) (2021).

9. *Dimensional reduction by geometrical frustration in a cubic antiferromagnet composed of tetrahedral clusters: R. Okuma, M. Kofu, S. Asai, M. Avdeev, A. Koda, H. Okabe, M. Hiraishi, S. Takeshita, K. M. Kojima, R. Kadono, T. Masuda, K. Nakajima and Z. Hiroi, Nat. Commun. **12**, 4382(1-7) (2021).

10. Dynamical Studies in Condensed Matter on High Resolution Chopper Spectrometer (HRC) —2nd Phase of HRC Project—: S. Itoh, T. Masuda, T. Yokoo, H. Yoshizawa, M. Soda, S. Asai, Y. Ikeda, S. Ibuka, M. Yoshida, T. Hawai, H. Saito, D. Kawana, R. Sugiura, T. Asami and Y. Ihata, JPS Conf. Proc. **33**, 011058(1-7) (2021).

11. Field-induced quantum spin disordered state in spin-1/2 honeycomb magnet $Na_2Co_2TeO_6$: G. Lin, J. Jeong, C. Kim, Y. Wang, Q. Huang, T. Masuda, S. Asai, S. Itoh, G. Günther, M. Russina, Z. Lu, J. Sheng, L. Wang, J. Wang, G. Wang, Q. Ren, C. Xi, W. Tong, L. Ling, Z. Liu, L. Wu, J. Mei, Z. Qu, H. Zhou, X. Wang, J.-G. Park, Y. Wan and J. Ma, Nat Commun **12**, 5559(1-8) (2021).

12. Triplon current generation in solids: Y. Chen, M. Sato, Y. Tang, Y. Shiomi, K. Oyanagi, T. Masuda, Y. Nambu, M. Fujita and E. Saitoh, Nat Commun **12**, 5199(1-7) (2021).

13. Nontrivial temperature dependence of magnetic anisotropy in multiferroic $Ba_2MnGe_2O_7$: S. Hasegawa, S. Hayashida, S. Asai, M. Matsuura, Z. Igor and T. Masuda, Phys. Rev. Research **3**, L032023(1-5) (2021).

14. Hybridized excitation of Higgs-amplitude and phase modes in frustrated quantum magnet: T. Masuda, S. Hayashida and M. Matsumoto, 日本物理学会誌 **76**, 23-27 (2021).

15. Novel Route for Analysis on Neutron Scattering Spectra: T. Masuda, JPSJ News Comments **18**, 03 (2021).

Nakajima group

Nakajima group has been studying magnetic materials showing cross-correlated phenomena related to topologically-nontrivial magnetic structures by means of neutron and X-ray scattering techniques. We are also responsible for a polarized-neutron triple-axis neutron spectrometer PONTA in the research reactor JRR-3 in Tokai. In this year, JRR-3 restarted its operation after the long shutdown since the east Japan great earthquake in 2011. We have updated components of the spectrometer and have supported the users who applied the joint-use user program of ISSP-NSL. One of the successful studies with the external users is the identification of complex magnetic orders in a centrosymmetric skyrmion host $EuAl_4$. Polarized neutron scattering at PONTA contributed to reveal successive magnetic phase transitions in this system at low temperatures in zero magnetic field. We are also collaborating with Kohama group in the international mega gauss laboratory in ISSP. By combining a long-pulse magnet developed by Kohama group with a pulsed neutron beam in J-PARC, we successfully performed time-of-flight neutron Laue diffraction measurements in long-pulse magnetic fields up to 14 T. We are planning to extend the limit of the magnetic field to 20-30 T in the future.

1. Direct Observation of Cycloidal Spin Modulation and Field-induced Transition in Néel-type Skyrmion-hosting $VOSe_2O_5$: T. Kurumaji, T. Nakajima, A. Feoktystov, E. Babcock, Z. Salhi, V. Ukleev, T.-H. Arima, K. Kakurai and Y. Tokura, J. Phys. Soc. Jpn. **90**, 024705 (2021).

2. Robust noncoplanar magnetism in band-filling-tuned $(Nd_{1-x}Ca_x)_2Mo_2O_7$: M. Hirschberger, Y. Kaneko, L. Spitz, T. Nakajima, Y. Taguchi and Y. Tokura, Phys. Rev. B **104**, 024436 (2021).

3. Phase correction method in a wide detector plane for MIEZE spectroscopy with pulsed neutron beams: T. Oda, H. Endo, H. Ohshita, T. Seya, Y. Yasu, T. Nakajima, M. Hino and Y. Kawabata, Nuclear Instruments and Methods in Physics Research Section A: Accelerators, Spectrometers, Detectors and Associated Equipment **1012**, 165616 (2021).

4. †*Above-ordering-temperature large anomalous Hall effect in a triangular-lattice magnetic semiconductor: M. Uchida, S. Sato, H. Ishizuka, R. Kurihara, T. Nakajima, Y. Nakazawa, M. Ohno, M. Kriener, A. Miyake, K. Ohishi, T. Morikawa, M. S. Bahramy, T.-H. Arima, M. Tokunaga, N. Nagaosa and M. Kawasaki, Sci. Adv. **7**, eabl5381(1-8)

† Joint research with outside partners.

(2021).

5. Emergence of spin-orbit coupled ferromagnetic surface state derived from Zak phase in a nonmagnetic insulator FeSi: Y. Ohtsuka, N. Kanazawa, M. Hirayama, A. Matsui, T. Nomoto, R. Arita, T. Nakajima, T. Hanashima, V. Ukleev, H. Aoki, M. Mogi, K. Fujiwara, A. Tsukazaki, M. Ichikawa, M. Kawasaki and Y. Tokura, Sci. Adv. **7**, eabj0498 (2021).

6. Square and rhombic lattices of magnetic skyrmions in a centrosymmetric binary compound: R. Takagi, N. Matsuyama, V. Ukleev, L. Yu, J. S. White, S. Francoual, J. R. L. Mardegan, S. Hayami, H. Saito, K. Kaneko, K. Ohishi, Y. Onuki, T.-H. Arima, Y. Tokura, T. Nakajima and S. Seki, Nat Commun **13**, 1472 (2022).

7. Zoology of Multiple-*Q* Spin Textures in a Centrosymmetric Tetragonal Magnet with Itinerant Electrons: N. D. Khanh, T. Nakajima, S. Hayami, S. Gao, Y. Yamasaki, H. Sagayama, H. Nakao, R. Takagi, Y. Motome, Y. Tokura, T. Arima and S. Seki, Advanced Science **9**, 2105452 (2022).

Mayumi group

Mayumi group has discovered that slide-ring gels, in which polymer chains are cross-linked by ring molecules, show reversible strain-induced crystallization of polymer chains in loading/unloading process, which realizes their remarkable mechanical toughness and high recoverability under repeated cyclic deformation. The formation process of strain-induced crystalline structure has been probed by time-resolved scattering technique.

1. Tough hydrogels with rapid self-reinforcement: C. Liu, N. Morimoto, L. Jiang, S. Kawahara, T. Noritomi, H. Yokoyama, K. Mayumi and K. Ito, Science **372**, 1078 (2021).

2. Softness, Elasticity, and Toughness of Polymer Networks with Slide-Ring Cross-Links: K. Mayumi, C. Liu, Y. Yasuda and K. Ito, Gels **7**, 91 (2021).

3. Overscreening Induced by Ionic Adsorption at the Ionic Liquid/Electrode Interface Detected Using Neutron Reflectometry with a Rational Material Design: N. Nishi, J. Uchiyashiki, T. Oda, M. Hino and N. L. Yamada, Bulletin of the Chemical Society of Japan **94**, 2914-2918 (2021).

4. Tri-branched gels: Rubbery materials with the lowest branching factor approach the ideal elastic limit: T. Fujiyabu, N. Sakumichi, T. Katashima, C. Liu, K. Mayumi, U.-I. Chung and T. Sakai, Science Advances **8**, eabk0010 (2022).

International MegaGauss Science Laboratory

Kindo group

We have found better approach to produce the Cu-Ag wire for the pulsed magnet. We can not tell the better wire from good one by comparing tensile strength or conductivity but only by generating field. Good Cu-Ag wire can generate 75 Tesla(T) field without destruction but better one can 85 T. The wire produced by better approach generated the highest field up to 86.1 T in this year.

1. [*]High-field phase diagram of $Ni_3V_2O_8$ studied by specific heat and magnetocaloric effect measurements: C. Dong, Y. Kohama, Z. Z. He, X. T. Han, K. Sato, A. Matsuo, K. Kindo, M. Yang and J. F. Wang, J. Phys.: Condens. Matter **33**, 205402 (2021).

2. Ligand dependent magnetism of the J = 3/2 Mott insulator Cs_2MX_6 (M = Ta, Nb, X = Br, Cl): H. Ishikawa, T. Yajima, A. Matsuo and K. Kindo, J. Phys.: Condens. Matter **33**, 125802(1-6) (2021).

3. GdV_6Sn_6: A Multi-carrier Metal with Non-magnetic 3d-electron Kagome Bands and 4f-electron Magnetism: H. Ishikawa, T. Yajima, M. Kawamura, H. Mitamura and K. Kindo, J. Phys. Soc. Jpn. **90**, 124704(4) (2021).

4. Magnetization Process in $EuCo_2P_2$ and EuT_2Ge_2 (T: transition metal): Comparison of Experiment and Theory: T. Takeuchi, T. Tahara, T. Kida, Y. Narumi, M. Hagiwara, K. Kindo, W. Iha, Y. Ashitomi, T. Yara, M. Nakashima, Y. Amako, M. Hedo, T. Nakama and Y. Onuki, J. Phys. Soc. Jpn. **90**, 034709(1-15) (2021).

5. †[*]Spin Excitations of the S = 1/2 One-Dimensional Ising-Like Antiferromagnet $BaCo_2V_2O_8$ in Transverse Magnetic Fields: A. Okutani, H. Onishi, S. Kimura, T. Takeuchi, T. Kida, M. Mori, A. Miyake, M. Tokunaga, K. Kindo and M. Hagiwara, J. Phys. Soc. Jpn. **90**, 044704(1-9) (2021).

---

[*] Joint research among groups within ISSP.

6. Experimental determination of the magnetic interactions of frustrated Cairo pentagon lattice materials: M. D. Le, E. M. Wheeler, J. Jeong, K. Ramesh Kumar, S. Lee, C.-H. Lee, M. J. Oh, Y.-J. Jo, A. Kondo, K. Kindo, U. Stuhr, B. Fåk, M. Enderle, D. Batuk, A. M. Abakumov, A. A. Tsirlin and J.-G. Park, Phys. Rev. B **103**, 104423 (2021).

7. *Ferroelectric polarization reversal in multiferroic $MnWO_4$ via a rotating magnetic field up to 52 T: J. F. Wang, W. X. Liu, Z. Z. He, C. B. Liu, M. Tokunaga, M. Li, C. Dong, X. T. Han, F. Herlach, C. L. Lu, Z. W. Ouyang, Z. C. Xia, K. Kindo, L. Li and M. Yang, Phys. Rev. B **104**, 014415 (2021).

8. †*Geometrical Hall effect and momentum-space Berry curvature from spin-reversed band pairs: M. Hirschberger, Y. Nomura, H. Mitamura, A. Miyake, T. Koretsune, Y. Kaneko, L. Spitz, Y. Taguchi, A. Matsuo, K. Kindo, R. Arita, M. Tokunaga and Y. Tokura, Phys. Rev. B **103**, L041111(1-6) (2021).

9. †High magnetic field properties in $Ru_{2-x}Fe_xCrSi$ with antiferromagnetic and spin-glass states: M. Hiroi, S. Nishiinoue, I. Shigeta, M. Ito, K. Koyama, A. Kondo, K. Kindo, I. Watanabe, M. Fujii, S. Kimura, H. Manaka and N. Terada, Phys. Rev. B **103**, 094428 (2021).

10. *Normal state specific heat in the cuprate superconductors $La_{2-x}Sr_xCuO_4$ and $Bi_{2+y}Sr_{2-x-y}LaxCuO_{6+\delta}$ near the critical point of the pseudogap phase: C. Girod, D. LeBoeuf, A. Demuer, G. Seyfarth, S. Imajo, K. Kindo, Y. Kohama, M. Lizaire, A. Legros, A. Gourgout, H. Takagi, T. Kurosawa, M. Oda, N. Momono, J. Chang, S. Ono, G. -q. Zheng, C. Marcenat, L. Taillefer and T. Klein, Phys. Rev. B **103**, 214506 (2021).

11. *Phase transition in the 5d(1) double perovskite Ba_2CaReO_6 induced by high magnetic field: H. Ishikawa, D. Hirai, A. Ikeda, M. Gen, T. Yajima, A. Matsuo, Y. H. Matsuda, Z. Hiroi and K. Kindo, Phys. Rev. B **104**, 174422(7) (2021).

12. †*Physical properties of liquid oxygen under ultrahigh magnetic fields: T. Nomura, A. Ikeda, M. Gen, A. Matsuo, K. Kindo, Y. Kohama, Y. H. Matsuda, S. Zherlitsyn, J. Wosnitza, H. Tsuda and T. C. Kobayashi, Phys. Rev. B **104**, 224423(10) (2021).

13. †*Quantum antiferromagnet bluebellite comprising a maple-leaf lattice made of spin-1/2 Cu^{2+} ions: Y. Haraguchi, A. Matsuo, K. Kindo and Z. Hiroi, Phys. Rev. B **104**, 174439(6) (2021).

14. *Quantum transport of topological spin solitons in a one-dimensional organic ferroelectric: S. Imajo, A. Miyake, R. Kurihara, M. Tokunaga, K. Kindo, S. Horiuchi and F. Kagawa, Phys. Rev. B **103**, L201117 (2021).

15. †*Spin-gap formation due to spin-Peierls instability in π-orbital-ordered NaO_2: M. Miyajima, F. Astuti, T. Fukuda, M. Kodani, S. Iida, S. Asai, A. Matsuo, T. Masuda, K. Kindo, T. Hasegawa, T. C. Kobayashi, T. Nakano, I. Watanabe and T. Kambe, Phys. Rev. B **104**, L140402(5) (2021).

16. Symmetry change of d-wave superconductivity in κ-type organic superconductors: S. Imajo, K. Kindo and Y. Nakazawa, Phys. Rev. B **103**, L060508(1-5) (2021).

17. Thermodynamic evidence for the formation of a Fulde-Ferrell-Larkin-Ovchinnikov phase in the organic superconductor λ−$(BETS)_2GaCl_4$: S. Imajo, T. Kobayashi, A. Kawamoto, K. Kindo and Y. Nakazawa, Phys. Rev. B **103**, L220501 (2021).

18. The FFLO State in the Dimer Mott Organic Superconductor κ-$(BEDT\text{-}TTF)_2Cu[N(CN)_2]Br$: S. Imajo and K. Kindo, Crystals **11**, 1358(11) (2021).

19. Ni deficiency effects on martensitic phase transition in Ni_2MnGa: M. Ito, S. Kuwahara, A. Taira, H. Matsuguma, A. Kondo and K. Kindo, Physica B: Condensed Matter **611**, 412794 (2021).

20. *Compact megajoule-class pulsed power supply for generating long-pulsed magnetic fields: K. Matsui, T. Kanda, Y. Ihara, K. Kindo and Y. Kohama, Review of Scientific Instruments **92**, 024711 (2021).

21. *High-resolution calorimetry in pulsed magnetic fields: S. Imajo, C. Dong, A. Matsuo, K. Kindo and Y. Kohama, Review of Scientific Instruments **92**, 043901 (2021).

22. †*Nuclear magnetic resonance measurements in dynamically controlled field pulse: Y. Ihara, K. Hayashi, T. Kanda, K. Matsui, K. Kindo and Y. Kohama, Review of Scientific Instruments **92**, 114709(8) (2021).

23. *Extraordinary π-electron superconductivity emerging from a quantum spin liquid: S. Imajo, S. Sugiura, H. Akutsu, Y. Kohama, T. Isono, T. Terashima, K. Kindo, S. Uji and Y. Nakazawa, Phys. Rev. Research **3**, 033026 (2021).

24. *Revealing three-dimensional quantum criticality by Sr substitution in Han purple: S. Allenspach, P. Puphal, J. Link, I. Heinmaa, E. Pomjakushina, C. Krellner, J. Lass, G. S. Tucker, C. Niedermayer, S. Imajo, Y. Kohama, K. Kindo, S. Kramer, M. Horvatic, M. Jaime, A. Madsen, A. Mira, N. Laflorencie, F. Mila, B. Normand, C. Ruegg, R. Stern and F. Weickert, Phys. Rev. Research **3**, 023177 (2021).

† Joint research with outside partners.

25. †*Nature of field-induced antiferromagnetic order in Zn-doped $CeCoIn_5$ and its connection to quantum criticality in the pure compound: M. Yokoyama, Y. Honma, Y. Oshima, ?. Rahmanto, K. Suzuki, K. Tenya, Y. Shimizu, D. Aoki, A. Matsuo, K. Kindo, S. Nakamura, Y. Kono, S. Kittaka and T. Sakakibara, Phys. Rev. B **105**, 054515(9) (2022).

26. Optical selection rules of the magnetic excitation in the S=1/2 one-dimensional Ising-like antiferromagnet $BaCo_2V_2O_8$: S. Kimura, H. Onishi, A. Okutani, M. Akaki, Y. Narumi, M. Hagiwara, K. Okunishi, K. Kindo, Z. He, T. Taniyama and M. Itoh, Phys. Rev. B **105**, 014417(9) (2022).

27. Reentrant ferroelectric phase induced by a tilting high magnetic field in $Ni_3V_2O_8$: C. Dong, J. F. Wang, Z. Z. He, Y. T. Chang, M. Y. Shi, Y. R. Song, S. M. Jin, Y. Q. Du, Z. Y. Wu, X. T. Han, K. Kindo and M. Yang, Phys. Rev. B **105**, 024427(6) (2022).

28. †Revised phase diagram of the high-T_c cuprate superconductor Pb-doped $Bi_2Sr_2CaCu_2O_{8+\delta}$ revealed by anisotropic transport measurements: K. Harada, Y. Teramoto, T. Usui, K. Itaka, T. Fujii, T. Noji, H. Taniguchi, M. Matsukawa, H. Ishikawa, K. Kindo, D. S. Dessau and T. Watanabe, Phys. Rev. B **105**, 085131(9) (2022).

29. †Quantum paramagnetism in the hyperhoneycomb Kitaev magnet β−$ZnIrO_3$: Y. Haraguchi, A. Matsuo, K. Kindo and H. A. Katori, Phys. Rev. Materials **6**, L021401(6) (2022).

30. †Spin-glass transition in the spin–orbit-entangled Jeff=0 Mott insulating double-perovskite ruthenate: H. Yatsuzuka, Y. Haraguchi, A. Matsuo, K. Kindo and H. A. Katori, Sci Rep **12**, 2429(6) (2022).

Tokunaga group

The topological Hall effect, which reflects the scalar spin chirality produced by magnetic ordering, was studied in various magnetic materials. Our experiments on magnetotransport properties in high magnetic fields have revealed that the anomalous Hall effect grows at high temperatures after arriving at a forced ferromagnetic state in some magnetic materials. Such phenomena suggest a new mechanism for the giant anomalous Hall effect.

1. †Anisotropic Physical Properties of Layered Antiferromagnet $U_2Pt_6Ga_{15}$: Y. Matsumoto, Y. Haga, E. Yamamoto, T. Takeuchi, A. Miyake and M. Tokunaga, J. Phys. Soc. Jpn. **90**, 074707(1-6) (2021).

2. Enhancement and Discontinuity of Effective Mass through the First-Order Metamagnetic Transition in UTe_2: A. Miyake, Y. Shimizu, Y. J. Sato, D. Li, A. Nakamura, Y. Homma, F. Honda, J. Flouquet, M. Tokunaga and D. Aoki, J. Phys. Soc. Jpn. **90**, 103702(1-5) (2021).

3. †*Spin Excitations of the S = 1/2 One-Dimensional Ising-Like Antiferromagnet $BaCo_2V_2O_8$ in Transverse Magnetic Fields: A. Okutani, H. Onishi, S. Kimura, T. Takeuchi, T. Kida, M. Mori, A. Miyake, M. Tokunaga, K. Kindo and M. Hagiwara, J. Phys. Soc. Jpn. **90**, 044704(1-9) (2021).

4. *Ferroelectric polarization reversal in multiferroic $MnWO_4$ via a rotating magnetic field up to 52 T: J. F. Wang, W. X. Liu, Z. Z. He, C. B. Liu, M. Tokunaga, M. Li, C. Dong, X. T. Han, F. Herlach, C. L. Lu, Z. W. Ouyang, Z. C. Xia, K. Kindo, L. Li and M. Yang, Phys. Rev. B **104**, 014415 (2021).

5. †*Field-induced valence fluctuations in YbB_{12}: R. Kurihara, A. Miyake, M. Tokunaga, A. Ikeda, Y. H. Matsuda, A. Miyata, D. I. Gorbunov, T. Nomura, S. Zherlitsyn, J. Wosnitza and F. Iga, Phys. Rev. B **103**, 115103(1-14) (2021).

6. †*Geometrical Hall effect and momentum-space Berry curvature from spin-reversed band pairs: M. Hirschberger, Y. Nomura, H. Mitamura, A. Miyake, T. Koretsune, Y. Kaneko, L. Spitz, Y. Taguchi, A. Matsuo, K. Kindo, R. Arita, M. Tokunaga and Y. Tokura, Phys. Rev. B **103**, L041111(1-6) (2021).

7. Quantum transport observed in films of the magnetic topological semimetal $EuSb_2$: M. Ohno, M. Uchida, R. Kurihara, S. Minami, Y. Nakazawa, S. Sato, M. Kriener, M. Hirayama, A. Miyake, Y. Taguchi, R. Arita, M. Tokunaga and M. Kawasaki, Phys. Rev. B **103**, 165144(1-6) (2021).

8. *Quantum transport of topological spin solitons in a one-dimensional organic ferroelectric: S. Imajo, A. Miyake, R. Kurihara, M. Tokunaga, K. Kindo, S. Horiuchi and F. Kagawa, Phys. Rev. B **103**, L201117 (2021).

9. †*Magnetoconduction in the Correlated Semiconductor FeSi in Ultrastrong Magnetic Fields up to a Semiconductor-to-Metal Transition: D. Nakamura, Y. H. Matsuda, A. Ikeda, A. Miyake, M. Tokunaga, S. Takeyama and T. Kanomata, Phys. Rev. Lett. **127**, 156601 (1-6) (2021).

10. †*Coexistence of Magnetoelectric and Antiferroelectric-like Orders in $Mn_3Ta_2O_8$: K. Kimura, N. Yagi, S. Hasegawa, M. Hagihala, A. Miyake, M. Tokunaga, H. Cao, T. Masuda and T. Kimura, Inorg. Chem. **60**, 15078(1-7) (2021).

11. †Enhancing Thermopower and Nernst Signal of High-Mobility Dirac Carriers by Fermi Level Tuning in the Layered

* Joint research among groups within ISSP.

Magnet $EuMnBi_2$: K. Tsuruda, K. Nakagawa, M. Ochi, K. Kuroki, M. Tokunaga, H. Murakawa, N. Hanasaki and H. Sakai, Adv. Funct. Mater. **31**, 2102275 (2021).

12. †Martensitic Transformation and Metamagnetic Transition in Co-V-(Si, Al) Heusler Alloys: K. Nakamura, A. Miyake, X. Xu, T. Omori, M. Tokunaga and R. Kainuma, Metals **11**, 226(1-12) (2021).

13. †*Above-ordering-temperature large anomalous Hall effect in a triangular-lattice magnetic semiconductor: M. Uchida, S. Sato, H. Ishizuka, R. Kurihara, T. Nakajima, Y. Nakazawa, M. Ohno, M. Kriener, A. Miyake, K. Ohishi, T. Morikawa, M. S. Bahramy, T.-H. Arima, M. Tokunaga, N. Nagaosa and M. Kawasaki, Sci. Adv. **7**, eabl5381(1-8) (2021).

14. †Observation of inverse magnetocaloric effect in magnetic-field-induced austenite phase of Heusler alloys $Ni_{50-x}Co_xMn_{31.5}Ga_{18.5}$ (x=9 and 9.7): T. Kihara, T. Roy, X. Xu, A. Miyake, M. Tsujikawa, H. Mitamura, M. Tokunaga, Y. Adachi, T. Eto and T. Kanomata, Phys. Rev. Materials **5**, 034416(1-13) (2021).

15. †Restoration of the collinear spin arrangement in non-magnetic-ion-substituted M-type hexaferrite by high magnetic fields: K. Kamishima, A. Yonezawa, K. Kakizaki, A. Miyake, H. Mitamura and M. Tokunaga, Journal of Magnetism and Magnetic Materials **538**, 168251(1-5) (2021).

16. †Giant anomalous Hall effect from spin-chirality scattering in a chiral magnet: Y. Fujishiro, N. Kanazawa, R. Kurihara, H. Ishizuka, T. Hori, F. S. Yasin, X. Yu, A. Tsukazaki, M. Ichikawa, M. Kawasaki, N. Nagaosa, M. Tokunaga and Y. Tokura, Nat Commun **12**, 317(1-6) (2021).

17. Molecular beam deposition of a new layered pnictide with distorted Sb square nets: M. Ohno, M. Uchida, Y. Nakazawa, S. Sato, M. Kriener, A. Miyake, M. Tokunaga, Y. Taguchi and M. Kawasaki, APL Materials **9**, 051107(1-4) (2021).

18. †Tunable spin-valley coupling in layered polar Dirac metals: M. Kondo, M. Ochi, T. Kojima, R. Kurihara, D. Sekine, M. Matsubara, A. Miyake, M. Tokunaga, K. Kuroki, H. Murakawa, N. Hanasaki and H. Sakai, Commun Mater **2**, 49(1-7) (2021).

19. Elastic Soft Mode and Electric Quadrupole Response in Excitonic Insulator Candidate $(Ta_{0.952}V_{0.048})_2NiSe_5$: Contribution of Electron–Phonon Interaction: R. Kurihara, Y. Hirose, S. Sano, K. Mitsumoto, A. Miyake, M. Tokunaga and R. Settai, J. Phys. Soc. Jpn. **91**, 024601(1-7) (2022).

20. †Magnetism of $Al_xFe_{2-x}GeO_5$ with Andalusite Structure: K. Kakimoto, S. Takada, H. Ohta, Y. Haraguchi, M. Hagihala, S. Torii, T. Kamiyama, H. Mitamura, M. Tokunaga, A. Hatakeyama and H. A. Katori, J. Phys. Soc. Jpn. **91**, 054704(1-7) (2022).

21. Extremely high upper critical field in $BiCh_2$-based (Ch: S and Se) layered superconductor $LaO_{0.5}F_{0.5}BiS_{2-x}Se_x$ (x = 0.22 and 0.69): K. Hoshi, R. Kurihara, Y. Goto, M. Tokunaga and Y. Mizuguchi, Sci Rep **12**, 288(1-8) (2022).

22. †Field-induced multiple metal-insulator crossovers of correlated Dirac electrons of perovskite $CaIrO_3$: R. Yamada, J. Fujioka, M. Kawamura, S. Sakai, M. Hirayama, R. Arita, T. Okawa, D. Hashizume, T. Sato, F. Kagawa, R. Kurihara, M. Tokunaga and Y. Tokura, npj Quantum Mater. **7**, 13(1-6) (2022).

Y. Matsuda group

The magnetic-field-induced insulator-metal transition in the correlated narrow gap semiconductor FeSi has been investigated using ultrahigh magnetic fields of up to 500 T generated by the electromagnetic flux compression technique. The critical magnetic field of the phase transition is found to be 270 T. It is found that the ingap state plays an important role in the mechanism of magnetoresistance in high magnetic fields. Closing of the energy gap due to the Zeeman shift of the electronic bands explains the metallization in an ultrahigh magnetic field. As for the single-turn coil technique, a development of the techniques for the generation of high magnetic fields has been made. A change in the weight of the single-turned coil affects the process of the magnetic field generation and the maximum magnetic field increases with increasing the weight. Another important technical development has been made for the ultrasound experiment and the technique has been applied for the study of liquid oxygen up to 140 T. The ultrasound experiment of Kondo insulator YbB_{12} has been performed in a relatively lower field range up to 60 T. Although the quantum oscillation has not been observed in the response of the ultrasound, the anomalous magnetic field dependence of the elastic constants was found at temperatures around 30 K, which suggests the magnetic-field-induced valence fluctuation of Yb ions.

1. †*Field-induced valence fluctuations in YbB_{12}: R. Kurihara, A. Miyake, M. Tokunaga, A. Ikeda, Y. H. Matsuda, A. Miyata, D. I. Gorbunov, T. Nomura, S. Zherlitsyn, J. Wosnitza and F. Iga, Phys. Rev. B **103**, 115103(1-14) (2021).

2. *Phase transition in the 5d(1) double perovskite Ba_2CaReO_6 induced by high magnetic field: H. Ishikawa, D. Hirai, A.

† Joint research with outside partners.

Ikeda, M. Gen, T. Yajima, A. Matsuo, Y. H. Matsuda, Z. Hiroi and K. Kindo, Phys. Rev. B **104**, 174422(7) (2021).

3. †*Physical properties of liquid oxygen under ultrahigh magnetic fields: T. Nomura, A. Ikeda, M. Gen, A. Matsuo, K. Kindo, Y. Kohama, Y. H. Matsuda, S. Zherlitsyn, J. Wosnitza, H. Tsuda and T. C. Kobayashi, Phys. Rev. B **104**, 224423(10) (2021).

4. †*Magnetoconduction in the Correlated Semiconductor FeSi in Ultrastrong Magnetic Fields up to a Semiconductor-to-Metal Transition: D. Nakamura, Y. H. Matsuda, A. Ikeda, A. Miyake, M. Tokunaga, S. Takeyama and T. Kanomata, Phys. Rev. Lett. **127**, 156601 (1-6) (2021).

5. †*Higher magnetic-field generation by a mass-loaded single-turn coil: M. Gen, A. Ikeda, S. Kawachi, T. Shitaokoshi, Y. H. Matsuda, Y. Kohama and T. Nomura, Review of Scientific Instruments **92**, 033902 (1-5) (2021).

6. *Ultrasound measurement technique for the single-turn-coil magnets: T. Nomura, A. Hauspurg, D. I. Gorbunov, A. Miyata, E. Schulze, S. A. Zvyagin, V. Tsurkan, Y. H. Matsuda, Y. Kohama and S. Zherlitsyn, Review of Scientific Instruments **92**, 063902(8) (2021).

7. *Ferroelectric Transition of a Chiral Molecular Crystal BINOL·2DMSO: T. Nomura, T. Yajima, Z. Yang, R. Kurihara, Y. Ishii, M. Tokunaga, Y. H. Matsuda, Y. Kohama, K. Kimura and T. Kimura, J. Phys. Soc. Jpn. **91**, 064702 (2022).

8. Generating 77 T using a portable pulse magnet for single-shot quantum beam experiments: A. Ikeda, Y. H. Matsuda, X. Zhou, S. Peng, Y. Ishii, T. Yajima, Y. Kubota, I. Inoue, Y. Inubushi, K. Tono and M. Yabashi, Appl. Phys. Lett. **120**, 142403 5pages (2022).

Kohama group

We have investigated various high-field properties. In $Pb(TiO)Cu_4(PO_4)_4$, Sn(SeS), and $MAPbX_3$ (X = I, Br, and Cl), the field induced phenomena have been investigated by magnetooptics in non-destructive and destructive magnetic fields. In $Ba_{0.9}Sr_{0.1}CuSi_2O$, graphite, and high-T_c superconductor, we have used specific heat and MCE techniques. The TDO and resistivity measurements have revealed rich transport phenomena in two dimensional materials, such as KZnBi and organic conductors. We have developed NMR measurement technique for measuring spin-lattice and spin-spin relaxation rates in pulsed magnetic fields. We also have developed the ultrasound experiemnt technique for investigations in destructive pulsed fields. We are now constructing new apparatus for the neutron scattering experiment in long pulse fields.

1. *High-field phase diagram of $Ni_3V_2O_8$ studied by specific heat and magnetocaloric effect measurements: C. Dong, Y. Kohama, Z. Z. He, X. T. Han, K. Sato, A. Matsuo, K. Kindo, M. Yang and J. F. Wang, J. Phys.: Condens. Matter **33**, 205402 (2021).

2. Emergence of Frustrated Short-Range Order above Long-Range Order in the S = 1/2 Kagome Antiferromagnet $CaCu_3(OD)_6Cl_2\cdot 0.6D_2O$: Y. Ihara, K. Matsui, Y. Kohama, S. Luther, D. Opherden, J. Wosnitza, H. Kühne and H. K. Yoshida, J. Phys. Soc. Jpn. **90**, 023703 (2021).

3. Nonreciprocal Directional Dichroism in a Magnetic-Field-Induced Ferroelectric Phase of $Pb(TiO)Cu_4(PO_4)_4$: T. Katsuyoshi, K. Kimura, Z. Yang, Y. Kato, S. Kimura, Y. Motome, Y. Kohama and T. Kimura, J. Phys. Soc. Jpn. **90**, 123701 (2021).

4. Combination of optical transitions of polarons with Rashba effect in methylammonium lead trihalide perovskites under high magnetic fields: Y. H. Shin, H. Choi, C. Park, D. Park, M. S. Jeong, H. Nojiri, Z. Yang, Y. Kohama and Y. Kim, Phys. Rev. B **104**, 035205 (2021).

5. Element-specific field-induced spin reorientation and tetracritical point in $MnCr_2S_4$: Sh. Yamamoto, H. Suwa, T. Kihara, T. Nomura, Y. Kotani, T. Nakamura, Y. Skourski, S. Zherlitsyn, L. Prodan, V. Tsurkan, H. Nojiri, A. Loidl and J. Wosnitza, Phys. Rev. B **103**, L020408 (2021).

6. Heavy carrier effective masses in van der Waals semiconductor Sn(SeS) revealed by high magnetic fields up to 150 T: Z. Yang, X. Wang, J. Felton, Z. Kudrynskyi, M. Gen, T. Nomura, X. Wang, L. Eaves, Z. D. Kovalyuk, Y. Kohama, L. Zhang and A. Patanè, Phys. Rev. B **104**, 085206 (2021).

7. *Normal state specific heat in the cuprate superconductors $La_{2-x}Sr_xCuO_4$ and $Bi_{2+y}Sr_{2-x-y}LaxCuO_{6+\delta}$ near the critical point of the pseudogap phase: C. Girod, D. LeBoeuf, A. Demuer, G. Seyfarth, S. Imajo, K. Kindo, Y. Kohama, M. Lizaire, A. Legros, A. Gourgout, H. Takagi, T. Kurosawa, M. Oda, N. Momono, J. Chang, S. Ono, G. -q. Zheng, C. Marcenat, L. Taillefer and T. Klein, Phys. Rev. B **103**, 214506 (2021).

8. †*Physical properties of liquid oxygen under ultrahigh magnetic fields: T. Nomura, A. Ikeda, M. Gen, A. Matsuo,

* Joint research among groups within ISSP.

K. Kindo, Y. Kohama, Y. H. Matsuda, S. Zherlitsyn, J. Wosnitza, H. Tsuda and T. C. Kobayashi, Phys. Rev. B **104**, 224423(10) (2021).

9. Wide Critical Fluctuations of the Field-Induced Phase Transition in Graphite: C. Marcenat, T. Klein, D. LeBoeuf, A. Jaoui, G. Seyfarth, J. Kacmarcik, Y. Kohama, H. Cercellier, H. Aubin, K. Behnia and B. Fauque, Phys. Rev. Lett. **126**, 106801 (2021).

10. *Compact megajoule-class pulsed power supply for generating long-pulsed magnetic fields: K. Matsui, T. Kanda, Y. Ihara, K. Kindo and Y. Kohama, Review of Scientific Instruments **92**, 024711 (2021).

11. †*Higher magnetic-field generation by a mass-loaded single-turn coil: M. Gen, A. Ikeda, S. Kawachi, T. Shitaokoshi, Y. H. Matsuda, Y. Kohama and T. Nomura, Review of Scientific Instruments **92**, 033902 1-5 (2021).

12. *High-resolution calorimetry in pulsed magnetic fields: S. Imajo, C. Dong, A. Matsuo, K. Kindo and Y. Kohama, Review of Scientific Instruments **92**, 043901 (2021).

13. †*Nuclear magnetic resonance measurements in dynamically controlled field pulse: Y. Ihara, K. Hayashi, T. Kanda, K. Matsui, K. Kindo and Y. Kohama, Review of Scientific Instruments **92**, 114709(8) (2021).

14. *Ultrasound measurement technique for the single-turn-coil magnets: T. Nomura, A. Hauspurg, D. I. Gorbunov, A. Miyata, E. Schulze, S. A. Zvyagin, V. Tsurkan, Y. H. Matsuda, Y. Kohama and S. Zherlitsyn, Review of Scientific Instruments **92**, 063902(8) (2021).

15. Tunable Berry curvature and transport crossover in topological Dirac semimetal KZnBi: J. Song, B. C. Park, K. I. Sim, J. Bang, S. Kim, Z. Yang, Y. Kohama, Y. Kim and S. W. Kim, npj Quantum Mater. **6**, 77 (2021).

16. *Extraordinary π-electron superconductivity emerging from a quantum spin liquid: S. Imajo, S. Sugiura, H. Akutsu, Y. Kohama, T. Isono, T. Terashima, K. Kindo, S. Uji and Y. Nakazawa, Phys. Rev. Research **3**, 033026 (2021).

17. *Revealing three-dimensional quantum criticality by Sr substitution in Han purple: S. Allenspach, P. Puphal, J. Link, I. Heinmaa, E. Pomjakushina, C. Krellner, J. Lass, G. S. Tucker, C. Niedermayer, S. Imajo, Y. Kohama, K. Kindo, S. Kramer, M. Horvatic, M. Jaime, A. Madsen, A. Mira, N. Laflorencie, F. Mila, B. Normand, C. Ruegg, R. Stern and F. Weickert, Phys. Rev. Research **3**, 023177 (2021).

18. *Ferroelectric Transition of a Chiral Molecular Crystal BINOL·2DMSO: T. Nomura, T. Yajima, Z. Yang, R. Kurihara, Y. Ishii, M. Tokunaga, Y. H. Matsuda, Y. Kohama, K. Kimura and T. Kimura, J. Phys. Soc. Jpn. **91**, 064702 (2022).

19. Quantum phase of the chromium spinel oxide $HgCr_2O_4$ in high magnetic fields: S. Kimura, S. Imajo, M. Gen, T. Momoi, M. Hagiwara, H. Ueda and Y. Kohama, Phys. Rev. B **105**, L180405 (2022).

Center of Computational Materials Science

Akai group

(1) The temperature dependence of intrinsic magnetic properties is one of the most important ingredients that determine the final performance of permanent magnets. In view of this, we have developed the methods that enable us to evaluate the magnetic properties under the influence of electron-magnon and electron-phonon scattering. (2) The hyperfine field distributions in the vicinity of the interface of Fe/MgO epitaxial films was detected layer by layer measurement using synchrotron Mössbauer source. We compare the experimental results with the first-principles calculation using KKR-CPA combined the optimized effective potential (OEP) method. The calculated hyperfine interactions provides important information about the electronic and lattice structure at the interfaces. (3) We have developed the method that enables us to calculate spin-wave dispersion and exchange stiffness of metallic magnet from first-principles. The exchange interactions between local spin density are calculated by Liechtenstein's method in the momentum space. The spin-wave dispersions are then directly calculated by diagonalizing the low energy effective Hamiltonian. (4) A new data assimilation methods that assimilate experimental and theoretical data obtained for permanent magnet materials. Based on a general framework for constructing a predictor from two data sets including missing values, a practical scheme for magnetic materials is formulated in which a small number of experimental data in limited composition space are integrated with a larger number of first-principles calculation data. Using this scheme we have evaluated the finite-temperature magnetization of permanent magnets over a high-dimensional composition space.

1. Spin-wave dispersion and exchange stiffness in $Nd_2Fe_{14}B$ and $RFe_{11}Ti$ (R=Y, Nd, Sm) from first-principles calculations: T. Fukazawa, H. Akai, Y. Harashima and T. Miyake, Phys. Rev. B **103**, 024418(1–7) (2021).

† Joint research with outside partners.

2. Direct observation of magnetic Friedel oscillation at Fe(001) surface: T. Mitsui, S. Sakai, S. Li, T. Ueno, T. Watanuki, Y. Kobayashi, R. Masuda, M. Seto and H. Akai, Hyperfine Interact **242**, 37 (2021).

3. Data assimilation method for experimental and first-principles data: Finite-temperature magnetization of (Nd, Pr, La, Ce)$_2$(Fe, Co, Ni)$_{14}$B: Y. Harashima, K. Tamai, S. Doi, M. Matsumoto, H. Akai, N. Kawashima, M. Ito, N. Sakuma, A. Kato, T. Shoji and T. Miyake, Phys. Rev. Materials **5**, 013806(1–10) (2021).

4. Atomistic theory of thermally activated magnetization processes in $Nd_2Fe_{14}B$ pemanent magnet: S. Miyashita, M. Nishino, Y. Toga, T. Hinokihara, I. E. Uysal, T. Miyake, H. Akai, S. Hirosawa and A. Sakuma, Science and Technology of Advanced Materials **22**, 658–682 (2021).

5. Understanding and optimization of hard magnetic compounds from first principles: T. Miyake, Y. Harashima, T. Fukazawa and H. Akai, Science and Technology of Advanced Materials **22**, 543–556 (2021).

6. 鉄の表面近傍の特異な磁性を発見—原子一層毎に磁気モーメントの大きさが増減する：三井 隆也，境誠 司，瀬戸 誠，赤井 久純，日本物理学会誌 **77**, 23-28 (2022).

7. First-principles investigation of Nd(Fe,M)$_{12}$ (M=k–Br) and Nd(Fe,Cr,Co,Ni,Ge,As): Possible enhancers of Curie temperature for $NdFe_{12}$ magnetic compounds: T. Fukazawa, H. Akai, Y. Harashima and T. Miyake, Acta Materialia **226**, 117597 (2022).

8. *Automatic exhaustive calculations of large material space by Korringa-Kohn-Rostoker coherent potential approximation method — Applied to equiatomic quaternary high entropy alloys: T. Fukushima, H. Akai, T. Chikyow and H. Kino, Pays. Rev. Mater. **6**, 023802(1-19) (2022).

Laser and Synchrotron Research Center

Kobayashi group

We are developing state-of-the-art laser system for laser processing and breath diagnosis. Process informatics is a new target to study.

1. *Direct generation of sub-picosecond pulse via multi-section gain switching: T. Nakamura, T. Ito, H. Nakamae, C. Kim, Y. Hazama, Y. Kobayashi, R. Kuroda and H. Akiyama, Opt. Lett. **46**, 1277 (2021).

2. レーザー加工の学理探索とデータ科学：小林 洋平，精密工学会誌 **87**, 601 (2021).

3. Independent contribution of optical attenuation length in ultrafast laser-induced structural change: T. Shibuya, K. Sakaue, H. Ogawa, D. Satoh, T.-H. Dinh, M. Ishino, M. Tanaka, M. Washio, T. Higashiguchi, M. Nishikino, A. Kon, Y. Kubota, Y. Inubushi, S. Owada, Y. Kobayashi and R. Kuroda, Opt. Express **29**, 33121 (2021).

4. 次世代レーザー及び加工の共通基盤技術開発：中里 智治，レーザー加工学会誌 **10**, 135 (2021).

5. Coherent control of acoustic phonons in a silica fiber using a multi-GHz optical frequency comb: M. Endo, S. Kimura, S. Tani and Y. Kobayashi, Commun Phys **4**, 73 (2021).

6. †Ultrafast laser processing of ceramics: Comprehensive survey of laser parameters: A. Narazaki, H. Takada, D. Yoshitomi, K. Torizuka and Y. Kobayashi, Journal of Laser Applications **33**, 012009 (2021).

7. †Fully Automated Data Acquisition for Laser Production Cyber-Physical System: Y. Kobayashi, T. Takahashi, T. Nakazato, H. Sakurai, H. Tamaru, K. Ishikawa, K. Sakaue and S. Tani, IEEE J. Select. Topics Quantum Electron. **27**, 1 (2021).

8. レーザー加工 CPS 開発：坂上 和之，田丸 博晴，小林 洋平，オプトロニクス **9**, 74 (2021).

9. † 次世代のモノづくり拠点を目指すレーザー加工プラットフォームとデータベース：中里 智治，高塚 肇，西林 一彦，田丸 博晴，小林 洋平，湯本 潤司，オプトロニクス **3**, 91 (2021).

10. Autonomous parameter optimization for femtosecond laser micro-drilling: K. Bamoto, H. Sakurai, S. Tani and Y. Kobayashi, Opt. Express **30**, 243 (2022).

11. Ultrafast laser ablation simulator using deep neural networks: S. Tani and Y. Kobayashi, Sci Rep **12**, 5837 (2022).

---

* Joint research among groups within ISSP.

12. Fiber lasers: Z. Z. K. Y. J. S, in: *Handbook of Laser Micro- and Nano-Engineering*, edited by Koji Sugioka, (Springer nature Switzerland, 2021), 1-32.

Harada group

We are developing instrumentation and exploring novel applications of soft X-ray emission spectroscopy in preparation for the next generation of synchrotron radiation. We discussed the segmented cross undulator as a novel polarization-controlled light source. Additionally, a soft X-ray CMOS image sensor with a wide dynamic range (WDR) is proposed (sxCMOS). We detected fully spin-polarized electronic states in the buried magnetic layer of Co_2MnSi, a prototype of semi-metallic Heusler alloys, using RIXS-MCD, as a pioneering application of the newly developed analytical approach. The minority-spin Fe-3d impurity band (IB) in (In,Fe)As, a typical n-type FMS, was studied using soft X-ray angle-resolved photoemission spectroscopy (SX-ARPES). The itinerant/localized nature of distinct dd excitations in TiO_2 nanocrystals with lattice multiphase was revealed by RIXS measurements on both Ti and O sites. In addition, various solutions and solid-liquid interfaces were investigated by RIXS. An isolated water molecule strongly interacting with an Li ion in a new high-salt concentration aqueous electrolyte solution "hydrate melt" was identified by RIXS and first-principles molecular dynamics simulation. RIXS of colloidal dispersions of multi-walled carbon nanotubes treated by solution plasma revealed the reconstruction of hydrogen-bonded network of water via orbital hybridization with the oxygen-containing functional groups generated by plasma treatment. In addition, we analyzed water encapsulated in the loop-shaped polyethylene glycol chain brushes and observed the absence of entropically-favored tetrahedrally coordinated water, which possibly regulates the biocompatibility.

1. †Minority-spin impurity band in n-type (In,Fe)As: A materials perspective for ferromagnetic semiconductors: M. Kobayashi, L. D. Anh, J. Minar, W. Khan, S. Borek, P. N. Hai, Y. Harada, T. Schmitt, M. Oshima, A. Fujimori, M. Tanaka and V. N. Strocov, Phys. Rev. B **103**, 115111 (1-10) (2021).

2. †Soft X-ray Emission Studies on Hydrate-Melt Electrolytes: T. Shimada, N. Takenaka, E. Watanabe, Y. Yamada, Y.-T. Cui, Y. Harada, M. Okubo and A. Yamada, J. Phys. Chem. B **125**, 11534-11539 (2021).

3. †Soft X-ray emission spectroscopy for the electronic state of water molecules influenced by plasma-treated multi-walled carbon nanotubes: N. Sakakibara, K. Inoue, S. Takahashi, T. Goto, T. Ito, K. Akada, J. Miyawaki, Y. Hakuta, K. Terashima and Y. Harada, Phys. Chem. Chem. Phys. **23**, 10468-10474 (2021).

4. A Global Shutter Wide Dynamic Range Soft X-Ray CMOS Image Sensor With Backside- Illuminated Pinned Photodiode, Two-Stage Lateral Overflow Integration Capacitor, and Voltage Domain Memory Bank: H. Shike, R. Kuroda, R. Kobayashi, M. Murata, Y. Fujihara, M. Suzuki, S. Harada, T. Shibaguchi, N. Kuriyama, T. Hatsui, J. Miyawaki, T. Harada, Y. Yamasaki, T. Watanabe, Y. Harada and S. Sugawa, IEEE Trans. Electron Devices **68**, 2056-2063 (2021).

5. †Detecting halfmetallic electronic structures of spintronic materials in a magnetic field: H. Fujiwara, R. Y. Umetsu, F. Kuroda, J. Miyawaki, T. Kashiuchi, K. Nishimoto, K. Nagai, A. Sekiyama, A. Irizawa, Y. Takeda, Y. Saitoh, T. Oguchi, Y. Harada and S. Suga, Sci Rep **11**, 18654 (1-9) (2021).

6. †*Fast and versatile polarization control of X-ray by segmented cross undulator at SPring-8: J. Miyawaki, S. Yamamoto, Y. Hirata, M. Horio, Y. Harada and I. Matsuda, AAPPS Bull. **31**, 25-1,-24 (2021).

7. †Hydrogen-Bonded Structure of Water in the Loop of Anchored Polyrotaxane Chain Controlled by Anchoring Density: K. Akada, K. Yamazoe, J. Miyawaki, R. Maeda, K. Ito and Y. Harada, Front. Chem. **9**, 743255 (1-8) (2021).

8. †Electronic surface reconstruction of TiO_2 nanocrystals revealed by resonant inelastic x-ray scattering: C.-H. Chuang, C.-M. Chen, Y.-C. Shao, P.-H. Yeh, C.-M. Chang, W.-F. Pong, M. Kapilashrami, P.-A. Glans, S. Gul, G. Wang, Y. Li, J. Zhang, J. Miyawaki, H. Niwa, Y. Harada, J.-M. Chen and J. Guo, Journal of Vacuum Science & Technology A **39**, 063204 (1-6) (2021).

9. †The Near Future of Synchrotron Radiation Operando Analysis : Development of Soft X-ray Absorption and Emission Spectroscopy for Functional Materials: Y. HARADA, Journal of the Japan Society for Precision Engineering **87**, 34-38 (2021).

10. † 放射光軟 X 線分光法によるリチウムイオン電池の電子状態オペランド計測：細野 英司 , 原田 慈久 , 朝倉 大輔 , 計測と制御 **60**, 207-212 (2021).

11. † 高分子内に入り込んだ水の電子状態観測：倉橋 直也 , 山添 康介 ,「【水】と機能性ポリマーに関する材料設計・最新応用」, 第 2 章 第 2 節 ,（株）技術情報協会 企画編集 , (（株）技術情報協会 , 2021), 42-52.

I. Matsuda group

† Joint research with outside partners.

The global pandemics of coronavirus disease (COVID-19) continued in 2021. We carried out research and user-supports with care at the beamline, SPring-8 BL07LSU. Since a project of the next-generation synchrotron radiation facility was launched, we participated devotedly in the construction and started technical developments, such as nano-focusing and scanning measurements. In the laboratory, we have succeeded in updating the soft X-ray non-linear optical effect into a spectroscopic method for materials science at X-ray free electron laser facility at SACLA.

1. Atomic arrangements of quasicrystal bilayer graphene: Interlayer distance expansion: Y. Fukaya, Y. Zhao, H.-W. Kim, J. R. Ahn, H. Fukidome and I. Matsuda, Phys. Rev. B **104**, L180202(1-5) (2021).

2. Polarization-Resolved Extreme-Ultraviolet Second-Harmonic Generation from $LiNbO_3$: C. B. Uzundal, S. Jamnuch, E. Berger, C. Woodahl, P. Manset, Y. Hirata, T. Sumi, A. Amado, H. Akai, Y. Kubota, S. Owada, K. Tono, M. Yabashi, J. W. Freeland, C. P. Schwartz, W. S. Drisdell, I. Matsuda, T. A. Pascal, A. Zong and M. Zuerch, Phys. Rev. Lett. **127**, 237402(1-8) (2021).

3. † ビスマス薄膜を通して「見る」表面物理学の新展開 : 伊藤 俊 , 松田 巌 , 日本物理学会誌 **76**, 566-574 (2021).

4. Recent Progress in Spectroscopies Using Soft X-ray Free-electron Lasers: I. Matsuda and Y. Kubota, Chem. Lett. **50**, 1336-1344 (2021).

5. †*Band Bending of n-GaN under Ambient H_2O Vapor Studied by X-ray Photoelectron Spectroscopy: Y. Imazeki, M. Sato, T. Takeda, M. Kobayashi, S. Yamamoto, I. Matsuda, J. Yoshinobu, M. Sugiyama and Y. Nakano, J. Phys. Chem. C **125**, 9011 (2021).

6. †*Comparative Study of H_2O and O_2 Adsorption on the GaN Surface: M. Sato, Y. Imazeki, T. Takeda, M. Kobayashi, S. Yamamoto, I. Matsuda, J. Yoshinobu, Y. Nakano and M. Sugiyama, J. Phys. Chem. C **125**, 25807 (2021).

7. †*Femtosecond Charge Density Modulations in Photoexcited $CuWO_4$: Y. Uemura, A. S. M. Ismail, S. H. Park, S. Kwon, M. Kim, Y. Niwa, H. Wadati, H. Elnaggar, F. Frati, T. Haarman, N. Höppel, N. Huse, Y. Hirata, Y. Zhang, K. Yamagami, S. Yamamoto, I. Matsuda, T. Katayama, T. Togashi, S. Owada, M. Yabashi, U. Halisdemir, G. Koster, T. Yokoyama, B. M. Weckhuysen and F. M. F. D. Groot, J. Phys. Chem. C **125**, 7329 (2021).

8. Influence of Stacking Order of Phthalocyanine and Fullerene Layers on the Photoexcited Carrier Dynamics in Model Organic Solar Cell: K. Ozawa, S. Yamamoto, T. Miyazawa, K. Yano, K. Okudaira, K. Mase and I. Matsuda, J. Phys. Chem. C **125**, 13963-13970 (2021).

9. Extreme Ultraviolet Second Harmonic Generation Spectroscopy in a Polar Metal: E. Berger, S. Jamnuch, C. B. Uzundal, C. Woodahl, H. Padmanabhan, A. Amado, P. Manset, Y. Hirata, Y. Kubota, S. Owada, K. Tono, M. Yabashi, C. Wang, Y. Shi, V. Gopalan, C. P. Schwartz, W. S. Drisdell, I. Matsuda, J. W. Freeland, T. A. Pascal and M. Zuerch, Nano Lett. **21**, 6095-6101 (2021).

10. A novel measurement approach for near-edge x-ray absorption fine structure: Continuous 2 π angular rotation of linear polarization: Y. Kudo, Y. Hirata, M. Horio, M. Niibe and I. Matsuda, Nuclear Instruments and Methods in Physics Research Section A: Accelerators, Spectrometers, Detectors and Associated Equipment **1018**, 165804(1-5) (2021).

11. †Electronic structure of a borophene layer in rare-earth aluminum/chromium boride and its hydrogenated derivative borophane: M. Niibe, M. Cameau, N. T. Cuong, O. I. Sunday, X. Zhang, Y. Tsujikawa, S. Okada, K. Yubuta, T. Kondo and I. Matsuda, Phys. Rev. Materials **5**, 084007-1,-8 (2021).

12. †Valence Fluctuations in Yb(Al,Fe)B_4 Studied by Nanosecond-time-resolved Photoemission Spectroscopy Using Synchrotron Radiation: M. Okawa, K. Akikubo, S. Yamamoto, I. Matsuda and T. Saitoh, e-J. Surf. Sci. Nanotechnol. **19**, 20-23 (2021).

13. *Ultrafast optical stress on $BaFe_2As_2$: T. Suzuki, Y. Kubota, A. Nakamura, T. Shimojima, K. Takubo, S. Ito, K. Yamamoto, S. Michimae, H. Sato, H. Hiramatsu, H. Hosono, T. Togashi, M. Yabashi, H. Wadati, I. Matsuda, S. Shin and K. Okazaki, Phys. Rev. Research **3**, 033222 (2021).

14. †*Fast and versatile polarization control of X-ray by segmented cross undulator at SPring-8: J. Miyawaki, S. Yamamoto, Y. Hirata, M. Horio, Y. Harada and I. Matsuda, AAPPS Bull. **31**, 25(1-24) (2021).

15. *Environmental effects on layer-dependent dynamics of Dirac fermions in quasicrystalline bilayer graphene: Y. Zhao, T. Suzuki, T. Iimori, H. -W. Kim, J. R. Ahn, M. Horio, Y. Sato, Y. Fukaya, T. Kanai, K. Okazaki, S. Shin, S. Tanaka, F. Komori, H. Fukidome and I. Matsuda, Phys. Rev. B **105**, 115304 (2022).

16. *Photoinduced transient states of antiferromagnetic orderings in $La_{1/3}Sr_{2/3}FeO_3$ and $SrFeO_{3-\delta}$ thin films observed through time-resolved resonant soft x-ray scattering: K. Yamamoto, T. Tsuyama, S. Ito, K. Takubo, I. Matsuda, N. Pontius, C. Schüßler-Langeheine, M. Minohara, H. Kumigashira, Y. Yamasaki, H. Nakao, Y. Murakami, T. Katase, T.

* Joint research among groups within ISSP.

Kamiya and H. Wadati, New J. Phys. **24**, 043012(1-9) (2022).

17. †*Functionalization of the MoS_2 basal plane for activation of molecular hydrogen by Pd deposition: F. Ozaki, S. Tanaka, W. Osada, K. Mukai, M. Horio, T. Koitaya, S. Yamamoto, I. Matsuda and J. Yoshinobu, Applied Surface Science **593**, 153313 (2022).

18. †*Hydrogen absorption and diffusion behaviors in cube-shaped palladium nanoparticles revealed by ambient-pressure X-ray photoelectron spectroscopy: J. Tang, O. Seo, D. S. R. Rocabado, T. Koitaya, S. Yamamoto, Y. Nanba, C. Song, J. Kim, A. Yoshigoe, M. Koyama, S. Dekura, H. Kobayashi, H. Kitagawa, O. Sakata, I. Matsuda and J. Yoshinobu, Applied Surface Science **587**, 152797 (2022).

19. Separating Non-linear Optical Signals of a Sample from High Harmonic Radiation in a Soft X-ray Free Electron Laser: T. Sumi, M. Horio, T. Senoo, T. Wada, Y. Tsujikawa, X. Zhang, P. Manset, M. Araki, Y. Hirata, W. S. Drisdell, J. W. Freeland, A. Amado, M. Zuerch, Y. Kubota, S. Owada, K. Tono, M. Yabashi, C. P. Schwartz and I. Matsuda, e-J. Surf. Sci. Nanotechnol. **20**, 31(1-5) (2022).

20. Electronic Structures of Polymorphic Layers of Borophane: I. Tateishi, X. Zhang and I. Matsuda, Molecules **27**, 1808(1-13) (2022).

21. †Measurement of X-ray Magnetic Linear Dichroism by Rotating Polarization Angle of Soft X-ray Generated by a Segmented Undulator: Y. Kudo, M. Horio, Y. Hirata, T. Ohkochi, T. Kinoshita and I. Matsuda, e-Journal of Surface Science and Nanotechnology (2022), accepted for publication.

22. 2D boron: Boraphene, Borophene, Boronene: I. Matsuda and K. Wu ed., (Springer Nature, Switzerland, 2021).

23. 物理科学，この 1 年　2022: 松田 巌 , 近藤 剛弘他 , (丸善出版 , 東京都千代田区 , 2022).

Itatani group

Advancements in soft x-ray attosecond spectroscopy and attosecond beamlines were also continued. First, quantum mechanical simulation revealed that the 2ω oscillations observed in a triatomic molecule (N_2O) arise from tunnel ionization of core-excited states, leading to a new understanding of transient absorption spectroscopy using soft x-ray attosecond pulses. Second, a water flat-jet system was developed for transient soft X-ray spectroscopy of liquids and solvents. High-order harmonics coupled with molecular vibrations were observed upon irradiation of intense mid-infrared pulses. Further experiments are now underway to elucidate molecular dynamics. Third, high-field electron scattering experiments were performed, and the cutoff behavior was successfully discussed in terms of quantum theory. Finally, a new infrared parametric light source using a Yb-based solid-state laser was developed, and phase-stable sub-30 fs pulses were obtained at repetition rates of 10 kHz and 100 kHz. In addition, a Yb-based solid-state laser was used to generate 6-eV pulses for angle-resolved photoemission spectroscopy.

1. *High-harmonic generation in GaAs beyond the perturbative regime: P. Xia, T. Tamaya, C. Kim, F. Lu, T. Kanai, N. Ishii, J. Itatani, H. Akiyama and T. Kato, Phys. Rev. B **104**, L121202(1-6) (2021).

2. †Observation of the quantum shift of a backward rescattering caustic by carrier-envelope phase mapping: T. Mizuno, N. Ishii, T. Kanai, P. Rosenberger, D. Zietlow, M. F. Kling, O. I. Tolstikhin, T. Morishita and J. Itatani, Phys. Rev. A **103**, 043121 (2021).

3. *Optical parametric amplification of phase-stable terahertz-to-mid-infrared pulses studied in the time domain: N. Kanda, N. Ishii, J. Itatani and R. Matsunaga, Optics Express **29**, 3479-3489 (2021).

4. †Time-domain spectroscopy of optical parametric amplification for phase-stable terahertz-to-midinfrared pulses: N. Kanda, N. Ishii, J. Itatani and R. Matsunaga, Optics Express **29(3)**, 3479-3489 (2021).

5. †Magnetic Domain Control of $ErFeO_3$ by Intense Terahertz Free Electron Laser Pulses: M. Nakajima, G. Isoyama and T. Kurihara, IEEE Trans. on Plasma Sci **49**, 3344-3350 (2021).

6. Attosecond electronic dynamics of core-excited states of N_2O in the soft x-ray region,: N. Saito, N. Douguet, H. Sannohe, N. Ishii, T. Kanai, Y. Wu, A. Chew, S. Han, B. I. Schneider, J. Olsen, L. Argenti, Z. Chang and J. Itatani, Phys. Rev. Res. **3**, 043222(1-8) (2021).

7. *Photo-Excitation Band-Structure Engineering of 2*H*-$NbSe_2$ Probed by Time- and Angle-Resolved Photoemission Spectroscopy: M. Watanabe, T. Suzuki, T. Someya, Y. Ogawa, S. Michimae, M. Fujisawa, T. Kanai, J. Itatani, T. Saitoh, S. Shin and K. Okazaki, J. Phys. Soc. Jpn. **91**, 064703 (2022).

8. †Ultrafast multidimensional spectroscopy with field resolution and noncollinear geometry at mid-infrared frequencies: T. Deckert, J. Allerbeck, T. Kurihara and D. Brida, New J. Phys. **24**, 023005(1-9) (2022).

† Joint research with outside partners.

9. †Spin canting in nonlinear terahertz magnon dynamics revealed by magnetorefractive probing in orthoferrite: T. Kurihara, M. Bamba, H. Watanabe, M. Nakajima and T. Suemoto, arXiv **2202**, 11365 (2022).

Kondo group

We gave the evidence for a higher-order topological insulator in a three-dimensional material built from van der Waals stacking of bismuth-halide chains and visualized the strain-induced topological phase transition in a quasi-one-dimensional superconductor $TaSe_3$.

1. Reduced Hall carrier density in the overdoped strange metal regime of cuprate supercond.: C. Putzke, S. Benhabib, W. Tabis, J. Ayres, Z. Wang, L. Malone, S. Licciardello, J. Lu, T. Kondo, T. Takeuchi, N. E. Hussey, J. R. Cooper and A. Carrington, Nature Phys. **17**, 826-831 (2021).
2. *Observation and control of the weak topological insulator state in $ZrTe_5$: P. Zhang, R. Noguchi, K. Kuroda, C. Lin, K. Kawaguchi, K. Yaji, A. Harasawa, M. Lippmaa, S. Nie, H. Weng, V. Kandyba, A. Giampietri, A. Barinov, Q. Li, G. D. Gu, S. Shin and T. Kondo, Nat. Commun. **12**, 406 (2021).
3. Anomalous vortex liquid in charge-ordered cuprate superconductors: Y.-T. Hsu, M. Berben, M. culo, S. Adachi, T. Kondo, T. Takeuchi, Y. Wang, S. Wiedmann, S. M. Hayden and N. E. Hussey, Proc. Natl. Acad. Sci. U.S.A. **118**, e2016275118(1-6) (2021).
4. *Evidence for a higher-order topological insulator in a three-dimensional material built from van der Waals stacking of bismuth-halide chains: R. Noguchi, M. Kobayashi, Z. Jiang, K. Kuroda, T. Takahashi, Z. Xu, D. Lee, M. Hirayama, M. Ochi, T. Shirasawa, P. Zhang, C. Lin, C. Bareille, S. Sakuragi, H. Tanaka, S. Kunisada, K. Kurokawa, K. Yaji, A. Harasawa, V. Kandyba, A. Giampietri, A. Barinov, T. K. Kim, C. Cacho, M. Hashimoto, D. Lu, S. Shin, R. Arita, K. Lai, T. Sasagawa and T. Kondo, Nature Materials **20**, 473-479 (2021).
5. *Visualization of the strain-induced topological phase transition in a quasi-one-dimensional superconductor $TaSe_3$: C. Lin, M. Ochi, R. Noguchi, K. Kuroda, M. Sakoda, A. Nomura, M. Tsubota, P. Zhang, C. Bareille, K. Kurokawa, Y. Arai, K. Kawaguchi, H. Tanaka, K. Yaji, A. Harasawa, M. Hashimoto, D. Lu, S. Shin, R. Arita, S. Tanda and T. Kondo, Nature Materials **20**, 1093-1099 (2021).
6. *Scaling law for Rashba-type spin splitting in quantum-well films: R. Noguchi, K. Kuroda, M. Kawamura, K. Yaji, A. Harasawa, T. Iimori, S. Shin, F. Komori, T. Ozaki and T. Kondo, Phys. Review B **103**, 180409(1-6) (2021).
7. *Multipole polaron in the devil's staircase of CeSb: Y. Arai, K. Kuroda, T. Nomoto, Z. H. Tin, S. Sakuragi, C. Bareille, S. Akebi, K. Kurokawa, Y. Kinoshita, W. -L. Zhang, S. Shin, M. Tokunaga, H. Kitazawa, Y. Haga, H. S. Suzuki, S. Miyasaka, S. Tajima, K. Iwasa, R. Arita and T. Kondo, Nat. Mater. **21**, 410(1-7) (2022).
8. Large anomalous Hall effect induced by weak ferromagnetism in the noncentrosymmetric antiferromagnet $CoNb_3S_6$: H. Tanaka, S. Okazaki, K. Kuroda, R. Noguchi, Y. Arai, S. Minami, S. Ideta, K. Tanaka, D. Lu, M. Hashimoto, V. Kandyba, M. Cattelan, A. Barinov, T. Muro, T. Sasagawa and T. Kondo, Phys. Review B **105**, 121102(1-7) (2022).
9. *Selective observation of surface and bulk bands in polar WTe_2 by laser-based spin- and angle-resolved photoemission spectroscopy.: Y. Wan, L. Wang, K. Kuroda, P. Zhang, K. Koshiishi, M. Suzuki, J. Kim, R. Noguchi, C. Bareille, K. Yaji, A. Harasawa, S. Shin, S.-W. Cheong, A. Fujimori and T. Kondo, Phys. Review B **105**, 085421 (2022).
10. *Visualization of optical polarization transfer to photoelectron spin vector emitted from a spin-orbit coupled surface state.: K. Kuroda, K. Yaji, R. Noguchi, A. Harasawa, S. Shin, T. Kondo and F. Komori, Phys. Review B **105**, 121106(1-6) (2022).

Matsunaga group

We have investigated light-matter interactions and light-induced nonequilibrium phenomena in solids by utilizing terahertz (THz) pulse. By using a Yb-based laser system and the multiplate broadening scheme, we realized phase-stable broadband multiterahertz pulses (10-45 THz, 40-180 meV, or 7-30 μm) with the pulse width of 28 fs. By using the multiterahertz pulse for time-resolved detection of complex response functions, we have investigated ultrafast dynamics of the photoexcited electrons in a 3D Dirac semimetal Cd_3As_2. We also demonstrate that a large reduction of the refractive index by 80% dominates the nonequilibrium infrared response of the Dirac semimetal, which can be utilized for designing ultrafast switches in active optoelectronics.

1. * ワイル反強磁性金属 Mn_3Sn 薄膜の室温テラヘルツ異常ホール効果：松田 拓也 , 肥後 友也 , 神田 夏輝 , 松永 隆佑 , 応

* Joint research among groups within ISSP.

用物理 **90**, 752 (2021).

2. テラヘルツパルス技術で拓く物性物理学と新奇機能性：松永 隆佑 , レーザー研究 **49**, 325 (2021).

3. *Optical parametric amplification of phase-stable terahertz-to-mid-infrared pulses studied in the time domain: N. Kanda, N. Ishii, J. Itatani and R. Matsunaga, Optics Express **29**, 3479-3489 (2021).

4. Topological Materials for Functional Optoelectronic Devices: H. Chorsi, B. Cheng, B. Zhao, J. Toudert, V. Asadchy, O. F. Shoron, S. Fan and R. Matsunaga, Advanced Functional Materials **32**, 2110655 (2022).

5. *Tracking Ultrafast Change of Multiterahertz Broadband Response Functions in a Photoexcited Dirac Semimetal Cd_3As_2 Thin Film: N. Kanda, Y. Murotani, T. Matsuda, M. Goyal, S. Salmani-Rezaie, J. Yoshinobu, S. Stemmer and R. Matsunaga, Nano Letters **22**, 2358 (2022).

Okazaki group

We have investigated superconducting-gap structures of unconventional superconductors by a low-temperature and high-resolution laser ARPES apparatus and transient electronic structures in photo-excited non-equilibrium states by a time-resolved ARPES apparatus using EUV and SX lasers. In the academic year 2021, we have revealed the two-fold symmetric superconducting gap of $FeSe_{0.78}S_{0.22}$ irrespective of its four-fold symmetric crystal structure by high-resolution laser ARPES. In addition, we have revealed a characteristic electron-phonon coupling during the photo-induced insulator-to-metal transition in 1*T*-TaS_2 from the FDARPES measurements by using HHG laser time-resolved ARPES.

1. *Detecting electron-phonon coupling during photoinduced phase transition: T. Suzuki, Y. Shinohara, Y. Lu, M. Watanabe, J. Xu, K. L. Ishikawa, H. Takagi, M. Nohara, N. Katayama, H. Sawa, M. Fujisawa, T. Kanai, J. Itatani, T. Mizokawa, S. Shin and K. Okazaki, Phys. Rev. B **103**, L121105 (2021).

2. *Ultrafast optical stress on $BaFe_2As_2$: T. Suzuki, Y. Kubota, A. Nakamura, T. Shimojima, K. Takubo, S. Ito, K. Yamamoto, S. Michimae, H. Sato, H. Hiramatsu, H. Hosono, T. Togashi, M. Yabashi, H. Wadati, I. Matsuda, S. Shin and K. Okazaki, Phys. Rev. Research **3**, 033222 (2021).

3. Discovery of Pressure-Induced Superconductivity in an Excitonic Insulator: K. Okazaki, JPSJ News Comments **18**, 11 (2021).

4. *Photo-Excitation Band-Structure Engineering of 2*H*-$NbSe_2$ Probed by Time- and Angle-Resolved Photoemission Spectroscopy: M. Watanabe, T. Suzuki, T. Someya, Y. Ogawa, S. Michimae, M. Fujisawa, T. Kanai, J. Itatani, T. Saitoh, S. Shin and K. Okazaki, J. Phys. Soc. Jpn. **91**, 064703 (2022).

5. *Environmental effects on layer-dependent dynamics of Dirac fermions in quasicrystalline bilayer graphene: Y. Zhao, T. Suzuki, T. Iimori, H. -W. Kim, J. R. Ahn, M. Horio, Y. Sato, Y. Fukaya, T. Kanai, K. Okazaki, S. Shin, S. Tanaka, F. Komori, H. Fukidome and I. Matsuda, Phys. Rev. B **105**, 115304 (2022).

6. HHG-laser-based time- and angle-resolved photoemission spectroscopy of quantum materials: T. Suzuki, S. Shin and K. Okazaki, Journal of Electron Spectroscopy and Related Phenomena **251**, 147105 (2021).

Kimura group

In FY2021, the Kimura group worked on the development of in-situ imaging techniques for mixing reactions of solution samples using the X-ray free-electron laser at SACLA and microscopic imaging techniques using soft X-rays at BL07LSU of SPring-8. In the experiment at SACLA, we succeeded in imaging nanoparticle structures in a mixed solution at sub-10-nanometer resolution; in the experiment at SPring-8 BL07LSU, we constructed a soft x-ray ptychography system using total-reflection Wolter mirror optics.

1. Copper electroforming replication process for soft x-ray mirrors: G. Yamaguchi, H. Motoyama, S. Owada, Y. Kubota, S. Egawa, T. Kume, Y. Takeo, M. Yabashi and H. Mimura, Review of Scientific Instruments **92**, 123106 (2021).
2. Current status of development of electroforming process for high precision soft x-ray mirrors: T. Kume, G. Yamaguchi, K. Hiraguri, Y. Matsuzawa, Y. Imamura, H. Miyashita, T. Saito, Y. Takeo, Y. Senba, H. Kishimoto, H. Ohashi, H. Hashizume, H. Mimura, C. Morawe, A. M. Khounsary and S. Goto, Proc. of SPIE **11837**(1-5) (2021).
3. Development of figure correction system for axisymmetric x-ray mirrors: S. Yokomae, Y. Takeo, T. Shimamura, Y. Matsuzawa, T. Kume, Y. Senba, H. Kishimoto, H. Ohashi, H. Mimura, C. Morawe, A. M. Khounsary and S. Goto, Proc. of SPIE **11837**(1-7) (2021).
4. Electrodeposition simulation for fabricating Wolter mirrors of x-ray telescopes: A. Ito, G. Yamaguchi, T. Watanabe, Y.

† Joint research with outside partners.

Takeo, T. Kume, Y. Matsuzawa, T. Saito, K. Hiraguri, K. Tamura, A. Takigawa, T. Kanoh, N. Ishida, I. Mitsuishi, H. Hashizume, H. Mimura, C. Morawe, A. M. Khounsary and S. Goto, Proc. of SPIE **11837**(1-9) (2021).
5. An arrayed-window microfluidic device for observation of mixed nanoparticles with an X-ray free-electron laser: Y. Matsumoto, Y. Takeo, S. Egawa, G. Yamaguchi, S. Yokomae, M. Takei, H. Yumoto, T. Koyama, H. Ohashi, K. Tono, M. Yabashi, H. Mimura and T. Kimura, Opt Rev **29**, 7 (2022).

* Joint research among groups within ISSP.

Subject of Joint Research

2021年度　共同利用課題一覧（前期）/ Joint Research List 2021 (First Term)

2021年度　共同利用課題一覧（後期）/ Joint Research List (Latter Term)

2021年度　中性子科学研究施設　共同利用課題一覧 / Joint Research List of Neutron Scattering Research Project 2021

2021年度　軌道放射物性研究施設 共同利用課題一覧 / Joint Research List of Synchrotron Radiation Research Project 2021

2021年度　スーパーコンピュータ共同利用課題一覧 / Joint Research List of Supercomputer System 2021

2021年度　CCMSスパコン共用事業枠課題一覧 / Supercomputing Consortium for Computational Materials Science Project List of Supercomputer System 2021

嘱託課題 / Commission Research Project

No.	課題番号	課題名	氏名	所属	分担者	Title	Name	Organization	Member of research project	担当所員
1	202012-CMBXX-0036	スピン偏極走査トンネル顕微鏡測定の安定動作手法の開発	吉田 靖雄	金沢大学		Development of stable measurements of spin-polarized scanning tunneling microscopy	Yasuo Yoshida	Kanazawa University		長谷川 幸雄
2	202012-CMBXX-0021	高圧下X線回折法の開発	江藤 徹二郎	久留米工業大学		Development of High Pressure X-ray diffraction measurements	Tetsujiro Eto	Kurume Institute of Technology		上床 美也
3	202012-CMBXX-0022	低次元有機物質の圧力下物性研究	糸井 充穂	日本大学		Study on pressure induced superconductivity of low dimension organic conductor	Miho Itoi	Nihon University		上床 美也
4	202012-CMBXX-0025	中性子回折用圧力発生装置の開発	宗像 孝司	総合科学研究機構　中性子科学センター		Development of high pressure apparatus for neutron diffraction	Koji Munakata	Comprehensive Research Organization for Science and Society, Neutron Science and Technology Center		上床 美也
5	202012-CMBXX-0026	希釈冷凍機温度で使用可能な10 GPa級超高圧発生装置の開発	松林 和幸	電気通信大学		Development of 10 GPa class high pressure apparatus for low temperature	Kazuyuki Matsubayashi	The University of Electro-Communications		上床 美也
6	202012-CMBXX-0027	高圧下量子振動観測システムの開発	摂待 力生	新潟大学		Development of quantum oscillation under high pressure	Rikio Settai	Niigata University		上床 美也
7	202012-CMBXX-0028	酸化物試料の作製と高圧下物性測定	川中 浩史	産業技術総合研究所		Sample preparation and high pressure experiments	Hirofumi Kawanaka	National Institute of Advanced Industrial Science and Technology		上床 美也
8	202012-CMBXX-0029	極低温下の磁気特性	鳥塚 潔	日本工業大学		Development of magnetic measurement method	Kiyoshi Torizuka	Nippon Institute of Technology		上床 美也
9	202012-CMBXX-0030	圧力下NMR測定法に関する開発	藤原 直樹	京都大学		Development of NMR measurement method under high pressure	Naoki Fujiwara	Kyoto University		上床 美也
10	202012-CMBXX-0033	有機伝導体の圧力効果	村田 惠三	大阪市立大学		Effect of pressure on the organic conductor	Keizo Murata	Osaka City University		上床 美也
11	202012-CMBXX-0034	トンネル分光による高圧下物性測定法の開発	本山 岳	島根大学		Development of high pressure measurement for tunneling spectroscopy	Gaku Motoyama	Shimane University		上床 美也
12	202012-CMBXX-0035	多重極限関連圧力装置の調整	高橋 博樹	日本大学		Adjustment of Cubic Anvil apparatus	Hiroki Takahashi	Nihon University		上床 美也
13	202102-CMBXX-0049	4Gにおける共同利用推進	佐藤　卓	東北大学		Research and Support of General-Use at 4G	Taku J Sato	Tohoku University		眞弓 皓一
14	202102-CMBXX-0050	4Gにおける共同利用推進	奥山　大輔	東北大学		Research and Support of General-Use at 4G	Daisuke Okuyama	Tohoku University		眞弓 皓一
15	202102-CMBXX-0056	4Gにおける共同利用推進	横山　淳	茨城大学		Research and Support of General-Use at T1-1	Makoto Yokoyama	Ibaraki University		眞弓 皓一
16	202102-CMBXX-0071	4Gにおける共同利用推進	坂倉　輝俊	東北大学		Research and Support of General-Use at T2-2 and T1-3	Terutoshi Sakakura	Tohoku University		眞弓 皓一
17	202012-CMBXX-0010	高分解能光電子分光による強相関物質の研究	横谷 尚睦	岡山大学		ultra-high resolution study on strongly correlated materials	Takayoshi Yokoya	Okayama University		近藤 猛
18	202012-CMBXX-0011	有機化合物の光電子分光	金井 要	東京理科大学		Photoemission study on organic compounds	Kaname Kanai	Tokyo University of Science		近藤 猛
19	202012-CMBXX-0018	トポロジカル超伝導体の探索	坂野 昌人	東京大学		Search for topological insulators	Masato Sakano	The University of Tokyo		近藤 猛

20	202012-CMBXX-0043	レーザースピン角度分解光分光による表面電子状態の研究	矢治 光一郎	物質・材料研究機構		SARPES studies of atomic layer materials at surfaces	Koichiro Yaji	National Institute for Materials Science		近藤 猛
21	202012-CMBXX-0016	60-eVレーザーを用いた時間分解光電子分光の開発	石坂 香子	東京大学		The development of time-resolved photoemission using 60eV laser	Kyoko Ishizaka	The University of Tokyo		岡﨑 浩三
22	202012-CMBXX-0042	鉄系超伝導体のレーザー光電子分光	下志万 貴博	理化学研究所　創発物性科学研究センター		Laser-ARPES on Fe superconductor	Takahiro Shimojima	RIKEN Center for Emergent Matter Science		岡﨑 浩三
23	202012-CMBXX-0002	三次元nanoESCAによる実デバイスのオペランド電子状態解析	永村 直佳	物質・材料研究機構		Operando analysis of the electronic structure of actual devices by 3DnanoESCA	Naoka Nagamura	National Institute for Materials Science		原田 慈久
24	202012-CMBXX-0006	軟Ｘ線発光・共鳴非弾性散乱分光の磁気円・線二色性測定システムの構築	菅 滋正	大阪大学産業科学研究所		Construction of a noble system for circular and linear dichroism in soft X-ray emission and　RIXS spectroscopy	Shigemasa Suga	ISIR, Osaka University		原田 慈久
25	202012-CMBXX-0007	高分解能光電子分光による酸化バナジウムの研究	藤原 秀紀	大阪大学		Study on vanadium oxides by high resolution Photoemission	Hidenori Fujiwara	Osaka University		原田 慈久
26	202012-CMBXX-0044	不均一触媒反応のオペランド光電子分光測定	小板谷 貴典	自然科学研究機構　分子科学研究所		Operando photoelectron spectroscopy of heterogeneous catalysts	Takanori Koitaya	National Institutes of Natural Sciences, Institute for Molecular Science		松田 巌
27	202012-CMBXX-0045	偏光制御型軟X線分光装置の開発	平田 靖透	防衛大学校		Developing a system for the polarization-controlled soft X-ray spectroscopy	Yasuyuki Hirata	National Defense Academy of Japan		松田 巌
28	202012-CMBXX-0047	雰囲気光電子分光装置の高度化	山本 達	東北大学　国際放射光イノベーション・スマート研究センター		Updates of the NAP-XPS machine	Susumu Yamamoto	Tohoku University, International Center for Synchrotron Radiation Innovation Smart		松田 巌
29	202104-CMBXX-0073	ESM-RISM法を実装したQuantum ESPRESSOの高度化	萩原 聡	筑波大学　計算科学研究センター		Improvement of Quantum ESPRESSO implementing the ESM-RISM method	Satoshi Hagiwara	Tsukuba University, Center for Computational Sciences		川島　直輝
30	202108-CMBXX-0147	光スピントロニクスに向けたスピン軌道ダイナミクスの研究	黒田 健太	広島大学		Studying spin-orbit dynamics for opt-spintronics	Kenta Kuroda	Hiroshima University		近藤 猛

一般課題 / General Research Project

No.	課題番号	課題名	氏名	所属	分担者	Title	Name	Organization	Member of research project	担当所員
1	202012-GNBXX-0045	双性イオン型新規中性ラジカル分子結晶の磁性・電気伝導性の解明	上田 顕	熊本大学	末棟 太朗	Elucidation of magnetic and electrical properties of novel zwitterionic neutral radical crystals	Akira Ueda	Kumamoto University	Taro Suemune	森 初果
2	202012-GNBXX-0075	高配向機能性分子層の合成によるプロトン－電子相関二分子膜の探求	加藤 浩之	大阪大学	棟安 陸	Study of proton-electron correlated bilayers by synthesis of highly oriented functional monolayer	Hiroyuki S. Kato	Osaka University	Riku Muneyasu	森 初果
3	202012-GNBXX-0030	重い電子系希土類化合物における異方的量子臨界現象の磁気的評価	河野 洋平	中央大学	橘高 俊一郎	Magnetic properties of anisotropic quantum critical phenomena in a heavy-fermion metal	Yohei Kono	Chuo University	Shunichiro Kittaka	山下 穣
4	202012-GNBXX-0074	アクチナイド系スピン三重項超伝導体における極低温磁化・熱膨張・磁歪測定	清水 悠晴	東北大学		Magnetization and thermal expansion measurements for actinide spin-triplet superconductors	Yusei Shimizu	Tohoku University		山下 穣
5	202012-GNBXX-0068	二次元銅酸化物のホール係数測定IV	神戸 士郎	山形大学	川村 桂太	Hall coefficient measurement of 2D cuprates (IV)	Shiro Kambe	Yamagata University	Keita Kawamura	勝本 信吾

6	202011-GNBXX-0010	真空転写法により形成したツイストグラフェンのSTM/STSによる構造・電子状態評価	田中 悟	九州大学	Visikovskiy Anton	Evaluation of structural and electronic states using STM/STS of twisted graphene fabricated by vacuum transfer technique	Satoru Tanaka	Kyushu University	Visikovskiy Anton Kyushu University	長谷川 幸雄
7	202012-GNBXX-0065	Si(110)3×2-Bi表面の原子構造	中辻 寛	東京工業大学	大内 拓実	Atomic structure of Si(110)3×2-Bi surface	Kan Nakatsuji	Tokyo Institute of Technology	Takumi Ouchi Tokyo Institute of Technology	長谷川 幸雄
8	202012-GNBXX-0086	超伝導ダイアモンド薄膜ー強磁性薄膜接合系の超伝導および磁性の直接観察	吉田 靖雄	金沢大学		Low-temperature STM study on a ferromagnet-superconducting diamond hybrid system	Yasuo Yoshida	Kanazawa University		長谷川 幸雄
9	202011-GNBXX-0021	基板での原子クラスター構造選別法の確立と, クラスター構造と磁性の関係の解明	塚原 規志	群馬工業高等専門学校		Establishment of selection method for atomic clusters on the substrate and elucidation of the relation between the cluster structure and its magnetic properties	Noriyuki Tsukahara	National Institute of Technology, Gunma College		吉信 淳
10	202012-GNBXX-0064	微傾斜Si(111)√3×√3-B基板上に成長したBi(110)超薄膜の電子状態	中辻 寛	東京工業大学	大内 拓実 小森 文夫	Electronic structure of Bi(110) thin films grown on vicinal Si(111)√3×√3-B substrates	Kan Nakatsuji	Tokyo Institute of Technology	Takumi Ouchi Fumio Komori	吉信 淳
11	202012-GNBXX-0066	窒素吸着Cu(001)表面におけるBi薄膜の成長と電子状態	中辻 寛	東京工業大学	永友 慶 森井 七生 小森 文夫	Growth process of Bi thin-film on nitrogen adsorbed Cu(001) surface and its electronic structure	Kan Nakatsuji	Tokyo Institute of Technology	Kei Nagatomo Morii Nanao Fumio Komori	吉信 淳
12	202011-GNBXX-0002	D-luciferin類似体を用いた絶対発光スペクトル測定	樋山 みやび	群馬大学	高橋 由太翔	Study for absolute emission spectra of D-luciferin analog	Miyabi Hiyama	Gunma University	Takahashi Yutaka	秋山 英文
13	202011-GNBXX-0003	DEACM-ケージドルシフェリンの光解離における高効率波長の調査	樋山 みやび	群馬大学	工藤 優斗	Study for photocleave wavelength of DEACM caged D-Luciferin	Miyabi Hiyama	Gunma University	Kudo Yuto	秋山 英文
14	202011-GNBXX-0004	新奇ケージド化合物の分光的特性の研究	樋山 みやび	群馬大学	勝見 渓太	Study of spectroscopic property for a new caged compound	Miyabi Hiyama	Gunma University	Katsumi Keita	秋山 英文
15	202012-GNBXX-0023	窒素デルタドープGaAs中の等電子トラップによる励起子分子発光の面方位依存性	矢口 裕之	埼玉大学	高宮 健吾 矢野 裕子	Surface orientation dependence of biexciton emission from isoelectronic traps in N delta-doped GaAs	Hiroyuki Yaguchi	Saitama University	Kengo Takamiya Yuko Yano	秋山 英文
16	202012-GNBXX-0012	Si基板上L10規則型CoPtナノロッドの磁化測定	山浦 淳一	東京工業大学	遠山 諒 真島 豊	Magnetization measurement of L10-ordered CoPt nanorods on Si substrates	Junichi Yamaura	Tokyo Institute of Technology	Ryo Toyama Yutaka Majima	広井 善二
17	202012-GNBXX-0035	ハニカム格子系van Vleckエキシトン磁性候補物質の物性	原口 祐哉	東京農工大学		Physical properties in candidates of van Vleck excitonic honeycomb lattice magnet	Yuya Haraguchi	Tokyo University of Agriculture and Technology		広井 善二
18	202012-GNBXX-0036	リチウムインターカレートされた欠損型スピネルにおけるスピン軌道結合金属相の探索	原口 祐哉	東京農工大学		Search for a spin-orbit-coupled metallic phase in lithium-Intercalated lacunar spinels	Yuya Haraguchi	Tokyo University of Agriculture and Technology		広井 善二
19	202012-GNBXX-0058	希土類4f電子数制御による新規体積変化アクチュエーター材料の創製	横山 泰範	名古屋大学	岡本 佳比古 渋谷 隼矢 竹中 康司 岸田 海斗	Development of novel volume-change-driven actuator materials by control of rare earth 4f electron number	Yasunori Yokoyama	Nagoya University	Yoshihiko Okamoto Junya Shibutani Koshi Takenaka Kishida Kaito	広井 善二
20	202012-GNBXX-0016	(Ce1-xRx)PtGe2の置換および圧力効果	中野 智仁	新潟大学	武藤 颯人	Substitution and pressure effect of (Ce1-xRx)PtGe2	Tomohito Nakano	Niigata University	Hayato Muto Niigata University	上床 美也
21	202012-GNBXX-0020	CeNiC2の結晶育成と物質評価	繁岡 透	山口大学	内間 清晴（沖縄キリスト教短期大学）	Crystal growth and characterization of CeNiC2	Toru Shigeoka	Yamaguchi University	Kiyoharu Uchima, Okinawa Christian Junior College	上床 美也

22	202012-GNBXX-0025	圧力媒体の高圧力物性	村田 惠三	大阪市立大学		High Pressure Properties of High Pressure Medium	Keizo Murata	Osaka City University		上床 美也
23	202012-GNBXX-0029	ウラン化合物の磁性の圧力効果	本多 史憲	九州大学アイソトープ統合安全管理センター	小泉 堯嗣（東北大学）	Effect of Pressure on the magnetism of uranium compounds	Fuminori Honda	Central Institute of Radioisotope Science and Safety Management, Kyushu University	Takatsugu Koizumi, Tohoku university	上床 美也
24	202012-GNBXX-0031	高圧下におけるEu化合物の価数転移の探索	本多 史憲	東北大学	小泉 堯嗣（東北大学）	Investigation of valence transition on Eu compounds under high pressure	Fuminori Honda	Tohoku university	Takatsugu Koizumi	上床 美也
25	202012-GNBXX-0038	ホイスラー化合物Fe3-xMnxSiの圧力下磁気相転移	廣井 政彦	鹿児島大学	赤石 幸起	Magnetic phase transitions under pressure in Heuser compounds Fe3-xMnxSi	Masahiko HIROI	Kagoshima University	Kouki Akaishi	上床 美也
26	202012-GNBXX-0043	S置換したFeSeの高圧低温NMR測定	藤原 直樹	京都大学	Yu Zhongyu	NMR studies on S-substituted FeSe at high pressures and low temperatures	Naoki Fujiwara	Kyoto University	Zhongyu Yu	上床 美也
27	202012-GNBXX-0044	Ba1-xRbxFe2As2における圧力下電子相図の研究	向笠 清隆	東京大学	岡田 昂	Studies on high-pressure phase diagrams in Ba1-xRbxFe2As2	Kiyotaka Mukasa	The University of Tokyo	Okada Ko	上床 美也
28	202012-GNBXX-0047	Ta2NiSe5 の置換物質における高圧力下電気抵抗測定	広瀬 雄介	新潟大学	土田 駿	Electrical resistivity measurement under pressure of substituted Ta2NiSe5	Yusuke Hirose	Niigata University	Shun Tsuchida	上床 美也
29	202012-GNBXX-0050	Ni2In型強磁性体の自発磁化の圧力効果	安達 義也	山形大学	井田 唯斗	Pressure effects on the spontaneous magnetization for Ni2In-type ferromagnets.	Yoshiya Adachi	Yamagata University	Yuino Ida	上床 美也
30	202012-GNBXX-0051	Ceジグザグ鎖を持つCe3TiSb5およびCe3TiBi5の圧力下電気抵抗測定	本山 岳	島根大学	篠﨑 真碩	Electrical resistivity measurements of Ce3TiSb5 and Ce3TiBi5 under pressure	Gaku Motoyama	Shimane University	Masahiro Shinozaki	上床 美也
31	202012-GNBXX-0061	超高圧下電気抵抗測定による反強磁性絶縁体 λ-(BEST)2FeCl4の温度圧力相図の決定と圧力誘起超伝導相の探索	谷口 弘三	埼玉大学	小林 拓矢 齋藤 陸丸（北海道大学） 小梁川 響子	Search for pressure-induced superconductivity and determination of the pressure-temperature phase diagram of antiferromagnetic insulator λ-(BEST)2FeCl4 by electrical resistivity measurement under ultra-high pressures	Hiromi Taniguchi	Saitama University	Takuya Kobayashi Saito Rikumaru, Hokkaido University Kyoko Koyanagawa	上床 美也
32	202012-GNBXX-0063	有機電荷移動錯体(DMET-TTF)2AuBr2の超高静水圧印加による超伝導相の探索	小林 拓矢	埼玉大学	谷口 弘三 加藤 大賀（北海道大学） 菅原 佳哉	Search for pressure-induced superconductivity by applying quasi-hydrostatic ultra-high pressures to organic charge-transfer salt (DMET-TTF)2AuBr2	Takuya Kobayashi	Saitama University	Hiromi Taniguchi Taiga Kato, Hokkaido University Yoshiya Sugawara	上床 美也
33	202012-GNBXX-0069	圧力誘起構造量子相転移を示す超伝導体のフェルミ面の研究	摂待 力生	新潟大学	三橋 大貴	Fermi surface study of superconductors with pressure-induced structural quantum phase transition	Rikio Settai	Niigata University	Daiki Mitsuhashi	上床 美也
34	202012-GNBXX-0080	CeZn2Ge2単結晶の高圧化磁化測定	藤原 哲也	山口大学	五反田 礼	Magnetization measurements under high pressures of CeZn2Ge2 single crystal	Tetsuya Fujiwara	Yamaguchi University	Rei Gotanda	上床 美也
35	202012-GNBXX-0081	GdCrGe2単結晶の磁化測定	藤原 哲也	山口大学	小林 遼平	Magnetization measurements of GdCrGe2 single crystal	Tetsuya Fujiwara	Yamaguchi University	Ryohei Kobayashi	上床 美也
36	202012-GNBXX-0082	TbCrGe2単結晶の磁化測定	藤原 哲也	山口大学	金子 達哉	Magnetization measurements of TbCrGe2 single crystal	Tetsuya Fujiwara	Yamaguchi University	Kaneko Tatsuya	上床 美也
37	202012-GNBXX-0083	HoCrGe2単結晶の磁化測定	藤原 哲也	山口大学	杉田 静留	Magnetization measurements of HoCrGe2 single crystal	Tetsuya Fujiwara	Yamaguchi University	Shizuru Sugita	上床 美也
38	202012-GNBXX-0084	重い電子系強磁性体の圧力下dHvA効果	摂待 力生	新潟大学	三橋 大貴	de Haas-van Alphen effect in heavy fermion ferromagnet under pressure	Rikio Settai	Niigata University	Daiki Mitsuhashi	上床 美也

39	202011-GNBXX-0005	金属ナノ構造の超高速発光による研究	末元 徹	電気通信大学		Studies on nanostructured metals by ultrafast luminescence spectroscopy	Suemoto Tohru	The University of Electro-Communications		小林 洋平
40	202012-GNBXX-0019	紫外光レーザー光源を用いた加工応用研究	藤本 靖	千葉工業大学	柴 優希	Research on laser processing application by ultraviolet laser light source	Yasushi Fujimoto	Chiba Institute of Technology	Yuki Shiba Chiba Institute of Technology	小林 洋平
41	202012-GNBXX-0032	次世代レーザーとレーザー加工の基礎技術研究	吉富 大	産業技術総合研究所	高田 英行 奈良崎 愛子 小川 博嗣 寺澤 英知 澁谷 達則 佐藤 大輔 黒田 隆之助 田中 真人	Basic research on next generation laser systems and laser machining technology	Dai Yoshitomi	National Institute of Advanced Industrial Science and Technology	Takada Hideyuki Aiko Narazaki Hiroshi Ogawa Eichi Terasawa Tatsunori Shibuya Daisuke Satoh Ryunosuke Kuroda Masahito Tanaka	小林 洋平
42	202012-GNBXX-0056	SmSの高強度中赤外パルス光を用いた光誘起相転移ダイナミクス	渡邊 浩	大阪大学	中村 拓人 陳 奕同	High power mid-infrared laser induced phase transition dynamics on SmS	Hiroshi Watanabe	Osaka University	Takuto Nakamura Yitong Chen	板谷 治郎
43	202012-GNBXX-0041	有機分子/貴金属界面におけるラシュバ分裂の増大	金井 要	東京理科大学	小久保 裕太	Enhancement of Rashba splitting on organic molecule/noble metal interface	Kaname Kanai	Tokyo University of Science	Yuta Kokubo	近藤 猛
44	202012-GNBXX-0048	Ti3SiC2のスピン分解角度分解光電子分光	伊藤 孝寛	名古屋大学	松永 和也 山本 凌 杉本 卓史 保科 拓海	Spin- and Angle-resolved photoemission study of Ti3SiC2	Takahiro Ito	Nagoya University	Matsunaga Kazuya Yamamoto Ryo Takafumi Sugimoto Hoshina Takumi	近藤 猛
45	202012-GNBXX-0053	超高品質4d強磁性酸化物SrRuO3薄膜におけるワイル半金属相の電子状態の解明	小林 正起	東京大学	武田 崇仁 岡野 諒	Unveiling of the electronic state of the Wyel semi-metal phase in ultra-high quality 4d ferromagnetic oxide SrRuO3 thin films	Masaki Kobayashi	the University of Tokyo	Takahito Takeda Ryo Okano	近藤 猛
46	202012-GNBXX-0054	バルク敏感高分解能スピン分解光電子分光を用いたハーフメタル強磁性体の多体効果の研究	横谷 尚睦	岡山大学	片岡 範行	Many-body interaction of half-metallic antiferromagnet studied by bulk sensitive high-resolution spin-resolved photoemission spectroscopy	Takayoshi Yokoya	Okayama University	Noriyuki Kataoka	近藤 猛
47	202012-GNBXX-0070	スピン角度分解光電子分光によるガリウム単結晶表面の電子状態研究	矢治 光一郎	物質・材料研究機構	永村 直佳	Electronic band structure of Ga single crystal studied by SARPES	Koichiro Yaji	National Institute for Materials Science	Naoka Nagamura	近藤 猛
48	202012-GNBXX-0042	高分解能レーザー励起光電子顕微鏡を用いた鉄系超伝導体の電子ネマティック状態の実空間観察III	橋本 顕一郎	東京大学	水上 雄太 大西 朝登 影山 遥一	Real-space observation of electronic nematicity in iron-based superconductors by using a high-resolution laser photoemission electron microscope III	Kenichiro Hashimoto	the University of Tokyo	Yuta Mizukami Asato Onishi Yoichi Kageyama	岡﨑 浩三
49	202012-GNBXX-0055	時間角度分解光電子分光による価数揺動物質の光誘起相転移ダイナミクス	中村 拓人	大阪大学	渡邊 浩 陳 奕同	Photo-induced phase transition dynamics on the valence fluctuate compound by TrARPES	Takuto Nakamura	Osaka University	Hiroshi Watanabe Yitong Chen	岡﨑 浩三
50	202012-GNBXX-0060	励起子絶縁体の原子層結晶における電子正孔相関の光誘起ダイナミクス	溝川 貴司	早稲田大学	大川 万里生	Photoinduced dynamics of electron-hole correlation in atomic layered excitonic insulators	Takashi Mizokawa	Waseda University	Mario Okawa	岡﨑 浩三
51	202012-GNBXX-0067	励起子絶縁体Ta2NiSe5及び高温超伝導体FeSeにおける光誘起相転移の研究	久保田 雄也	理化学研究所		Investigation of the photo-induced phase transitions in an exitonic insulator Ta2NiSe5 and a superconductor FeSe	Yuya Kubota	RIKEN		岡﨑 浩三

物質合成・評価設備Gクラス / Materials Synthesis and Characterization G Class Research Project

No.	課題番号	課題名	氏名	所属	分担者	Title	Name	Organization	Member of research project	実験室
1	202012-MCBXG-0040	泥岩中の化学的浸透に伴う岩石の変形に関する実験的・数値的検討	廣田 翔伍	東京大学		Experimental and numerical investigation of rock deformation caused by chemical osmosis	Shogo Hirota	the University of Tokyo		X線測定室
2	202011-MCBXG-0001	金属間化合物の構造解析	齋藤 哲治	千葉工業大学		Study of intermetallic compounds	Tetsuji Saito	Chiba Institute of Technology		電子顕微鏡室
3	202012-MCBXG-0032	MOF を鋳型とした極細無機ナノワイヤーの創製	北尾 岳史	東京大学	細野 暢彦 飯塚 知也 松田 一輝	Synthesis of ultrathin inorganic nanowire templated by MOFs	Takashi Kitao	the University of Tokyo	Nobuhiko Hosono Tomoya Iizuka Ikki Matsuda	電子顕微鏡室
4	202012-MCBXG-0031	交流磁化率測定による反強磁性絶縁体に近接した層状有機超伝導体における相分離した超伝導相の研究	谷口 弘三	埼玉大学	高橋 啓太	Studies on phase-separated superconducting phase in layered organic superconductors bordering on antiferromagnetic insulating phase by ac susceptibility measurements	Hiromi Taniguchi	Saitama University	Takahashi Keita	電磁気測定室
5	202012-MCBXG-0039	新規スピン軌道結合磁性体の物性評価	香取 浩子	東京農工大学	原口 祐哉 柿本 和勇	Characterization of novel spin-orbit coupled magnetic materials	Hiroko Katori	Tokyo University of Agriculture and Technology	Yuya Haraguchi Kazuo Kakimoto	電磁気測定室
6	202011-MCBXG-0013	六方晶フェライトSrCo2-Wの磁気異方性制御	和氣 剛	京都大学	中井 慎司	Controlling the magnetic anisotropy of the hexaferrite SrCo2-W	Takeshi Waki	Kyoto University	Shinji Nakai	高圧合成室
7	202012-MCBXG-0007	希土類元素およびアルカリ土類金属元素を充填した新規スクッテルダイト型熱電材料の高圧合成	関根 ちひろ	室蘭工業大学	本間 さくら	High-pressure synthesis of new rare-earth and alkaline-earth filled skutterudite-type thermolectric materials	Chihiro Sekine	Muroran Institute of Technology	Sakura Homma	高圧合成室
8	202012-MCBXG-0042	高温高圧中性子回折測定を用いた鉄ーケイ素系での水素原子のサイト決定と溶存量の測定	鍵 裕之	東京大学	森 悠一郎 磯部 隆仁	Solubility and site occupancy of hydrogen in Fe-Si system using in-situ neutron diffraction measurement under high pressure and high temperature	Hiroyuki Kagi	the University of Tokyo	Mori Yuichiro Ryuto Isobe	高圧合成室
9	202011-MCBXG-0006	α-RuBr3の高圧合成	今井 良宗	東北大学	藤原 秀行	High pressure synthesis of α-RuBr3	Yoshinori Imai	Tohoku university	Hideyuki Fujihara	高圧合成室、X線測定室
10	202012-MCBXG-0030	磁気多極子の強的秩序に基づく物質機能の開発	有馬 孝尚	東京大学	車地 崇 池田 凜太郎 木村 真栄 佐藤 樹 海本 祐真 渡辺 義人 柳田 真佑 石崎 大悟 徳永 祐介 厳 正輝	Development of material functions based on ferroic multipole order	Taka-hisa Arima	the University of Tokyo	Takashi Kurumaji Rintaro Ikeda Shin-Ei Kimura Tatsuki Sato Yuma Umimoto Yoshito Watanabe Shinsuke Yanagida Daigo Ishizaki Yusuke Tokunaga Masaki Gen	X線測定室 電磁気測定室
11	202012-MCBXG-0017	カルシウムループ法によるメタン化プロセスの研究	大友 順一郎	東京大学	李 智漢	Development of Ca looping process for production of methane	Junichiro Otomo	the University of Tokyo	Jihan Lee	X線測定室 電子顕微鏡室

12	202012-MCBXG-0018	イオン及び電子伝導特性の制御によるSOEC性能の改善	大友 順一郎	東京大学	Ortiz Julian	Improvement of solid-oxide electrolysis cells performance by controlling ionic and electronic transport properties	Junichiro Otomo	the University of Tokyo	Julian Andres Ortiz Corrales	X線測定室 電子顕微鏡室
13	202012-MCBXG-0019	イオン・電子混合電解質の界面輸送特性制御と新規電気化学セル設計	大友 順一郎	東京大学	田島 星也	Control of interfacial transport properties of ion-electron mixed electrolytes and design of new electrochemical cells	Junichiro Otomo	the University of Tokyo	Tajima Seiya	X線測定室
14	202012-MCBXG-0020	プロトン伝導性固体電解質膜の異相接合界面における輸送現象の研究	大友 順一郎	東京大学	中根 健太	Study of the transport phenomenon at heterojunction of proton conductor	Junichiro Otomo	the University of Tokyo	Nakane Kenta	X線測定室 電子顕微鏡室
15	202012-MCBXG-0021	赤外分光法を用いた反応吸着種のその場測定用電解セルの作製とCO2吸着種の反応追跡	大友 順一郎	東京大学	平子 睦海	Preparation of electrolytic cell for in-situ measurement of reaction adsorbed species and observation of CO2 adsorbed species using infrared spectroscopy	Junichiro Otomo	the University of Tokyo	Mutsumi Hirako	X線測定室
16	202012-MCBXG-0022	プロトン伝導形燃料電池を用いた二酸化炭素の電解還元	大友 順一郎	東京大学	黄 睿	Electrolytic reduction of carbon dioxide using proton-conducting fuel cells	Junichiro Otomo	the University of Tokyo	Rui Huang	X線測定室 電子顕微鏡室
17	202012-MCBXG-0036	in-situ生成触媒を用いた連続式超臨界水ガス化プロセスの検討	布浦 鉄兵	東京大学	張 鵬	Continuous supercritical water gasification process using in-situ generation of catalyst	Teppei Nunoura	the University of Tokyo	Peng Zhang	X線測定室 電子顕微鏡室
18	202012-MCBXG-0037	ニッケル触媒を用いた地溝油の水熱ガス化反応に関する検討	布浦 鉄兵	東京大学	温 雅茹	Hydrothermal gasification of hogwash oil using nickel catalyst	Teppei Nunoura	the University of Tokyo	Yaru Wen	X線測定室 電子顕微鏡室
19	202011-MCBXG-0004	高脂質含有量のバイオマスの超臨界水ガス化における水素生産のための2段階接触分解装置と改質装置の開発	グバタンガ ダイアン	東京大学		Development of a two-stage catalytic cracker and reformer for hydrogen production in supercritical water gasification of biomass with high lipid content	Diane Valenzuela Gubatanga	the University of Tokyo		X線測定室 電子顕微鏡室 光学測定室
20	202012-MCBXG-0034	合金ナノ粒子のキャラクタリゼーション	佐々木 岳彦	東京大学	張 凱朝	Characterization of alloy nanoparticles	Takehiko Sasaki	the University of Tokyo	Kaichao Zhang	X線測定室 電子顕微鏡室
21	202012-MCBXG-0015	電子不足型量体化分子の内部構造の解明	片山 尚幸	名古屋大学	塩見 学 小島 慶太 原 武史	Elucidation of the internal structure of electron-deficient dimerized molecules	Naoyuki Katayama	Nagoya University	Manabu Shiomi Keita Kojima Takeshi Hara	化学分析室 X線測定室 電磁気測定室
22	202012-MCBXG-0016	量体化直前の金属における圧力誘起相転移の探索	片山 尚幸	名古屋大学	松田 悠大 塩見 学 小島 慶太	Search for pressure-induced phase transitions in metals just before dimerization	Naoyuki Katayama	Nagoya University	Matsuda Yudai Manabu Shiomi Keita Kojima	化学分析室 X線測定室 電磁気測定室
23	202012-MCBXG-0010	超臨界水熱合成法を利用したZrO2微粒子のその場有機修飾技術の研究	秋月 信	東京大学	李 雪	In-situ organic modification of ZrO2 nanoparticles using supercritical hydrothermal method	Makoto Akizuki	the University of Tokyo	Li Xue	化学分析室 X線測定室 電子顕微鏡室
24	202012-MCBXG-0011	超臨界水を用いたペロブスカイト構造金属酸化物微粒子の合成	秋月 信	東京大学	朱 崢琿	Synthesis of perovskite structure metal oxide nanoparticles using supercritical water	Makoto Akizuki	the University of Tokyo	Zhenghui Zhu	化学分析室 X線測定室 電子顕微鏡室
25	202012-MCBXG-0012	超臨界水と亜臨界水の二段階反応による結晶性の高いBaZrO3ナノ粒子の合成	秋月 信	東京大学	王 咏旭	Synthesis of highly crystalline BaZrO3 nanoparticles by a two-step reaction of supercritical water and subcritical water	Makoto Akizuki	the University of Tokyo	Yongxu Wang	X線測定室 電子顕微鏡室
26	202012-MCBXG-0024	幾何学的フラストレート格子を持つキタエフ・ハイゼンベルグ磁性体の物性研究	原口 祐哉	東京農工大学		Study of Physical Properties of Kitaev-Heisenberg Magnets with Geometric Frustrated Lattice	Yuya Haraguchi	Tokyo University of Agriculture and Technology		電磁気測定室

27	202012-MCBXG-0028	三角格子反強磁性体ACrS2 (A = Ag, Au)の磁場誘起歪	岡本 佳比古	名古屋大学		Magnetostriction in Triangular Antiferromagnet ACrS2 (A = Ag, Au)	Yoshihiko Okamoto	Nagoya University		電磁気測定室
28	202012-MCBXG-0033	キラルな無機蛍光体単結晶の育成	木崎 和郎	生産技術研究所		Single Crystal Growth of Chiral Inorganic Phosphors	Kazuro Kizaki	Institute of Industrial Science		X線測定室 物質合成質室
29	202012-MCBXG-0035	トポロジカル超伝導体の新規物質開発と物性評価	水上 雄太	東京大学	今村 薫平 原澤 龍平 向笠 清隆 石原 滉大 影山 遥一 広瀬 夏彦 岡田 昂 六本木 雅生 大西 朝登 ファン センジェ	Synthesis and characterization of novel topological superconductors	Yuta Mizukami	the University of Tokyo	Kumpei Imamura Ryuhei Harasawa Kiyotaka Mukasa Kota Ishihara Yoichi Kageyama Natsuhiko Hirose Okada Ko Masaki Roppongi Asato Onishi Shengjie Fang	物質合成質室 X線測定室 電磁気測定室
30	202012-MCBXG-0008	新規フェロイック秩序物性の創成に関する研究	木村 剛	東京大学	林 悠生 大島 貴彦 林田 健志 荒川 慶人 木村 健太 三澤 龍介	Exploration of new ferroic properties	Tsuyoshi Kimura	the University of Tokyo	Yuki Hayashi Takahiko Oshima Takeshi Hayashida Keito Arakawa Kenta Kimura Ryusuke Misawa	物質合成質室 X線測定室 電子顕微鏡室

物質合成・評価設備Uクラス / Materials Synthesis and Characterization U Class Research Project

No.	課題番号	課題名	氏名	所属	分担者	Title	Name	Organization	Member of research project	担当所員
1	202104-MCBXU-0048	新規量子マテリアルの単結晶合成	中辻 知	東京大学	酒井 明人 王 陽明 Fu Mingxuan 見波 将 中村 紘人 Ray Mayukh Kumar Feng Zili 唐 楠	Single crystal growth of new quantum matter	Satoru Nakatsuji	the University of Tokyo	Akito Sakai Yangming Wang Fu Mingxuan Susumu Minami Hiroto Nakamura Ray Mayukh Kumar Feng Zili Nan Tang	物質合成質室 化学分析室 電子顕微鏡室
2	202104-MCBXU-0051	月資源利用を目指したレーザーによるアルミナ還元	田中 聖也	東京大学	西井 啓太 田中 直輝	Laser alumina reduction toward utilization of lunar resources	Seiya Tanaka	the University of Tokyo	Keita Nishii Naoki Tanaka	電子顕微鏡室
3	202105-MCBXU-0052	中温作動のアンモニア電解合成システムに向けたプロトン伝導型固体セルと電気化学反応器の開発	岡﨑 萌	東京大学		Development of solid proton-conducting cells and electrochemical reactors for an ammonia electrosynthesis system operating at intermediate temperatures	Moe Okazaki	the University of Tokyo		X線測定室
4	202105-MCBXU-0053	多孔金属支持型プロトン伝導性セラミックス燃料電池の作製および物性評価	山手 駿	東京大学		Fabrication of Porous Metal Supported Proton Conducting Fuel Cells and Evaluation of Physical Properties	Shun Yamate	the University of Tokyo		X線測定室

No.	課題番号	課題名	氏名	所属	分担者	Title	Name	Organization	Member of research project	担当所員
1	202012-HMBXX-0004	重い電子系化合物が示す非従来型超伝導と非フェルミ液体状態の相関	横山 淳	茨城大学	平山 堅理	Relationship between unconventional superconductivity and non-Fermi-liquid state in heavy-fermion compounds	Makoto Yokoyama	Ibaraki University	Takatoshi Hirayama	金道 浩一
2	202012-HMBXX-0009	パルス強磁場中c軸抵抗率測定による銅酸化物高温超伝導体における前駆クーパー対形成の検証	渡辺 孝夫	弘前大学	藤井 武則（東京大学）	Observation of preformed Cooper pairing in high-Tc cuprates using out-of-plane resistivity measurements of Bi(Pb)-2212 single crystals under high pulsed magnetic fields	Takao Watanabe	Hirosaki University	Takenori Fujii, the University of Tokyo	金道 浩一
3	202012-HMBXX-0014	中性イオン性物質における相転移の磁場制御と磁気抵抗現象の探索	福岡 脩平	北海道大学	伊藤 悠馬	Magnetic-field control of phase transitions and search for magnetoresistance phenomena in neutral-ionic materials	Shuhei Fukuoka	Hokkaido University	Ito Yuma	金道 浩一
4	202012-HMBXX-0018	CeAgxCu1-xSb2の磁気相図と新規遍歴電子フラストレーション系における強磁場磁化過程に関する研究	道岡 千城	京都大学	森山 広大	Study of the magnetic phase diagram in CeAgxCu1-xSb2 and magnetization curves in novel itinerant frustrated systems	Michioka Chishiro	Kyoto University	Kodai Moriyama	金道 浩一
5	202012-HMBXX-0020	α-Ru(Br,Cl)3の磁場配向試料の作製と強磁場磁化過程の測定	今井 良宗	東北大学	藤原 秀行	Preparation of magnetically oriented α - Ru(Br,Cl)3 and high-field magnetization measurements	Yoshinori Imai	Tohoku university	Hideyuki Fujihara	金道 浩一
6	202012-HMBXX-0021	フラストレートしたハニカム格子磁性体における新奇磁場誘起相の探索	原口 祐哉	東京農工大学	八束 波椰斗	Search for novel magnetic field-induced phases in frustrated honeycomb lattice magnets	Yuya Haraguchi	Tokyo University of Agriculture and Technology	Yatsuzuka Hayato	金道 浩一
7	202012-HMBXX-0023	有機超伝導体のFFLO超伝導相に対する乱れの効果	杉浦 栞理	東北大学		Disorder effect on FFLO superconductivity of organic superconductors	Shiori Sugiura	Institute for Materials Research, Tohoku University		金道 浩一
8	202012-HMBXX-0034	高圧合成新規希土類ホウ化物RB12（R=Ce, Pr, Nd）とErB6の強磁場磁化と輸送特性	伊賀 文俊	茨城大学	山田 健介	Magnetic and transport properties under high magnetic field of novel rare-earth dodecaborides RB12（R=Ce, Pr, Nd）and ErB6 prpduced by high-pressure synthesis	Fumitoshi Iga	Ibaraki University	Kensuke Yamada	金道 浩一
9	202012-HMBXX-0003	ハニカム近藤格子系CePt6Al3におけるフラストレーション効果の強磁場磁化・抵抗測定による研究	鬼丸 孝博	広島大学	高畠 敏郎 大石 遼平 志村 恭通	Role of frustration in the honeycomb Kondo lattice CePt6Al3 studied by magnetization and magnetoresistance measurements in high magnetic fields	Takahiro Onimaru	Hiroshima university	Toshiro Takabatake Oishi Ryohei Yasuyuki Shimura	徳永 将史
10	202012-HMBXX-0024	新規スピン軌道結合モット絶縁体の強磁場磁化過程	香取 浩子	東京農工大学	原口 祐哉 柿本 和勇	Magnetization process of novel spin-orbit coupled Mott insulators in high magnetic fields	Hiroko Katori	Tokyo University of Agriculture and Technology	Yuya Haraguchi Kazuo Kakimoto	徳永 将史
11	202012-HMBXX-0028	ヨウ素輸送法で育成したFe(Te,S) における超伝導状態の磁気光学イメージングによる観測	矢口 宏	東京理科大学	山中 隆義 藤川 俊樹	Observations of superconducting states in Fe(Te,S) grwon by an iodine-transport method using an MO imaging technique	Hiroshi Yaguchi	Tokyo University of Science	Takayoshi Yamanaka Toshiki Fujikawa	徳永 将史
12	202012-HMBXX-0032	鉄系超伝導体Fe(Te, Se)における超伝導空間分布の磁気光学イメージングによる観測	山中 隆義	東京理科大学	矢口 宏 打川 景大	Observation of the distribution of superconductivity in Fe(Te, Se) using a magnet optical imaging technique	Takayoshi Yamanaka	Tokyo University of Science	Hiroshi Yaguchi Keita Uchikawa	徳永 将史
13	202012-HMBXX-0041	パルス強磁場を用いた Ni-Co-Mn-Sn 系合金のメタ磁性相転移の実験的調査	許 畠	東北大学	宮川 寅矢	Metamagnetic transition behaviors in Ni-Co-Mn-Sn alloys under pulsed high magnetic fields	Xiao Xu	Tohoku University	Tomoya Miyakawa	徳永 将史

14	202012-HMBXX-0044	強磁場中におけるクラスター磁気多極子に起因した特異物性の探索	木村 健太	東京大学		Explorations of peculiar high-field behaviors due to cluster magnetic multipoles	Kenta Kimura	the University of Tokyo		徳永 将史
15	202012-HMBXX-0008	クロムスピネル酸化物におけるスピンネマティック相の探索	木村 尚次郎	東北大学		Explorations of the spin nematic phase in the chromium spinel oxide	Shojiro Kimura	Tohoku University		小濱 芳允
16	202012-HMBXX-0026	有機スピン液体候補物質の超強磁場物性研究	宮川 和也	東京大学	杉浦 栞理（東北大学） 浦井 瑞紀	Physical property measurements of organic spin liquid candidate materials under ultra-high magnetic field	Kazuya Miyagawa	the University of Tokyo	Shiori Sugiura, Tohoku University Mizuki Urai	小濱 芳允
17	202103-HMBXX-0046	強磁場下における分子材料励起三重項状態の磁気光学分光	石井 和之	東京大学		Magneto-Optical Spectroscopy of Molecular Materials in the Excited Triplet States under Strong Magnetic Fields	Kazuyuki Ishii	the University of Tokyo		小濱 芳允
18	202104-HMBXX-0047	トポロジカル磁性体候補物質の量子振動の研究	酒井 英明	大阪大学	近藤 雅起	Study of the quantum oscillation of a putative topological magnet	Hideaki Sakai	Osaka University	Masaki Kondo	徳永 将史
19	202104-HMBXX-0050	ブリージングパイロクロア格子磁性体の新規磁場誘起物性および機能性の開拓	巌　正輝	東京大学		Search for novel field-induced properties and functionalities in breathing pyrochlore magnets	Masaki Gen	Department of Advanced Materials Science		松田 康弘
20	202104-HMBXX-0051	新規スキルミオン候補物質Eu化合物における格子歪みの研究	車地 崇	東京大学	巌 正輝	Study of lattice distortions in a possible skyrmion host Eu compound	Takashi Kurumaji	the University of Tokyo	Masaki Gen	小濱 芳允
21	202104-HMBXX-0052	異方的三角格子を組んだ5d遷移金属量子磁性体の磁場中物性	巌　正輝	東京大学		Magnetic-field induced properties of 5d transition metal quantum magnets on the anisotropic triangular lattice	Masaki Gen	Department of Advanced Materials Science		小濱 芳允
22	202106-HMBXX-0095	鉄系超伝導体Fe(Se, Te)のネマティック量子臨界点近傍における輸送現象の研究	芝内 孝禎	東京大学	向笠 清隆 劉 蘇鵬	Electrical transport studies on Fe(Se, Te) superconductors near the nematic quantum critical point	Takasada Shibauchi	the University of Tokyo	Kiyotaka Mukasa SUPENG LIU	金道 浩一

大阪大学大学院理学研究科附属先端強磁場科学研究センター / Center for Advanced High Magnetic Field Science, Graduate School of Science, Osaka University

No.	課題番号	課題名	氏名	所属	分担者	Title	Name	Organization	Member of research project	担当所員
1	202011-HMOXX-0001	空間反転対称性の破れや磁気フラストレーションに誘発された特異な磁気特性と強磁場物性	竹内 徹也	大阪大学	大貫 惇睦（理化学研究所）	Magnetic-field induced properties of 5d transition metal quantum magnets on the anisotropic triangular lattice	Tetsuya Takeuchi	Osaka University	Yoshichika Onuki, RIKEN	萩原 政幸 (大阪大学)
2	202012-HMOXX-0010	マンガン窒化物Mn3XN (X= Cu, Sb)の磁化・磁歪の高速磁場応答性の研究	左近 拓男	龍谷大学		Research on time dependences of magnetization and magnetstriction of Mn3XN(X = Cu, Sb)	Takuo Sakon	Ryukoku University		萩原 政幸 (大阪大学)
3	202012-HMOXX-0011	ホイスラー合金Ni2MnX(X = Al, Sb)およびPd2MnSnの磁化・磁歪の高速磁場応答性の研究	左近 拓男	龍谷大学		Research on time dependences of magnetstriction of Ni2MnX(X = Al, Sb) type and Pd2MnSn type Heusler alloys	Takuo Sakon	Ryukoku University		萩原 政幸 (大阪大学)
4	202012-HMOXX-0012	量子スピン系の電場励起ESRと方向二色性	木村 尚次郎	東北大学	大月 保直	Electric dipole active ESR and nonreciprocal directional dichroism in quantum spin systems	Shojiro Kimura	Tohoku University	Yasunao Otsuki	萩原 政幸 (大阪大学)
5	202012-HMOXX-0015	ショートパルスマグネットを用いた圧力下ESR装置の開発	櫻井 敬博	神戸大学	赤木 暢	Development of high-pressure ESR system using short pulse magnet	Takahiro Sakurai	Kobe University	Mitsuru Akaki	萩原 政幸 (大阪大学)

6	202012-HMOXX-0017	強いスピン-軌道相互作用を活かした酸化物スピントロニクス	松野 丈夫	大阪大学		Oxide spintronics utilizing strong spin-orbit coupling	Jobu Matsuno	Osaka University		萩原 政幸 (大阪大学)
7	202012-HMOXX-0025	トポロジカル磁性体の巨大磁気抵抗効果の研究	村川 寛	大阪大学		High magnetic field study of giant magnetoresistance in topological magnets	Hiroshi Murakawa	Osaka University		萩原 政幸 (大阪大学)
8	202012-HMOXX-0035	層状磁性体EuMg2Bi2の磁気特性の解明	酒井 英明	大阪大学	奥田 裕貴 近藤 雅起 阪口 駿也	Study of magnetic properties for layered magnet EuMg2Bi2	Hideaki Sakai	Osaka University	Yuki Okuda Masaki Kondo Shunya Sakaguchi	萩原 政幸 (大阪大学)
9	202012-HMOXX-0039	Coスピン系CoSeO3の強磁場磁気相の解明	大久保 晋	神戸大学	赤木 暢 木田 孝則（大阪大学） 菊池 彦光（福井大学）	Investigation of High-field magnetic phase of CoSeO3	Susumu Okubo	Kobe University	Mitsuru Akaki Takanori Kida, Osaka University Hikomitsu Kikuchi, University of Fukui	萩原 政幸 (大阪大学)
10	202012-HMBXX-0013	精密電子スピン共鳴測定用パルスマグネットの開発	赤木 暢	神戸大学		Development of pulsed magnet for precise electron spin resonance measurements	Mitsuru Akaki	Kobe University		萩原 政幸 (大阪大学)
11	202012-HMBXX-0030	有機ラジカルから成るフラストレート系の低温物性測定	山口 博則	大阪府立大学		Low temperature physical properties of frustrated spin systems composed of organic radicals	Hironori Yamaguchi	Osaka Prefecture University		萩原 政幸 (大阪大学)
12	202104-HMOXX-0049	非従来型超伝導体のパルス強磁場下輸送特性	掛谷 一弘	京都大学	孫 悦（青山学院大学）	Transport measurements on unconventional superconductors under pulsed high magnetic fields	Itsuhiro Kakeya	Kyoto University	Yue Sun, Aoyama Gakuin University	萩原 政幸 (大阪大学)
13	202105-HMOXX-0053	遷移金属フタロシアニン及びフタロシアニン重合体の圧力下における磁性	本多 善太郎	埼玉大学		Magnetic properties of transition metal phthalocyanines and poly-phthalocyanines under pressure	Zentaro Honda	Saitama University		萩原 政幸 (大阪大学)
14	202105-HMOXX-0054	高磁場下の脂質膜特性の解析	岡本 行広	大阪大学	尾澤 知紘	Investigation of lipid membrane properties under high magnetic field	Yukihiro Okamoto	Grad. Sch. of Engineering Science Osaka University	Ozawa Tomohiro	萩原 政幸 (大阪大学)
15	202105-HMOXX-0056	タンパク質結晶の熱物性値の異方性に関する予備実験	牧 祥	岡山理科大学		Preliminary experiment on anisotropy of thermophysical properties of protein crystals	Syou Maki	Okayama University of Science		萩原 政幸 (大阪大学)
16	202107-HMOXX-0096	キラル磁性体CrTa3S6の強的もしくは反強的キラルソリトン格子の検証	高阪 勇輔	大阪府立大学		Ferro- or antiferro-based chiral soliton lattice in CrTa3S6	Yusuke Kousaka	Osaka Prefecture University		萩原 政幸 (大阪大学)

強磁場コラボラトリー / The High Magnetic Field Collaboratory

No.	課題番号	課題名	氏名	所属	分担者	Title	Name	Organization	Member of research project	担当所員
1	202012-HMBXX-0030	有機ラジカルから成るフラストレート系の低温物性測定	山口 博則	大阪府立大学		Low temperature physical properties of frustrated spin systems composed of organic radicals	Hironori Yamaguchi	Osaka Prefecture University		金道 浩一
2	202012-HMCXX-0006	微視的プローブによる強磁場誘起電子相の探索とその周辺ダイナミクス観測	井原 慶彦	北海道大学		NMR study for magnetic field induced electronic states and their dynamics	Yoshihiko Ihara	Hokkaido University		小濱 芳允
3	202012-HMBXX-0013	精密電子スピン共鳴測定用パルスマグネットの開発	赤木 暢	神戸大学		Development of pulsed magnet for precise electron spin resonance measurements	Mitsuru Akaki	Kobe University		小濱 芳允

留学研究課題 / External Research Project Long / Short -term

No.	課題番号	課題名	氏名	所属	分担者	Title	Name	Organization	Member of research project	担当所員

1	202012-VSBXL-0003	ケージド化合物光解離の時間分解測定	崎元 柊	群馬大学		Time-resolved measurement of photodissociation of caged compounds	Shu Sakimoto	Gunma University		秋山 英文

2021年度　共同利用課題一覧（後期）/ Joint Research List (Latter Term)

※実施課題一覧、所属は申請時のデータ

嘱託課題 / Commission Research Project

No.	課題番号	課題名	氏名	所属	分担者	Title	Name	Organization	Member of research project	担当所員
1	202104-CMBXX-0075	Materials Foundryのための材料開発システム構築に向けた薄膜合成装置の開発	高橋 竜太	日本大学		Development of Film Deposition Systems for High-throughput-Material Exploration	Ryota Takahashi	Nihon University		Mikk Lippmaa
2	202110-CMBXX-0149	ESM-RISM法を実装したQuantum ESPRESSOの高度化	萩原 聡	筑波大学計算科学研究センター		Improvement of Quantum ESPRESSO implementing the ESM-RISM method	Satoshi Hagiwara	Tsukuba University, Center for Computational Sciences		川島 直輝
3	202106-CMBXX-0096	低次元有機物質の圧力下物性研究	糸井 充穂	日本大学		Study on pressure induced superconductivity of low dimension organic conductor	Miho Itoi	Nihon University		上床 美也
4	202106-CMBXX-0088	圧力下NMR測定法に関する開発	藤原 直樹	京都大学		Development of NMR measurement method under high pressure	Naoki Fujiwara	Kyoto University		上床 美也
5	202106-CMBXX-0097	高圧下X線回折法の開発	江藤 徹二郎	久留米工業大学		Development of High Pressure X-ray diffraction measurements	Tetsujiro Eto	Kurume Institute of Technology		上床 美也
6	202106-CMBXX-0087	希土類122化合物における圧力効果	繁岡 透	山口大学		Pressure effect of rare earth 122 compounds	Toru Shigeoka	Yamaguchi University		上床 美也
7	202107-CMBXX-0144	4Gにおける共同利用推進	那波 和宏	東北大学		Research and Support of General-Use at 4G	Kazuhiro Nawa	Tohoku University		眞弓 皓一
8	202107-CMBXX-0145	4Gにおける共同利用推進	奥山 大輔	東北大学		Research and Support of General-Use at 4G	Daisuke Okuyama	Tohoku University		眞弓 皓一
9	202107-CMBXX-0146	4Gにおける共同利用推進	佐藤 卓	東北大学		Research and Support of General-Use at 4G	Taku J Sato	Tohoku University		眞弓 皓一
10	202110-CMBXX-0150	超強磁場におけるスピン格子強結合系の研究	池田 暁彦	電気通信大学		Study of the strongly spin-lattice-coupled systems in ultrahigh magnetic fields	Akihiko Ikeda	University of Electro-Communications		松田 康弘
11	202106-CMBXX-0102	有機化合物の光電子分光	金井 要	東京理科大学		Photoemission study on organic compounds	Kaname Kanai	Tokyo University of Science		近藤 猛
12	202106-CMBXX-0101	レーザースピン角度分解光分光による表面電子状態の研究	矢治 光一郎	物質・材料研究機構		SARPES studies of atomic layer materials at surfaces	Koichiro Yaji	National Institute for Materials Science		近藤 猛
13	202106-CMBXX-0117	反強磁性を示す近似結晶の精密光電子分光測定	津田 俊輔	物質・材料研究機構		Laser-Photoemission Study on antiferromagnetic approximant crystals	Shunsuke Tsuda	National Institute for Materials Science		近藤 猛
14	202105-CMBXX-0081	軟X線吸収/発光分光法によるリチウムイオン電池電極材料の電子物性研究	朝倉 大輔	産業技術総合研究所		Study on the electronic property of electrode materials for Li-ion batteries by soft X-ray absorption/emission spectroscopy	Daisuke Asakura	AIST		原田 慈久
15	202105-CMBXX-0079	三次元nanoESCAによる実デバイスのオペランド電子状態解析	永村 直佳	物質・材料研究機構		Operando analysis of the electronic structure of actual devices by 3DnanoESCA	Naoka Nagamura	National Institute for Materials Science		原田 慈久
16	202106-CMBXX-0113	偏光制御型軟X線分光装置の開発	平田 靖透	防衛大学校		Developing a system for the polarization-controlled soft X-ray spectroscopy	Yasuyuki Hirata	National Defense Academy of Japan		松田 巌

一般課題 / General Research Project

No.	課題番号	課題名	氏名	所属	分担者	Title	Name	Organization	Member of research project	担当所員

1	202105-GNBXX-0117	分子性超薄膜単結晶のX線構造解析	熊谷 翔平	東京大学	岡本 敏宏 荒井 勇太郎 沢辺 千鶴 黒澤 忠法 山中 大輔	X-ray structure determination of molecular single crystal ultrathin films	Shohei Kumagai	Department of Advanced Materials Science, Graduate School of Frontier Sciences	Toshihiro Okamoto Yutaro Arai Chizuru Sawabe Tadanori Kurosawa Daisuke Yamanaka	森 初果
2	202201-GNBXX-0187	高いプロトン伝導度を示すスルホン酸有機塩の創製	岡 弘樹	大阪大学	森 初果（東京大学）	Sulfonic Acid Organic Salts with High Proton Conductivity	Kouki Oka	Osaka University	Hatsumi Mori, The University of Tokyo	森 初果
3	202106-GNBXX-0134	ウラン系微小純良単結晶試料における磁化測定と高感度磁力計の開発	清水 悠晴	東北大学金属材料研究所		Magnetization measurements for uranium-based high-quality single crystals and development of high-resolution magnetometers	Yusei Shimizu	Tohoku University, Institute for Materials Research		山下 穣
4	202106-GNBXX-0160	インデンター型高圧セルを応用した極低温磁化測定技術の開発	清水 悠晴	東北大学金属材料研究所	佐藤 芳樹	Development of Faraday magnetometers for sub-kelvin-temperature region under high pressures using indenter-type pressure cell	Yusei Shimizu	Tohoku University, Institute for Materials Research	Yoshiki Sato, Tohoku University	山下 穣
5	202110-GNBXX-0176	古典スピンアイス Ho2Ti2O7 の極低温低周波磁化率測定	柄木 良友	琉球大学		Low-temperature ;low-frequency magnetic susceptibility measurement of classical spin ice Ho2Ti2O7	Yoshitomo Karaki	University of the Ryukyus		山下 穣
6	202105-GNBXX-0152	重い電子系化合物YbRh2Zn20における極低温磁化測定	北澤 崇文	東北大学	池田 陽一 清水 悠晴 川又 雅広	Magnetization measurements at very low temperatures on the heavy fermion compound YbRh2Zn20	Kitazawa Takafumi	Tohoku university	Yoichi Ikeda Yusei Shimizu Masahiro Kawamata	山下 穣
7	202106-GNBXX-0154	ファラデー法による反転対称性を持つ磁性体における極低温磁化測定	南部　雄輔	東北大学	川又 雅広	Low-temperature magnetization measurement of centrosymmetric compounds with a capacitive Faraday magnetometer	Yusuke Nambu	Tohoku Univ.	Masahiro Kawamata	山下 穣
8	202111-GNBXX-0185	古典スピンアイス Ho2Ti2O7 の極低温低周波磁化率測定	柄木 良友	琉球大学	唐 楠（東京大学）	Low-temperature low-frequency magnetic susceptibility measurement of classical spin ice Ho2Ti2O7	Yoshitomo Karaki	University of the Ryukyus	Nan Tang, The University of Tokyo	山下 穣
9	202105-GNBXX-0114	重い電子系希土類化合物における異方的量子臨界現象の磁気的評価	河野 洋平	中央大学	辻 貴丹 木元 大介 綱島 海斗 加藤 謙介	Magnetic properties of anisotropic quantum critical phenomena in a heavy-fermion metal	Yohei Kono	Chuo University	Kitami Tsuji Daisuke Kimoto Kaito Tsunashima Kensuke Kato	山下 穣
10	202105-GNBXX-0112	c軸磁場下におけるCeCoIn5の極低温精密磁歪測定	橘高 俊一郎	中央大学	辻 貴丹 木元 大介 綱島 海斗 加藤 謙介	Low-temperature high-resolution magnetostriction measurement on CeCoIn5 in a magnetic field along the c axis	Shunichiro Kittaka	Chuo University	Kitami Tsuji Daisuke Kimoto Kaito Tsunashima Kensuke Kato	山下 穣
11	202105-GNBXX-0106	スピン軌道結合金属Cd2Re2O7の酸素NMRと電流誘起効果	瀧川 仁	高エネルギー加速器研究機構・物質構造科学研究所		Oxygen NMR and current-induced effects in the spin-orbit coupled metal Cd2Re2O7	Masashi Takigawa	High Energy Accelerator Research Organization, Institute of Materials Structure Science		山下 穣
12	202105-GNBXX-0122	二次元銅酸化物のホール係数測定IV	神戸 士郎	山形大学大学院理工学研究科	川村 桂太 南光 伸哉	Hall coefficient measurement of 2D cuprates (IV)	Shiro Kambe	Graduate School of Science and Engineering, Yamagata University	Keita Kawamura Shinya Nanko	勝本 信吾

13	202104-GNBXX-0093	量子ホール効果のための高移動度半導体試料作製と超低温での測定	福田 昭	兵庫医科大学		Development of the high mobility semiconductor samples for the quantum Hall state and their measurements in very low temperature	Akira Fukuda	Hyogo College of Medicine		勝本 信吾
14	202109-GNBXX-0181	希土類金属間化合物の強磁場低温物性研究	海老原 孝雄	静岡大学		Physical properties in rare earth intermetallic compounds at high magnetic fields in low temperature	Takao Ebihara	Shizuoka University		大谷 義近
15	202105-GNBXX-0150	窒素吸着Cu(001)表面におけるBi薄膜の成長と電子状態	中辻 寛	東京工業大学	永友 慶 森井 七生 小森 文夫	Growth process of Bi thin-film on nitrogen adsorbed Cu(001) surface and its electronic structure	Kan Nakatsuji	Tokyo Institute of Technology	Kei Nagatomo Morii Nanao Fumio Komori	吉信 淳
16	202105-GNBXX-0151	微傾斜Si(111)√3×√3-B基板上に成長したBi(110)超薄膜の電子状態	中辻 寛	東京工業大学	大内 拓実 小森 文夫	Electronic structure of Bi(110) thin films grown on vicinal Si(111)√3×√3-B substrates	Kan Nakatsuji	Tokyo Institute of Technology	Takumi Ouchi Fumio Komori	吉信 淳
17	202105-GNBXX-0107	基板での原子クラスター構造選別法の確立と, クラスター構造と磁性の関係の解明	塚原 規志	群馬工業高等専門学校		Establishment of selection method for atomic clusters on the substrate and elucidation of the relation between the cluster structure and its magnetic properties	Noriyuki Tsukahara	National Institute of Technology, Gunma College		吉信 淳
18	202106-GNBXX-0128	貴金属表面における水素結合を有する有機分子薄膜の成長過程の観測	金井 要	東京理科大学	小久保 裕太 馬上 怜奈	Observation of the growth process of organic molecular thin films with hydrogen bonding on noble metal surfaces	Kaname Kanai	Tokyo University of Science	Yuta Kokubo Rena Moue	吉信 淳
19	202105-GNBXX-0101	遷移金属酸化物ナノシート表面への欠陥導入による外来分子吸着の制御	野内 亮	大阪府立大学	前山 滉貴	Control of molecular adsorption on transition metal oxide nanosheet films by introduction of surface defects	Ryo Nouchi	Osaka Prefecture University	Hirotaka Maeyama	吉信 淳
20	202105-GNBXX-0110	GaAs中のエルビウムからの複数の発光線の識別	矢口 裕之	埼玉大学	矢野 裕子 伊藤 駿平	Identification of emission lines from erbium in GaAs	Hiroyuki Yaguchi	Saitama University	Yuko Yano Shunpei Ito	秋山 英文
21	202106-GNBXX-0129	新奇ケージド化合物の分光的特性の研究	樋山 みやび	群馬大学	勝見 渓太	Study of spectroscopic property for a new caged compound	Miyabi Hiyama	Gunma University	Katsumi Keita	秋山 英文
22	202106-GNBXX-0138	DEACM-ケージドルシフェリンの蛍光測定	樋山 みやび	群馬大学	工藤 優斗	Study for photoluminescence of DEACM caged D-Luciferin	Miyabi Hiyama	Gunma University	Kudo Yuto	秋山 英文
23	202106-GNBXX-0127	自動定量測定法の開発	樋山 みやび	群馬大学	高橋 由太翔	Development of automatic quantitative measurements	Miyabi Hiyama	Gunma University	Takahashi Yutaka	秋山 英文
24	202110-GNBXX-0179	Si基板上に直接成長させたGaNの成長条件が光学特性に及ぼす影響	石川 由依	香川大学	石川 由依 田中 慈大	Influence of growth conditions of GaN on Si substrate on optical properties	Yui Ishikawa	Kagawa University	Yui Ishikawa Tanaka Shigehiro	秋山 英文
25	202110-GNBXX-0180	分子線エピタキシー法を用いて作製したGaN/AlN半導体超格子のフォトルミネッセンスによる光学特性評価	土居 虹介	香川大学	土居 虹介 田中 慈大	Photoluminescence study of GaN/AlN superlattices grown by MBE.	Kosuke Doi	Kagawa University	Kosuke Doi Tanaka Shigehiro	秋山 英文
26	202110-GNBXX-0179	Si基板上に直接成長させたGaNの成長条件が光学特性に及ぼす影響	小柴 俊	香川大学	石川 由依 田中 慈大	Influence of growth conditions of GaN on Si substrate on optical properties	Shyun Koshiba	Kagawa University	Yui Ishikawa Tanaka Shigehiro	秋山 英文
27	202111-GNBXX-0183	Si基板上に成長したGaN系pn素子の電気特性と光学特性	宮川 勇人	香川大学	森 健	Electrical and optical properties of GaN pn-junction grown on Si substrates	Hayato Miyagawa	Kagawa University	Takeshi Mori	秋山 英文
28	202106-GNBXX-0124	ハニカム格子系van Vleckエキシトン磁性候補物質の物性	原口 祐哉	東京農工大学		Physical properties in candidates of van Vleck excitonic honeycomb lattice magnet	Yuya Haraguchi	Tokyo University of Agriculture and Technology		広井 善二

29	202105-GNBXX-0119	反強磁性体Eu-Pt-Ga化合物の高圧下における電子状態の研究	本多 史憲	九州大学アイソトープ統合安全管理センター	小泉 堯嗣（東北大学）	Electronic properties of an antiferromagnetic Eu-Pt-Al compound under high pressures	Fuminori Honda	Central Institute of Radioisotope Science and Safety Management, Kyushu University	Takatsugu Koizumi, Tohoku university	上床 美也
30	202106-GNBXX-0167	ウラン化合物の磁性の圧力効果	本多 史憲	九州大学アイソトープ統合安全管理センター		Effect of Pressure on the magnetism of uranium compounds	Fuminori Honda	Central Institute of Radioisotope Science and Safety Management, Kyushu University		上床 美也
31	202106-GNBXX-0132	Ni2In型強磁性体の自発磁化の圧力効果	安達 義也	山形大学	井田 唯斗	Pressure effects on the spontaneous magnetization for Ni2In-type ferromagnets	Yoshiya Adachi	Yamagata University	Yuino Ida	上床 美也
32	202106-GNBXX-0157	CDWや励起子絶縁体転移に伴う構造相転移温度の圧力依存性	広瀬 雄介	新潟大学	土田 駿	Study of pressure effect on structural transition in CDW and excitonic orderings	Yusuke Hirose	Niigata University	Shun Tsuchida	上床 美也
33	202106-GNBXX-0145	多重極限下における点接合分光測定法の開発	本山 岳	島根大学	篠﨑 真碩	Improvement of point-contact spectroscopy for multiple extreme conditions	Gaku Motoyama	Shimane University	Masahiro Shinozaki	上床 美也
34	202106-GNBXX-0143	奇パリティ多極子秩序候補物質Ce3TiSb5の圧力下電気抵抗測定	篠﨑 真碩	島根大学	本山 岳	Electrical resistivity measurements of Ce3TiSb5 under pressure	Masahiro Shinozaki	Shimane University	Gaku Motoyama	上床 美也
35	202106-GNBXX-0166	高スピン分極ホイスラー合金における圧力誘起量子臨界現象の探索	重田 出	鹿児島大学	辻川 聡一朗	Search for pressure-induced quantum critical phenomenon in highly spin polarized Heusler alloys	Iduru Shigeta	Kagoshima University	Soichiro Tsujikawa	上床 美也
36	202106-GNBXX-0158	HoRh2Si2のPd置換系化合物の単結晶育成 (3)	藤原 哲也	山口大学	五反田 礼	Single crystal growth of Pd substituted compounds HoRh2-xPdxSi2 (3)	Tetsuya Fujiwara	Yamaguchi University	Rei Gotanda	上床 美也
37	202106-GNBXX-0159	TmRh2Si2の単結晶育成 (3)	藤原 哲也	山口大学	金子 達哉	Single crystal growth of TmRh2Si2 (3)	Tetsuya Fujiwara	Yamaguchi University	Kaneko Tatsuya	上床 美也
38	202106-GNBXX-0163	CeZn2Ge2単結晶の高圧化磁化測定 (2)	藤原 哲也	山口大学	杉田 静留	Magnetization measurements under high pressures of CeZn2Ge2 single crystal (2)	Tetsuya Fujiwara	Yamaguchi University	Shizuru Sugita	上床 美也
39	202106-GNBXX-0162	YbMn2Ge2の圧力誘起価数転移と高圧力下の磁気状態に関する研究	藤原 哲也	山口大学	小林 遼平	Investigation for pressure induced valence transition and magnetic phase of YbMn2Ge2	Tetsuya Fujiwara	Yamaguchi University	Ryohei Kobayashi	上床 美也
40	202106-GNBXX-0153	ホイスラー化合物Fe3-xMnxSiの圧力下磁気相転移	廣井 政彦	鹿児島大学	赤石 幸起	Magnetic phase transitions under pressure in Heuser compounds Fe3-xMnxSi	Masahiko HIROI	Kagoshima University	Kouki Akaishi	上床 美也
41	202106-GNBXX-0144	高圧物性測定に適した圧力媒体の探索	村田 惠三	大阪市立大学		Search for high pressure medium suitable for high pressure experiment on material properties	Keizo Murata	Osaka City University		上床 美也
42	202111-GNBXX-0186	Eu3Bi2S4F4における圧力効果の研究	石垣 賢卯	兵庫県立大学		Research of pressure effect on Eu3Bi2S4F4	Kento Ishigaki	University of Hyogo		上床 美也
43	202105-GNBXX-0100	S置換したFeSeの高圧低温NMR測定	藤原 直樹	京都大学	Yu Zhongyu	NMR studies on S-substituted FeSe at high pressures and low temperatures	Naoki Fujiwara	Kyoto University	Zhongyu Yu	上床 美也
44	202105-GNBXX-0108	擬三元化合物Ce1-xLaxNiC2の結晶育成と物質評価 3	繁岡 透	山口大学	内間 清晴（沖縄キリスト教短期大学）	Crystal growth and characterization of pseude-ternary compounds Ce1-xLaxNiC2 3	Toru Shigeoka	Yamaguchi University	Kiyoharu Uchima, Okinawa Christian Junior College Professor	上床 美也
45	202105-GNBXX-0109	CeNiC2の結晶育成と物質評価	繁岡 透	山口大学	内間 清晴（沖縄キリスト教短期大学）	Crystal growth and characterization of CeNiC2	Toru Shigeoka	Yamaguchi University	Kiyoharu Uchima, Okinawa Christian Junior College Professor	上床 美也

46	202111-GNBXX-0184	立方晶ラーベス相化合物PrIr2の高圧下物性測定による強磁性量子臨界現象の探索	菅原 仁	神戸大学		Search of the ferromagnetic quantum critical phenomenon by the high pressure physical property measurement of cubic Laves-phase compound PrIr2	Hitoshi Sugawara	Kobe university		上床 美也
47	202105-GNBXX-0149	ベリル中の水分子の量子常誘電状態における同位体効果	山根 崚	東北大学		Deuterium isotope effect of quantum paraelectric state of water confined in beryl	Ryo Yamane	Tohoku university		益田 隆嗣
48	202109-GNBXX-0172	セリウム系金属間化合物の物性測定	植田 大地	高エネルギー加速器研究機構		Magnetic properties of cerium-based intermetallic compounds	Daichi Ueta	High Energy Accelerator Research Organization		益田 隆嗣
49	202105-GNBXX-0103	金属ナノ構造の超高速発光による研究	末元 徹	電気通信大学		Studies on nanostructured metals by ultrafast luminescence spectroscopy	Suemoto Tohru	The University of Electro-Communications		小林 洋平
50	202105-GNBXX-0104	次世代レーザーとレーザー加工の基礎技術研究	吉富 大	産業技術総合研究所	高田 英行 奈良崎 愛子 小川 博嗣 寺澤 英知 澁谷 達則 佐藤 大輔 黒田 隆之助 田中 真人	Basic research on next generation laser systems and laser machining technology	Dai Yoshitomi	National Institute of Advanced Industrial Science and Technology	Takada Hideyuki Aiko Narazaki Hiroshi Ogawa Eichi Terasawa Tatsunori Shibuya Daisuke Satoh Ryunosuke Kuroda Masahito Tanaka	小林 洋平
51	202106-GNBXX-0146	炭素材料におけるレーザー照射による構造変化に関する研究	山口 誠	秋田大学	高林 圭佑	Structural changes induced by laser irradiation in carbon materials	Yamaguchi Makoto	Akita University	Keisuke Takabayashi	小林 洋平
52	202105-GNBXX-0115	パルス時間幅がレーザー加工プロセスに与える影響	三村 一暉	徳島大学	三村 一暉	Influence of laser pulse duration on laser ablation process	Mimura Kazuki	Tokushima University	Mimura Kazuki	小林 洋平
53	202105-GNBXX-0121	有機分子/貴金属界面におけるラシュバ分裂の増大	金井 要	東京理科大学	小久保 裕太 馬上 怜奈	Enhancement of Rashba splitting on organic molecule/noble metal interface	Kaname Kanai	Tokyo University of Science	Yuta Kokubo Rena Moue	近藤 猛
54	202105-GNBXX-0121	有機分子/貴金属界面におけるラシュバ分裂の増大	小久保 裕太	東京理科大学	小久保 裕太 馬上 怜奈	Enhancement of Rashba splitting on organic molecule/noble metal interface	yuta kokubo	Tokyo University of Science	Yuta Kokubo Rena Moue	近藤 猛
55	202106-GNBXX-0137	Ti3SiC2のスピン分解角度分解光電子分光	伊藤 孝寛	名古屋大学	松永 和也 山本 凌 杉本 卓史 保科 拓海	Spin- and Angle-resolved photoemission study of Ti3SiC2	Takahiro Ito	Nagoya University	Matsunaga Kazuya Yamamoto Ryo Takafumi Sugimoto Hoshina Takumi	近藤 猛
56	202106-GNBXX-0130	バルク敏感高分解能スピン分解光電子分光を用いたハーフメタル強磁性体の多体効果の研究	横谷 尚睦	岡山大学	片岡 範行 瀬戸口 太朗	Many-body interaction of half-metallic antiferromagnet studied by bulk sensitive high-resolution spin-resolved photoemission spectroscopy	Takayoshi Yokoya	Okayama University	Noriyuki Kataoka Taro Setoguchi	近藤 猛
57	202106-GNBXX-0155	励起子絶縁体の原子層結晶における電子正孔相関の光誘起ダイナミクス(2)	大川 万里生	早稲田大学	高橋 優	Photoinduced dynamics of electron-hole correlation in atomic-layered excitonic insulators (2)	Mario Okawa	Waseda University	Yu Takahashi	岡﨑 浩三
58	202109-GNBXX-0171	カロリメトリーによる金属試料の赤外吸収率測定	末元 徹	電気通信大学		Measurement of infrared absorptivity on metal samples by calorimetry	Suemoto Tohru	The University of Electro-Communications		岡﨑 浩三

No.	課題番号	課題名	氏名	所属	分担者	Title	Name	Organization	Member of research project	実験室
1	202104-MCBXG-0054	Nd1-x(Sr0.5Ca0.5)xFeO3 (0.1≦x≦0.9) の高温における磁性と熱電特性に関する研究	中津川 博	横浜国立大学	鎌谷 雄大	Magnetism and thermoelectric properties at high temperature in Nd1-x(Sr0.5Ca0.5)xFeO3 (0.1≦x≦0.9)	Hiroshi Nakatsugawa	Yokohama National University	Yudai Kamatani	電磁気測定室
2	202105-MCBXG-0055	量体化直前の金属における圧力誘起相転移の探索	片山 尚幸	名古屋大学	松田 悠大 塩見 学 小島 慶太	Search for pressure-induced phase transitions in metals just before dimerization	Naoyuki Katayama	Nagoya University	Matsuda Yudai Manabu Shiomi Keita Kojima	化学分析室 X線測定室 電磁気測定室
3	202105-MCBXG-0056	電子不足型量体化分子の内部構造の解明	片山 尚幸	名古屋大学	塩見 学 小島 慶太 原 武史	Elucidation of the internal structure of electron-deficient dimerized molecules	Naoyuki Katayama	Nagoya University	Manabu Shiomi Keita Kojima Takeshi Hara	化学分析室 X線測定室 電磁気測定室
4	202105-MCBXG-0060	高温高圧下での斜方輝石と水流体の間の界面エネルギー	松影 香子	帝京科学大学		Interfacial energy between orthopyroxene and aqueous fluid in high pressure and high temperature conditions	Kyoko N. Matsukage	Teikyo University of Science		電子顕微鏡室 高圧合成室
5	202105-MCBXG-0061	希土類元素およびアルカリ土類金属元素を充填した新規スクッテルダイト型熱電材料の高圧合成	関根 ちひろ	室蘭工業大学	本間 さくら	High-pressure synthesis of new rare-earth and alkaline-earth filled skutterudite-type thermoelectric materials	Chihiro Sekine	Muroran Institute of Technology	Sakura Homma	高圧合成室
6	202105-MCBXG-0062	磁気多極子の強的秩序に基づく物質機能の開発	渡辺 義人（有馬 孝尚）	東京大学	車地 崇 池田 凜太郎 木村 真栄 佐藤 樹 海本 祐真 渡辺 義人 柳田 真佑 徳永 祐介 石崎 大悟 厳 正輝 吉田 健斗	Development of material functions based on ferroic multipole order	Yoshito Watanabe	Department of Advanced Materials Science	Takashi Kurumaji Rintaro Ikeda Shin-Ei Kimura Tatsuki Sato Yuma Umimoto Shinsuke Yanagida Yusuke Tokunaga Daigo Ishizaki Masaki Gen Kento Yoshida	X線測定室 電磁気測定室
7	202105-MCBXG-0063	一次元テルル化物Nb2Pd3Te5における超伝導	岡本 佳比古	名古屋大学		Superconductivity in one-dimensional telluride Nb2Pd3Te5	Yoshihiko Okamoto	Nagoya University		化学分析室 電磁気測定室
8	202106-MCBXG-0065	幾何学的フラストレート格子を持つキタエフ・ハイゼンベルグ磁性体の物性研究	原口 祐哉	東京農工大学		Study of Physical Properties of Kitaev-Heisenberg Magnets with Geometric Frustrated Lattice	Yuya Haraguchi	Tokyo University of Agriculture and Technology		化学分析室 電磁気測定室
9	202106-MCBXG-0066	合金ナノ粒子のキャラクタリゼーション	佐々木 岳彦	東京大学	張 凱朝 フェ ジシュン	Characterization of alloy nanoparticles	Takehiko Sasaki	Graduate School of Frontier Sciences, Department of Complexity Science and Engineering	Kaichao Zhang He Zixuan	X線測定室 電子顕微鏡室 光学測定室
10	202106-MCBXG-0070	二次元銅酸化物の磁化率測定	神戸 士郎	山形大学	川村 桂太 南光 伸哉	Magnetic susceptibility measurement of 2D cuprates	Shiro Kambe	Graduate School of Science and Engineering, Yamagata University	Keita Kawamura Shinya Nanko	電磁気測定室

11	202106-MCBXG-0073	ハニカム格子を持つRuI3の高圧合成	今井 良宗	東北大学	藤原 秀行	High pressure synthesis of RuI3 with the honeycomb structure	Yoshinori Imai	Tohoku university	Hideyuki Fujihara	X線測定室 高圧合成室
12	202106-MCBXG-0076	奇パリティ磁気多極子秩序を持つ物質の単結晶育成と物性評価	阿部 伸行	日本大学		Crystal growth and physical properties measurement in odd parity multipole ordering materials	Nobuyuki Abe	Nihon University		物質合成室 X線測定室 電磁気測定室
13	202106-MCBXG-0079	ホイスラー化合物での反強磁性の研究	廣井 政彦	鹿児島大学	赤石 幸起 鹿児島大学 大学院生（前期・修士課程）	Study on antiferromagnetism in Heusler compounds	Masahiko Hiroi	Kagoshima University	Kouki Akaishi Kagoshima University	電磁気測定室
14	202106-MCBXG-0082	高度に制御された凝縮相と高圧非平衡プラズマの相互作用による金属等の表面改質および微粒子合成の研究	宗岡 均	東京大学	新田 魁洲 黒田 知暉 羽藤 健	Surface modification of metals and synthesis of fine metal particles by interaction between highly controlled condensed phases and high-pressure non-equilibrium plasmas	Hitoshi Muneoka	The University of Tokyo	Kaishu Nitta Kuroda Tomoki Takeru Hato	電子顕微鏡室
15	202106-MCBXG-0083	交流磁化率測定による反強磁性絶縁体に近接した層状有機超伝導体における相分離した超伝導相の研究	谷口 弘三	埼玉大学	高橋 啓太	Studies on phase-separated superconducting phase in layered organic superconductors bordering on antiferromagnetic insulating phase by ac susceptibility measurements	Hiromi Taniguchi	Saitama University	Takahashi Keita	電磁気測定室
16	202106-MCBXG-0094	高スピン分極ホイスラー合金の磁気特性のスピンゆらぎ理論による解析に関する研究	重田 出	鹿児島大学	横山 喬亮	Study on analysis of magnetic properties for highly spin polarized Heusler alloys by the spin fluctuation theory	Iduru Shigeta	Kagoshima University	Takaaki Yokoyama	電磁気測定室

物質合成・評価設備Uクラス / Materials Synthesis and Characterization U Class Research Project

No.	課題番号	課題名	氏名	所属	分担者	Title	Name	Organization	Member of research project	実験室
1	202109-MCBXU-0104	Sm1-x(Sr0.5Ca0.5)xFeO3 (0.1≦x≦0.9) の高温における磁性と熱電特性に関する研究	中津川 博	横浜国立大学	鎌谷 雄大	Magnetism and thermoelectric properties at high temperature in Sm1-x(Sr0.5Ca0.5)xFeO3 (0.1≦x≦0.9)	Hiroshi Nakatsugawa	Yokohama National University	Yudai Kamatani	電磁気測定室
2	202109-MCBXU-0106	Sr-Al-O系ウイスカー結晶の高温磁性評価	鄭 旭光	佐賀大学		High-temperature magnetization for Sr-Al-O whisker crystals	Xu-Guang Zheng	Saga University		電磁気測定室
3	202111-MCBXU-0110	YnConGa型遍歴電子磁性体の単結晶X線構造解析	和氣 剛	京都大学		X-ray Single-Crystal Structural Analysis of YnConGa-type itinerant electron magnets	Takeshi Waki	Kyoto University		X線測定室
4	202111-MCBXU-0111	ハイドロゲル中に吸着されたポリヨウ化物イオンの同定	周 泓遥	東京大学	松野 稜平	Identification of polyiodide ions adsorbed in hydrogel	Hongyao Zhou	The University of Tokyo	Ryohei Matsuno	光学測定室
5	202109-MCBXU-0107	セリウム系金属間化合物のarc溶解による合成	植田 大地	高エネルギー加速器研究機構		Sample growth of a cerium-based intermetallic compounds by arc melting method	Daichi Ueta	High Energy Accelerator Research Organization		物質合成室

国際超強磁場科学施設 / International MegaGauss Science Laboratory

No.	課題番号	課題名	氏名	所属	分担者	Title	Name	Organization	Member of research project	担当所員

1	202105-HMBXX-0059	重い電子系化合物が示す非従来型超伝導と非フェルミ液体状態の相関	横山 淳	茨城大学	平山 堅理	Relationship between unconventional superconductivity and non-Fermi-liquid state in heavy-fermion compounds	Makoto Yokoyama	Ibaraki University	Takatoshi Hirayama	金道 浩一
2	202105-HMBXX-0064	フラストレート格子をもつダブルペロブスカイト鉄酸化物の強磁場磁性	後藤 真人	京都大学	小杉 佳久 飯星 眞	Magnetic properties of double-perovskite-Fe oxides with frustrated lattices under high magnetic fields	Masato Goto	Kyoto University	Yoshihisa Kosugi Makoto Iihoshi	金道 浩一
3	202105-HMBXX-0065	幾何学的フラストレート磁性体の強磁場磁化測定	菊池 彦光	福井大学		Magnetization measurements of the frustrated magnets	Hikomitsu Kikuchi	University of Fukui		金道 浩一
4	202105-HMBXX-0067	超伝導相近傍に位置する有機反強磁性体の磁気構造決定	小林 拓矢	埼玉大学	安村 乃絵瑠	Determination of the magnetic structure of organic antiferromagnets located in the vicinity of the superconducting phase	Takuya Kobayashi	Saitama University	Noeru Yasumura	金道 浩一
5	202106-HMBXX-0066	フラストレートしたハニカム格子磁性体における新奇磁場誘起相の探索	原口 祐哉	東京農工大学	八束 波椰斗	Search for novel magnetic field-induced phases in frustrated honeycomb lattice magnets	Yuya Haraguchi	Tokyo University of Agriculture and Technology	Yatsuzuka Hayato	金道 浩一
6	202106-HMBXX-0071	パルス強磁場中c軸抵抗率測定による銅酸化物高温超伝導体における前駆クーパー対形成の検証	渡辺 孝夫	弘前大学	藤井 武則（東京大学）	Observation of preformed Cooper pairing in high-Tc cuprates using out-of-plane resistivity measurements of Bi(Pb)-2212 single crystals under high pulsed magnetic fields	Takao Watanabe	Hirosaki University	Takenori Fujii, The University of Tokyo	金道 浩一
7	202106-HMBXX-0073	有機超伝導体のFFLO超伝導相に対する乱れの効果	杉浦 栞理	東北大学 金属材料研究所		Disorder effect on FFLO superconductivity of organic superconductors	Shiori Sugiura	Institute for Materials Research, Tohoku University		金道 浩一
8	202106-HMBXX-0081	S = 1/2カゴメ格子反強磁性体A2BTi3F12および擬二次元遍歴電子系ACo2X2の高磁場下における磁気特性	道岡 千城	京都大学	森山 広大	Magnetic properties of S = 1/2 kagome lattice antiferromagnets A2BTi3F12 and quasi-two-dimensional itinerant electron system ACo2X2 in high magnetic fields	Michioka Chishiro	Kyoto University	Kodai Moriyama	金道 浩一
10	202109-HMBXX-0099	高磁場における１イオン磁気異方性の回復過程の観測と常磁性良導体試料に対するパルス強磁場磁化測定の最適条件の検討	池田 陽一	東北大学金属材料研究所	北澤 崇文	Recovery of the single-ion anisotropy at high magnetic fields and verification of the optimum condition on magnetization measurements for paramagnetic metals in pulsed high magnetic field	Yoichi Ikeda	Institute for materials research, Tohoku university	Kitazawa Takafumi	金道 浩一
11	202110-HMBXX-0104	三角格子磁性体NaPrTe2の強磁場磁化過程	岡本 佳比古	名古屋大学		High-Field Magnetization Measurement of a Triangular Magnet NaPrTe2	Yoshihiko Okamoto	Nagoya University		金道 浩一
12	202110-HMBXX-0105	λ型有機導体の示す負の巨大磁気抵抗、磁場誘起絶縁体金属転移の解明	福岡 脩平	北海道大学		Study of giant negative magnetoresistance and magnetic field-induced insulator-metal transition in λ-type organic conductors	Shuhei Fukuoka	Hokkaido University		金道 浩一
13	202110-HMBXX-0106	トポロジカル磁気相転移に伴う格子歪みの研究	巌 正輝	東京大学		Study of lattice distortions associated with topological phase transition	Masaki Gen	The University of Tokyo		松田 康弘
14	202201-HMBXX-0110	超高磁場下で巨大な異方性磁場を持つ Sm-Co-B ベースの化合物の調査	トズマン カラニコラス ペリン	物質・材料研究機構		Investigation of Sm-Co-B-based compounds with giant anisotropy field under ultrahigh magnetic field	Pelin Tozman Karanikolas	National Institute for Materials Science		松田 康弘
15	202106-HMBXX-0069	ヨウ素輸送法で育成したFe(Te,S) における超伝導状態の磁気光学イメージングによる観測	矢口 宏	東京理科大学	藤川 俊樹 山中 隆義	Observations of superconducting states in Fe(Te,S) grown by an iodine-transport method using an MO imaging technique	Hiroshi Yaguchi	Tokyo University of Science	Toshiki Fujikawa Takayoshi Yamanaka	徳永 将史

16	202106-HMBXX-0074	鉄系超伝導体Fe(Te, Se)における超伝導空間分布の磁気光学イメージングによる観測	山中 隆義	東京理科大学	矢口 宏 打川 景大	Observation of the distribution of superconductivity in Fe(Te, Se) using a magnet optical imaging technique	Takayoshi Yamanaka	Tokyo University of Science	Hiroshi Yaguchi Keita Uchikawa	徳永 将史
17	202106-HMBXX-0079	磁性元素をドープした極性ディラック電子系の強磁場物性	酒井 英明	大阪大学	近藤 雅起	Study of high-field phenomena in magnetic-ion-doped polar Dirac materials	Hideaki Sakai	Osaka University	Masaki Kondo	徳永 将史
18	202106-HMBXX-0085	マルチフェロイック物質の外場による相転移現象の研究	河智 史朗	兵庫県立大学		Study of phase transition phenomena in multiferroic materials under external fields	Kawachi Shiro	University of Hyogo		徳永 将史
19	202106-HMBXX-0090	反強磁性体EuPt3Al5の強磁場磁化測定	本多 史憲	九州大学アイソトープ統合安全管理センター	小泉 堯嗣（東北大学）	High-field magnetization measurement on a new antiferromagnet EuPt3Al5	Fuminori Honda	Central Institute of Radioisotope Science and Safety Management, Kyushu University	Takatsugu Koizumi, Tohoku university	徳永 将史
20	202110-HMBXX-0103	マルチフェロイック物質(NH4)2[FeCl5(H2O)]の電気磁気効果	木原 工	岡山大学異分野基礎科学研究所		Magnetoelectric effect of multiferroic (NH4)2[FeCl5(H2O)]	Takumi Kihara	Research Institute for Interdisciplinary Science, Okayama University		徳永 将史
21	202112-HMBXX-0109	強磁性/常磁性半導体ヘテロ接合における磁気近接効果と量子輸送現象	レデゥック アイン	東京大学	白谷 治憲 瀧口 耕介	Magnetic proximity effect and quantum transport phenomena in ferromagnetic/nonmagnetic semiconductor heterostructures	Le Duc Anh	The University of Tokyo	Harunori Shiratani Takiguchi Kosuke	徳永 将史
22	202106-HMBXX-0088	ブリージングパイロクロア格子磁性体の新規磁場誘起物性および機能性の開拓	厳 正輝	東京大学		Search for novel field-induced properties and functionalities in breathing pyrochlore magnets	Masaki Gen	The University of Tokyo		小濱 芳允
23	202109-HMBXX-0100	有機スピン液体候補物質の超強磁場物性研究	宮川 和也	東京大学	杉浦 栞理（東北大学） 浦井 瑞紀	Physical property measurements of organic spin liquid candidate materials under ultra-high magnetic field	Kazuya Miyagawa	The University of Tokyo	Shiori Sugiura, Tohoku University Mizuki Urai	小濱 芳允
24	202109-HMBXX-0101	強磁場下における分子材料励起三重項状態の磁気光学分光	石井 和之	生産技術研究所		Magneto-Optical Spectroscopy of Molecular Materials in the Excited Triplet States under Strong Magnetic Fields	Kazuyuki Ishii	Institute of Industrial Science		小濱 芳允
25	202111-HMBXX-0108	30テスラ級小型パルス電磁石の立ち上げとマルチフェロイック物質研究への応用	河智 史朗	兵庫県立大学		Start-up of a 30-Tesla-class portable pulsed magnet and its application to the study of multiferroic materials	Kawachi Shiro	University of Hyogo		小濱 芳允

大阪大学大学院理学研究科附属先端強磁場科学研究センター / Center for Advanced High Magnetic Field Science, Graduate School of Science, Osaka University

No.	課題番号	課題名	氏名	所属	分担者	Title	Name	Organization	Member of research project	担当所員
1	202105-HMOXX-0063	パルス強磁場用極低温実験装置の開発	野口 悟	大阪公立大学	吉田 勝一	Development of the cryostat for pulsed high magnetic field	Satoru Noguchi	Osaka Metropolitan University	Yoshida	萩原 政幸
2	202106-HMOXX-0072	強いスピン-軌道相互作用を活かした酸化物スピントロニクス	松野 丈夫	大阪大学		Oxide spintronics utilizing strong spin-orbit coupling	Jobu Matsuno	Osaka University		萩原 政幸
3	202105-HMOXX-0062	RInCu4単結晶のパルス強磁場磁化測定	和氣 剛	京都大学		Pulse high field magnetization measurement of RInCu4	Takeshi Waki	Kyoto University		萩原 政幸
4	202105-HMOXX-0061	ショートパルスマグネットを用いた圧力下ESR装置の開発	櫻井 敬博	神戸大学	赤木 暢	Development of high-pressure ESR system using short pulse magnet	Takahiro Sakurai	Kobe University	Mitsuru Akaki	萩原 政幸

5	202111-HMOXX-0107	ハニカム構造を持つBaPt(As1-xSbx)の超伝導物性	工藤 一貴	大阪大学		Superconducting properties of BaPt(As1-xSbx) with honeycomb networks	Kazutaka Kudo	Osaka University		萩原 政幸
6	202109-HMOXX-0098	非従来型超伝導体のパルス強磁場下輸送特性	掛谷 一弘	京都大学		Transport measurements on unconventional superconductors under pulsed high magnetic fields	Itsuhiro Kakeya	Kyoto University		萩原 政幸
7	202106-HMOXX-0080	磁性を有する極性金属における磁気秩序の解明	酒井 英明	大阪大学	奥田 裕貴 近藤 雅起 湯浅 直輝	Study of magnetic order in a magnetic polar metal	Hideaki Sakai	Osaka University	Yuki Okuda Masaki Kondo Naoki Yuasa	萩原 政幸
8	202105-HMOXX-0058	空間反転対称性の破れや磁気フラストレーションに誘発された特異な磁気特性と強磁場物性	竹内 徹也	大阪大学	大貫 惇睦（理化学研究所）	Characteristic magnetic properties and high-field magnetism in materials with a lack of inversion symmetry and/or magnetic frustration.	Tetsuya Takeuchi	Osaka University	Yoshichika Onuki, RIKEN	萩原 政幸
9	202105-HMOXX-0057	辺及び頂点共有Cu4四面体フラストレート系の強磁場物性	浅野 貴行	福井大学		High-field properties of frustrated systems with corner- and edge-sharing Cu4 tetrahedra	Takayuki Asano	University of Fukui		萩原 政幸
10	202106-HMOXX-0075	S＝5/2バックルドハニカム反強磁性体Cs3Fe2Cl9の強磁場ESR測定	吉田 紘行	北海道大学		High-field ESR measurements on S = 5/2 buckled-honeycomb antiferromagnet Cs3Fe2Cl9	Hiroyuki Kura Yoshida	Hokkaido University		萩原 政幸

強磁場コラボラトリー / The High Magnetic Field Collaboratory

No.	課題番号	課題名	氏名	所属	分担者	Title	Name	Organization	Member of research project	担当所員
1	202106-HMBXX-0089	有機ラジカルからなるフラストレート磁性体の強磁場物性	山口 博則	准教授		High-field magnetic properties of frustrated materials composed of organic radicals	Hironori Yamaguchi	Osaka Prefecture University		金道 浩一
2	202108-HMCXX-0097	微視的プローブによる強磁場誘起電子相の探索とその周辺ダイナミクス観測	井原 慶彦	北海道大学大学院		NMR study for magnetic field induced electronic states and their dynamics	Yoshihiko Ihara	Hokkaido University		萩原 政幸

留学研究課題 / External Research Project Long / Short -term

No.	課題番号	課題名	氏名	所属	分担者	Title	Name	Organization	Member of research project	担当所員
1	202012-VSBXL-0004	π電子ープロトン相関型有機伝導体κ-H3(Cat-EDT-ST)2における圧力誘起超伝導	北山 元晴	東邦大学		Pressure-induced superconductivity in π-electron–proton coupled organic conductor κ-H3(Cat-EDT-ST)2	Motoharu Kitayama	TOHO University		森 初果
2	202011-VSBXL-0001	クマリンケージド D-ルシフェリンの蛍光測定	熊谷 遼	群馬大学		Photoluminescence spectroscopy of coumarin-caged D-luciferin	Ryo Kumagai	Gunma University		秋山 英文
3	202012-VSBXL-0002	ルシフェリン-ルシフェラーゼ反応における触媒金属としてのカドミウムの作用	齋藤 啓輔	群馬大学		Influence of cadmium on luciferin - luciferase reaction as catalytic metals	Keisuke Saito	Gunma University		秋山 英文
4	202012-VSBXL-0003	ケージド化合物光解離の時間分解測定	崎元 柊	群馬大学		Time-resolved measurement of photodissociation of caged compounds	Shu Sakimoto	Gunma University		秋山 英文

※実施課題一覧、所属は申請時のデータ

No.	課題番号	課題名	氏名	所属	分担者（共同研究者）	Title	Name	Organization	Member of research project	装置	ビームポート
1		GPTAS（汎用3軸中性子分光器）IRT課題	佐藤 卓	東北大学	奥山 大輔, 那波 和宏, Wu Hung-Cheng, 横山 淳, 田畑 吉計, 村崎 遼, 平岡 巧, 宮田 颯	IRT project of GPTAS	Taku J Sato	Tohoku University	Daisuke Okuyama, Kazuhiro Nawa, Wu Hung-Cheng, Makoto Yokoyama, Yoshikazu Tabata, Ryo Murasaki, Takumi Hiraoka, Hayato Miyata	GPTAS	4G
2		a-Cu2V2O7 の非相反マグノンに対するbc面内磁場効果	佐藤 卓	東北大学	那波 和宏, Pharit Piyawongwatthana, 奥山 大輔	Effect of in-plane magnetic field for the nonreciprocal magnon in a-Cu2V2O7	Taku J Sato	Tohoku University	Kazuhiro Nawa, Pharit Piyawongwatthana, Daisuke Okuyama	GPTAS	4G
3		準一次元量子反強磁性体 Cu2(MoO4)(SeO3)の磁気励起	佐藤 卓	東北大学	Pharit Piyawongwatthana, 奥山 大輔, 那波 和宏	Magnetic Excitation of the Quasi-1D Quantum Antiferromagnet Cu2(MoO4)(SeO3)	Taku J Sato	Tohoku University	Pharit Piyawongwatthana, Daisuke Okuyama, Kazuhiro Nawa	GPTAS	4G
4		量子三角格子磁性体Ba3Yb(BO3)3の結晶場、短距離相関および磁気励起	佐藤 卓	東北大学	松坂 信之介, 奥山 大輔, 那波 和宏	CEF, short-range correlation, and spin excitations in the new quantum triangular-lattice compound Ba3Yb(BO3)3	Taku J Sato	Tohoku University	Shinnosuke Matsuzaka, Daisuke Okuyama, Kazuhiro Nawa	GPTAS	4G
5		Sr2RuO4の磁気揺らぎの超伝導発現機構への関連性の証明	古川 はづき	お茶の水女子大学	左右田 稔, Foley Edward, 石田 茜, 河村 聖子, 井上 凜香, 中村 琴美, 植木 萌	Mechanism of superconductivity and magnetic fluctuations in Sr2RuO4	Hazuki Furukawa	Ochanomizu University	Minoru Soda, Edward Foley, Akane Ishida, Seiko Kawamura, Rika Inoue, Kotomi Nakamura, Moe Ueki	GPTAS	4G
6		反強磁性量子臨界的挙動がもたらす異常超伝導物性	横山 淳	茨城大学	平山 堅理, 川崎 郁斗	Anomalous superconducting properties generated by antiferromagnetic quantum criticality	Makoto Yokoyama	Ibaraki University	Takatoshi Hirayama, Ikuto Kawasaki	GPTAS	4G
7		キタエフ候補物質α-RuBr3における分数スピン励起	那波 和宏	東北大学	今井 良宗, 大串 研也, 佐藤 卓	Fractional spin excitations in the Kitaev candidate compound α-RuBr3	Kazuhiro Nawa	Tohoku University	Yoshinori Imai, Kenya Ohgushi, Taku J Sato	GPTAS	4G
8		スピンアイスにおけるトポロジカル相転移	門脇 広明	東京都立大学	佐藤 卓	Topological phase transition in spin ice	Hiroaki Kadowaki	Tokyo Metropolitan University	Taku J Sato	GPTAS	4G
9		価数揺動希土類化合物における電荷・フォノン結合現象の検証	筒井 智嗣	高輝度光科学研究センター	李 哲虎, 光田 暁弘, 和田 裕文, 坂上 良介	Investigation of Valence-Lattice Coupling Phenomenon in Valence-Fluctuating Rare-Earth Intermetallics	Satoshi Tsutsui	Japan Synchrotron Radiation Research Institute	Chul-Ho Lee, Akihiro Mitsuda, Hirofumi Wada, Ryosuke Sakagami	GPTAS	4G
10		液体ベンゼンの部分構造因子	亀田 恭男	山形大学	天羽 優子, 臼杵 毅	Partial structure factors of liquid benzene	Yasuo Kameda	Yamagata University	Yuko Amo, Takeshi Usui	GPTAS	4G
11		反転対称性を持つスキルミオン物質Gd2PdSi3の磁気構造の検証	中島 多朗	東京大学	齋藤 開, 車地 崇, 有馬 孝尚, Ju Jiwon	Magnetic structures in a centrosymmetric skyrmion-host compound Gd2PdSi3	Taro Nakajima	The University of Tokyo	Hiraku Saito, Takashi Kurumaji, Takahisa Arima, Ju Jiwon	PONTA	5G

12		ワイルー近藤半金属を含むトポロジカル希土類物質における磁気状態	岩佐 和晃	茨城大学	下田 愛海, 桑原 慶太郎	Magnetic states of topological rare-earth materials including Weyl–Kondo semimetals	Kazuaki Iwasa	Ibaraki University	Ami Shimoda, Keitaro Kuwahara	PONTA	5G
13		Eu系ダイアモンド格子物質におけるスピンテクスチャの探索	車地 崇	東京大学	徳永 祐介, 有馬 孝尚, 中島 多朗	Search for spin textures in a Eu-based diamond-lattice magnet	Takashi Kurumaji	The University of Tokyo	Yusuke Tokunaga, Takahisa Arima, Taro Nakajima	PONTA	5G
14		空間反転対称性の破れた化合物CeNiC2の磁気構造	郷地 順	東京大学	上床 美也, Ma Hanming, 繁岡 透, 中島 多朗, 齋藤 開	Magnetic structure of non-centrosymmetric compound CeNiC2	Jun Gouchi	The University of Tokyo	Yoshiya Uwatoko, Ma Hanming, Toru Shigeoka, Taro Nakajima, Hiraku Saito	PONTA	5G
15		偏極中性子散乱によるCoTa3S6の磁気構造解析	関 真一郎	東京大学	中島 多朗, 高木 里奈, 高木 寛貴	Magnetic structure analysis for CoTa3S6 by polarized neutron scattering	Shinichiro Seki	The University of Tokyo	Taro Nakajima, Rina Takagi, Hirotaka Takagi	PONTA	5G
16		偏極中性子散乱法によるEuAl4の磁気構造解析	高木 里奈	東京大学	中島 多朗, 関 真一郎	Magnetic structure analysis of EuAl4 by polarized neutron scattering	Rina Takagi	The University of Tokyo	Taro Nakajima, Shinichiro Seki	PONTA	5G
17		中性子弾性散乱によるCeRh2Si2の一軸圧下磁気構造の探査	齋藤 開	東京大学	中島 多朗, 網塚 浩, 今 布咲子	Search for the magnetic structure of CeRh2Si2 under uniaxial pressure by means of elastic neutron diffraction	Hiraku Saito	The University of Tokyo	Taro Nakajima, Hiroshi Amitsuka, Fusako Kon	PONTA	5G
18		三角格子反強磁性体 CuFeO2の圧力誘起磁気相転移に伴う磁気励起の探査	寺田 典樹	物質材料研究機構	中島 多朗	Investigation of magnetic excitation in high pressure condition for triangular lattice antiferromagnet CuFeO2	Noriki Terada	National Institute for Materials Science	Taro Nakajima	PONTA	5G
19		Mn3TX系におけるスピンカイラリティー転移	社本 真一	総合科学研究機構	松浦 直人, 池内 和彦, 山内 宏樹, Chang Lieh-Jeng, 池内 和彦, 山内 宏樹	Spin chirality transition in Mn3TX system	Shinichi Shamoto	Comprehensive Research Organization for Science and Society	Masato Matsuura, Kazuhiko Ikeuchi, Hiroki Yamauchi, Chang Lieh-Jeng, Kazuhiko Ikeuchi, Hiroki Yamauchi	PONTA	5G
20		MnO酸化物の磁気相転移とスピンカレントに関する研究	古川 はづき	お茶の水女子大学	左右田 稔, 中村 琴美, Foley Edward, 植木 萌	Contribution of magnetism on spin current in MnO	Hazuki Furukawa	Ochanomizu University	Minoru Soda, Kotomi Nakamura, Edward Foley, Moe Ueki	PONTA	5G
21		PONTA（高性能偏極中性子散乱装置）IRT課題	中島 多朗	東京大学	益田 隆嗣, 浅井 晋一郎, 齋藤 開, 上床 美也, 郷地 順, 寺田 典樹, Ju Jiwon	IRT project of PONTA	Taro Nakajima	Tokyo University	Takatsugu Masuda, Shinichiro Asai, Hiraku Saito, Yoshiya Uwatoko, Jun Gouchi, Noriki Terada, Ju Jiwon	PONTA	5G
22		YbNi3Al9の結晶場励起	松村 武	広島大学	塚越 舜, 比嘉 野乃花, 岸田 卓	Crystal Field Excitation of YbNi3Al9	Takeshi Matsumura	Hiroshima University	Mitsuru Tsukagoshi, Nonoka Higa, Suguru Kishida	TOPAN	6G
23		電子添加型銅酸化物PLCCOの格子振動を通じたギャップ対称性の観測	池内 和彦	総合科学研究機構		Observation of the gap symmetry due to lattice vibrations in e-doped cuprate PLCCO	Kazuhiko Ikeuchi	Comprehensive Research Organization for Science and Society		TOPAN	6G

24		TOPAN（東北大理：３軸型偏極中性子分光器）IRT課題	藤田 全基	東北大学	南部 雄亮, 池田 陽一, 谷口 貴紀, 木村 宏之, 岩佐 和晃, 大山 研司, Xie Peiao, Pang Xiaoqi, Wang Tong, 唐 一飛, Chen Yizhou, 大里 耕太郎, 北山 慎之介, 橋本 勇輝	IRT project of TOPAN	Masaki Fujita	Tohoku University	Yusuke Nambu, Yoichi Ikeda, Takanori Taniguchi, Hiroyuki Kimura, Kazuaki Iwasa, Kenji Ohoyama, Xie Peiao, Pang Xiaoqi, Wang Tong, Tang Yife, Chen Yizho, Koichiro Ohsato, Shinnosuke Kitayama, Yuki Hashimoto	TOPAN	6G
25		空間反転対称性を持つ磁気スキルミオン物質Gd2PdSi3の磁気励起	中島 多朗	東京大学	齋藤 開, Ju Jiwon	Magnetic excitations of a centrosymmetric skyrmion-host material Gd2PdSi3	Taro Nakajima	The University of Tokyo	Hiraku Saito, Ju Jiwon	HER	C1-1
26		a-Cu2V2O7 の非相反マグノンに対するbc面内磁場効果	佐藤 卓	東北大学	那波 和宏, Pharit Piyawongwatthana, 奥山 大輔	Effect of in-plane magnetic field for the nonreciprocal magnon in a-Cu2V2O7	Taku J Sato	Tohoku University	Kazuhiro Nawa, Pharit Piyawongwatthana, Daisuke Okuyama	HER	C1-1
27		量子三角格子磁性体Ba3Yb(BO3)3の結晶場、短距離相関および磁気励起	佐藤 卓	東北大学	松坂 信之介, 奥山 大輔, 那波 和宏	CEF, short-range correlation, and spin excitations in the new quantum triangular-lattice compound Ba3Yb(BO3)3	Taku J Sato	Tohoku University	Shinnosuke Matsuzaka, Daisuke Okuyama, Kazuhiro Nawa	HER	C1-1
28		Magnon dispersion relations in a 2D Dresselhaus magnet	南部 雄亮	東北大学		Magnon dispersion relations in a 2D Dresselhaus magnet	Yusuke Nambu	Tohoku University		HER	C1-1
29		フラストレーション磁性体YBaCo4O7における磁気散漫散乱	左右田 稔	お茶の水女子大学		magnetic diffuse scattering of frustrated magnet YBaCo4O7	Minoru Soda	Ochanomizu University		HER	C1-1
30		GaV4Se8における巨大な熱ホール効果を生む磁気スキルミオン凝縮状態の研究	有馬 孝尚	東京大学	徳永 祐介, 車地 崇, Su Dan, 中島 多朗, 井出 竜鳳	Magnetic Skyrmion States in GaV4Se8 with Large Thermal Hall Effect	Takahisa Arima	The University of Tokyo	Yusuke Tokunaga, Takashi Kurumaji, Su Dan, Taro Nakajima, Ryuho Ide	HER	C1-1
31		スピンギャップ系KCuCl3における圧力誘起量子相転移と磁気励起	栗田 伸之	東京工業大学	益田 隆嗣, 田中 秀数	Pressure-induced quantum phase transition and magnetic excitation in the spin gap system KCuCl3	Nobuyuki Kurita	Tokyo Institute of Technology	Takatsugu Masuda, Hidekazu Tanaka	HER	C1-1
32		反強磁性量子臨界的挙動がもたらす異常超伝導物性	横山 淳	茨城大学	平山 堅理, 川崎 郁斗	Anomalous superconducting properties generated by antiferromagnetic quantum criticality	Makoto Yokoyama	Ibaraki University	Takatoshi Hirayama, Ikuto Kawasaki	HER	C1-1
33		Inelastic neutron scattering study on the optical-acoustic phonon interactions in InSe	益田 隆嗣	東京大学	Ma Jie, 浅井 晋一郎	Inelastic neutron scattering study on the optical-acoustic phonon interactions in InSe	Takatsugu Masuda	The University of Tokyo	Ma Jie, Shinichiro Asai	HER	C1-1
34		T'構造銅酸化物Pr2-xCaxCuO4における磁気相関と超伝導の研究	藤田 全基	東北大学	谷口 貴紀, 池田 陽一, 高濱 元史, 陳 逸舟, Wang Tong	Study of spin correlations and superconductivity in T'-structured cuprate oxide Pr2-xCaxCuO4	Masaki Fujita	Tohoku University	Takanori Taniguchi, Yoichi Ikeda, Motofumi Takahama, Chen Yizhou, Wang Tong	HER	C1-1
35		量子スピン鎖におけるスピノンラシュバ分裂	那波 和宏	東北大学	村崎 遼, 佐藤 卓	Spinon Rashba splitting on the quantum spin chain	Kazuhiro Nawa	Tohoku University	Ryo Murasaki, Taku J Sato	HER	C1-1
36		交替した内部磁場が印加されるスピン鎖物質Tb3RuO7の磁気励起の研究	長谷 正司	物質・材料研究機構	益田 隆嗣, 浅井 晋一郎	Study of magnetic excitations of spin chain material Tb3RuO7 to which staggered internal magnetic fields are applied	Masashi Hase	National Institute for Materials Science	Takatsugu Masuda, Shinichiro Asai	HER	C1-1
37		三角格子反強磁性体 CuFeO2の圧力誘起磁気相転移に伴う磁気励起の探査	寺田 典樹	物質材料研究機構	中島 多朗	Investigation of magnetic excitation in high pressure condition for triangular lattice antiferromagnet CuFeO2	Noriki Terada	National Institute for Materials Science	Taro Nakajima	HER	C1-1

38		HER (高エネルギー分解能３軸型中性子分光器) IRT課題	益田 隆嗣	東京大学	浅井 晋一郎, 佐藤 卓, 横山 淳, 斎藤 開, 中島 多朗, 阿曽 尚文, 田中 秀数, 栗田 伸之, 三宅 岳志, 菊地 帆高	IRT project of HER	Takatsugu Masuda	The University of Tokyo	Shinichiro Asai, Taku J Sato, Makoto Yokoyama, Hiraku Saito, Taro Nakajima, Naofumi Aso, Hidekazu Tanaka, Nobuyuki Kurita, Takeshi Miyake, Hodaka Kikuchi	HER	C1-1
39		小角中性子散乱によるテトラポリアクリル酸ゲルの構造解析	Li Xiang	東京大学	Gupit Caidric, 辻 優衣, 光上 義郎	Structure characterization of model tetra-poly(acrylic acid) gel by small-angle neutron scattering	Li Xiang	The University of Tokyo	Gupit Caidric, Yui Tsuji, Yoshiro Mitsukami	SANS-U	C1-2
40		小角中性子散乱を用いた４分岐星型Poly(ethylene glycol)の内部相関の解明	Li Xiang	東京大学	辻 優依, 大平 征史	The elucidation of the internal correlation of star poly(ethylene glycol) with small-angle neutron scattering	Li Xiang	The University of Tokyo	Yui Tsuji, Masashi Ohira	SANS-U	C1-2
41		タンパク質複合体中の天然変性タンパク質の選択的構造解析	井上 倫太郎	京都大学	小田 隆, 杉山 正明, 守島 健, 佐藤 信浩	Selective strutural analysis of intrisically dioredерd protein in the protein complex	Rintaro Inoue	Kyoto University	Takashi Oda, Masaaki Sugiyama, Ken Morishima, Nobuhiro Sato	SANS-U	C1-2
42		コントラスト変調中性子小角散乱による食品タンパク質複合体の構造解析	佐藤 信浩	京都大学	杉山 正明, 裏出 令子, 井上 倫太郎, 守島 健, 奥田 綾, 清水 将裕	Structural analysis of food protein complex by contrast-variation small-angle neutron scattering	Nobuhiro Sato	Kyoto University	Masaaki Sugiyama, Reiko Urade, Rintaro Inoue, Ken Morishima, Aya Okuda, Shimizu Masahiro	SANS-U	C1-2
43		中性子小角散乱実験によるSr2RuO4の異常金属状態の研究	古川 はづき	お茶の水女子大学	Foley Edward, 左右田 稔, 石田 茜, 中村 琴美, 石田 茜, 奥村 練	Anomalous vortex state in Sr2RuO4 studied by SANS experiments	Hazuki Furukawa	Ochanomizu University	Foley Edward, Minoru Soda, Akane Ishida, Kotomi Nakamura, Akane Ishida, Ren Okumura	SANS-U	C1-2
44		空間反転対称性の破れた超伝導体のヘリカル磁束格子の観測	古川 はづき	お茶の水女子大学	左右田 稔, 石田 茜, Foley Edward, 伊藤 未希	Herical vortex phase on non-centrosymmetric superconductors	Hazuki Furukawa	Ochanomizu University	Minoru Soda, Akane Ishida, Edward Foley, Miki Ito	SANS-U	C1-2
45		ポリエチレンカーボネート型新規固体電解質の小角中性子散乱測定による構造評価	土肥 侑也	名古屋大学	Ohl Michael	Evaluation of structures of poly(ethylene carbonate) solid electrolytes by small-angle neutron scattering (SANS) measurements	Yuya Doi	Nagoya University	Ohl Michael	SANS-U	C1-2
46		逆転コントラスト同調中性子小角散乱法によるER-60/CNX複合体の構造解析	奥田 綾	京都大学	清水 将裕, 守島 健, 佐藤 信浩, 井上 倫太郎, 裏出 令子, 杉山 正明	Structural analysis of the ER-60/CNX complex using inverse contrast-matching small-angle neutron scattering	Aya Okuda	Kyoto University	Shimizu Masahiro, Ken Morishima, Nobuhiro Sato, Rintaro Inoue, Reiko Urade, Masaaki Sugiyama	SANS-U	C1-2
47		逆転コントラスト同調中性子小角散乱と超遠心分析の複合解析による時計蛋白質複合体の構造解明	守島 健	京都大学	杉山 正明, 井上 倫太郎, 佐藤 信浩, 奥田 綾, 矢木 宏和, 柚木 康弘	Integrated structural analysis with inverse contrast-matching small-angle neutron scattering and analytical ultracentrifugation for clock protein complex	Ken Morishima	Kyoto University	Masaaki Sugiyama, Rintaro Inoue, Nobuhiro Sato, Aya Okuda, Hirokazu Yagi, Yasuhiro Yunoki	SANS-U	C1-2

48		レゾルシナレン系逆ミセルの構造と触媒活性の相関関係の解明	櫻井 和朗	北九州市立大学	藤井 翔太, 西村 智貴, 秋葉 勇, 金丸 拓磨	Solvent dependence of resorcinarene-based capsules on their platonic structures and catalytic ability	Kazuo Sakurai	The University of Kitakyushu	Shota Fujii, Tomoki Nishimura, Isamu Akiba, Takuma Kanamaru	SANS-U	C1-2
49		均一構造を有する過渡的網目の構造・物性評価	片島 拓弥	東京大学	酒井 崇匡, Li Xiang, 大平 征史	Relationship between structures and mechanical properties of transient networks with uniform network strands	Takuya Katashima	The University of Tokyo	Takamasa Sakai, Li Xiang, Masashi Ohira	SANS-U	C1-2
50		環状分子被覆率の均一性が環動ゲルの網目変形挙動に与える影響	眞弓 皓一	東京大学	乗富 貴子, Liu Chang, 河原 聡平	Effect of homogeneity of ring coverage on network deformation of slide-ring gels	Koichi Mayumi	The University of Tokyo	Takako Noritomi, Liu Chang, Sohei Kawahara	SANS-U	C1-2
51		ロバスト強靭化ゲルにおける伸長誘起結晶化の形成メカニズム	眞弓 皓一	東京大学	Liu Chang, 乗富 貴子, 河原 聡平, 酒井 崇匡, Li Xiang	Strain-induced crystallization of tough and robust polymer gels	Koichi Mayumi	The University of Tokyo	Liu Chang, Takako Noritomi, Sohei Kawahara, Takamasa Sakai, Li Xiang	SANS-U	C1-2
52		コントラストマッチング中性子散乱法によるリン脂質/ブロックポリマー ハイブリッドベシクルの構造解析	西村 智貴	京都大学	櫻井 和朗, 藤井 翔太, 秋葉 勇, 高野 心	Structural analysis of phospholipid/block copolymer hybrid vesicles by contrast-matching SANS measurements	Tomoki Nishimura	Kyoto University	Kazuo Sakurai, Shota Fujii, Isamu Akiba, Shin Takano	SANS-U	C1-2
53		高圧条件下における2成分混合溶液の新奇な臨界挙動	貞包 浩一朗	同志社大学	青山 航大, 荒木田 怜那, 吉良 康弘, 後藤 篤子	Novel critical behavior in a mixture of water / organic solvent under high-pressure condition	Koichiro Sadakane	Doshisha University	Kodai Aoyama, Reina Arakida, Yasuhiro Kira, Atsuko Goto	SANS-U	C1-2
54		ポリアルキルスチレン類とポリイソプレンの相溶性評価と相溶化機構の検討	高野 敦志	名古屋大学	織戸 列, 織戸 烈, 土肥 侑也	Evaluation of miscibility of poly(4-alkylstyrene)/polyisoprene blend systems	Atsushi Takano	Nagoya University	Tsuyoshi Orido, Tsuyoshi Orido, Yuya Doi	SANS-U	C1-2
55		一次粒径が異なるフュームドシリカの混合サスペンション中における相互分散効果	鳥飼 直也	三重大学	池田 莉紗子, 小暮 準才	Interplay of Binary Fumed Silica with Different Primary Particle Sizes Dispersed in Suspension	Naoya Torikai	Mie University	Masako Ikeda, Junsai Kogure	SANS-U	C1-2
56		水素添加レシチン／非イオン界面活性剤混合系リポソームの 中性子小角散乱を用いた構造解析	吉村 倫一	奈良女子大学	矢田 詩歩, 王 珊, 天野 沙耶, 小林 礼実, 水口 裕恵	Structural analysis of liposome formed by mixed system of hydrogenated lecithin and nonionic surfactant using small-angle neutron scattering	Tomokazu Yoshimura	Nara Women's University	Shiho Yada, Wang Shan, Saya Amno, Ayami Kobayashi, Hiroe Mizuguchi	SANS-U	C1-2
57		SANS-U（二次元位置測定小角散乱装置）IRT課題	Li Xiang	東京大学	杉山 正明, 井上 倫太郎, 守島 健, 眞弓 皓一, 辻 優依, 大平 征史, 千葉 文野, 伊藤 大基, 貞包 浩一朗, 土肥 侑也, 小田 達郎, 花房 明宏, 乗富 貴子, 河原 聡平, 廣井 卓思	IRT project of SANS-U	Li Xiang	The University of Tokyo	Masaaki Sugiyama, Rintaro Inoue, Ken Morishima, Koichi Mayumi, Yui Tsuji, Masashi Ohira, Ayano Chiba, Hiroki Ito, Koichiro Sadakane, Yuya Doi, Tatsuro Oda, Akihiro Hanahusa, Takako Noritomi, Sohei Kawahara, Takushi Hiroi	SANS-U	C1-2

58		iNSE（中性子スピンエコー分光器)IRT課題	眞弓 皓一	東京大学	Li Xiang, 井上 倫太郎, 日野 正裕, 守島 健, 小田 達郎	IRT project of iNSE	Koichi Mayumi	The University of Tokyo	Li Xiang, Rintaro Inoue, Masahiro Hino, Ken Morishima,Tatsuro Oda	iNSE	C2-3-1
59		アニオン交換型電解質膜に水和した水分子のダイナミクス測定	吉田 亨次	福岡大学	犬飼 潤治, 川本 鉄平, 西山 博通, 白勢 裕登, Solomon Wekesa, Anna Kapulwa	Water dynamics in Anion Exchange Membrane	Koji Yoshida	Fukuoka University	Junji Inukai, Teppei Kawamoto, Hiromichi Nishiyama, Yuuto Shirase, Solomon Wekesa, Anna Kapulwa	AGNES	C3-1-1
60		アモルファス水素ハイドレートの水素拡散ダイナミクス	秋葉 宙	東京大学	山室 修, 國澤 昌史, 佐藤 創	Diffusion dynamics of hydrogen in amorphous hydrogen hydrate	Hiroshi Akiba	The University of Tokyo	Osamu Yamamuro, Masashi Kunizawa, Hajime Sato	AGNES	C3-1-1
61		LEA蛋白質の脱水折り畳みに伴うガラス化状態の解析	中川 洋	日本原子力研究開発機構	味戸 聡志	Analysis of vitrification of LEA protein upon desiccation-induced folding	Hiroshi Nakagawa	Japan Atomic Energy Agency	Ajito Satoshi	AGNES	C3-1-1
62		糊化過程における澱粉の水和状態に対する塩の影響の解析	中川 洋	日本原子力研究開発機構	味戸 聡志	Analysis of effect of salt on hydration state of starch during gelatinization process	Hiroshi Nakagawa	Japan Atomic Energy Agency	Ajito Satoshi	AGNES	C3-1-1
63		澱粉の加熱過程における水の分子運動に対する水分量依存性の解析	中川 洋	日本原子力研究開発機構	味戸 聡志	Analysis of dependence of water content on water dynamics in starch during heating	Hiroshi Nakagawa	Japan Atomic Energy Agency	Ajito Satoshi	AGNES	C3-1-1
64		微生物の乾燥耐性機構の解明を目指したガラス転移の水分活性依存性の解析	中川 洋	日本原子力研究開発機構	川井 清司, 小関 成樹, 曽我部 知史	Water activity dependent glass transition of microorganisms for elucidation of the desiccation tolerance mechanism	Hiroshi Nakagawa	Japan Atomic Energy Agency	Kiyoshi Kawai, Shigenobu Koseki, Tomochika Sogabe	AGNES	C3-1-1
65		bcc金属水素化物中の水素の量子ダイナミクスの観測	古府 麻衣子	日本原子力研究開発機構		Observation of quantum dynamics of hydrogen in bcc metal hydrides	Maiko Kofu	Japan Atomic Energy Agency		AGNES	C3-1-1
66		ボソンピークを指標とした出土琥珀の産地推定	山口 繁生	公益財団法人 元興寺文化財研究所	中川 洋, 植田 直見	Provenance study of excavated amber by the observation of boson peak.	Shigeo Yamaguchi	Gangoji institute for research of cultural property	Hiroshi Nakagawa, Naomi Ueda	AGNES	C3-1-1
67		AGNES（高分解能パルス冷中性子分光器）IRT課題	山室 修	東京大学	秋葉 宙, 大政 義典, 楡井 真実, Zhao Yuansheng, Wu Xuejun, 山根 崚, 湊 広章, 関口 崚, 山田 武, 伊藤 華苗, 佐藤 創, 國澤 昌史	IRT project of AGNES	Osamu Yamamuro	The University of Tokyo	Hiroshi Akiba, Yoshinori Ohmasa, Nirei Masami, Zhao Yuansheng, Wu Xuejun, Ryo Yamane, Hiroaki Minato, Shun Sekiguchi, Takeshi Yamada, Kanae Ito, Hajime Sato, Shun Sato, Masashi Kunizawa	AGNES	C3-1-1

68		中性子基礎物理実験のためのデバイス開発	北口 雅暁	名古屋大学	広田 克也, 清水 裕彦, 嶋 達志, 吉川 大幹, 吉岡 瑞樹, 藤岡 宏之, 藤家 拓大, 奥平 琢也, 遠藤 駿典, 河村 しほり	Development of neutron devices for fundamental physics	Masaaki Kitaguchi	Nagoya University	Katsuya Hirota, Hirohiko Shimizu, Tatsushi Shima, Hiromoto Yoshikawa, Tamaki Yoshioka, Hiroyuki Fujioka,Takuhiro Fujiie, Takuya Okudaira, Syunsuke Endo, Shihori Kawamura	MINE	C3-1-2
69		中性子反射率測定に基づく気体透過薄膜の収着挙動に関する研究	川口 大輔	九州大学	田中 敬二, 古賀 弘樹, 原田 怜, 阿部 建樹, 種子田 英伸, 松野 寿生, 山口 晃, 川原 啓吾, 川畑 建人, 川野 雅恭, 田村 隼太	Sorption Behavior in Gas Separation Thin Films Studied by Neutron Reflectivity	Daisuke Kawaguchi	Kyushu University	Keiji Tanaka, Hiroki Koga, Rei Harada, Tatsuki Abe, Hidenobu Taneda, Hisao Matsuno, Kou Yamaguchi, Keigo Kawahara, Kento Kawabata, Masayasu Kawano, Shunta Tamura	MINE	C3-1-2
70		多層膜性中性子ミラーの高度化と集光デバイス開発	日野 正裕	京都大学	小田 達郎, 細畠 拓也	Development of multilayer neutron mirrors and focusing devices	Masahiro Hino	Kyoto University	Tatsuro Oda, Takuya Hosobata	MINE	C3-1-2
71		細孔ガラスプレートMPGDを用いた中性子イメージング検出器の開発	門叶 冬樹	山形大学	住吉 孝行, 日野 正裕, 杉山 浩之, 近藤 治靖, 森谷 透	Development of neutron imager based on hole-type MPGD with glass capillary plate	Fuyuki Tokanai	Yamagata University	Takayuki Sumiyoshi, Masahiro Hino, Hiroyuki Sugiyama, Haruyasu Kondo, Toru Moriya	MINE	C3-1-2
72		MINE（京大複合研：多層膜中性子干渉計・反射率計）IRT課題	日野 正裕	京都大学	田崎 誠司, 小田 達郎, 細畠 拓也, 北口 雅暁, 平山 朋子, 中村 吏一朗	MINE (Multilayer neutron interferometer and reflectometer)	Masahiro Hino	Kyoto University	Seiji Tasaki, Tatsuro Oda, Takuya Hosobata, Masaaki Kitaguchi, Tomoko Hirayama, Riichiro Nakamura	MINE	C3-1-2
73		π電子量子スピン系物質CsO2の結晶構造および磁気構造解析	中野 岳仁	茨城大学	神戸 高志, 宮島 瑞樹, 大山 研司, 林 明弘, 紺谷 駿, 原島 周平, 岡田 健吾, 三田 魁人	Magnetic and crystal structural studies on π-orbital quantum spin system CsO2	Takehito Nakano	Ibaraki University	Kambe Takashi, Mizuki Miyajima, Kenji Ohoyama, Akihiro Hayashi, Shun Kontani, Shuhei Harashima, Kengo Okada, Kaito Mita	HQR	T1-1
74		単結晶NdCo2Zn20における磁気揺らぎによる一次相転移の秩序変数の決定	鬼丸 孝博	広島大学	山本 理香子, 志村 恭通, 岩佐 和晃, 下田 愛海	Determination of the order parameter of magnetic-fluctuation-induced first-order transition in singlecrystalline NdCo2Zn20	Takahiro Onimaru	Hiroshima University	Rikako Yamamoto, Yasuyuki Shimura, Kazuaki Iwasa, Ami Shimoda	HQR	T1-1

75		HQR(高分解能中性子散乱装置)IRT課題	大山 研司	茨城大学	岩佐 和晃, 桑原 慶太郎, 横山 淳, 伊賀 文俊, 中野 岳仁, 中島 多朗, 西口 日向, 尾本 星太, 熊田 隆伸, 下田 愛海, 荒瀬 将太朗, 石﨑 嵩人, 野田 新太, 菅野 友哉, 高野 元輝, 星 翔太, KEIKO WIDYANISA, 小林 洋大, 富松 優花	IRT project of HQR	Kenji Ohoyama	Ibaraki University	Kazuaki Iwasa, Keitaro Kuwahara, Makoto Yokoyama, Fumitoshi Iga, Takehito Nakano, Taro Nakajima, Hyuga Nishiguchi, Seita Omoto, Takanobu Kumada, Ami Shimoda, Shoutaro Arase, Takato Ishizaki, Shinta Noda, Tomoya Kanno, Motoki Takano, Syota Hoshi, KEIKO WIDYANISA, Youdai Kobayashi, Yuka Tomimatsu	HQR	T1-1
76		AKANE（東北大金研：三軸型中性子分光器）IRT課題	藤田 全基	東北大学	南部 雄亮, 池田 陽一, 谷口 貴紀, 猪野 隆, 奥 隆之, 上床 美也, 川本 陽, 梅本 好日古, Xie Peiao, Pang Xiaoqi, Wang Tong, 北澤 崇文, 唐 一飛, 川又 雅広, Chen Yizhou, 大里 耕太郎, 北山 慎之介	IRT project of AKANE	Masaki Fujita	Tohoku University	Yusuke Nambu, Yoichi Ikeda, Takanori Taniguchi, Takashi Ino, Takayuki Oku, Yoshiya Uwatoko,Yo Kawamoto, Yoshihiko Umemoto, Xie Peiao, Pang Xiaoqi, Wang Tong, Takahumi Kitazawa, Tang Yifei, Masahiro Kawamata, Chen Yizhou, Koichiro Ohsato, Shinnosuke Kitayama	AKANE	T1-2
77		Magnetic structure of a new Dresselhaus magnet	南部 雄亮	東北大学	Pang Xiaoqi, 川又 雅広	Magnetic structure of a new Dresselhaus magnet	Yusuke Nambu	Tohoku University	Pang Xiaoqi, Masahiro Kawamata	HERMES	T1-3
78		カイラル磁性体Ce5Ru3Al2の低温の磁気秩序構造	奥山 大輔	東北大学	佐藤 卓	Magnetic structure of chiral magnet Ce5Ru3Al2	Daisuke Okuyama	Tohoku University	Taku J Sato	HERMES	T1-3
79		(111)p欠損面を有するペロブスカイト酸化物の結晶構造・磁気構造解析	山本 隆文	東京工業大学	長瀬 鉄平, 大見 拓也	Structural and magnetic refinements of perovskite oxide with (111)p defect	Takafumi Yamamoto	Tokyo Institute of Technology	Teppei Nagase, Takuya Omi	HERMES	T1-3
80		中性子粉末回折測定によるベリル中の水分子の量子常誘電状態の研究	山根 崚	東京大学	山室 修, 秋葉 宙	Neutron powder diffraction study on quantum paraelectric state of water confined in beryl	Ryo Yamane	The University of Tokyo	Osamu Yamamuro, Hiroshi Akiba	HERMES	T1-3
81		ワイルー近藤半金属を含むトポロジカル希土類物質における磁気状態	岩佐 和晃	茨城大学	下田 愛海	Magnetic states of topological rare-earth materials including Weyl–Kondo semimetals	Kazuaki Iwasa	Ibaraki University	Ami Shimoda	HERMES	T1-3
82		電気磁気交差相関現象を示すCe3TiSb5の複雑な磁場中の磁気構造の解明	本山 岳	島根大学	阿曽 尚文, 篠﨑 真碩, 金城 龍廣	Magnetic structure studies of complex magnetic phases in a magnetoelectric material of Ce3TiSb5	Gaku Motoyama	Shimane University	Naofumi Aso, Masahiro Shinozaki, Tatsuhiro Kinjo	HERMES	T1-3
83		中性子回折法によるハイパーカゴメ反強磁性体の研究	気谷 卓	東京工業大学	川路 均	Neutron Diffraction Study of Hyperkagome Antiferromagnets	Suguru Kitani	Tokyo Institute of Technology	Hitoshi Kawaji	HERMES	T1-3

84		ミディアムエントロピー合金中の短距離秩序に対する元素置換効果	池田 陽一	東北大学	梅本 好日古, 藤田 全基	Impurity effects to the short-range ordering in medium-entropy alloys	Yoichi Ikeda	Tohoku University	Yoshihiko Umemoto, Masaki Fujita	HERMES	T1-3
85		新規キタエフ模型候補物質CaCo2TeO6の中性子回折	浅井 晋一郎	東京大学	益田 隆嗣	Neutron Diffraction on new Kitaev model candidate CaCo2TeO6	Shinichiro Asai	The University of Tokyo	Takatsugu Masuda	HERMES	T1-3
86		新規酸化物イオン伝導体の結晶構造解析とイオン伝導経路の解明	藤井 孝太郎	東京工業大学	八島 正知, 張 文鋭, 矢口 寛, 松崎 航平	Crystal Structure Analysis and Investigation of Ion Diffusion Path of Novel Oxide-Ion Conductors	Kotaro Fujii	Tokyo Institute of Technology	Masatomo Yashima, ZHANG Wenrui, Hiroshi Yaguchi, Kohei Matsuzaki	HERMES	T1-3
87		T'構造銅酸化物の超伝導発現と結晶構造の関係	藤田 全基	東北大学	谷口 貴紀, 池田 陽一, 高濱 元史, 陳 逸舟, 南部 雄亮, Wang Tong, Xie Peiao, Chen Yizhou, 北山 慎之介	Relationship between the mechanism of superconductivity and crystal structure in T' cuprate oxide	Masaki Fujita	Tohoku University	Takanori Taniguchi, Yoich Ikeda, Motofumi Takahama, Chen Yizhou, Yusuke Nambu, Wang Tong, Xie Peiao, Chen Yizhou, Shinnosuke Kitayama	HERMES	T1-3
88		電気磁気交差相関現象を示す重い電子系反強磁性体Ce3TiBi5の磁気構造	阿曽 尚文	琉球大学	本山 岳, 篠﨑 真碩, 金城 龍廣	Magnetic structure in a heavy fermion antiferromagnet Ce3TiBi5 exhibiting electromagnetic cross-correlation phenomenon	Naofumi Aso	University of the Ryukyus	Gaku Motoyama, Masahiro Shinozaki, Tatsuhiro Kinjo	HERMES	T1-3
89		量子臨界点近傍にあるYbCo2Zn20の置換系試料の結晶構造	阿曽 尚文	琉球大学	金城 龍廣	Crystal structure in doped systems of YbCo2Zn20 in vicinity of a quantum critical point	Naofumi Aso	University of the Ryukyus	Tatsuhiro Kinjo	HERMES	T1-3
90		構造相転移を示すヒドリド導電体A2H3Xの構造解析および拡散経路の可視化	陰山 洋	京都大学	生方 宏樹, タッセル セドリック	Structural analysis of Hydride conductors A2H3X exhibiting a phase transition	Hiroshi Kageyama	Kyoto University	Hiroki Ubukata, Tassel Cedric	HERMES	T1-3
91		液体イオウの光誘起重合転移における局所構造の研究	坂口 佳史	総合科学研究機構	有馬 寛	Investigations on the local structure of liquid sulfur at photo-induced polymerization transition	Yoshifumi Sakaguchi	Comprehensive Research Organization for Science and Society	Hiroshi Arima	HERMES	T1-3
92		熱電材料122ジントル相の結晶構造	李 哲虎	産業技術総合研究所	木方 邦宏, 小野 圭吾, 和嶋 宏虎, 坂上 良介	Crystal structure analysis of thermoelectric compounds of 122 Zintl phase	Chul-Ho Lee	National Institute of Advanced Industrial Science and Technology	Kunihiro Kihou, Keigo Ono, Hirotora Wajima, Ryosuke Sakagami	HERMES	T1-3

93		HERMES（東北大金研：中性子粉末回折装置）IRT課題	南部 雄亮	東北大学	藤田 全基, 池田 陽一, 谷口 貴紀, 大山 研司, 八島 正知, 藤井 孝太郎, 川本 陽, 梅本 好日古, Xie Peiao, Pang Xiaoqi, Wang Tong, 北澤 崇文, 唐 一飛, 川又 雅広, Chen Yizhou, 大里 耕太郎, 北山 慎之介, 宮崎 司, 岩瀬 裕希, 鈴木 孝行, 渡邊 正理, 大野 真之, 石橋 広記, 芦谷 拓嵩, 正木 秀知, 成瀬 卓弥, 高濱 元史, 大坂 恵一, 佐藤 眞直	IRT project of HERMES	Yusuke Nambu	Tohoku University	Masaki Fujita, Yoichi Ikeda, Takanori Taniguchi, Kenji Ohoyama, Masatomo Yashima, Kotaro Fujii,Yo Kawamoto, Yoshihiko Umemoto, Xie Peiao, Pang Xiaoqi, Wang Ton, Takahumi Kitazawa, Tang Yifei, Masahiro Kawamata, Chen Yizhou, Koichiro Ohsato, Shinnosuke Kitayama, Tsukasa Miyazaki, Yuki Iwase, Takayuki Suzuki, Masari Watanabe, Saneyuki Ohno, Hiroki Ishibashi, Hirotaka Ashitani, Hidetomo Masaki, Takuya Naruse, Motohumi Takahama, Keichi Ohsaka, Masugu	HERMES	T1-3
94		FONDER(中性子4軸回折装置)IRT課題	木村 宏之	東北大学	坂倉 輝俊, 山本 孟, 土肥 優紀, 戸田 薫, 上山 幸子, 山神 玄蔵, 野田 幸男, 石井 祐太	IRT proposal for FONDER (Neutron 4-circle diffractometer)	Hiroyuki Kimura	Tohoku University	Terutoshi Sakakura, Hajime Yamamoto, Yuki Dohi, Kaoru Toda, Sachiko Kamiyama, Genzo Yamagami, Yukio Noda, Yuta Ishii	FONDER	T2-2
95		磁気スキルミオン物質Gd2PdSi3における磁気秩序と超格子構造	中島 多朗	東京大学	齋藤 開, Ju Jiwon	Magnetic and superlattice structures in a centrosymmetric skyrmion-host material Gd2PdSi3	Taro Nakajima	The University of Tokyo	Hiraku Saito, Ju Jiwon	FONDER	T2-2
96		塑性歪みを加えたPt3Fe反強磁性体における強磁性の発現機構	小林 悟	岩手大学	野村 英志, 松尾 咲琴, 堀田 侑里	Mechanism of ferromagnetism in plastically deformed Pt3Fe antiferromagnet	Satoru Kobayashi	Iwate University	Eiji Nomura, Sakoto Matsuo, Yuri Hotta	FONDER	T2-2
97		スピン軌道結合絶縁体Ba2MgReO6における 四極子秩序によって安定化される磁気秩序の研究	平井 大悟郎	東京大学	佐賀山 基, 室井 利彦	Study of magnetic structure stabilized by quadrupolar order in Spin-orbit-coupled insulator Ba2MgReO6	Daigorou Hirai	The University of Tokyo	Hajime Sagayama,Toshihiko Muroi	FONDER	T2-2
98		T'-type Pr2CuO4における結晶構造の還元効果	木村 宏之	東北大学	坂倉 輝俊	Oxygen reduction effect on the crystal structure in the T'-structure of Pr2CuO4+y	Hiroyuki Kimura	Tohoku University	Terutoshi Sakakura	FONDER	T2-2
99		共線磁気構造が介在する一軸応力誘起強誘電相の探査	満田 節生	東京理科大学	内原 猛, 小澤 竜也, 藤原 理賀, 玉造 博夢	Investigation of uniaxial stress-induced ferroelectric phase with collinear magnetic structure	Setsuo Mitsuda	Tokyo University of Science	Takeru Uchihara, Tatsuya Ozawa, Masayoshi Fujihara, Hiromu Tamatsukuri	FONDER	T2-2

100		Co2+が二等辺デルタ鎖を形成する新物質NaCo2(SO4)2Clの磁気構造の解明	藤原 理賀	東京理科大学	満田 節生, 塚原 隆史, 内原 猛, 玉造 博夢	Investigation of magnetic structure of Co-delta chain NaCo2(SO4)2Cl	Masayoshi Fujihara	Tokyo University of Science	Setsuo Mitsuda, Takashi Tsukahara, Takeshi Uchihara, Hiromu Tamatsukuri	FONDER	T2-2
101		反強磁性体eNiC2の磁気構造	郷地 順	東京大学	上床 美也, Ma Hanmin, 繁岡 透, 中島 多朗, 齋藤 開	Magnetic structure of antiferromagnetic compound CeNiC2	Jun Gouchi	The University of Tokyo	Yoshiya Uwatoko, Ma Hanmin, Toru Shigeoka, Tar Nakajima, Hiraku Saito	FONDER	T2-2

播磨分室　BL07LSU/Harima Branch BL07LSU

No.	課題番号	課題名	氏名	所属	分担者（共同研究者）	Title	Name	Organization	Member of research project	担当所員
1	202012-SRBXG-0010	レドックスフロー電池における有機酸化還元中心の静置および電気化学反応下での水和構造解析	細野 英司	産業技術総合研究所	朝倉 大輔、大平 昭博、佐藤 縁、原田 慈久、舩木 敬、張 文雄	Analysis of hydration structure for organic redox centers in redox flow batteries under static and electrochemical reactions	Eiji Hosono	National Institute of Advanced Industrial Science and Technology	Daisuke Asakura,Akihiro Ohira,Yukari Sato,Yoshihisa Harada,Takashi Funaki,Humio Chou	原田 慈久
2	202012-SRBXG-0007	全固体リチウムイオン電池を用いた電極材料のオペランド軟X線発光分光	朝倉 大輔	産業技術総合研究所	細野 英司、石山 智大、小林 正起	Operando soft X-ray emission spectroscopy of electrode materials by using all-solid-state Li-ion battery	Daisuke Asakura	National Institute of Advanced Industrial Science and Technology	Eiji Hosono,Tomohiro Ishikawa,Masaki Kobayashi	原田 慈久
3	202012-SRBXG-0004	Co2MnZ (Z = Ge and Ga)ホイスラー合金バルク単結晶の磁場中共鳴非弾性軟X線散乱(SX-RIXS)によるハーフメタル型電子状態の解明	梅津 理恵	東北大学	藤原 秀紀、菅 滋正、笠原 理加、西岡 拓真、宮脇 淳	Half-metallic electronic states of bulk-single crystal Co2MnZ (Z = Ge and Ga) Heusler alloys probed by resonant inelastic soft X-ray scattering (SX-RIXS) in magnetic field	Rie Umetu	Tohoku University	Hideki Fujiwara,Shigemasa Suga,Rika Kasahara,Takuma Nishioka,Jun Miyawaki	原田 慈久
4	202012-SRBXG-0013	二次電池の高エネルギー密度化を目指した酸化物電極における酸素レドックス反応の機構解明	大久保 將史	東京大学	朝倉 大輔	Study on oxygen-redox reaction mechanism in oxide cathodes for higher energy-density batteries	Masashi Okubo	The University of Tokyo	Daisuke Asakura	原田 慈久
5	202012-SRBXG-0015	軟X線発光分光法による二酸化炭素分離膜中でのCO2の収着状態評価	高原 淳	九州大学	西堀 麻衣子、宮野 陽、二宮 翔、松野 亮介、小椎尾 謙、藤川 茂紀	Analysis of Sorption State of Carbon Dioxide in Separation Membrane	Atsushi Takahara	Kyushu University	Maiko Nishibori,Akira Miyano,Kakeru Ninomiya,Ryousuke Matsuno,Ken Kojio,Shigenori Fujikawa	原田 慈久
6	202012-SRBXG-0025	高分子電解質膜中の水分子電子状態に関する研究	倉橋 直也	東京大学物性研究所	山添 康介、UGALINO RALPH	Study on electronic state of water molecules in polymer electrolyte membranes.	Naoya Kurahashi	The Institute for Solid State Physics, The University of Tokyo	Kousuke Yamazoe,Ugalino Ralph	原田 慈久
7	202012-SRBXG-0016	共鳴非弾性軟X線回折における中間状態のコヒーレンス効果	宮脇 淳	量子科学技術研究開発機構	原田 慈久、倉橋 直也、山添 康介	Coherence Effect of Intermediate State in Resonant Inelastic Soft X-ray Diffraction	Jun Miyawaki	National Institutes for Quantum Science and Technology	Yoshihisa Harada,Naoya Kurahashi,Kousuke Yamazoe	原田 慈久
8	202012-SRBXG-0017	三次元走査型光電子顕微鏡を利用した微粒子光触媒の電子状態の解析	久富 隆史	信州大学	原田 慈久、尾嶋 正治、永村 直佳、張 文雄、吉成 朝子、竹澤 伸吾	Analysis of electronic states of particulate photocatalysts by 3D nano-ESCA	Takashi Hisatomi	Shinsyu University	Yoshihisa Harada,Masaharu Oshima,Naoka Nagamura,Humio Chou,Asako Yoshinari,Shingo Takezawa	原田 慈久

9	202012-SRBXG-0018	顕微分光を活用した原子層シートのポイントプローブ電場印加オペランド電位分布計測技術開発	永村 直佳	物質・材料研究機構	尾嶋 正治、小嗣 真人、矢治 光一郎、吉成 朝子、竹澤 伸吾、津田 俊輔、大石 健太	Development of operando electric potential distribution analysis technique of atomic layer nano sheets with point-probe using spectromicroscopy	Naoka Nagamura	National Institute for Materials Science	Masaharu Oshima,Masato Kotsugi,Koichiro Yaji,Asako Yoshinari,Shingo Takezawa,Shunsuke Tsuda,Kenta Oishi	原田 慈久
10	202012-SRBXG-0022	RIXS-MCD Study of Chromium Trihalides	原田 慈久	東京大学物性研究所		RIXS-MCD Study of Chromium Trihalides	Yoshihisa Harada	The Institute for Solid State Physics, The University of Tokyo		原田 慈久
11	202012-SRBXG-0023	Investigation of electronic structure of Fe-Co spinels by 2p3d RIXS and L-edge XAS	原田 慈久	東京大学物性研究所	宮脇 淳	Investigation of electronic structure of Fe-Co spinels by 2p3d RIXS and L-edge XAS	Yoshihisa Harada	The Institute for Solid State Physics, The University of Tokyo	Jun Miyawaki	原田 慈久
12	202106-SRBXG-0054	セルロースの分子間/分子内水素結合と水の役割の解明	原田 慈久	東京大学物性研究所	倉橋 直也、木内 久雄	Elucidating the intermolecular/intramolecular hydrogen bonding and the role of water in cellulose	Yoshihisa Harada	The Institute for Solid State Physics, The University of Tokyo	Naoya Kurahashi,Hisao Kiuchi	原田 慈久
13	202105-SRBXG-0034	角度分解軟X線発光分光法の開拓	倉橋 直也	東京大学物性研究所	原田　慈久、宮脇　淳、張　文雄、山添　康介、UGALINO　RALPH、寶田 唯以	Development of angle-resolved soft X-ray emission spectroscopy	Naoya Kurahashi	The Institute for Solid State Physics, The University of Tokyo	Yoshihisa Harada,Jun Miyawaki,Humio Chou,Kousuke Yamazoe,Ugalino Ralph,Yui Hoda	原田 慈久
14	202106-SRBXG-0035	T*構造ホールドープ型銅酸化物超伝導体における電荷秩序および電荷励起	藤田 全基	東北大学	谷口　貴典、北山　慎之介、谢 佩翱、王 彤、原田　慈久	Charge order and excitations in T*-type hole-doped cuprate superconductors	Masaki Fuiita	Tohoku University	Takanori Taniguchi,Shinnosuke Kitayama,Shiie Peiao,Wan Ton,Yoshihisa Harada	原田 慈久
15	202106-SRBXG-0038	全固体リチウムイオン電池を用いた電極材料のオペランド軟X線発光分光 2	朝倉 大輔	産業技術総合研究所	細野 英司、石山 智大、小林 正起	Operando soft X-ray emission spectroscopy of electrode materials by using all-solid-state Li-ion battery 2	Daisuke Asakura	National Institute of Advanced Industrial Science and Technology	Eiji Hosono,Tomohiro Ishikawa,Masaki Kobayashi	原田 慈久
16	202106-SRBXG-0039	マルチフェロイックCuOの反強磁性相におけるアナポール秩序観測およびその電場印加効果	木村 剛	東京大学	原田 慈久、荒川　慶人、三澤　龍介、田中　良和、宮脇　淳、上田　大貴	Observation of anapole order and their electric-field-induced effect in antiferromagnetic phases of multiferroic CuO	Tsuyoshi Kimura	The University of Tokyo	Yoshihisa Harada,Keito Arakawa,Ryusuke Misawa,Yosikazu Tanaka,Jun Miyawaki,Hiroki Ueda	原田 慈久
17	202106-SRBXG-0044	共鳴非弾性 X 線散乱法を用いた全固体フッ化物電池酸フッ化物正極の電子状態分析	山本 健太郎	京都大学	原田　慈久、木内　久雄	Study on the electronic structure of oxyfluoride cathode for all-solid-state fluoride ions batteries by resonant inelastic X-ray scattering	Kentaro Yamamoto	Kyoto University	Yoshihisa Harada,Hisao Kiuchi	原田 慈久
18	202106-SRBXG-0050	温度応答性高分子ブラシ内の水分子の構造解析	長瀬 健一	慶應義塾大学	原田　慈久	Observation of local structure of water confined in a thermoresponsive polymer brush	Kenichi Nagase	Keio University	Yoshihisa Harada	原田 慈久
19	202106-SRBXG-0051	顕微分光を活用した原子層シートのポイントプローブ電場印加オペランド電位分布計測技術開発II	永村 直佳	物質・材料研究機構	尾嶋 正治、小嗣 真人、吉成 朝子、竹澤 伸吾、大石 健太	Development of operando electric potential distribution analysis technique of atomic layer nano sheets with point-probe using spectromicroscopy (II)	Naoka Nagamura	National Institute for Materials Science	Masaharu Oshima,Masato Kotsugi,,Asako Yoshinari,Shingo Takezawa,Kenta Oishi	原田 慈久

20	202106-SRBXG-0048	顕微分光による新奇合金系熱電材料"FAST材"の電子状態解析	高際 良樹	物質・材料研究機構	尾嶋 正治、永村　直佳、小嗣 真人、吉成 朝子、竹澤 伸吾、大石 健太	Electronic state analysis of earth-abundant Fe–Al–Si thermoelectric (FAST) materials using scanning photoelectron microscopy	Yoshiki Takagiwa	National Institute for Materials Science	Masaharu Oshima,Nagamura Naoka,Masato Kotsugi,,Asako Yoshinari,Shingo Takezawa,Kenta Oishi	原田 慈久
21	202106-SRBXG-0059	共鳴軟X線非弾性散乱による銅結合タンパク質の電子状態解析	藤井 健太郎	量子科学技術研究開発機構	原田 慈久、宮脇　淳、倉橋 直也、安達　基泰、横谷　明徳	Analysis for Electronic States of Cu-binding Proteins using Resonant Inelastic X-ray Scattering Spectroscopy	Kentaro Fujii	National Institutes for Quantum Science and Technology	Yoshihisa Harada,Jun Miyawaki,Naoya Kurahashi,Motoyasu Adachi,Akinari Yokoya	原田 慈久
22	202012-SRBXG-0008	オペランド光電子分光によるパラジウム金合金の水素吸蔵過程のリアルタイム観測	小板谷 貴典	自然科学研究機構　分子科学研究所		Real-time observation of hydrogen absorption in Pd-Au alloys by operando XPS	Takanori Koitaya	Institute for Molecular Science		松田 巌
23	202012-SRBXG-0014	分割クロスアンジュレータを用いた新たなX線線２色性実験法の開発	小嗣 真人	東京理科大学	松田 巌	Development of novel XMCD method by using segmented cross undulator	Masato Kotsugi	Tokyo University of Science	Iwao Matsuda	松田 巌
24	202012-SRBXG-0026	雰囲気軟X線光電子分光による水素の吸脱着過程に伴う機能性材料の電子状態の研究	吉信 淳	東京大学物性研究所	向井 孝三、尾崎 文彦、田中 駿介	Electronic states of functional materials induced by hydrogen adsorption/desorption studied by ambient pressure soft X-ray photoelectron spectroscopy	Jun Yoshinobu	The Institute for Solid State Physics, The University of Tokyo	Kozo Mukai,Fumihiko Ozaki,Syunsuke Tanaka	松田 巌
25	202012-SRBXP-0027	高速偏光スイッチングを利用した磁気光学測定による鉄コバルト合金薄膜の複素誘電率の決定	平田 靖透	防衛大学校	松田 巌、三輪 真嗣	Determination of the complex permittivity of FeCo alloy thin film by magneto-optical measurement using fast polarizationswitching	Yasuyuki Hirata	National Defense Academy of Japan	Iwao Matsuda,Shinji Miwa	松田 巌
26	202103-SRBXS-0030	軟X線オペランド計測の高度化が拓く次世代触媒科学	山本　達	東北大学	吉信　淳、松田　巌、小板谷　貴典、田中　駿介、向井　孝三、長田　渉、崔　永賢、杉山　正和、佐藤　正寛、今関　裕貴、小林　正起、武田　崇仁、堀尾　眞史、佐藤　祐輔、趙　宇豪、工藤　佳生、鷲見　寿秀、和田　哲弥	Next Generation Catalysis Science Opened by Sophistication of Operando Soft X-ray Spectroscopies	Susumu Yamamoto	Tohoku University	Jun Yoshinobu,Iwao Matsuda,Takanori Koitaya,Syunsuke Tanaka,Kozo Mukai,Wataru Osada,Che Yonhyun,Masakazu Sugiyama,Masahiro Sato,Yuki Imazeki,Masaki Kobayashi,Takahito Takeda,Masafumi Horio,Yusuke Sato,Chou Ugo,Yoshio Kudo,Toshihide Sumi,Tetsuya Wada	松田 巌
27	202103-SRBXS-0030	軟X線オペランド計測の高度化が拓く次世代触媒科学	山本　達	東北大学		Next Generation Catalysis Science Opened by Sophistication of Operando Soft X-ray Spectroscopies	Susumu Yamamoto	Tohoku University		松田 巌

28	202106-SRBXG-0033	CoFe/Cu/Al2O3における軌道トルク: 重金属を用いない巨大磁気トルクの起源解明	金 俊延	理化学研究所	松田　巌、大谷　義近、堀尾　眞史、妹尾　共晃、辻川　夕貴	Orbital torque in CoFe/Cu/Al2O3: Revealing the mechanism of giant magnetic-torque generation without heavy metals	Kimu Junyon	Riken	Iwao Matsuda,Yoshitika Otani,Masafumi Horio,Tomoaki Senoo,Yuki Tujikawa	松田 巌
29	202106-SRBXG-0036	異常ホール効果を示すVNb3S6における磁気状態の徹底解明	堀尾 眞史	東京大学物性研究所	松田　巌、妹尾　共晃、鷲見　寿秀、和田　哲弥	Unambiguous elucidation of the magnetic state of the anomalous Hall-effect compound VNb3S6	Masafumi Horio	The Institute for Solid State Physics, The University of Tokyo	Iwao Matsuda,Tomoaki Senoo,Toshihide Sumi,Tetsuya Wada	松田 巌
30	202106-SRBXG-0040	回転直線偏光を用いた強磁性単原子層薄膜の共鳴光電子分光：磁性制御パラメータとしての界面軌道混成	山本 航平	自然科学研究機構　分子科学研究所	松田　巌、小森　文夫、堀尾　眞史、和田　哲弥、工藤　佳生	Resonance photoemission spectroscopy of monolayer ferromagnetic films using rotational linear polarization: interfacial orbital hybridization as a control parameter of magnetism	Kohei Yamamoto	Institute for Molecular Science	Iwao Matsuda,Fumio Komori,Masafumi Horio,Tetsuya Wada,Yoshio Kudo,	松田 巌
31	202106-SRBXG-0046	機能化したMoS2基底面およびエッジ面の評価と化学反応のオペランド雰囲気光電子分光による研究	吉信 淳	東京大学物性研究所	向井 孝三、尾崎 文彦、田中 駿介	Operando ambient pressure photoelectron spectroscopy of chemical reaction on the functionalized basal and edge surfaces of MoS2	Jun Yoshinobu	The Institute for Solid State Physics, The University of Tokyo	Kozo Mukai,Fumihiko Ozaki,Syunsuke Tanaka	松田 巌
32	202012-SRBXS-0009	次世代光源に向けた全反射ウォルターミラーを利用した新規X線イメージング技術の開発	木村　隆志	東京大学物性研究所	原田　慈久、松田　巌、志村　まり、三村　秀和、江川　悟	Development of Novel X-ray Imaging Technology using Total Reflection Walter Mirror for Next Generation Light Source.	Takashi Kimura	The Institute for Solid State Physics, The University of Tokyo	Yoshihisa Harada,Iwao Matsuda,Mari Shimura,Hidekazu Mimura, Satoru Egawa,Noboru Furuya,Yoko Takeo,Kai Sakurai	木村　隆志
33	202012-SRBXS-0009	次世代光源に向けた全反射ウォルターミラーを利用した新規X線イメージング技術の開発	木村 隆志	東京大学物性研究所	原田　慈久、松田　巌、志村　まり、三村　秀和、江川　悟、古谷　登、竹尾　陽子、櫻井　快	Development of Novel X-ray Imaging Technology using Total Reflection Walter Mirror for Next Generation Light Source.	Takashi Kimura	The Institute for Solid State Physics, The University of Tokyo	Yoshihisa Harada,Iwao Matsuda,Mari Shimura,Hidekazu Mimura, Satoru Egawa	木村　隆志

柏キャンパスE棟/Laser and Synchrotron Radiation Laboratory in Kashiwa

No.	課題番号	課題名	氏名	所属	分担者	Title	Name	Organization	Member of research project	担当所員
1		Spin measurement of 2m-WS_2	Huh, Soonsang	東京大学物性研究所		Spin measurement of 2m-WS_2	Soonsang Huh	The University of Tokyo		
2		Zr_3SnC_2のスピン分解角度分解光電子分光	伊藤　孝寛	名古屋大学		Spin- and Angle-resolved photoemission study of Zr_3SnC_2	Takahiro Ito	Nagoya University		
3		有機分子/貴金属界面におけるラシュバ分裂の増大	金井　要	東京理科大学		Enhancement of Rashba splitting on organic molecule/noble metal interface	Kaname Kanai	Tokyo University of Science		
4		スピン・角度分解光電子分光によるトポロジカル半金属の電子状態の研究	万 宇軒	東京大学		Electronic states of topological semimetals studied by spin- and angle-resolved photoemission spectroscopy	Yuxuan Wan	The University of Tokyo		
5		レーザースピン角度分解光分光による表面電子状態の研究	矢治　光一郎	物質材料研究機構		SARPES studies of atomic layer materials at surfaces	Koichiro Yaji	National Institute for Materials Science		

6		Pb系トポロジカル絶縁体のスピン角度分解光電子分光	矢治　光一郎	物質材料研究機構		SARPES study of a Pb-based topological insulator	Koichiro Yaji	National Institute for Materials Science		
7		バルク敏感高分解能スピン分解角度分解光電子分光によるハーフメタル強磁性体$La_{1-x}Sr_xMnO_3$のNQP状態の観測	横谷　尚睦	岡山大学		Observation of NQP state in half metal ferromagnet $La_{1-x}Sr_xMnO_3$ by bulk sensitive high-resolution spin and angle resolved photoemission spectroscopy	Takayoshi Yokoya	Okayama University		

※採択課題一覧、所属は申請時のデータ

1. 第一原理計算 / First-Principles Calculation of Materials Properties

No.	課題番号	課題名	氏名	所属	Title	Name	Organization
1	2021-Ea-0004	量子論大規模計算による半導体薄膜成長とデバイス界面形成の微視的機構解明	押山　淳	名古屋大学未来材料・システム研究所	Clarification of Microscopic Mechanisms of Semiconductor Epitaxial Growth and Device-Interface Formation by Large-Scale Quantum-Theory-Based Computations	Atsushi Oshiyama	Institute of Materials and Systems for Sustainability
2	2021-Eb-0005	量子論大規模計算による半導体薄膜成長とデバイス界面形成の微視的機構解明	押山　淳	名古屋大学未来材料・システム研究所	Clarification of Microscopic Mechanisms of Semiconductor Epitaxial Growth and Device-Interface Formation by Large-Scale Quantum-Theory-Based Computations	Atsushi Oshiyama	Institute of Materials and Systems for Sustainability
3	2021-Ea-0005	固液界面における電気化学反応シミュレーション手法の開発とその応用	大谷　実	筑波大学計算科学研究センター	Development and Application of electrochemical-reaction simulation methods at the solid/solution interfaces	Minoru Otani	Center for Computational Sciences, The University of Tsukuba
4	2021-Ea-0006	水素の機能性に関する第一原理計算	杉野　修	東京大学物性研究所	First-principles calculation of functionality of hydrogen	Osamu Sugino	Institute for Solid State Physics, University of Tokyo
5	2021-Eb-0001	酸化物等複雑物質の安定性と機能性予測のための第一原理計算	杉野　修	東京大学物性研究所	First-principles prediction of stability and functionality of complex materials	Osamu Sugino	Institute for Solid State Physics, University of Tokyo
6	2021-Ca-0098	全電子混合基底法プログラムの改良と応用	大野　かおる	横浜国立大学大学院工学研究院	Improvement and application of all-electron mixed basis program	Kaoru Ohno	Graduate School of Engineering, Yokohama National University
7	2021-Ca-0118	量子シミュレーションによる動的不均一触媒理論	森川　良忠	大阪大学 大学院工学研究科 物理学系専攻	Quantum simulations on dynamical heterogeneous catalysts	Yoshitada Morikawa	Department of Precision Engineering, Graduate School of Engineering, Osaka University
8	2021-Ca-0063	第一原理計算による新規蓄電デバイス材料の解析	山田　淳夫	東京大学工学系研究科	First principles analysis on novel energy storage device materials	Atsuo Yamada	Faculty of Engineering, The University of Tokyo
9	2021-Cb-0022	フラッシュメモリ応用を目指したSi3N4中のN空孔の第一原理計算による研究	白石　賢二	名古屋大学　未来材料・システム研究所	First Pricnciples Study of N Vacancies in Si3N4 for Flash Memory Application	Kenji Shiraishi	Institute of Materials and Systems for Sustainability, Nagoya University
10	2021-Ca-0101	高密度水素を用いた超機能性材料の機構解明と理論予測	常行　真司	東京大学大学院理学系研究科物理学専攻	Elucidation of mechanism and theoretical prediction of super-functional materials using high-density hydrogen	Shinji Tsuneyuki	Department of Physics, University of Tokyo
11	2021-Cb-0030	表面、界面、欠陥等の複雑構造における原子構造と原子ダイナミク スに関する解析	渡邉　聡	東京大学大学院工学系研究科マテリアル工学専攻	Analyses related to atomic structures and atom dynamics at complex structures such as surfaces, interfaces and defects	Satoshi Watanabe	Department of Materials Engineering, School of Engineering, The University of Tokyo
12	2021-Ca-0001	高圧力下における共有結合性液体・ガラスの構造と電子状態の第一原理計算	下條　冬樹	熊本大学大学院先端科学研究部	First-Principles Molecular-Dynamics Study of Structural and Electronic Properties of Covalent Liquids and Glasses under Pressure	Fuyuki Shimojo	Department of Physics, Kumamoto University
13	2021-Ca-0018	第一原理GW+Bethe-Salpeter法によるXAS計算	野口　良史	静岡大学工学部	XAS simulations by first-principles GW+Bethe-Salpeter method	Yoshifumi Noguchi	Graduate School of Engineering, Shizuoka University
14	2021-Ca-0068	Bayes最適化を用いた界面電気磁気結合の最大化	合田　義弘	東京工業大学物質理工学院材料系	Maximization of interface magnetoelectric coupling with Bayesian optimization	Yoshihiro Gohda	Department of Materials Science and Engineering, Tokyo Institute of Technology
15	2021-Ca-0075	機械学習を用いた結晶構造探索手法の開発	山下　智樹	長岡技術科学大学	Development of crystal structure prediction methods using machine learning	Tomoki Yamashita	Nagaoka University of Technology
16	2021-Ca-0100	パワー半導体における界面欠陥構造の特定とその低減法の提案: 第一原理計算からのアプローチ	松下　雄一郎	東京工業大学	Identification of interface-state defects in power semiconductors: Approach from ab-initio calculations	Yu-Ichiro Matsushita	Tokyo Institute of Technology
17	2021-Ca-0048	次世代スピントロニクス応用に向けたトポロジカル界面の第一原理設計	山内　邦彦	大阪大学工学研究科	First-principles design of topological interfaces toward next-generation spintronics application	Kunihiko Yamauchi	Graduate School of Engineering Osaka University
18	2021-Ca-0069	遷移金属化合物における電子局在化の第一原理計算	レービガー　ハンネス	横浜国立大学　大学院工学研究院　物理工学コース	First principles theory of carrier localization in transition metal compounds	Hannes Raebiger	Department Physics, Yokohama National University

19	2021-Ca-0072	不規則物質系の超イオン伝導性	笠松　秀輔	山形大学学術研究院	Understanding superionic conduction in disordered materials systems	Shusuke Kasamatsu	Academic Assembly, Yamagata University
20	2021-Ca-0070	固体中ミュオンの第一原理計算	斎藤　峯雄	金沢大学理工研究域数物科学系	First-principles calculations on muon in solids	Mineo Saito	Division of Mathematical and Physical Sciences Kanazawa University
21	2021-Ca-0112	第一原理電子状態・輸送特性計算コードRSPACEの開発とデバイスシミュレーション	小野　倫也	神戸大学大学院工学研究科電気電子工学専攻	Development of first-principles electronic-structure and transport calculation code RSPACE and simulations for device	Tomoya Ono	Department of Electrical and Electronic Engineering, Graduate School of Engineering, Kobe University
22	2021-Cb-0006	三元系最密充填構造に基づく結晶構造探索	尾崎　泰助	東京大学物性研究所	Prediction of new crystal structures based on the densest ternary sphere packings	Taisuke Ozaki	Institute for Solid State Physics, The University of Tokyo
23	2021-Cb-0052	機械学習ポテンシャル分子動力学計算による不規則物質系の超イオン伝導性の解明	笠松　秀輔	山形大学学術研究院	Understanding superionic conductivity in disordered systems using machine learning potential molecular dynamics	Shusuke Kasamatsu	Academic Assembly, Yamagata University
24	2021-Ca-0052	表面、界面、欠陥等の複雑構造における原子構造と原子ダイナミクスに 関する解析	渡邉　聡	東京大学大学院工学系研究科マテリアル工学専攻	Analyses related to atomic structures and atom dynamics at complex structures such as surfaces, interfaces and defects	Satoshi Watanabe	Department of Materials Engineering, School of Engineering, The University of Tokyo
25	2021-Cb-0031	原子層エッチングプロセスにおける表面反応解析	浜口　智志	大阪大学工学研究科	Analysis of Surface Reactions in Atomic Layer Etching Processes	Satoshi Hamaguchi	Graduate School of Engineering, Osaka University
26	2021-Ca-0091	大規模界面構造における第一原理電子輸送計算手法の開発と応用	江上　喜幸	北海道大学大学院工学研究院	Development and application of first-principles method for electron-transport calculations of large-scale interface structures	Yoshiyuki Egami	Faculty of Engineering, Hokkaido University
27	2021-Ca-0003	機械学習を用いた環境発電用ポリマーエレクトレット材料の開発	鈴木　雄二	東京大学大学院工学系研究科機械工学専攻	Development of Polymer Electret Materials for Energy Harvesting Using Machine Learning	Yuji Suzuki	Dept. of Mechanical Engineering, The University of Tokyo
28	2021-Ca-0061	原子層エッチングプロセスにおける表面反応解析	浜口　智志	大阪大学工学研究科	Analysis of Surface Reactions in Atomic Layer Etching Processes	Satoshi Hamaguchi	Graduate School of Engineering, Osaka University
29	2021-Ca-0109	氷惑星・氷衛星内部の熱力学的状態の統一的理解	小松　勇	自然科学研究機構アストロバイオロジーセンター＆国立天文台	A unified understanding of thermodynamic properties in icy planets and icy moons	Yu Komatsu	National Institutes of Natural Sciences AstroBiology Center & National Astronomical Observatory of Japan
30	2021-Cb-0040	半導体界面構造における第一原理電子輸送研究	江上　喜幸	北海道大学大学院工学研究院	First-principles study on electron-transport through semiconductor interface structures	Yoshiyuki Egami	Faculty of Engineering, Hokkaido University
31	2021-Cb-0045	パワー半導体における界面欠陥構造の特定とその低減法の提案: 第一 原理計算からのアプローチ	松下　雄一郎	東京工業大学	Identification of interface-state defects in power semiconductors: Approach from ab-initio calculations	Yu-Ichiro Matsushita	Tokyo Institute of Technology
32	2021-Ca-0019	ギ酸分解触媒及び酸素吸蔵材料の省貴金属化	國貞　雄治	北海道大学大学院工学研究院　附属エネルギー・マテリアル融合領域研究センター	Reduction of Rare Metals in Formic Acid Decomposition Catalysts and Oxygen Storage Materials	Yuji Kunisada	Center for Advanced Research of Energy and Materials, Faculty of Engineering, Hokkaido University
33	2021-Cb-0048	第一原理電子状態・輸送特性計算コードRSPACEの開発とデバイスシミュレーション	小野　倫也	神戸大学大学院工学研究科電気電子工学専攻	Development of first-principles electronic-structure and transport calculation code RSPACE and simulations for device	Tomoya Ono	Department of Electrical and Electronic Engineering, Graduate School of Engineering, Kobe University
34	2021-Ca-0080	金属絶縁体超格子熱電材料の機械学習の最適化	邵　成	東京大学機械工学塩見研究室	Machine-learning optimization of metal-insulator superlattice thermoelectric materials	Cheng Shao	Shiomi Lab, Mechanical engineering, The University of Tokyo
35	2021-Ca-0119	エネルギー変換物質におけるスピン分裂と異常ホール伝導度の第一原理計算	石井　史之	金沢大学ナノマテリアル研究所	First-Principles Calculation of Spin Splitting and Anomalous Hall Conductivity in Energy Conversion Materials	Fumiyuki Ishii	Kanazawa University
36	2021-Cb-0001	高圧力下における共有結合性液体･ガラスの構造と電子状態の第一 原理計算	下條　冬樹	熊本大学大学院先端科学研究部	First-Principles Molecular-Dynamics Study of Structural and Electronic Properties of Covalent Liquids and Glasses under Pressure	Fuyuki Shimojo	Department of Physics, Kumamoto University
37	2021-Eb-0007	量子シミュレーションによる動的不均一触媒理論	森川　良忠	大阪大学 大学院工学研究科 物理学系専攻	Quantum Simulations on Dynamical Heterogeneous Catalysts	Yoshitada Morikawa	Department of Precision Engineering, Graduate School of Engineering, Osaka University

38	2021-Ca-0086	分子接合の第一原理伝導計算	大戸　達彦	大阪大学大学院基礎工学研究科	First-principles transport calculations for single-molecular junctions	Tatsuhiko Ohto	Graduate School of Engineering Science, Osaka University
39	2021-Cb-0041	新奇熱電物質における欠陥形成に関する第一原理計算による研究	黒木　和彦	大阪大学	First principles study on defect formations in new thermoelectric materials	Kazuhiko Kuroki	Osaka University
40	2021-Ca-0027	GaN中の転位と不純物の複合体の第一原理計算による研究	白石　賢二	名古屋大学　未来材料・システム研究所	First principles studies of impurity-dislocation complexes in GaN	Kenji Shiraishi	Institute of Materials and Systems for Sustainability, Nagoya University
41	2021-Ca-0066	帯電が誘起する薄膜酸化物の構造相転移：第一原理計算による研究	中山　隆史	千葉大学理学部物理学科	First-principles study on charging-induced structure phase transitions of thin film oxides	Takashi Nakayama	Department of Physics, Chiba University
42	2021-Ca-0058	van der Waals 相互作用が生み出す低熱伝導	大西　正人	東京大学機械工学専攻	Low Thermal Conductance Generated by van der Waals Interaction	Masato Ohnishi	Department of Mechanical Engineering, The University of Tokyo
43	2021-Ca-0108	ナノ構造の量子伝導の第一原理計算	小林　伸彦	筑波大学 数理物質系　物理工学域	First-principles study of quantum transport in nanostructures	Nobuhiko Kobayashi	Department of Applied Physics, University of Tsukuba
44	2021-Cb-0011	機械学習を用いた環境発電用ポリマーエレクトレット材料の開発	鈴木　雄二	東京大学大学院工学系研究科機械工学専攻	Development of Polymer Electret Materials for Energy Harvesting Using Machine Learning	Yuji Suzuki	Dept. of Mechanical Engineering, The University of Tokyo
45	2021-Ca-0085	密度汎関数法と溶液理論を用いた電気化学反応の解析 3	春山　潤	東京大学物性研究所	Electrochemical reaction analysis using density functional calculation + implicit solvation model 3	Jun Haruyama	Institute for Solid State Physics, The University of Tokyo
46	2021-Ca-0087	遷移金属合金の磁気熱量効果	小口　多美夫	大阪大学産業科学研究所	Magnetocaloric Effect of Transition-Metal Alloys	Tamio Oguchi	ISIR, Osaka University
47	2021-Ca-0028	人工ニューラルネットワーク力場構築のための効率的な学習データ生成法の模索III	島村　孝平	熊本大学大学院先端科学研究部	Study of Efficient Training Data Generation Method for Constructing Artificial Neural Network Force Field III	Kohei Shimamura	Faculty of Advanced Science and Technology, Kumamoto University
48	2021-Ca-0111	高分子系有機半導体の電子状態・界面準位の第一原理的研究	柳澤　将	琉球大学理学部物質地球科学科物理系	First-principles investigation on the electronic properties of polymer organic semiconductors	Susumu Yanagisawa	Department of Physics and Earth Sciences, Faculty of Science, University of the Ryukyus
49	2021-D-0008	π電子－プロトン相関型分子性導体群の圧力下構造及び電子状態の系統的予測	出倉　駿	東京大学物性研究所	Systematic elucidation of structure and electronic state of π-electron-proton coupled molecular conductors under pressure	Shun Dekura	Institute for Solid State Physics, The University of Tokyo
50	2021-Cb-0010	燃料電池電極触媒及び水素透過膜の省貴金属化	坂口　紀史	北海道大学大学院工学研究院　附属エネルギー・マテリアル融合領域研究センター	Reduction of Rare Metals in Fuel Cell Catalysts and Hydrogen Permeable Membrane	Norihito Sakaguchi	Center for Advanced Research of Energy and Materials, Faculty of Engineering, Hokkaido University
51	2021-Ca-0084	還元CeO$_{2}$（100）上での水の反応による水素生成	横　哲	東北大学材料科学高等研究所	Hydrogen formation by reaction of water on reduced CeO$_{2}$ (100) surface	Akira Yoko	WPI-AIMR, Tohoku University
52	2021-Cb-0012	高機能スピントロニクス磁性材料の電子構造解析および電気磁気効果解析	小田　竜樹	金沢大学理工研究域数物科学系	Analyses on electronic structure and magnetoelectric effect in high-performance spintronics and magnetic materials	Tatsuki Oda	Faculty of Mathematics and Physics, Institute of Science and Engineering, Kanazawa University
53	2021-Ca-0024	ワイドギャップ酸化物材料における点欠陥の構造安定性と電子状態	籾田　浩義	大阪大学産業科学研究所	Structure stability and electronic structures of point defects in wide-gap oxide materials	Hiroyoshi Momida	Institute of Scientific and Industrial Research, Osaka University
54	2021-Cb-0028	第一原理計算による有限温度下での有機半導体のバンド計算	柳澤　将	琉球大学理学部物質地球科学科物理系	First-principles band structure calculation of organic crystals at finite-temperature	Susumu Yanagisawa	Department of Physics and Earth Sciences, Faculty of Science, University of the Ryukyus
55	2021-Ca-0012	第一原理計算による磁性元素を含む表面・界面の理論解析	立津　慶幸	名桜大学	Theoretical analyses for surfaces and grain boundaries with magnetic elements from first-principles calculations	Yasutomi Tatetsu	Meio University
56	2021-Ca-0064	進化論的アルゴリズムによる高速化学反応過程シミュレーション手法の開発	草部　浩一	兵庫県立大学大学院理学研究科	Evolutionary algorithm for simulation of fast chemical reaction process	Koichi Kusakabe	Graduate School of Science, University of Hyogo
57	2021-Ca-0094	Mg-Si-O系ポストポストペロブスカイト相における秩序無秩序転移	梅本　幸一郎	東京工業大学地球生命研究所	Order-disorder transitions in post-post-perovskite phases in Mg-Si-O system	Koichiro Umemoto	Earth-Life Science Institute, Tokyo Institute of Technology

58	2021-Ca-0020	燃料電池電極触媒及び水素透過膜の省貴金属化	坂口　紀史	北海道大学大学院工学研究院　附属エネルギー・マテリアル融合領域研究センター	Reduction of Rare Metals in Fuel Cell Catalysts and Hydrogen Permeable Membrane	Norihito Sakaguchi	Center for Advanced Research of Energy and Materials, Faculty of Engineering, Hokkaido University
59	2021-Ca-0056	高機能スピントロニクス磁性材料の電子構造解析および電気磁気効果解析	小田　竜樹	金沢大学理工研究域数物科学系	Analyses on electronic structure and magnetoelectric effect in high-performance spintronics and magnetic materials	Tatsuki Oda	Faculty of Mathematics and Physics, Institute of Science and Engineering, Kanazawa University
60	2021-Ca-0096	第一原理計算によるセロビオースの加水分解反応過程の研究	佐々木　岳彦	東京大学　大学院新領域創成科学研究科	Study on Hydration Process of Cellobiose by First Principles Calculations	Takehiko Sasaki	Graduate School of Frontier Sciences, The University of Tokyo
61	2021-Cb-0008	固体中ミュオンの第一原理計算	斎藤　峯雄	金沢大学理工研究域数物科学系	First-principles calculations on muon in solids	Mineo Saito	Division of Mathematical and Physical Sciences Kanazawa University
62	2021-Ca-0008	純水による Si 単結晶の触媒表面基準エッチングのメカニズム解明	BUI　VANPHO	大阪大学大学院工学研究科	Study on removal mechanism of single crystalline Si planarized by catalyst referred etching in pure water	Vanpho Bui	Graduate School of Engineering, Osaka University
63	2021-Ca-0047	ペロブスカイト型酸化物の光励起状態におけるイオン伝導に関する第一原理分子動力学研究	大村　訓史	広島工業大学　工学部	Ab initio molecular dynamics study on ion-conduction mechanisms of perovskite-type oxide	Satoshi Ohmura	Faculty of Engineering, Hiroshima Institute of Technology
64	2021-Ca-0113	第一原理計算による金属酸化物中の水素同位体ミクロ挙動に関する研究	毛　偉	東京大学工学部研究科	First-principles calculation of microscopic behaviors of hydrogen in metal oxides	Wei Mao	School of Engineering, The University of Tokyo
65	2021-Ca-0071	玄武岩メルトとガラスの構造と物性	飯高　敏晃	理化学研究所	Structure and Property of Basalt Melt and Glass	Toshiaki Iitaka	Riken
66	2021-D-0006	第一原理計算による銀(111)表面上ヘリセン吸着構造の数値的研究	濱本　雄治	大阪大学 大学院工学研究科 物理学系専攻	First principles study of the adsorption structure of helicene on the Ag(111) surface	Yuji Hamamoto	Department of Precision Engineering, Osaka University
67	2021-Ca-0011	有機無機材料界面における二次元秩序構造形成過程の第一原理計算	折本　裕一	九州大学大学院総合理工学研究院物質科学部門	First principles calculations of two-dimensional ordering process at organic/inorganic materials interface	Yuuichi Orimoto	Department of Material Sciences, Faculty of Engineering Sciences, Kyushu University
68	2021-Ca-0107	RSDFT計算による非接触原子間力顕微鏡のエネルギー散逸チャンネルで捉えた原子変位機構の解明	新井　豊子	金沢大学	RSDFT calculation of atomic displacement captured by energy dissipation channel of noncontact atomic force microscope	Toyoko Arai	Kanazawa University
69	2021-Ca-0060	第一原理計算による有機強誘電体・圧電体の物性予測	石橋　章司	産業技術総合研究所	Prediction of properties of organic ferroelectrics and piezoelectrics by first-principles calculation	Shoji Ishibashi	National Institute of Advanced Industrial Science and Technology
70	2021-Cb-0018	Sb系テラヘルツトランジスタのための歪バンド構造設計	藤代　博記	東京理科大学	Strained Band-Structure Engineering for Antimonide-Based Terahertz Transistors	Hiroki Fujishiro	Tokyo University of Science
71	2021-Cb-0053	界面構造予測と電子状態に関する第一原理的研究	石井　史之	金沢大学ナノマテリアル研究所	First-principles study of interface structure prediction and electronic structures	Fumiyuki Ishii	Kanazawa University
72	2021-Cb-0034	基于第一原理的铁磁体声子-磁子耦合研究	邵　成	東京大学機械工学塩見研究室	First principles based investigation of phonon-magnon coupling in ferromagnetic insulator	Cheng Shao	Shiomi Lab, Mechanical engineering, The University of Tokyo
73	2021-Cb-0035	van der Waals 相互作用が生み出す低熱伝導	大西　正人	東京大学機械工学専攻	Low Thermal Conductance Generated by van Der Waals Interaction	Masato Ohnishi	Department of Mechanical Engineering, The University of Tokyo
74	2021-Ca-0116	ガウス過程回帰による二次元物質構造の大域的探索	濱本　雄治	大阪大学 大学院工学研究科 物理学系専攻	Global search for the structures of two-dimensional materials by Gaussian process regression	Yuji Hamamoto	Department of Precision Engineering, Osaka University
75	2021-Cb-0023	ギ酸分解触媒及び酸素吸蔵材料の省貴金属化	國貞　雄治	北海道大学大学院工学研究院　附属エネルギー・マテリアル融合領域研究センター	Reduction of Rare Metals in Formic Acid Decomposition Catalysts and Oxygen Storage Materials	Yuji Kunisada	Center for Advanced Research of Energy and Materials, Faculty of Engineering, Hokkaido University
76	2021-Ca-0090	マグネシウム合金系の相安定性と物性制御因子の解明：第一原理計算による研究	圓谷　貴夫	熊本大学　大学院先導機構	Origins of phase stabilities and physical properties in Mg based alloys: A first-principles study	Takao Tsumuraya	Priority Organization for Innovation and Excellence, Kumamoto University
77	2021-Ca-0026	第一原理分子動力学法に基づくガラスの静的構造に関する研究	高良　明英	熊本大学技術部	*Ab initio* molecular dynamics study on static structure of glass materials	Akihide Koura	Technical Division, Kumamoto University

78	2021-Ca-0082	第一原理計算による光触媒反応メカニズムの解明	城塚　達也	茨城大学	Elucidation of Photocatalytic Reaction Mechanism by Ab Initio Calculations	Tatsuya Joutsuka	Ibaraki University
79	2021-Ca-0114	第一原理計算による粒界安定構造探索	幾原　雄一	東京大学大学院工学系研究科総合研究機構	Determining grain-boundary stable atomic structure by first-principle calculations	Yuichi Ikuhara	Institute of Engineering Innovation, University of Tokyo
80	2021-Cb-0029	準フォノニック結晶によるナノ熱輸送の究極抑制	LIAO　YUXUAN	東京大学機械工学専攻	Ultimate Suppression of Nanoheat Transport with Quasi-phononic Crystal	Yuxuan Liao	Department of Mechanical Engineering, the University of Tokyo
81	2021-Cb-0033	SrVO3/SrTiO3 および CaCuO2/SrTiO3 多層膜およびCa5Ir3O12に対する反射スペクトルの第一原理計算	中村　和磨	九州工業大学	Ab initio calculation for reflectivity for SrVO3/SrTiO3, CaCuO2/SrTiO3, and Ca5Ir3O12	Kazuma Nakamura	Kyushu Institute of Technology
82	2021-Ca-0030	半導体表面界面における構造的素励起の研究	影島　博之	島根大学大学院自然科学研究科	Study on structural elementary excitations at semiconductor surfaces and interfaces	Hiroyuki Kageshima	Graduate School of Natural Science and Technology, Shimane University
83	2021-Ca-0041	固体光吸収の原子論的シミュレーション	篠原　康	東京大学工学系研究科附属光量子科学研究センター	Atomistic simulations for optical absorption of solids	Yasushi Shinohara	Photon Science Center, School of Engineering, the University of Tokyo
84	2021-Ca-0092	SrVO3/SrTiO3 および CaCuO2/SrTiO3 多層膜に対する第一原理有効模型導出	中村　和磨	九州工業大学	Ab initio derivation of effective low-energy models for SrVO3/SrTiO3 and CaCuO2/SrTiO3 multilayer system	Kazuma Nakamura	Kyushu Institute of Technology
85	2021-Ca-0046	分子修飾ナノ界面設計のための第一原理および人工ニューラルネット分子動力学計算	鶴田　健二	岡山大学学術研究院自然科学学域	Ab-initio and artificial neural-network molecular-dynamics calculations for molecule-modified nanointerfaces	Kenji Tsuruta	Graduate School of Natural Science and Technology, Okayama University
86	2021-D-0003	イリジウム酸化物Ca$_{5}$Ir$_{3}$O$_{12}$の光学伝導度の第一原理計算	河野　翔也	九州工業大学	Optical conductivity of Ca$_{5}$Ir$_{3}$O$_{12}$ by first-principles calculations	Shoya Kawano	Kyushu Institute of Technology
87	2021-Ca-0006	原子層合金の安定性	小野　頌太	岐阜大学	Stability of atomically thin alloys	Shota Ono	Gifu University
88	2021-Ca-0065	Sb系テラヘルツトランジスタのための歪バンド構造設計	藤代　博記	東京理科大学	Strained Band-Structure Engineering for Antimonide-Based Terahertz Transistors	Hiroki Fujishiro	Tokyo University of Science
89	2021-Ca-0088	複雑な構造を持つ合金表面の第一原理計算	野澤　和生	鹿児島大学理学部物理科学科	First-principles calculations of complex metallic alloy surfaces	Kazuki Nozawa	Department of Physics and Astronomy, Kagoshima University
90	2021-Cb-0004	金属表面での置換反応の分子動力学シュミレーション	福田　常男	大阪公立大学大学院工学研究科電子物理系専攻	Molecular dynamics simulation of substitution reaction on metal surface	Tuneo Fukuda	Depart. of Physics and Electronics, Graduate School of Eng., Osaka Metroolitan University
91	2021-Ba-0041	永久磁石材料の有限温度磁性	赤井　久純	東京大学物性研究所	Finite temperature magnetic properties of permanent magnet materials	Hisazumi Akai	Institute for Solid State Physics, The University of Tokyo
92	2021-Ba-0020	超伝導密度汎関数理論に基づく第一原理Tc計算手法の高度化	明石　遼介	量子科学技術研究開発機構	Development of the first-principles method for calculating Tc based on density functional theory for superconductors	Ryosuke Akashi	National Institutes for Quantum Science and Technology
93	2021-Bb-0036	永久磁石材料の結晶磁気異方性の第一原理計算	赤井　久純	東京大学物性研究所	First-principles calculation of magnetocrystalline anisotropy of permanent magnet materials	Hisazumi Akai	Institute for Solid State Physics, The University of Tokyo
94	2021-Ba-0026	対称性指標を用いた網羅的なトポロジカル物質探索	渡邉　悠樹	東京大学工学系研究科物理工学専攻	Comprehensive material search based on symmetry indicators	Haruki Watanabe	Department of Applied Physics, The University of Tokyo
95	2021-Ca-0044	積層グラフェンの物性解明	藤本　義隆	九州大学工学研究院	Physical properties of layered graphene	Yoshitaka Fujimoto	Faculty of Engineering, Kyushu University
96	2021-Cb-0039	不純物半導体の金属絶縁体転移の臨界濃度とクーロンギャップ	原嶋　庸介	奈良先端科学技術大学院大学	Critical concentration of metal-insulator transition in doped semiconductors and Coulomb gap	Yosuke Harashima	Nara Institute of Science and Technology
97	2021-Cb-0051	第一原理によるペロブスカイト型酸化物粒界の安定構造探索	幾原　雄一	東京大学大学院工学系研究科総合研究機構	First principles calculations for proving stable grain-boundary structures in perovskite oxides	Yuichi Ikuhara	Institute of Engineering Innovation, University of Tokyo

98	2021-Ba-0022	触媒インフォマティクスに向けた新奇表面サイト探索	日沼　洋陽	産業技術総合研究所	Exploration of exotic surface sites for catalyst informatics	Yoyo Hinuma	National Institute of Advanced Industrial Science and Technology
99	2021-Bb-0017	一様電場下における磁性絶縁体の第一原理計算	山口　直也	金沢大学ナノマテリアル研究所	First-principles Calculations of Magnetic Insulators Under Uniform Electric Fields	Naoya Yamaguchi	Nanomaterials Research Institute, Kanazawa University
100	2021-Bb-0020	機械学習による振動スペクトルの予測方法の検証	平塚　将起	工学院大学機械工学科	Validation of a Machine Learning Method for Predicting Vibration Spectra	Masaki Hiratsuka	Department of Mechanical Engineering, Kogakuin University
101	2021-Bb-0041	銀・銅カルコゲナイド熱電材料の計算機マテリアルデザイン	佐藤　和則	大阪大学大学院工学研究科	Computational materials design of Ag, Cu chalcogenide based thermoelectric materials	Kazunori Sato	Graduate School of Engineering, Osaka University
102	2021-Ba-0024	第一原理計算と機械学習に基づく非平衡現象の大規模分子動力学シミュレーション	三澤　賢明	岡山大学大学院自然科学研究科	Large-Scale Molecular Dynamics Simulations on Non-Equilibrium Phenomena Using First-Principles Calculation and Machine Leaning	Masaaki Misawa	Graduate School of Natural Science and Technology, Okayama University
103	2021-Bb-0005	原子層合金の安定性: II	小野　頌太	岐阜大学	Stability of atomically thin alloys: II	Shota Ono	Gifu University
104	2021-Bb-0012	硫化ホウ素薄膜の電子状態における膜厚依存性	豊田　雅之	東京工業大学　理学院物理学系	Thickness-dependent electronic structure of exfoliated boron monosulfide	Masayuki Toyoda	Department of Physics, School of Science, Tokyo Institute of Technology
105	2021-Ba-0011	ネオジム永久磁石副相および界面の構造と交換結合定数の第一原理計算的解析	寺澤　麻子	高度情報科学技術研究機構	First-principles analysis of structure and exchange coupling constants of subphases and interface in Nd-based permanent magnets	Asako Terasawa	Research Organization for Information Science and Technology
106	2021-Ba-0054	機械学習と第一原理MDによる赤外およびラマンスペクトルの計算方法の検討	平塚　将起	工学院大学機械工学科	Calculation of Infrared and Raman spectra by molecular dynamics simulation using machine learning	Masaki Hiratsuka	Department of Mechanical Engineering, Kogakuin University
107	2021-Ba-0007	新たなナノスケール表面界面の電子物性に関する理論的研究	小林　功佳	お茶の水女子大学理学部物理学科	Theoretical study on electronic properties of new nanoscale surfaces and interfaces	Katsuyoshi Kobayashi	Department of Physics, Faculty of Science, Ochanomizu University
108	2021-Ba-0017	MLOを用いた第一原理有効模型の自動生成システムの研究	榊原　寛史	鳥取大学大学院工学研究科	Automatic generation of first-principle effective models based on MLO	Hirofumi Sakakibara	Graduate School of Engineering, Tottori University
109	2021-Ba-0019	有機分子を活用したスピン流-電流変換物質の第一原理計算	山口　直也	金沢大学ナノマテリアル研究所	First-principles Calculations of Spin-to-charge Conversion Materials Utilizing Organic Molecules	Naoya Yamaguchi	Nanomaterials Research Institute, Kanazawa University
110	2021-Ba-0025	Pb系トポロジカル絶縁体の欠陥形成エネルギーおよびバンド構造	徳本　有紀	東京大学生産技術研究所	Defect formation energy and band structure of Pb-based topological insulators	Yuki Tokumoto	Institute of Industrial Science, The University of Tokyo
111	2021-Ba-0028	大きな分子量を持つ有機半導体結晶の電子状態の計算	島田　敏宏	北海道大学　大学院工学研究院	Electronic structure calculation of organic crystals with high molecular weight	Toshihiro Shimada	Faculty of Engineering, Hokkaido University
112	2021-Ba-0046	量子液晶の電子状態計算	池田　浩章	立命館大学理工学部物理科学科	Electronic structure calculations in quantum liquid crystals	Hiroaki Ikeda	Department of Physics, Ritsumeikan University
113	2021-Ba-0057	液晶におけるオーダーパラメータと電子輸送機構との相関	大野　玲	東京工業大学	Correlation between Order Parameter and Electron Transport Mechanism in Liquid Crystal	Akira Ohno	Tokyo Institute of Technology
114	2021-Ba-0058	網羅的DFT計算によるAB型2次元物質探索	福田　将大	東京大学物性研究所	AB type 2D materials search by high-throughput DFT calculations	Masahiro Fukuda	Institute for Solid State Physics, The University of Tokyo
115	2021-Ba-0059	ダイヤモンド表面のグラファイト化とその剥離プロセスの第一原理計算	稲垣　耕司	大阪大学大学院工学研究科	First-principles calculation of graphitization of diamond surface and its exfoliation process	Kouji Inagaki	Graduate school of Engineering, Osaka University
116	2021-Bb-0032	異方的結晶構造を持つ磁性体と誘電体/磁性体界面系の解析	小幡　正雄	金沢大学理工研究域	Analysis of insulator-ferromagnetic interface and magnetic material with an anisotropic crystal structure	Masao Obata	Institute of Science and Engineering, Kanazawa University
117	2021-Bb-0016	硫化物系固体電解質を用いた全固体キャパシタの開発	大久保　將史	早稲田大学	Development of all-solid-state capacitors using sulfide-based solid electrolytes	Masashi Okubo	Waseda University
118	2021-Bb-0039	不安定結晶面CeO2(100)と担持金属単原子の相互作用	横　哲	東北大学材料科学高等研究所	Interaction between metallic atom and instable CeO2 (100) facet	Akira Yoko	WPI-AIMR, Tohoku University

119	2021-Ba-0033	化学気相成長における金属膜成長メカニズムの理論解析	城塚　達也	茨城大学	Theoretical Analysis of Metal Film Growth Mechanism in Chemical Vapor Deposition	Tatsuya Joutsuka	Ibaraki University
120	2021-Bb-0021	分子吸着表面における光励起過程における光電子角度分布に関する計算	二木　かおり	千葉大学	Calculation of photoelectron angle distribution in the photoexcitation process on the organic molecules adsorbed surface	Kaori Niki	Chiba University
121	2021-Bb-0031	第一原理計算を用いた金属とプラズマ処理したフッ素樹脂界面の接着メカニズムの解明	大久保　雄司	大阪大学大学院工学研究科	Clarification of atomistic mechanism application of process design for adhesion interface between metal and plasma-treated fluoropolymers using first principles calculation	Yuji Ohkubo	Graduate School of Engineering, Osaka University
122	2021-Ca-0034	照射損傷と格子間原子との相互作用の研究	大澤　一人	九州大学応用力学研究所	Study of interaction between radiation damage and interstitial atom	Kazuhito Ohsawa	Research Institute for Applied Mechanics, Kyushu University
123	2021-Ca-0051	第一原理計算によるダブルペロブスカイト型光触媒の研究	西館　数芽	岩手大学理工学部	First-principles electronic structure calculation of double-perovskite photocatalyst	Kazume Nishidate	Faculty of Science and Engineering, IWATE University
124	2021-Ca-0062	不純物半導体の金属絶縁体転移の臨界指数とスピン秩序	原嶋　庸介	奈良先端科学技術大学院大学	Critical exponent of metal-insulator transition in doped semiconductors and spin ordering	Yosuke Harashima	Nara Institute of Science and Technology
125	2021-Cb-0054	ナノ構造の量子伝導の第一原理計算	小林　伸彦	筑波大学 数理物質系　物理工学域	First-principles study of quantum transport in nanostructures	Nobuhiko Kobayashi	Department of Applied Physics, University of Tsukuba
126	2021-Ba-0055	金属２原子膜と磁性金属フタロシアニン分子の相互作用	有賀　哲也	京都大学理学研究科化学専攻	Interaction between magnetic metal phthalocyanine molecules and bi-layer metal films	Aruga Tetsuya	Dept. Chem., School of Science, Kyoto University
127	2021-Ba-0056	強誘電体/強磁性体界面系と異方的結晶構造を持つ磁性体の解析	小幡　正雄	金沢大学理工研究域	Analysis of ferroelectric-ferromagnetic interface and magnetic material with an anisotropic crystal structure	Masao Obata	Institute of Science and Engineering, Kanazawa University
128	2021-Ba-0029	シリサイド薄膜系の原子構造と電子状態	服部　賢	奈良先端科学技術大学院大学物質創成科学研究科	Atomic structure and electronic states for silicide films	Ken Hattori	Graduate School of Materials Science, Nara Institute of Science and Technology
129	2021-Bb-0022	グラフェンナノリボンの電子状態計算と加工用触媒としての反応性調査	有馬　健太	大阪大学 大学院 工学研究科	First-principles simulation of graphene nanoribbon and investigation of reactivity as machining catalyst	Kenta Arima	Graduate School of Engineering, Osaka University
130	2021-Bb-0040	d電子系化合物の電子構造とフェルミオロジー	眞榮平　孝裕	琉球大学　理学部	Electronic Structure and Fermiology of d-electron compounds	Takahiro Maehira	Faculty of Science, University of the Ryukyus
131	2021-Ba-0030	酸化物における電場印加下での電子格子相互作用	牧野　哲征	福井大学遠赤外領域開発研究センター	Electron-phonon interaction under electric fields in oxides	Takayuki Makino	Research Center for Development of Far-Infrared Region, University of Fukui
132	2021-Ba-0053	第一原理計算に基づくマグネシウム合金の欠陥場の解析	松中　大介	信州大学工学部機械システム工学科	First-principles Study of Defects of Magnesium Alloys	Matsunaka Daisuke	Department of Mechanical Systems Engineering, Shinshu University
133	2021-Bb-0006	触媒インフォマティクスに向けた新奇表面サイト探索	日沼　洋陽	産業技術総合研究所	Exploration of exotic surface sites for catalyst informatics	Yoyo Hinuma	National Institute of Advanced Industrial Science and Technology
134	2021-Ca-0010	分子結晶表面状態の時間分解解析手法の確立	二木　かおり	千葉大学	Development of time-resolved analysis method for molecular crystal surface	Kaori Niki	Chiba University
135	2021-A-0004	硫化物系固体電解質を用いた全固体キャパシタの開発	大久保　將史	早稲田大学	Development of all-solid-state capacitors using sulfide-based solid electrolytes	Masashi Okubo	Waseda University
136	2021-A-0005	ドープされたFe$_{2}$VAlにおける熱電性と磁性の第一原理的研究	西口　和孝	神戸大学大学院システム情報学研究科	First-principles study of thermoelectric and magnetic properties in doped Fe$_{2}$Val	Kazutaka Nishiguchi	Graduate School of System Informatics, Kobe University
137	2021-A-0007	トポロジカル絶縁体系のバンド計算	秋山　了太	東京大学理学系研究科物理学専攻	Band calculation of topological insulator systems	Ryota Akiyama	Department of Physics, The University of Tokyo
138	2021-A-0010	第一原理計算による光熱変換原理の解明	江目　宏樹	山形大学	Study of the principle of photothermal conversion by ab initio calculations	Hiroki Gonome	Yamagata University
139	2021-A-0011	種々の磁性材料における物理特性の第一原理計算	小田　洋平	福島工業高等専門学校	First-principles calculation of physical properties in various magnetic materials	Yohei Kota	National Institute of Technology, Fukushima College

140	2021-A-0013	ハイエントロピー合金の相安定性	御手洗　容子	東京大学新領域創成科学研究科	Phase stability of high-entropy alloys	Yoko Mitarai	Graduate School of Frontier Sciences, The University of Tokyo
141	2021-A-0015	半導体および金属基板へ吸着した有機ハロゲン分子の吸着状態	塚原　規志	群馬工業高等専門学校	Adsorption states of an organic halogen molecule on semiconductor and metal surfaces	Noriyuki Tsukahara	National Institute for Technology, Gunma College
142	2021-A-0016	Quantum Espressoを用いた無機固体材料の電子状態計算	鈴木　義和	筑波大学数理物質系	Electronic state calculation of inorganic solid materials using Quantum Espresso	Yoshikazu Suzuki	Faculty of Pure and Applied Sciences, University of Tsukuba
143	2021-A-0017	タングステンブロンズの熱伝導度計算	内田　建	東京大学 大学院工学系研究科 マテリアル工学専攻	Calculation of thermal conductivity of Hexagonal Tungsten Bronze	Ken Uchida	Materials Engineering, The University of Tokyo
144	2021-A-0021	ワイドギャップ半導体電子光素子のフォノン制御のためのフォノン物性計算	石谷　善博	千葉大学	Phonon-property analysis for phonon control in electronic/photonic devices by wide-bandgap semiconductors	Ishitani Yoshihiro	Chiba University

2. 強相関 / Strongly Correlated Quantum Systems

No.	課題番号	課題名	氏名	所属	Title	Name	Organization
1	2021-Eb-0006	テンソルネットワーク繰り込み群による臨界現象の研究	川島　直輝	東京大学物性研究所	Tensor-Network Renormalization-Group Study of Critical Phenomena	Naoki Kawashima	Institute for Solid State Physics, University of Tokyo
2	2021-Ea-0007	テンソルネットワーク繰り込み群による臨界現象の研究	川島　直輝	東京大学物性研究所	Tensor-Network Renormalization-Group Studey of Critical Phenomena	Naoki Kawashima	Institute for Solid State Physics, University of Tokyo
3	2021-Eb-0004	高温超伝導の設計に資する非局所クーロン相互作用の効果の解明	今田　正俊	早稲田大学理工学術院	Studies on Effects of Non-Local Coulomb Interaction for High Termperature Superconductivity	Masatoshi Imada	Research Institute for Science and Engineering, Waseda University
4	2021-Ea-0008	量子スピン液体物質におけるモット転移の数値的研究	山地　洋平	物質・材料研究機構	Numerical studies of Mott transitions in quantum spin liquid candidates	Youhei Yamaji	National Institute for Materials Science
5	2021-Ea-0001	パイロクロア格子上の量子スピン液体	今田　正俊	早稲田大学理工学術院	Quantum Spin Liquids on Pyrochlore Lattice	Masatoshi Imada	Research Institute for Science and Engineering, Waseda University
6	2021-Ca-0079	新規ニッケル系超伝導体の多軌道模型に基づく研究	黒木　和彦	大阪大学	Study on new-type of nickelate superconductors based on multiorbital models	Kazuhiko Kuroki	Osaka University
7	2021-Ca-0050	電荷・スピン・軌道結合系に現れる対称性の破れと量子輸送現象の理論的研究	求　幸年	東京大学大学院工学系研究科	Theoretical study of symmetry breaking and quantum transport phenomena in charge-spin-orbital coupled systems	Yukitoshi Motome	Department of Applied Physics, The University of Tokyo
8	2021-Cb-0014	電荷・スピン・軌道結合系に現れる対称性の破れと量子輸送現象の理論的研究	求　幸年	東京大学大学院工学系研究科	Theoretical study of symmetry breaking and quantum transport phenomena in charge-spin-orbital coupled systems	Yukitoshi Motome	Department of Applied Physics, The University of Tokyo
9	2021-Ca-0025	ボルツマンマシンを用いた量子多体系の有限温度計算	野村　悠祐	慶應義塾大学	Finite-temperature calculations for quantum many-body systems using Boltzmann machine	Yusuke Nomura	Keio University
10	2021-Ca-0083	強相関系のトポロジカル相・輸送現象と例外点効果	川上　則雄	京都大学大学院理学研究科物理学宇宙物理学専攻	Topological phases, transport phenomena and effects of exceptional points in strongly correlated systems	Norio Kawakami	Department of Physics, Kyoto University
11	2021-Ca-0103	強相関効果と非エルミート・トポロジーが織りなす異常物性	吉田　恒也	筑波大学　数理物質系	Exotic phenomena induced by strong correlations and non-Hermitian topology	Tsuneya Yoshida	Department of Physics, University of Tsukuba
12	2021-Ca-0117	イリジウム酸化物における電荷スピン軌道エンタングルメント	諏訪　秀麿	東京大学大学院理学系研究科物理学専攻	Charge-spin-orbital entanglement of iridates	Hidemaro Suwa	Department of Physics, The University of Tokyo
13	2021-Ca-0055	重希土類イオンに創出するマルチチャンネル近藤効果の研究	堀田　貴嗣	東京都立大学理学研究科物理学専攻	Research of multi-channel Kondo effect emerging from heavy rare-earth ions	Takashi Hotta	Department of Physics, Graduate School of Science, Tokyo Metropolitan University

14	2021-Ca-0054	キタエフ関連模型におけるトポロジカル熱伝導の数値解析	那須　譲治	東北大学	Numerical study of topological thermal transport in Kitaev-related systems	Joji Nasu	Tohoku University
15	2021-Ca-0009	変分モンテカルロ法によるツイスト二層グラフェンの研究	岡田　健	大阪大学量子情報・量子生命研究センター	Variational Monte Carlo study of twisted bilayer graphene	Ken Okada	Center for Quantum Information and Quantum Biology, Osaka University
16	2021-Ca-0042	遍歴磁性体におけるメロン結晶の探索	速水　賢	東京大学大学院工学系研究科	Searching for meron crystal in itinerant magnets	Satoru Hayami	Department of Applied Physics, The University of Tokyo
17	2021-Ca-0032	キャリアドープされた二次元モット絶縁体の光学伝導度に現れるストリング励起の解析	遠山　貴己	東京理科大学理学部応用物理学科	Analysis of string excitations in the optical conductivity of doped Mott insulators	Takami Tohyama	Department of Applied Physics, Tokyo University of Science
18	2021-Cb-0032	強相関系の励起モードと輸送現象	川上　則雄	京都大学大学院理学研究科物理学宇宙物理学専攻	Excitation modes and transport phenomena in strongly correlated systems	Norio Kawakami	Department of Physics, Kyoto University
19	2021-D-0004	EDXTオリゴマー電荷移動塩のクーロン反発の計算	藤野　智子	東京大学物性研究所	Estimation of Coulomb repulsion in charge transfer salts of EDXT oligomers	Tomoko Fujino	Institute for Solid State Physics, The University of Tokyo
20	2021-Ca-0022	強相関電子系での超伝導状態、および磁性状態のハバードモデルによる研究。	山田　篤志	千葉大学理学研究科	Studies of the superconductivity and magnetic states in the strongly correlated electron systems based on Hubbard models.	Atsushi Yamada	Department of Physics, Chiba University
21	2021-Ba-0005	Kitaevスピン液体のトポロジカル・ネマティック相転移	藤本　聡	大阪大学基礎工学研究科	Topological nematic phase transition in Kitaev spin liquid	Satoshi Fujimoto	Department of Materials Engineering Science, Osaka University
22	2021-Bb-0004	散逸のある周期駆動系における非平衡相の数値的研究	池田　達彦	東京大学物性研究所	Numerical study of nonequilibrium phases in periodically driven systems with dissipation	Tatsuhiko Ikeda	Institute for Solid State Physics, The University of Tokyo
23	2021-Ba-0051	強相関電子系における励起状態のためのニューラルネットワーク量子状態	井戸　康太	東京大学物性研究所	Neural network quantum states for excited states in strongly correlated electron systems	Kota Ido	Institute for Solid State Physics, The University of Tokyo
24	2021-Ba-0015	数値シミュレーションによる金属磁性体中のスキルミオン格子が示す光誘起現象の研究	望月　維人	早稲田大学先進理工学部応用物理学科	Numerical studies on the photoinduced phenomena of magnetic skyrmion lattices in metallic magnets	Masahito Mochizuki	Waseda university
25	2021-Ba-0018	有機導体の強相関ディラック電子系における秩序状態の解明	小林　晃人	名古屋大学　大学院理学研究科	Ordered states in strongly correlated Dirac electron systems of organic conductors	Akito Kobayashi	Graduate School of Science, Nagoya University
26	2021-Ba-0043	4バンドd-p模型を用いた銅酸化物高温超伝導体の解析	渡部　洋	立命館大学	Study of cuprate high-temperature superconductors using 4-band d-p model	Hiroshi Watanabe	Ritsumeikan University
27	2021-Bb-0010	強相関多体電子系における新規量子現象の研究	柳沢　孝	産業技術総合研究所	New quantum phenomena in strongly correlated many-body electron systems	Takashi Yanagisawa	National Institute of Advanced Industrial Science and Technology
28	2021-Bb-0037	Coナノ薄膜の厚み方向磁化分布計算	首藤　健一	横浜国立大学・工学部	Vertical Magnetic distribution of nano-scale Co film	Ken-Ichi Shudo	Yokohama National University
29	2021-Ba-0035	相関電子系における光誘起非平衡ダイナミクス	小野　淳	東北大学大学院理学研究科	Photoinduced nonequilibrium dynamics in correlated electron systems	Atsushi Ono	Department of Physics, Tohoku University

3. 巨視系の協同現象 / Cooperative Phenomena in Complex, Macroscopic Systems

No.	課題番号	課題名	氏名	所属	Title	Name	Organization
1	2021-Eb-0002	音波に対するキャビテーションの影響	浅野　優太	東北大学金属材料研究所	Effects of cavitation on soundwaves	Yuta Asano	Institute for Materials Research, Tohoku University
2	2021-Ea-0002	全原子・粗視化力場によるソフトマターの分子シミュレーション	篠田　渉	岡山大学異分野基礎科学研究所	Molecular Simulation of Soft Materials using All-Atom and Coarse-Grained Force Field	Wataru Shinoda	Okayama University, Research Institute for Interdisciplinary Science
3	2021-Ea-0003	分子動力学シミュレーションによる複雑流体の解析	浅野　優太	東北大学金属材料研究所	Molecular Dynamics Simulation of Complex Fluids	Yuta Asano	Institute for Materials Research, Tohoku University
4	2021-D-0002	多重Qヘッジホッグ型磁気構造のスピン波励起および関連現象の理論的解明	望月　維人	早稲田大学先進理工学部応用物理学科	Theoretical study on the spin-wave excitations of multiple-Q magnetic hedgehogs	Masahito Mochizuki	Waseda university

5	2021-Ca-0089	キタエフスピン液体の有限温度物性の解明	大久保　毅	東京大学大学院理学系研究科知の物理学研究センター	Finite temperature property of the Kitaev spin liquid	Tsuyoshi Okubo	Institute for Physics of Intelligence, The University of Tokyo
6	2021-Ca-0078	生体膜の構造形成	野口　博司	東京大学物性研究所	structure formation of biomembrane	Hiroshi Noguchi	Institute for Solid State Physics, University of Tokyo
7	2021-Ca-0081	量子多体系におけるトポロジカルな秩序と量子操作	藤堂　眞治	東京大学大学院理学系研究科物理学専攻	Topological order and quantum operation in quantum many-body systems	Synge Todo	Department of Physics, University of Tokyo
8	2021-Ca-0016	蛋白質物性に強く関与するソフトモードの効率的サンプリングシミュレー ション	北尾　彰朗	東京工業大学生命理工学院	Efficient sampling simulation of the soft modes significantly contribute to protein properties	Akio Kitao	Institute of Molecular and Cellular Biosciences, University of Tokyo
9	2021-Ca-0005	アンダーソン転移の新奇な普遍クラスの臨界現象	大槻　東巳	上智大学理工学部	Critical phenomena in novel Anderson transitions	Tomi Ohtsuki	Faculty of Science and Technology, Sophia University
10	2021-Ca-0115	分子動力学シミュレーションによるタンパク質凝集体の離合集散の研究	奥村　久士	自然科学研究機構生命創成探究センター	Molecular dynamics simulations for assembly and disassembly of protein aggregates	Hisashi Okumura	Exploratory Research Center on Life and Living Systems, Institute for Molecular Science
11	2021-Ca-0014	量子スピン液体に対するスピン非対角相互作用と双極子相互作用の効果	加藤　雄介	東京大学総合文化研究科広域科学専攻相関基礎科学系	Effects of non-diagonal spin interactions and dipole interaction on quantum spin liquids	Yusuke Kato	Department of Basic Science, The University of Tokyo
12	2021-Cb-0036	マルチスケールシミュレーションを用いた熱機能材料の性能解析	塩見　淳一郎	東京大学工学系研究科	Analysis for Thermal Functional Materials using Multi-scale Simulation	Junichiro Shiomi	School of Engineering, The University of Tokyo
13	2021-Cb-0013	生体膜の構造形成	野口　博司	東京大学物性研究所	structure formation of biomembrane	Hiroshi Noguchi	Institute for Solid State Physics, University of Tokyo
14	2021-Ca-0033	吸水した結晶性高分子の構造と機械的特性	樋口　祐次	九州大学情報基盤研究開発センター	Structure and mechanical properties of crystalline polymers absorbing water molecules	Yuji Higuchi	Research Institute for Information Technology, Kyushu University
15	2021-Ca-0038	HPCを基盤とした実験解析・シミュレーション・データ駆動科学の融合	星　健夫	鳥取大学大学院工学研究科機械宇宙工学専攻応用数理工学講座	HPC-based fusion of experiment analysis, simulation and data-driven science	Takeo Hoshi	Department of Applied Mathematics and Physics, Tottori University
16	2021-Ca-0035	キタエフ量子スピン液体におけるスピン輸送特性	古賀　昌久	東京工業大学	Spin transport through Kitaev spin liquids	Akihisa Koga	Tokyo Institute of Technology
17	2021-Ca-0106	マルチスケールシミュレーションを用いた熱機能材料の性能解析	塩見　淳一郎	東京大学工学系研究科	Analysis for Thermal Functional Materials using Multi-scale Simulation	Junichiro Shiomi	School of Engineering, The University of Tokyo
18	2021-Cb-0025	定常熱伝導下における相界面の解析解析	渡辺　宙志	慶応義塾大学理工学部	Analysis of the phase boundary under the steady-state heat conduction	Hiroshi Watanabe	Faculty of Science and Technology, Keio University
19	2021-Cb-0049	拡張キタエフ模型の有限温度物性の解明	大久保　毅	東京大学大学院理学系研究科知の物理学研究センター	Finite temperature property of the Kitaev models	Tsuyoshi Okubo	Institute for Physics of Intelligence, The University of Tokyo
20	2021-Ca-0102	マルチスケール流動シミュレーション用プラットフォーム(MSSP)を用いた流体―粘弾性体膜の連成シミュレーション	川勝　年洋	東北大学大学院理学研究科物理学専攻	Hybrid simulations on fluid-viscoelastic membrane system using multiscale simulation platform on complex fluids (MSSP)	Toshihiro Kawakatsu	Department of Physics, Faculty of Science, Tohoku University
21	2021-Ca-0053	大域熱力学的釣り合いによりもたらされる非平衡特有の現象	中川　尚子	茨城大学理学部	Steady states realized by a global thermodynamic balance in nonequilibrium	Naoko Nakagawa	Department of Physics, Ibaraki University
22	2021-Cb-0037	厳密対角化法を用いた量子格子模型シミュレーションデータベースCOMPAREDの構築	井戸　康太	東京大学物性研究所	Development of COMPutation ARchive of Exact Diagonalization(COMPARED)	Kota Ido	Institute for Solid State Physics, The University of Tokyo
23	2021-Ca-0043	スピン・フラストレーション系の量子相転移の数値対角化による研究	坂井　徹	兵庫県立大学大学院理学研究科	Numerical Diagonalization Study on Quantum Phase Transitions of Frustrated Spin Systems	Toru Sakai	Graduate School of Science, University of Hyogo
24	2021-Ca-0093	ウイルス感染を阻害する新規人工タンパク質の理論的設計	新井　宗仁	東京大学大学院総合文化研究科	Theoretical Design of Novel Artificial Proteins to Inhibit Viral Infection	Munehito Arai	Graduate School of Arts and Sciences, The University of Tokyo
25	2021-Cb-0027	量子多体系におけるスクランブリングと散逸の効果	手塚　真樹	京都大学大学院理学研究科物理学・宇宙物理学専攻	Scrambling and effect of dissipation in quantum many-body systems	Masaki Tezuka	Department of Physics, Kyoto University

26	2021-Ca-0095	全原子分子動力学シミュレーションによる実在系バイオポリマーの力学的特性及び熱的特性発現の分子機構の解明	岡崎　進	東京大学大学院新領域創成科学研究科物質系専攻	Investigation of the molecular origins of the mechanical and thermal properties of realistic bio-polymers using all-atomistic molecular dynamics	Susumu Okazaki	Department of Advanced Materials Science, The University of Tokyo
27	2021-Ca-0007	ロバスト強靭化高分子ゲルにおける伸長誘起結晶化の分子動力学シミュレーション	眞弓　皓一	東京大学物性研究所	Molecular Dynamics Simulations of Strain-Induced Crystallization in Robust and Tough Polymer Gels	Koichi Mayumi	Institute for Solid State Physics, The University of Tokyo
28	2021-Ca-0049	無秩序キタエフ模型におけるグラス転移	山田　昌彦	大阪大学基礎工学研究科	Glass transition in the disordered Kitaev model	Masahiko Yamada	Department of Materials Engineering Science, Osaka University
29	2021-Ca-0013	ホタル生物発光関連分子の吸収・蛍光スペクトル解析	樋山　みやび	群馬大学	Theoretical analysis of absorption and fluorescence spectra for firefly bioluminescence related molecules	Miyabi Hiyama	Gunma University
30	2021-Cb-0005	非平衡条件下にある表面ナノバブルの分子動力学シミュレーション	中野　裕義	慶応義塾大学理工学部物理情報工学科	Molecular dynamics study of surface nanobubbles under non-equilibrium conditions	Hiroyoshi Nakano	Keio University, Faculty of Science and Technology, Department of Applied Physics and Physico-Informatics
31	2021-Cb-0020	臨界現象のための動的スケーリング解析の開発と改良 II	尾関　之康	電気通信大学情報理工学研究科	Development and improvement of dynamical scaling analysis for critical phenomena II	Yukiyasu Ozeki	Department of Applied Physics and Chemistry, The University of Electro-Communications
32	2021-Ca-0015	トポロジカル相とバルクエッジ対応の科学に関する数値的研究	初貝　安弘	筑波大学大学院数理物質科学研究科物理学専攻	Topological phases and science of bulk-edge correspondence by numerical methods	Yasuhiro Hatsugai	Institute of Physics, University of Tsukuba
33	2021-Cb-0026	三元系クロムカルコゲナイドの磁性と超伝導	Jeschke　Harald	岡山大学異分野基礎科学研究所	Magnetism and superconductivity in ternary chromium chalcogenides	Harald Jeschke	Research Institute for Interdisciplinary Science Okayama University
34	2021-Ca-0036	BaTiO$_{3}$ナノ構造の分子動力学シミュレーション	橋本　保	産業技術総合研究所	Molecular dynamics simulation of BaTiO$_{3}$ nano structure	Tamotsu Hashimoto	National Institute of Advanced Industrial Science and Technology (AIST)
35	2021-Ca-0039	臨界現象のための動的スケーリング解析の開発と改良	尾関　之康	電気通信大学情報理工学研究科	Development and improvement of dynamical scaling analysis for critical phenomena	Yukiyasu Ozeki	Department of Applied Physics and Chemistry, The University of Electro-Communications
36	2021-Ca-0074	MP-SRP法を活用した架橋ネットワークのトポロジー効果のDPDシミュレーション研究	萩田　克美	防衛大学校応用科学群応用物理学科	DPD simulations of cross-linked networks to study topological effect using MP-SRP method	Katsumi Hagita	Department of Applied Physics, School of Applied Sciences, National Defense Academy
37	2021-Ca-0077	ポリマー材料の巨大熱物性データベースの機械学習支援開発	LIAO　YUXUAN	東京大学機械工学専攻	Machine-learning-assisted Development of Giant Thermal-Property Database for Polymer Materials	Yuxuan Liao	Department of Mechanical Engineering, the University of Tokyo
38	2021-Cb-0024	カイラル磁性体における量子効果	加藤　雄介	東京大学総合文化研究科広域科学専攻相関基礎科学系	Quantum effects on chiral magnets	Yusuke Kato	Department of Basic Science, The University of Tokyo
39	2021-Cb-0042	医療・産業応用を指向した新規タンパク質の合理的設計	新井　宗仁	東京大学大学院総合文化研究科	Rational design of novel proteins for medical and industrial applications	Munehito Arai	Graduate School of Arts and Sciences, The University of Tokyo
40	2021-Ca-0099	フラストレート磁性体における新奇秩序	川村　光	神戸大学分子フォトサイエンス研究センター	Novel order in frustrated magnets	Hikaru Kawamura	Molecular Photoscience Research Center, Kobe University
41	2021-Cb-0043	フラストレートした量子磁性体に対する熱ゆらぎの効果	下川　統久朗	沖縄科学技術大学院大学	Thermal effects on quantum frustrated magnetisms	Tokuro Shimokawa	Okinawa Institute of Science and Technology Graduate University
42	2021-Ca-0073	固体間摩擦の3次元有限要素解析	大槻　道夫	大阪大学基礎工学研究科	Three-Dimensional Finite Element Analysis of Friction between solids	Michio Otsuki	Graduate school of engineering science
43	2021-Cb-0017	双極子相互作用を持つ三角格子上のボーズハバード模型における超固体探索	鈴木　隆史	兵庫県立大学　大学院工学研究科	Supersolid phases in the hard-core bosonic Hubbard model on a triangular lattice	Takafumi Suzuki	Graduate School of Engineering, University of Hyogo
44	2021-Ca-0059	希土類永久磁石材料における計測・計算データ同化	松本　宗久	信越化学工業磁性材料研究所	Data assimilation of measurement and simulation for rare-earth permanent magnets	Munehisa Matsumoto	Institute for Magnetic Materials, Shin-Etsu Chemical Engineering

45	2021-Cb-0046	Ground state and dynamical properties of the J_1J_2K-Heisenberg model on the square lattice	ゴウケ　マティアス	沖縄科学技術大学院大学	Ground state and dynamical properties of the J_1J_2K-Heisenberg model on the square lattice	Matthias Gohlke	Okinawa Institute of Science and Technology Graduate University
46	2021-Ca-0021	セラミックス界面におけるナノスケールフォノン散乱機構の解明	藤井　進	大阪大学大学院工学研究科マテリアル生産科学専攻	Nanoscale phonon transport across ceramics interfaces	Susumu Fujii	Division of Materials and Manufacturing Science, Graduate School of Engineering, Osaka University
47	2021-Ca-0110	センサー材料のためのノイズを考慮した量子古典混合アルゴリズム計算	水上　渉	大阪大学 量子情報・量子生命研究センター	Simulations of quantum-classical-hybrid algorithms for sensor materials with considering noise	Wataru Mizukami	Center for Quantum Information and Quantum Biology
48	2021-Cb-0002	SU(N)ハイゼンベルク模型の比熱と磁化率	山田　昌彦	大阪大学基礎工学研究科	Heat capacity and magnetic susceptibility of the SU(N) Heisenberg models	Masahiko Yamada	Department of MaterialsMaterials Engineering Science, Osaka University
49	2021-Cb-0007	ポリマー材料開発の次世代統合工学	吉本　勇太	東京大学 大学院工学系研究科 機械工学専攻	Next-generation integrated engineering for developing polymer materials	Yuta Yoshimoto	Department of Mechanical Engineering, The University of Tokyo
50	2021-Ca-0017	ハニカム格子スピン系の数値的研究	安田　千寿	琉球大学理学部	Numerical study of spin systems on the honeycomb lattice	Chitoshi Yasuda	Department of Physics and Earth Sciences, University of the Ryukyus
51	2021-Ca-0105	Ground state and dynamical properties of the J_1J_2K-Heisenberg model on the square lattice	ゴウケ　マティアス	沖縄科学技術大学院大学	Ground state and dynamical properties of the J_1J_2K-Heisenberg model on the square lattice	Matthias Gohlke	Okinawa Institute of Science and Technology Graduate University
52	2021-Ca-0076	摩擦の物理	松川　宏	青山学院大学理工学部	Physics of Friction	Hiroshi Matsukawa	Faculty of Science and Engineering, Aoyama Gakuin University
53	2021-Cb-0019	スカーミオン等の磁気構造の安定性とダイナミクスの数値解析	近藤　憲治	北海道大学電子科学研究所	Numerical Analysis for Stability and Dynamics of Magnetic Structures such as Skyrmions	Kenji Kondo	Research Institute for Electronic Science
54	2021-Cb-0016	相転移キネティクスとポリアモルフィズム	渕崎　員弘	愛媛大学理工学研究科	Kinetics of phase transition and polyamorphism	Kazuhiro Fuchizaki	Department of Physics, Ehime University
55	2021-Ca-0029	ダイポール相互作用を持つ２次元正方格子上のボーズハバード模型における超固体状態	鈴木　隆史	兵庫県立大学　大学院工学研究科	Supersolid state in a square-lattice Bose-Hubbard model with dipole interactions	Takafumi Suzuki	Graduate School of Engineering, University of Hyogo
56	2021-Ca-0040	量子スピン系の低エネルギー状態に関する数値的研究	中野　博生	兵庫県立大学大学院理学研究科	Numerical study on low-energy states of quantum spin systems	Hiroki Nakano	Graduate School of Science, University of Hyogo
57	2021-Ca-0004	機械学習を用いた代替燃料の低温酸化反応モデル構築	李　敏赫	東京大学大学院工学系研究科機械工学専攻	Development of the Low-Temperature Oxidation Model for Alternative Fuels Using Machine Learning	Minhyeok Lee	Department of Mechanical Engineering, The University of Tokyo
58	2021-Ca-0037	分子動力学シミュレーションを用いた脂質ラフト形成に関する研究	伊藤　暁	分子科学研究所	Formation of lipid rafts studied by molecular dynamics simulation	Satoru Itoh	Institute for Molecular Science
59	2021-Cb-0044	Fe基アモルファス合金の原子間ポテンシャルの作成と結晶化過程の分子動力学シミュレーション	平山　尚美	島根大学次世代たたら協創センター	Development of inter-atomic potentials of Fe-based amorphous alloys and MD simulation of crystallization process	Naomi Hirayama	Next Generation Tatara Co-Creation Centre, Shimane University
60	2021-Ca-0104	フラストレートした量子磁性体に対する熱ゆらぎの効果	下川　統久朗	沖縄科学技術大学院大学	Thermal effects on quantum frustrated magnetisms	Tokuro Shimokawa	Okinawa Institute of Science and Technology Graduate University
61	2021-Cb-0009	磁気スキルミオン結晶における余剰自由度が生み出す新規ダイナミクス	望月　維人	早稲田大学先進理工学部応用物理学科	Novel dynamics of magnetic skyrmion crystal phases due to extra degrees of freedom	Masahito Mochizuki	Waseda university
62	2021-Cb-0050	センサー材料のためのノイズを考慮した量子古典混合アルゴリズム 計算	水上　渉	大阪大学 量子情報・量子生命研究センター	Simulations of quantum-classical-hybrid algorithms for sensor materials with considering noise	Wataru Mizukami	Center for Quantum Information and Quantum Biology
63	2021-Cb-0047	テンソルネットワーク表現を用いたデータ分析手法	原田　健自	京都大学大学院情報学研究科	Data analysis method using a tensor network representation	Kenji Harada	Graduate school of Informatics, Kyoto University
64	2021-Ca-0045	相転移キネティクスとポリアもルフィズム	渕崎　員弘	愛媛大学理工学研究科	Kinetics of phase transition and polyamorphism	Kazuhiro Fuchizaki	Department of Physics, Ehime University

65	2021-Cb-0015	フラストレート磁性体における新奇秩序	川村　光	神戸大学分子フォトサイエンス研究センター	Novel order in frustrated magnets	Hikaru Kawamura	Molecular Photoscience Research Center, Kobe University
66	2021-Ca-0067	テンソルネットワーク表現を用いたデータ分析手法	原田　健自	京都大学大学院情報学研究科	Data analysis method using a tensor network representation	Kenji Harada	Graduate school of Informatics, Kyoto University
67	2021-Ca-0031	大規模メタダイナミクスシミュレーションによるイオン液体の結晶化経路解明	灘　浩樹	産業技術総合研究所環境創生研究部門	Elucidation of pathways for the crystallization of ionic liquids by large-scale metadynamics simulation	Hiroki Nada	Environmental Management Research Institute, National Institute for Advanced Industrial Science and Technology
68	2021-Ba-0001	量子モンテカルロ法を用いたスピンホール磁気抵抗効果の理論研究	加藤　岳生	東京大学物性研究所	Theoretical study of spin Hall magnetoresistance by the quantum Monte Carlo method	Takeo Kato	Institute for Solid State Physics, The University of Tokyo
69	2021-Ba-0016	高次元系におけるテンソルネットワークくりこみ群の改良	森田　悟史	東京大学物性研究所	Improvement of tensor network renormalization for high-dimensional systems	Satoshi Morita	Institute for Solid State Physics, The University of Tokyo
70	2021-Ba-0037	連続体と分子動力学法連成のマルチスケールシミュレーション手法開発	村島　隆浩	東北大学大学院理学研究科	Development of multiscale simulation technique for liquids and solids	Takahiro Murashima	東北大学大学院理学研究科
71	2021-Ba-0045	量子スピン系におけるギャップレスSPT相の研究	押川　正毅	東京大学物性研究所	Study on gapless SPT phases in quantum spin systems	Masaki Oshikawa	Institute for Solid State Physics, University of Tokyo
72	2021-Ba-0002	メゾスコピック素子を介した熱輸送の数値計算	加藤　岳生	東京大学物性研究所	Numerical study of heat transport through a mesoscopic device	Takeo Kato	Institute for Solid State Physics, The University of Tokyo
73	2021-Ba-0012	パイロクロア反強磁性体で実現するスピンテクスチャへの磁気異方性の効果	青山　和司	大阪大学大学院理学研究科宇宙地球専攻	Effect of magnetic anisotropy on spin textures in pyrochlore antiferromagnets	Kazushi Aoyama	Department of Earth and Space Science, Graduate School of Science, Osaka University
74	2021-Ba-0047	１次元・２次元磁性体の有限温度熱力学量の計算手法の開発と実装	堀田　知佐	東京大学総合文化研究科	Development and application of methods to calculate thermodynamic properties in low dimensional magnets	Chisa Hotta	Department of Basic Science, The University of Tokyo
75	2021-Ba-0050	ガウス過程回帰を用いた効率的な相図探索手法の開発	渡辺　宙志	慶応義塾大学理工学部	Development of an Efficient Phase Diagram Exploration Method Using Gaussian Process Regression	Hiroshi Watanabe	Faculty of Science and Technology, Keio University
76	2021-Cb-0021	Biquadratic相互作用のある量子スピン鎖の磁化過程の数値対角化による研究	坂井　徹	兵庫県立大学大学院理学研究科	Numerical Diagonalization Study on Magnetization Process of Quantum Spin Chain with the Biquadratic Interaction	Toru Sakai	Graduate School of Science, University of Hyogo
77	2021-Bb-0034	ブリージングパイロクロア反強磁性体におけるヘッジホッグ格子相の安定性	青山　和司	大阪大学大学院理学研究科宇宙地球専攻	Stability of the hedgehog-lattice topological spin texture in breathing-pyrochlore antiferromagnets	Kazushi Aoyama	Department of Earth and Space Science, Graduate School of Science, Osaka University
78	2021-Ba-0027	ソフトマテリアルの秩序構造とそのダイナミクス、光学的性質の計算	福田　順一	九州大学　大学院理学研究院	Calculation of ordered structures, dynamics and optical properties of soft materials	Jun-Ichi Fukuda	Faculty of Science, Kyushu University
79	2021-Ba-0034	量子近似最適化アルゴリズムに相転移現象が与える影響の探求	白井　達彦	早稲田大学基幹理工学部	The effect of quantum phase transition on the performance of QAOA	Tatsuhiko Shirai	School of Fundamental Science and Engineering, Waseda University
80	2021-Bb-0014	メタダイナミクス法によるスケール形成制御分子デザイン方法の構築	灘　浩樹	産業技術総合研究所環境創生研究部門	Creation of a Method for Design of Scale Formation Control Molecules by a Metadynamics Method	Hiroki Nada	Environmental Management Research Institute, National Institute for Advanced Industrial Science and Technology
81	2021-Bb-0015	2DMATによる２次元物質の構造解析	高山　あかり	早稲田大学	Structure analysis of 2D materials by using 2DMAT	Akari Takayama	Waseda University
82	2021-Bb-0026	高密剛体球系における平衡緩和と相転移	礒部　雅晴	名古屋工業大学	Equilibration and phase transition in the dense hard sphere systems	Masaharu Isobe	Nagoya Institute of Technology
83	2021-Bb-0038	１次元・２次元磁性体の有限温度熱力学量の計算手法の開発と実装2	堀田　知佐	東京大学総合文化研究科	Development and application of methods to calculate thermodynamic properties in low dimensional magnets	Chisa Hotta	Department of Basic Science, The University of Tokyo
84	2021-Ba-0009	トポロジカル超伝導体におけるMajorana量子ビットの数値シミュレーションによる耐性評価	水島　健	大阪大学基礎工学研究科	Numerical study on the tolerance of Majorana-based qubits in topological superconductors	Takeshi Mizushima	Osaka University

85	2021-Ba-0039	タンパク質中の不均一な熱輸送物性の解析	倭　剛久	名古屋大学	Non-uniform thermal transport properties in proteins	Takahisa Yamato	Nagoya University
86	2021-Ba-0052	多元球充填を指導原理とする結晶構造探索	河村　光晶	東京大学物性研究所	Crystal structure search guided by multicomponent sphere packing	Mitsuaki Kawamura	Institute for Solid State Physics, The University of Tokyo
87	2021-Ba-0006	１次元フラストレート量子スピン系の数値的研究	飛田　和男	埼玉大学大学院理工学研究科物質科学部門	Numerical Study of One Dimensional Frustrated Quantum Spin Systems	Kazuo Hida	Division of Material Science, Graduate School of Science and Engineering, Saitama University
88	2021-Ba-0023	有向グラフのスペクトル解析によるクラスタリングの手法開発	羽田野　直道	東京大学生産技術研究所	Novel Spectral Clustering Method of Directed Networks	Naomichi Hatano	Institute of Industrial Science, University of Tokyo
89	2021-Ba-0044	統計力学に基づくイジングマシンの新規アルゴリズム構築	田中　宗	慶應義塾大学理工学部物理情報工学科	Development of Algorithms for Ising Machines Based on Statistical Mechanics	Shu Tanaka	Dept. Applied Physics and Physico-Informatics, Keio University
90	2021-Ba-0048	量子パイロクロア磁性体の磁気励起研究	佐藤　卓	東北大学多元物質科学研究所	Magnetic excitations in the quantum pyrochlore magnet	Taku Sato	Institute of Multidisciplinary Research for Advanced Materials, Tohoku University
91	2021-Bb-0002	Patchy粒子系における構造形成	寺尾　貴道	岐阜大学工学部	Structural formation of patchy particles	Takamichi Terao	Faculty of Engineering, Gifu University
92	2021-Bb-0007	テンソルネットワーク法によるSU(N) Heisenberg模型の磁化過程の研究	金子　隆威	近畿大学	tensor-network study of the magnetization process of the SU(N) Heisenberg model	Ryui Kaneko	Kindai University
93	2021-Bb-0035	イジングモデルを利用した量子シミュレーション	関　優也	慶應義塾大学	Quantum simulation using Ising models	Yuya Seki	Keio University
94	2021-Ba-0032	S=1/2球体カゴメ系{W$_{72}$V$_{30}$}, {Mo$_{72}$V$_{30}$}の熱力学的性質の統一的理解へ向けて	福元　好志	東京理科大学	Towards a unified understanding of thermodynamic properties in S=1/2 spherical kagome systems {W$_{72}$V$_{30}$} and {Mo$_{72}$V$_{30}$}	Fukumoto Yoshiyuki	Tokyo University of Science
95	2021-Bb-0013	ソフトマテリアルの秩序構造とそのダイナミクス，光学的性質の計算	福田　順一	九州大学　大学院理学研究院	Calculation of ordered structures, dynamics and optical properties of soft materials	Jun-Ichi Fukuda	Faculty of Science, Kyushu University
96	2021-Bb-0018	トポロジカルネマティック超流動の分数渦	正木　祐輔	東北大学	Fractional Vortices in Topological Nematic Superfluids	Yusuke Masaki	Tohoku University
97	2021-Bb-0023	高圧下におけるシリカメルトおよびガラスの大規模分子動力学シミュレーションのためのANNポテンシャルの能動学習	若林　大佑	高エネルギー加速器研究機構物質構造科学研究所	Large-scale molecular-dynamics simulation of silica melt and glass under high pressure with ANN potentials by active learning	Daisuke Wakabayashi	Institute of Materials Structure Science, High Energy Accelerator Research Organization (KEK)
98	2021-Bb-0027	量子近似最適化アルゴリズムにおける回路深さ依存性の探求	白井　達彦	早稲田大学基幹理工学部	Circuit-depth dependence of quantum approximate optimization algorithm	Tatsuhiko Shirai	School of Fundamental Science and Engineering, Waseda University
99	2021-Bb-0033	ドープされたFe$_{2}$VAlの熱電性能に関する理論的研究：弱結合理論からのアプローチ	西口　和孝	神戸大学大学院システム情報学研究科	Theoretical study of thermoelectric properties in doped Fe$_{2}$VAl: A weak-coupling approach	Kazutaka Nishiguchi	Graduate School of System Informatics, Kobe University
100	2021-Ba-0010	異なる幅を持つグラフェンナノリボンの電子状態と反応性調査	有馬　健太	大阪大学 大学院 工学研究科	Investigations of electronic structures and reactivity of graphene nanoribbons with different widths	Kenta Arima	Graduate School of Engineering, Osaka University
101	2021-Ba-0049	有機電荷秩序材料における電気伝導度変調の起源に関する研究	酒井　正俊	千葉大学大学院工学研究院電気電子	Origin of the electronic conductivity on organic charge order materials	Masatoshi Sakai	Department of Electrical and Electronic Engineering, Chiba University
102	2021-Ba-0004	Patchy粒子系における構造形成	寺尾　貴道	岐阜大学工学部	Structural formation of patchy particles	Takamichi Terao	Faculty of Engineering, Gifu University
103	2021-Ba-0014	テンソルネットワーク法による2次元冷却原子系の実時間ダイナミクスの計算	金子　隆威	近畿大学	tensor-network calculation of real time dynamics in two-dimensional cold atom systems	Ryui Kaneko	Kindai University
104	2021-Bb-0008	可逆架橋ゴムの分子動力学シミュレーション	保田　侑亮	国立研究開発法人　産業技術総合研究所	Molecular Dynamics Simulations of Reversibly Crosslinked Rubbers	Yusuke Yasuda	National Institute of Advanced Industrial Science and Technology
105	2021-Ba-0003	空間構造をもつ一次元量子スピン系の数値的研究	利根川　孝	神戸大学大学院理学研究科	Numerical Study of the One-Dimensional Quantum Spin Systems with Spatial Structures	Takashi Tonegawa	Graduate School of Science, Kobe University

106	2021-Ba-0008	高密剛体球系における非平衡応答と相転移	礒部　雅晴	名古屋工業大学	Nonequilibrium response and phase transition in the dense hard sphere systems	Masaharu Isobe	Nagoya Institute of Technology
107	2021-Ba-0040	非整合積層系の電子状態：モデル化の検証と応用	苅宿　俊風	物材機構	Electronic structure in mismatched multilayer systems: evaluation and application of the modeling scheme	Toshikaze Kariyado	NIMS
108	2021-Bb-0003	空間構造をもつ一次元量子スピン系の数値的研究	利根川　孝	神戸大学大学院理学研究科	Numerical Study of the One-Dimensional Quantum Spin Systems with Spatial Structures	Takashi Tonegawa	Graduate School of Science, Kobe University
109	2021-Bb-0009	固体電解質材料における粒界イオン伝導の分子動力学解析	小林　亮	名古屋工業大学	Molecular dynamics analyses of ion migration at grain boundaries in solid state electrolyte	Ryo Kobayashi	Nagoya Institute of Technology
110	2021-Bb-0029	三角格子及びかごめ格子上のハイゼンベルグ反強磁性体の励起スペクトルの数値的研究	福元　好志	東京理科大学	Numerical studies on excitation spectra of Heisenberg antiferromagnets on the triangular and Kagome lattices	Fukumoto Yoshiyuki	Tokyo University of Science
111	2021-Ca-0023	細胞の集団回転運動のシミュレーション	松下　勝義	大阪大学理学研究科	Simulation of Cell Collective Rotation	Katsuyoshi Matsushita	Graduate School of Science, Osaka University
112	2021-Ba-0042	有効モデル推定の誤差評価手法開発	田村　亮	国立研究開発法人 物質・材料研究機構	Evaluation method of error in effective model estimation	Ryo Tamura	National Institute for Materials Science
113	2021-Ba-0021	スピン量子ビット伝導機構の解明	棚本　哲史	帝京大学	Analysis of transport properties of spin-qubit based on FinFET	Tetsufumi Tanamoto	Teikyo University
114	2021-Bb-0025	反転対称なハバード模型における多重Q秩序の自発形成	内田　尚志	北海道科学大学	Spontaneous formation of multiple-Q orders in inversion-symmetric Hubbard models	Takashi Uchida	Hokkaido University of Science
115	2021-Bb-0028	有機電荷秩序材料における秩序構造と電気伝導性に関する研究	酒井　正俊	千葉大学大学院工学研究院電気電子	Charge order structure in organic charge order materials	Masatoshi Sakai	Department of Electrical and Electronic Engineering, Chiba University
116	2021-Cb-0003	細胞塊の回転-並進運動遷移の数値研究	松下　勝義	大阪大学理学研究科	Numerical Study of Rotation-Translation Motion Transition of Cell Clusters	Katsuyoshi Matsushita	Graduate School of Science, Osaka University
117	2021-Ba-0013	固有値ソルバの統一的インターフェースRokkoの開発と量子スピン系への応用	坂下　達哉	大阪大学　世界最先端研究機構　量子情報・量子生命研究センター	Development of integrated interface of eigensolvers Rokko and application to quantum spin systems	Tatsuya Sakashita	Center for Quantum Information and Quantum Biology, International Advanced Research Institute, Osaka University
118	2021-Ba-0036	反転対称な二次元ハバード模型における多重スピン密度波	内田　尚志	北海道科学大学	Multiple spin density waves in inversion-symmetric two-dimensional Hubbard models	Takashi Uchida	Hokkaido University of Science
119	2021-A-0002	トポロジカル超流動の分数渦に対する微視的計算	正木　祐輔	東北大学	Microscopic calculations of fractional vortices in topological superfluids	Yusuke Masaki	Tohoku University
120	2021-A-0003	ANNポテンシャルを用いた高圧下におけるシリカメルトの大規模分子動力学シミュレーション	若林　大佑	高エネルギー加速器研究機構物質構造科学研究所	Large-scale molecular-dynamics simulation of silica melt under high pressure with ANN potentials	Daisuke Wakabayashi	Institute of Materials Structure Science, High Energy Accelerator Research Organization (KEK)
121	2021-A-0008	電子豊富なオリゴマー型有機伝導体の電子構造解析	藤野　智子	東京大学物性研究所	Electronic states of electron-rich oligomer-based conductors	Tomoko Fujino	Institute for Solid State Physics, The University of Tokyo
122	2021-A-0014	THz光が誘起するグラフェン中の電子ダイナミクスの理論的研究	佐藤　駿丞	筑波大学計算科学研究センター	Theoretical investigation on THz-field induced electron dynamics in graphene	Shunsuke Sato	Center for Computational Sciences, University of Tsukuba
123	2021-A-0018	複合材料用マトリクス樹脂の分子動力学計算	大矢　豊大	東京理科大学先進工学部	Molecular dynamics simulation of matrix resin for composite materials	Yutaka Oya	Faculty of Advanced Engineering, Tokyo University of Science
124	2021-A-0019	カイロ-フラクタル格子における基底状態	岩瀬　文達	東京医科大学	The ground state of cairo-fractal lattice	Fumitatsu Iwase	Tokyo Medical University
125	2021-A-0020	フラックス法単結晶育成のための核成長用素材スクリーニング	北川　健太郎	東京大学理学系研究科物理学専攻	Screening test for crystal nucleation of flux method	Kentaro Kitagawa	Department of physics, University of Tokyo
126	2021-Bb-0024	固有値ソルバの統一的インターフェースRokkoの開発と量子スピン系への応用	坂下　達哉	大阪大学　世界最先端研究機構　量子情報・量子生命研究センター	Development of integrated interface of eigensolvers Rokko and application to quantum spin systems	Tatsuya Sakashita	Center for Quantum Information and Quantum Biology, International Advanced Research Institute, Osaka University

127	2021-Bb-0030	ゆっくり地震との相互作用による通常の地震の周期変化	鈴木　岳人	青山学院大学	Change in period of ordinary earthquakes due to the interaction with slow earthquakes	Takehito Suzuki	Aoyama Gakuin University
128	2021-Ba-0031	既存Juliaパッケージを活用した分光データの非線形回帰分析の並列化	牧野　哲征	福井大学遠赤外領域開発研究センター	Parallel nonlinear regression analysis for spectroscopic data with existing Julia packages	Takayuki Makino	Research Center for Development of Far-Infrared Region, University of Fukui

2021年度　CCMSスパコン共用事業枠課題一覧 / Supercomputing Consortium for Computational Materials Science Project List of Supercomputer System 2021

※共同利用ではなく共用事業の採択課題一覧。所属は申請時のデータ

前期課題/ The first half term

No.	課題番号	課題名	氏名	所属	Title	Name	Organization
1		希薄電解液の界面張力の大規模分子シミュレーション	芝　隼人	東京大学	Interfacial tension of dilute electrolyte liquid: large-scale molecular simulation study	Hayato Shiba	University of Tokyo
2		擬二次元有機物質κ型BEDT-TTF分子性導体に対する第一原理有効ハミルトニアンの網羅的解析	吉見 一慶	東京大学	A systematic ab initio study of quasi-two-dimensional molecular conductors κ-type BEDT-TTF salts	Kazuyoshi Yoshimi	University of Tokyo
3		大規模GW/BSE法による金属-有機ハイブリッド系の電子状態計算	藤田　貴敏	分子科学研究所	Large-Scale GW/BSE electronic structure calculations for metal-organic hybrid materials	Takatoshi Fujita	Institute for Molecular Science
4		二次電池材料の電子論	小口　多美夫	大阪大学	Electron Theory on Secondary-Battery Materials	Tamio Oguchi	Osaka University
5		貴金属フリーの汎用元素ナノ触媒に向けた第一原理計算	武次　徹也	北海道大学大学院	Ab initio study toward abundant element nanocatalysts with less precious metals	Tetsuya Taketsugu	Hokkaido University
6		分光実験と第一原理計算解析の統合解析による非従来型超伝導機構の解明	今田　正俊	早稲田大学/豊田理化学研究所	Integrated analyses on spectroscopic experiments and ab initio electronic structure calculations for mechanisms of unconventional superconductors	Masatoshi Imada	Waseda University/Toyota Physical and Chemical Research Institute
7		省エネルギー次世代半導体デバイス開発のための量子論マルチシミュレーション	押山 淳	名古屋大学	Quantum-theory-based multiscale simulation for next-generation power devices	Atsushi Oshiyama	Nagoya University
8		第一原理自動網羅計算に基づいた高精度・高速度のハイスループット材料計算ソフトウェアの開発・拡張と磁気特性の評価	福島 鉄也	東京大学	Development of high-throughput calculation tools and evaluation of magnetic properties in hard magnetic materials	Tetsuya Fukushima	University of Tokyo
9		全固体ナトリウム金属電池創成のための新規塩化物固体電解質材料の探索(2)	中山　将伸	名古屋工業大学	Novel chloride solid electrolytes for all solid-state sodium metal battery (2)	Masanobu Nakayama	Nagoya Institute of Technology
10		大規模計算とデータ駆動手法による高性能永久磁石の開発	三宅　隆	産業技術総合研究所	Development of high-performance permanent magnets by large-scale simulation and data-driven approach	Takashi Miyake	National Institute of Advanced Industrial Science and Technology
11		固体電解質界面におけるイオン液体の最適状態探索	鷲津　仁志	兵庫県立大学大学院	Search for the optimum state of the ionic liquid at the solid electrolyte interface	Hitoshi Washizu	University of Hyogo

後期課題/ The second half term

No.	課題番号	課題名	氏名	所属	Title	Name	Organization
1		希薄電解液のイオン解離結合の長時間分子シミュレーション	芝　隼人	東京大学	Ion dissociation and association in dilute electrolyte liquid: long-time molecular dynamics study	Hayato Shiba	University of Tokyo
2		擬二次元有機物質Pd(dmit)2塩の第一原理有効ハミルトニアンの温度依存性とその解析	吉見 一慶	東京大学	Finite temperature dependence of ab-initio Hamiltonians and its analysis for Pd(dmit)2 Salts	Kazuyoshi Yoshimi	University of Tokyo
3		電子状態計算をベースとした非線形光学応答理論の確立とバイオ系・ナノ系への応用	藤田　貴敏	量子科学技術研究開発機構	Developments of non-linear optical response theory based on electronic structure calculations and their applications to nano and biological systems	Takatoshi Fujita	National Institutes for Quantum Science and Technology
4		貴金属フリーの汎用元素ナノ触媒に向けた第一原理計算	武次　徹也	北海道大学大学院	Ab initio study toward abundant element nanocatalysts with less precious metals	Tetsuya Taketsugu	Hokkaido University
5		炭素導電助剤へのアニオン挿入機構の理論的解析	山田 淳夫	東京大学	Theoretical Analysis of Anion Insertion Mechanism into Conductive Carbon	Atsuo Yamada	University of Tokyo
6		電子デバイス応用に向けた軽元素B, C, Nからなる原子膜積層系の設計と物性予測	斎藤　晋	東京工業大学	Electronic properties and materials design of stacked B-C-N atomic layers for next-generation devices	Susumu Saito	Tokyo Institute of Technology

7		銅酸化物の超伝導機構解析	今田　正俊	早稲田大学/豊田理化学研究所	Analysis on Superconducting Mechanism of Cuprate Superconductors	Masatoshi Imada	Waseda University/Toyota Physical and Chemical Research Institute
8		省エネルギー次世代半導体デバイス開発のための量子論マルチシミュレーション	押山 淳	名古屋大学	Quantum-theory-based multiscale simulation for next-generation power devices	Atsushi Oshiyama	Nagoya University
9		磁性界面の第一原理計算	合田 義弘	東京工業大学	First-principles study of magnetic interfaces	Yoshihiro Gohda	Tokyo Institute of Technology
10		次世代型燃料電池のための酸化物電極物質の設計	杉野 修	東京大学	Design of oxide electrocatalyst for next-generation fuel cells	Osamu Sugino	University of Tokyo
11		永久磁石材料を対象とした磁気異方性エネルギーのハイスループット計算	福島 鉄也	東京大学	High-throughput calculation of magnetic anisotropy energy in permanent magnet materials	Tetsuya Fukushima	University of Tokyo

The Institute for Solid State Physics (ISSP), The University of Tokyo

Address	5-1-5 Kashiwanoha, Kashiwa, Chiba, 277-8581, Japan
Phone	+81-4-7136-3207
Home Page	https://www.issp.u-tokyo.ac.jp